Environmental Chemistry for a Sustainable World

Inamuddin
Mohd Imran Ahamed
Abdullah M. Asiri
Eric Lichtfouse *Editors*

Nanophotocatalysis and Environmental Applications

Energy Conversion and Chemical Transformations

Springer

Environmental Chemistry for a Sustainable World

Volume 31

Other Publications by the Editors

Books
Environmental Chemistry
http://www.springer.com/978-3-540-22860-8

Organic Contaminants in Riverine and Groundwater Systems
http://www.springer.com/978-3-540-31169-0

Sustainable Agriculture
Volume 1: http://www.springer.com/978-90-481-2665-1
Volume 2: http://www.springer.com/978-94-007-0393-3

Book series
Environmental Chemistry for a Sustainable World
http://www.springer.com/series/11480

Sustainable Agriculture Reviews
http://www.springer.com/series/8380

Journals
Environmental Chemistry Letters
http://www.springer.com/10311

More information about this series at http://www.springer.com/series/11480

Inamuddin • Mohd Imran Ahamed
Abdullah M. Asiri • Eric Lichtfouse
Editors

Nanophotocatalysis and Environmental Applications

Energy Conversion and Chemical Transformations

Springer

Editors
Inamuddin
Chemistry Department, Faculty of Science
King Abdulaziz University
Jeddah, Saudi Arabia

Mohd Imran Ahamed
Department of Chemistry
Aligarh Muslim University
Aligarh, India

Abdullah M. Asiri
Chemistry Department, Faculty of Science
King Abdulaziz University
Jeddah, Saudi Arabia

Eric Lichtfouse
CEREGE, CNRS, IRD, INRA, Coll France
Aix-Marseille University
Aix-en-Provence, France

ISSN 2213-7114 ISSN 2213-7122 (electronic)
Environmental Chemistry for a Sustainable World
ISBN 978-3-030-04948-5 ISBN 978-3-030-04949-2 (eBook)
https://doi.org/10.1007/978-3-030-04949-2

Library of Congress Control Number: 2019932801

This Springer imprint is published by the registered company Springer Nature Switzerland AG.
The registered company address is: Gewerbestrasse 11, 6330 Cham, Switzerland

Preface

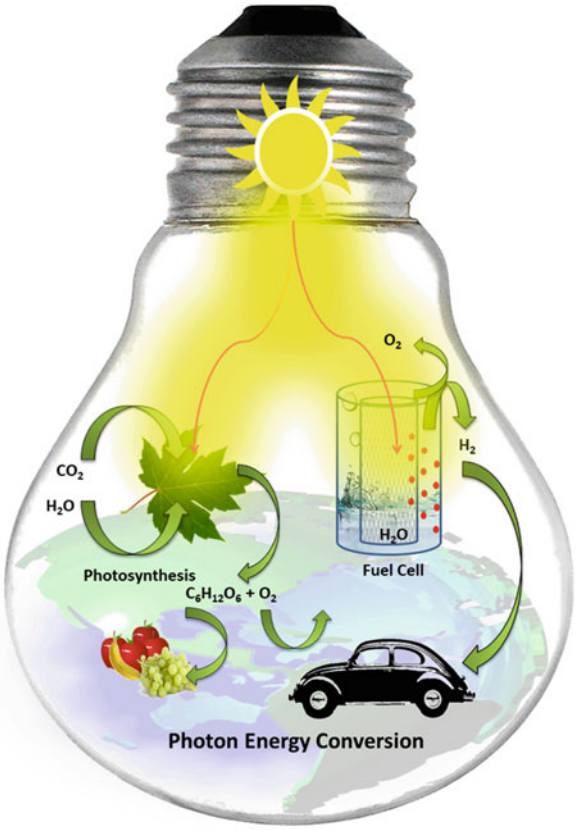
O_2
H_2
CO_2
H_2O
H_2O
Photosynthesis
$C_6H_{12}O_6 + O_2$
Fuel Cell
Photon Energy Conversion

The global energy crisis and climate change have been labelled as the most critical environmental challenges in terms of both research and remediation. Non-renewable energy resources fulfil nearly 85% of world energy demands leading to global warming and depletion of resources. The exhaustion of finite fuels should be addressed for a sustainable energy future. Therefore, research is ongoing to harness the renewable energy during the processes such as photocatalytic and bioproduction of hydrogen and other fuels. The use of renewable sources of energy and the mitigation of climate change or global warming are interrelated, and, if both are worked upon simultaneously, it certainly will make a difference.

The increasing global demand for energy is a result of a population explosion, which is demanding the intention towards the development of effective strategies for energy conversion and the reduction of greenhouse gas emissions. This can obviously be achieved by focussing on non-fossil sources of energy such as solar, thermal, hydrogen and nuclear energy as well as CO_2 capture and photoconversion of CO_2 into fuels. Advanced oxidation processes have evolved during the years, and scientists are using photocatalysis for energy conversion especially harnessing of solar energy.

Photocatalytic water splitting for H_2 and O_2 production using semiconductors is the most promising fields as a green technology that is accounted for economic importance. The direct semiconductors mediated water splitting for hydrogen generation as clean fuel can be performed on a large scale for practical applications. In general, there are many efficient catalysts reported for the same, but these are active in ultraviolet light only. The challenge still lies in designing low-cost catalysts that show high quantum efficiency, ability to work under visible and sunlight as well as the ability to work without noble metals as co-catalysts. Many works with high quantum efficiencies have reported on solar- and visible-powered hydrogen emission by designing novel catalysts by surface modifications, sensitizations, immobilization, formation of Z-scheme junctions, dye-sensitized solar cells, etc. Recently, significant progress is made to develop and engineer various photocatalysts for this purpose. The prime solution is bandgap engineering that involves bandgap broadening or narrowing, interparticle electron coupling, reducing recombination of charge carriers, plasmon-exciton coupling and high surface energy of the catalysts.

Additionally, combustion of fuels and industrial effluents has been threatening as they release alarming amounts of greenhouse gas as CO_2. According to the various studies, the CO_2 level may reach 750 ppm and raise the global temperature further. Photocatalytic reduction of CO_2 into syngas, methane, carbon monoxide, methanol, formic acid and formaldehyde has its own advantages as lowering of greenhouse gas levels and energy production simultaneously. Photocatalytic reduction of CO_2 into fuels is, however, more complicated process as compared to water splitting. This is because of its dependence on thermodynamics and kinetics of light absorption, band potentials, charge separation and largely the activation of catalyst, i.e. adsorption of CO_2. Various organic materials as part of catalysts or supports such as carbon nanotubes, graphene, graphene oxide, carbon nitride, etc. for CO_2 activation as adsorption and interaction with the catalyst is an important requirement of the reaction. In addition, very few solar active catalysts are available which are capable

of reducing carbon dioxide. The photocatalytic conversion of CO_2 into fuels is in its embryonic stage, and a substantial development and progress are still required. It is therefore important to study and analyse various catalysts and technologies developed so far for better modification and upgradation. Among various energy conversion applications, photocatalysis has also been promising for removal of NO_x gases, volatile organic carbon removal, air clean-up filters and catalytic converters for vehicle exhausts.

Nanophotocatalysis and Environmental Applications: Energy Conversion and Chemical Transformations is focussed on fuel production as a source of renewable energy using photocatalysis. The application of photocatalysis is discussed in areas such as fuel production including carbon monoxide, formic acid, methanol, methane and hydrogen and CO_2 reduction and water splitting, water purification and purification of food industry wastewater and organic synthesis using various types of photocatalytic materials such as quantum dots, graphitic carbon nitride, metal oxides, Z-scheme photocatalysts, metal organic frameworks, composites and polymeric semiconductors. This is beneficial for analysing the current progress underway, which certainly paves ways for new directions for breakthrough technologies to be developed. Based on thematic topics, the book edition contains the following nine chapters:

Chapter 1 gives an overview of the main methods to obtain quantum dots and some examples of their use as a photocatalyst for fuel production.

Chapter 2 summarizes the works on the photocatalytic hydrogen production using highly stable TiO_2-based heterostructured photocatalysts. The emphasis is given on three important characteristics, namely, UV-active TiO_2-based photocatalysts, visible-active TiO_2-based photocatalysts and the effects of various carbon nanostructures on the photocatalytic hydrogen production efficacy of TiO_2-based heterostructured photocatalysts.

Chapter 3 highlights the method of synthesis of photocatalysts and their possible modification for performance enhancement in water splitting and CO_2 reduction.

Chapter 4 provides the basic principles, terminologies, concepts, state-of-the-art achievements and the charge transfer mechanism of the photocatalytic reduction of CO_2 using artificial Z-scheme photocatalysts. In spite of these, the development on semiconductor photocatalytic materials from the perspective of light harvesting as well as the co-catalyst strategy for potentially boosting the activity and/or product selectivity for the photocatalytic reduction of CO_2 along with the future direction of research using Z-scheme systems are also discussed and highlighted.

Chapter 5 deals with the importance of photocatalysts and their applications for artificial photosynthesis. The primary photosynthetic applications of photocatalysts such as supramolecular artificial photosynthetic systems, covalently linked molecular systems and general mechanism of photosynthesis are also discussed in detail.

Chapter 6 discusses various chemical methodologies, properties and photocatalytic applications of polymeric semiconductors (carbon nitride, C_3N_4), graphene, and metal-organic framework (MOF)-based hybrid nanostructured photocatalysts for the water purification and the solar hydrogen production.

Chapter 7 summarizes the innovative aspects of the applicability of photocatalysis and technological advances with particular attention to the photocatalytic energy recovery, organic synthesis and new reactor configurations. In particular, the chapter discusses the possibility to produce an energy source such as hydrogen and/or methane from the degradation of organic substance present in wastewater by heterogeneous photocatalysis. The chapter also reports simultaneous valorization and purification of food industry wastewater using structured photocatalysts.

Chapter 8 focusses on some important nano-semiconductor photocatalysts like TiO_2, ZnO and graphitic carbon nitride and various strategies adopted for improving their photocatalytic activity under sunlight. Different methods for improving visible light active photocatalysts including metal/nonmetal doping, the addition of photosensitive materials, the incorporation of other nanoparticles, the composite formation with other semiconductors and the formation of heterojunctions and nanohybrids are discussed.

Chapter 9 reviews the state-of-the-art progresses in the use of common photocatalytic materials for the purpose of four important classes of organic synthesis, namely, oxidation of alcohols, oxidative cleavage of olefins, reduction of nitro compounds and cyclisation; carbon-hetero bond formation and alkylation will be reviewed.

Jeddah, Saudi Arabia — Inamuddin
Aligarh, India — Mohd Imran Ahamed
Jeddah, Saudi Arabia — Abdullah M. Asiri
Aix-en-Provence, France — Eric Lichtfouse

Contents

Contributors

Annelise Kopp Alves Universidade Federal do Rio Grande do Sul, Porto Alegre, RS, Brazil

K. S. Ambili Research Department of Chemistry, Kuriakose Elias College, Kottayam, Kerala, India

R. Badri Narayan Department of Chemical Engineering, Sri Sivasubramaniya Nadar College of Engineering, Chennai, Tamil Nadu, India

Busra Balli Sen Research Group, Biochemistry Department, Faculty of Arts and Science, Dumlupınar University, Kütahya, Turkey

U. Bhargava Nano Catalysis and Solar Fuels Research Laboratory, Department of Materials Science & Nanotechnology, Yogi Vemana University, Kadapa, Andhra Pradesh, India

Chiranjib Bhattacharjee Chemical Engineering Department, Jadavpur University, Kolkata, West Bengal, India

Paolo Ciambelli Department of Industrial Engineering, University of Salerno, Fisciano, SA, Italy

Buse Demirkan Sen Research Group, Biochemistry Department, Faculty of Arts and Science, Dumlupınar University, Kütahya, Turkey

K. P. Gopinath Department of Chemical Engineering, Sri Sivasubramaniya Nadar College of Engineering, Chennai, Tamil Nadu, India

R. Goutham Department of Chemical Engineering, Sri Sivasubramaniya Nadar College of Engineering, Chennai, Tamil Nadu, India

Enamul Haque School of Medicine and Centre for Molecular and Medical Research, Deakin University, Waurn Ponds, VIC, Australia

Giuseppina Iervolino Department of Industrial Engineering, University of Salerno, Fisciano, SA, Italy

Raghava Reddy Kakarla The School of Chemical and Biomolecular Engineering, The University of Sydney, Sydney, NSW, Australia

Sudesh Kumar Department of Chemistry, Banasthali University, Banasthali Vidyapith, Vanasthali, Rajasthan, India

Murikinati Mamatha Kumari Nano Catalysis and Solar Fuels Research Laboratory, Department of Materials Science & Nanotechnology, Yogi Vemana University, Kadapa, Andhra Pradesh, India

S. Naveen School of Basic Sciences, Jain University, Bangalore, India

A. Ramprasath Department of Chemical Engineering, Sri Sivasubramaniya Nadar College of Engineering, Chennai, Tamil Nadu, India

N. Ramesh Reddy Nano Catalysis and Solar Fuels Research Laboratory, Department of Materials Science & Nanotechnology, Yogi Vemana University, Kadapa, Andhra Pradesh, India

Ch. Venkata Reddy School of Mechanical Engineering, Yeungnam University, Gyeongsan, South Korea

Veera Sadhu School of Physical Sciences, Banasthali University, Banasthali Vidyapith, Vanasthali, Rajasthan, India

Santanu Sarkar Environment Research Group, R&D, Tata Steel Ltd., Jamshedpur, Jharkhand, India

Shubhrajit Sarkar Chemical Engineering Department, Jadavpur University, Kolkata, West Bengal, India

Supriya Sarkar Environment Research Group, R&D, Tata Steel Ltd., Jamshedpur, Jharkhand, India

Betul Sen Sen Research Group, Biochemistry Department, Faculty of Arts and Science, Dumlupınar University, Kütahya, Turkey

Fatih Sen Sen Research Group, Biochemistry Department, Faculty of Arts and Science, Dumlupınar University, Kütahya, Turkey

M. V. Shankar Nano Catalysis and Solar Fuels Research Laboratory, Department of Materials Science & Nanotechnology, Yogi Vemana University, Kadapa, Andhra Pradesh, India

S. K. Soni Sustainable Living Lab, School of Science, RMIT University, Melbourne, VIC, Australia

B. Srikanth Department of Chemical Engineering, Sri Sivasubramaniya Nadar College of Engineering, Chennai, Tamil Nadu, India

Song Sun National Synchrotron Radiation Laboratory, Collaborative Innovation Center of Chemistry for Energy Materials, University of Science & Technology of China, Hefei, China

Jesty Thomas Research Department of Chemistry, Kuriakose Elias College, Kottayam, Kerala, India

Vincenzo Vaiano Department of Industrial Engineering, University of Salerno, Fisciano, SA, Italy

Xiaodi Zhu National Synchrotron Radiation Laboratory, Collaborative Innovation Center of Chemistry for Energy Materials, University of Science & Technology of China, Hefei, China

Chapter 1
Nanophotocatalysts for Fuel Production

Annelise Kopp Alves

Contents

Abstract Quantum dots, particles with diameters from 2 up to 20 nm, are one of the sweethearts of nanotechnology because their properties are intermediate between bulk and discrete molecules and can be tuned according to their size and shape. Nowadays, quantum dots are one of the most common nanophotocatalysts used to produce fuel using ultraviolet, visible, or solar light. Traditional methods such as sol-gel, hydrothermal synthesis, e-beam lithography, microwave synthesis, and chemical vapor deposition, among others, are suitable for produced quantum dot photocatalysts. In this context, the most common fuels obtained using photocatalysts are carbon monoxide, formic acid, methanol, methane, and hydrogen. In this chapter, it will be given an overview of the main methods to obtain quantum dots and some examples of their use as a photocatalyst for fuel production.

Keywords Quantum dots · Photocatalysis · Fuel · Hydrogen · Semiconductors · Solar light

A. K. Alves (✉)
Universidade Federal do Rio Grande do Sul, Porto Alegre, RS, Brazil
e-mail: annelise.alves@ufrgs.br

Inamuddin et al. (eds.), *Nanophotocatalysis and Environmental Applications*,
Environmental Chemistry for a Sustainable World 31,
https://doi.org/10.1007/978-3-030-04949-2_1

1.1 Introduction

The search for an alternative to fossil fuels as an energy source is more in evidence than ever. The number of gases in the atmosphere that may cause climate changes is ever growing due to industrialization, the need to transport goods and people, and the increasing consumption of energy in general. There are already different approaches to harvest energy in a not-so-environmentally damaging way. Energy is available from the wind, the tides, and the sun at practically no cost. All that is needed is a mechanism that collects, stores, and transfers efficiently the energy nature already offers to the human been use.

In this regard, researches have tried to find similar results to what happens in plants, the photosynthesis. It is a complex group of chemical reactions that basically transforms CO_2 and water into carbohydrates (fuels) using the sun's light. In the last 10 years (up to April 2018), there are approximately 3921 scientific papers published regarding the synthesis and application of photocatalysts for fuel production (Fig. 1.1).

The most common fuel photocatalytic produced is, by far, hydrogen, followed by methanol and methane. In these processes, UV, visible light, or solar simulators as light sources and different types of photocatalysts were used. This chapter will describe a review of the most recent publications relating to the synthesis of nanophotocatalysts for fuel production.

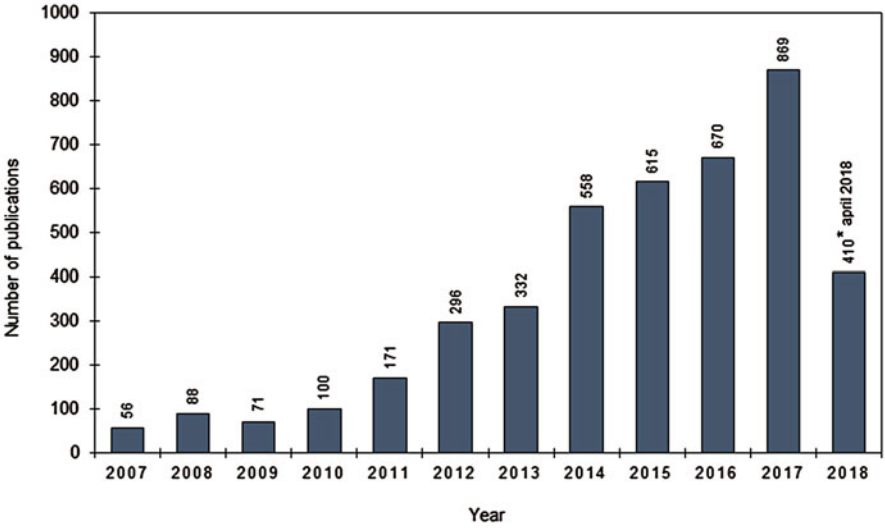

Fig. 1.1 A number of publications by year, consulting the term "photocatalyst fuel production" in the Web of Science database

1.2 Quantum Dot Semiconductors

Quantum dots are semiconductors particles with diameters from 2 up to 20 nm. They are one of the sweethearts of nanotechnology because their properties are intermediate between bulk and discrete molecules and can be tuned according to their size and shape.

Different routes have been used to synthesize quantum dots using both top-down and bottom-up techniques. Top-down methods include molecular beam epitaxy (Biswas et al. 2018), ion implantation (Kwak et al. 2018), e-beam lithography (Kaganskiy et al. 2018), and X-ray lithography (Bertino et al. 2007). In bottom-up methods, wet chemical and vapor phase methods are used. Wet chemical methods are generally microemulsion (Liu et al. 2014), sol-gel (Adhikari et al. 2017), competitive reaction chemistry (Liu et al. 2018a), and microwave synthesis (Lia et al. 2018). Vapor phase methods include sputtering (Hong et al. 2017), vapor phase epitaxy (Tile et al. 2018), and chemical vapor deposition (Yang et al. 2016). The process mechanism of quantum dot-based photocatalysis is not yet fully understood. In homogeneous photocatalysis, the light can be absorbed by both the quantum dot and the pollutant molecule. According to a proposed pathway for the photocatalytic activity of the quantum dots, electrons in the valence band of quantum dots could be excited to the conduction band and electron-hole pairs could be generated. The photogenerated electrons can produce superoxide and hydrogen peroxide radicals. The valence band holes can directly oxidize the pollutants adsorbed on the surface of quantum dots or mineralize them indirectly through hydroxyl radicals generated by the reaction of holes and water molecules (Rajabi 2016). Table 1.1 summarizes some of the most recent application of quantum dot used in the photocatalytic process.

1.3 Synthesis of Quantum Dots

The most traditional approach for the synthesis of quantum dots is called hot-injection organometallic synthesis. It is based on the heating of organic solvents and the rapid injection of the semiconductor precursor, under an inert atmosphere in a batch reactor. This technique was introduced by Murray et al. in 1993 (1993). In this foundational work, a series of quantum dots (CdE; E=S, Se, Te) with sizes from 1.5 to 11.5 nm was obtained by controlling the growth temperature.

In 2016, Mir et al. (2016) compared the structural, optical, and sensing properties of CdSe synthesized using the hot-injection method and a room temperature synthesis protocol. In the first method, the quantum dot had sizes from 2.5 up to 6.3 nm, compared to the practically monomodal 3.3 nm obtained using the room temperature method. It was observed by the authors that despite the versatility of the hot-injection synthesis that may be considered to be supreme as room temperature methods regarding the production of particles of different size, it yields products that have limited sensing capability compared to those synthesized at room temperature.

Table 1.1 Application of quantum dots in the photocatalytic process

Type of quantum dot	Synthesis method	Parameter evaluated	Reference
Carbon quantum dots/graphene aerogel	Hydrothermal	Photoreduction of Cr (VI)	Wang et al. (2018a)
N-rich carbon quantum dots decorated two-phase TiO_2	Microwave assisted	CO_2 photoreduction	Li et al. (2018)
ZnO_{1-x}/carbon dots composite	Aerosol	CO_2 photoreduction	Lin et al. (2018)
Carbon dots modified MoO_3/g-C_3N_4	Hydrothermal	Tetracycline photocatalysis	Xie et al. (2018)
TiO_2 quantum dots embedded in SiO_2 foams	Sol-gel	Photocatalytic H_2 evolution	Panb et al. (2018)
CdS quantum dots/BiOCl nanocomposites	Conventional wet-chemistry precipitation	Methyl orange and phenol photodegradation	Pan et al. (2018)
CdS quantum dots/Ti_3^+-TiO_2 nanobelts	Hydrothermal-chemical bath deposition	Methylene blue visible light photocatalysis and hydrogen production	Zhao et al. (2018)
Carbon dots and AgCl over g-C_3N_4 nanosheets	Sol-gel and microwave assisted	Rhodamine B, methylene blue, methyl orange, and phenol photocatalysis	Asadzadeh-Khaneghah et al. (2018)
Carbon dots and CdS quantum dot – TiO_2 composite	Carbo dots: hydrothermal treatment; CdS quantum dots: conventional wet-chemistry precipitation	Visible light photocatalysis of benzene and toluene	Wang et al. (2018b)
Vanadate quantum dots/g-C_3N_4	Ultrasound	Salmonella under visible light disinfection	Wang et al., (2018c)

Reactive direct current magnetron sputtering method is one of the methods used to obtain quantum dots for large-scale production. In the work of Patel et al. (2018), NiO quantum dots were produced by this method using Ni target of 99.999% purity, with flowing Ar and O_2. They have used a sputtering power of 50 W and working pressure of 3 mTorr. The NiO quantum dot was deposited over glass or fluorine-doped tin oxide (FTO) glass substrates and presents an average diameter from 5 to7 nm (Fig. 1.2).

Alternatively, the group of Hong et al. (2018) produced NiO quantum dot embedded into TiO_2 particles using the temperature-programmed method. This method consists of mixing TiO_2 powder, urea, and nickel nitrate and heating this mixture under an N_2 atmosphere at 500 °C, followed by annealing at 800 °C, obtaining N-doped carbon coating. To remove the carbon the temperature was

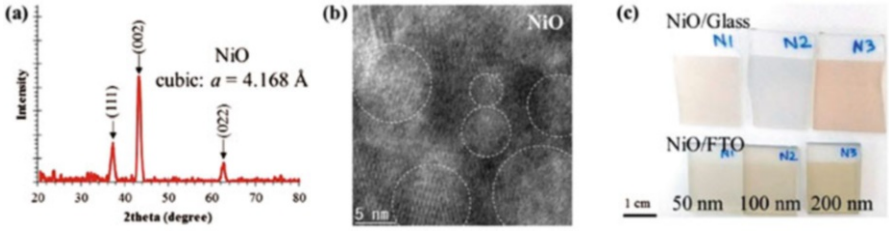

Fig. 1.2 NiO quantum dot obtained by magnetron sputtering method: (**a**) X-ray diffraction analysis; (**b**) transmission electron microscopy image of the NiO quantum dot; (**c**) thickness of the samples obtained over glass and fluorine-doped tin oxide glass (Reprinted with permission from Patel et al. 2018)

maintained at 800 °C in air. NiO quantum dot of 2 nm covered TiO_2 nanoparticles of 50–200 nm (Fig. 1.3) were synthesized by this method.

Colloidal quantum dots can be obtained using water as a solvent. In the work of Li et al. (2017), $AgInSe_2$ quantum dot for sensitized solar cell was produced using a direct aqueous synthesis using glutathione as a stabilizer. The method was based on the dissolution of SeO_2 and $NaBH_4$ in deionized water at room temperature and the mixture of this solution to an $AgNO_3$ and $I(NO_3)_3$ solution. The final mixture was microwaved in the presence of a stabilizer (thioglycolic acid, 3-mercaptopropionic acid, or glutathione) at 160 °C for 10 min. Agglomerated particles of average diameter of 50 nm were obtained (Fig. 1.4a) and the incident photon to current efficiency (IPCE) of the samples synthesized using different stabilizers was measured. The glutathione was the best stabilizer using the proposed synthesis protocol, due to the functional moieties that promote a strong coordination with the quantum dots, facilitating electron injection between the quantum dots and TiO_2 in solar cells.

Typically, quantum dots synthesized via colloidal methods have an insulating layer of a long-chain organic ligand. This prevents their direct use in electronic devices due to the weak interparticle coupling (Choi et al. 2017). To overcome this issue, considering a large-scale method for the production of quantum dot films, the spray synthesis is an interesting alternative. Among these methods, supersonic (Choi et al. 2017), ultrasonic (Ji et al. 2017), and thermal spray coating (Yadav et al. 2016) are the most suitable for the production of quantum dot.

Choi et al. (2017) produced quantum dot films over fluorine-doped tin oxide glass substrates by supersonic spraying technique using PbS quantum dot inks, prepared by solution-phase ligand exchange using methylammonium lead iodide ($MAPbI_3$) (Fig. 1.5). This method promotes the rapid evaporation of the solvent and the deposition of the PbS quantum dot without further annealing treatments. Varying the number of sweeps during the deposition process, it was possible to obtain different film thickness, with an average roughness of 3.4 nm.

The ultrasonic spray coating method was used by Ji et al. (2017) to deposit ZnCdSSE/ZnS core/shell-structured quantum dot (Fig. 1.6b), over indium tin oxide (ITO)-coated glass substrate and multilayers of NiO, Al_2O_3, and NiO (Fig. 1.6a). In the deposition process, the solution precursor (using toluene for the

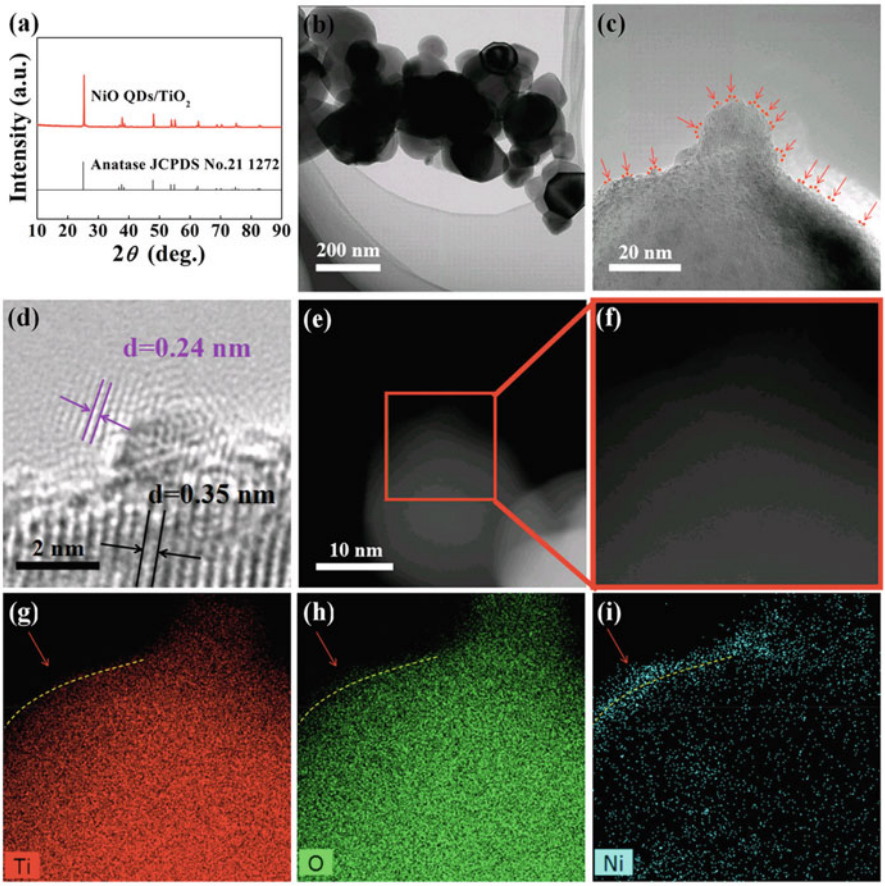

Fig. 1.3 NiO quantum dot/TiO_2 obtained by temperature-programmed method: (**a**) X-ray diffraction pattern, (**b**) transmission electron microscopy image of NiO quantum dots/TiO_2, (**c**, **d**) high-resolution transmission electron microscopy image of NiO quantum dots/TiO_2, (**e**, **f**) high-angle annular dark-field images of NiO quantum dots/TiO_2 and elemental mapping results of (**g**) Ti, (**h**) O, and (**i**) Ni (Reprinted with permission from Hong et al. 2018. Copyright 2018 American Chemical Society)

quantum dot and ethanol for the other precursors) flowed into an atomizer, using N_2 as a carrier gas and subsequently atomized at a spray rate of 0.3 mL/min. The thicknesses of the layers were around 40 nm.

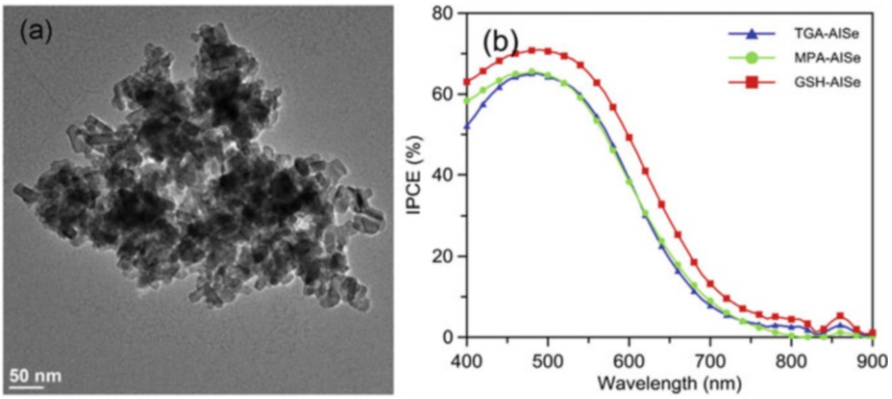

Fig. 1.4 (**a**) Transmission electron microscopy image of $AgInSe_2$ quantum dot for sensitized solar cell produced using a direct aqueous synthesis using glutathione as a stabilizer. (**b**) $AgInSe_2$ quantum dot incident photon to current efficiency results comparing different stabilizers (Adapted and reprinted with permission from Li et al. 2017)

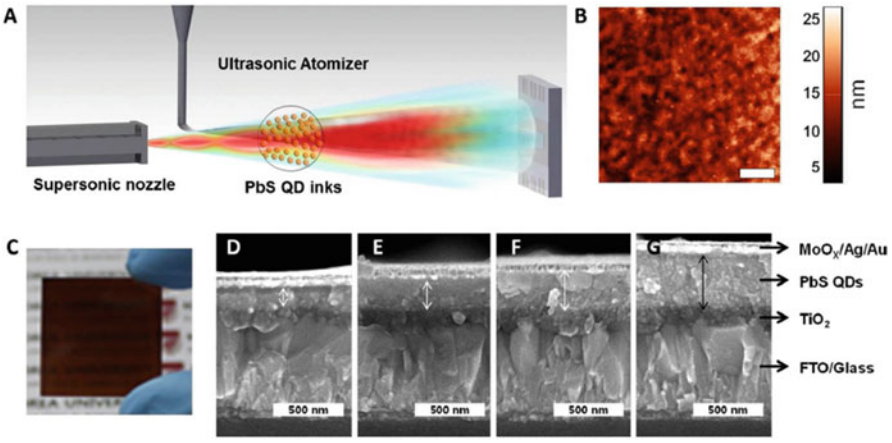

Fig. 1.5 (**a**) Schematic of ultrasonic spray deposition of PbS quantum dot ink. (**b**) Atomic force microscopy image (scale bar 1 μm), (**c**) photographic image, and (**d**–**g**) cross-sectional scanning electron microscopy images (scale bars 500 nm) of PbS quantum dot films deposited by ultrasonic spray coating for (**d**) 8 sweeps, (**e**) 10 sweeps, (**f**) 12 sweeps, and (**g**) 14 sweeps (Reprinted with permission from Choi et al. 2017)

1.4 Application of Quantum Dots for Fuel Production

The use of photocatalytic processes to obtain fuels using nanoparticles (quantum dots) is a focus of research around the world. The most common fuels produced using these methods are methane, methanol, and formic acid (via CO_2 fixation) and hydrogen (via water splitting into electrochemical cells).

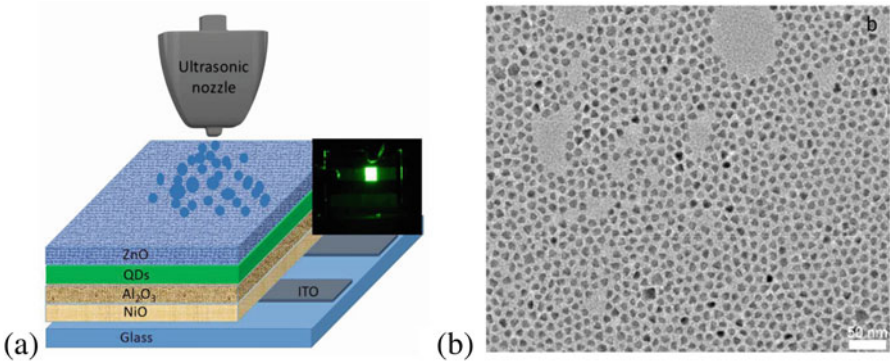

Fig. 1.6 (**a**) Schematic diagram of an ultrasonic spray nozzle and deposited layers. (**b**) Transmission electron microscopy image of the ZnCdSSe/ZnS quantum dots (Reprinted with permission from Ji et al. 2017. Copyright 2018 American Chemical Society)

The group of Yadav et al. (2016) synthesized graphene quantum dot photocatalysts to produce formic acid from CO_2 using visible light. The graphene quantum dot was functionalized with a chromophore organic molecule. To promote the selective production of formic acid, an enzyme (formate dehydrogenase) was added to the photocatalysis reaction flask. A Rh complex was used as proton transfer molecule. The reaction occurs at room temperature using a 450 W xenon lamp (100 $mWcm^2$), under a CO_2 flow (0.5 ml/min). The authors achieved a selective production of formic acid in these conditions at a rate of 1.658 μmol/min, when using functionalized graphene quantum dot as a photocatalyst, in comparison with a rate of 0.0475 μmol/min when pristine graphene quantum dot where used.

Another way to transform CO_2 in useful compounds using photocatalysis is exemplified in the work of Xu et al. (2018). In their work, TiO_2 nanofibers obtained using the electrospinning technique were doped with $CuInS_2$ quantum dot (1, 2.5, 5 and 10 wt%) via hydrothermal synthesis (Fig. 1.7).

These doped fibers had their capacity to reduce CO_2 to methane and methanol evaluated via photocatalysis under the illumination of a solar simulator (350 W, Xe arc lamp). The photocatalytic reaction occurs in a CO_2/water vapor atmosphere. The suspension of the catalyst and water was previously purged with nitrogen to assure an anaerobic environment. The author found out that the presence of CO_2 and light is fundamental to the production of the hydrocarbons. The maximum efficiency of the system was achieved using a TiO_2 composite fiber doped with 2.5 wt% of $CuInS_2$ quantum dot, which yield 2.5 μmol h^{-1} g^{-1} for CH_4 and 0.86 μmol h^{-1} g^{-1} for CH_3OH.

Another common product (fuel) obtained from the photocatalytic reduction of CO_2 is CO. The work of Lin et al. (2018) studied this photoreduction phenomenon using a ZnO_{1-x}/carbon dots composite as a photocatalyst (Fig. 1.8). Carbon dots are a class of carbon particles with sizes below 10 nm that have unique photoinduced electron transfer properties. The composite particles were obtained using the furnace aerosol reactor (FuAR) method, where hollow particles were obtained. The ZnO

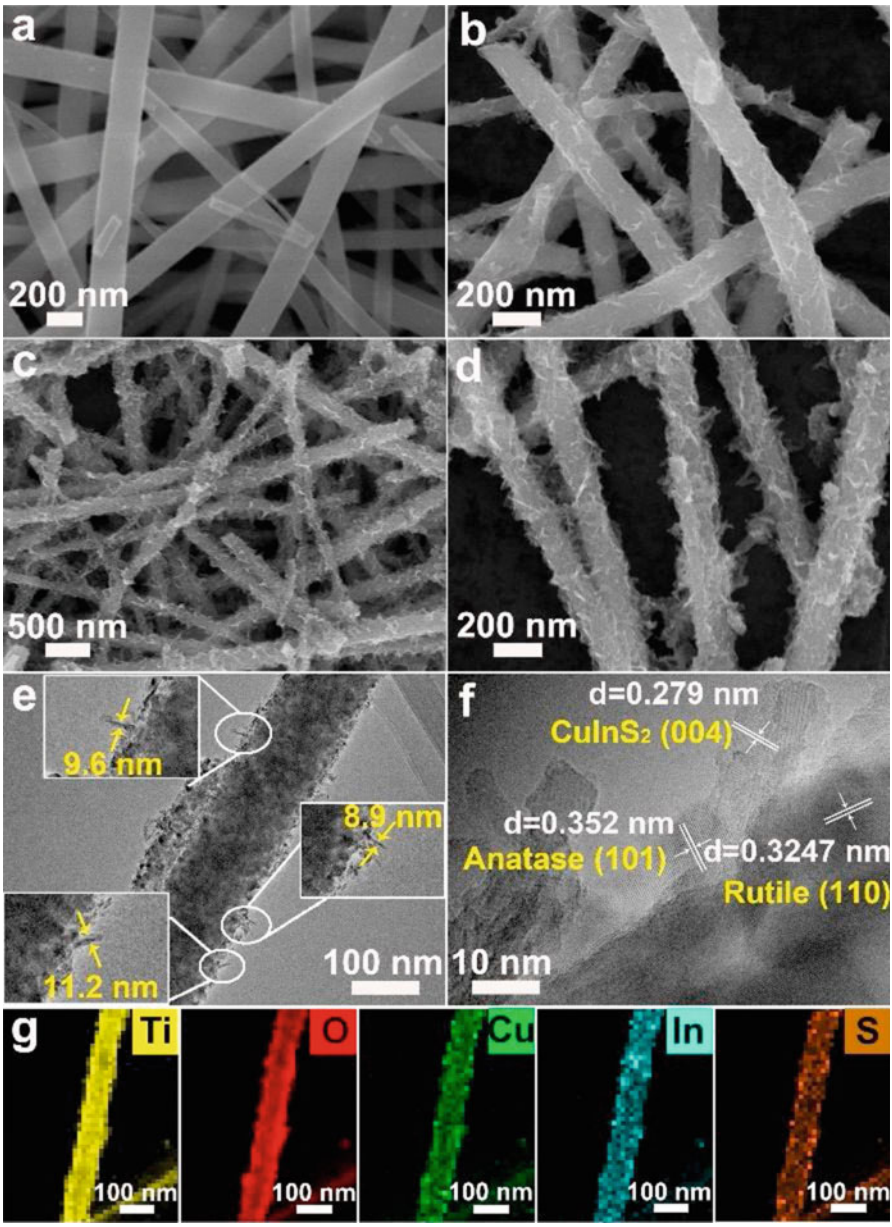

Fig. 1.7 Scanning electron microscopy images of pristine TiO_2 fibers before (**a**) and after (**b**) NaOH etching. (**c**, **d**) TiO_2 composite fibers with 2.5 wt% $CuInS_2$ quantum dot. Transmission electron microscopy image (**e**) and high-resolution transmission electron microscopy image (**f**) of fibers with 2.5 wt% $CuInS_2$ quantum dot. (**g**) Energy-dispersive X-ray spectroscopy element mappings of the elements Ti, O, Cu, In, and S in the fibers with 2.5 wt% $CuInS_2$ quantum dot (Reprinted with permission from Xu et al. 2018)

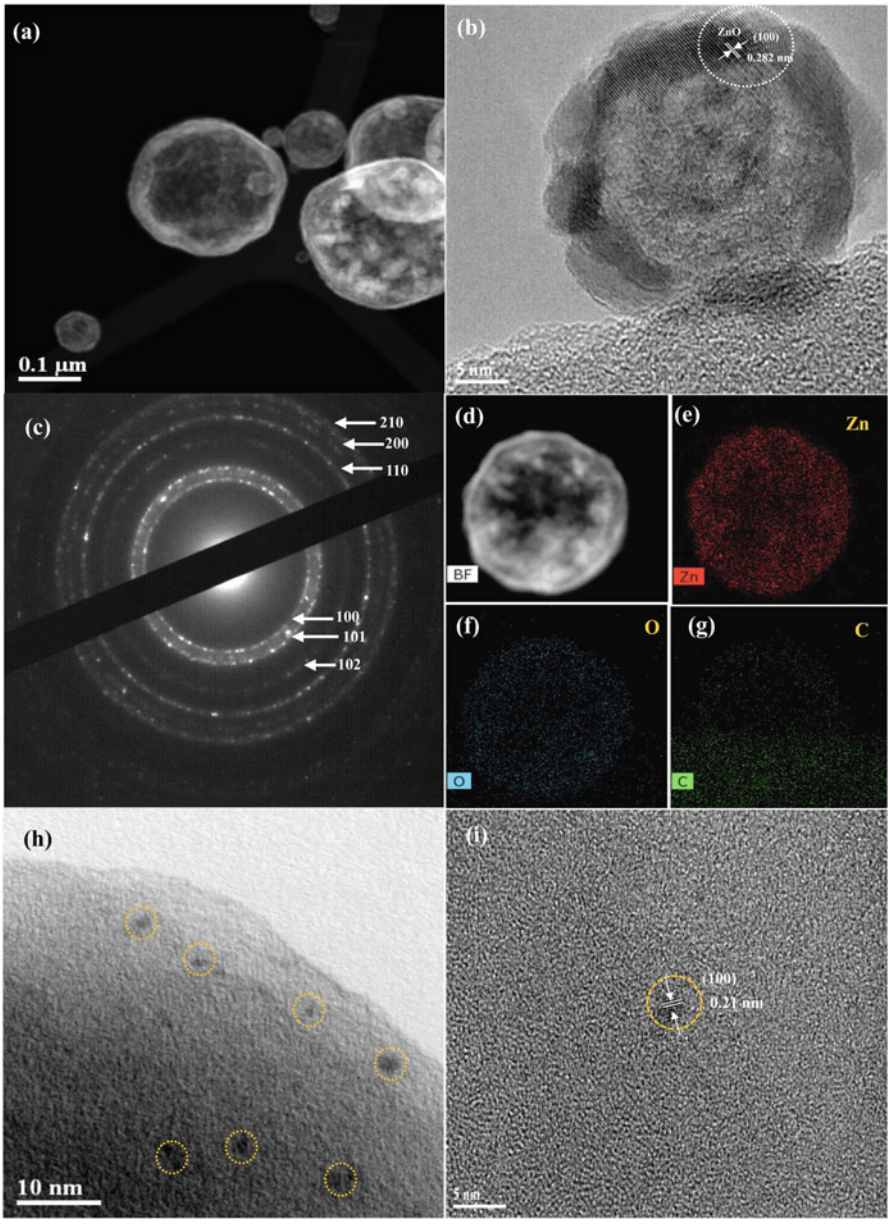

Fig. 1.8 (**a**, **b**) High-resolution transmission electron microscopy images, (**c**) Selected area (electron) diffraction pattern. (**d**–**g**) Energy-dispersive X-ray spectroscopy elemental mapping images of the ZnO_{1-x}/C composite particles. (**h**, **i**) High-resolution transmission electron microscopy images of Zn-free C (Reprinted with permission from Lin et al. 2018)

particles have around 2 nm in diameter and the carbon quantum dot have around 0,21 nm in diameter. The photocatalytic reaction was carried out using a 400 W Xe arc lamp, in a previously CO_2 purged reactor, under CO_2 and water vapor atmosphere. The authors observed that in the conditions that the reaction occurs using this catalyst, only CO was produced, preferably over methane or methanol, at a rate of 34.1 μmol h^{-1} g^{-1}. This is probably because CO needs a minimum number of electrons and protons to be reduced than CH_4.

One of the most researched fuels synthesized using photocatalysis is hydrogen, especially when derived from the water-splitting reaction in a photoelectrochemical cell. Although the storage of hydrogen is difficult nowadays, the idea of using a fuel that generates only water as emission and that the water is the main source of the fuel is very appealing.

One of the most recent works regarding hydrogen production using nanophotocatalysts was published by Liu et al. (2018b). In their work, two-dimensional (2D) SnS_2/g-C_3N_4 catalysts were produced using microwave-assisted hydrothermal technique. Graphitic carbon nitride (g-C_3N_4) is a layered 2D nonmetal photocatalyst that has a conduction band (−1.22 eV) interesting for H_2 generation and also a valence band (1.56 eV) interesting for the photodecomposition of pollutants. Usually, to promote a better photocatalysis activity, this material is exfoliated using ultrasound. In the work of Liu et al., after synthesis and exfoliation of SnS_2/g-C_3N_4, hydrogen production performance was evaluated using a 300 W Xe lamp. The authors produced samples doping the g-C_3N_4 with 1, 3, 5 and 10% of SnS_2 (named 1-SCNNs, 3-SCNNs, 5-SCNNs, and 10-SCNNs, respectively). The results in Fig. 1.9, reprinted with authorization from the authors, show that the best H_2 generation rate reached 972 μmol·h^{-1}·g^{-1} when doping the nitride with 5% of SnS_2. This sample was evaluated considering its reusability and stability in recycling experiments (Fig. 1.9b). After five cycles, the hydrogen rate was stable, suggesting great stability of this catalyst.

Usually, the photocatalysts have a specific selectivity toward CO_2 reduction or H_2 production; rarely there is a catalyst that is effective to both reactions. However, as observed in the work of Roy et al. (2018), metal-nitrogen-carbon (m-n-c) electrocatalysts, synthesized using the sacrificial support method, are active to produce CO from CO_2 and hydrogen from water splitting at the same time. They have used as metals Cu, Mo, Pr, and Ce and aminoantipyrine as a source of nitrogen and carbon. After the synthesis, the catalysts particles have a diameter from 20 up to 50 nm. Although H_2 and CO are produced during electrolysis in a CO_2 environment for all the m-n-c tested catalysts, the results showed that in controlling the amount of nitrogen present in the catalyst, it is possible to guide the reaction to the formation of one of the products. A 50/50 CO/H_2 ratio (the highest ratio observed) was achieved for the metal-free catalyst. Adjusting this system to more negative potentials, the ratio, in this case, shifts toward H_2 production (30% CO_2–70% H_2). In a nitrogen-rich catalyst, the reaction products shift to the production of hydrogen, preferably. When using Cu or Mo, the main product was H_2. Just trace amounts of CO (less than 1%) were formed when using these metals in the metal-nitrogen-carbon catalysts.

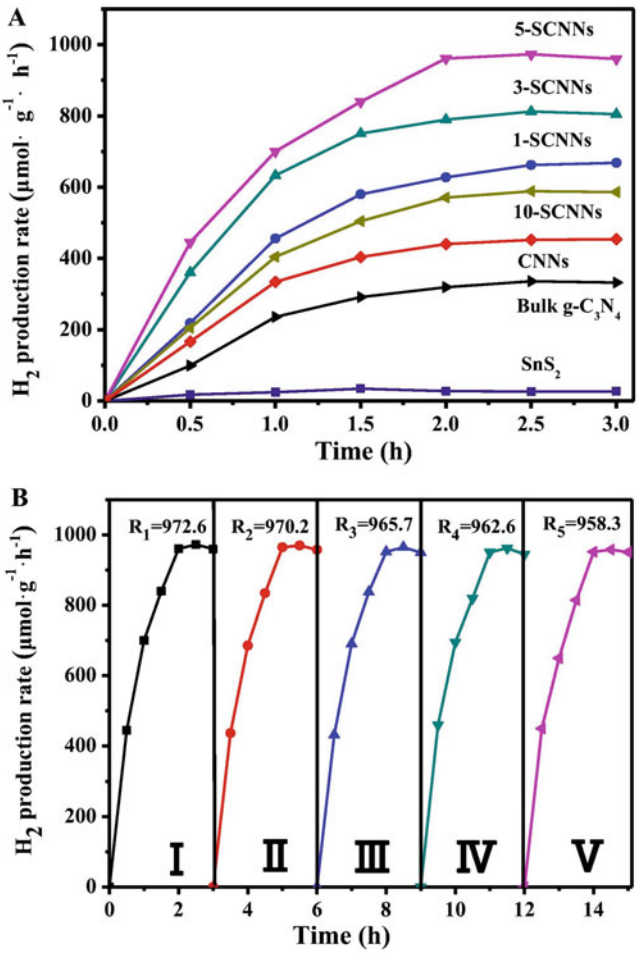

Fig. 1.9 (**a**) H_2 production rate for the different catalysis synthesized. (**b**) The H_2 production rate of five-layer SnS_2/g-C_3N_4 catalyst in a circulation experiment (Reprinted with permission from Liu et al. 2018b)

Thus, in controlling the composition of the catalyst and the medium where the photoelectrolysis works, it is possible to control the composition of the product.

1.5 Conclusion

In summary, quantum dots are a trend in the photocatalysis for fuel production scientific community due their superior and tunable catalytic properties. Different methods are used to produce quantum dots, each one adapted to achieve the desired

characteristic for a specific fuel production. The most common fuels obtained using photocatalysts are methane, methanol, formic acid, and hydrogen. Among the catalysts applied for this purpose, it is possible to highlight the transformation of CO_2 using enzymes to produce formic acid, TiO_2-$CuInS_2$ quantum dots to produce methane and methanol, and ZnO-carbon dots to produce CO and the synthesis of H_2 using SnS_2-g-C_3N_4 as catalyst. Despite the increased number of publication over the recent years, there is no standard solution to attend the energetic conundrum, mainly because scalable, reliable, and reproductive results in large scale are practically nonexistent. More investment is necessary from companies and governments to promote the effective use of photocatalyst for fuel production.

References

Adhikari T, Pathak D, Wagner T, Jambor R, Jabeen U, Aamir M, Nunzi J-M (2017) Structural, optical, electrochemical and photovoltaic studies of spider web like silver indium diselenide quantum dots synthesized by ligand mediated colloidal sol-gel approach. Opt Mater 73:70–76. https://doi.org/10.1016/j.optmat.2017.08.005

Asadzadeh-Khaneghah S, Habibi-Yangjeh A, Abedi M (2018) Decoration of carbon dots and AgCl over g-C_3N_4 nanosheets: novel photocatalysts with substantially improved activity under visible light. Sep Purif Technol 199:64–77. https://doi.org/10.1016/j.seppur.2018.01.023

Bertino MF, Gadipalli RR, Martin LA, Rich LE, Yamilov A, Heckman BR, Leventis N, Guha S, Katsoudas J, Divan R, Mancini DC (2007) Quantum dots by ultraviolet and x-ray lithography. Nanotechnology 18:315603. https://doi.org/10.1088/0957-4484/18/31/315603

Biswas M, Singh S, Balgarkashi A, Makkar R, Bhatnagar A, Sreedhara S, Chakrabarti S (2018) Vertical strain-induced dot size uniformity and thermal stability of InAs/GaAsN/GaAs coupled quantum dots. J Alloys Compd 748:601–607. https://doi.org/10.1016/j.jallcom.2018.03.163

Choi H, Lee J-G, Mai XD, Beard MC, Yoon SS, Jeong S (2017) Supersonically spray-coated colloidal quantum dot ink solar cells. Sci Rep 7(622):1–8. https://doi.org/10.1038/s41598-017-00669-9

Hong X, Xu Z, Zhang F, He C, Gao X, Liu Q, Guo W, Liu X, Ye M (2017) Sputtered seed-assisted growth of CuS nanosheet arrays as effective counter electrodes for quantum dot-sensitized solar cells. Mater Lett 203:73–76. https://doi.org/10.1016/j.matlet.2017.05.078

Hong W, Zhou Y, Lv C, Han Z, Chen G (2018) NiO quantum dot modified TiO_2 toward robust hydrogen production performance. ACS Sustain Chem Eng 6:889–896. https://doi.org/10.1021/acssuschemeng.7b03250

Ji W, Liu S, Zhang H, Wang R, Xie W, Zhang H (2017) Ultrasonic spray processed, highly efficient all-inorganic quantum-dot light-emitting diodes. ACS Photon 4:1271–1278. https://doi.org/10.1021/acsphotonics.7b00216

Kaganskiy A, Fischbach S, Strittmatter A, Rodt S, Heindel T, Reitzenstein S (2018) Enhancing the photon-extraction efficiency of site-controlled quantum dots by deterministically fabricated microlenses. Opt Commun 413:162–166. https://doi.org/10.1016/j.optcom.2017.12.032

Kwak GY, Kim TG, Hong S, Kim A, Ha MH, Kim KJ (2018) Efficiency improvement of Si quantum dot solar cells by activation with boron implantation. Sol Energy 164:89–93. https://doi.org/10.1016/j.solener.2018.02.029

Li P-N, Ghule AV, Chang J-Y (2017) Direct aqueous synthesis of quantum dots for high-performance $AgInSe_2$ quantum-dot-sensitized solar cell. J Power Sources 354:100–107. https://doi.org/10.1016/j.jpowsour.2017.04.040

Li M, Wang M, Zhu L, Li Y, Yan Z, Shen Z, Cao X (2018) Facile microwave assisted synthesis of N-rich carbon quantum dots/dualphase TiO_2 heterostructured nanocomposites with high activity

in CO_2 photoreduction. Appl Catal B Environ 231:269–276. https://doi.org/10.1016/j.apcatb.2018.03.027

Lia M, Wang M, Zhu L, Li Y, Yan Z, Shen Z, Cao X (2018) Facile microwave assisted synthesis of N-rich carbon quantum dots/dual-phase TiO_2 heterostructured nanocomposites with high activity in CO_2 photoreduction. Appl Catal B Environ 231:269–276. https://doi.org/10.1016/j.apcatb.2018.03.027

Lin L-Y, Kavadiya S, Karakocak BB, Nie Y, Raliya R, Wang ST, Berezin MY, Biswas P (2018) ZnO_{1-x}/carbon dots composite hollow spheres: facile aerosol synthesis and superior CO_2 photoreduction under UV, visible and near-infrared irradiation. Appl Catal B Environ 230:36–48. https://doi.org/10.1016/j.apcatb.2018.02.018

Liu L, Wang Y, An W, Hu J, Cui W, Liang Y (2014) Photocatalytic activity of PbS quantum dots sensitized flower-like Bi_2WO_6 for degradation of rhodamine B under visible light irradiation. J Mol Catal A Chem 394:309–315. https://doi.org/10.1016/j.molcata.2014.07.029

Liu Q, Jiang M, Ju Z, Qiao X, Xu Z (2018a) Development of direct competitive biomimetic immunosorbent assay based on quantum dot label for determination of trichlorfon residues in vegetables. Food Chem 250:134–139. https://doi.org/10.1016/j.foodchem.2017.12.079

Liu E, Chen J, Ma Y, Feng J, Jia J, Fan J, Hu X (2018b) Fabrication of 2D SnS2/g-C3N4 heterojunction with enhanced H_2 evolution during photocatalytic water splitting. J Colloid Interface Sci 524:313–324. https://doi.org/10.1016/j.jcis.2018.04.038

Mir IA, Das K, Rawat K, Bohidar HB (2016) Hot injection versus room temperature synthesis of CdSe quantum dots: a differential spectroscopic and bioanalyte sensing efficacy evaluation. Colloids Surf A Physicochem Eng Asp 494:162–169. https://doi.org/10.1016/j.colsurfa.2016.01.002

Murray CB, Norris DJ, Bawendi MG (1993) Synthesis and characterization of nearly monodisperse CdE (E = sulfur, selenium, tellurium) semiconductor nanocrystallites. J Am Chem Soc 115:8706–8715. https://doi.org/10.1021/ja00072a025

Pan J, Liu J, Zuo S, Khan UA, Yu Y, Li B (2018) Synthesis of cuboid BiOCl nanosheets coupled with CdS quantum dots by region-selective deposition process with enhanced photocatalytic activity. Mater Res Bull 103:216–224. https://doi.org/10.1016/j.materresbull.2018.03.043

Panb D, Hanb Z, Miao Y, Zhang D, Li G (2018) Thermally stable TiO_2 quantum dots embedded in SiO_2 foams: characterization and photocatalytic H_2 evolution activity. Appl Catal B Environ 229:130–138. https://doi.org/10.1016/j.apcatb.2018.02.022

Patel M, Kim JS, Kim BS, Kim Y-H, Kim J (2018) Optical and photoelectrochemical properties of transparent NiO quantum dots. Mater Lett 218:123–126. https://doi.org/10.1016/j.matlet.2018.01.162

Rajabi HR (2016) Photocatalytic activity of quantum dots, semiconductor photocatalysis – materials, mechanisms and applications, Prof. Wenbin Cao (Ed.), InTech. https://doi.org/10.5772/63435

Roy A, Hursán D, Artyushkova K, Atanassov P, Janáky C, Serov A (2018) Nanostructured metal-N-C electrocatalysts for CO_2 reduction and hydrogen evolution reactions. Appl Catal B Environ 232:512–520. https://doi.org/10.1016/j.apcatb.2018.03.093

Tile N, Ahia CC, Olivier J, Botha JR (2018) Atmospheric pressure-MOVPE growth of GaSb/GaAs quantum dots. Phys B Condens Matter 535:20–23. https://doi.org/10.1016/j.physb.2017.06.014

Wang R, K-Q. L, Zhang F, Tang Z-R, Xu Y-J (2018a) 3D carbon quantum dots/graphene aerogel as a metal-free catalyst for enhanced photosensitization efficiency. Appl Catal B Environ 233:11–18. https://doi.org/10.1016/j.apcatb.2018.03.108

Wang M, Hu J, Yang Y (2018b) Fabrication of CDs/CdS-TiO_2 ternary nano-composites for photocatalytic degradation of benzene and toluene under visible light irradiation. Spectrochim Acta A Mol Biomol Spectrosc 199:102–109. https://doi.org/10.1016/j.saa.2018.03.041

Wang R, Kong X, Zhang W, Zhu W, Huang L, Wang J, Zhang X, Liu X, Hu N, Suo Y, Wang J (2018c) Mechanism insight into rapid photocatalytic disinfection of Salmonella based on vanadate QDs-interspersed g-C_3N_4 heterostructures. Appl Catal B Environ 225:228–237. https://doi.org/10.1016/j.apcatb.2017.11.060

Xie Z, Feng Y, Wang F, Chen D, Zhang Q, Zeng Y, Lv W, Liu G (2018) Construction of carbon dots modified MoO_3/g-C_3N_4 Z-scheme photocatalyst with enhanced visible-light photocatalytic activity for the degradation of tetracycline. Appl Catal B Environ 229:96–104. https://doi.org/10.1016/j.apcatb.2018.02.011

Xu F, Zhang J, Zhu B, Yu J, Xu J (2018) $CuInS_2$ sensitized TiO_2 hybrid nanofibers for improved photocatalytic CO_2 reduction. Appl Catal B Environ 230:194–202. https://doi.org/10.1016/j.apcatb.2018.02.042

Yadav D, Yadav RK, Kumar A, Park N-J, Baeg J-O (2016) Functionalized graphene quantum dots as efficient visible-light photocatalysts for selective solar fuel production from CO_2. ChemCatChem 8:3389–3393. https://doi.org/10.1002/cctc.201600905

Yang D, Wang L, Hao Z-B, Luo Y, Sun C, Han Y, Xiong B, Wang J, Li H (2016) Dislocation analysis of InGaN/GaN quantum dots grown by metal organic chemical vapor deposition. Superlattice Microst 99:221–225. https://doi.org/10.1016/j.spmi.2016.02.016

Zhao T, Xing Z, Xiu Z, Li Z, Shen L, Cao Y, Hu M, Yang S, Zhou W (2018) CdS quantum dots/Ti^{3+}-TiO_2 nanobelts heterojunctions as efficient visible light-driven photocatalysts. Mater Res Bull 103:114–121. https://doi.org/10.1016/j.materresbull.2018.03.029

Chapter 2
Highly Stable Metal Oxide-Based Heterostructured Photocatalysts for an Efficient Photocatalytic Hydrogen Production

Murikinati Mamatha Kumari, Raghava Reddy Kakarla, N. Ramesh Reddy, U. Bhargava, M. V. Shankar, and S. K. Soni

Contents

Abstract The need for fuel generated by renewable resources has become important in the global scenario. Solar energy is an abundantly available renewable resource for the earth. There is a huge potential for H_2 derived from clean energy resources for commercial applications such as generation of electricity, fuel for transportation, domestic usage, rocket propulsion, etc. With H_2 as a fuel, a zero-emission process using fuel cells produces electricity with only water as the

M. Mamatha Kumari (✉) · N. R. Reddy · U. Bhargava · M. V. Shankar
Nano Catalysis and Solar Fuels Research Laboratory, Department of Materials Science & Nanotechnology, Yogi Vemana University, Kadapa, Andhra Pradesh, India

R. R. Kakarla (✉)
The School of Chemical and Biomolecular Engineering, The University of Sydney, Sydney, NSW, Australia

S. K. Soni
Sustainable Living Lab, School of Science, RMIT University, Melbourne, VIC, Australia

Inamuddin et al. (eds.), *Nanophotocatalysis and Environmental Applications*,
Environmental Chemistry for a Sustainable World 31,
https://doi.org/10.1007/978-3-030-04949-2_2

by-product. Global demand for hydrogen (H_2) as an energy carrier is steadily increasing. Researchers are therefore working towards the development of efficient materials for hydrogen (H_2) production by solar photocatalysis. For efficient H_2 fuel production, development of novel/modified photocatalysts that are efficient, stable and recyclable remains a challenge.

Titanium dioxide (TiO_2), with a band gap of 3.2 eV and suitable band potential, has demonstrated efficient H_2 production under UV light irradiation. Significant research had been carried out to modify TiO_2-based photocatalysts for enhanced H_2 production under UV light and solar/visible light irradiation since in its pure form, it can absorb only UV light (<5% of solar light). This chapter briefs and summarizes about the recent works on the photocatalytic hydrogen production of highly stable TiO_2-based heterostructured photocatalysts. This book chapter also aims to concentrate on three important characteristics: (a) UV-active TiO_2-based photocatalysts, (b) visible active TiO_2-based photocatalysts and (c) the effects of various carbon nanostructures on the photocatalytic hydrogen production efficacy of TiO_2-based heterostructured photocatalysts.

Keywords Semiconducting metal oxides · TiO_2 · Heterostructured photocatalysts · Doped photocatalysts · Functionalization · Carbon materials (carbon nanotube graphene) · Catalyst properties · Crystal phases · Band edge · Band gap · Noble metals · Sacrificial reagents · Photocatalysis · Catalytic kinetics · Photocatalytic mechanism · Photocatalytic water splitting · Visible and UV light irradiation · Hydrogen production

2.1 Photocatalysis

Research in photocatalysis has significantly increased in recent years due to its potential use in environmental applications such as hydrogen generation, organic synthesis and water treatment technologies. Photocatalysis is a process which uses light to activate a substance, photocatalyst, responsible to modify the rate of a reaction without being part of it. Semiconductors are the most common photocatalysts used due to its special light absorption properties, morphological structures, electronic structure, controlling band gap properties, charge transport characteristics and excited states lifetime. Semiconductor photocatalysis has been applied for water splitting, hydrogen production, removing organic pollutants in the wastewater and air, controlling odour and so on (Hoffmann et al. 1995; Nakata and Fujishima 2012).

2.1.1 Photocatalytic Mechanism

Semiconductors are characterized to have an energy gap between the filled valence band and empty conductive band (Patsoura et al. 2007). To promote an electron from

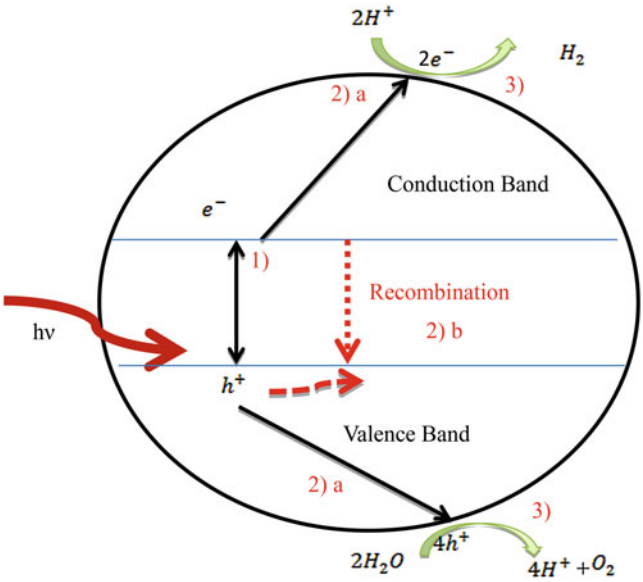

Fig. 2.1 Major processes in semiconductor photocatalysis for water splitting into H_2 and O_2 gas generation. (Reprinted from Robertson 1996 with permission of Elsevier)

valence band to conduction band, a quantity of energy correspondent or greater to this gap should be provided to have an electron transition. In the semiconductor photocatalysis, electrons absorb energy from a photon leaving behind holes. After that, electrons can return to holes dissipating energy as heat or reacting with electron donors and electron acceptors adsorbed on the semiconductor surface and initiate a chemical reaction (Hoffmann et al. 1995). Scheme 1 shows the possible reaction for a semiconductor (Robertson 1996).

$$\text{Light absorption} : \text{Semiconductor} + h\upsilon \rightarrow e^- + h^+$$
$$\text{Recombination} : e^- + h^+ \rightarrow \text{heat}$$
$$\text{Oxidation} : D + h^+ \rightarrow D^+$$
$$\text{Reduction} : A + e^- \rightarrow A^-$$

where e^- is an electron, h^+ is the hole, D is the species to be oxidized, A is the species to be reduced.

The schematic process (Fig. 2.1) is illustrated to explain the photocatalytic mechanism of TiO_2 as follows:

1. When an incident photon energy is greater than the energy band gap of the semiconductor, there will be electron transfer from valance band to conduction band and a hole generated in the valance band of the semiconductor.
2. (a) These photo-generated electrons and holes migrate onto the surface of the semiconductor, or (b) some of these photo-generated electrons may recombine.

Table 2.1 The oxidation potential of common reactants

Oxidant agent	Oxidation potential (volts)
TiO_2 conduction band	3.10
Hydroxyl radical	2.80
Ozone	2.07
Silver (+2)	1.98
Hydrogen peroxide	1.78
Hypochlorous acid	1.49
Chlorine	1.36
Chromium (+6)	1.33

3. Photo-generated electrons and holes, without any recombination, can move to the surface active sites and can, respectively, reduce and oxidize the reactants adsorbed by the semiconductor (Robertson 1996) as shown below (Fig. 2.1). The reduction and oxidation reactions are basic mechanisms of hydrogen production and air/water purification, respectively.

To have a reduction reaction, the conduction band of the semiconductor should have a lower reduction potential than the acceptor species (Robertson 1996). The redox potential of valence bands varies between +1.0 and 3.5 V vs normal hydrogen electrode (NHE), while the conduction bands are powerful reducing agents, from +0.5 to −1.5 V vs NHE (2). Therefore, to have an effective reaction, the material chosen should have an adequate redox potential. Comparing the valence band of TiO_2 with other oxidizing agents, it is seen that TiO_2 has a higher potential as shown in Table 2.1.

The oxidizing potential valence band of some semiconductors is higher than traditional oxidizing agents used in the industry such as Cr^{+6} and Ag^{2+}. For instance, the valence band of TiO_2 (+3.2 V vs NHE) is much stronger than Ag^{2+} (1.98 V vs NHE). This comparison shows the importance of reaction performances by semiconductors.

2.1.2 Band Edge Positions

The primary criteria for good semiconductor photocatalyst depend on the energy band gap and the positions of valance and conduction bands.

- To reduce water, the potential of the bottom of conduction band must be more negative than the hydrogen reduction potential.
- For oxidation reaction, the top of valence band should be more positive than the oxidation potential of water.
- Theoretically, water splitting requires a minimum band gap of 1.23 eV, which corresponds to wavelength of about 992 nm calculated from the formula:

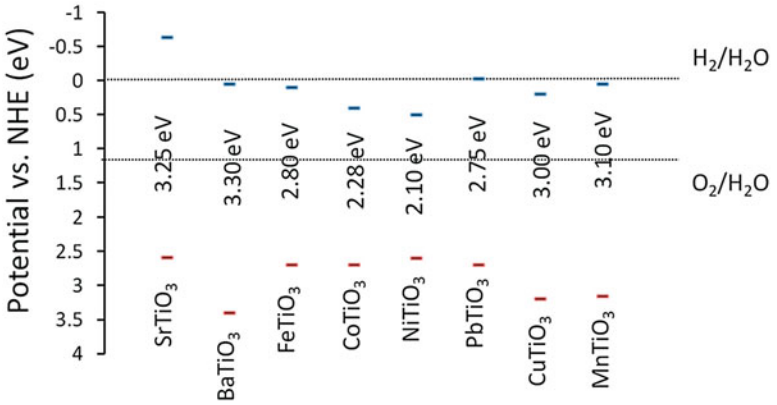

Fig. 2.2 Band position of selected semiconductor materials in contact with an aqueous electrolyte (pH 0) evolution. (Reproduced from Kanhere and Chen 2014, MDPI publisher)

$$\text{Band gap(eV)} = 1240/\lambda(\text{nm}) \tag{2.5}$$

Redox potentials of H_2/H_2O (0 eV) and O_2/H_2O (1.23 eV) and band gap energies of various semiconductor photocatalysts are as shown in Fig. 2.2. The positions are derived from flat-band potentials in a contact solution of the aqueous electrolyte at pH = 0. The pH of the electrolyte solution influences the band edge positions of the various semiconductors compared to the redox potential of adsorbate. The energy level at the bottom of the conduction band is actually the reduction potential of the photoelectrons. The energy level at the top of the valance band determines the oxidizing ability of the system to promote reduction and oxidation reactions, respectively.

Semiconductors like TiO_2 (E_g = 3.2 eV), $KTaO_3$ (E_g = 3.4 eV), $SrTiO_3$ (E_g = 3.2 eV), ZnS (E_g = 3.2 eV), CdS (E_g = 2.4 eV) and SiC (E_g = 3.0 eV) are thermodynamically suitable for photocatalytic water splitting reaction to produce hydrogen and oxygen simultaneously. However, the other factors like thermodynamic losses due to solar energy utilization, photo-generation of electron-hole pairs, transportation of electron-holes to the water molecules, recombination of electrons-holes, kinetic losses, etc. also need to be taken into account. In addition to this, another essential requirement of the photocatalyst is stability under solid/liquid interface. For example, semiconductors like CdS, GaP and ZnO can undergo photocorrosion under band gap excitation. The other semiconductors are active for water splitting when they are modified with suitable ions. The remaining semiconductors can generate hydrogen or oxygen depending on their conduction and valence band positions (Kanhere and Chen 2014).

2.2 Semiconducting Metal Oxides for Photocatalytic Water Splitting

2.2.1 Metal Oxide-Based Heterostructured Photocatalysts

The research work in the area of photocatalytic water splitting into hydrogen and oxygen has led to the development of many photocatalytic systems. Heterogeneously dispersed photocatalysts such as TiO_2, $SrTiO_3$, ZnO, CdS, Fe_2O_3, etc. have been extensively researched. Several investigations have focused on TiO_2 when compared to other semiconducting photocatalysts. TiO_2 is much more promising as it is stable under UV light irradiation, non-corrosive, environmentally friendly, abundant and cost-effective. Moreover, it shows relatively high activity and chemical stability.

2.2.1.1 Energy Structure of TiO_2

Energy structure of titanium dioxide is such that it consists of 2p orbital of oxygen (O) in the valence band and 3d orbital of titanium (Ti) in the conduction band. In large band gap semiconductors, electrons cannot be transferred from valance band to conduction band. However, when external energy greater than the band gap of the semiconductor is applied, electrons can be transferred from valance band to conduction band, leaving the equal number of holes in the valence band. This transfer of electrons is equivalent to electrons' movement from the bonding orbital to the antibonding orbital. Generally, the photoexcited states of these kinds are unstable and can break down. However, photoexcited titanium dioxide remains stable which makes titania an excellent photocatalyst.

2.2.1.2 Lattice Structure of TiO_2

Titanium dioxide as shown in Fig. 2.3 exists in any of the following three crystal forms: (a) anatase, (b) rutile and (c) brookite (Cheng et al. 2003a, b; Kolen'ko et al. 2006; Yin et al. 2007). Anatase and rutile exist in tetragonal crystal geometry, whereas brookite exists in orthorhombic crystal geometry, and their physical properties are as shown in Table 2.2. Anatase is stable at lower temperatures (<500 °C) and gets converted into rutile at higher temperatures.

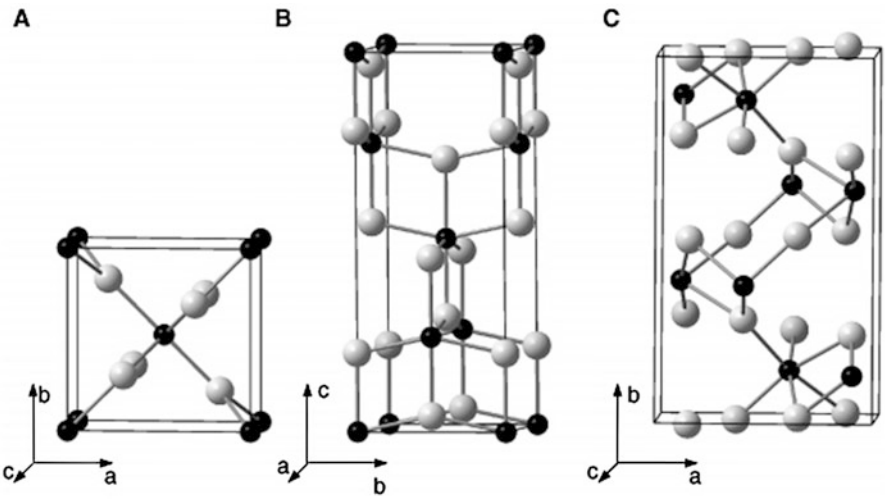

Fig. 2.3 Crystal structures of (**a**) rutile, (**b**) anatase and (**c**) brookite evolution. (Reprinted from Janisch et al. 2005 with permission of IOP publisher)

Table 2.2 Different TiO_2 crystal phases and their physical properties (Janisch et al. 2005)

	Anatase	Rutile	Brookite
Crystal structure	Tetragonal	Tetragonal	Orthorhombic
Lattice constants (Å)	$a = 3.784$	$a = 4.5936$	$a = 9.184$
	$c = 9.515$	$c = 2.9587$	$b = 5.447$
			$c = 5.145$
Ti-O bond length (Å)	1.937–1.965	1.949–1.980	1.87–2.04
O-Ti-O bond angle	77.7–92.6°	81.2–90.0°	81.2–90°
Density (g/cm^3)	3.79	4.13	3.99
TiO_2 molecule/cell	4	2	8

2.3 The Challenges in Photocatalytic H_2 Production Using TiO_2 Particulate Systems

Anatase TiO_2 possesses both band gap and band potential suitable for water splitting reactions. However, surface and semiconducting properties of anatase TiO_2 restrict its efficiency owing to the following reasons:

- Only UV light (5% of solar energy, 200–400 nm) can be utilized. The inability to utilize visible light (about 50%, 400–700 nm) limits the efficiency of TiO_2 photocatalyst.
- Rapid recombination of electron-hole during the photocatalytic process.
- The backward reaction (recombination of H_2 and O_2 into H_2O) easily proceeds.

2.4 Strategies for Improving TiO_2 Photocatalytic Activity

Major attempts have been made:

1. To overcome the surface potential for reduction and oxidation reactions, cocatalyst is often deposited on the catalyst surface. In addition to this, cocatalysts provide catalytic active sites for adsorption and surface reactions besides suppressing the recombination of charge carriers in the photocatalysis.
2. To minimize electron-hole recombination and improve the H_2 production efficiency, inorganic or organic sacrificial reagents are added to react with the photo-generated electrons-holes and get oxidized/reduced. This ensures the photocatalyst becomes enriched with electrons-holes leading to enhanced photocatalytic H_2 production.
3. To extend the light absorption in visible region, energy band engineering and other suitable surface modification techniques were required.

The addition of electron-hole scavengers, noble metal ion doping, cation doping, anion doping, dye sensitization, composite semiconductors, metal ion implantation, multicomponent semiconductors, Z-scheme and morphology control have been used to resolve the above-listed problems and to enhance the solar photocatalytic H_2 production. These techniques can be grouped under two broad categories as chemical additives and photocatalytic modification techniques which are described below.

2.4.1 Addition of Sacrificial Reagents

As photocatalytic pure water splitting is a tough reaction, sacrificial reagents were used to estimate the photocatalytic activity. Photocatalytic reactions can be carried out in the presence of an aqueous solution of reducing agents like electron donors or hole scavengers, such as sulphide ions and alcohols. Thus, the reducing reagent gets irreversibly oxidized by photo-generated holes instead of water. This leads to a large number of electrons in a photo catalyst and hence enhanced H_2 evolution reaction. For practical and effective H_2 production, sacrificial agents abundantly available in nature and industrial/biomass-derived by-products are good choices.

Photocatalytic reactions can also be carried out resulting in O_2 evolution by the reduction of oxidizing agents like electron acceptors or electron scavengers, such as Fe^{3+} and Ag^{+} by the photo-generated electrons in the conduction band of the photocatalyst. These H_2 and O_2 evolution reactions are known as half reactions of water splitting. An illustration of half reactions of photocatalytic water splitting in the presence of heterostructured photocatalyst is shown in Fig. 2.4.

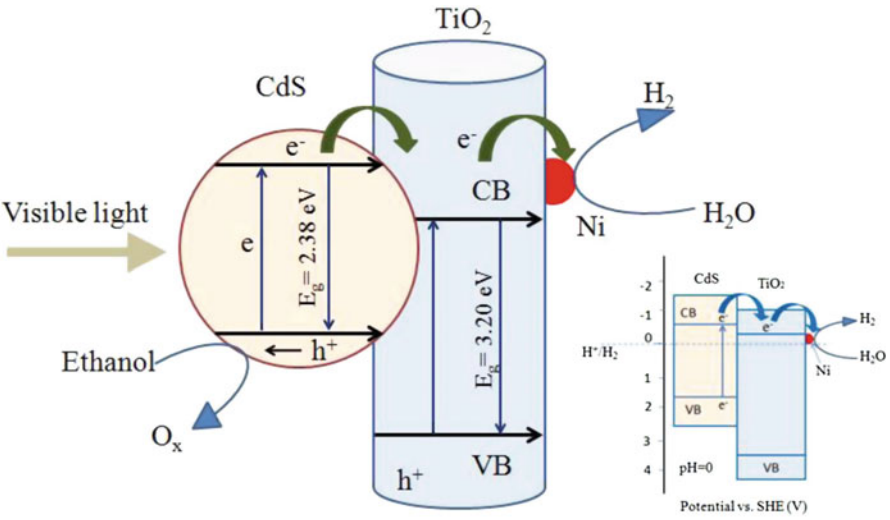

Fig. 2.4 Schematic diagram of photocatalytic water splitting in the presence of Ni-TiO_2@CdS heterostructured photocatalyst for H_2 evolution. (Reprinted from Vu et al. 2014 with permission of American Chemical Society)

2.4.2 *TiO_2-Based Semiconductors Under UV Light Irradiation*

Various non-metals like C, N, S, F, etc. were doped to TiO_2 nanostructures to enhance the photocatalytic H_2 production under UV light irradiation. The N-doped TiO_2 nanofibres synthesized by the hydrothermal approach and annealed in air/ammonia had higher photocatalytic efficiency in the generation of hydrogen from ethanol-water mixtures under UV-A and UV-B light irradiation compared to undoped counterparts (Xu et al. 2013). Wu et al. produced 1D nanofibres as a support for noble metallic Pd and Pt nanoparticles decorated. The results showed a high catalytic efficiency in hydrogen generation from ethanol-water 1:3 molar ratio under UV-A and UV-B irradiation with 100 mg of catalyst is used in 1 L of ethanol-water mixture. The H_2 evolution rate was greater than 700 μmol/h (UV-A) and 2250 μ mol/h (UV-B), and the photo-energy conversions were approximately 3.6% and 12.3%, respectively. Different non-metals have been applied to improve the hydrogen evolution performance of TiO_2 as shown in Table 2.4.

Another new photocatalyst synthesized for application under UV light photocatalysis was the hybrid TiO_2/graphene nanocrystals (Pan et al. 2013). It was synthesized by two steps, coating TiO_2 on GO nanosheets using hydrolysis method followed by a hydrothermal method to obtain anatase nanocrystals. The hybrid material showed a better photocatalytic activity under UV irradiation compared to pristine TiO_2 produced by the same method and commercial P25. The enhanced photocatalytic efficiency was due to the power coupling between TiO_2 and 3D GO

Table 2.3 UV light active photocatalysts using various heterostructured metal oxides

Photocatalyst	Cocatalyst	QY (%)	H_2 production μmol. h^{-1} g^{-1}_{cat}	References
TiO_2 (anatase)	Rh	29	449	Yamaguti and Sato (1985)
Colloid TiO_2	Pt-RuO_2	30		Duonghong et al. (1981)
TiO_2:Sn/Eu	Pd	40.4	540	Sasikala et al. (2008)
$Sr_4Ti_3O_{10}$	NiO_x	4.5	160	Ya-hui et al. (2009)
$Rb_2La_2Ti_3O_{10}$	NiO_x	5	869	Takata et al. (1998)
$La_2Ti_2O_7$	NiO_x	27	440	Kim et al. (2003)
$La_2Ti_2O_7$:Ba	NiO_x	50	2010	Kim et al. (2005)
$NaTaO_3$:La	NiO_x	56	384	Kato et al. (2003)

nanosheets that facilitated the interfacial charge transfer with GO acting as an electron acceptor and decreasing electron-hole recombination. Additionally, nanohybrid photocatalyst material had a larger surface area than nano TiO_2 and P25. This experiment conducted by Liang et al. (Pan et al. 2013) expected to apply this novel photocatalyst as high-efficiency water splitting electrode, material for DSSCs and Li-ion batteries.

Different semiconductor oxides, nitrides and sulphides over 130 were reported in the literature for photocatalytic hydrogen production. Among these photocatalysts, NiO/$NaTaO_3$ (Kato et al. 2003) and Ba-doped $La_2Ti_2O_7$ (Kato et al. 2003) showed higher quantum yields of 56% and 50% for pure water splitting under UV light, respectively (Table 2.3).

However, this progressive novel materials contribution is limited value for practical hydrogen production as UV light accounts for only about 3–4% of solar radiation energy. Hence, it is crucial to develop visible light active photocatalysts for water splitting. The band gap of visible light photocatalyst should be less than 3.0 eV. Hence, suitable band engineering is necessary for the design of photocatalysts with a visible light response.

2.4.3 *Photocatalytic Performance of TiO_2 Under Visible Irradiation*

The photocatalytic activity of surface-modified TiO_2 under visible light irradiation has been widely studied (Jamalluddin and Abdullah 2011; Asiri et al. 2014). The majority of the research reported the doped TiO_2 in the presence of inorganic anion as $S_2O_8^{2-}$, $S_2O_3^{2-}$ and I^-, and the doped material was prepared in an autoclave at higher temperatures. To shift the sensibility of TiO_2 from UV light to visible light, non-metallic elements have been doped to the TiO_2 structure as nitrogen, sulphur,

carbon and phosphorus elements; and other modification techniques are the addition of small-sized noble metallic particles, narrow band gap semiconductor coupling agents and sensitizers (Wu et al. 2011). Nitrogen- and sulphur-doped TiO_2 has advantages over other non-metal dopants (carbon and phosphorus) since they introduce a band gap near the TiO_2 valence band. So, when electrons are excited to the conduction band, they are promoted first to these localized states.

The N-Ti-O has a better catalytic performance than other non-metals (C, P and S). N-doped can be more effective than S-doped because the energy requirest for the former S-substitution is greater than N-substitution (Wu et al. 2011). The results showed an improvement of photocatalytic efficiency for N- and S-doped TiO_2 compared to undoped TiO_2 due to the doping effect the presence of the inorganic anion donors such as $S_2O_8^{2-}$, $S_2O_3^{2-}$ and I^- led to the prevention of the electron-hole recombination due to trapping of the valence band holes by the inorganic anions. The activity showed to have a better efficiency in the presence of $S_2O_3^{2}$ (Wu et al. 2011).

An approach that has become the focus of research is the modification of titanium dioxide nanotubes arrays (TiO_2 NT arrays) by addition of silver nanoparticles to the TiO_2 structure. Nanosized Ag particles have been widely used over other noble metallic particles due to its low cost compared to Au or Pt and strong resonance wavelength of 400–550 nm (Liang et al. 2010).

Chen et al. (Liang et al. 2010) have investigated the improvement obtained in the photocatalytic activity under sunlight irradiation by using silver nanoparticles decorated on TiO_2 nanotube (NT) arrays, which was fabricated by two steps, an electrochemical anodization process followed by a photochemical reduction method. The photocatalytic activities were measured under visible light irradiation. The results showed that silver nanoparticles have an effect on the catalytic efficiency of the TiO_2 NT arrays. They found that Ag nanoparticles promoted the separation and transfer of photo-generated charge carriers that is a crucial feature for improving considerably photocatalytic activity. The new material synthesized with high efficiency has a potential use in the numerous photocatalysis technologies such as hydrogen generation and dye-sensitized solar cells.

Hydrogen evolution performance of TiO_2 hybrids with different noble metal and metal oxide particles is shown in Table 2.4. Among all the possible noble metal-based metal oxide photocatalysts, Pt and Ag observed to show higher photocatalytic H_2 production activity due to efficient electron transfer and reduced electron-hole recombination.

Table 2.5 shows the visible light active oxide, doped (non-metals) oxides photocatalysts for O_2 and H_2 evolution under visible light irradiation. So far, GaN/ZnO-Cr/Rh photocatalyst achieved a maximum 2.5% quantum yield (Maeda et al. 2006) for pure water splitting under visible light irradiation which is no way near the marked minimum quantum yield 10% for practical utilization (Shet et al. 2010). Therefore, the need for the development of novel photocatalysts is still a major issue.

Table 2.4 The summary of hydrogen generation performance of TiO_2/noble metal or metal oxide hybrid-based photocatalysts

Modified with noble metals/ metal oxides	Reaction solution	Light source	H_2 production $\mu mol.\ h^{-1}\ g^{-1}_{cat}$	References
2.5 Pt wt%	CH_3OH+H_2O	UV-Vis	1023	Liang et al. (2017)
1.25 Pt wt%	CH_3OH+H_2O	Light at 254 nm	30	Antony et al. (2012)
Pt with Ce^{3+}	CH_3OH+H_2O	Visible	4.5	Kozlova et al. (2009)
Pt-CdS	CH_3OH+H_2O	Visible	290	Li et al. (2008)
Ag_2O	CH_3OH+H_2O	Visible	3350	Lalitha et al. (2010)
Au	$C_3H_8O_3+H_2O$	Solar	15.8	Naldoni et al. (2013)
1 wt% Pt-Bi_2O_3	CH_3OH+H_2O	Visible (λ >400 nm)	1025	Naik et al. (2011)
Au	Glycerol $+H_2O$	UV-Vis	29	Dosado et al. (2015)
Ni	C_2H_5OH $+H_2O$	UV-Vis	11.6	Chen et al. (2015)
0.5 wt% Ni-Au	CH_3OH+H_2O	UV-Vis	318	Luna et al. (2016)
Au	C_2H_5OH $+H_2O$	UV-Vis	34	Jovic et al. (2013)
1 wt% Au-Ag	CH_3OH+H_2O	UV-Vis	12.82	Chiarello et al. (2010)
Fe^{3+}	CH_3OH+H_2O	UV	12.5	Khan et al. (2008)

Table 2.5 Visible light active heterostructured photocatalysts

Photocatalyst	Reaction solution	Light source	H_2 production $\mu mol.\ h^{-1}\ g^{-1}_{cat}$	References
Fe/TiO_2	CH_3OH+H_2O	Visible	12.5	Khan et al. (2008)
Bi_2O_3/TiO_2	CH_3OH+H_2O	Visible	198.4	Naik et al. (2011)
SiC/TiO_2	CH_3OH+H_2O	Visible	1254 μmol	Mishra et al. (2015)

2.4.4 Functionalization of TiO_2 with Carbon Nanomaterials

As mentioned above, various carbon nanostructured materials such as 2D graphene nanosheets, 1D carbon nanotubes (MWCNTs and SWCNTs) and graphene quantum dots (GQDs) play a key role to enhance the photocatalytic applicability of TiO_2.

Carbon nanomaterials have outstanding mechanical, electrical, thermal and optical properties (Bai et al. 2012).

2.4.4.1 Carbon Nanotubes

The combinations of different carbon nanotubes (SWCNTs, DWCNTs, MWCNTs) with TiO_2 have been intensely studied due to the enhanced photocatalytic activity of TiO_2. It has been reported that CNTs can act either by a heat sink in CNT-TiO_2 hybrid or by reducing electron-hole recombination (Dai et al. 2014a). The inefficient dispersion of TiO_2 on the surface of nanotubes is the main challenge involved in the increase of photocatalytic activity. Yang et al. proposed a new method to improve TiO_2 performance by depositing TiO_2 into a hydrophilic carbon nanotube surface. The modified surface was achieved by the treatment with acid and L-lysine. The improvement of photocatalytic activity under UV and visible light was attributed to the larger surface area achieved which facilitates the adsorption capacity of reactive and the absorbance of photons. Another reason for the enhancement was due to the great dispersion of TiO_2 particles on CNTs and the efficient contact, which lead to dense hetero-junctions at the interface of TiO_2 and CNTs.

Electron spinning and sol-gel methods were used to prepare the mesoporous CNT-TiO_2 nanocomposite with titanium ethoxide using TiO_2 precursor. In this report, they have also discussed the electrospun effect for photocatalytic hydrogen production under UV irradiation and oxygen vacancies effect on the phase transformation and oxide crystallization (Moya et al. 2015). The interface between the CNT-TiO_2 is confirmed through TEM and FTIR spectra. In the FTIR spectra, rocking and stretching peaks at 1160, 1090 and 1030 cm^{-1} are assigned to Ti-O-C bonding between the CNT-TiO_2. Complex structural evolution in the synthesis process and structure, morphology and porosity is compared with pure TiO_2 fibres (electrospun) and TiO_2 nanoparticles for hydrogen production. The electrospun catalyst showed the highest activity due to oxygen vacancies between CNT-TiO_2 interfaces, useful to the inter-band gap states, reducing the band gap of TiO_2, mesoporosity structure favours to the charge transformation and CNTs acts as electron acceptor (Saleh and Gupta 2012).

Synthesis methods play a crucial role in forming the interface between CNT and TiO_2 which greatly influences its optical, electrical and photocatalytic properties. Uniform dispersion, good contact between CNT and TiO_2 was achieved with CNT-TiO_2 nanocomposites prepared by hydrothermal methods. Though in some cases this method could not extend the light absorption edge of the composite to the visible light, it could still enhance the photocatalytic H_2 production due to uniform dispersion and better surface contact which facilitates efficient electron transfer with minimization of electron-hole recombination. TEM image (Fig. 2.5) shows the uniformly dispersed TiO_2 nanoparticles on the CNT surface of CNT-TiO_2 nanocomposite synthesized by hydrothermal method.

In order to enhance the electron transfer efficiency and minimize electron-hole recombination, nanocomposites of CNTs as well as TiO_2 nanotubes (TiNT) were

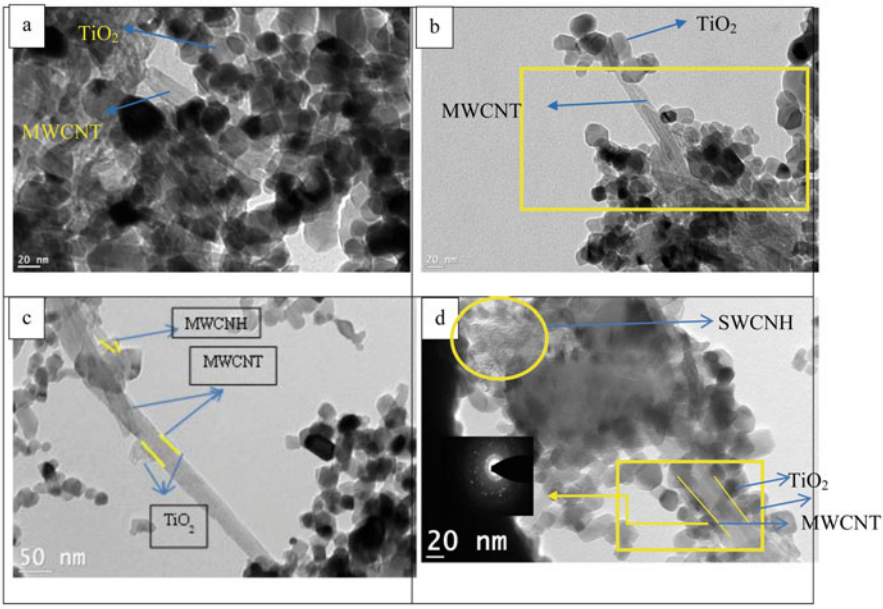

Fig. 2.5 TEM images of MWCNT-TiO_2 hybrid catalysts. (Reprinted from Mamathakumari et al. 2015 with permission from Elsevier)

also synthesized by simple impregnation method which had shown improved photocatalytic H_2 production than CNT-TiO_2 nanoparticle nanohybrid and P25 under solar irradiation with 5 vol.% glycerol aqueous solution. Even though both the two nanocomposites showed the extension of the absorption edge to the visible region, CNT-TiNT nanocomposite showed improved efficacy under similar experimental conditions. This leads to an inference that tubular morphology or general morphology plays an important role for the improved photocatalytic activity (Mamathakumari et al. 2015; Kumari et al. 2017). XPS confirmed the Ti-O-C bond formation in the nanocomposites. The nature of bonding between CNT and TiO_2 affects the charge transfer which further influences its photocatalytic activity. Formation of Ti-O-C bonding leads to efficient electron transfer, effective utilization of electron-hole pair and hence enhanced photocatalytic H_2 production. In these composites, CNTs worked as both sensitizer and cocatalyst and possible photocatalytic H_2 production mechanism as shown in Fig. 2.6.

For effective utilization of incident light, proper uniform dispersion of the photocatalyst in the sacrificial solution is necessary. This could be achieved by optimizing different amounts (mg/L) of the photocatalyst for photocatalytic H_2 production under solar irradiation. Among different amounts of the photocatalysts (3–100 mg), 5 mg of the catalyst showed the highest H_2 production due to less

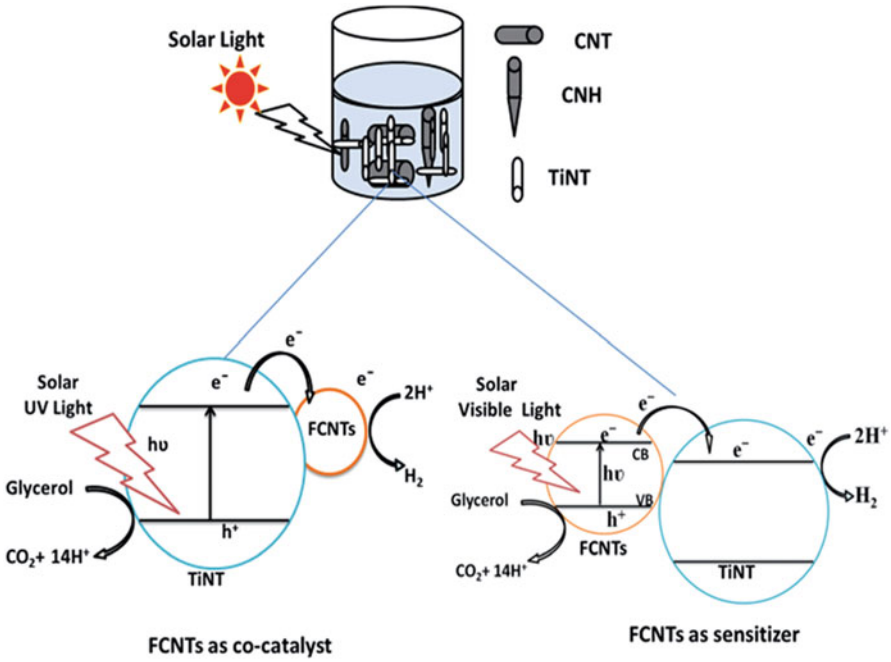

Fig. 2.6 Schematic illustration of hydrogen production mechanism of FCNT-TiNT composite evolution. (Reprinted from Kumari et al. 2017 with permission of the Royal Society of Chemistry)

Table 2.6 The summary of hydrogen generation performance of elements-doped TiO_2 photocatalysts

Doped elements (non-metals)	Reaction solution	Light source	H_2 production μmol. h^{-1} g^{-1}_{cat}	References
N	CH_3OH+H_2O	Solar	6.5	Sreethawong et al. (2008)
N	CH_3OH+H_2O	Solar	8.5	Jayakumar et al. (2012)
N-In	CH_3OH+H_2O	Visible	14	Sasikala et al. (2010)
S-SiC	CH_3OH+H_2O	Visible	1200	Mishra et al. (2015)

agglomeration between the particles, uniformly dispersed in the glycerol aqueous solution with improved division of charge carriers and operation for redox reactions (Kato et al. 2003; Cheng et al. 2014). The H_2 production rates of different CNT-TiO_2 nanocomposites are as shown in Table 2.6. Interestingly, some of the research work on CNT-TiO_2 nanocomposites (Table 2.7) employ biodegradable, cost-effective, eco-friendly glycerol used as the hole trapping agent due to its additional benefit for the improvement of H_2 production (Chi et al. 2007).

Table 2.7 Photocatalytic H_2 generation rates of CNT-TiO_2 hybrid photocatalysts

Photocatalyst	Catalyst (mg)	Light source	Sacrificial agent	Activity (μ mol h^{-1} g^{-1})	References
CNT-CNH/ TiO_2	5	Sunlight	Glycerol	24,048	Mamathakumari et al. (2015)
CNT-TiNT	5	Sunlight	Glycerol	29,904	Kumari et al. (2017)
MWCNT-TiO_2	40	UV-Vis	TEOA	8092	Dai et al. (2014b)
Pt@MWCNT-TiO_2	50	UV-Vis	Na_2S and Na_2SO_3	8718	Haldorai et al. (2015)
Pt@CNT- TiO_2	500	UV	Methanol	3803	Moya et al. (2015)
MWNT/TiO_2/ Ni	1000	Visible	Methanol	381	Ou et al. (2006)
MWCNT-TNT	50	UV-Vis	Na_2S and Na_2SO_3	1610	Li et al. (2012)
Pd@MWCNTs-TiO_2	10	UV-Vis	Ethanol and methanol	2400	Beltram et al. (2017)

2.4.4.2 Graphene Oxide/Reduced Graphene Oxide (RGO)

Functionalizing TiO_2 with graphene provides significant gains in photoelectrocatalytic efficiencies due to electron transport characteristics of graphene (Nazeeruddin et al. 2011). Graphene oxides have been widely studied due to the reactivity of the oxygen in the material. For instance, TiO_2-GO, the oxygen acts as a support to anchor the TiO_2 (Li et al. 2011a). In addition, GO has special features such as large surface area, lightweight and a large amount of delocalized electrons (Matsuoka et al. 2007). GO has an important role when coupling with TiO_2 because light absorption of GO is largely reduced than graphene favouring light irradiation on TiO_2 surface (Matsuoka et al. 2007).

The combination of the advantages of nitrogen and graphene has enhanced the TiO_2 photocatalytic performance (Liang et al. 2010). TiO_2/N-graphene nanohybrid photocatalyst synthesized by in situ sol-gel approach followed by hydrothermal method, showed the ultrasmaller diameter of 1 nm for the new particles. The results of this methodology indicate that the band gap was redshifted from neat TiO_2 nanoparticles to TiO_2/N-graphene hybrid catalysts. Photocatalytic activity results showed that TiO_2/N-graphene hybrid photocatalyst with 5 wt.% N-graphene has a 2.5 higher catalytic activity than pristine TiO_2 nanoparticles, illustrating that the novel hybrid material has better photocatalytic performance than a pristine one. This improvement is due to the narrowing of band gap and the optimized light absorption in sunlight.

Comparing to carbon nanotubes (CNTs) and activated carbon (AC), graphene oxide (GO) has a better conductivity and better surface area. These characteristics can enhance TiO_2 photocatalytic performance (9). Dai et al. (10) reported a scalable method to synthesize surface-fluorinated TiO_2 (F-TiO_2) nanosheets hybridized with GO through a hydrothermal treatment and colloidal self-assembly approach. F-TiO_2

nanosheets were anchored on the surface of the GO nanosheets. The photocatalytic activities were analysed under UV light, and the results showed that the F-TiO_2-GO hybrid photocatalyst with exposed facet (001) having a higher photocatalytic performance than commercial P25 and pure TiO_2. The enhancement of photocatalytic activity was mainly due to the reinforcement of electron-hole separation which can be attributed to the GO presence. One of the reasons was that GO acted as recombination centre rather than provides an electron pathway. 3 wt.% GO was the optimum ratio value found for best and efficient TiO_2-GO photocatalyst.

Differently of Dai et al. (10), the novel hybrid TiO_2-GO photocatalyst obtained by Cong et al. (2013) (9) was visible light active. TiO_2-GO hybrid was synthesized by two steps, in-situ growth of a uniform TiC layer on graphene oxide sheets using a molten salt method followed by oxidation conversion of TiC to anatase TiO_2 layer in airflow. The formation of the bond Ti-O-C introduced a mid-band gap near TiO_2 valence band and allows absorption of light to a longer-wavelength region. This improvement resulted in a better photocatalytic performance under visible light than P25. Finally, they explained that to achieve a reasonable absorption capability and photocatalytic activity, the ratio between GO and TiO_2 should be adjusted.

There was an improvement in the synthesis of reduced TiO_2-rGO catalyst with the development of the new technique named electrophoretic deposition-anodization method (CEPDA) (Yun et al. 2012). This has an advantage of fabricating hybrid electrodes because it requires just one single step which provides an anodic growth of TiO_2 nanotubes and electrophoretic-driven attachment of rGO at the same time. It achieved a balance between oxygen functional group and electron conductivity which allows a better catalytic performance to the TiO_2. Graphite has a greater conductivity than GO; however, the absence of oxygen makes the interaction with TiO_2 difficult. Therefore, the right condition found using the technique CEPDA represents a potential mechanism to improve the photoelectrochemical performance of TiO_2. Graphene accepts the electrons generated during the photocatalysis and worked beneficially as the acceptor, which lengthens the charge carrier's lifetime (Cheng et al. 2012). The mechanism involved in this charge carrier transfer has been shown in Fig. 2.7.

Various nanostructured carbons have used to improve the photocatalytic hydrogen generation performance of TiO_2 nanostructures, and the results are summarized in Table 2.8.

2.5 Future Scope/Conclusions

In this, we have covered different TiO_2-based heterostructures which are highly influencing the photocatalytic efficiency in a positive manner. The properties of most promising semiconductor materials like TiO_2 were discussed; a view has been given about its composites since TiO_2 in alone condition is facing several difficulties regarding fast recombination and efficient light absorption. In order to compensate for these difficulties and to work TiO_2 efficiently at sunlight/visible irradiation, TiO_2

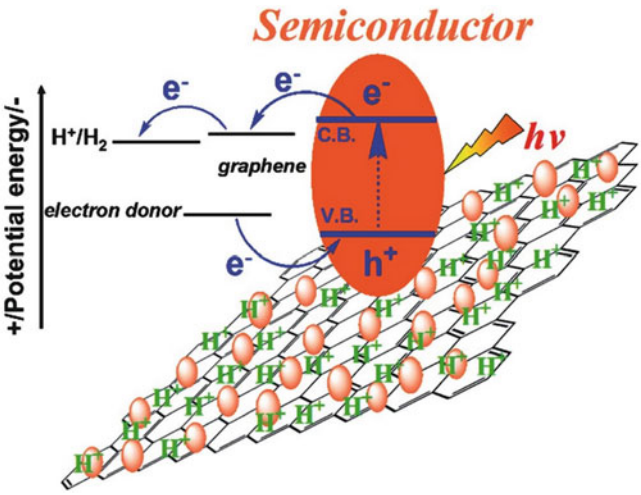

Fig. 2.7 A schematic diagram of the possible charge transfer in the TiO_2/graphene evolution. (Reprinted from Lv et al. 2012 with permission from the Royal Society of Chemistry)

surface has been modified with noble metallic particles (e.g. gold, silver, palladium, platinum, etc.), non-metals (e.g. carbon, nitrogen, sulphur, phosphorus, its co- and tri-doping) and nanostructured carbons (e.g. carbon black, carbon nanotubes, graphene, reduced graphene oxide, porous carbons, carbon quantum dots, carbon fibres, etc.). Such modifications change the morphological and TiO_2 band gap characteristics to enhance the photocatalytic activity.

Functionalization of TiO_2 with carbonaceous materials is a spectacular thought which adds another milestone in TiO_2-based photocatalysis. Since some of the carbonaceous materials possess high surface area and better charge conduction properties as described, noble metal loading creates a channel to hinder the charge carrier recombination, whereas cation-anion doping offers the modular band gap to make TiO_2 visible light active. In another aspect, crucial properties such as size, amount of the catalyst and morphology were also explained along with their significance.

- Efficient utilization of TiO_2 as photocatalyst leads to eye-countable values of H_2 production, which curtails the usage of toxic fossils and saves the environment. So TiO_2 should be utilized in a better manner, for the composites with high light-absorbing capabilities and retarded electron-hole recombination rates were needed to be synthesized through simple routes.
- Availability (occurrence) of TiO_2 is literally good, but finding a way to recycle the compound after utilization is needed to look upon.

Table 2.8 The summary of hydrogen generation performance of various TiO_2/nanocarbon hybrid-based photocatalysts

Nanocarbon used for TiO_2 hybridization	Reaction solution	Light source	H_2 production $\mu mol.\ h^{-1}\ g^{-1}{}_{cat}$	References
Graphene	$CH_3OH + H_2O$	Solar	186	Zhou et al. (2017)
Pt-rGO	$CH_3OH + H_2O$	UV-Vis	1016	Shinde et al. (2017)
Graphene	$CH_3OH + H_2O$	UV-Vis	80	Li et al. (2011b)
P25/rGO	$CH_3OH + H_2O$	UV-Vis	668	Cheng et al. (2012)
Pt-rGO	$CH_3OH + H_2O$	Xenon lamp with >300 nm	670	El-Bery et al. (2017)
CNT-graphene	$CH_3OH + H_2O$	Solar	29	Bellamkonda et al. (2017)
CNTs	$CH_3OH + H_2O$	Solar	8	Dai et al. (2009)
Graphene	$CH_3OH + H_2O$	Solar	22	Bellamkonda et al. (2017)
RGO	$CH_3OH + H_2O$	Solar	550	Gupta et al. (2015)
Graphene	$CH_3OH + H_2O$	Solar	400	Qiu et al. (2015)
NS-rGO	$CH_3OH + H_2O$	UV-Vis	13,996	Chen et al. (2016)
N-rGO	$CH_3OH + H_2O$	Solar	13.3	Mou et al. (2014)
RGO	$CH_3OH + H_2O$	Solar	8.6	Zhang et al. (2010)
C_3N_4	$CH_3OH + H_2O$	Solar	40	Zhang et al. (2017)

References

Antony RP, Mathews T, Ramesh C, Murugesan N, Dasgupta A, Dhara S, Dash S, Tyagi AK (2012) Efficient photocatalytic hydrogen generation by Pt modified TiO 2 nanotubes fabricated by rapid breakdown anodization. Int J Hydrog Energy 37:8268–8276. https://doi.org/10.1016/j.ijhydene.2012.02.089

Asiri AM, Al-Amoudi MS, Bazaid SA, Adam AA, Alamry KA, Anandan S (2014) Enhanced visible light photodegradation of water pollutants over N-, S-doped titanium dioxide and n-titanium dioxide in the presence of inorganic anions. J Saudi Chem Soc 18:155–163. https://doi.org/10.1016/j.jscs.2011.06.008

Bai H, Liu Z, Sun DD (2012) The design of a hierarchical photocatalyst inspired by natural forest and its usage on hydrogen generation. Int J Hydrog Energy 37:13998–14008. https://doi.org/10.1016/j.ijhydene.2012.07.041

Bellamkonda S, Thangavel N, Hafeez HY, Neppolian B, Ranga Rao G (2017) Highly active and stable multi-walled carbon nanotubes-graphene-TiO2nanohybrid: an efficient non-noble metal photocatalyst for water splitting. Catal Today 321–322:120–127. https://doi.org/10.1016/j.cattod.2017.10.023

Beltram A, Melchionna M, Montini T, Nasi L, Fornosiero P, Proto M (2017) Making H2 from light and biomass-derived alcohols: The outstanding activity newly designed hierarchical MWCNT/Pd@TiO2 hybrid catalyst Green chemistry. RSC Adv 19:2379–2389. https://doi.org/10.1039/C6GC01979J

Chen WT, Chan A, Sun-Waterhouse D, Moriga T, Idriss H, Waterhouse GIN (2015) Ni/TiO2: a promising low-cost photocatalytic system for solar H2 production from ethanol-water mixtures. J Catal 326:43–53. https://doi.org/10.1016/j.jcat.2015.03.008

Chen D, Zou L, Li S, Zheng F (2016) Nanospherical like reduced graphene oxide decorated TiO 2 nanoparticles: an advanced catalyst for the hydrogen evolution reaction. Sci Rep 6:1–8. https://doi.org/10.1038/srep20335

Cheng H-L, Mostoslavsky R, Saito S, Manis JP, Gu Y, Patel P, Bronson R, Appella E, Alt FW, Chua KF (2003a) Developmental defects and p53 hyperacetylation in Sir2 homolog (SIRT1)-deficient mice. Proc Natl Acad Sci 100:10794–10799. https://doi.org/10.1073/pnas.1934713100

Cheng P, Zheng M, Jin Y, Huang Q, Gu M (2003b) Preparation and characterization of silica-doped titania photocatalyst through sol-gel method. Mater Lett 57:2989–2994. https://doi.org/10.1016/S0167-577X(02)01409-X

Cheng P, Yang Z, Wang H, Cheng W, Chen M, Shangguan W, Ding G (2012) TiO2-graphene nanocomposites for photocatalytic hydrogen production from splitting water. Int J Hydrog Energy 37:2224–2230. https://doi.org/10.1016/j.ijhydene.2011.11.004

Cheng W-Y, Yu T-H, Chao K-J, Lu S-Y (2014) Cu2O-decorated mesoporous TiO2 beads as a highly efficient photocatalyst for hydrogen production. ChemCatChem 6:293–300. https://doi.org/10.1002/cctc.201300681

Chi Z, Pyle D, Wen Z, Frear C, Chen S (2007) A laboratory study of producing docosahexaenoic acid from biodiesel-waste glycerol by microalgal fermentation. Process Biochem 42:1537–1545. https://doi.org/10.1016/j.procbio.2007.08.008

Chiarello GL, Aguirre MH, Selli E (2010) Hydrogen production by photocatalytic steam reforming of methanol on noble metal-modified TiO2. J Catal 273:182–190. https://doi.org/10.1016/j.jcat.2010.05.012

Cong Y, Long M, Cui Z, Li X, Dong Z, Yuan G, Zhang J (2013) Anchoring a uniform TiO2 layer on graphene oxide sheets as an efficient visible light photocatalyst. Appl Surf Sci 282:400–407. https://doi.org/10.1016/j.apsusc.2013.05.143

Dai K, Peng T, Ke D, Wei B (2009) Photocatalytic hydrogen generation using a nanocomposite of multi-walled carbon nanotubes and TiO2 nanoparticles under visible light irradiation. Nanotechnology 20:125603. https://doi.org/10.1088/0957-4484/20/12/125603

Dai K, Lu L, Liu Q, Zhu G, Liu Q, Liu Z (2014a) Graphene oxide capturing surface-fluorinated TiO_2 nanosheets for advanced photocatalysis and the reveal of synergism reinforce mechanism. Dalton Trans 43:2202–2210. https://doi.org/10.1039/C3DT52542B

Dai K, Zhang X, Fan K, Zeng P, Peng T (2014b) Multiwalled carbon nanotube-TiO_2 nanocomposite for visible-light-induced photocatalytic hydrogen evolution. J Nanomater 2014:1–8

Dosado AG, Chen WT, Chan A, Sun-Waterhouse D, Waterhouse GIN (2015) Novel Au/TiO<inf>2</inf> photocatalysts for hydrogen production in alcohol-water mixtures based on hydrogen titanate nanotube precursors. J Catal 330:238–254. https://doi.org/10.1016/j.jcat.2015.07.014

Duonghong D, Borgarello E, Grätzel M (1981) Dynamics of light-induced water cleavage in colloidal systems. J Am Chem Soc 103:4685–4690. https://doi.org/10.1021/ja00406a004

El-Bery HM, Matsushita Y, Abdel-moneim A (2017) Fabrication of efficient TiO2-RGO heterojunction composites for hydrogen generation via water-splitting: comparison between RGO, Au and Pt reduction sites. Appl Surf Sci 423:185–196. https://doi.org/10.1016/j.apsusc.2017.06.130

Gupta B, Melvin AA, Matthews T, Dhara S, Dash S, Tyagi AK (2015) Facile gamma radiolytic methodology for TiO2-rGO synthesis: effect on photo-catalytic H_2 evolution. Int J Hydrog Energy 40:5815–5823. https://doi.org/10.1016/j.ijhydene.2015.02.102

Haldorai Y, Rengaraj A, Lee JB, Huh YS, Han YK (2015) Highly efficient hydrogen production via water splitting using Pt@MWNT/TiO2 ternary hybrid composite as a catalyst under UV-visible light. Synth Met 199:345–352. https://doi.org/10.1016/j.synthmet.2014.12.014

Hoffmann MR, Martin ST, Choi W, Bahnemann DW (1995) Environmental applications of semiconductor photocatalysis. Chem Rev 95:69–96. https://doi.org/10.1021/cr00033a004

Jamalluddin NA, Abdullah AZ (2011) Reactive dye degradation by combined Fe(III)/TiO2 catalyst and ultrasonic irradiation: effect of Fe(III) loading and calcination temperature. Ultrason Sonochem 18:669–678. https://doi.org/10.1016/j.ultsonch.2010.09.004

Janisch R, Gopal P, Spaldin NA (2005) Transition metal doped TiO2 and ZnO-present status of the field. J Phys Condens Matter 17:R657–R689

Jayakumar OD, Sasikala R, Kadam RM, Kienle L, Adelung R, Mittal JP, Tyagi AK (2012) Photochemical hydrogen generation using nitrogen-doped TiO 2 − Pd nanoparticles: facile synthesis and effect of Ti 3+ incorporation. J Phys Chem C 116:12642–12467

Jovic V, Chen WT, Sun-Waterhouse D, Blackford MG, Idriss H, Waterhouse GIN (2013) Effect of gold loading and TiO2 support composition on the activity of Au/TiO2 photocatalysts for H_2 production from ethanol-water mixtures. J Catal 305:307–317. https://doi.org/10.1016/j.jcat.2013.05.031

Kanhere P, Chen Z (2014) A review on visible light active perovskite-based photocatalysts. Molecules 19:19995–20022. https://doi.org/10.3390/molecules191219995

Kato H, Asakura K, Kudo A (2003) Highly efficient water splitting into H_2 and O_2 over lanthanum-doped NaTaO3 photocatalysts with high crystallinity and surface nanostructure. J Am Chem Soc 125:3082–3089. https://doi.org/10.1021/ja027751g

Khan MA, Woo SI, Yang OB (2008) Hydrothermally stabilized Fe(III) doped titania active under visible light for water splitting reaction. Int J Hydrog Energy 33:5345–5351. https://doi.org/10.1016/j.ijhydene.2008.07.119

Kim HG, Hwang DW, Bae SW, Jung JH, Lee JS (2003) Photocatalytic water splitting over $La_2Ti_2O_7$ synthesized by the polymerizable complex method. Catal Lett 91:193–198

Kim J, Hwang DW, Kim HG, Bae SW, Lee JS, Li W, Oh SH (2005) Highly efficient overall water splitting through optimization of preparation and operation conditions of layered perovskite photocatalysts. Top Catal 35:295–303. https://doi.org/10.1007/s11244-005-3837-x

Kolen'ko YV, Kovnir KA, Gavrilov AI, Garshev AV, Frantti J, Lebedev OI, Churagulov BR, Van Tendeloo G, Yoshimura M (2006) Hydrothermal synthesis and characterization of nanorods of various titanates and titanium dioxide. J Phys Chem B 110:4030–4038. https://doi.org/10.1021/jp055687u

Kozlova EA, Korobkina TP, Vorontsov AV (2009) Overall water splitting over Pt/TiO2 catalyst with Ce3+/Ce4+ shuttle charge transfer system. Int J Hydrog Energy 34:138–146. https://doi.org/10.1016/j.ijhydene.2008.09.101

Kumari MM, Priyanka A, Marenna B, Haridoss P, Kumar DP, Shankar MV (2017) Benefits of tubular morphologies on electron transfer properties in CNT/TiNT nanohybrid photocatalyst for enhanced H $_2$ production. RSC Adv 7:7203–7209. https://doi.org/10.1039/C6RA26693B

Lalitha K, Reddy JK, Phanikrishna Sharma MV, Kumari VD, Subrahmanyam M (2010) Continuous hydrogen production activity over finely dispersed Ag2O/TiO2 catalysts from methanol: water mixtures under solar irradiation: a structure-activity correlation. Int J Hydrog Energy 35:3991–4001. https://doi.org/10.1016/j.ijhydene.2010.01.106

Li Y, Du J, Peng S, Xie D, Lu G, Li S (2008) Enhancement of photocatalytic activity of cadmium sulfide for hydrogen evolution by photoetching. Int J Hydrog Energy 33:2007–2013. https://doi.org/10.1016/j.ijhydene.2008.02.023

Li J, Chen X, Ai N, Hao J, Chen Q, Strauf S, Shi Y (2011a) Silver nanoparticle doped TiO2 nanofiber dye sensitized solar cells. Chem Phys Lett 514:141–145. https://doi.org/10.1016/j.cplett.2011.08.048

Li N, Liu G, Zhen C, Li F, Zhang L, Cheng HM (2011b) Battery performance and photocatalytic activity of mesoporous anatase TiO2 nanospheres/graphene composites by template-free self-assembly. Adv Funct Mater 21:1717–1722. https://doi.org/10.1002/adfm.201002295

Li H, Zhang X, Cui X, Lin Y (2012) TiO $_2$ nanotubes/MWCNTs nanocomposite photocatalysts: synthesis, characterization and photocatalytic hydrogen evolution under UV-Vis light illumination. J Nanosci Nanotechnol 12:1806–1811. https://doi.org/10.1166/jnn.2012.5161

Liang Y, Wang H, Casalongue HS, Chen Z, Dai H (2010) TiO2 Nanocrystals grown on graphene as advanced photocatalytic hybrid materials. Nano Res 3:701–705. https://doi.org/10.1007/s12274-010-0033-5

Liang S, Zhou Y, Kang K, Zhang Y, Cai Z, Pan J (2017) Synthesis and characterization of porous TiO2 -NS/Pt/GO aerogel: a novel three-dimensional composite with enhanced visible-light photoactivity in degradation of chlortetracycline. J Photochem Photobiol A Chem 346:1–9. https://doi.org/10.1016/j.jphotochem.2017.05.036

Luna AL, Novoseltceva E, Louarn E, Beaunier P, Kowalska E, Ohtani B, Valenzuela MA, Remita H, Colbeau-Justin C (2016) Synergetic effect of Ni and Au nanoparticles synthesized on titania particles for efficient photocatalytic hydrogen production. Appl Catal B Environ 191:18–28. https://doi.org/10.1016/j.apcatb.2016.03.008

Lv X-J, Fu W-F, Chang H-X, Zhang H, Cheng J-S, Zhang G-J, Song Y, Hu C-Y, Li J-H (2012) Hydrogen evolution from water using semiconductor nanoparticle/graphene composite photocatalysts without noble metals. J Mater Chem 22:1539–1546. https://doi.org/10.1039/C1JM14502A

Maeda K, Teramura K, Lu D, Takata T, Saito N, Inoue Y, Domen K (2006) Characterization of Rh-Cr mixed-oxide nanoparticles dispersed on (Ga1-xZnx)(N1-xOx) as a cocatalyst for visible-light-driven overall water splitting. J Phys Chem B 110:13753–13758. https://doi.org/10.1021/jp061829o

Mamathakumari M, Praveen Kumar D, Haridoss P, Durgakumari V, Shankar MV (2015) Nanohybrid of titania/carbon nanotubes – nanohorns: a promising photocatalyst for enhanced hydrogen production under solar irradiation. Int J Hydrog Energy 40:1665–1674. https://doi.org/10.1016/j.ijhydene.2014.11.117

Matsuoka M, Kitano M, Takeuchi M, Tsujimaru K, Anpo M, Thomas JM (2007) Photocatalysis for new energy production. Recent advances in photocatalytic water splitting reactions for hydrogen production. Catal Today 122:51–61. https://doi.org/10.1016/j.cattod.2007.01.042

Mishra G, Parida KM, Singh SK (2015) Facile fabrication of S-TiO2/??-SiC nanocomposite photocatalyst for hydrogen evolution under visible light irradiation. ACS Sustain Chem Eng 3:245–253. https://doi.org/10.1021/sc500570k

Mou Z, Wu Y, Sun J, Yang P, Du Y, Lu C (2014) TiO2 nanoparticles-functionalized N-doped graphene with superior interfacial contact and enhanced charge separation for photocatalytic hydrogen generation. ACS Appl Mater Interfaces 6:13798–13806. https://doi.org/10.1021/am503244w

Moya A, Cherevan A, Marchesan S, Gebhardt P, Prato M, Eder D, Vilatela JJ (2015) Oxygen vacancies and interfaces enhancing photocatalytic hydrogen production in mesoporous CNT/TiO2 hybrids. Appl Catal B Environ 179:574–582. https://doi.org/10.1016/j.apcatb.2015.05.052

Naik B, Martha S, Parida KM (2011) Facile fabrication of Bi2O3/TiO2-xN x nanocomposites for excellent visible light driven photocatalytic hydrogen evolution. Int J Hydrog Energy 36:2794–2802. https://doi.org/10.1016/j.ijhydene.2010.11.104

Nakata K, Fujishima A (2012) TiO2 photocatalysis: design and applications. J Photochem Photobiol C: Photochem Rev 13:169–189. https://doi.org/10.1016/j.jphotochemrev.2012.06.001

Naldoni A, D'Arienzo M, Altomare M, Marelli M, Scotti R, Morazzoni F, Selli E, Dal Santo V (2013) Pt and Au/TiO2 photocatalysts for methanol reforming: role of metal nanoparticles in tuning charge trapping properties and photoefficiency. Appl Catal B Environ 130–131:239–248. https://doi.org/10.1016/j.apcatb.2012.11.006

Nazeeruddin MK, Baranoff E, Grätzel M (2011) Dye-sensitized solar cells: a brief overview. Sol Energy 85:1172–1178. https://doi.org/10.1016/j.solener.2011.01.018

Ou Y, Lin J, Fang S, Liao D (2006) MWNT-TiO2:Ni composite catalyst: a new class of catalyst for photocatalytic H_2 evolution from water under visible light illumination. Chem Phys Lett 429:199–203. https://doi.org/10.1016/j.cplett.2006.08.024

Pan L, Zou JJ, Wang S, Huang ZF, Zhang X, Wang L (2013) Enhancement of visible-light-induced photodegradation over hierarchical porous TiO2by nonmetal doping and water-mediated dye sensitization. Appl Surf Sci 268:252–258. https://doi.org/10.1016/j.apsusc.2012.12.074

Patsoura A, Kondarides DI, Verykios XE (2007) Photocatalytic degradation of organic pollutants with simultaneous production of hydrogen. Catal Today 124:94–102. https://doi.org/10.1016/j.cattod.2007.03.028

Qiu B, Zhou Y, Ma Y, Yang X, Sheng W, Xing M, Zhang J (2015) Facile synthesis of the Ti3+ self-doped TiO2-graphene nanosheet composites with enhanced photocatalysis. Sci Rep 5:8591–8596. https://doi.org/10.1038/srep08591

Robertson PKJ (1996) Semiconductor photocatalysis: an environmentally acceptable alternative production technique and effluent treatment process. J Clean Prod 4:203–212. https://doi.org/10.1016/S0959-6526(96)00044-3

Saleh TA, Gupta VK (2012) Photo-catalyzed degradation of hazardous dye methyl orange by use of a composite catalyst consisting of multi-walled carbon nanotubes and titanium dioxide. J Colloid Interface Sci 371:101–106. https://doi.org/10.1016/j.jcis.2011.12.038

Sasikala R, Sudarsan V, Sudakar C, Naik R, Sakuntala T, Bharadwaj SR (2008) Enhanced photocatalytic hydrogen evolution over nanometer sized Sn and Eu doped titanium oxide. Int J Hydrog Energy 33:4966–4973. https://doi.org/10.1016/j.ijhydene.2008.07.080

Sasikala R, Shirole AR, Sudarsan V, Jagannath, Sudakar C, Naik R, Rao R, Bharadwaj SR (2010) Enhanced photocatalytic activity of indium and nitrogen co-doped TiO2-Pd nanocomposites for hydrogen generation. Appl Catal A Gen 377:47–54. https://doi.org/10.1016/j.apcata.2010.01.039

Shet S, Ahn KS, Deutsch T, Wang HI, Ravindra N, Yan Y, Turner J, Al-Jassim M (2010) Synthesis and characterization of band gap-reduced ZnO:N and ZnO:(Al,N) films for photoelectrochemical water splitting. J Mater Res 25:69–75. https://doi.org/10.1557/jmr.2010.0017

Shinde Y, Wadhai S, Ponkshe A, Kapoor S, Thakur P (2017) Decoration of Pt on the metal free RGO-TiO 2 composite photocatalyst for the enhanced photocatalytic hydrogen evolution and photocatalytic degradation of pharmaceutical pollutant β blocker. Int J Hydrog Energy 43:4015–4027. https://doi.org/10.1016/j.ijhydene.2017.10.089

Sreethawong T, Laehsalee S, Chauadej S (2008) Comparative investigation of mesoporous- and non-mesoporous-assembled TiO2 nanocrystals for photocatalytic H2 production over N-doped TiO2 under visible light irradiation. Int J Hydrog Energy 33:5947–5957. https://doi.org/10.1016/j.ijhydene.2008.08.007

Takata T, Tanaka A, Hara M, Kondo JN, Domen K (1998) Recent progress of photocatalysts for overall water splitting. Catal Today 44:17–26. https://doi.org/10.1016/S0920-5861(98)00170-9

Vu TTD, Mighri F, Ajji A, Do T (2014) Synthesis of titanium dioxide/cadmium sulfide nanosphere particles for photocatalyst applications. Ind Eng Chem Res 53:3888–3897. https://doi.org/10.1021/ie403718n

Wu MC, Hiltunen J, Sápi A, Avila A, Larsson W, Liao HC, Huuhtanen M, Tóth G, Shchukarev A, Laufer N, Kukovecz Á, Kónya Z, Mikkola JP, Keiski R, Su WF, Chen YF, Jantunen H, Ajayan

PM, Vajtai R, Kordás K (2011) Nitrogen-doped anatase nanofibers decorated with noble metal nanoparticles for photocatalytic production of hydrogen. ACS Nano 5:5025–5030. https://doi.org/10.1021/nn201111j

Xu H, Ouyang S, Li P, Kako T, Ye J (2013) High-active anatase TiO 2 nanosheets exposed with 95% {100} facets toward efficient H 2 evolution and CO 2 photoreduction. ACS Appl Mater Interfaces 5:1348–1354.

Ya-hui Y, Qi-yuan C, Zhou-lan Y, Jie L (2009) Applied surface science study on the photocatalytic activity of K 2 La 2 Ti 3 O 10 doped with zinc (Zn). Appl Surf Sci 255:8419–8424. https://doi.org/10.1016/j.apsusc.2009.05.146

Yamaguti K, Sato S (1985) Photolysis of water over metallized powdered titanium dioxide. J Chem Soc Faraday Trans 1 Phys Chem Condens Phases 81:1237. https://doi.org/10.1039/f19858101237

Yin S, Ihara K, Liu B, Wang Y, Li R, Sato T (2007) Preparation of anatase, rutile and brookite type anion doped titania photocatalyst nanoparticles and thin films. Phys Scr T T129:268–273. https://doi.org/10.1088/0031-8949/2007/T129/060

Yun J-H, Wong RJ, Ng YH, Du A, Amal R (2012) Combined electrophoretic deposition–anodization method to fabricate reduced graphene oxide–TiO2 nanotube films. RSC Adv 2:8164–8171. https://doi.org/10.1039/c2ra20827j

Zhang X-Y, Li H-P, Cui X-L, Lin Y (2010) Graphene/TiO2 nanocomposites: synthesis, characterization and application in hydrogen evolution from water photocatalytic splitting. J Mater Chem 20:2801–2806. https://doi.org/10.1039/b917240h

Zhang H, Liu F, Wu H, Cao X, Sun J, Lei W (2017) In situ synthesis of g-C $_3$ N $_4$/TiO $_2$ heterostructures with enhanced photocatalytic hydrogen evolution under visible light. RSC Adv 7:40327–40333. https://doi.org/10.1039/C7RA06786K

Zhou G, Shen L, Xing Z, Kou X, Duan S, Fan L, Meng H, Xu Q, Zhang X, Li L, Zhao M, Mi J, Li Z (2017) Ti 3+ self-doped mesoporous black TiO 2/graphene assemblies for unpredicted-high solar-driven photocatalytic hydrogen evolution. J Colloid Interface Sci 505:1031–1038. https://doi.org/10.1016/j.jcis.2017.06.097

Chapter 3
Novelty in Designing of Photocatalysts for Water Splitting and CO_2 Reduction

Santanu Sarkar, Shubhrajit Sarkar, Chiranjib Bhattacharjee, and Supriya Sarkar

Contents

Abstract The photocatalytic CO_2 reduction and water splitting in the presence of solar illumination are very attractive in the current decade for production of alternative fuel in terms of hydrocarbon and hydrogen. The present chapter has highlighted the method of synthesis of photocatalyst and their possible modification for performance enhancement in the mentioned area. It also includes the scope of opportunity for further development of the present methodology to commercialize in the near future.

Keywords CO_2 photoreduction · Water splitting · Oxides · Synthesis of oxides · Bandgap engineering

S. Sarkar · S. Sarkar
Environment Research Group, R&D, Tata Steel Ltd., Jamshedpur, Jharkhand, India

S. Sarkar · C. Bhattacharjee (✉)
Chemical Engineering Department, Jadavpur University, Kolkata, West Bengal, India
e-mail: cbhattacharyya@chemical.jdvu.ac.in

Inamuddin et al. (eds.), *Nanophotocatalysis and Environmental Applications*,
Environmental Chemistry for a Sustainable World 31,
https://doi.org/10.1007/978-3-030-04949-2_3

3.1 Introduction

In the twenty-first century, increasing demand for energy results in maximization of utilization of fossil fuel. Thus, GHG (greenhouse gas) emission has increased simultaneously. By the year 2050, there will be a huge crisis of fossil fuel. Therefore, development of new technology is very essential for resource allocation of alternative fuel, and establishment of clean energy source for our future generation is very challenging. As per the understanding, the solar energy is the cleanest and most abundant source of energy for our society without any detrimental effect to the environment. The supply of solar energy to earth is $4.3*10^2$ J per hour, whereas annual consumption of energy on our planet is approximately $4.1*10^{20}$ J. However, the consumption of solar energy is very limited till date and the contribution of solar energy is almost 2% of the global consumption. Hence, there is a huge potential area of research for utilization of solar energy and to mitigate the gap between availability and utilization of solar energy.

On the other hand, increasing demand of utilization of fossil fuel is responsible for the enhancement of GHG emission which results in an increment of CO_2 concentration in the atmosphere. It has already been predicted that the global average temperature will rise by 1.9 °C if CO_2 concentration reaches to 590 ppm by 2100 which will have an adverse effect on global climate. Therefore, it is essential to reduce the consumption of fossil fuel by replacing it with renewable sources and reducing CO_2 to other alternative fuel.

In recent years, several methods have been developed for the production of alternative fuel from CO_2 via photochemical reduction, electrochemical reduction, photoelectrochemical reduction, thermochemical reduction, etc. (Froehlich and Kubiak 2012; Bonin et al. 2014; Beley et al. 1984; Laitar et al. 2005; Cokoja et al. 2011; Morris et al. 2009; Savéant 2008; Halmann 1978; Taniguchi et al. 1984; Blajeni et al. 1983; Hori et al. 1985; Le et al. 2011; Ashley et al. 2009; Rodriguez et al. 2015; Jadhav et al. 2014; Saeidi et al. 2014). Among all photochemical reactions, several researchers have paid lots of attention on photocatalysis using solar energy as a source of energy, e.g., water splitting, H_2O_2 production, pollutant degradation (Wenderich and Mul 2016; Ong et al. 2016; Shi et al. 2017a; Ong 2017; Kar et al. 2015; Zeng et al. n.d.; Chu et al. 2017; Li et al. 2016; Shiraishi et al. 2014; Asahi et al. 2001; Rahman et al. 2012), etc.

There are several photocatalysts have been developed so far for CO_2 reduction which can be categorized as semiconductors (oxide or non-oxide) (Inoue et al. 1979; Chen et al. 2017), metal oxides and sulfides except titanium (Navalón et al. 2013; Kar et al. 2014; Zhu et al. 2017a), and nonmetallic compounds (Kumar et al. 2013; Mömming et al. 2009), catalysts work in molecular state (Rakowski Dubois and Dubois 2009; Collin and Sauvage 1989), etc. (Ong et al. 2017; Zhu et al. 2017b; Pan et al. 2017; Rechberger and Niederberger 2017; Yang et al. 2017a, b; Wang et al. 2015a; Takeda et al. 2017; Li et al. 2017; Maina et al. 2017). However, above all, perovskites pose better photovoltaic and reduction potential of CO_2 (Luo et al. 2014;

Bin et al. 2016; Wang et al. 2017; Hou et al. 2017; Schreier et al. 2015; Xu et al. 2017). The earth-abundant elements are present in perovskites.

Nowadays, water splitting for production of hydrogen and oxygen (alternative fuel) using catalyst has become very lucrative for research fraternity. In this regard, researchers have paid lots of attention to the photoelectrochemical cell (PEC) for water splitting to oxygen and hydrogen using solar energy. Water splitting was initiated in 1972, using TiO_2 electrodes under UV illumination inside PEC (Fujishima and Honda 1972), though the process is very inefficient. After that many research initiatives have been taken to develop efficient photocatalyst-based energy and visible light-driven water splitting process (Lin et al. 2011; Chen et al. 2012a; Li et al. 2013a; Hisatomi et al. 2014).

In this chapter, special attention has been paid to the advancement of different types of photocatalyst used for water splitting and CO_2 reduction considering all challenges. This article also highlights catalytic mechanisms, improvement of performance of photocatalyst, and challenges for commercialization of water splitting and CO_2 reduction.

3.2 CO_2 Reduction

3.2.1 Principles of CO_2 Reduction

The electron is transferred from valence band (VB) to conduction band (CB) when light energy is higher than or equal to its bandgap (Eg) energy, and at the same time a hole is generated in the VB. The reduction potential of an electron depends on the energy level of the CB. Similarly, the oxidation is carried out with the help of hole, and thus oxidation potential is decided by the energy stored in the VB. The reduction of CO_2 by perovskite oxide photocatalyst in the presence of water, the energy of VB of the catalyst should be less than the redox potential of H_2O. Henceforth, the energy of CB should be greater than the redox potential of the CO_2 (Shi et al. 2017b; Xie et al. 2011; Zhou et al. 2013). Thus, perovskite oxide is a very important photocatalyst for a CO_2 reduction in the presence of water. Moreover, the availability of electron acceptor and the donor is very easy on the mentioned catalyst surface as well as such nanoparticle is excited in the femtosecond, but de-excitation takes the time in the range of picosecond/nanosecond. Hence, availability of electron and hole is maximized on the surface of the catalyst for effective reduction of CO_2.

The principle of reduction of CO_2 is the same in the presence of H_2 or water vapor, but as H_2 is highly reactive in nature, it is very difficult to control the reaction (Xie et al. 2011; Zhou et al. 2013; Varghese et al. 2009; Rani et al. 2014; Kar et al. 2016). During the reaction, the proton is released by oxidation of H_2 or water to reduce CO_2. It was reported that the proton might convert CO_2 into CO_2^- (Jia et al. 2009a) on the surface of the in perovskite oxides or it might be possible that CO_2 is activated by an electron in the semiconductor. Both phenomena could occur simultaneously. Kar et al. (2014, 2015, 2016) also reported that CO_2 could be converted

Table 3.1 Nanoparticles with corresponding by-products after CO_2 reduction

Catalyst	By-product	References
$SrTiO_3$-δ	CH_4	Xie et al. (2011)
$SrTiO_3$	CO and CH_4	Zhou et al. (2013)
C-$LaCoO_3$	HCHO, HCOOH	Jia et al. (2009a)
$CaTaO_2N$	HCOOH	Yoshitomi et al. (2015)
$NaNbO_3$	CH_4	Li et al. (2012)
$SrTiO_3$	CH_4	Hemminger et al. (1978)
$NaNbO_3$	CH_4	Shi et al. (2011)
g-C_3N_4/$NaNbO_3$	CH_4	Shi et al. (2014)
g- C3N_4/$KNbO_3$	CH_4	Shi et al. (2015)
$NaNbO_3$ and $KNbO_3$		Shi and Zou (2012)
$NaTaO_3$	CO and CH_4	Zhou et al. (2015)
$NaNbO_3$ and $NaTaO_3$	CO, CH_4, H_2, CH_3OH	Fresno et al. (2017)
$LiNbO_3$	HCOOH and HCHO	Nath et al. (2012)
$PbTiO_3$	CH_4	Do et al. (2016)
$LaCoO_3$ (doped with C and Fe)	HCHO, HCOOH	Jia et al. (2009b)
$CaLa_4Ti_4O_{15}$/$SrLa_4Ti_4O_{15}$/$BaLa_4Ti_4O_{15}$	H2, O2, CO, HCOOH	Iizuka et al. (2011)
Bi_2WO_6	CO	Sun et al. (2014)
Bi_2WO_6	Methanol	Liang et al. (2015)
Bi_2WO_6	CH_4	Kong et al. (2017)
Bi_2WO_6	CH_4	Zhou et al. (2011a)
$MnCo_2O_4$	CO, H_2	Wang et al. (2015b)
$ZnGa_2O_4$	CH_4	Liu et al. (2014a)

into hydrocarbons with the formation of the carbine at the electron-rich surface. In the first step CO_2 reduced to CO and then into carbon radical (·C). After that, a carbon radical is converted to ·CH, ·CH_2, and ·CH_3 by reacting with electron and proton generated from the oxidation of water. Finally, ·CH_3 is converted to CH_4. On the other hand, in the formaldehyde pathway, CO_2 is directly converted to formaldehyde, formic acid, methanol, and methane in electron-deficient environment.

3.2.2 By-Products of CO_2 Reduction

It has been confirmed that during the photocatalytic reduction, CO_2 is converted into carbon monoxide, and some other hydrocarbons (Jia et al. 2009a; Yoshitomi et al. 2015). In 1994, Hori et al. have established the pathway of CO_2 into CO (Hori et al. 1994) with intermediate formation of CO_2 radical. Several by-products and corresponding nanoparticles for CO_2 reduction have been tabulated in Table 3.1.

Table 3.2 Typical chemical methods for synthesis of perovskite oxides

Method of preparation	References
Hydrothermal: aqueous solutions at high pressure and at moderate to high temperatures	Xu et al. (2014)
Solvothermal: nonaqueous solvents at a higher temperature than hydrothermal	Caruntu et al. (2015)
Sol gel: preparation of colloidal solution using monomers	Parida et al. (2010)
Polymerized complex: polymer complex precursor using various metal ions	Phokha et al. (2014)
Solid-state reaction: very high temperature reaction	Yin et al. (2014)
Molten salt: molten salt as the medium	Vradman et al. (2017)
Sonochemical: ultrasound treatment	Wattanawikkam and Pecharapa (2016)
Microwave: electromagnetic wave for synthesis	Tang et al. (2013)

3.2.3 Synthesis of Nanoparticles

Perovskite oxide nanoparticle is commonly used for the reduction of CO_2, and typical methods for preparation of such nanoparticle have been listed in Table 3.2. Several methods have been developed for the preparation of perovskite oxides by improving surface morphology, carrier mobility, bandgap energy, etc. (Zhu et al. 2014a).

Kwak et al. (Kwak and Kang 2015) synthesized $Ca_xTi_yO_3$ perovskite oxides via hydrothermal process (453 °K for 8 h) from hydrated $CaCl_2$ and titanium isopropoxide at a certain stoichiometric ratio, and during the synthesis, pH was adjusted using sodium hydroxide. SrTiO3 perovskite oxides have been produced by Zheng et al. and Dong et al. (Zheng et al. 2011; Dong et al. 2012). The solgel method was also very attractive for generation of formation of $CoTiO_3$ in the presence of polymeric fugitive agents (Sobhani-Nasab et al. 2015), and in sonochemical method ultra-sonication was used to initiate the synthesis (Moghtada and Ashiri 2016).

3.2.3.1 Doping of Photocatalyst

The performance of photocatalyst depends on the bandgap energy of any semiconductor. Doping and substitution are two typical synthesis processes for reduction of bandgap to enhance the catalytic performance. In this regard, metallic and nonmetallic elements are used for such purpose, i.e., Au, Pd, Pt, Ni, Bi, Mn, N, Ph, F, Cu, Ag, C, Cr, Ru, Pb, Rh, Br, S, etc. Proper dopant could improve the bandgap, but at the same time, the improper dopant can create defects in semiconductor. Ta and Ni (Kato and Kudo 2002) and Sb and Cr (Niishiro et al. 2005) are called co-dopants as those reduce bandgap by minimizing non-radiative recombination. Ni and Co are more electronegative than Ti thus, those two elements can be used for reduction of the bandgap of titanate perovskite oxides, e.g., SrTiO3-AgNbO3 (Wang et al.

2009a). Therefore, to obtain the best performance of the semiconductors, suitable dopant needs to be identified based on the electronegativity of both mother and doping elements.

3.2.4 Commercial Challenges of CO_2 Reduction

The technical feasibility has already been established for CO_2 reduction using photocatalyst. However, the commercialization of CO_2 reduction largely depends on some factors of catalytic performance such as availability, a wide range of applicability, physicochemical properties, and stability during the reaction (Zhu et al. 2014a). Moreover, the process must be energy efficient so that solar to fuel conversion efficiency (ratio of energy required for CO_2 conversion to incident energy) should be at least 10% (Jacobsson et al. 2013). Considering above factors, the perovskite oxide is the probable catalyst can be developed as a commercialized system for CO_2 reduction. Moreover, the thermal stability of perovskite oxides has not been well established; thus, it is not suitable for gas phase reaction with a variation of temperature. Henceforth, application of perovskite oxides is limited inside the laboratory. In addition, the presence of acidic gases reduces the performance of the catalyst as well (Simakov 2017). However, very few literatures are available on the perspective of commercialization in the present process. Hence, further research is required considering real parametric condition before commercialization.

3.3 Water Splitting

3.3.1 The Basic Principle of Water Splitting

In general, the reaction of the water splitting can be presented using below equation (ΔG^0-Gibbs free energy).

$$H_2O\ (l) \rightarrow H_2(g) + O_2(g) a \ldots\ldots\ldots\ldots \Delta G^0 = 238 \frac{\text{kJ}}{\text{mol}} \text{ OR } 1.23 \text{ eV}$$

$$\text{Oxidation} : H_{2,}O + 2h^+ \rightarrow \frac{1}{2}O_2 + 2H^+$$

$$\text{Reduction} : 2H^+ + 2e \rightarrow H_2$$

Working principle of the photocatalyst is very similar as mentioned earlier in Sect. 3.2.1. Generally, the visible light energy, i.e., 2–2.4 eV, is greater than Gibbs free energy of water splitting. However, the bandgap energy should be greater than 1.23 eV as there are several losses on the catalyst surface. The losses of energy

include the change of entropy of water, transportation and recombination of electron and hole, etc. (Navarro et al. 2009). According to the principle of the reaction, to achieve the best reaction condition, the electronegativity of the CB of the photocatalyst should be greater than the reduction potential of the conversion from hydrogen ion to gaseous hydrogen, and similarly, the electropositivity of the VB should be more than the oxidation potential of the conversion from H_2O to O_2 (Gratzel 2001). In this regard, the mechanism of separation and transportation of electron and hole should be very efficient so that the loss of carriers could be minimized, and that can be achieved with the highly crystalline semiconductor. At the same time, the catalyst should be stable in a hostile environment such as increment of temperature and change in pH. Though, there are several photocatalysts, e.g., CdS, GaP, and TaON, which are very suitable for water splitting under sunlight. However, those have limited stability during the reaction (Ellis et al. 1977). It is very common that particle size of the catalyst should very less so that higher available active surface for water splitting can be achieved. Lower particle size also ensures better transportation of the charge carrier to the surface of the catalyst. Therefore, nanostructured material provides all the necessary properties of a photocatalyst for water splitting. In the next subsequent sections, an elaborate discussion on nanostructured photocatalyst has been presented.

3.3.2 Photocatalyst for Water Splitting

3.3.2.1 Oxide-Based Photocatalyst

The common catalyst for water splitting used by several researchers is TiO_2 due to its superior stability during reaction and surface activity (Gratzel 2001; Ellis et al. 1977; Navarro et al. 2010; Zhang et al. 2013a; Chen and Mao 2007; Chen et al. 2010, 2012b; Ni et al. 2007; Mor et al. 2006). It is also available in different forms like nanotubes and nanowires, which have larger surface area and lower carrier diffusion length (Chen and Mao 2007; Chen et al. 2010, 2012b; Ni et al. 2007; Mor et al. 2006) with all other potential properties of photocatalyst as earlier. However, UV illumination is required as its bandgap energy is higher, i.e., 3.2 eV, and consequently, the efficiency is less. The light penetration in TiO_2 is poor due to quantum confinement effect, and this property can be improved with the help of doping, coating, functionalization, and defect engineering (Chen and Mao 2007; Chen et al. 2010; Ni et al. 2007; Mor et al. 2006; Khan et al. 2002; Hwang and Lewis 2005; Asahi et al. 2001; Borgarello et al. 1982; In et al. 2007; Pan et al. 2009a, b, 2011; Wang et al. 2010; Wendt et al. 2008; Das et al. 2011; Chowdhury et al. 2011; Dholam et al. 2010; Yu et al. 2010; Dashora et al. 2014; Albuquerque et al. 2014), heterojunction (with another semiconductor) (Li et al. 2014a; Ai et al. 2011; Yan et al. 2014; Liu et al. 2014b), the introduction of plasmonic effect (Chen et al. 2011a; Warren and Thimsen 2012), etc. The synthesis of nonstructured photocatalyst has been briefly described in Table 3.3.

Table 3.3 Method of performance improvement of the photocatalyst

Method of preparation	References
Codoping: To increase the light penetration and decrease the bandgap energy. Anion doping using N_2, C, S, F, etc. (replacement of oxygen) and cation doping (replacement of Ti) using Fe, W, Cr, V, Mo, and Mn. Both cation and anion could be performed together (V-N doped TiO_2, 2.3 eV; Cr-N doped TiO_2, 1.5 eV	Khan et al. (2002, 2012), Hwang and Lewis (2005), Asahi et al. (2001), Dholam et al. (2010), Yu et al. (2010), Pan et al. (2011), Dashora et al. (2014), Albuquerque et al. (2014), Guo et al. (2010), Zhu et al. (2009), Shao (2009), Sadanandam et al. (2014), Xia et al. (2012), Kim et al. (2008), Yang et al. (2004), Low et al. (2013), Clarizia et al. (2014), Inturia et al. (2014), Jaiswal et al. (2012), Isimjan et al. (2010), Chen et al. (2011b), and Naldoni et al. (2012)
Tri-dopping: TiO_2 doped with Fe-N-C performed under solar illumination (2.7 eV)	
Hydrogenation: Doping with hydrogen creates different phases of TiO_2 (nanocrystal as a core which is surrounded by highly disordered surface, 1.85 eV)	
Defect engineering or self-dopping: Removal of oxygen from the catalyst selectively, improves visible light adsorption with effective charge transfer, electrical conductivity (1.3 eV)	Mao et al. (2013), Boerio-Goates et al. (2013), Nowontny et al. (2006, 2008), Zhang et al. (2013b), and Pan (2015)
Sensitization and formation of heterojunction: Two types of semiconductors TiO_2 (host) and CdS or quantum dots or dye molecule (sensitizer) are used to enhance visible absorption and carrier mobility. Such configuration drives to move electron and hole in opposite direction which results in better separation of electron and hole	Wang et al. (2013a), Antoniadou et al. (2014), Cai et al. (2014), Lee et al. (2010), and Pany et al. (2014)
Surface plasmon resonance effect (coating of TiO_2 with noble metals, i.e., Au, Ag, Pt): Noble metal nanoparticles attract the photogenerated electron to separate it from a hole in TiO_2, and such metal can improve the visible light adsorption. Thus, availability of the electron is much better on the catalyst surface	Rayalu et al. (2013), Zhao et al. (2014), Li et al. 2013b, Wu et al. (2013), Yang et al. (2014), Pu et al. 2013, Zhang et al. (2014a, 2013c, 2013d), Bumajdad and Madkour (2014), and Wang et al. (2013b)

Though, several methods have already been developed for the performance improvement of TiO_2 nanoparticle in the application of water splitting for production of hydrogen, there are other nanoparticles which have been used for the same purpose with improved efficiency and reduced cost such as WO_3 (Liu et al. 2012; Liew et al. 2014; Valentin et al. 2013; Ng et al. 2013; Fujimoto et al. 2014), ZnO (Kumari et al. 2014; Lv et al. 2014; Li et al. 2014b; Zhang et al. 2014b; Kargar et al. 2013; Hsu et al. 2013), $BiVO_4$ (Cao et al. 2012; Rao et al. 2014; Xie et al. 2014; Saito et al. 2012), $SrTiO_3$ (Chen et al. 2012c; Zhou et al. 2011b; Wang et al. 2014a; Shi and Xiong 2011; Yu et al. 2012; Sharma et al. 2014; Ma et al. 2015), Fe_2O_3 (Ohmori et al. 2000; Mao et al. 2011; Hou et al. 2012a), and Ta_2O_5 (Yang et al. 2014; Pu et al. 2013; Zhang et al. 2014a, 2013c, d; Bumajdad and Madkour 2014; Wang et al. 2013b; Liu et al. 2012; Liew et al. 2014).

It has been reported that S/I-doped WO_3 (Liu et al. 2012) and $WO_3/BiVO_4$ (Kumari et al. 2014; Xie et al. 2014) can be used for water splitting under visible light with improved performance. Au-coated ZnO (Kargar et al. 2013) and $BiVO_4$ (Xie et al. 2014) nanoparticle has better efficiency than the normal one. It has been reported that the photocathodic current can be improved using the heterojunction of ZnO and CuO (Hsu et al. 2013) and PdS and ZnO (Cao et al. 2012) for water splitting. Xie et al. (Saito et al. 2012) developed TiO_2-$BiVO_4$ nanocomposite with 5% of TiO_2 having better stability and higher efficiency than normal $BiVO_4$. The application of n-Type hematite (α-Fe_2O_3) with 2–2.2 eV bandgap in water splitting has been examined (Ohmori et al. 2000); however, it failed due to a higher rate of recombination and shorter length for hole diffusion (Mao et al. 2011). Hou et al. (2012a) have tried to eliminate those limitations using heterojunction of α-Fe_2O_3/graphene/$BiV_{1-x}Mo_xO_4$.

Many researchers have proven that tantalum pentoxide (Ta_2O_5) is an outstanding photocatalyst for water splitting under UV as Ta has 5d orbital for which conduction band Ta_2O_5 is more negative (Mao et al. 2014; Goncalves et al. 2012; Takahara et al. 2001). Thus, a better thermal dynamic force acts upon for reduction of H_2O into gaseous hydrogen in the absence of cocatalysts too (Mao et al. 2014; Goncalves et al. 2012; Takahara et al. 2001). The performance of this photocatalyst can be improved by those methods as mentioned in Table 3.3 (Nashed et al. 2014; Zhou et al. 2014; Goncalves et al. 2012; Cherevan et al. 2014).

Several developments have already been done in oxide-based photocatalyst though upscaling of the oxide-based process is still limited. The major improvement is required to achieve better stability of catalyst in a hostile environment.

3.3.2.2 Nitride-Based Photocatalyst

The difference between oxide- and nitride-based catalyst is that for oxide d orbital electron takes part in the reaction and for s/p orbital electrons participate in catalysis resulting in high mobility. Mainly graphitic carbon nitride (Wang et al. 2009b; Liu et al. 2010; Liao et al. 2012; Zhu et al. 2014b; Chu et al. 2014; Cao et al. 2013; Cheng et al. 2013; Feng et al. 2014; Kroke and Schwarz 2004; Liu and Wang 2009) and gallium nitride (Pan et al. 2010; Kida et al. 2006; Maeda et al. 2005; Yashima et al. 2006; Wei et al. 2008; Wang and Wang 2010; Pan and Zhang 2012; Kibria et al. 2013; Caccamo et al. 2014) are major photocatalysts which have been used for the production of hydrogen from water.

Carbon nitride has several phases based on the ratio of carbon and nitrogen as well as atomic structure (Liu and Wang 2009). Among all, graphitic carbon nitride (g-C_3N) is the most stable form (Pan et al. 2010). Wang et al. found that g-C_3N_4 having a bandgap of 2.7 eV was very useful for generation of hydrogen from water under solar illumination (Wang et al. 2009b). However, the carrier mobility is not up to the mark due to its porous geometry. The performance of g-C_3N_4 can be improved by doping (Liu et al. 2010; Feng et al. 2014; Kroke and Schwarz 2004), hybridization (Zhu et al. 2014b; Cao et al. 2013), defect engineering (Chu et al. 2014), and Au

modification (Cheng et al. 2013). Liu et al. (2010) found that doping with sulfur can improve hydrogen evolution up to seven to eight times than normal g-C_3N_4. Moreover, the presence of graphene oxide (Liao et al. 2012) and Au (Cheng et al. 2013) improves the separation of photogenerated electron and hole.

The utilization of gallium nitride (GaN) has been paid lots of attention due to its high stability under harsh conditions under UV illumination with bandgap energy of 3.4 eV (Pan et al. 2010; Kida et al. 2006). It has been reported that gallium and zinc nitrogen oxide ($Ga_{1-x}Zn_xN_{1-x}O_x$) can split water under visible light (Maeda et al. 2005; Yashima et al. 2006) as it has bandgap energy less than GaN (Wei et al. 2008; Wang and Wang 2010). Moreover, the doping with CrO also improves the ability of visible light adsorption of GaN (Wei et al. 2008). Similar to another photocatalyst, the performance of GaN can be improved with the help of heterojunction (Pan and Zhang 2012; Kibria et al. 2013; Caccamo et al. 2014), codoping with ZnO (Lim et al. 2013).

Except for above, two nitrides tantalum nitride (Ta_3N_5) (Li et al. 2013c; Zhen et al. 2013; Pinaud et al. 2012; Higashi et al. 2011; Yokoyama et al. 2011; Wang et al. 2014b; Pinaud et al. 2014) and tantalum oxynitride (TaON) (Allam et al. 2014; Wang et al. 2013c; Higashi et al. 2012; Hou et al. 2012b; Maeda et al. 2010; Abe et al. 2010; Masanobu et al. 2009) having bandgap energy of 2.1 eV and 2.2–2.5 eV, respectively, can be used for water splitting under visible light. Their catalytic activity can also be improved as mentioned earlier (Table 3.3). Though, the stability of Ta_3N_5 and TaON is very less as those are easily oxidized. Therefore, application of those catalysts is very challenging.

3.3.3 Commercial Challenges of Water Splitting

The first and foremost challenge for commercialization of water splitting process is to develop efficient photoelectrochemical cell for water splitting. Till date, the tandem cell is commonly used for the same purpose (Brillet et al. 2012; Prevot and Sivula 2013; Weber and Dignam 1984; Khaselev and Turner 1998) where a p-type semiconductor is used as photoanode and an n-type semiconductor represents the photocathode. In the tandem cell, the maximum efficiency achieved till date is 12.4% under solar illumination (Khaselev and Turner 1998). However, the commercialization of tandem cell is very limited due to high installation cost, poor stability, and complex fabrication (Brillet et al. 2012). Several initiatives have already been taken to improve the overall performance of photoelectrochemical cell under solar illumination, but those are not adequate. Thus, there is a huge scope of research in the future for commercialization of water splitting process.

3.4 Conclusion and Way Forward

The storage of fossil fuel is decreasing rapidly, and by 2050, very limited amount of fossil will remain globally. Thus, it is very high time to find new alternative fuel for the future. Thus, in last two decades, several types of research have been initiated for the development of carbon-neutral fuel for reduction of dependency on fossil fuel as well as reduction of GHG emission. This chapter has already represented several processes for the production of green fuel using photocatalyst. It has been already proven that the biggest green energy is the solar energy. Therefore, the solar-driven process for water splitting and CO_2 reduction is most attractive in the current scenario. In this regard, a wide range of photocatalyst is available for the development of such processes. Unfortunately, all processes are limited inside the laboratory. Therefore, huge development is essential for commercialization of CO_2 reduction and water splitting so that in the near future solarB26-based alternative fuel can replace fossil fuel.

References

Abe R, Higashi M, Domen K (2010) Facile fabrication of an efficient oxynitride TaON photoanode for overall water splitting into H_2 and O_2 under visible light irradiation. J Am Chem Soc 132:11828–11829. https://doi.org/10.1021/ja1016552

Ai G, Sun WT, Gao XF, Zhang YL, Peng LM (2011) Hybrid CdSe/TiO_2 nanowire photoelectrodes: fabrication and photoelectric performance. J Mater Chem 21:8749–8755. https://doi.org/10.1039/C0JM03867A

Albuquerque AR, Bruix A, dos Santos IMG, Sambrano JR, Illas F (2014) DFT study on Ce-doped anatase TiO_2: nature of Ce^{3+} and Ti^{3+} centers triggered by oxygen vacancy formation. J Phys Chem C 118:9677–9689. https://doi.org/10.1021/jp501757f

Allam NK, Shaheen BS, Hafez AM (2014) Layered tantalum oxynitride nanorod array carpets for efficient photoelectrochemical conversion of solar energy: experimental and DFT insights. ACS Appl Mater Interfaces 6:4609–4615. https://doi.org/10.1021/am500286n

Antoniadou M, Sfaelou S, Lianos P (2014) Quantum dot sensitized titania for photo-fuel-cell and for water splitting operation in the presence of sacrificial agents. Chem Eng J 254:45–251. https://doi.org/10.1016/j.cej.2014.05.106.

Asahi R, Morikawa T, Ohwaki T, Aoki K, Taga Y (2001) Visible-light photocatalysis in nitrogen-doped titanium oxides. Science 293:269–271. https://doi.org/10.1126/science.1061051

Ashley AE, Thompson AL, O'Hare D (2009) Non-metal-mediated homogeneous hydrogenation CO_2 to CH_3OH. Angew Chem 121:10023–10027. https://doi.org/10.1002/anie.200905466l

Beley M, Collin J-P, Ruppert R, Sauvage J-P (1984) Nickel (II)-cyclam: an extremely selective electrocatalyst for reduction of CO_2 in water. J Chem Soc Chem Commun 19:1315–1316

Bin AR, Yusoff M, Jang J (2016) Highly efficient photoelectrochemical water splitting by a hybrid tandem perovskite solar cell. Chem Commun 52:5824–5827. https://doi.org/10.1039/C6CC01249C

Blajeni B, Halmann M, Manassen J (1983) Electrochemical measurements on the photoelectrochemical reduction of aqueous carbon-dioxide on p-gallium phosphide and p-gallium arsenide semiconductor electrodes. Sol Energ Mater 8:425–440. https://doi.org/10.1016/0165-1633(83)90007-2

Boerio-Goates J, Smith SJ, Liu SF, Lang BE, Li GS, Woodfield BF, Navrotsky A (2013) Characterization of surface defect sites on bulk and nanophase anatase and rutile TiO_2 by low-temperature specific heat. J Phys Chem C 117(9):4544–4550. https://doi.org/10.1021/jp310993w

Bonin J, Chaussemier M, Robert M, Routier M (2014) Homogeneous photocatalytic reduction of CO_2 to CO using iron (0) porphyrin catalysts: mechanism and intrinsic limitations. Chem Cat Chem 6:3200–3207. https://doi.org/10.1002/cctc.201402515

Borgarello E, Kiwi J, Gratzel M, Pelizzetti E, Visca M (1982) Visible light induced water cleavage in colloidal solutions of chromium-doped titanium dioxide particles. J Am Chem Soc 104:2996–3002. https://doi.org/10.1021/ja00375a010

Brillet J, Yum JH, Cornuz M, Hisatomi T, Solarska R, Augustynski J, Graetzel M, Sivul K (2012) Highly efficient water splitting by a dual-absorber tandem cell. Nat Photonics 6:824–828. http://nature.com/articles/nphoton.2012.265

Bumajdad A, Madkour M (2014) Understanding the superior photocatalytic activity of noble metals modified Titania under UV and visible light irradiation. Phys Chem Chem Phys 16:7146–7158. https://doi.org/10.1039/C3CP54411G

Caccamo L, Hartmann J, Fabrega C, Estrade S, Lilienkamp G, Prades JD, Hoffmann MWG, Ledig J, Wagner A, Wang X, Lopez-Conesa L, Peiro F, Rebled JM, Wehmann HH, Daum W, Shen H, Waag A (2014) Band engineered epitaxial 3D GaN-InGaN core–shell rod arrays as an advanced photoanode for visible-light-driven water splitting. ACS Appl Mater Interface 6:2235–2240. https://doi.org/10.1021/am4058937

Cai H, Yang Q, Hu ZQ, Duan ZH, You QH, Sun J, Xu N, Wu JD (2014) Enhanced photoelectrochemical activity of vertically aligned ZnO-coated TiO_2 nano-tubes. Appl Phys Lett 104:053114. https://doi.org/10.1063/1.4863852

Cao SW, Yin Z, Barber J, Boey FYC, Loo SCJ, Xue C (2012) Preparation of Au–$BiVO_4$ heterogeneous nanostructures as highly efficient visible-light photocatalysts. ACS Appl Mater Interfaces 4:418–423. https://doi.org/10.1021/am201481b

Cao SW, Yuan YP, Fang J, Shahjamali MM, Boey FYC, Barber J, Loo SCJ, Xue C (2013) In-situ growth of CdS quantum dots on g-C3N4 nanosheets for highly efficient photocatalytic hydrogen generation under visible light irradiation. Int J Hydrog Energy 38:1258–1266. https://doi.org/10.1016/j.ijhydene.2012.10.116

Caruntu D, Rostamzadeh T, Costanzo T, Salemizadeh Parizi S, Caruntu G (2015) Solvothermal synthesis and controlled self-assembly of monodisperse titanium-based perovskite colloidal nanocrystals. Nanoscale 7:12955–12969. https://doi.org/10.1039/C5NR00737B

Chen X, Mao SS (2007) Titanium dioxide nanomaterials: synthesis, properties, modifications, and applications. Chem Rev 107:2891–2959. https://doi.org/10.1021/cr0500535

Chen XB, Shen SH, Guo LJ, Mao SS (2010) Semiconductor-based photocatalytic hydrogen generation. Chem Rev 110:6503–6570. https://doi.org/10.1021/cr1001645

Chen JJ, Wu JCS, Wu PC, Tsai DP (2011a) Plasmonic photocatalyst for H_2 evolution in photocatalytic water splitting. J Phys Chem C 115:210–216. https://doi.org/10.1021/jp1074048

Chen X, Liu L, Yu PY, Mao SS (2011b) Increasing solar absorption for photocatalysis with black hydrogenated titanium dioxide nanocrystals. Science 331(6018):746–750. https://doi.org/10.1126/science.1200448

Chen HM, Chen CK, Liu RS, Zhang L, Zhang LJ, Wilkinson DP (2012a) Nano- architecture and material designs for water splitting photoelectrodes. Chem Soc Rev 41:5654–5671. https://doi.org/10.1039/C2CS35019J

Chen XB, Li C, Graetzel M, Kostecki R, Mao SS (2012b) Nanomaterials for renewable energy production and storage. Chem Rev Soc 41:7909–7937. https://doi.org/10.1039/C2CS35230C

Chen HC, Huang CW, Wu JCS, Lin ST (2012c) Theoretical investigation of the metal-doped $SrTiO_3$ photocatalysts for water splitting. J Phys Chem C 116:7897–7903. https://doi.org/10.1021/jp300910e

Chen Y, Chuang C-H, Qin Z, Shen S, Doane T, Burda C (2017) Electron-transfer dependent photocatalytic hydrogen generation over cross-linked CdSe/TiO_2 type-II heterostructure. Nanotechnology 28:084002. https://doi.org/10.1088/1361-6528/aa5642/meta

Cheng NY, Tian JQ, Liu Q, Ge CJ, Qusti AH, Asiri AM, Al-Youbi AO, Sun XP (2013) Au-nanoparticle-loaded graphitic carbon nitride nanosheets: green photo-catalytic synthesis and application toward the degradation of organic pollutants. ACS Appl Mater Interface 5:6815–6819. https://doi.org/10.1021/am401802r

Cherevan AS, Gebhardt P, Shearer CJ, Matsukawa M, Domen K, Eder D (2014) Interface engineering in nanocarbon-Ta_2O_5 hybrid photocatalysts. Energy Environ Sci 7:791–796. https://doi.org/10.1039/C3EE42558D

Chowdhury P, Gomaa H, Ray AK (2011) Factorial design analysis for dye-sensitized hydrogen generation from water. Int J Hydro Energy 36:13442–13451. https://doi.org/10.1016/j.ijhydene.2011.07.093

Chu S, Wang CC, Feng JY, Wang Y, Zou ZG (2014) Melem: a metal-free unit for photocatalytic hydrogen evolution. Int J Hydrog Energy 39:13519–13526. https://doi.org/10.1016/j.ijhydene.2014.02.052

Chu S, Li W, Yan Y, Hamann T, Shih I, Wang D, Mi Z (2017) Roadmap on solar water splitting: current status and future prospects. Nano Futures 1(2):022001. https://doi.org/10.1088/2399-1984/aa88a1

Clarizia L, Spasiano D, Di Somma I, Marotta R, Andreozzi R, Dionysiou DD (2014) Copper modified-TiO_2 catalysts for hydrogen generation through photo-reforming of organics. A short review. Int J Hydrog Energy 39(30):16812–16831. https://doi.org/10.1016/j.ijhydene.2014.08.037

Cokoja M, Bruckmeier C, Rieger B, Herrmann WA, Kühn FE (2011) Transformation of carbon dioxide with homogeneous transition – metal catalysts: a molecular solution to a global challenge? Angew Chem Int Ed 50:8510–8537. https://doi.org/10.1002/anie.201102010

Collin J, Sauvage J (1989) Electrochemical reduction of carbon dioxide mediated by molecular catalysts. Coord Chem Rev 93:245–268. https://doi.org/10.1016/0010-8545(89)80018-9

Das C, Roy P, Yang M, Jha H, Schmuki P (2011) Nb doped TiO_2 nanotubes for enhanced photoelectrochemical water-splitting. Nanoscale 3:3094–3096. https://doi.org/10.1039/C1NR10539F

Dashora A, Patel N, Kothari DC, Ahuja BL, Miotello A (2014) Formation of an intermediate band in the energy gap of TiO_2 by Cu–N-codoping: first principles study and experimental evidence. Sol Energy Mater Sol Cells 125:120–126. https://doi.org/10.1016/j.solmat.2014.02.032

Dholam R, Patel N, Santini A, Miotello A (2010) Efficient indium tin oxide/Cr-doped- TiO_2 multilayer thin films for H_2 production by photocatalytic water-splitting. Int J Hydro Energy 25:9581–9590. https://doi.org/10.1016/j.ijhydene.2010.06.097

Do JY, Im Y, Kwak BS, Park S-M, Kang M (2016) Preparation of basalt fiber@ perovskite $PbTiO_3$ core–shell composites and their effects on CH_4 production from CO_2 photoreduction. Ceram Int 42:5942–5951. https://doi.org/10.1016/j.ceramint.2015.12.142

Dong W, Li X, Yu J, Guo W, Li B, Tan L, Li C, Shi J, Wang G (2012) Porous $SrTiO_3$ spheres with enhanced photocatalytic performance. Mater Lett 67:131–134. https://doi.org/10.1016/j.matlet.2011.09.045

Ellis AB, Kaiser SW, Bolts JM, Wrighton MS (1977) Study of n-type semiconducting cadmium chalcogenide-based photoelectrochemical cells employing poly- chalcogenide electrolytes. J Am Chem Soc 99:2839–2848. https://doi.org/10.1021/ja00451a001

Feng LL, Zou YC, Li CG, Gao S, Zhou LJ, Sun QS, Fan MH, Wang HJ, Wang DJ, Li GD, Zou XX (2014) Nanoporous sulfur-doped graphitic carbon nitride microrods: a durable catalyst for visible-light-driven H2 evolution. Int J Hydrog Energy 39(28):15373–15379. https://doi.org/10.1016/j.ijhydene.2014.07.160

Fresno F, Jana P, Renones P, Coronado JM, Serrano DP, de la Pena O'Shea VA (2017) CO_2 reduction over $NaNbO_3$ and $NaTaO_3$ perovskite photocatalysts. Photochem Photobiol Sci 16:17–23. https://doi.org/10.1039/C6PP00235H

Froehlich JD, Kubiak CP (2012) Homogeneous CO_2 reduction by Ni (cyclam) at a glassy carbon electrode. Inorg Chem 51:3932–3934. https://doi.org/10.1021/ic3001619

Fujimoto I, Wang NN, Saito R, Miseki Y, Gunji T, Sayama K (2014) WO_3/$BiVO_4$ composite photoelectrode prepared by improved auto-combustion method for highly efficient water splitting. Int J Hydrog Energy 39:2454–2461. https://doi.org/10.1016/j.ijhydene.2013.08.114

Fujishima A, Honda K (1972) Electrochemical photolysis of water at a semi-conductor electrode. Nature 238:37–38. https://doi.org/10.1038/238037a0

Goncalves RV, Migowski P, Wender H, Eberhardt D, Weibel DE, Sonaglio FC, Zapata MJM, Dupont J, Feil AF, Teixeira SR (2012) Ta_2O_5 nanotubes obtained by anodization: effect of thermal treatment on the photocatalytic activity for hydrogen production. J Phys Chem C 116 (26):14022–14030. https://doi.org/10.1021/jp303273q

Gratzel M (2001) Photoelectrochemical cells. Nature 414:338–344. https://doi.org/10.1038/35104607

Guo ML, Zhang XD, Liang CT, Jia GZ (2010) Mechanism of visible photoactivity of F-doped TiO_2. Chin Phys Lett 27:057103. https://doi.org/10.1088/0256-307X/27/5/057103/meta.

Halmann M (1978) Photoelectrochemical reduction of aqueous carbon dioxide on p-type gallium phosphide in liquid junction solar cells. Nature 275:115–116. https://doi.org/10.1038/275115a0

Hemminger JC, Carr R, Somorjai GA (1978) The photoassisted reaction of gaseous water and carbon dioxide adsorbed on the $SrTiO_3$ (111) crystal face to form methane. Chem Phys Lett 57:100–104. https://doi.org/10.1016/0009-2614(78)80359-5

Higashi M, Domen K, Abe R (2011) Fabrication of efficient TaON and Ta_3N_5 photo-anodes for water splitting under visible light irradiation. Energy Environ Sci 4:4138–4147. https://doi.org/10.1039/C1EE01878G

Higashi M, Domen K, Abe R (2012) Highly stable water splitting on oxynitride TaON photoanode system under visible light irradiation. J Am Chem Soc 134:6968–6971. https://doi.org/10.1021/ja302059g

Hisatomi T, Kubota J, Domen K (2014) Recent advances in semiconductors for photocatalytic and photoelectrochemical water splitting. Chem Soc Rev 43:7520–7535. https://doi.org/10.1039/C3CS60378D

Hori Y, Kikuchi K, Suzuki S (1985) Production of CO and CH_4 in electrochemical reduction of CO_2 at metal electrodes in aqueous hydrogen carbonate solution. Chem Lett 14:1695–1698. https://doi.org/10.1246/cl.1985.1695

Hori Y, Wakebe H, Tsukamoto T, Koga O (1994) Electrocatalytic process of CO selectivity in electrochemical reduction of CO_2 at metal electrodes in aqueous media. Electrochim Acta 39:1833–1839. https://doi.org/10.1016/0013-4686(94)85172-7

Hou Y, Zuo F, Dagg A, Feng PY (2012a) Visible light-driven α-Fe_2O_3 nanorod/graphene/$BiV_{1-x}Mo_xO_4$ core/shell heterojunction array for efficient photoelectrochemical water splitting. Nano Lett 12:6464–6473. https://doi.org/10.1021/nl303961c

Hou J, Wang Z, Kan WB, Jiao SQ, Zhu HM, Kumar RV (2012b) Efficient visible-light-driven photocatalytic hydrogen production using CdS@TaON core–shell composites coupled with graphene oxide nanosheets. J Mater Chem 22:7291–7299. https://doi.org/10.1039/C2JM15791H

Hou J, Cao S, Wu Y, Gao Z, Liang F, Sun Y, Lin Z, Sun L (2017) Inorganic colloidal Perovskite quantum dots for robust solar CO_2 reduction. Chem-Eur J 23:9481–9485. https://doi.org/10.1002/chem.201702237l

Hsu CH, Chen CH, Chen DH (2013) Decoration of PbS nanoparticles on Al-doped ZnO nanorod array thin film with hydrogen treatment as a photoelectrode for solar water splitting. J Alloy Compd 554:45–50. https://doi.org/10.1016/j.jallcom.2012.11.192

Hwang H, Lewis JP (2005) Effects of dopant states on photoactivity in carbon-doped TiO_2. J Phys Conden Matter 17:L209–L213. https://doi.org/10.1088/0953-8984/17/21/L01

Iizuka K, Wato T, Miseki Y, Saito K, Kudo A (2011) Photocatalytic reduction of carbon dioxide over Ag cocatalyst-loaded $ALa_4Ti_4O_{15}$ (A= Ca, Sr, and Ba) using water as a reducing reagent. J Am Chem Soc 133:20863–20868. https://doi.org/10.1021/ja207586e

In S, Orlov A, Berg R, Garcia F, Pedrosa-Jimenez S, Tikhov MS, Wright DS, Lambert RM (2007) Effective visible light-activated B-doped and B, N-codoped TiO_2 photocatalysts. J Am Chem Soc 129:13790–13791. https://doi.org/10.1021/ja0749237

Inoue T, Fujishima A, Konishi S, Honda K (1979) Photoelectrocatalytic reduction of carbon dioxide in aqueous suspensions of semiconductor powders. Nature 277:637–638. https://doi.org/10.1038/277637a0

Inturia SNR, Boningaria T, Suidanb M, Smirniotis PG (2014) Visible-light-induced photodegradation of gas phase acetonitrile using aerosol-made transition metal (V, Cr, Fe, Co, Mn, Mo, Ni, Cu, Y, Ce, and Zr) doped TiO_2. Appl Catal B 144:333–342. https://doi.org/10.1016/j.apcatb.2013.07.032

Isimjan TT, Ruby AE, Rohani S, Ray AK (2010) The fabrication of highly ordered and visible-light-responsive Fe–C–N codoped TiO_2 nanotubes. Nanotechnology 21:055706. https://doi.org/10.1088/0957-4484/21/5/055706

Jacobsson TJ, Fjällström V, Sahlberg M, Edoff M, Edvinsson T (2013) A monolithic device for solar water splitting based on series interconnected thin film absorbers reaching over 10% solar-to-hydrogen efficiency. Energy Environ Sci 6:3676–3683. https://doi.org/10.1039/C3EE42519C

Jadhav SG, Vaidya PD, Bhanage BM, Joshi JB (2014) Catalytic carbon dioxide hydrogenation to methanol: a review of recent studies. Chem Eng Res Des 92:2557–2567. https://doi.org/10.1016/j.cherd.2014.03.005

Jaiswal R, Patel N, Kothari DC, Miotello A (2012) Improved visible light photo-catalytic activity of TiO_2 co-doped with vanadium and nitrogen. Appl Catal B 126:47–54. https://doi.org/10.1016/j.apcatb.2012.06.030

Jia L, Li J, Fang W, Song H, Li Q, Tang Y (2009a) Visible-light-induced photocatalyst based on C-doped $LaCoO_3$ synthesized by novel microorganism chelate method. Catal Commun 10:1230–1234. https://doi.org/10.1016/j.catcom.2009.01.025

Jia L, Li J, Fang W (2009b) Enhanced visible-light active C and Fe co-doped $LaCoO_3$ for reduction of carbon dioxide. Catal Commun 11:87–90. https://doi.org/10.1016/j.catcom.2009.08.016

Kar P, Farsinezhad S, Zhang X, Shankar K (2014) Anodic Cu_2S and CuS nanorod and nanowall arrays: preparation, properties and application in CO_2 photoreduction. Nanoscale 6:14305–14318. https://doi.org/10.1039/C4NR05371K

Kar P, Zhang Y, Farsinezhad S, Mohammadpour A, Wiltshire BD, Sharma H, Shankar K (2015) Rutile phase n-and p-type anodic titania nanotube arrays with square-shaped pore morphologies. Chem Commun 51:7816–7819. https://doi.org/10.1039/C5CC01829C

Kar P, Farsinezhad S, Mahdi N, Zhang Y, Obuekwe U, Sharma H, Shen J, Semagina N, Shankar K (2016) Enhanced CH_4 yield by photocatalytic CO_2 reduction using TiO_2 nanotube arrays grafted with Au, Ru, and ZnPd nanoparticles. Nano Res 9:3478–3493. https://doi.org/10.1007/s12274-016-1225-4

Kargar A, Jing Y, Kim SJ, Riley CT, Pan XQ, Wang DL (2013) ZnO/CuO heterojunction branched nanowires for photoelectrochemical hydrogen generation. ACS Nano 7:11112–11120. https://doi.org/10.1021/nn404838n

Kato H, Kudo A (2002) Visible-light-response and photocatalytic activities of TiO_2 and $SrTiO_3$ photocatalysts codoped with antimony and chromium. J Phys Chem B 106:5029–5034. https://doi.org/10.1021/jp0255482

Khan SU, Al-Shahry M, Ingler WB Jr (2002) Efficient photochemical water splitting by a chemically modified n-TiO_2. Science 297:2243–2245. https://doi.org/10.1126/science.1075035

Khan M, Xu J, Chen N, Cao W (2012) Electronic and optical properties of pure and Mo doped anatase TiO_2 using GGA and GGA+U calculations. Physica B 407:3610–3616. https://doi.org/10.1016/j.physb.2012.05.037

Khaselev O, Turner J (1998) A monolithic photovoltaic–photoelectrochemical device for hydrogen production via water splitting. Science 280:425–427. https://doi.org/10.1126/science.280.5362.425.

Kibria MG, Nguyen HPT, Cui K, Zhao SR, Liu DP, Guo H, Trudeau ML, Paradis S, Hakima AR, Mi ZT (2013) One-step overall water splitting under visible light using multiband InGaN/GaN nanowire heterostructures. ACS Nano 7:7886–7893. https://doi.org/10.1021/nn4028823

Kida T, Minami Y, Guan G, Nagand M, Akiyama M, Yoshida A (2006) Photocatalytic activity of gallium nitride for producing hydrogen from water under light irradiation. J Mater Sci 41:3527–3534. https://doi.org/10.1007/s10853-005-5655-8

Kim HY, Lee HM, Pala RGS, Shapovalov V, Metiu H (2008) CO oxidation by rutile TiO_2 (110) doped with V, W, Cr, Mo, and Mn. J Phys Chem C 112:12398–12408. https://doi.org/10.1021/jp802296g

Kong XY, Tan WL, Ng B-J, Chai S-P, Mohamed AR (2017) Harnessing Vis–NIR broad spectrum for photocatalytic CO_2 reduction over carbon quantum dots-decorated ultrathin Bi_2WO_6 nanosheets. Nano Res 10:1720–1731. https://doi.org/10.1007/s12274-017-1435-4

Kroke E, Schwarz M (2004) Novel group 14 nitrides. Coord Chem Rev 248:493–532. https://doi.org/10.1016/j.ccr.2004.02.001

Kumar B, Asadi M, Pisasale D, Sinha-Ray S, Rosen BA, Haasch R, Abiade J, Yarin AL, Salehi-Khojin A (2013) Renewable and metal-free carbon nanofibre catalysts for carbon dioxide reduction. Nat Commun 4:2819. https://doi.org/10.1038/ncomms3819

Kumari B, Sharma S, Singh N, Verma A, Satsangi VR, Dass S, Shrivastav R (2014) ZnO thin films, surface embedded with biologically derived Ag/Au nanoparticles, for efficient photoelectrochemical splitting of water. Int J Hydrog Energy 39(32):18216–18229. https://doi.org/10.1016/j.ijhydene.2014.09.025

Kwak BS, Kang M (2015) Photocatalytic reduction of CO_2 with H_2O using perovskite $CaxTiyO_3$. Appl Surf Sci 337:138–144. https://doi.org/10.1016/j.apsusc.2015.02.078

Laitar DS, Müller P, Sadighi JP (2005) Efficient homogeneous catalysis in the reduction of CO_2 to CO J. Am Chem Soc 127:17196–17197. https://doi.org/10.1002/cctc.201402515

Le M, Ren M, Zhang Z, Sprunger PT, Kurtz RL, Flake JC (2011) Electrochemical reduction of CO_2 to CH_3OH at copper oxide surfaces. J Electrochem Soc 158:E45–EE9. https://doi.org/10.1149/1.3561636

Lee Y-L, Chi C-F, Liau S-Y (2010) CdS/CdSe co-sensitized TiO_2 photoelectrode for efficient hydrogen generation in a photoelectrochemical cell. Chem Mater 22:922–927. https://doi.org/10.1021/cm901762h

Li P, Ouyang S, Xi G, Kako T, Ye J (2012) The effects of crystal structure and electronic structure on photocatalytic H_2 evolution and CO_2 reduction over two phases of perovskite-structured NaNbO3. J Phys Chem C 116:7621–7628. https://doi.org/10.1021/jp210106b

Li ZS, Luo WJ, Zhang ML, Feng JY, Zou ZG (2013a) Photoelectrochemical cells for solar hydrogen production: current state of promising photoelectrodes, methods to improve their properties, and outlook. Energy Environ Sci 6:347–370. https://doi.org/10.1039/C2EE22618A

Li YK, Yu HM, Zhang CK, Fu L, Li GF, Shao ZG, Yi BL (2013b) Enhancement of photoelectrochemical response by Au modified in TiO_2 nanorods. Int J Hydrog Energy 38:13023–13030. https://doi.org/10.1016/j.ijhydene.2013.03.122

Li Y, Takata T, Cha D, Takanabe K, Minegishi T, Kubota J, Domen K (2013c) Vertically aligned Ta_3N_5 nanorod arrays for solar-driven photoelectrochemical water splitting. Adv Mater 25:125–131. https://doi.org/10.1002/adma.201202582

Li TT, Li XY, Zhao QD, Teng W (2014a) Preparation of $CuInS_2/TiO_2$ nanotube heterojunction arrays electrode and investigation of its photoelectrochemical properties. Mater Res Bull 59:227–233. https://doi.org/10.1016/j.materresbull.2014.07.031

Li Q, Sun X, Lozano K, Mao YB (2014b) Facile and scalable synthesis of "Caterpillar-like" ZnO nanostructures with enhanced photoelectrochemical water splitting effect. J Phys Chem C 118 (25):13467–13475. https://doi.org/10.1021/jp503155c

Li S, Dong G, Hailili R, Yang L, Li Y, Wang F, Zeng Y, Wang C (2016) Effective photocatalytic H_2O_2 production under visible light irradiation at g-C3N4 modulated by carbon vacancies. Appl Catal B-38 Environ 190:26–35. https://doi.org/10.1016/j.apcatb.2016.03.004

Li N, Chen X, Ong W-J, MacFarlane DR, Zhao X, Cheetham AK, Sun C (2017) Understanding of electrochemical mechanisms for CO_2 capture and conversion into hydrocarbon fuels in transition-metal carbides (MXenes). ACS Nano 11(11):10825–10833. https://doi.org/10.1021/acsnano.7b03738

Liang L, Lei F, Gao S, Sun Y, Jiao X, Wu J, Qamar S, Xie Y (2015) Single unit cell bismuth tungstate layers realizing robust solar CO_2 reduction to methanol. Angew Chem Int Ed 54:13971–13974. https://doi.org/10.1002/anie.201506966l

Liao GZ, Chen S, Quan X, Yu HT, Zhao HM (2012) Graphene oxide modified g-C_3N_4 hybrid with enhanced photocatalytic capability under visible light irradiation. J Mater Chem 22:2721–2726. https://doi.org/10.1039/C1JM13490F

Liew SL, Zhang Z, Goh TWG, Subramanian GS, Seng HLD, Hor TSA, Luo HK, Chi DZ (2014) Yb-doped WO_3 photocatalysts for water oxidation with visible light. Int J Hydrog Energy 39 (9):4291–4298. https://doi.org/10.1016/j.ijhydene.2013.12.204

Lim YK, Koh E, Zhang YW, Pan H (2013) Ab initio design of GaN-based photo-catalyst: ZnO-codoped GaN nanotubes. J Power Sources 232:323–331. https://doi.org/10.1016/j.jpowsour.2013.01.066

Lin YL, Yuan GB, Liu R, Zhou S, Sheehan SW, Wang DW (2011) Semiconductor nanostructure-based photoelectrochemical water splitting: a brief review. Chem Phys Lett 507:209–215. https://doi.org/10.1016/j.cplett.2011.03.074

Liu M, Wang JG (2009) Study on mechanical properties and blood compatibility of carbon nitride film deposited on NiTi alloy. J Inorg Mater 24:491–496. https://doi.org/10.3724/SP.J.1077.2009.00491

Liu G, Niu P, Sun CH, Smith SC, Chen ZG, Lu GQ, Cheng HM (2010) Unique electronic structure induced high photoreactivity of sulfur-doped graphitic C_3N_4. J Am Chem Soc 132:11642–11648. https://doi.org/10.1021/ja103798k

Liu XE, Wang FY, Wang Q (2012) Nanostructure-based WO_3 photoanodes for photoelectrochemical water splitting. Phys Chem Chem Phys 14:7894–7911. https://doi.org/10.1039/C2CP40976C

Liu Q, Wu D, Zhou Y, Su H, Wang R, Zhang C, Yan S, Xiao M, Zou Z (2014a) Single-crystalline, ultrathin $ZnGa_2O_4$ nanosheet scaffolds to promote photocatalytic activity in CO_2 reduction into methane. ACS Appl Mater Inter 6:2356–2361. https://doi.org/10.1021/am404572g

Liu J, Yu XL, Liu QY, Liu RJ, Shang XK, Zhang SS, Li WH, Zheng WQ, Zhang GJ, Cao HB, Gu ZJ (2014b) Surface-phase junctions of branched TiO_2 nanorod arrays for efficient photoelectron chemical water splitting. Appl Catal B 158–159:296–300. https://doi.org/10.1016/j.apcatb.2014.04.032

Low IM, Albetran H, Prida VM, Vega V, Manurung P, Ionescu M (2013) A comparative study on crystallization behavior, phase stability, and binding energy in pure and Cr-doped TiO_2 nanotubes. J Mater Res 28:304–312. https://doi.org/10.1557/jmr.2012.275

Luo J, Im J-H, Mayer MT, Schreier M, Nazeeruddin MK, Park N-G, Tilley SD, Fan HJ, Grätzel M (2014) Water photolysis at 12.3% efficiency via perovskite photovoltaics and earth-abundant catalysts. Science 345:1593. https://doi.org/10.1126/science.1258307

Lv R, Wang T, Su FL, Zhang P, Li CJ, Gong JL (2014) Facile synthesis of ZnO nano-pencil arrays for photoelectrochemical water splitting. Nano Energy 7:143–150. https://doi.org/10.1016/j.electacta.2013.12.095.

Ma ZQ, Pan H, Wang Z, Wong PK (2015) Effects of non-metal dopants and defects on electronic properties of barium titanate as photocatalyst. Int J Hydrog Energy 40:4766–4776. https://doi.org/10.1016/j.ijhydene.2015.02.002

Maeda K, Takata T, Hara M, Saito N, Inoue Y, Kobayashi H, Domen K (2005) GaN:ZnO solid solution as a photocatalyst for visible-light-driven overall water split- ting. J Am Chem Soc 127:8286–8287. https://doi.org/10.1021/ja0518777

Maeda K, Higashi M, Lu D, Abe R, Domen K (2010) Efficient nonsacrificial water splitting through two-step photoexcitation by visible light using a modified oxynitride as a hydrogen evolution photocatalyst. J Am Chem Soc 132:5858–5868. https://doi.org/10.1021/ja1009025

Maina JW, Pozo-Gonzalo C, Kong L, Schutz J, Hill M, Dumee LF (2017) Metal organic framework based catalysts for CO_2 conversion. Mater Horiz 4:345–361. https://doi.org/10.1039/C6MH00484A

Mao A, Shin K, Kim JK, Wang DH, Han GY, Park JH (2011) Controlled synthesis of vertically aligned hematite on conducting substrate for photoelectrochemical cells: nanorods versus nanotubes. ACS Appl Mater Interfaces 3:1852–1858. https://doi.org/10.1021/am200407t

Mao XC, Lang XF, Wang ZQ, Hao QQ, Wen B, Ren ZF, Dai DX, Zhou CY, Liu LM, Yang XM (2013) Band-gap states of TiO_2(110): major contribution from surface defects. J Phys Chem Lett 4:3839–3844. https://doi.org/10.1021/jz402053p

Mao L, Zhu SM, Ma J, Shi D, Chen YX, Chen ZX, Yin C, Li Y, Zhang D (2014) Superior H_2 production by hydrophilic ultrafine Ta_2O_5 engineered covalently on graphene. Nanotechnology 25:215401. https://doi.org/10.1088/0957-4484/25/21/215401

Masanobu H, Abe R, Takata T, Domen K (2009) Photocatalytic overall water splitting under visible light using $ATaO_2N$ (A= Ca, Sr, Ba) and WO_3 in a IO_3^- /I^- shuttle redox mediated system. Chem Mater 21:1543–1549. https://doi.org/10.1021/cm803145n

Moghtada A, Ashiri R (2016) Enhancing the formation of tetragonal phase in perovskite nanocrystals using an ultrasound assisted wet chemical method. Ultrason Sonochem 33:141–149. https://doi.org/10.1016/j.ultsonch.2016.05.002

Mömming CM, Otten E, Kehr G, Fröhlich R, Grimme S, Stephan DW, Erker G (2009) Reversible metal-free carbon dioxide binding by frustrated Lewis pairs. Angew Chem Int Ed 48:6643–6646. https://doi.org/10.1002/anie.200901636

Mor GK, Varghese OK, Paulose M, Shankar K, Grimes CA (2006) A review on highly ordered, vertically oriented TiO_2 nanotube arrays: fabrication, material properties, and solar energy applications. Sol Energy Mater Solar Cells 90:2011–2075. https://doi.org/10.1016/j.solmat.2006.04.007

Morris AJ, Meyer GJ, Fujita E (2009) Molecular approaches to the photocatalytic reduction of carbon dioxide for solar fuels. Acc Chem Res 42:1983–1994. https://doi.org/10.1021/ar9001679

Naldoni A, Allieta M, Santangelo S, Marelli M, Fabbri F, Cappelli S, Bianchi CL, Psaro R, Santo VD (2012) Effect of nature and location of defects on bandgap narrowing in black TiO_2 nanoparticles. J Am Chem Soc 134:7600–7603. https://doi.org/10.1021/ja3012676

Nashed R, Szymanski P, El-Sayed MA, Allam NK (2014) Self-assembled nanostructured photoanodes with staggered bandgap for efficient solar energy conversion. ACS Nano 8:4915–4923. https://doi.org/10.1021/nn5009066

Nath RK, Zain MFM, Kadhum AAH (2012) New material $LiNbO_3$ for photocatalytically improvement of indoor air – an overview. Adv Nat Appl Sci 6:1030–1035. https://ukm.pure.elsevier.com/en/publications/new-material-linbosub3sub-for-photocatalytically-improvement-of-i

Navalón S, Dhakshinamoorthy A, Álvaro M, Garcia H (2013) Photocatalytic CO_2 reduction using non-titanium metal oxides and sulfides. Chem Sus Chem 6:562–577. https://doi.org/10.1002/cssc.201200670l

Navarro RM, Del Valle F, Villoria de la Mano JA, Alvarez-Galván MC, Fierro JLG (2009) Photocatalytic water splitting under visible light: concept and catalysts development. Adv Chem Eng 36:111–143. https://doi.org/10.1016/S0065-2377(09)00404-9.

Navarro RM, Alvarez-Galván MC, Villoria de la Mano JA, Al-Zahrani SM, Fierro JLG (2010) A framework for visible-light water splitting. Energy Environ Sci 3:1865–1882. https://doi.org/10.1039/C001123A

Ng KH, Minggu LJ, Kassim MB (2013) Gallium-doped tungsten trioxide thin film photoelectrodes for photoelectrochemical water splitting. Int J Hydrog Energy 38:9585–9591. https://doi.org/10.1016/j.ijhydene.2013.02.144

Ni M, Leung MKH, Leung DYC, Sumathy K (2007) A review and recent developments in photocatalytic water-splitting using TiO_2 for hydrogen production. Renew Sust Energ Rev 11:401–425. https://doi.org/10.1016/j.rser.2005.01.009

Niishiro R, Kato H, Kudo A (2005) Nickel and either tantalum or niobium-codoped TiO_2 and $SrTiO_3$ photocatalysts with visible-light response for H_2 or O_2 evolution from aqueous solutions. Phys Chem Chem Phys 7:2241–2245. https://doi.org/10.1039/B502147B

Nowontny J, Bak T, Nowontny MK (2006) Defect disorder of titanium dioxide. J Phys Chem B 110:21560–21567. https://doi.org/10.1021/jp063700k

Nowontny MK, Sheppard LR, Bak T, Nowontny J (2008) Defect chemistry of titanium dioxide. Application of defect engineering in processing of TiO_2-based photocatalysts. J Phys Chem C 112:5275–5300. https://doi.org/10.1021/jp077275m

Ohmori T, Takahashi H, Mametsuka H, Suzuki E (2000) Photocatalytic oxygen evolution on α-Fe_2O_3 films using Fe^{3+} ion as a sacrificial oxidizing agent. Phys Chem Chem Phys 2:3519–3522. https://doi.org/10.1039/B003977M

Ong W-J (2017) 2D/2D graphitic carbon nitride (g-C_3N_4) heterojunction nanocomposites for photocatalysis: why does face-to-face interface matter? Adv Mater Res-Switz 4:1–10. https://doi.org/10.3389/fmats.2017.00011

Ong W-J, Tan L-L, Ng YH, Yong S-T, Chai S-P (2016) Graphitic carbon nitride (g-C_3N_4)-based photocatalysts for artificial photosynthesis and environmental remediation: are we a step closer to achieving sustainability? Chem Rev 116:7159–7329. https://doi.org/10.1021/acs.chemrev.6b00075

Ong W-J, Putri LK, Tan Y-C, Tan L-L, Li N, Ng YH, Wen X, Chai S-P (2017) Unravelling charge carrier dynamics in protonated g-C_3N_4 interfaced with carbon nanodots as co-catalysts toward enhanced photocatalytic CO_2 reduction: a combined experimental and first-principles DFT study. Nano Res 10:1673–1696. https://doi.org/10.1007/s12274-016-1391-4

Pan H (2015) Bandgap engineering of oxygen-rich TiO_{2+x} for photocatalyst with enhanced visible-light photocatalytic ability. J Mater Sci 50:4324–4329. https://doi.org/10.1007/s10853-015-8984-2

Pan H, Zhang YW (2012) GaN-ZnO superlattice nanowires as photocatalyst for hydrogen generation – a first-principles study on electronic and magnetic properties. Nano Energy 1:488–493. https://doi.org/10.1016/j.nanoen.2012.03.001

Pan H, Guo B, Zhang Z (2009a) Phase-dependent photocatalytic ability of TiO_2: a first-principles study. J Chem Theory Comput 5:3074–3078. https://doi.org/10.1021/ct9002724

Pan H, Qiu XF, Ivanovc IN, Meyer HM, Wang W, Zhu WG, Paranthaman MP, Zhang ZY, Eres G, Gu BH (2009b) Fabrication and characterization of brookite-rich, visible light-active TiO_2 films for water splitting. Appl Catal B 93:90–95. https://doi.org/10.1016/j.apcatb.2009.09.016

Pan H, Gu BH, Eres G, Zhang ZY (2010) Ab initio study on non-compensated CrO codoping of GaN for enhanced solar energy conversion. J Chem Phys 132:104501. https://doi.org/10.1063/1.3337919

Pan H, Zhang YW, Shenoy V, Gao HJ (2011) Effects of H-, N-, and (H, N)-doping on the photocatalytic activity of TiO_2. J Phys Chem C 115:12224–12231. https://doi.org/10.1021/jp202385q

Pan B, Zhou Y, Su W, Wang X (2017) Self-assembly synthesis of $LaPO_4$ hierarchical hollow spheres with enhanced photocatalytic CO_2-reduction performance. Nano Res 10:534–545. https://doi.org/10.1007/s12274-016-1311-7

Pany S, Naik B, Martha S, Parida K (2014) Plasmon induced nano Au particle decorated over S, N-modified TiO_2 for exceptional photocatalytic hydrogen evolution under visible light. ACS Appl Mater Interfaces 6(2):839–846. https://doi.org/10.1021/am403865r

Parida KM, Reddy KH, Martha S, Das DP, Biswal N (2010) Fabrication of nanocrystalline $LaFeO_3$: an efficient sol–gel auto-combustion assisted visible light responsive photocatalyst for water decomposition. Int J Hydrog Energy 35:12161–12168. https://doi.org/10.1016/j.ijhydene.2010.08.029

Phokha S, Pinitsoontorn S, Maensiri S, Rujirawat S (2014) Structure, optical and magnetic properties of $LaFeO_3$ nanoparticles prepared by polymerized complex method. J Sol-Gel Sci Technol 71:333–341. https://doi.org/10.1007/s10971-014-3383-8

Pinaud B, Vesborg PCK, Jaramillo TF (2012) Effect of film morphology and thickness on charge transport in Ta_3N_5/Ta photoanodes for solar water splitting. J Phys Chem C 116:15918–15924. https://doi.org/10.1021/jp3041742

Pinaud BA, Vailionis A, Jaramillo TF (2014) Controlling the structural and optical properties of Ta_3N_5 films through nitridation temperature and the nature of the Ta metal. Chem Mater 26:1576–1582. https://doi.org/10.1021/cm403482s

Prevot MS, Sivula K (2013) Photoelectrochemical tandem cells for solar water splitting. J Phys Chem C 117:17879–17893. https://doi.org/10.1021/jp405291g

Pu YC, Wang GM, Chang KD, Ling YC, Lin YK, Fitzmorris BC, Liu CM, Lu XH, Tong YX, Zhang JZ, Hsu YJ, Li Y (2013) Au nanostructure-decorated TiO_2 nanowires exhibiting photoactivity across entire UV–visible region for photoelectrochemical water splitting. Nano Lett 13:3817–3823. https://doi.org/10.1021/nl4018385

Rahman QI, Ahmad M, Misra SK, Lohani M (2012) Efficient degradation of methylene blue dye over highly reactive Cu doped strontium titanate (SrTiO3) nanoparticles photocatalyst under visible light. J Nanosci Nanotechnol 12:7181–7186. https://doi.org/10.1166/jnn.2012.6494

Rakowski Dubois M, Dubois DL (2009) Development of molecular electrocatalysts for CO_2 reduction and H_2 production/oxidation. Acc Chem Res 42:1974–1982. https://doi.org/10.1021/ar900110c

Rani S, Bao N, Roy SC (2014) Solar spectrum photocatalytic conversion of CO_2 and water vapor into hydrocarbons using TiO_2 nanoparticle membranes. Appl Surf Sci 289:203–208. https://doi.org/10.1016/j.apsusc.2013.10.135

Rao PM, Cai LL, Liu C, Cho IS, Lee CH, Weisse JM, Yang PD, Zheng XL (2014) Simultaneously efficient light absorption and charge separation in WO_3/ $BiVO_4$ core/shell nanowire photoanode for photoelectrochemical water oxidation. Nano Lett 14:1099–1105. https://doi.org/10.1021/nl500022z

Rayalu SS, Jose D, Joshi MV, Mangrulkar PA, Shrestha K, Klabunde K (2013) Photo-catalytic water splitting on Au/TiO_2 nanocomposites synthesized through various routes: enhancement in photocatalytic activity due to SPR effect. Appl Catal B 142:684–692. https://doi.org/10.1016/j.apcatb.2013.05.057

Rechberger F, Niederberger M (2017) Translucent nanoparticle-based aerogel monoliths as 3-dimensional photocatalysts for the selective photoreduction of CO_2 to methanol in a continuous flow reactor. Mater Horiz 4:1115–1121. https://doi.org/10.1039/C7MH00423K

Rodriguez JA, Liu P, Stacchiola DJ, Senanayake SD, White MG, Chen JG (2015) Hydrogenation of CO_2 to methanol: importance of metal–oxide and metal–carbide interfaces in the activation of CO_2. ACS Catal 5:6696–6706. https://doi.org/10.1021/acscatal.5b01755

Sadanandam G, Lalitha K, Kumari VD, Shankar MV, Subrahmanyam M (2014) Cobalt doped TiO_2: a stable and efficient photocatalyst for continuous hydrogen production from glycerol: water mixtures under solar light irradiation. Int J Hydrog Energy 38:9655–9664. https://doi.org/10.1021/jp810923r.

Saeidi S, Amin NAS, Rahimpour MR (2014) Hydrogenation of CO_2 to value-added products—a review and potential future developments. J CO2 Util 5:66–81. https://doi.org/10.1016/j.jcou.2013.12.005

Saito R, Miseki Y, Sayama K (2012) Highly efficient photoelectrochemical water splitting using a thin film photoanode of $BiVO_4$/SnO_2/WO_3 multi-composite in a carbonate electrolyte. Chem Commun 48:3833–3835. https://doi.org/10.1039/C2CC30713H

Savéant J-M (2008) Molecular catalysis of electrochemical reactions. Mechanistic aspects. Chem Rev 108:2348–2378. https://doi.org/10.1021/cr068079z

Schreier M, Curvat L, Giordano F, Steier L, Abate A, Zakeeruddin SM, Luo J, Mayer MT, Grätzel M (2015) Efficient photosynthesis of carbon monoxide from CO_2 using perovskite photovoltaics. Nat Commun 6:7326. https://doi.org/10.1038/ncomms8326

Shao G (2009) Red shift in manganese- and iron-doped TiO_2: a DFT+U analysis. J Phys Chem C 113:6800–6808. https://doi.org/10.1021/jp810923r

Sharma D, Verma A, Satsangi VR, Shrivastav R, Dass S (2014) Nanostructured $SrTiO_3$ thin films sensitized by Cu_2O for photoelectrochemical hydrogen generation. Int J Hydrog Energy 39:4189–4197. https://doi.org/10.1016/j.ijhydene.2013.12.201

Shi WJ, Xiong SJ (2011) Ab initio study on band-gap narrowing in $SrTiO_3$ with Nb–C–Nb codoping. Phys Rev B 84:205210. https://doi.org/10.1103/PhysRevB.84.205210.

Shi H, Zou Z (2012) Photophysical and photocatalytic properties of $ANbO_3$ (A= Na, K) photocatalysts. J Phys Chem Solids 73:788–792. https://doi.org/10.1016/j.jpcs.2012.01.026

Shi H, Wang T, Chen J, Zhu C, Ye J, Zou Z (2011) Photoreduction of carbon dioxide over $NaNbO_3$ nanostructured photocatalysts. Catal Lett 141:525–530. https://doi.org/10.1007/s10562-010-0482-1

Shi H, Chen G, Zhang C, Zou Z (2014) Polymeric g-C_3N_4 coupled with $NaNbO_3$ nanowires toward enhanced photocatalytic reduction of CO_2 into renewable fuel. ACS Catal 4:3637–3643. https://doi.org/10.1021/cs500848f

Shi H, Zhang C, Zhou C, Chen G (2015) Conversion of CO_2 into renewable fuel over Pt-g-C3N4/KNbO3 composite photocatalyst. RSC Adv 5:93615–93622. https://doi.org/10.1039/C5RA16870H

Shi J, Zhang D, Zi W, Wang P, Liu SZ (2017a) Recent advances in Photoelectrochemical applications of silicon materials for solar-to-chemicals conversion. ChemSusChem 10:4324–4341. https://doi.org/10.1002/cssc.201701674

Shi R, Waterhouse GI, Zhang T (2017b) Recent progress in photocatalytic CO_2 reduction over Perovskite oxides. Solar RRL 1(11). https://doi.org/10.1002/solr.201700126

Shiraishi Y, Kanazawa S, Sugano Y, Tsukamoto D, Sakamoto H, Ichikawa S, Hirai T (2014) Highly selective production of hydrogen peroxide on graphitic carbon nitride (g-C3N4) photocatalyst activated by visible light. ACS Catal 4:774–780. https://doi.org/10.1021/cs401208c

Simakov DS (2017) Renewable synthetic fuels and chemicals from carbon dioxide: fundamentals, catalysis, design considerations and technological challenges. Springer, New York. ISBN 978-3-319-61112-9

Sobhani-Nasab A, Hosseinpour-Mashkani SM, Salavati-Niasari M, Bagheri S (2015) Controlled synthesis of $CoTiO_3$ nanostructures via two-step sol–gel method in the presence of 1, 3, 5-benzenetricarboxylic acid. J Clust Sci 26:1305–1318. https://doi.org/10.1007/s10876-014-0814-1

Sun Z, Yang Z, Liu H, Wang H, Wu Z (2014) Visible-light CO_2 photocatalytic reduction performance of ball-flower-like Bi_2WO_6 synthesized without organic precursor: effect of post- calcination and water vapor. Appl Surf Sci 315:360–367. https://doi.org/10.1016/j.apsusc.2014.07.153

Takahara Y, Kondo JN, Takata T, Lu D, Domen K (2001) Mesoporous tantalum oxide 1: characterization and photocatalytic activity for the overall water decomposition. Chem Mater 13:1194–1199. https://doi.org/10.1021/cm000572i

Takeda H, Cometto C, Ishitani O, Robert M (2017) Electrons, photons, protons and earth abundant metal complexes for molecular catalysis of CO_2 reduction. ACS Catal 7:70–88. https://doi.org/10.1021/acscatal.6b02181

Tang P, Tong Y, Chen H, Cao F, Pan G (2013) Microwave-assisted synthesis of nanoparticulate perovskite $LaFeO_3$ as a high active visible-light photocatalyst. Curr Appl Phys 13:340–343. https://doi.org/10.1016/j.cap.2012.08.006

Taniguchi I, Aurian-Blajeni B, Bockris JOM (1984) The mediation of the photoelectrochemical reduction of carbon dioxide by ammonium ions. J Electroanal Chem 161:385–388. https://doi.org/10.1016/S0022-0728(84)80195-3

Valentin CD, Wang FG, Pacchioni G (2013) Tungsten oxide in catalysis and photocatalysis: hints from DFT. Top Catal 56:1404–1419. https://doi.org/10.1007/s11244-013-0147-6

Varghese OK, Paulose M, LaTempa TJ, Grimes CA (2009) High-rate solar photocatalytic conversion of CO_2 and water vapor to hydrocarbon fuels. Nano Lett 9:731–737. https://doi.org/10.1021/nl803258p

Vradman L, Friedland E, Zana J, Vidruk-Nehemya R, Herskowitz M (2017) Molten salt synthesis of $LaCoO_3$ perovskite. J Mater Sci 52:11383–11390. https://doi.org/10.1007/s10853-017-1332-y

Wang S, Wang LW (2010) Atomic and electronic structures of GaN/ZnO alloys. Phys Rev Lett 104:065501. https://doi.org/10.1103/PhysRevLett.104.065501.

Wang D, Kako T, Ye J (2009a) New series of solid-solution semiconductors $(AgNbO_3)_{1-x}(SrTiO_3)_x$ with modulated band structure and enhanced visible-light photocatalytic activity. J Phys Chem C 113:3785–3792. https://doi.org/10.1021/jp807393a

Wang X, Maeda K, Thomas A, Takanabe K, Xin G, Carlsson JM, Domen K, Markus AM (2009b) A metal-free polymeric photocatalyst for hydrogen production from water under visible light. Nat Mater 8:76–80. https://doi.org/10.1038/nmat2317

Wang JW, Mao BD, Gole JL, Burda C (2010) Visible-light-driven reversible and switchable hydrophobic to hydrophilic nitrogen-doped titania surfaces: correlation with photocatalysis. Nanoscale 2:2257–2261. https://doi.org/10.1039/C0NR00313A

Wang YJ, Wang QS, Zhan XY, Wang FM, Safdar M, He J (2013a) Visible light driven type II heterostructures and their enhanced photocatalysis properties: a review. Nanoscale 5:8326–8339. https://doi.org/10.1039/C3NR01577G

Wang Z, Yang CY, Lin TQ, Yin H, Chen P, Wan DY, Xu FF, Huang FQ, Lin JH, Xie XM, Jiang MH (2013b) H-doped black Titania with very high solar absorption and excellent photocatalysis enhanced by localized surface plasmon resonance. Adv Funct Mater 23:5444–5450. https://doi.org/10.1002/adfm.201300486

Wang Z, Hou JG, Yang C, Jiao SQ, Huang K, Zhu HM (2013c) Hierarchical metastable γ-TaON hollow structures for efficient visible-light water splitting. Energy Environ Sci 6:2134–2144. https://doi.org/10.1039/C3EE24370B

Wang CD, Qiu H, Inoue T, Yao QW (2014a) Highly active $SrTiO_3$ for visible light photocatalysis: a first-principles prediction. Solid State Commun 181:5–8. https://doi.org/10.1016/j.ssc.2013.11.026.

Wang JJ, Feng JY, Zhang L, Li ZS, Zou ZG (2014b) Role of oxygen impurity on the mechanical stability and atomic cohesion of Ta_3N_5 semiconductor photo-catalyst. Phys Chem Chem Phys 16:15375–15380. https://doi.org/10.1039/C4CP00120F

Wang W-H, Himeda Y, Muckerman JT, Manbeck GF, Fujita E (2015a) CO_2 hydrogenation to formate and methanol as an alternative to photo-and electrochemical CO_2 reduction. Chem Rev 115:12936–12973. https://doi.org/10.1021/acs.chemrev.5b00197

Wang S, Hou Y, Wang X (2015b) Development of a stable $MnCo_2O_4$ cocatalyst for photocatalytic CO_2 reduction with visible light. ACS Appl Mater Inter 7:4327–4335. https://doi.org/10.1021/am508766s

Wang C, Yang S, Chen X, Wen T, Yang HG (2017) Surface-functionalized perovskite films for stable photoelectrochemical water splitting. J Mater Chem A 5:910–913. https://doi.org/10.1039/C6TA08812K

Warren SC, Thimsen E (2012) Plasmonic solar water splitting. Energy Environ Sci 5:5133–5146. https://doi.org/10.1039/C1EE02875H

Wattanawikkam C, Pecharapa W (2016) Sonochemical synthesis, characterization, and photocatalytic activity of perovskite $ZnTiO_3$ nanopowders. IEEE T Ultrason Ferr 63:1663–1667. https://doi.org/10.1109/TUFFC.2016.2593002

Weber M, Dignam M (1984) Efficiency of splitting water with semiconducting photoelectrodes. J Electrochem Soc 131:1258–1265. https://doi.org/10.1149/1.2115797

Wei W, Dai Y, Yang K, Guo M, Huang B (2008) Origin of the visible light absorption of GaN-rich $Ga_{1-x}Zn_xN_{1-x}O_x$ (x-0.125) solid solution. J Phys Chem C 112:15915–15919. https://doi.org/10.1021/jp804146a

Wenderich K, Mul G (2016) Methods, mechanism, and applications of photodeposition in photocatalysis: a review. Chem Rev 116:14587–14619. https://doi.org/10.1021/acs.chemrev.6b00327

Wendt S, Sprunger PT, Lira E, Madsen GKH, Li Z, Hansen JØ, Matthiesen J, Blekinge-Rasmussen-A, Lægsgaars E, Hammer B, Besenbacger F (2008) The role of interstitial sites in the Ti_3d defect state in the band gap of titania. Science 320:1755–1759. https://doi.org/10.1126/science.1159846

Wu F, Hu XY, Fan J, Liu EZ, Sun T, Kang LM, Hou WQ, Zhu CJ, Liu HC (2013) Photocatalytic activity of Ag/TiO_2 nanotube arrays enhanced by surface plasmon resonance and application in hydrogen evolution by water splitting. Plasmonics 8:501–508. https://doi.org/10.1007/s11468-012-9418-5

Xia XH, Lu L, Walton AS, Ward M, Han XP, Brydson R, Luo JK, Shao G (2012) Origin of significant visible-light absorption properties of Mn-doped TiO_2 thin films. Acta Mater 60:1974–1985. https://doi.org/10.1016/j.actamat.2012.01.006

Xie K, Umezawa N, Zhang N, Reunchan P, Zhang Y, Ye J (2011) Self-doped $SrTiO_3$-[small delta] photocatalyst with enhanced activity for artificial photosynthesis under visible light. Energy Environ Sci 4:4211–4219. https://doi.org/10.1039/C1EE01594J

Xie MZ, Fu XD, Jing LQ, Luan P, Feng YJ, Fu HG (2014) Long-lived, visible-light-excited charge carriers of TiO_2/$BiVO_4$ nanocomposites and their unexpected photoactivity for water splitting. Adv Energy Mater 4:1300995. https://doi.org/10.1002/aenm.201300995

Xu G, Huang X, Krstic V, Chen S, Yang X, Chao C, Shen G, Han G (2014) Hydrothermal synthesis of single-crystalline tetragonal perovskite $PbTiO_3$ nanosheets with dominant (001) or (111) facets. Cryst Eng Comm 16:4373–4376. https://doi.org/10.1039/C4CE00234B

Xu Y-F, Yang M-Z, Chen B-X, Wang X-D, Chen H-Y, Kuang D-B, Su C-Y (2017) A $CsPbBr_3$ Perovskite quantum dot/graphene oxide composite for photocatalytic CO_2 reduction. J Am Chem Soc 139:5660–5663. https://doi.org/10.1021/jacs.7b00489

Yan Y, Wang C, Yan X, Xiao LS, He JH, Gu W, Shi WD (2014) Graphene acting as surface phase junction in anatase–graphene–rutile heterojunction photo-catalysts for H_2 production from water splitting. J Phys Chem C 118:23519–23526. https://doi.org/10.1021/jp507087k

Yang Y, Li X, Chen J, Wang L (2004) Effect of doping mode on the photocatalytic activities of Mo/TiO_2. J Photochem Photobiol A 163:517–522. https://doi.org/10.1016/j.jphotochem.2004.02.008

Yang YH, Liu EZ, Dai HZ, Kang LM, Wu HT, Fan J, Hu XY, Liu HC (2014) Photocatalytic activity of Ag–TiO_2–graphene ternary nanocomposites and application in hydrogen evolution by water splitting. Int J Hydrog Energy 39:7664–7671. https://doi.org/10.1016/j.ijhydene.2013.09.109

Yang G, Chen D, Ding H, Feng J, Zhang JZ, Zhu Y, Hamid S, Bahnemann DW (2017a) Well-designed 3D $ZnIn_2S_4$ nanosheets/TiO_2 nanobelts as direct Z-scheme photocatalysts for CO_2 photoreduction into renewable hydrocarbon fuel with high efficiency. Appl Catal B-Environ 219:611–618. https://doi.org/10.1016/j.apcatb.2017.08.016

Yang KD, Lee CW, Jang JH, Ha TR, Nam KT (2017b) Rise of nano effects in electrode during electrocatalytic CO_2 conversion. Nanotechnology 28:352001. https://doi.org/10.1088/1361-6528/aa7b0b

Yashima M, Teramura K, Lu DL, Takata T, Saito N, Inoue Y, Domen K (2006) Photo-catalyst releasing hydrogen from water. Nature 440:295. https://doi.org/10.1038/440295a

Yin S, Zhu Y, Ren Z, Chao C, Li X, Wei X, Shen G, Han Y, Han G (2014) Facile synthesis of $PbTiO_3$ truncated octahedra via solid-state reaction and their application in low-temperature CO oxidation by loading Pt nanoparticles. J Mater Chem A 2:9035–9039. https://doi.org/10.1039/C4TA00374H

Yokoyama D, Hashiguchi H, Maeda K, Minegishi T, Takata T, Abe R, Kubota J, Domen K (2011) Ta_3N_5 photoanodes for water splitting prepared by sputtering. Thin Solid Film 519:2087–2092. https://doi.org/10.1016/j.tsf.2010.10.055

Yoshitomi F, Sekizawa K, Maeda K, Ishitani O (2015) Selective formic acid production via CO_2 reduction with visible light using a hybrid of a perovskite tantalum oxynitride and a binuclear ruthenium (II) complex. ACS Appl Mater Inter 7:13092–13097. https://doi.org/10.1021/acsami.5b03509

Yu JG, Qi LF, Jaroniec M (2010) Hydrogen production by photocatalytic water-splitting over Pt/TiO_2 nanosheets with exposed (001) facets. J Phys Chem C 114:13118–13125. https://doi.org/10.1021/jp104488b

Yu H, Yan SC, Li ZS, Yu T, Zou ZG (2012) Efficient visible-light-driven photocatalytic H_2 production over Cr/N-codoped $SrTiO_3$. Int J Hydrog Energy 37:12120–12127. https://doi.org/10.1016/j.ijhydene.2012.05.097

Zeng D, Xiao L, Ong W-J, Wu P, Zheng H, Chen Y, Peng D-L (n.d.) Hierarchical $ZnIn_2S_4$/$MoSe_2$ nanoarchitectures for efficient noble-metal-free photocatalytic hydrogen evolution under visible light. Chem Sus Chem 10:4624–4631. https://doi.org/10.1002/cssc.201701345

Zhang QF, Uchaker E, Candelaria SL, Cao GZ (2013a) Nanomaterials for energy conversion and storage. Chem Rev Soc 42:3127–3171. https://doi.org/10.1039/C3CS00009E

Zhang ZH, Hedhili MN, Zhu HB, Wang P (2013b) Electrochemical reduction induced self-doping of Ti^{3+} for efficient water splitting performance on TiO_2 based photoelectrodes. Phys Chem Chem Phys 15:15637–15644. https://doi.org/10.1039/C3CP52759J

Zhang ZY, Wang Z, Cao SW, Xue C (2013c) Au/Pt nanoparticle-decorated TiO_2 nanofibers with plasmon-enhanced photocatalytic activities for solar-to-fuel conversion. J Phys Chem C 117:25939–25947. https://doi.org/10.1021/jp409311x

Zhang ZH, Zhang LB, Hedhili MN, Zhang HN, Wang P (2013d) Plasmonic gold nanocrystals coupled with photonic crystal seamlessly on TiO_2 nanotube photoelectrodes for efficient visible light photoelectrochemical water splitting. Nano Lett 13:14–20. https://doi.org/10.1021/nl3029202

Zhang X, Liu Y, Lee ST, Yang SH, Kang ZH (2014a) Coupling surface plasmon resonance of gold nanoparticles with slow-photon-effect of TiO_2 photonic crystals for synergistically enhanced photoelectrochemical water splitting. Energy Environ Sci 7:1409–1419. https://doi.org/10.1039/C3EE43278E

Zhang X, Liu Y, Kang ZH (2014b) 3D branched ZnO nanowire arrays decorated with plasmonic Au nanoparticles for high-performance photoelectrochemical water splitting. ACS Appl Mater Interfaces 6:4480–4489. https://doi.org/10.1021/am500234v

Zhao WR, Ai ZY, Dai JS, Zhang M (2014) Enhanced photocatalytic activity for H_2 evolution under irradiation of UV–vis light by Au-modified nitrogen-dopedTiO2. PLoS One 9:e103671. https://doi.org/10.1371/journal.pone.0103671

Zhen C, Wang LZ, Liu G, Lu GQ, Cheng HM (2013) Template-free synthesis of Ta_3N_5 nanorod arrays for efficient photoelectrochemical water splitting. Chem Commun 49:3019–3021. https://doi.org/10.1039/C3CC40760H

Zheng Z, Huang B, Qin X, Zhang X, Dai Y (2011) Facile synthesis of $SrTiO_3$ hollow microspheres built as assembly of nanocubes and their associated photocatalytic activity. J Colloid Interface Sci 358:68–72. https://doi.org/10.1016/j.jcis.2011.02.032

Zhou Y, Tian Z, Zhao Z, Liu Q, Kou J, Chen X, Gao J, Yan S, Zou Z (2011a) High-yield synthesis of ultrathin and uniform Bi_2WO_6 square nanoplates benefitting from photocatalytic reduction of CO_2 into renewable hydrocarbon fuel under visible light. ACS Appl Mater Inter 3:3594–3601. https://doi.org/10.1021/am2008147

Zhou X, Shi JY, Li C (2011b) Effect of metal doping on electronic structure and visible light absorption of $SrTiO_3$ and $NaTaO_3$ (Metal=Mn, Fe, and Co). J Phys Chem C 115:8305–8311. https://doi.org/10.1021/jp200022x

Zhou H, Guo J, Li P, Fan T, Zhang D, Ye J (2013) Leaf-architectured 3D hierarchical artificial photosynthetic system of Perovskite Titanates towards CO_2 photoreduction into hydrocarbon fuels. Sci Rep-UK 3:1667. https://doi.org/10.1038/srep01667

Zhou C, Shang L, Yu HJ, Bian T, Wu LZ, Tung CH, Zhang TR (2014) Mesoporous plasmonic Au-loaded Ta_2O_5 nanocomposites for efficient visible light photocatalysis. Catal Today 225:158–163. https://doi.org/10.1016/j.cattod.2013.10.085

Zhou H, Li P, Guo J, Yan R, Fan T, Zhang D, Ye J (2015) Artificial photosynthesis on tree trunk derived alkaline tantalates with hierarchical anatomy: towards CO_2 photo-fixation into CO and CH_4. Nanoscale 7:113–120. https://doi.org/10.1039/C4NR03019B

Zhu W, Qiu XF, Iancu V, Chen XQ, Pan H, Wang W, Dimitrijevic NM, Rajh T, Meyer HM, Paranthaman M, Stocks GM, Weitering HH, Gu BH, Eres G, Zhang ZY (2009) Band gap narrowing of titanium oxide semiconductors by non-compensated anion-cation codoping for enhanced visible-light photo-activity. Phys Rev Lett 103:226401. https://doi.org/10.1103/PhysRevLett

Zhu J, Li H, Zhong L, Xiao P, Xu X, Yang X, Zhao Z, Li J (2014a) Perovskite oxides: preparation, characterizations, and applications in heterogeneous catalysis. ACS Catal 4:2917–2940. https://doi.org/10.1021/cs500606g

Zhu YS, Xu Y, Hou YD, Ding ZX, Wang XC (2014b) Cobalt sulfide modified graphitic carbon nitride semiconductor for solar hydrogen production. Int J Hydrog Energy 39 (23):11873–11879. https://doi.org/10.1016/j.apsusc.2016.09.086.

Zhu C, Jiang Z, Chen L, Qian K, Xie J (2017a) L-cysteine-assisted synthesis of hierarchical NiS2 hollow spheres supported carbon nitride as photocatalysts with enhanced lifetime. Nanotechnology 28:115708. https://doi.org/10.1088/1361-6528/aa5cf2

Zhu Y, Gao C, Bai S, Chen S, Long R, Song L, Li Z, Xiong Y (2017b) Hydriding Pd cocatalysts: an approach to giant enhancement on photocatalytic CO_2 reduction into CH_4. Nano Res 10:3396–3406. https://doi.org/10.1007/s12274-017-1552-0

Chapter 4
Z-Scheme Photocatalysts for the Reduction of Carbon Dioxide: Recent Advances and Perspectives

Xiaodi Zhu and Song Sun

Contents

Abstract Photocatalytic reduction of carbon dioxide, i.e. CO_2 using artificial Z-scheme systems, appears to be a promising approach to convert CO_2 into useful chemicals. In this chapter, basic principles for the photocatalytic reduction of CO_2 as well as terminologies, concepts, and the charge transfer mechanism in artificial Z-scheme systems are described in general. The state-of-the-art achievements of Z-scheme photocatalysts for the reduction of CO_2 are thoroughly summarized and discussed in detail by presenting selected systems in terms of different Z-scheme constructions, including (i) aqueous shuttle redox-mediated Z-scheme systems, denoted as PS-A/D-PS; (ii) all-solid-state Z-scheme systems with/without a conductor electron mediator, denoted as PS-C-PS and PS-PS, respectively; and (iii) semiconductor/metal-complex hybrid Z-scheme systems, denoted as SC-MC. In spite of these, the development on semiconductor photocatalyst materials from the perspective of light harvesting and the cocatalyst strategy for potentially boosting the activity and/or product selectivity for the photocatalytic reduction of CO_2 using Z-scheme systems are also discussed and highlighted. Finally, a concise perspective

X. Zhu · S. Sun (✉)
National Synchrotron Radiation Laboratory, Collaborative Innovation Center of Chemistry for Energy Materials, University of Science & Technology of China, Hefei, China
e-mail: suns@ustc.edu.cn

Inamuddin et al. (eds.), *Nanophotocatalysis and Environmental Applications*,
Environmental Chemistry for a Sustainable World 31,
https://doi.org/10.1007/978-3-030-04949-2_4

for the future direction of research on photocatalytic conversion of CO_2 using Z-scheme photocatalyst is proposed.

Keywords Energy conversion · Photocatalysis · Z-scheme · CO_2 reduction · Activity · Selectivity · Cocatalyst · Light harvesting · Charge transfer · Solar fuel

4.1 Introduction

Over the past 30 years, the concentration of carbon dioxide, i.e. CO_2, which is one of the main greenhouse gases, has been increasing rapidly because of the excessive dependence on fossil resources. The Intergovernmental Panel on Climate Change has predicted that by 2100, the atmospheric CO_2 level could reach up to 590 ppm, leading to the increase in the global mean temperature by 1.9 °C (IPCC 2007). The impact of massive CO_2 emission, such as melting of ice at the Earth's poles, rapidly rising sea levels, and increasing insect pests and freak weather, as well as the inevitable depleting fossil fuel, will be global and be the most serious problem faced by humans (Khatib 2012). Therefore, growing concerns have driven research activities towards the three main routes for reducing the amount of CO_2 in atmosphere, i.e. direct decrease of CO_2 emissions, CO_2 capture and storage, and CO_2 utilization (Hurst et al. 2012). Thus far, the techniques available for CO_2 utilization include catalysed chemical, electrochemical, photochemical, and photoelectrochemical processes, which have been applied to convert CO_2 into useful chemicals (Kondratenko et al. 2013). Among these methods, using solar-light-driven photocatalytic conversion of CO_2 with H_2O into energy-rich chemicals over semiconductors is a promising yet challenging approach. The photocatalytic conversion of CO_2 occurs under relatively mild conditions such as low temperature and normal pressure without secondary pollution, which will potentially address issues related to the booming energy demands and increasingly serious environmental risks (Tu et al. 2014; Li et al. 2016a). Nevertheless, photocatalytic conversion efficiencies for hydrocarbon fuels obtained by CO_2 reduction are still far behind in the race of performance with cost.

Typically, semiconductor photocatalysts are materials that can absorb photons to generate excited electrons and holes exhibiting redox ability. These photogenerated carriers can drive reduction and oxidation if charge injections into the reactants are thermodynamically favourable. As CO_2 reduction with H_2O oxidation is uphill reaction processes ($\Delta G > 0$), sufficient input energy from the reactive electrons and holes is needed to break the chemical bonds of CO_2 and H_2O. Therefore, the photocatalyst is required to satisfy two conditions: (i) excitation with energy equivalent to or greater than its band-gap and (ii) its bottom of the conduction band and the top of the valence band should straddle the redox potential of CO_2 and H_2O. However, few semiconductors can meet these two requirements simultaneously, because broadening the band-gap for the suitable thermodynamic potential of redox reactions and narrowing the band-gap for utilizing as much light as possible

are mutually exclusive. Moreover, in single-component photocatalysts, the photogenerated electrons in the conduction band easily return to the valence band and recombine with the photogenerated holes.

Fortunately, inspired by natural photosynthesis in green plants, A. Bard had originally introduced a new photocatalytic system known as an artificial Z-scheme system for water splitting, which is composite of two functional photocatalysts with/without an appropriate shuttle redox mediator (Bard 1979; Hisatomi et al. 2014; Maeda 2013). It allows the multi-semiconductor photocatalyst systems to satisfy both the thermodynamic and kinetic requirements since it can utilize light more efficiently while simultaneously maintaining the superior reduction/oxidation ability of the individual semiconductor. Although historically Z-scheme photocatalytic systems were predominantly used for water splitting, increased attention has been paid to the exploration of Z-scheme systems for the degradation of pollutants and for the reduction of CO_2 recently. As the reduction of CO_2 over semiconductor photocatalysts is accomplished by photogenerated electrons simultaneously with the consumption of photogenerated holes by electron donor species, such as H_2O, these photocatalysts used in Z-scheme water splitting systems can be potentially applied in the Z-scheme systems for the reduction of CO_2. In the last 5 years, studies reporting the photocatalytic reduction of CO_2 using Z-scheme systems have steadily increased, and significant efforts have been made on different constructions of Z-scheme systems, the development of novel photocatalysts, loaded cocatalysts, optimization of reaction conditions, and control of selectivity. These studies share common perspectives with respect to the design and fabrication of multi-semiconductor composite systems to promote solar energy conversion efficiency and product selectivity.

This chapter will focus on the state-of-the-art Z-scheme photocatalytic systems for CO_2 reduction with a review of the most studied photocatalysts, cocatalysts, reaction conditions, CO_2 conversion efficiencies, and the corresponding primary products. The construction strategies for Z-scheme systems from the viewpoint of enhancement of light harvesting, facilitation of charge separation and transfer, and the promotion of the two-step cycles are highlighted. Considering the Z-scheme CO_2 reduction process is very complicated, this chapter starts with a snapshot of the basic principles of the photocatalytic reduction of CO_2 and charge transfer mechanism of Z-scheme systems. It ends up with a short perspective on the challenges and potential directions in this field.

4.2 Basic Principles of the Z-Scheme Reduction of CO_2

To achieve photocatalytic overall water splitting using a single-component photocatalyst, the bottom of conduction band and the top of valence band of the semiconductor must straddle the reduction and oxidation potentials of water, which are −0.41 and +0.82 eV vs. the normal hydrogen electrode, respectively, at a reactant solution pH of 7 (Fig. 4.1a). Regarding the photocatalytic reduction of

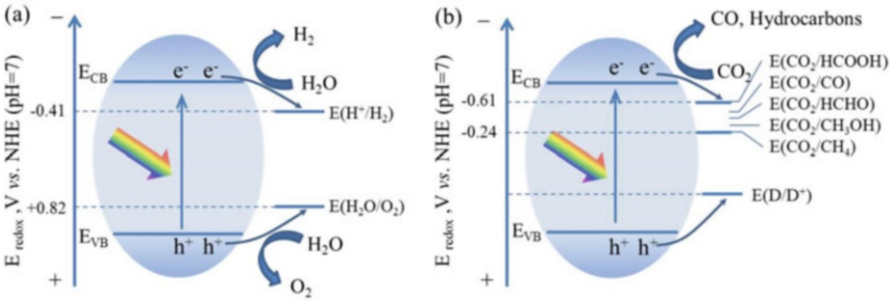

Fig. 4.1 Mechanisms for the one-step excited photocatalytic (**a**) water splitting and (**b**) CO_2 reduction. NHE refers to the normal hydrogen electrode, and E_{CB} and E_{VB} represent the potential of the bottom of conduction band and the top of valence band, respectively. e^-, photogenerated electron; h^+, photogenerated hole

CO_2, it typically demands various energy inputs to break the C=O bond (750 kJ mol^{-1}) and form the C-H bond (411 kJ mol^{-1}), C-O bond (327 kJ mol^{-1}), and C-C bond (336 kJ mol^{-1}) (Xie et al. 2016). Therefore, in order to reduce CO_2 into carbon monoxide, i.e. CO or hydrocarbons, photogenerated electrons in the conduction band are required to exhibit a chemical potential more negative than that of various CO_2 reduction reactions. As shown in Fig. 4.1b, the photocatalytic reduction of CO_2 requires that materials efficiently absorb light to generate electron-hole pairs with the final goal of achieving a carbon-neutral artificial photosynthesis cycle by coupling the reductive half-reaction of CO_2 reduction with a matched oxidative half-reaction such as water oxidation. From a thermodynamic viewpoint, the formation of methane, i.e. CH_4, and methanol, i.e. CH_3OH, is more favourable in CO_2 reduction, because these reactions take place at lower potentials. However, the kinetic drawback makes the formation of CH_4 and CH_3OH more difficult than that of CO; formaldehyde, i.e. HCHO; and formic acid, i.e. HCOOH, because more electrons are required for the former reactions. Equations 4.1–4.7 show the multielectron steps for the reduction of CO_2. As is well known, CO_2 molecules are extremely stable with a closed-shell electronic configuration and linear geometry. The single-electron reduction of CO_2 to the anion radical $CO_2^{\bullet -}$ has a strongly negative electrochemical potential of −1.9 eV vs. the normal hydrogen electrode (Eq. 4.2) (Indrakanti et al. 2009). Few semiconductors can provide sufficient potential to mediate the one-electron reduction of CO_2 under visible light irradiation because the conduction band of most semiconductors lies below the homogeneous reduction potential of CO_2. Fortunately, the proton-assisted transfer of multiple electrons leads to a higher potential for the photocatalytic reduction of CO_2, accomplishing the processes expressed in Eqs. 4.3–4.7. H_2O is a preferred candidate of proton source due to its richness, non-toxicity, and effectiveness, particularly in different operating circumstances. Since the photocatalytic reduction of CO_2 with H_2O into hydrocarbon fuels such as CH_4 and CH_3OH are uphill reactions in which the Gibbs free energy increases by 702.2 kJ mol^{-1} and 818.3 kJ mol^{-1}, for $CO_2 + 2H_2O \rightarrow CH_3OH + 3/2O_2$ and $CO_2 + 2H_2O \rightarrow CH_4 + 2O_2$, respectively, the input energy provided by

incident light should overcome these reaction barriers. Besides, the hydrogen evolution reaction expressed in Eq. 4.8 should be considered with H_2O as the proton source in the system because this reaction invariably competes with the reduction of CO_2 (White et al. 2015). As the counterpart half-reaction for CO_2 reduction reaction, the water oxidation reaction (Eq. 4.9) is an indispensable consideration for attempting to advance the CO_2 photocatalytic conversion efficiency.

$$\text{Photocatalyst} + h\nu \rightarrow e^- + h^+ \tag{4.1}$$

$$CO_2 + e^- \rightarrow CO_2 \bullet^- \quad -1.90\ \text{eV} \tag{4.2}$$

$$CO_2 + 2e^- + 2H^+ \rightarrow HCOOH \quad -0.61\ \text{eV} \tag{4.3}$$

$$CO_2 + 2e^- + 2H^+ \rightarrow CO + H_2O \quad -0.53\ \text{eV} \tag{4.4}$$

$$CO_2 + 4e^- + 4H^+ \rightarrow HCHO + H_2O \quad -0.48\ \text{eV} \tag{4.5}$$

$$CO_2 + 6e^- + 6H^+ \rightarrow CH_3OH + H_2O \quad -0.38\ \text{eV} \tag{4.6}$$

$$CO_2 + 8e^- + 8H^+ \rightarrow CH_4 + H_2O \quad -0.24\ \text{eV} \tag{4.7}$$

$$2H^+ + 2e^- \rightarrow H_2 \quad -0.41\ \text{eV} \tag{4.8}$$

$$2H_2O + 4h^+ \rightarrow 4H^+ + O_2 \quad +0.82\text{eV} \tag{4.9}$$

Since the 1980s, more than 200 studies related to the single-semiconductor photocatalytic reduction of CO_2 have been reported. Currently, the semiconductors investigated for photocatalytic reduction of CO_2 include, but are not limited to, metal oxides (Yu et al. 2014; Habisreutinger et al. 2013), metal sulphides (Zhang et al. 2004; Hiroshi Inoue et al. 1995), nitrides (Li et al. 2015a; Tahir et al. 2017), and phosphides (Barton et al. 2008). Figure 4.2 shows some representative photocatalysts and their relative redox potentials vs. the normal hydrogen electrode at pH 7. Although the photocatalytic reduction of CO_2 has been investigated for a long time and has developed considerably, it is still limited by the extremely low conversion efficiency. The major obstacle to progress the development of photocatalysts driven by one-step CO_2 reduction includes the lack of a suitable compound that can simultaneously satisfy the thermodynamic and kinetic requirements as explained in the introduction. Moreover, the photocatalytic CO_2 reduction is a heterogeneous catalytic process and inevitably involves the adsorption and activation of CO_2, which makes the process more complicated. The adsorption and activation of CO_2 are not the main topic of this chapter and can be referred to in some reviews (Kondratenko et al. 2013; Habisreutinger et al. 2013). Here, we will skip over these aspects and concentrate on the next general issue about fundamental concepts and the charge transfer mechanisms of photocatalytic reduction of CO_2 using Z-scheme systems.

Figure 4.3 shows the Z-scheme photocatalytic system originating from natural photosynthesis in green plants, which was initially proposed for water splitting. This Z-scheme photocatalytic system is regarded as a two-step photoexcitation system.

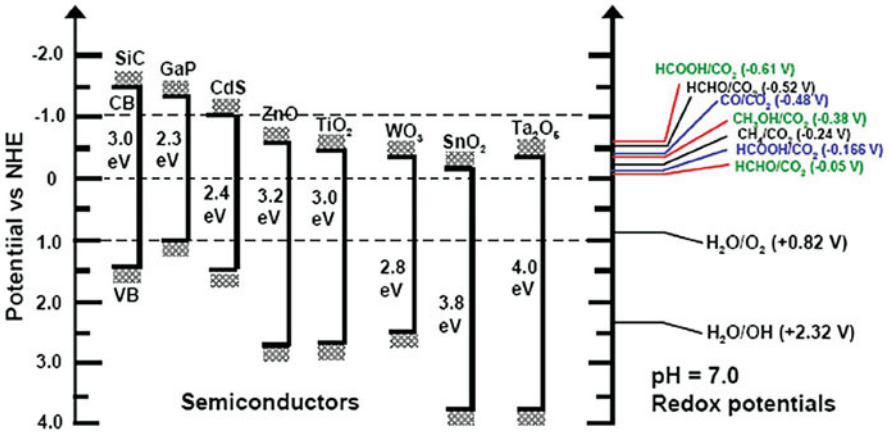

Fig. 4.2 Conduction band, valence band potentials, and band-gap energies of various semiconductor photocatalysts relative to the redox potentials at pH 7 of compounds involved in CO_2 reduction. (Reprinted from Kondratenko et al. 2013 with permission of Royal Society of Chemistry)

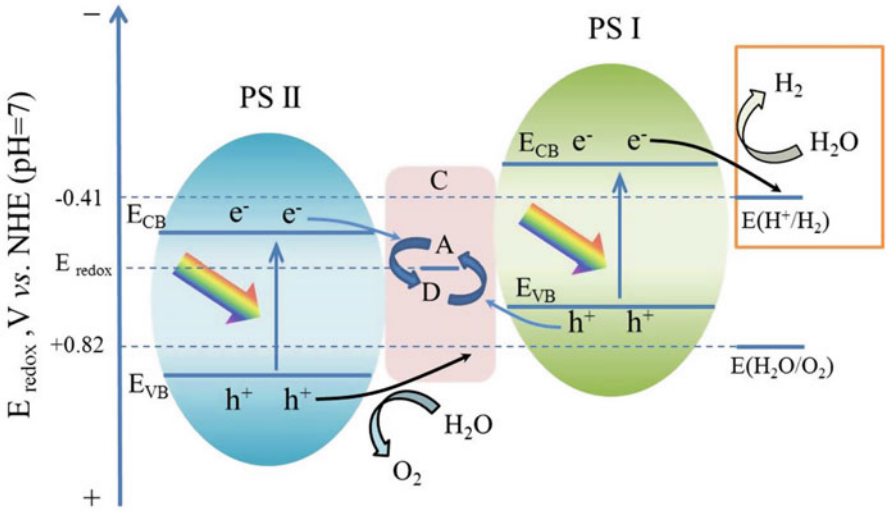

Fig. 4.3 Schematic of water splitting mechanism using Z-scheme photocatalysts. In this case, PS I and PS II are also known as hydrogen evolution photocatalyst and oxygen evolution photocatalyst, respectively. E_{CB} and E_{VB} represent the potential of the bottom of conduction band and the top of valence band, respectively. e^-, photogenerated electron; h^+, photogenerated hole

Redox reactions are spatially separated and carried out at two different functional photocatalysts, photocatalysts I and II, labelled as PS I and PS II, where the water reduction and water oxidation occur, respectively. An aqueous shuttle redox mediator or a solid-state electron mediator is usually necessary to complete the whole photocatalytic cycle via consumption of photogenerated electrons and holes from the

oxygen evolution photocatalyst, i.e. PS II, and hydrogen evolution photocatalyst, i.e. PS I, respectively. In the case of shuttle redox-mediated system, electron transfer is strongly dependent on the redox reactions of the shuttle redox mediator. An electron acceptor with an appropriate reduction potential will be reduced into the electron donor by a photogenerated electron from the conduction band of PS II. Simultaneously, the electron donor with an appropriate oxidation potential will be oxidized into the electron acceptor by the photogenerated hole from the valence band of PS I expressed as Eqs. 4.10 and 4.11.

$$A + e^- \rightarrow D \text{ (conduction band of PS II)} \tag{4.10}$$

$$D + h^+ \rightarrow A \text{ (valence band of PS I)} \tag{4.11}$$

While in the case of solid-state electron mediator-mediated system, thanks to the ohmic contact with a low resistance between the conductor and semiconductor, the photogenerated electrons in the conduction band of PS II can easily transfer to the conductor mediator and recombine with holes coming from the valence band of PS I, besides, in some other Z-scheme systems, electron mediators are not necessary. A similar ohmic contact can be formed at the interface between two semiconductors and the photogenerated charge carriers, which obey an analogous transfer mechanism with solid-state electron mediator-mediated systems and directly recombine at the interface. Compared to the one-step excited photocatalytic systems, thermodynamically unsatisfactory semiconductors in the one-step photoexcitation systems with either a conduction band more positive than the potential of H_2/H_2O or a valence band more negative than the potential of O_2/H_2O can be used in two-step photoexcitation Z-scheme systems.

For the reduction of CO_2 using water as an electron donor (Fig. 4.4), a similar water oxidation process involves, while the reduction process is the reduction of CO_2 to yield CO/hydrocarbon. Many strategies adopted for Z-scheme water splitting can be exploited for the reduction of CO_2 with advantages of not only offering complimentary light absorption in different spectral regions and spatial separation of electrons from holes but also maintaining the energy levels of the remaining electrons and holes with thermodynamic requirements for sufficient reactivity. Nevertheless, it should be pointed out that in Z-scheme systems, the possible backward electron transfer routes are increased because of the additional elementary steps. As represented by the dashed arrows shown in Fig. 4.4, except for the general backward reactions including oxygen reduction reaction, hydrogen oxidation reaction, CO/hydrocarbon oxidation reaction, and competitive reactions such as hydrogen evolution reaction, the reactions between redox mediator and electrons from the conduction band of PS I and holes from the valence band of PS II (Eqs. 4.12 and 4.13) make the scheme of CO_2 reduction kinetically more challenging than that in the one-step photoexcitation approach. Therefore, the suppression of the redox-involved backward reactions is crucial to achieving efficient conversion according to the Z-scheme principle.

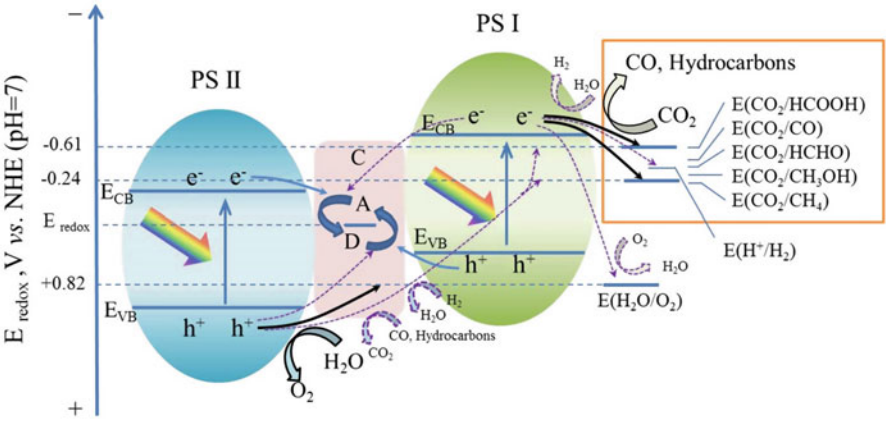

Fig. 4.4 Schematic of the photocatalytic reduction of CO_2 with water in Z-scheme system. Unlike water splitting, PS I and PS II in this case photoinduced the CO_2 reduction and water oxidation, respectively. The dash arrows in purple represent the possible backward reactions. A and D represent the electron acceptor and donor, respectively; C represents the conductor mediator; E_{CB} and E_{VB} represent the potential of the bottom of conduction band and the top of valence band, respectively. e^-, photogenerated electron; h^+, photogenerated hole

$$A + e^- \rightarrow D \text{ (conduction band of PS I)} \tag{4.12}$$

$$D + h^+ \rightarrow A \text{(valence band of PS II)} \tag{4.13}$$

4.3 Advances in Z-Scheme Photocatalytic Reduction of CO_2

Since the pioneering work of Inoue and coworkers (Inoue et al. 1979), intensive studies in both one-step and two-step excitation photocatalytic systems have conducted on the photocatalytic reduction of CO_2 to valuable fuels. So far, the explored two-step excitation systems, referring to Z-scheme CO_2 reduction systems, have demonstrated the success in fuel production of CH_4, CO, CH_4OH, and so on, as summarized in Table 4.1. These systems can be divided into three main categories: (i) Z-scheme systems with aqueous redox mediator or solid conductive mediator undergoing the photocatalytic cycle via the recombination of photogenerated electrons and holes from the donor species oxidation photocatalyst and CO_2 reduction photocatalyst, respectively; (ii) Z-scheme systems without specific electrons transfer mediator; and (iii) Z-scheme systems composed of semiconductor and metal-complex light absorber. The state-of-the-art existing Z-scheme photocatalyst systems for the photocatalytic reduction of CO_2 are selectively exemplified to demonstrate the charge transfer mechanism from the point of view of Z-scheme constructions. In particular, the exploration of composite semiconductor materials and the modification strategy of applying cocatalyst layer aiming at improving the

Table 4.1 Summary of the Z-scheme systems for the photocatalytic reduction of CO_2

Z-scheme photocatalysts							
PS II (available wavelength/nm)	PS I (available wavelength/nm)	Mediators	Cocatalysts	Reactants	Light source	Products	References
g-C_3N_4 (<450)	$Bi_4O_5I_2$ (<570)	I_3^-/I^-	None	5 mL H_2SO_4 (4 M) + $NaHCO_3$ to achieve 1 atm CO_2 gas	300 W high-pressure Xe arc lamp with a UV cutoff filter (λ > 400 nm)	CO CH_4 H_2 O_2	Bai et al. (2016a)
g-C_3N_4 (<460)	BiOI (<708)	I_3^-/I^-	None	CO_2 gas was passed through a water bubbler to generate a mixture of CO_2 and water vapour	300 W Xe arc lamp with a UV cutoff filter (λ > 400 nm)	CH_4 CO H_2 O_2	Wang et al. (2016)
TiO_2 (<387)	CdS (<496)	Cys/CySS	Phthalocyanine for TiO_2	Defined photosynthesis media (DPM) + 0.1 wt.% cysteine·HCl and 250 kPa H_2:CO_2 (80:20)	A filtered 75 W Xe lamp (AM1.5G, 5% sun)	CH_3COOH, O_2	Sakimoto et al. (2016)
BiOBr (<520)	g-C_3N_4 (<460)	Au	None	5 mL H_2SO_4 (4 M) + 1.3 g $NaHCO_3$ to achieve 1 atm CO_2 gas	300 W high-pressure Xe arc lamp (350/550 nm)	CO CH_4	Bai et al. (2016b)
Ag_3PO_4 (<523)	g-C_3N_4 (<473)	Ag	None	0.4 MPa CO_2 + 4 mL H_2O	500 W Xe arc lamp with a UV cutoff filter (λ > 420 nm)	CO CH_3OH CH_4 CH_3CH_2OH	He et al. (2015a)
Bi_2WO_6 (<430)	CdS (<496)	Au	None	1 atm CO_2 + 0.4 mL H_2O	300 W Xe arc lamp	CH_4	Wang et al. (2017a)
IO-TiO_2 (<387)	CdS (<496)	Au	None	CO_2 and water vapour mixture (the pressure of CO_2 was regulated to 0.1 MPa)	300 W Xe arc lamp	H_2 CH_4 CO O_2	Wei et al. (2015)

(continued)

Table 4.1 (continued)

Z-scheme photocatalysts		Mediators	Cocatalysts	Reactants	Light source	Products	References
PS II (available wavelength/nm)	PS I (available wavelength/nm)						
WO_3 (<442)	In_2S_3 (<496)	Au	None	1 atm high-purity CO_2 gas +0.4 mL H_2O	300 W Xe arc lamp with a UV cutoff filter (λ > 420 nm)	CH_4	Li et al. (2016b)
$BiVO_4$ (<516)	Metal sulphide ($CuGaS_2$)	RGO	Pt for metal sulphide, CoO_x for $BiVO_4$	1 atm CO_2 gas flow in H_2O	300 W Xe arc lamp with a long-pass filter (λ > 420 nm) and a solar simulator	CO	Iwase et al. (2016)
TiO_2 (<387)	CdS (<516)	RGO	None	1 atm CO_2 + 0.4 mL H_2O	300 W Xe arc lamp	CH_4	Kuai et al. (2015)
CdS (<516)	$Fe_2V_4O_{13}$ (<677)	RGO	None	0.4 mL H_2O vapourized in the presence of high-purity CO_2	300 W Xe lamp	CH_4 O_2	Li et al. (2015b)
TiO_2 (<387)	Metal sulphides	RGO	None	CO_2 gas was bubbled into the suspension containing catalysts and 120 mL H_2O	300 W Xe lamp without any cutoff filters (λ > 330 nm)	CO for $CuGaS_2$ HCOOH for Ni-doped ZnS	Takayama et al. (2017)
TiO_2 (<390)	Cu_2O (<600)	None	None	1 atm CO_2 with water vapour	1 kW high-pressure Hg (Xe) arc lamp with a water filter and a cutoff filter (λ ≥ 305 nm)	CO	Aguirre et al. (2017)
SnS_2 (<590)	g-C_3N_4 (<443)	None	None	84 mg $NaHCO_3$ + 0.3 mL H_2SO_4 (0.2 M) aqueous solution	300 W Xe lamp with a cutoff filter (λ > 420 nm)	CH_4 CH_3OH	Di et al. (2017)
MoO_3 (<450)	g-C_3N_4 (<470)	None	None	0.3 MPa CO_2 + 4 mL H_2O	350 W Xe lamp equipped with a UV cut and an IR cut filters (800 nm > λ > 420 nm)	CH_4 CH_3OH CO	Feng et al. (2017)

SnO_{2-x} (<496)	g-C_3N_4 (<460)	None	None	0.3 MPa CO_2 + 4 mL H_2O	500 W Xe lamp	CH_4 CH_3OH CO	He et al. (2015b)
WO_3 (<442)	CdS (<540)	None	None	0.12 g $NaHCO_3$ + 0.25 mL HCl (4 M) aqueous solution	300 W Xe arc lamp with a UV cutoff filter ($\lambda \geq$ 420 nm)	CH_4	Jin et al. (2015)
$Ti_{0.91}O_2$ (<387)	CdS (<540)	None	None	High purity of CO_2 + 0.4 mL of deionized water	300 W Xe arc lamp	CH_4	Tu et al. (2015)
g-C_3N_4 (<460)	Bi_2WO_6 (<450)	None	None	A mixture of CO_2 and water vapour	300 W Xe arc lamp with a 420 nm cutoff filter	CO	Li et al. (2015c)
TiO_2 (<387)	Si (<1127)	None	None	50 psi CO_2 + 100 mL H_2O	The third harmonic of the pulsed Nd:YAG laser (λ = 355 nm)	CH_3OH	Liu et al. (2014)
WO_3 (<496)	g-C_3N_4 (<450)	None	Au or Ag for g-C_3N_4	5 mL ion-exchanged water saturated with CO_2	LED (Epitex, 30M32L, λ = 435 nm, I = 3.0 mW cm^{-2})	CH_3OH	Ohno et al. (2014)
TiO_2 (<390)	$ZnFe_2O_4$ (<700)	None	None	CO_2 was bubbled through 10 mL cyclohexanol	250 W high-pressure mercury lamp (λ = 360 nm)	HCOOH	Song et al. (2015)
α-Fe_2O_3 (<630)	g-C_3N_4 (<460)	None	None	CO_2 gas was passed through water into the reactor containing 5 mL H_2O	300 W Xe arc lamp	CO CH_4 O_2	Wang et al. (2018)
α-Fe_2O_3 (<630)	Cu_2O (<605)	None	None	CO_2 gas was passed through a water bubbler to generate a mixture of CO_2 and water vapour	300 W Xe arc lamp	CO CH_4	Wang et al. (2015)
TiO_2 (<380)	$ZnIn_2S_4$ (<468)	None	None	0.4 mL H_2O, CO_2 gas was injected into the vacuumed reaction system	300 W Xe lamp	CH_4	Yang et al. (2017a)
ZnO (<381)	g-C_3N_4 (<450)	None	None	0.12 g $NaHCO_3$ + 0.25 mL 4 M HCl aqueous solution	300 W simulated solar Xe arc lamp	CH_3OH	Yu et al. (2015)
ZnO (<381)	Cu_2ZnSnS_4 (<712)	None	None	A mixture of CO_2 and water vapour formed by passing CO_2 through a water bubbler	100 W Xe solar simulator with an AM 1.5 filter	CH_4	Zubair et al. (2017)

(continued)

Table 4.1 (continued)

Z-scheme photocatalysts		Mediators	Cocatalysts	Reactants	Light source	Products	References
PS II (available wavelength/nm)	PS I (available wavelength/nm)						
YTaON (<580)	Ru (II) binuclear complex (<600)	Ag	None	4 mL of a 20 vol% TEOA solution in DMA, purging CO_2 before reaction	400 W high-pressure Hg lamp with a $NaNO_2$ solution filter	HCOOH	Muraoka et al. (2016)
TiO_2 (<387)	InP/[MCE2-A + MCE4] (<918)	None	Pt for TiO_2	5 ml of electrolyte solution (10 mM $NaHCO_3$/Na_3PO_4/Na_2SO_4) bubbled with CO_2 gas	Xe lamp equipped with an optical filter ($\lambda > 400$ nm)	HCOOH	Sato et al. (2011)
Reduced $SrTiO_3$ (<400)	InP/[RuCP] (<900)	Ag	None	10 ml of 0.1 M $NaHCO_3$ aqueous solution mixed with phosphoric acid, bubbled with CO_2 gas	Solar simulator AM1.5	HCOOH	Arai et al. (2013)
$CaTaO_2N$ (<496)	Ru (II) binuclear complex (<600)	Ag	None	4 mL of a 20 vol% TEOA solution in DMA, purging CO_2 before reaction	Visible light ($\lambda > 400$ nm)	HCOOH	Yoshitomi et al. (2015)

TaON, $CaTaO_2N$, C_3N_4, and YTaON (<580)	Ru (II) binuclear complex (<600)	Ag	None	CH_3OH under CO_2 atmosphere	450 or 400 W high-pressure Hg lamp with an aqueous $NaNO_2$ solution (λ > 400 nm)	HCOOH CO H_2	Maeda (2016)
mpg-C_3N_4 (<450)	Ru (II) binuclear complex (<600)	Ag	None	CO_2 gas +4 mL10 mM EDTA·2Na aqueous solution with K_2CO_3 or $K_2C_2O_4$	400 W high-pressure Hg lamp, with an aqueous $NaNO_2$ solution (λ > 400 nm)	HCOOH CO H_2	Kuriki et al. (2016)
NS-C_3N_4 (<450)	Ru (II) binuclear complex (<600)	Ag	None	CO_2 gas +4 mL10 mM EDTA·2Na aqueous solution with 0.1 M K_2CO_3	400 W high-pressure Hg lamp, with an aqueous $NaNO_2$ solution filter (λ > 400 nm)	HCOOH H_2	Kuriki et al. (2017)
TaON(<500)	Ru (II) binuclear complex (<600)	Ag/Pt	None	4 mL CH_3OH + CO_2	500 W high-pressure Hg lamp with an aqueous $NaNO_2$ solution filter (λ > 400 nm)	HCOOH CO H_2 HCHO	Sekizawa et al. (2013)

light-harvesting capability, photocatalytic activity, and/or product selectivity are highlighted for a thorough perspective on the current developments in this field as well as for the further promotion on the performance of Z-scheme photocatalyst systems.

4.3.1 *Z-Scheme Systems with Aqueous Shuttle Redox Mediator*

Various artificial Z-scheme systems have been constructed focusing on the development of both new semiconductor materials and suitable redox mediators (Ozin 2015; Kudo 2011; Zhou et al. 2014). In Z-scheme photocatalytic systems, the electron acceptor/donor pair is a common electron mediator (Maeda 2013; Abe et al. 2005). The most frequently used electron acceptor/donor pairs in Z-scheme systems for photocatalytic water splitting include IO^{3-}/I^-, Fe^{3+}/Fe^{2+}, $[Co(bpy)_3]^{3+/2+}$, $[Co(phen)_3]^{3+/2+}$, and NO_3^-/NO_2^- (Abe et al. 2013; Sasaki et al. 2008; Sasaki et al. 2013; Sayama et al. 2006). At present, however, I_3^-/I^- is typically used in the reported Z-scheme systems for the photocatalytic reduction of CO_2. Bai et al. (2016a) have demonstrated an enhanced photocatalytic activity towards g-C_3N_4/$Bi_4O_5I_2$ heterojunction using an I_3^-/I^- redox mediator. As shown in Fig. 4.5a, CO,

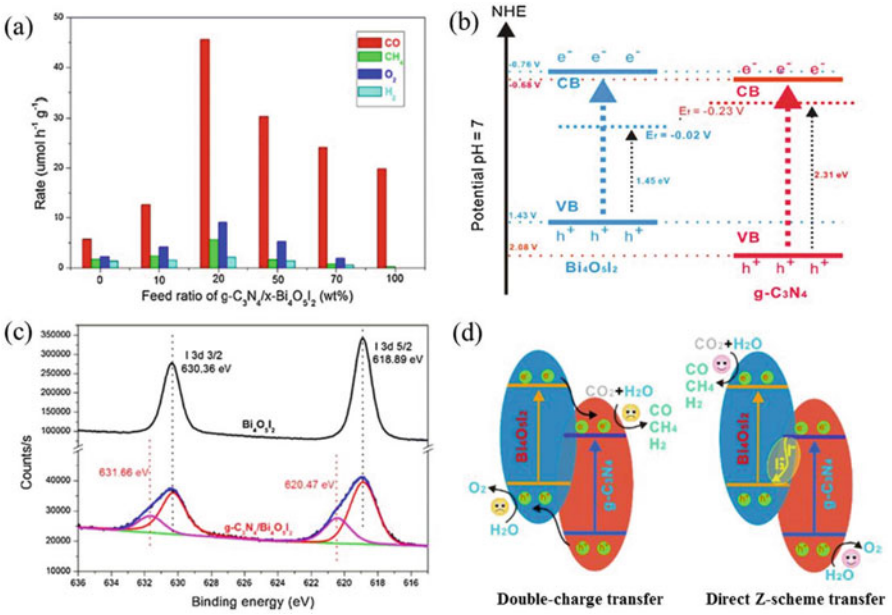

Fig. 4.5 (**a**) Rates of products for g-C_3N_4/x-$Bi_4O_5I_2$ ($x = 0$, 10, 20, 50, 70, and 100) under visible light irradiation for 5 h; (**b**) diagram of the band energy of $Bi_4O_5I_2$ and g-C_3N_4; (**c**) I 3d X-ray photoelectron spectra of $Bi_4O_5I_2$ and g-C_3N_4/20-$Bi_4O_5I_2$; and (**d**) photocatalytic charge transfer mechanism of g-C_3N_4/$Bi_4O_5I_2$. (Reprinted from Bai et al. 2016a with permission of Elsevier)

CH_4, O_2, and H_2 were generated in the g-C_3N_4/x-$Bi_4O_5I_2$ system. The generation rate of the CO is 7.9 times higher than that of pure g-C_3N_4 and 2.3 times higher than that of pure $Bi_4O_5I_2$ at optimal conditions. To understand the performance enhancement, energy band structures of pure g-C_3N_4 and $Bi_4O_5I_2$ (Fig. 4.5b) were firstly determined by the comprehensive analysis of UV-visible diffuse reflectance spectra, Mott-Schottky plots, and valence band X-ray photoelectron spectroscopy. Afterwards, the quantification of specific reactive oxygen species by detecting the production of superoxide radical (O_2•$^-$) and hydroxyl radical (•OH) intermediates was carried out to discount the possibility of type-II heterojunction double-charge transfer mechanism. Furthermore, the existence of the I_3^-/I^- redox which was in situ formed in the system via the photocatalytic oxidation of I^- in $Bi_4O_5I_2$ was confirmed by I 3d X-ray photoelectron spectra (Fig. 4.5c). Based on these results, the enhancement of the photocatalytic conversion of CO_2 is confirmed to result from an I_3^-/I^- redox-assisted Z-scheme mechanism (Fig. 4.5d). Wang et al. (2016) also verified the indirect Z-scheme charge transfer mechanism with the assistance of I_3^-/I^- redox in a similar material system, i.e. BiOI/g-C_3N_4. Besides, the thiol amino acid cysteine/the disulphide form cysteine has been recently reported as a molecular redox shuttle in a *Moorella thermoacetica*-CdS+TiO_2-MnPc system for a potential biomimetic approach to complete oxygenic solar-to-chemical production via the photocatalytic reduction of CO_2 coupling with water oxidation reaction. This work provided new options for redox mediators applied in Z-scheme CO_2 reduction systems.

However, the characteristics of a shuttle redox mediator significantly affect the efficiency of a given Z-scheme system with aqueous shuttle redox mediator. For one thing, it is typically difficult to maintain long-term stability in a wide pH range for these electron acceptor/donor pairs, which in turn decrease the actual amount of the available electron acceptor/donor pairs. In most cases, each electron acceptor/donor redox has its own suitable operating pH range. For instance, the available reaction pH in a Fe^{3+}/Fe^{2+} redox system is limited to the acidic condition because iron ions undergo precipitation to give iron hydroxide in neutral and basic conditions (Maeda 2013). Also, these shuttle redox mediators absorb light to a different extent, which probably decreases the number of absorbed photons by the photocatalysts (Zhou et al. 2014; Abe et al. 2013; Sasaki et al. 2013). Moreover, the aforementioned electron acceptor/donor redox-involved backward reactions inevitably decrease the amount of the available photogenerated carriers for target reactions. Consequently, the electron transfer rate between PS II and PS I in Z-scheme system is decreased. To avoid these disadvantages, the electron acceptor/donor -free Z-scheme photocatalytic systems attract more and more scientific attention and are considerably developed in recent years as exemplified in the following sections.

4.3.2 All-Solid-State Z-Scheme Systems

The electron acceptor/donor pair-free Z-scheme systems are also referred to as all-solid-state Z-scheme systems, which can be further categorized into two types. By the replacement of electron acceptor/donor shuttle redox mediator, a conductor is

employed as the solid electron mediator in an all-solid-state Z-scheme system, denoted as PS-C-PS (Figs. 4.3 and 4.4). Relative to electron acceptor/donor redox mediators, solid electron mediators such as noble metal nanoparticles and reduced graphene oxide are more favourable in terms of ensuring a continuous flow of electrons between two photocatalysts because of the intimate photocatalyst-conductor-photocatalyst contact (Yu et al. 2013). The insertion of a conductor between PS I and PS II forms an ohmic contact with low resistance, resulting in direct recombination of electrons from the conduction band of PS II and the holes from the valence band of PS I through the conductor (Kochuveedu et al. 2013; Byun et al. 2013; Ou et al. 2011). In 2006, TiO_2-Au-CdS was reported as the first example of a PS-C-PS Z-scheme system, where Au nanoparticles were photodeposited on the TiO_2 surface serving as the electron mediator, and CdS was further grown on the surface of Au nanoparticles to yield CdS-coated Au nanocrystals on the TiO_2 surface (Tada et al. 2006). Because of the large work function of Au, photogenerated electrons in the conduction band of TiO_2 can be transferred through Au to combine with the photogenerated holes in the valence band of CdS, leaving electrons in the conduction band of CdS and holes in the valence band of TiO_2 to participate in reduction and oxidation, respectively. The recombination of photogenerated carriers was effectively suppressed while simultaneously maintaining the superior oxidation potential of TiO_2 and reduction potential of CdS. In the same manner, the photocatalytic reduction of CO_2 was successfully implemented on the inverse opal TiO_2-supported Au@CdS core-shell nanoparticles synthesized by the two-step process of gas bubbling-assisted membrane procedures (Wei et al. 2015). As illustrated in Fig. 4.6, the core-shell-structured Au@CdS nanoparticles were uniformly

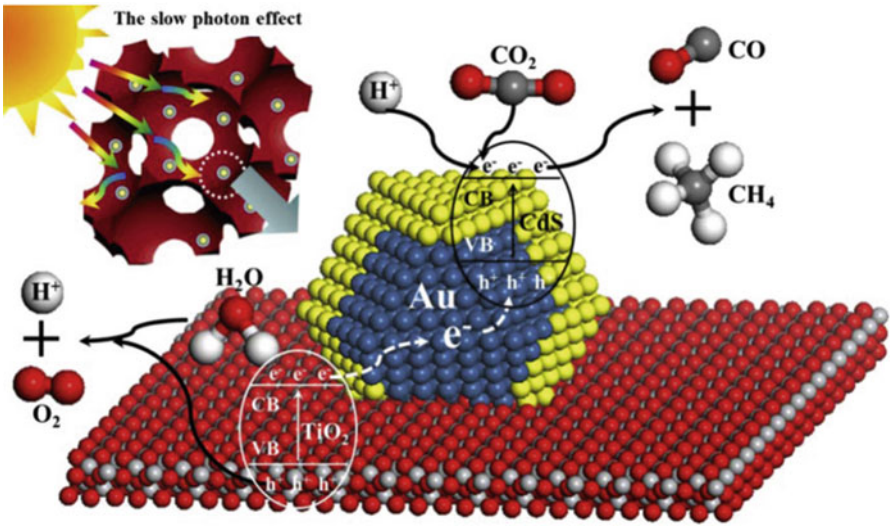

Fig. 4.6 The mechanism for the photoreduction of CO_2 with H_2O over Au@CdS/IO-TiO_2 photocatalysts. (Reprinted from Wei et al. 2015 with permission of Elsevier)

dispersed on the inner walls of the uniform macropores of inverse opal TiO_2. On the one hand, improved light-harvesting efficiency was achieved due to the slow photon effect of inverse opal-structured TiO_2 with moderate pore sizes, which contributed to the superior performance. On the other hand, vectorial electron transfer (TiO_2→Au→CdS) is favourable for the separation of photogenerated electrons and holes, resulting in superior performance for the photocatalytic reduction of CO_2 with H_2O.

Apparently, the work function of the metal or/and the conductivity, as well as the interfacial contact property, is crucial to the charge carrier transfer between two semiconductors. Therefore, the choice of conductors and synthesis conditions may significantly affect the formation of ohmic contacts at the interfaces. Except for metal Au, Ag also serves as conductor mediator in PS-C-PS Z-scheme systems due to its excellent conductivity. Taking Ag_3PO_4/g-C_3N_4 hybrids as an example, Ag nanoparticles were in situ generated by the photoreduction of Ag^+ under light irradiation (He et al. 2015a). The authors have attributed the enhanced photocatalytic performance for the reduction of CO_2 to the promoted separation efficiency of electron-hole pairs by Ag nanoparticle-bridged Z-scheme construction and the improved capacity for light absorption arising from the surface plasma resonance effect of Ag nanoparticles. Actually, the surface plasma resonance-enhanced light absorption is a common phenomenon in noble metal nanoparticles (Zhang et al. 2011; Ding et al. 2014). Thus, the role of noble metal nanoparticles and the extent of its contribution made to the enhancement of the photocatalytic performance in this case really depend on the specific material systems and photocatalytic reaction conditions. For example, in the study of Yang Bai et al. (Wei et al. 2015), big Au nanoparticles with size of 100–150 nm are thought to mainly exhibit a Z-scheme bridge role, and g-C_3N_4/BiOBr mediated with big size Au nanoparticles shows higher photocatalytic activity than that of g-C_3N_4/BiOBr under 380 nm monochromatic light irradiation. While small Au nanoparticles with size of 10–20 nm mainly exhibit the role of surface plasma resonance, g-C_3N_4/BiOBr mediated with small size Au nanoparticles shows higher photocatalytic activity than that of g-C_3N_4/BiOBr under 550 nm monochromatic light irradiation (Fig. 4.7). These studies suggested that identification of the contribution of the Z-scheme charge transfer mechanism to the improved photocatalytic performance needs to be carefully examined with sufficient experimental evidence to draw the reliable conclusions.

Except for the noble metals discussed above, some cost-effective metal oxides and nonmetal materials with excellent conductivity have also been used as the electron mediators in PS-C-PS systems, especially for metal-free material graphene (Xiang et al. 2012; Xie et al. 2013). However, it is rather difficult to prepare an intact graphene layer due to the generation of numerous defects. Thus, graphene is typically used as the reduced graphene oxide denoted as RGO in practical applications. Since CdS is well known as an efficient photocatalyst for hydrogen evolution and is also active for CO_2 reduction, metal sulphides have been considered to be promising candidates for CO_2 reduction under visible light irradiation. Unfortunately, self-oxidation by photogenerated holes, i.e. photocorrosion, still remains an issue that hinders the use of metal sulphides. Taking these into consideration,

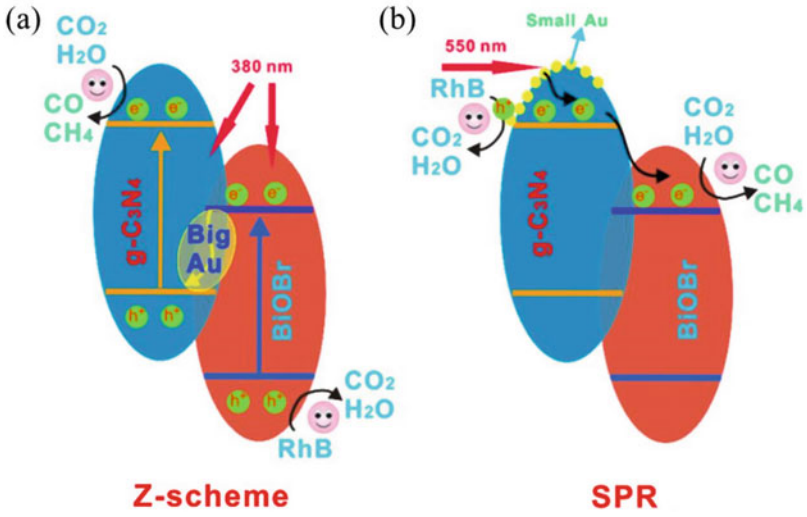

Fig. 4.7 Schematic of the photocatalytic reduction mechanism of CO_2 and dye degradation: (**a**) g-C_3N_4/BiOBr/Au-B under 380 nm and (**b**) g-C_3N_4/BiOBr/Au-S under 550 nm. (Reprinted from Bai et al. 2016b with permission of Elsevier)

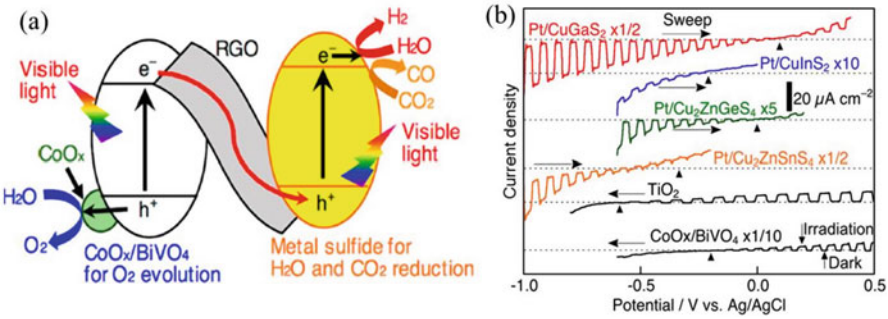

Fig. 4.8 (**a**) Pt-loaded metal sulphide and RGO-CoO_x/$BiVO_4$ composite photocatalytic Z-scheme system for water splitting and CO_2 reduction under visible light irradiation; (**b**) Current-potential curves of various metal sulphides, TiO_2, and CoO_x/$BiVO_4$. Electrolyte, 0.1 mol L^{-1} K_2SO_4 + 0.025 mol L^{-1} KH_2PO_4 + 0.025 mol L^{-1} Na_2HPO_4; light source, 300 W Xe arc lamp ($\lambda > 300$ nm for TiO_2 and $\lambda > 420$ nm for others). (Reprinted from Iwase et al. 2016 with permission of American Chemical Society)

Akihiko Kudo's group has made intense efforts on developing Z-scheme systems with different metal sulphides as PS I, suitable semiconductor as PS II, and RGO as an electron mediator for the reduction of CO_2. They have successfully proceeded the visible-light-driven photocatalytic reduction of CO_2 using an RGO-CoO_x/$BiVO_4$ and Pt/$CuGaS_2$ powder Z-scheme system (Iwase et al. 2016). As shown in Fig. 4.8a, the electron flow through the RGO electron mediator definitely reduces the photogenerated carriers' recombination in the individual photocatalyst

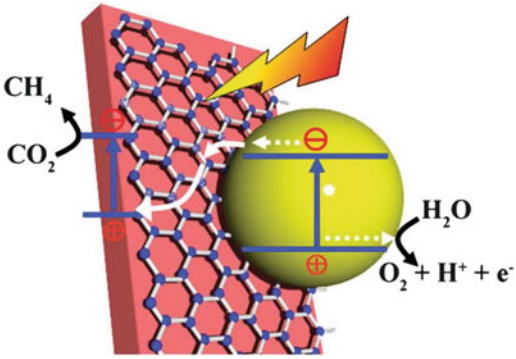

Fig. 4.9 Schematic illustration of photocatalytic conversion of CO_2 into CH_4 over $Fe_2V_4O_{13}$/RGO/CdS Z-scheme system. $Fe_2V_4O_{13}$ E_{CB}, -0.55 eV; E_{VB}, 1.28 eV; CdS E_{CB}, −0.52 eV; E_{VB}, 1.88 eV vs. the normal hydrogen electrode. (Reprinted from Li et al. 2015b with permission of Royal Society of Chemistry)

simultaneously maintaining the superior reduction ability of Pt-loaded metal sulphides and the oxidation ability of RGO-CoO_x/$BiVO_4$. Yet, due to the relatively low reduction ability of $BiVO_4$, the available metal sulphide photocatalysts coupled with CoO_x/$BiVO_4$ to construct the Z-scheme systems are currently limited. In contrast, TiO_2 exhibits a better reduction ability (Fig. 4.8b). Herein, more metal sulphides, such as $CuGaS_2$, $CuInS_2$, Cu_2ZnGeS_4, and Cu_2ZnSnS_4, function well as PS I with TiO_2 and as PS II by an RGO electron mediator (Takayama et al. 2017).

As the aforementioned works demonstrated, most of the reported Z-scheme photocatalysts to date are powder systems. For practical applications, it is desirable to construct an integrated nanosystem of two individual components closely connected by a charge transport unit. From this viewpoint, Zou et al. (Li et al. 2015b) have designed a $Fe_2V_4O_{13}$/RGO/CdS Z-scheme system on a stainless steel mesh for the photoconversion of CO_2 into CH_4. As an interlayer, RGO offers a high-speed charge transfer channel, resulting in the enhancement of the charge separation efficiency and protection of CdS against photocorrosion (Fig. 4.9). A broad solid-solid contact interface between the quasi-two-dimensional $Fe_2V_4O_{13}$ nanoribbon and the RGO nanosheet provided extensive channels for the carrier transfer in the Z-scheme mechanism. This work provided a suggestive model for designing a solid mediator integrated system for the future practical application of the photocatalytic conversion of CO_2 into renewable solar fuels.

In the other type of all-solid-state Z-scheme system, PS I and PS II directly contact with each other forming heterojunction, which is labelled as PS-PS system. Since large amounts of defects can be easily aggregated at the interface, the energy levels of this contact interface are quasi-continuous, which is similar to those of the conductor/semiconductor interface. Therefore, in PS-PS systems, ohmic contact can also be formed, which serves as a combination centre and proceeds by an analogous charger transfer path directly through the junction region instead of the additional electron mediator (Zhou et al. 2014). Various heterostructural composites such as Cu_2O/TiO_2 (Aguirre et al. 2017), α-Fe_2O_3/Cu_2O (Wang et al. 2015), TiO_2/CdS (Tu et al. 2015), WO_3/CdS (Jin et al. 2015), Si/TiO_2 (Liu et al. 2014), $ZnIn_2S_4$/TiO_2 (Yang et al. 2017a), and g-C_3N_4-coupled systems (Di et al. 2017; He et al. 2015b; Li et al. 2015c; Wang et al. 2018) have been demonstrated for successfully

photocatalytic reduction of CO_2 in a manner of direct Z-scheme charge transfer mechanism. For example, in Cu_2O/TiO_2 composite, octahedral Cu_2O covered with fine TiO_2 nanoparticles as shown in Fig. 4.10a, b synthesized by a solvothermal method has been reported recently (Aguirre et al. 2017). The generation rate of CO through the selective photoreduction of CO_2 in the presence of water vapour on the Cu_2O/TiO_2 composite has been demonstrated to be four times greater than that on

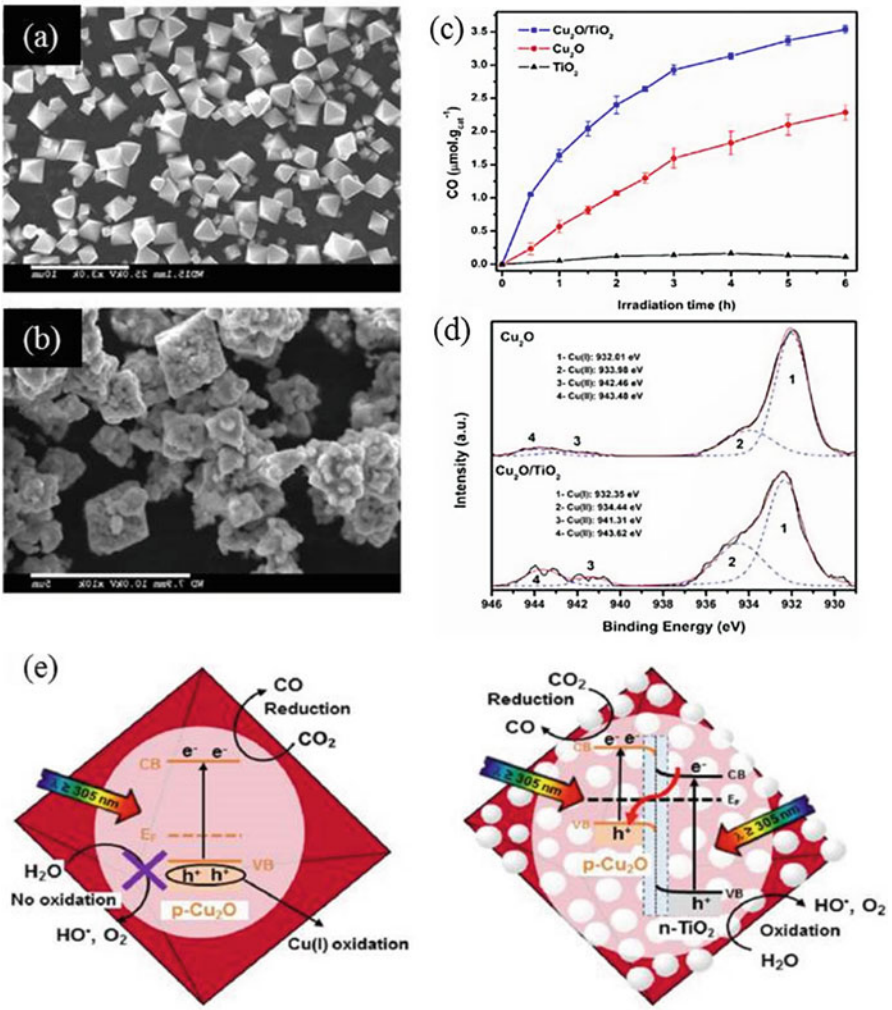

Fig. 4.10 Scanning electron microscope images of Cu_2O (**a**) and Cu_2O/TiO_2 (**b**); (**c**) CO evolution over Cu_2O/TiO_2 heterostructure, Cu_2O and TiO_2 under UV-visible irradiation ($\lambda \geq 305$ nm); (**d**) high-resolution X-ray photoelectron spectra for Cu $2p_{3/2}$; and (**e**) sketch of the proposed mechanism to account for CO_2 reduction induced by UV-visible irradiation ($\lambda \geq 305$ nm) towards pure Cu_2O (left) and Cu_2O/TiO_2 composite (right). (Reprinted from Aguirre et al. 2017 with permission of Elsevier)

pure Cu_2O under identical conditions (Fig. 4.10c). X-ray photoelectron spectra under operation and the formation of HO• radicals in the Cu_2O/TiO_2 system at variance with the results for pure Cu_2O (Fig. 4.10d) unequivocally prove a Z-scheme mechanism as illustrated in Fig. 4.10e. Several heterostructural composites comprising of TiO_2 and other semiconductors have been reported and verified to follow the direct Z-scheme charge transfer mechanism for the photocatalytic conversion of CO_2 (Tu et al. 2015; Liu et al. 2014; Yang et al. 2017a).

Shi et al. (Li et al. 2015c) have reported the highly selective photoreduction of CO_2 to CO over g-C_3N_4/Bi_2WO_6 composites under visible light irradiation, in which a direct Z-scheme charge transfer mechanism has been proposed as a possibility to explain the promoted efficient separation of photogenerated carriers. Similar results of other PS-PS composites were also explained by a direct Z-scheme charge transfer mechanism. Notably, seldom of them have provided consolidate evidence for the transfer behaviour of interfacial charge carriers, which arises arguments or doubts about the authenticity of the proposed charge transfer mechanism and thereby misinterprets the Z-schemes for double-charge transfer. Delightedly, a direct Z-scheme mechanism on some specific composites such as SnO_{2-x}/g-C_3N_4 (He et al. 2015b) and WO_3/CdS (Jin et al. 2015) has been sufficiently verified. Taking SnO_{2-x}/g-C_3N_4 as an example, to discover the origin of the promoted charger transfer, the formed heterojunction structure was first verified to suppress the recombination of the photogenerated electron-hole pairs through photoluminescence spectroscopy, electrochemical impedance spectroscopy, and photocurrent analysis. By detecting the products from the photocatalytic reduction of CO_2 (Fig. 4.11a), a double-charge transfer mechanism was excluded then. To further prove the direct Z-scheme mechanism, a series of radical trapping experiments were performed using

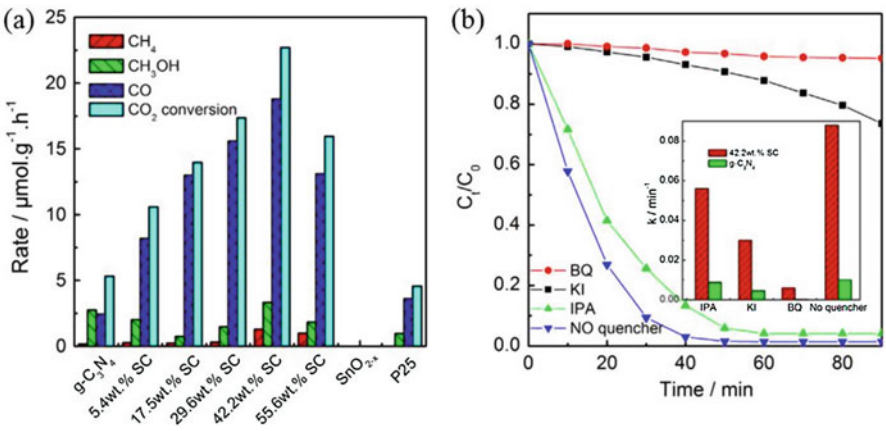

Fig. 4.11 (**a**) Photocatalytic activities of SnO_{2-x}/g-C_3N_4 composites on the photocatalytic reduction of CO_2 under simulated sunlight irradiation; (**b**) Photodegradation of RhB over a 42.2 wt% SnO_{2-x}/g-C_3N_4 photocatalyst with different quenchers ($\lambda > 420$ nm). BQ, KI, and IPA are benzoquinone, potassium iodide, and isopropanol, respectively. (Reprinted from He et al. 2015b with permission of Elsevier)

benzoquinone, potassium iodide, and isopropanol scavengers (Fig. 4.11b). Besides, it should be pointed out that the mass ratio of PS I and PS II is crucial for the photocatalytic activities of the PS-PS Z-scheme system. An optimized value usually exists which is significantly affected by the geometry architectures of the two-component semiconductors.

Generally, when the individual components of the PS-PS system are simultaneously excited, two different charge transfer mechanisms, (i) double-charge transfer mechanism and (ii) direct Z-scheme transfer mechanism, can be envisaged to rationalize the charge transfer across the interface as exemplified above. The double-charge transfer mechanism promotes charge separation at the expense of the decrease in reduction and oxidation abilities of electrons and holes, respectively. Moreover, the excess photogenerated charges in two-component photocatalysts probably lead to the photocorrosion in the absence of a suitable electron donor, for example, Cu_2O and CdS. Instead, in the Z-scheme mechanism, the electrons in the conduction band of PS II transfer across the interface and immediately combine with holes from the valence band of PS I, which apparently provides a way to prevent the photocatalyst from photocorrosion and maintain the high reduction ability of electrons in PS I and oxidation ability of holes in PS II. Both mechanisms have been previously invoked to explain the higher photocatalytic efficiency of the heterostructures in comparison with the individual counterparts; however, the factors favouring one of the two mechanisms remain elusive.

Although the mediator-free Z-scheme heterojunctions provide energetically favourable band alignment to promote the effective separation of photogenerated carriers and subsequent facile migration across the interface in the heterojunction region, the lattice mismatch, surface relaxation, and a number of defect sites at the interface of the heterojunctions may seriously reduce the interfacial transfer of the photogenerated charge carriers at the junction region. Hence, it is essential to introduce a conductive layer at the interface of two semiconductors for promoting excellent interfacial charge transfer during the photocatalytic reaction (Yu et al. 2013; Tada et al. 2006; Xie et al. 2011; Wang et al. 2012).

4.3.3 Semiconductor/Metal-Complex Hybrid Z-Scheme Systems

In addition to the aforementioned progress for the Z-scheme photocatalytic reduction of CO_2, it's worth noting that the novel semiconductor/metal-complex Z-scheme system has become a hot topic currently. A proof-of-concept of the metal-complex/semiconductor Z-scheme for the reduction of CO_2 was demonstrated to yield HCOOH as the main product under visible light using a Ru binuclear complex (RuRu′) containing a photosensitizer and catalytic units and Ag/TaON, but with moderate selectivity (∼60%) (Sekizawa et al. 2013). Recently, Kazuhiko Maeda et al. (Kuriki et al. 2016) have developed a graphitic C_3N_4/Ru binuclear complex (RuRu′) composite photocatalyst for the selective reduction of CO_2 into HCOOH

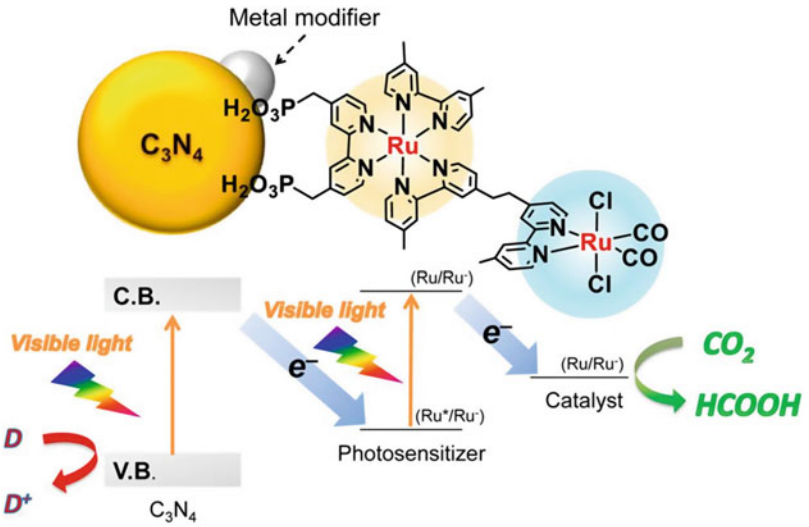

Fig. 4.12 Z-Scheme CO_2 reduction using a hybrid of C_3N_4 and a binuclear Ru complex. (Reprinted from Kuriki et al. 2016 with permission of American Chemical Society)

under visible light. It was found to follow a Z-scheme charge transfer mechanism involving the step-by-step photoexcitation of C_3N_4 and RuRu′. As shown in Fig. 4.12, the photogenerated electrons in the conduction band of C_3N_4 recombine with the photogenerated holes in the valence band of photosensitizer in the molecular metal complex, while the corresponding photogenerated holes in the valence band of C_3N_4 undergo water oxidation and the photogenerated electrons in the conduction band of photosensitizer transfer to the catalytic units in the complex to reduce CO_2. The hybrid photocatalyst reduced CO_2 into HCOOH with a catalytic turnover number greater than 33,000 and a selectivity of 87–99% under optimal conditions with an organic electron donor, which are much greater than those reported for similar metal-complex/semiconductor hybrid systems. Unfortunately, moderate values for the turnover number and selectivity (660% and 80% at most, respectively) are observed for this system during the reduction of CO_2 in aqueous solution (Kuriki et al. 2016).

Therefore, they alter the morphology of C_3N_4 from mesoporous nanoparticles to nanosheets and revealed a unique ability of these C_3N_4 nanosheets strong binding on their surface even in basic aqueous solution, which allowed the reduction of CO_2 using the RuRu′/Ag/NS-C_3N_4 photocatalyst under visible light to obtain HCOOH with a good turnover number (>2000) and high selectivity (>90%) (Kuriki et al. 2017). These values are by far the highest yet reported for a heterogeneous photocatalyst system in an aqueous solution. Notably, a metal complex such as RuRu′ could desorb from the inorganic semiconductor surface under various reaction conditions, such as solution pH, salt additives, and irradiation (Nakada et al. 2016). This loss of a metal complex can become a major factor in the deterioration of the photocatalytic activity of semiconductor/metal-complex hybrid Z-scheme systems.

4.3.4 Light Harvesting of Photocatalysts Utilized for the Z-Scheme CO_2 Reduction

Visible light can be utilized more efficiently in Z-scheme systems compared to conventional one-step systems because the energy required to drive each photocatalyst is reduced. The efficient light harvesting of the photocatalyst can thermodynamically guarantee the generation of charge carriers, while the migration of charge carriers from the bulk to the surface, as well as the subsequent redox reactions, will kinetically affect the overall efficiency of the solar-to-fuel conversion. Meantime, the band structures of semiconductors determine the feasibility of the reduction of CO_2, and the surface state and area, morphology, crystal facet, and phase effects must be considered for the design and fabrication of CO_2 reduction systems (Li et al. 2016a). In this section, we will summarize the development of photocatalysts for Z-scheme CO_2 reduction systems from the perspective of light harvesting.

Most metal oxide photocatalysts consist of metal cations with d^0, e.g. Ti^{4+}, V^{5+}, Mo^{6+}, and W^{+6}, and d^{10}, e.g. In^{3+}, Ga^{3+}, Ge^{4+}, and Sn^{4+}, configurations (Kudo and Miseki 2009). For many years, TiO_2 has been the most widely studied photocatalyst (Sakimoto et al. 2016; Wei et al. 2015; Kuai et al. 2015; Takayama et al. 2017; Aguirre et al. 2017; Tu et al. 2015; Liu et al. 2014; Ohno et al. 2014; Song et al. 2015; Yang et al. 2017a; Sato et al. 2011). However, in most cases, TiO_2 only responds to UV light because of its large band-gap of 3.2 eV. Yang et al. (Yang et al. 2017a) have reported a three-dimensional $ZnIn_2S_4/TiO_2$ Z-scheme system to reduce CO_2 into CH_4. The generation rate of CH_4 using this artificial Z-scheme system is 39 times higher than that using bare $ZnIn_2S_4$ nanosheets. Although the authors have reported that the system exhibits excellent light-harvesting properties, the performance of the system is still limited by the light absorption of TiO_2. Thus, the effective separation of the charge carriers between $ZnIn_2S_4$ and TiO_2 via the direct Z-scheme mechanism is the possible reason for the activity improvement rather than the light harvesting. By loading a manganese phthalocyanine cocatalyst on TiO_2, Sakimoto et al. (2016) have realized the reduction of CO_2 over a tandem TiO_2/CdS Z-scheme (Fig. 4.13). Similarly, the limited light absorption of TiO_2 and CdS likely bottlenecks the solar-to-chemical efficiency of the current system.

Similar to TiO_2, ZnO with a relatively wide band-gap (ca. 3.4 eV) was employed as PS II for the Z-scheme reduction of CO_2 (Yu et al. 2015; Zubair et al. 2017). Notably, the g-C_3N_4/ZnO photocatalytic system exhibits improved light absorption in the visible light range compared to pure g-C_3N_4, resulting from the increased amount of defect states in the g-C_3N_4 phase introduced by the interference of ZnO crystals. The enhancement of light harvesting, in fact, does not originate from ZnO itself. On the contrary, two single-metal oxides, WO_3 and α-Fe_2O_3, are selected as PS II because of their excellent visible light absorption in addition to their oxidation ability. For WO_3, WO_3/Au/In_2S_3 (Li et al. 2016b), WO_3/C_3N_4 (Ohno et al. 2014), and WO_3/CdS (Jin et al. 2015) have been precisely constructed. All the systems exhibit enhanced visible light activity towards the photocatalytic reduction of CO_2 into renewable hydrocarbon fuels in the presence of water vapour or water solution

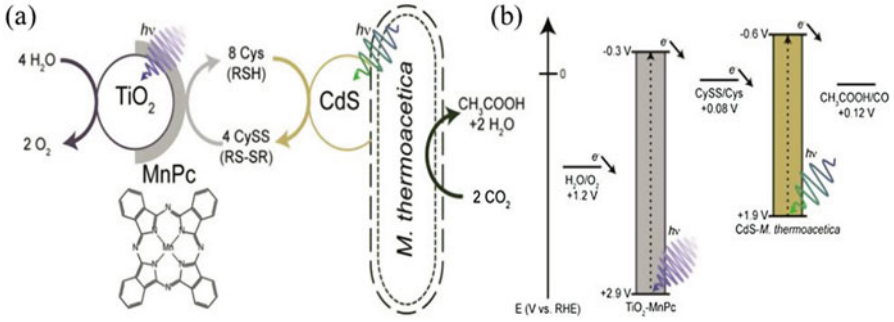

Fig. 4.13 Schematic of the *Moorella thermoacetica*-CdS+TiO_2-MnPc tandem system. (**a**) Illumination of *Moorella thermoacetica*-CdS drives the reduction of CO_2 into acetic acid, which is coupled to the oxidation of Cys to CySS. The co-illumination of TiO_2-MnPc drives the reduction of CySS back into Cys, which is coupled to the oxidation of H_2O to O_2. (**b**) Energy level diagram depicting the relative alignment of the TiO_2 and CdS with the relevant redox reactions. (Reprinted from Sakimoto et al. 2016 with permission of American Chemical Society)

in comparison to single composite in Z-scheme system. α-Fe_2O_3 is a visible-light-driven n-type semiconductor with a band-gap energy of 2.0–2.2 eV. The narrow band-gap in addition to the top of the valence band (2.48 eV) makes α-Fe_2O_3 an excellent PS II candidate for the Z-scheme reduction of CO_2. In the cases of C_3N_4/α-Fe_2O_3 (Wang et al. 2018) and α-Fe_2O_3/Cu_2O (Wang et al. 2015), PS I materials are also visible light responsive semiconductors.

Cuprous oxide is an interesting p-type semiconductor with a considerably more energetic conduction band than that of the commonly used semiconductors with wide band-gap. Another inspiration for developing a Z-scheme system with Cu_2O comes from the photostability problem of Cu_2O, considering that the electron transport in Z-scheme system can effectively address these issues (Kondratenko et al. 2013; Maeda 2013; Wang et al. 2015). These results not only capitalize on the advantages of light harvesting but also prevent these photocatalysts from photocorrosion via the Z-scheme design wherein the accumulation of extra holes can be avoided since they are combined with electrons from the other component semiconductor. Alternative examples of these single-metal oxides in the Z-scheme reduction of CO_2 include MoO_3 (Feng et al. 2017) and SnO_{2-x} (He et al. 2015b), which will be discussed later in the cases of C_3N_4.

In addition, the present oxide-based Z-schemes for the reduction of CO_2 have revealed the applications of multi-metal oxides, including Bi_2WO_6/CdS (Wang et al. 2017a), $BiVO_4$/metal sulphides (Iwase et al. 2016), $Fe_2V_4O_{13}$/CdS (Li et al. 2015b), Bi_2WO_6/g-C_3N_4 (Li et al. 2015c), $ZnFe_2O_4$/TiO_2 (Song et al. 2015), and $SrTiO_3$/InP (Arai et al. 2013). It should be pointed out that in contrast to TiO_2/InP (Sato et al. 2011), $SrTiO_3$/InP sacrificed a sort of light absorption, but a higher solar energy conversion efficiency was obtained because $SrTiO_3$ as a reduction site with a more negative conduction band potential facilitates the electron transfer from the conduction band of PS II to the valence band of the PS I.

Metal sulphides are highly active photocatalysts for water reduction and CO_2 reduction under visible light irradiation even without any assistance of cocatalysts (Hisatomi et al. 2014; Simon et al. 2014; Yan et al. 2009; Moriya et al. 2013; Jiao et al. 2017; Wang et al. 2017b; Kuehnel et al. 2017). The valence band of the metal (oxy)sulphide photocatalysts consists of S 3p and O 2p, resulting in the formation of narrow band-gap and correspondingly utilizing visible light up to 500–600 nm. CdS with a band-gap of 2.4 eV is a well-known metal sulphide photocatalyst. Recently, CdS/TiO_2 (Sakimoto et al. 2016; Wei et al. 2015; Kuai et al. 2015; Tu et al. 2015), CdS/Bi_2WO_6 (Wang et al. 2017a), and CdS/WO_3(Jin et al. 2015) have been reported to be efficient Z-scheme photocatalysts for the reduction of CO_2. By using a gas bubbling-assisted membrane reduction-precipitation method, the core-shell-structured Au@CdS/TiO_2 Z-scheme is favourable for the separation of photogenerated electrons and holes due to the vectorial electron transfer of $TiO_2 \rightarrow Au \rightarrow CdS$, which has been explained in Fig. 4.6 (Wei et al. 2015). Except for this, the high light-harvesting efficiency arising from CdS contributes to the superior photocatalytic performance for the reduction of CO_2. A different core-shell construction of CdS/TiO_2 likewise allows the enrichment of photogenerated electrons on the CdS semiconductor and holes on the TiO_2. As expected, the photocatalytic efficiency of the Z-scheme system exhibits remarkable enhancement compared to those of pure CdS and CdS/TiO_2 (Tu et al. 2015). Instead of applying CdS as PS I, Li et al. (Li et al. 2015b) have reported a Z-scheme system using CdS as PS II. As shown in Fig. 4.9, the photogenerated electrons from the CB of CdS may transfer to RGO and release to the VB of $Fe_2V_4O_{13}$, finally recombining with the existing holes of $Fe_2V_4O_{13}$. The holes remained in CdS oxidize H_2O to O_2, whereas the electrons remained in $Fe_2V_4O_{13}$ reduce CO_2 to CH_4. Notably, the system retains its performance in a long-term run without using any hole scavengers such as S^{2-} and SO_3^{2-} which are supposed to address the drawback of instability for metal sulphide photocatalysts (Kudo and Miseki 2009). The authors attributed it to that the presence of RGO bridged between CdS and $Fe_2V_4O_{13}$ constructing a PS-C-PS Z-scheme system possibly prevents CdS from oxidation by extra holes (Li et al. 2015b).

In_2S_3 (Li et al. 2016b), SnS_2 (Di et al. 2017), $ZnIn_2S_4$ (Yang et al. 2017a), Cu_2ZnSnS_4 (Zubair et al. 2017), and $CuGa_2S_2$ (Iwase et al. 2016; Takayama et al. 2017) further contribute to the development of metal sulphide-based Z-scheme photocatalysts for the reduction of CO_2 into chemical fuels. However, as a typical example, the solid solution of sulphides has not attracted attention in the field. It may provide a chance to realize high solar-to-fuel conversion considering that many sulphide solid solution photocatalysts can utilize visible light with wavelengths of up to ~700 nm (Tong et al. 2011; Nandy et al. 2017; Tsuji et al. 2004).

With the partial or complete substitution of O atoms in a metal oxide by N atoms, the material is expected to exhibit a higher valence band maximum compared with that of the corresponding oxide owing to the higher potential of N 2p orbitals compared to the O 2p orbital, without affecting the conduction band minimum. This hypothesis has also been confirmed in the cases of oxysulphides whose valence bands consist of S 3p and O 2p. Therefore, in comparison to metal oxides photocatalysts, either (oxy)nitrides or (oxy)sulphides may be more interesting

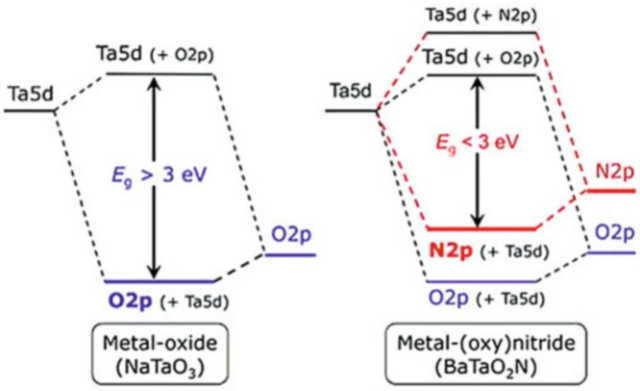

Fig. 4.14 Schematic band structures of a metal oxide ($NaTaO_3$) and metal oxynitride ($BaTaO_2N$) with a perovskite structure. (Reprinted from Maeda and Domen 2007 with permission of American Chemical Society)

compounds for application in Z-scheme water splitting and CO_2 reduction because of their better light-harvesting properties and suitable band edge positions. For instance, as shown in Fig. 4.14, the band-gap is narrowed to respond to visible light with the formation of N 2p orbitals after nitridation, leaving the bottom of the conduction band unchanged (Maeda and Domen 2007). Therefore, in theory, the oxides that exhibit activity for the reduction of CO_2 with H_2O or water reduction can remain the reduction ability after nitridation. However, few successful single (oxy) nitride examples have been reported for overall water splitting or CO_2 reduction. In such situations, (oxy)nitrides have been used to develop Z-scheme system (Muraoka et al. 2016; Yoshitomi et al. 2015; Maeda 2016; Sekizawa et al. 2013). So far, the longest wavelength response for the reduction of CO_2 has been reported over an oxynitride-based Z-scheme system in which YTaON and a Ru binuclear complex can utilize the light up to 580 nm (Muraoka et al. 2016; Maeda 2016).

Since the first report in 2009, g-C_3N_4, a metal-free semiconductor, has become one of the most promising visible light-responsive photocatalysts for water splitting due to its suitable band-gap (ca. 2.7 eV), appropriate band positions (conduction band of ca. −1.1 eV and valence band of ca. 1.6 eV, vs. normal hydrogen electrode), non-toxicity, abundance, and facile fabrication (Wang et al. 2008). g-C_3N_4 was reported to exhibit a thermodynamic ability for the overall water splitting and a high solar-to-hydrogen efficiency close to the theoretical value of 6% (Liu et al. 2015). Furthermore, because of the presence of abundant surface groups and the ability to exhibit negative charge when it is dispersed in water, g-C_3N_4 is an ideal supporting material for depositing or coupling with other photocatalysts (Yang et al. 2017b). Therefore, g-C_3N_4 can be used as PS I, e.g. g-C_3N_4/BiOBr (Bai et al. 2016b), g-C_3N_4/Ag_3PO_4 (He et al. 2015a), g-C_3N_4/SnS_2 (Di et al. 2017), g-C_3N_4/MO_3 (Feng et al. 2017), g-C_3N_4/SnO_{2-x} (He et al. 2015b), g-C_3N_4/WO_3 (Ohno et al. 2014), g-C_3N_4/α-Fe_2O_3 (Wang et al. 2018), and g-C_3N_4/ZnO (Yang et al. 2017a), or PS II, e.g. g-C_3N_4/$Bi_4O_5I_2$ (Bai et al. 2016a), g-C_3N_4/BiOI (Wang et al. 2016),

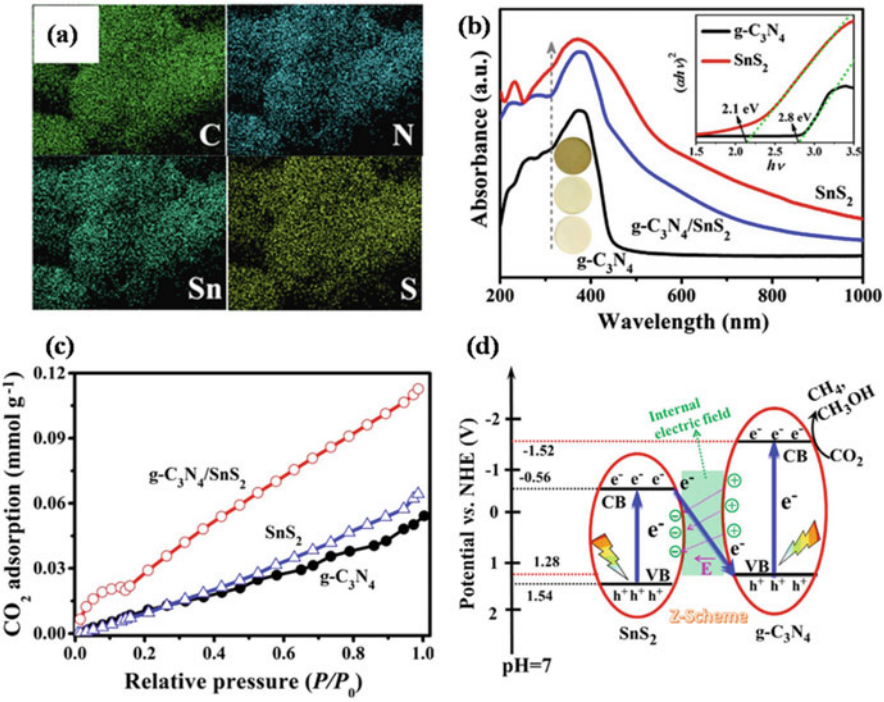

Fig. 4.15 (**a**) Elemental mapping images of C, N, Sn, and S of a typical g-C_3N_4/SnS_2 sample; (**b**) UV-visible diffuse reflectance spectra and the corresponding optical pictures of g-C_3N_4, g-C_3N_4/SnS_2, and SnS_2; (**c**) CO_2 adsorption isotherms of g-C_3N_4, g-C_3N_4/SnS_2, and SnS_2 samples; and (**d**) Z-scheme charge transfer mechanism for g-C_3N_4/SnS_2 in the photocatalytic reduction of CO_2. (Reprinted from Di et al. 2017 with permission of Elsevier)

g-C_3N_4/Bi_2WO_6 (Li et al. 2015c), and g-C_3N_4/Ru binuclear complex (Kuriki et al. 2017), in Z-scheme configurations for the reduction of CO_2.

As shown in Fig. 4.15, a C_3N_4/SnS_2 Z-scheme system was constructed by the in situ deposition of SnS_2 quantum dots on the g-C_3N_4 surface via a simple one-step hydrothermal method (Di et al. 2017). SEM and elemental mapping images (Fig. 4.15a) have revealed the uniform coating of SnS_2 quantum dots on g-C_3N_4. The appearance colour and optical UV-visible diffuse reflectance spectrum (Fig. 4.15b) exhibited the visible light response of the samples. Importantly, the g-C_3N_4/SnS_2 composite showed a considerably higher CO_2 adsorption capacity (Fig. 4.15c), which is related to the anchoring of amine groups on g-C_3N_4 surface during the hydrothermal reaction, wherein L-cysteine served as the sulphur source and meanwhile provided the amine groups, which have been widely employed to increase the CO_2 adsorption capacity of the material owing to their alkalinity (Xing et al. 2012). This characteristic for CO_2 adsorption as well as the merit from the Z-scheme cycle (Fig. 4.15d) leads to the increased photocatalytic efficiency, yielding CH_3OH and CH_4 from CO_2.

In 2013, Ishitani's group first reported a supermolecular metal complex as PS I in Z-scheme system for the reduction of CO_2 (Sekizawa et al. 2013). This development allows the conversion of light energy of less than 500 nm into chemical energy using TaON as PS II for CH_3OH oxidation. Afterwards, different PS II semiconductors, including C_3N_4 (Kuriki et al. 2016, 2017), $CaTaO_2N$ (Yoshitomi et al. 2015; Maeda 2016), and YTaON (Muraoka et al. 2016; Maeda 2016), have been employed to couple with such complex. Very recently, Maeda et al. (Kuriki et al. 2017) have found that C_3N_4 nanosheets undergo robust binding with a RuRu′ complex even without distinct chemical bonding, which expanded the possible applications of functional metal complexes.

Bismuth oxyhalides (BiOX, X = Cl, Br, I) have been widely used as a new branch of photocatalysts due to their intensive visible light absorption ability with appropriate band-gap and their layered structure (Ye et al. 2014). Wang et al. (Wang et al. 2016) have designed Z-scheme photocatalysts using BiOI as PS I for the reduction of CO_2 under visible light irradiation ($\lambda > 400$ nm). However, Bai et al. (2016b) have hypothesized that BiOX usually does not exhibit effective photocatalytic reduction activity under neutral conditions due to the lower position of the conduction band minimum. Thus, a g-C_3N_4/BiOBr Z-scheme system is constructed by utilizing BiOBr as a PS II photocatalyst (Bai et al. 2016b). Theoretical calculations indicated that the position of the conduction band of BiOX is mainly dependent on the Bi 6p (Huang 2009). The adjustment of the bismuth content is possibly feasible for promoting the conduction band position of BiOX. For this reason, Bai et al. (2016a) have prepared bismuth-rich $Bi_xO_yX_z$ composite photocatalysts as PS I for constructing a Z-scheme system for CO_2 reduction. This work not only enhanced the photocatalytic CO_2 conversion under visible light but also provided a method to use bismuth oxyhalides as reduction sites in Z-schemes.

According to the previous reports, different kinds of semiconductors have been attempted in the Z-scheme reduction of CO_2. However, compared with those applied in Z-scheme water splitting, neither the long wavelength response nor photocatalytic conversion is satisfactory as a result of inadequate attempts for existing potential photocatalysts. On the other hand, in most cases, only reduction products were obtained, while the oxidation products were missing to present. Note that PS I and PS II harvest photons of different wavelength but reduce CO_2 and oxidize H_2O, respectively, with a quantum yield close to unity. Therefore, it is essential to show both reduction and oxidation yields to demonstrate the Z-scheme mechanism in these studies.

4.3.5 Cocatalyst Strategies for Z-Scheme CO_2 Reduction

As schematically illustrated in Figs. 4.1 and 4.4 in Sect. 4.2, the photocatalytic reduction of CO_2 with H_2O can be divided into three main steps: (i) the photocatalyst absorbs photon energy greater than its band-gap energy and generates photogenerated electron-hole pairs in the bulk, (ii) the photogenerated carriers

separate and migrate to the surface without recombination, and (iii) the electrons and holes that reach the surface reduce CO_2 and oxidize H_2O, respectively. The first two steps are strongly dependent on the structural and electronic properties of the photocatalyst, while the third step can be promoted by cocatalysts (Maeda 2013; Yang et al. 2013). In general, cocatalysts play four important roles: (i) boosting charge separation/transfer, (ii) improving the activity and selectivity for the reduction of CO_2, (iii) enhancing the stability of photocatalysts, and (iv) suppressing side- or backward reactions (Maeda 2013; Chen et al. 2017). Specifically, loading cocatalyst was found to improve the durability of the Z-scheme cycle (Ohno et al. 2012). However, thus far, only a few studies have reported the Z-scheme reduction of CO_2 with the cocatalysts.

Sato et al. (2011) have reported the Z-scheme photoelectrochemical reduction of CO_2 over p-type InP/Ru complex polymer combining with TiO_2 which is cocatalysed by Pt for water oxidation. In this work, the Pt cocatalyst significantly facilitates O_2 production from H_2O_2 originated from H_2O. Sakimoto et al (2016) have developed a biomimetic approach based on the tandem Z-scheme design, in which photoreduction and photooxidation are carried out by two separate light harvesters and cocatalysts using a biocompatible CySS/Cys redox couple. The TiO_2 nanoparticle loaded with a manganese phthalocyanine cocatalyst denoted as MnPc is used to reduce CySS back into Cys, rendering the formerly sacrificial reductant into a regenerative redox couple. It was found that CySS reduction rate of MnPc-loaded TiO_2 photocatalysts is strongly correlated to the type and amount of the cocatalyst (Table 4.2). The combination of *Moorella thermoacetica*-CdS + bare TiO_2 yielded more acetic acid than that obtained using only *Moorella thermoacetica* but less than that obtained using TiO_2-MnPc, indicative of the catalytic action of MnPc for the selective reduction of CySS, leading to a more effective regenerative redox couple and longer sustained acetic acid photosynthesis.

A hybrid g-C_3N_4/WO_3 has been demonstrated as an efficient Z-scheme photocatalyst system once the g-C_3N_4 was loaded with Au or Ag (Ohno et al. 2014). Au or Ag particles

Table 4.2 CySS reduction rate of phthalocyanine-loaded TiO_2 photocatalysts

Catalyst	Rate (μM Cys h^{-1})
No catalyst	53.0 ± 9.3
MnPc (0.1 wt%)[a]	65.9 ± 4.6
MnPc (0.05 wt%)[a]	130.1 ± 8.4
MnPc (0.01 wt%)[a]	75.9 ± 3.3
FePc[b]	61.9 ± 4.5
CoPc[b]	56.4 ± 2.2
NiPc[b]	87.7 ± 18.7
CuPc[b]	68.7 ± 5.8
ZnPc[b]	45.2 ± 5.7
H2Pc[b]	75.5 ± 12.8

Sakimoto et al. (2016)
[a]Catalyst loading relative to the mass of TiO_2
[b]Equimolar to 0.05 wt% MnPc. The standard deviation represents error associated with linear regression of kinetic data

as cocatalysts were loaded only on g-C_3N_4 of the prepared hybrid photocatalysts by photodeposition because g-C_3N_4 serves as a reduction photocatalyst for the reduction of CO_2, whereas water oxidation as a counterreaction possibly proceeds on WO_3. The amount of CH_3OH generated by the reduction of CO_2 exhibited a volcano-like relationship with the amount of the loaded cocatalyst. The optimum amount of loaded Au or Ag for CH_3OH generation was 0.5 wt%, respectively. Increase in the generation of CH_3OH by CO_2 reduction was presumably due to the prevention of recombination and/or improvement of selectivity for the reduction of CO_2 via the capture of electrons on metal particles because the reduction of protons to hydrogen usually competes with the reduction of CO_2. Decrease in the generation of CH_3OH with an excess amount of the cocatalyst may be attributed to the decreased dispersibility and increased particle size of the cocatalyst.

Recently, Kudo's group has reported a Z-scheme reduction of CO_2 under visible light irradiation by the combination of metal sulphides as a CO_2-reducing photocatalyst, RGO electron mediator, and a visible-light-driven CoO_x-loaded $BiVO_4$ as an O_2-evolving photocatalyst (Iwase et al. 2016). The role of the CoO_x cocatalyst in the developed Z-scheme system was investigated and determined to be the key factor that regulates the overall activities. Meantime, the authors have also investigated the water splitting performance by applying a Pt cocatalyst on $CuGaS_2$. Because a Pt cocatalyst does not work as active sites for the photocatalytic reduction of CO_2, pristine $CuGaS_2$ is used for the reduction of CO_2. On the contrary, some cocatalyst strategies from water splitting have also been demonstrated to be effective in the reduction of CO_2. In other words, the cocatalyst strategies for water splitting can be used as a reference for the Z-scheme reduction of CO_2. Although cocatalysts also play important roles in the selectivity improvement of CO_2 reduction, the stability enhancement of photocatalysts, and suppression of backward reactions over single-component photocatalyst, there is no relative study in Z-scheme systems.

4.4 Summary and Outlook

The photocatalytic conversion of CO_2 to chemical fuels using semiconductor photocatalysts is totally a "one stone kills two birds" strategy in terms of reducing global warming and producing sustainable energy. This chapter descriptively presented the basic mechanism for the Z-scheme CO_2 reduction from the point of view of the thermodynamic and kinetic requirements. Different constructions of Z-scheme systems for the photocatalytic reduction of CO_2 including shuttle redox-mediated systems, all-solid-state systems, and semiconductor/metal-complex hybrid systems are reviewed. They exhibit the obvious differences in the preparation methodology, working mechanism, and applications. The all-solid-state Z-scheme systems avoid the acceptor/donor pair involved backward reactions which are common issues in the shuttle redox mediator systems. Besides, the electron transfer path in the former is shorter than that in the latter, which probably can decrease the bulk electron-hole recombination. Moreover, the latter systems can only work in liquid-phase, while the all-solid-state systems can work in the gas-phase and liquid-

phase environments. Thus, the all-solid-state systems have been widely used in CO_2 reduction. In addition, the development of the photocatalysts from the perspective of light-harvesting and cocatalyst strategies is summarized and discussed. Since the first report of Z-scheme research on CO_2 reduction, 7 years passed during which only less than 40 scientific papers have been published. Fortunately, it can be seen that visible-light-driven Z-scheme CO_2 reduction was accomplished. The key factors governing the reaction have also attracted wide attention. Nevertheless, the stability, light harvesting, redox ability, charge separation, and transportation of the existing Z-scheme systems for the photocatalytic reduction of CO_2 are far from fulfilling the requirements of practical applications and need to be further investigated. The following aspects are suggested for the future study in this area.

First, it is crucial to explore more active photocatalysts that effectively work in half-reactions with a considerable light harvesting. Given that the two semiconductors in the Z-scheme system undergo reduction and oxidation reaction, respectively, it is possible to apply an existing photocatalyst that has demonstrated the potential for half-reaction. For water splitting, the solar-to-hydrogen conversion efficiency for the photocatalytic system is expected to reach ~10% for H_2 production for the process to be cost-competitive to conventional industrial processes (Pinaud et al. 2013). Hence, it is impossible for a photocatalyst with an absorption edge around 500 nm to meet this goal, even with an apparent quantum yield of 100%. For this reason, likewise in CO_2 reduction, employment of photocatalysts with an adsorption edge of greater than 600 nm is a necessity. On the other hand, some representative photocatalysts only respond to UV light but exhibit superior properties, such as $SrTiO_3$ and TiO_2, and could be taken full advantages of them to construct Z-scheme. Furthermore, the findings obtained with the use of loaded cocatalysts in water splitting and CO_2 reduction in single-component photocatalysts could be used as a reference for Z-scheme CO_2 reduction. Alternatively, integrated sensitizers, supermolecular complex with facet-dependent or one-dimensional structure, should be a promising strategy, whereby both light harvesting and efficient charge separation can be obtained through preferential light absorption and carrier transport.

Second, the Z-scheme mechanism is suggested to be addressed adequately and reliably in the future. The authors have observed that some investigations provide insufficient control experiments and structural characterization to support the Z-scheme cycles, which are probably assigned to heterostructures or coupled semiconductors. Particularly, both oxidation and reduction products should be shown to verify the yield from the two separate but dependent reactions in the Z-scheme close to unity. Otherwise, the investigation is not complete and the conclusion lacks a scientific basis. Based on the fact, new construction strategies and fabrications methodologies can be adopted. As an example, in all-solid-state Z-scheme, the introduction of a hierarchical coaxial structure may further facilitate the targeted transfer of photogenerated carriers.

In summary, new advanced materials, structures, and mechanisms in other fields are needed to be considered for application in this study. Breakthrough discoveries may stem from the collaboration in a broad range of research areas. The authors truly believe it will contribute to address the global energy and environmental issues in the future through the incessant efforts of scientists in related fields.

Acknowledgements This work was supported by the National Key Research and Development Program (2016YFB0700205), National Natural Science Foundation of China (U1632273 and 11205159), and Hefei Center for Physical Science and Technology (2016FXZY002).

References

Abe R, Sayama K, Sugihara H (2005) J Phys Chem B 109:16052. https://doi.org/10.1021/jp052848l

Abe R, Shinmei K, Koumura N, Hara K, Ohtani B (2013) J Am Chem Soc 135:16872. https://doi.org/10.1021/ja4048637

Aguirre ME, Zhou R, Eugene AJ, Guzman MI, Grela MA (2017) Appl Catal B Environ 217:485. https://doi.org/10.1016/j.apcatb.2017.05.058

Arai T, Sato S, Kajino T, Morikawa T (2013) Energy Environ Sci 6:1274. https://doi.org/10.1039/c3ee24317f

Bai Y, Ye L, Wang L, Shi X, Wang P, Bai W, Wong PK (2016a) Appl Catal B Environ 194:98. https://doi.org/10.1016/j.apcatb.2016.04.052

Bai Y, Chen T, Wang P, Wang L, Ye L, Shi X, Bai W (2016b) Sol Energy Mater Sol Cells 157:406. https://doi.org/10.1016/j.solmat.2016.07.001

Bard JA (1979) J Photochem 10:59. https://doi.org/10.1016/0047-2670(79)80037-4

Barton EE, Rampulla DM, Bocarsly AB (2008) J Am Chem Soc 130:6342. https://doi.org/10.1021/ja0776327

Byun KE, Chung HJ, Lee J, Yang H, Song HJ, Heo J, Seo DH, Park S, Hwang SW, Yoo I, Kim K (2013) Nano Lett 13:4001. https://doi.org/10.1021/nl402367y

Chen S, Takata T, Domen K (2017) Nat Rev Mater 2:17050. https://doi.org/10.1038/natrevmats.2017.50

Di T, Zhu B, Cheng B, Yu J, Xu J (2017) J Catal 352:532. https://doi.org/10.1016/j.jcat.2017.06.006

Ding X, Liow CH, Zhang M, Huang R, Li C, Shen H, Liu M, Zou Y, Gao N, Zhang Z, Li Y, Wang Q, Li S, Jiang J (2014) J Am Chem Soc 136:15684. https://doi.org/10.1021/ja508641z

Feng Z, Zeng L, Chen Y, Ma Y, Zhao C, Jin R, Lu Y, Wu Y, He Y (2017) J Mater Res 32:3660. https://doi.org/10.1557/jmr.2017.271

Habisreutinger SN, Schmidt-Mende L, Stolarczyk JK (2013) Angew Chem Int Ed Eng 52:7372. https://doi.org/10.1002/anie.201207199

He Y, Zhang L, Teng B, Fan M (2015a) Environ Sci Technol 49:649. https://doi.org/10.1021/es5046309

He Y, Zhang L, Fan M, Wang X, Walbridge ML, Nong Q, Wu Y, Zhao L (2015b) Sol Energy Mater Sol Cells 137:175. https://doi.org/10.1016/j.solmat.2015.01.037

Hiroshi Inoue HM, Maeda K, Yoneyama H (1995) J Photochem Photobiol A Chem 86:191. https://doi.org/10.1016/1010-6030(94)03936-o

Hisatomi T, Kubota J, Domen K (2014) Chem Soc Rev 43:7520. https://doi.org/10.1039/c3cs60378d

Huang WL (2009) J Comput Chem 30:1882. https://doi.org/10.1002/jcc.21191

Hurst TF, Cockerill TT, Florin NH (2012) Energy Environ Sci 5:7132. https://doi.org/10.1039/c2ee21204h

Indrakanti VP, Kubicki JD, Schobert HH (2009) Energy Environ Sci 2:745. https://doi.org/10.1039/b822176f

Inoue T, Fujishima A, Konishi S, Honda K (1979) Nature 277:637. https://doi.org/10.1038/277637a0

IPCC (2007) Climate change 2007, contribution of working group 2 to the fourth assessment. https://doi.org/10.2134/jeq2008.0015br

Iwase A, Yoshino S, Takayama T, Ng YH, Amal R, Kudo A (2016) J Am Chem Soc 138:10260. https://doi.org/10.1021/jacs.6b05304

Jiao X, Li X, Jin X, Sun Y, Xu J, Liang L, Ju H, Zhu J, Pan Y, Yan W, Lin Y, Xie Y (2017) J Am Chem Soc 139:18044. https://doi.org/10.1021/jacs.7b10287
Jin J, Yu J, Guo D, Cui C, Ho W (2015) Small 11:5262. https://doi.org/10.1002/smll.201500926
Khatib H (2012) Energy Policy 48:737. https://doi.org/10.1016/j.enpol.2012.06.007
Kochuveedu ST, Jang YH, Kim DH (2013) Chem Soc Rev 42:8467. https://doi.org/10.1039/c3cs60043b
Kondratenko EV, Mul G, Baltrusaitis J, Larrazábal GO, Pérez-Ramírez J (2013) Energy Environ Sci 6:3112. https://doi.org/10.1039/c3ee41272e
Kuai L, Zhou Y, Tu W, Li P, Li H, Xu Q, Tang L, Wang X, Xiao M, Zou Z (2015) RSC Adv 5:88409. https://doi.org/10.1039/c5ra14374h
Kudo A (2011) MRS Bull 36:32. https://doi.org/10.1557/mrs.2010.3
Kudo A, Miseki Y (2009) Chem Soc Rev 38:253. https://doi.org/10.1039/b800489g
Kuehnel MF, Orchard KL, Dalle KE, Reisner E (2017) J Am Chem Soc 139:7217. https://doi.org/10.1021/jacs.7b00369
Kuriki R, Matsunaga H, Nakashima T, Wada K, Yamakata A, Ishitani O, Maeda K (2016) J Am Chem Soc 138:5159. https://doi.org/10.1021/jacs.6b01997
Kuriki R, Yamamoto M, Higuchi K, Yamamoto Y, Akatsuka M, Lu D, Yagi S, Yoshida T, Ishitani O, Maeda K (2017) Angew Chem Int Ed Eng 56:4867. https://doi.org/10.1002/anie.201701627
Li H, Gan S, Wang H, Han D, Niu L (2015a) Adv Mater 27:6906. https://doi.org/10.1002/adma.201502755
Li P, Zhou Y, Li H, Xu Q, Meng X, Wang X, Xiao M, Zou Z (2015b) Chem Commun (Camb) 51:800. https://doi.org/10.1039/c4cc08744e
Li M, Zhang L, Fan X, Zhou Y, Wu M, Shi J (2015c) J Mater Chem A 3:5189. https://doi.org/10.1039/c4ta06295g
Li K, Peng B, Peng T (2016a) ACS Catal 6:7485. https://doi.org/10.1021/acscatal.6b02089
Li H, Gao Y, Zhou Y, Fan F, Han Q, Xu Q, Wang X, Xiao M, Li C, Zou Z (2016b) Nano Lett 16:5547. https://doi.org/10.1021/acs.nanolett.6b02094
Liu Y, Ji G, Dastageer MA, Zhu L, Wang J, Zhang B, Chang X, Gondal MA (2014) RSC Adv 4:56961. https://doi.org/10.1039/c4ra10670a
Liu J, L Y, Liu N, Han Y, Zhang X, Huang H, Lifshitz Y, Lee S, Zhong J, Kang Z (2015) Science 347:970. https://doi.org/10.1126/science.aaa3145
Maeda K (2013) ACS Catal 3:1486. https://doi.org/10.1021/cs4002089
Maeda K (2016) Proc SPIE 9935:99350J. https://doi.org/10.1117/12.2258625
Maeda K, Domen K (2007) J Phys Chem C 111:7851. https://doi.org/10.1021/jp070911w
Moriya M, Minegishi T, Kumagai H, Katayama M, Kubota J, Domen K (2013) J Am Chem Soc 135:3733. https://doi.org/10.1021/ja312653y
Muraoka K, Kumagai H, Eguchi M, Ishitani O, Maeda K (2016) Chem Commun (Camb) 52:7886. https://doi.org/10.1039/c6cc03627a
Nakada A, Nakashima T, Sekizawa K, Maeda K, Ishitani O (2016) Chem Sci 7:4364. https://doi.org/10.1039/c6sc00586a
Nandy S, Goto Y, Hisatomi T, Moriya Y, Minegishi T, Katayama M, Domen K (2017) ChemPhotoChem 1:265. https://doi.org/10.1002/cptc.201700005
Ohno T, Bai L, Hisatomi T, Maeda K, Domen K (2012) J Am Chem Soc 134:8254. https://doi.org/10.1021/ja302479f
Ohno T, Murakami N, Koyanagi T, Yang Y (2014) J CO2 Utilization 6:17. https://doi.org/10.1016/j.jcou.2014.02.002
Ou F, Buchholz DB, Yi F, Liu B, Hseih C, Chang RP, Ho ST (2011) ACS Appl Mater Interfaces 3:1341. https://doi.org/10.1021/am2001357
Ozin GA (2015) Energy Environ Sci 8:1682. https://doi.org/10.1039/c5ee00907c
Pinaud BA, Benck JD, Seitz LC, Forman AJ, Chen Z, Deutsch TG, James BD, Baum KN, Baum GN, Ardo S, Wang H, Miller E, Jaramillo TF (2013) Energy Environ Sci 6:1983. https://doi.org/10.1039/c3ee40831k

Sakimoto KK, Zhang SJ, Yang P (2016) Nano Lett 16:5883. https://doi.org/10.1021/acs.nanolett.6b02740
Sasaki Y, Iwase A, Kato H, Kudo A (2008) J Catal 259:133. https://doi.org/10.1016/j.jcat.2008.07.017
Sasaki Y, Kato H, Kudo A (2013) J Am Chem Soc 135:5441. https://doi.org/10.1021/ja400238r
Sato S, Arai T, Morikawa T, Uemura K, Suzuki TM, Tanaka H, Kajino T (2011) J Am Chem Soc 133:15240. https://doi.org/10.1021/ja204881d
Sayama K, Abe R, Arakawa H, Sugihara H (2006) Catal Commun 7:96. https://doi.org/10.1016/j.catcom.2005.09.008
Sekizawa K, Maeda K, Domen K, Koike K, Ishitani O (2013) J Am Chem Soc 135:4596. https://doi.org/10.1021/ja311541a
Simon T, Bouchonville N, Berr MJ, Vaneski A, Adrovic A, Volbers D, Wyrwich R, Doblinger M, Susha AS, Rogach AL, Jackel F, Stolarczyk JK, Feldmann J (2014) Nat Mater 13:1013. https://doi.org/10.1038/nmat4049
Song G, Xin F, Yin X (2015) J Colloid Interface Sci 442:60. https://doi.org/10.1016/j.jcis.2014.11.039
Tada H, Mitsui T, Kiyonaga T, Akita T, Tanaka K (2006) Nat Mater 5:782. https://doi.org/10.1038/nmat1734
Tahir B, Tahir M, Amin NAS (2017) Appl Surf Sci 419:875. https://doi.org/10.1016/j.apsusc.2017.05.117
Takayama T, Sato K, Fujimura T, Kojima Y, Iwase A, Kudo A (2017) Faraday Discuss 198:397. https://doi.org/10.1039/c6fd00215c
Tong H, Ouyang S, Bi Y, Umezawa N, Oshikiri M, Ye J (2011) Adv Mater 24:229. https://doi.org/10.1002/adma.201102752
Tsuji I, Kato H, Kobayashi H, Kudo A (2004) J Am Chem Soc 126:13406. https://doi.org/10.1021/ja048296m
Tu W, Zhou Y, Zou Z (2014) Adv Mater 26:4607. https://doi.org/10.1002/adma.201400087
Tu W, Zhou Y, Feng S, Xu Q, Li P, Wang X, Xiao M, Zou Z (2015) Chem Commun (Camb) 51:13354. https://doi.org/10.1039/c5cc03905c
Wang X, Maeda K, Thomas A, Takanabe K, Xin G, Carlsson JM, Domen K, Antonietti M (2008) Nat Mater 8:76. https://doi.org/10.1038/nmat2317
Wang X, Liu G, Wang L, Chen Z-G, Lu GQM, Cheng H-M (2012) Adv Energy Mater 2:42. https://doi.org/10.1002/aenm.201100528
Wang JC, Zhang L, Fang WX, Ren J, Li YY, Yao HC, Wang JS, Li ZJ (2015) ACS Appl Mater Interfaces 7:8631. https://doi.org/10.1021/acsami.5b00822
Wang JC, Yao HC, Fan ZY, Zhang L, Wang JS, Zang SQ, Li ZJ (2016) ACS Appl Mater Interfaces 8:3765. https://doi.org/10.1021/acsami.5b09901
Wang M, Han Q, Li L, Tang L, Li H, Zhou Y, Zou Z (2017a) Nanotechnology 28:274002. https://doi.org/10.1088/1361-6528/aa6bb5
Wang S, Guan BY, Lu Y, Lou XWD (2017b) J Am Chem Soc 139:17305. https://doi.org/10.1021/jacs.7b10733
Wang J, Qin C, Wang H, Chu M, Zada A, Zhang X, Li J, Raziq F, Qu Y, Jing L (2018) Appl Catal B Environ 221:459. https://doi.org/10.1016/j.apcatb.2017.09.042
Wei Y, Jiao J, Zhao Z, Liu J, Li J, Jiang G, Wang Y, Duan A (2015) Appl Catal B Environ 179:422. https://doi.org/10.1016/j.apcatb.2015.05.041
White JL, Baruch MF, Pander Iii JE, Hu Y, Fortmeyer IC, Park JE, Zhang T, Liao K, Gu J, Yan Y, Shaw TW, Abelev E, Bocarsly AB (2015) Chem Rev 115:12888. https://doi.org/10.1021/acs.chemrev.5b00370
Xiang Q, Yu J, Jaroniec M (2012) Chem Soc Rev 41:782. https://doi.org/10.1039/c1cs15172j
Xie K, Wu Q, Wang Y, Guo W, Wang M, Sun L, Lin C (2011) Electrochem Commun 13:1469. https://doi.org/10.1016/j.elecom.2011.09.023
Xie G, Zhang K, Guo B, Liu Q, Fang L, Gong JR (2013) Adv Mater 25:3820. https://doi.org/10.1002/adma.201301207

Xie S, Zhang Q, Liu G, Wang Y (2016) Chem Commun (Camb) 52:35. https://doi.org/10.1039/c6cc00590j
Xing W, Liu C, Zhou Z, Zhang L, Zhou J, Zhuo S, Yan Z, Gao H, Wang G, Qiao SZ (2012) Energy Environ Sci 5:7323. https://doi.org/10.1039/c2ee21653a
Yan H, Yang J, Ma G, Wu G, Zong X, Lei Z, Shi J, Li C (2009) J Catal 266:165. https://doi.org/10.1016/j.jcat.2009.06.024
Yang J, Wang D, Han H, Li C (2013) Acc Chem Res 46:1900. https://doi.org/10.1021/ar300227e
Yang G, Chen D, Ding H, Feng J, Zhang JZ, Zhu Y, Hamid S, Bahnemann DW (2017a) Appl Catal B Environ 219:611. https://doi.org/10.1016/j.apcatb.2017.08.016
Yang Y, Wang S, Li Y, Wang J, Wang L (2017b) Chem Asian J 12:1421. https://doi.org/10.1002/asia.201700540
Ye L, Su Y, Jin X, Xie H, Zhang C (2014) Environ Sci Nano 1:90. https://doi.org/10.1039/c3en00098b
Yoshitomi F, Sekizawa K, Maeda K, Ishitani O (2015) ACS Appl Mater Interfaces 7:13092. https://doi.org/10.1021/acsami.5b03509
Yu ZB, Xie YP, Liu G, Lu GQ, Ma XL, Cheng H-M (2013) J Mater Chem A 1:2773. https://doi.org/10.1039/c3ta01476b
Yu J, Low J, Xiao W, Zhou P, Jaroniec M (2014) J Am Chem Soc 136:8839. https://doi.org/10.1021/ja5044787
Yu W, Xu D, Peng T (2015) J Mater Chem A 3:19936. https://doi.org/10.1039/c5ta05503b
Zhang XV, Martin ST, Friend CM, Schoonen MAA, Holland HD (2004) J Am Chem Soc 126:11247. https://doi.org/10.1021/ja0476415
Zhang H, Fan X, Quan X, Chen S, Yu H (2011) Environ Sci Technol 45:5731. https://doi.org/10.1021/es2002919
Zhou P, Yu J, Jaroniec M (2014) Adv Mater 26:4920. https://doi.org/10.1002/adma.201400288
Zubair M, Razzaq A, Grimes CA, In S-I (2017) J CO2 Utilization 20:301. https://doi.org/10.1016/j.jcou.2017.05.021

Chapter 5
Photocatalysts for Artificial Photosynthesis

Busra Balli, Buse Demirkan, Betul Sen, and Fatih Sen

Contents

Abstract By the help of the novel nanocomposites and nanoparticles, photocatalysis for artificial photosynthesis is an important area of application due to the problems related to global warming and the renewed interest in the development of non-fossil fuel sources of energy. Thus, there has been a resurgence of research into the electrochemical and photochemical reaction and conversion into energy-rich products. Addressed herein, the importance of photocatalysts and their applications for artificial photosynthesis in our daily life has been stressed out for human beings. Further, the properties of photocatalysts as a result of nanoscale are also discussed here. Besides, the primary photosynthetic systems applications of photocatalysts, supramolecular artificial photosynthetic systems, covalently linked molecular systems**;** general photosynthesis mechanism are also pointed out here in detail.

B. Balli · B. Demirkan · B. Sen · F. Sen (✉)
Sen Research Group, Biochemistry Department, Faculty of Arts and Science, Dumlupınar University, Kütahya, Turkey
e-mail: fatih.sen@dpu.edu.tr

Inamuddin et al. (eds.), *Nanophotocatalysis and Environmental Applications*,
Environmental Chemistry for a Sustainable World 31,
https://doi.org/10.1007/978-3-030-04949-2_5

Keywords Artificial photosynthesis · Porphyrin · Subphthalocyanines · BODIPY · Porphyrins/naphthalocyanines

5.1 Introduction

Though still disputable, scientific studies suggest that the greenhouse effect or global warming is directly associated with the burning of fossil fuels that leads to an increase in the concentration of carbon dioxide in the atmosphere. Fossil fuels have been the primary source of cheap energy for the industrial development since the nineteenth century. Notwithstanding the debate on the association between global warming and the use of fossil fuels, the fact remains that these sources are limited. So the question is when, not if, fossil fuels will run out, and according to some pessimistic scenarios, it will be sooner than we would hope for. This is mainly a big challenge for developed and developing countries, which will have to make a paradigm shift in the way in which they produce and consume energy.

This situation will, of course, have social, political, and economic repercussions as well. The Kyoto Protocol on global warming demands that countries reduce their greenhouse gas emissions significantly. However, not all countries are willing to take the necessary steps to make that happen. This reluctance indicates that the much-needed paradigm shift in energy production and consumption cannot be achieved only by using the excellent responsibility card. Nanomaterials offer very promising solutions to the ongoing problems of the world (Sen et al. 2013a, b, 2014a, b). Fuel cell (Eris et al. 2018a, b, c) catalyst materials (Sen et al. 2017a, b), thermopower applications (Abrahamson et al. 2013), capacitors (Chen and Dai 2013), solar cells (Demir et al. 2017a, b), and sensors (Bozkurt et al. 2017; Baskaya et al. 2017a, b; Sen et al. 2018; Giraldo et al. 2014) are some examples of these solutions. Materials used as nanoparticles (Sahin et al. 2017; Goksu et al. 2016a, b, c; Akocak et al. 2017; Erken et al. 2016a, b; Sahin et al. 2018) or composite materials combine the superior properties of different molecules and different materials (Ayranci et al. 2017a, b; Dasdelen et al. 2017; Celik et al. 2016a, b, c, d; Karatepe et al. 2016). Composite materials are widely studied in developing appropriate materials for electronic applications such as conductive polymers and other electronically active materials. Graphene and graphene oxide (Yildiz et al. 2017a, b; Sen et al. 2016; Akocak et al. 2017; Goksu et al. 2016a, b, c; Demirci et al. 2016), carbon nanotubes (CNTs) (Sen et al. 2015; Yildiz et al. 2016a, b, c, d, e; Goksu et al. 2016a, b, c), activated carbon (AC) (Erken et al. 2015), vulcanized carbon (VC) (Yildiz et al. 2016a, b, c, d, e; Eris et al. 2018a, b, c), carbon black (Baskaya et al. 2017a, b), and graphene-derived materials which have different structure and morphologies as reduced graphene oxide (Esirden et al. 2015; Goksu et al. 2016a, b, c; Aday et al. 2016; Yildiz et al. 2017a, b; Eris et al. 2018a, b, c), graphene nanosheets, graphene nanoribbons, and graphene nanoplatelets may be thought as active materials in different applications.

Economic arguments should also bring skeptics and economical hardliners to reason, and societal and technical modifications should be compensated by the invention and manufacturing of new products. Nevertheless, these economic arguments and the difficulty of restorative initiatives and financing of solutions will diversify with time.

Artificial or bioengineered photosynthesis is one feasible solution to the challenges introduced by global warming. The idea behind this is imitating the natural processes of energy production and reintroducing it with advancement in science and technology. One of the concepts is making use of the light and dark to produce energy and biopolymers. This solution involves the use of solar energy and may result in analog systems to (i) produce clean energy, (ii) to produce photohydrogen, (iii) to manufacture carbon products, and (iv) to capture carbon dioxide. These artificial photosynthetic systems can be of capital importance for reducing greenhouse gaseous emissions and water requirements and for decreasing and even breaking our dependence on fossil fuels (Collings and Critchley 2005).

Recently, artificial photosynthesis has magnetized much attention from scientific and technological perspectives. Researchers have desired to disclose the rudimental principle of photosynthetic energy and electron transfer processes in nature. Currently, artificial photosynthesis has become of more significant interest due to scientific and technological reasons. Studies have been conducted to reveal the elementary laws of photosynthetic energy and electron transfer. Functional problems regarding artificial photosynthesis are building photonic microscopic instruments, which belong to the fields of nanoscience and nanotechnology. Photocatalysts and organic solar cells that mimic photosynthesis are likely to help us eliminate global and climate issues. Various researchers have, therefore, turned their attention to artificial photosynthesis. Photosynthesis is the most complex nanoscale natural phenomenon (Deisenhofer and Norris 1993; Blankenship et al. 1995). It converts light energy into chemical energy that fuels all living organisms. The basis of photosynthesis is an avalanche of photon energy and electron transfer among donors and acceptors in light-harvesting complexes and reaction center (Blankenship et al. 1995).

Artificial photosynthesis aims to imitate plants and photoautotrophs using solar energy to produce high-energy chemicals (Balzani et al. 1987; Gust and Moore 1999; Balzani et al. 2003). This is a difficult task as achievement calls for a combination of numerous synthetic activities in a steady chemical system. Therefore, the improvement in artificial photosynthesis technology has become slower than that in other technological fields (Alstrum-Acevedo et al. 2005).

5.2 General Photosynthesis Mechanism

Natural photosynthesis involves organisms converting solar energy using systematized bodies of photofunctional chromophores and catalysts within proteins supplying categorically arranged media for chemical reactions. Mimicking natural

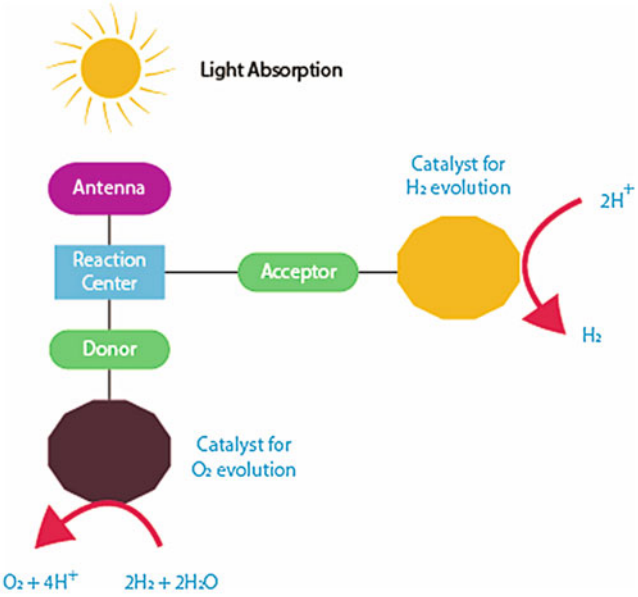

Fig. 5.1 Schematic representation of artificial photosynthesis

photosynthesis, artificial photosynthetic systems should also accumulate solar energy, create separate charges, and transfer them to substrates. Though promising efforts have been exerted on every phase of this complicated process, scientists are yet to construct autonomous components and categorically arranged media to achieve a self-reliant artificial system. A schematic representation of an artificial photosynthesis mechanism is shown in Fig. 5.1.

The elaborate molecular structure of natural photosynthesis is not only a lesson to be learned about the challenges of developing state-of-the-art technology but also a source of inspiration (Britt 1996; Wheeler 2004; Danks et al. 1985). If achieved, artificial photosynthesis could bypass the evolutionary process that has produced perfectly functioning photosynthetic membranes. Employing chemical structures and the laws of chemistry and physics, the aim of artificial photosynthesis is more manageable and less ambitious. Photosynthesis by higher green plants involves utilizing complex reaction mechanisms to convert water into oxygen and reducing equivalents as nicotinamide adenine dinucleotide phosphate. Photosystem I employs lowering equivalents in nicotinamide adenine dinucleotide phosphate to reduce carbon dioxide to carbohydrates (Eq. 5.1). Bacteria also utilize reducing equivalents directly as a reductive energy source (Britt 1996; Wheeler 2004; Danks et al. 1985). Artificial photosynthesis aims to use solar energy to achieve high-energy small-molecule reactions such as water splitting (Eq. 5.2) or carbon dioxide reduction (Eq. 5.3).

$$6H_2O + 6CO_2 + 48h\nu \rightarrow C_6H_{12}O_6 + 6O_2 \quad (5.1)$$

$$2H_2O + 4h\nu \rightarrow 2H_2 + O_2 \quad (5.2)$$

$$2H_2O + 2CO_2 + 4h\nu \rightarrow 2HCOOH + O_2 \quad (5.3)$$

There are two main approaches in this area of study. One of these approaches focuses on porphyrins and metalloporphyrins as chromophores and their inclusion into molecular assemblies (Gust et al. 1993, 2001; Gust and Moore 1999). The second approach addresses metal-to-ligand charge transfer to excited states of metal polypyridyl complexes. These two approaches adopt the same fundamental physical laws and precise molecular assembly designs (Alstrum-Acevedo et al. 2005).

5.3 Covalently Linked Molecular Systems for Artificial Photosynthesis

5.3.1 Porphyrin-Based Donor-Acceptor Molecular Systems

Porphyrins compose a pervasive class of naturally occurring biomolecules. They vigorously incorporate the visible spectrum and resist change under the light; they have combined structures widely and can moderate photon-electron conversion (Panda et al. 2012; Tsuda and Osuka 2001; Kim 2012; Urban et al. 2014). Therefore, researchers have comprehensively examined covalently linked porphyrin-based systems as artificial photosynthetic systems. To establish these effective photosynthetic designs, electron-donating porphyrins were incorporated with different electron acceptors, one of which is fullerene C_{60}. It is widely used since it has a 3-D scheme, numerous photoreduction processes, and limited rearrangement energy that speeds up polarization and slows down back energy transfer (Nierengarten 2014; Fukuzumi et al. 2001; Imahori et al. 2003).

Artificial photosynthetic systems include that the artificial reaction centers include the photogenerated electron transfer. The first report published addressed dyad 1 and developed various norms (Liddell et al. 1994). Utilizing the laser photolysis methods, the research on H_2P-C_{60} indicated the facilitation of dyad 1a to yield ^1H_2P*-C_{60} followed by singlet-singlet energy transformation to yield H_2P-1C60*, which, in turn, had a commonly useful intersystem crossing to populate H_2P-$3C_{60}$*. The performance of 1a in polar benzonitrile had various properties in which electron transfer occurred at the singlet state of H_2P to electron accepting C_{60} yielding the polarization state H_2P •+-C_{60} •− (Liddell et al. 1994). The corresponding dyad 1b in toluene and benzonitrile is subjected to electron transfer (kCS = 1011 s^{-1}) to yield the polarization state ZnP•+-C_{60} •−. Variations in the energy of light of dyads 1a and 1b were justified with regard to powers of different moderators (Liddell et al. 1994; El-Khouly et al. 2017).

When we look at the most up-to-date studies in this area, it is seen a successful and arresting progress that Pan and co-workers (2018) investigate the porphyrin dyes with dithieno[3,2-b:2,3-d] pyrrole for enhanced photosynthetic systems, and they synthesized different dyes with modified dithieno[3,2-b:2,3-d] pyrrole. They reported that the dithieno[3,2-b:2,3-d] pyrrole unit broadly included in the solar cell gadgets has demonstrated to be a promising and capable electron donor for manufacturing porphyrin-based dye-sensitized solar cells. Three novel porphyrin photosensitizers JY47–49 developed from dithieno[3,2-b:2,3-d] pyrrole donor, porphyrin bridge, and benzoic acceptor all appear exceedingly productive photoelectric change capability. In comparison with the reference molecule YD2−o−C8, benefitting from the progressed Jsc by supplanting the diphenylamine giver with dithieno [3,2-b:2,3-d] pyrrole, colors JY47 and JY48 both donate higher gadget proficiency even though their open circuit potential values somewhat diminish. Dye JY48 primarily based−device has eventually great photocatalytic efficiency of 8.44% (Voc: 717 mV; Jsc: 18.43 mA cm^{-2}; electrolyte: I2/I3 – couple). Also, broadening the conjugation system with other acetylene group outcomes in JY49 a substantially reduced Voc and a comparable photocatalytic efficiency of YD2-o-C8. So the dithieno[3,2-b:2,3-d] pyrrole unit can be used to develop different dyes for highly efficient dye-sensitized solar cells not only as a good π-spacer but also as a promising donor (Pan et al. 2018).

5.3.2 Subphthalocyanine-Based Light-Harvesting Complexes

Among numerous porphyrinoids used as an antenna, subphthalocyanines (SubPcs) have currently attracted particular interest due to their unique properties such as their π electrons and cone-shaped aromatic surfaces. These unique properties make subphthalocyanines exceptional from the similar materials (Claessens et al. 2002; Kietaibl 1974; Rauschnabel and Hanack 1995; Kuninobu et al. 1996; del Rey et al. 1998; Aminur Rahman et al. 2009; El-Khouly et al. 2006, 2010, 2012a, b; Verrett et al. 2011; Luhman and Holmes 2011; Shimizu et al. 2011; Gonzalez-Rodríguez et al. 2009; Solntsev et al. 2012; Gonzalez Rodríguez and Bottari 2009; Brothers 2008; Torres 2006; Sastre et al. 1996). Because of the versatile chemical structures of subphthalocyanines (Claessens et al. 2002), they can be performed by the help of various ways such as peripheral (del Rey and Torres 1997) and/or axial (Kietaibl 1974; Rauschnabel and Hanack 1995; Kuninobu et al. 1996). The axial way is more superior compared to the peripheral one because of the electronic properties of cycles and the substitution patterns. They have a particular interest in the redox reactions as compared to the other structures. So, subphthalocyanines can be used as electron accepting or donating group and antennas (Geyer et al. 1996; Romero-Nieto et al. 2011, 2012; Gonzalez-Rodríguez et al. 2002, 2006; El-Khouly et al. 2008, 2009; Kim et al. 2008; El-Khouly 2010).

El-Khouly and co-workers worked on artificial photosynthesis with the help of subphthalocyanine ferrocenophane and subphthalocyanine naphthalene diimide

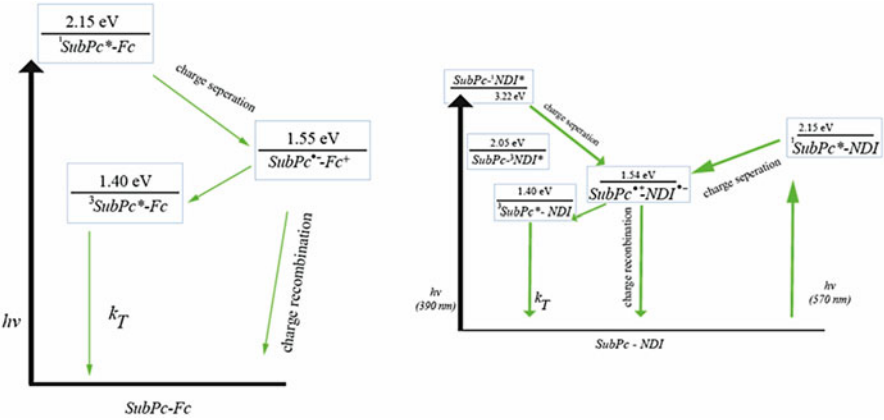

Fig. 5.2 Energy level diagrams of photochemical properties of dyads by indicating the photoinduced intramolecular events of the molecules

dyads (El-Khouly et al. 2012a, b, c). The energy level diagrams in Fig. 5.2 summarize the photochemical properties of dyads by indicating the photoinduced intramolecular events of the materials in the current figure schematically.

5.3.3 BODIPY-Based Light-Harvesting Systems

These days, 4,4-difluoro-4-bora-3a,4a-diaza-s-indacene – otherwise called BODIPY – is at the bleeding edge of fluorophores for life sciences. Without a doubt, its high brightness and its tunable excitation and emission wavelengths alongside its high synthetic and photochemical steadiness draw the enthusiasm of specialists increasingly. In the most recent decade, scientific experts have exploited the variability of the union of BODIPY to configuration-refined items like simulated photosynthesis-based sunlight-based cells.

It is a very likely issue that synthesis and photophysical investigations of porphyrin e4,4-difluoro-4-bora-3a,4a-diaza-s-indacene (BODIPY) compounds linked either with different covalent bonds or with axial coordination to metalloporphyrin. BODIPY moiety considerably increases the light absorption capability of porphyrins by using efficient BODIPY to porphyrin excitation electricity transfer. The energy transfer efficiency is dramatically affected by the type of linkage between two chromophores. The most efficient energy transfer was indicated for compounds linked via a cyanuric chloride bridge (~99% quenching). Accordingly, this type of bond seems to be a more appropriate choice in constructing porphyrin BODIPY assemblies for light-harvesting applications.

Furthermore, the functionalization of the conjugates with fullerenes appears to be exciting electron transfer dynamics in the excited state. As demonstrated in various

studies (Mao et al. 2015; Liao et al. 2015, 2016; Zhao et al. 2015; Cabrera-Espinoza et al. 2018; Ladomenou et al. 2017), covalently or noncovalently linked dimeric and trimeric porphyrin BODIPY moieties were examined, regarding the impact of different linkages in the energy transfer efficiency. In all reported cases herein, BODIPY acts as an energy donor, transferring energy to porphyrin, because the singlet state energy level of the BODIPY is higher compared to the porphyrin. It was verified that the linkages, namely, (1) cyanuric chloride bridge, (2) amino group, (3) ethynyl bridge, and (4) metal coordination, strongly affect the efficiency in the energy transfer process (Kim et al. 2010).

Some recent studies have shown that some derivatives of BODIPY-based dyes such as isoxazoline(60)fullerene and pyrrolidine(60)fullerene (Cabrera-Espinoza et al. 2018) electron-withdrawing BODIPY motif as the central core, and several types of electron-donating segments, including thiophene, bithiophene, fluorene, and carbazole, flanked at its 2,6 positions as terminal groups (Liao et al. 2016), are useful for organic solar cells. In the study of Espinoza et al. (Cabrera-Espinoza et al. 2018), it is reported that the BODIPY-C_{60} systems built using with 2,6-dialkoxyphenylethynyl- BODIPY as the central unit and C_{60} as acceptor, in which a pyrrolidine (B2-Pyr) and isoxazoline ring (B2-Is) were employed as linker between the two electroactive groups, revealed several exciting features. First, based on their photophysical and electrochemical properties, the new B2-Is derivative showed a better electron affinity compared to B2-Pyr and C_{60}. As a result of extended π-conjugation and strong electronic interactions between the alkoxyphenylethynyl substituents and BODIPY core, these systems offered better spectral capture covering a broad spectral portion. Strong electronic interactions between BODIPY core and C_{60} fragments take place in the excited states of the two derivatives. Electrochemical and theoretical studies helped in evaluating redox potentials of different entities of the BODIPY-C_{60} systems, suggesting the existence of electron transfer from BODIPY group to a C_{60} moiety.

In another study (Liao et al. 2016), developed some organic dyes based on BODIPY that electron-withdrawing BODIPY motif as the central core, and several types of electron-donating segments, including thiophene, bithiophene, fluorene, and carbazole, flanked at its 2,6-positions as terminal groups. They reported that the organic solar cell used one of these dyes reached 2.15% power conversion efficiency value. Also, BODIPY-backboned polymers are used as electron donor in bulk heterojunction solar cells (Kim et al. 2010)

5.4 Supramolecular Artificial Photosynthetic Systems

Despite the fact that molecular bond donor-acceptor systems have perfect base and higher energy state features including considerable longevity of polarized states, they are primarily distinguished from natural systems, particularly regarding transfer between donor and acceptor in which photo- and redox non-innocent components in bacterial photosynthetic reaction centers are organized by non-molecular bond

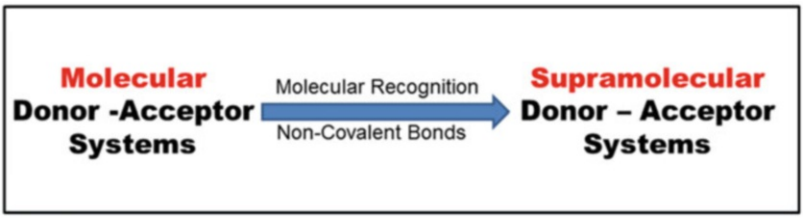

Fig. 5.3 Supramolecular system mechanism

interactions into a protein matrix (Chitta 2002). Essentially, non-molecular bonds ensure regulation over the harmonization of the composition and therefore offer the opportunity to manage precise and rigorous forms which possess great directionality and discrimination (El-Khouly et al. 2014; D'Souza and Ito 2012; Lehn 1990; KC and D'Souza 2016; Lehn 1993). Therefore, investigation of non-ionically linked electron donor-acceptor systems is on the rise for building systems to mimic natural photosynthetic processes. Currently, many non-ionically supramolecular systems have been constructed and combined by using various forms of binding in order to mimic living organisms and to comprehend the central notion behind photogenerated energy transformation and electron transfer reactions in antenna-reaction centers by using the way seen in Fig. 5.3 (El-Khouly et al. 2014; D'Souza and Ito 2012; Lehn 1990, 1993; KC and D'souza 2016).

5.4.1 Metal-Ligand Interactions of Porphyrins/ Naphthalocyanines with Electron Acceptors

Porphyrins possess remarkably adjustable photochemical and electrochemical processes and are likely to be able to construct complexes (Panda et al. 2012; Tsuda and Osuka 2001; Ding et al. 2016). Some research has been performed on porphyrins with ionically linked axial ligands being designed mixtures to figure out the workings of different reduction-oxidation reactions (Chitta 2002; D'Souza and Ito 2012). Various research has pointed out the presence of five steady metallophthalocyanine overlayers, therefore, imitating the operating regions of different hemoproteins where axial ligands are supplied to the heme through the "R" groups of the protein. Various studies have addressed the notion of penta-coordination of porphyrins to design artificial photosynthetic systems (Chitta 2002; D'Souza and Ito 2012). The supramolecular assembly approach based on coordination compounds is primarily directed by the metal-ligand affinities, stereochemistry, and substitution properties of the complexes involved.

A more significant part of the metals from the periodic table is equipped for framing metal buildings with tetrapyrroles of square planar geometry, for example, porphyrins and phthalocyanines. In a few cases, the focal metal molecule in these

buildings is coordinatively unsaturated accordingly showing their desire for extra maybe a couple of ligands. Frequently, a second molecular entity (energy or electron acceptor/donor) is functionalized with an N-ligand and permitted to tie to some metal tetrapyrrole buildings. This metal-ligand axial interaction gives directly to high stability for the following supramolecular light energy harvesting systems (KC and D'Souza 2016).

Porphyrins are employed as building blocks efficiently in artificial photosynthetic systems due to their being excellent donors as well as sensitizers in the visible light region (Guldi 2000). Manufactured photosynthetic systems use porphyrins as foundations, as they are perfect donors and antennas in the visible spectrum. They are employed together with buckyballs as electron acceptors to construct antenna compounds and polarization instruments (Guldi 2000; Ohkubo and Fukuzumi 2009; El-Khouly et al. 2004). Because of their exclusive electrochemical and photophysical properties, buckyballs are considered perfect acceptors, because they are capable of reversibly accept six electrons at most in the lowest unoccupied molecular orbitals and have limited inner and solvent restructuring energies. This is crucial for electron transfer to come up with a permanent polarized state with high quantum yield. Zero-dimensional nanoarchitectures function as nano-scaffolds to build stratified donor-acceptor nanocomposites. Porphyrins and buckyballs are three-dimensionally converted into noncovalent compounds by utilizing dendrimers (Hasobe et al. 2004; Hosomizu et al. 2007), oligomers (Hasobe et al. 2005, 2007), and nano- and microparticles. Imahori et al. manufactured three-dimensional donor-acceptor noncovalent compounds by combining buckyballs in the void spaces between porphyrin moieties bound to zero-dimensional nanoarchitectures by alkanethiolate chains (Imahori et al. 2005a, b, 2006a, b, 2006a, b). These composite assemblies have carbon nanotube intake and discharge bands because p compound construction between the porphyrins and buckyball ensures useful polarization at the donor-acceptor interface. The related solar cells exhibit conversion ability by about 1.5%. To bring directional transfer features to composite core-shell architectures, semiconducting nanocolumns that are commonly utilized in photovoltaics thanks to their exclusive charge carrier features are promising entities as nanoscaffolds (Sagawa et al. 2010; Shah et al. 2012).

Some porphyrin-based donor-acceptor binds have recently been built and employed to work on the tracks of electron transfer in which the layout of different components was perpendicular to the porphyrin plane. The aluminum porphyrin in this study was one of a kind and synthetically superior because it introduced a reaction site on both faces of the porphyrin plane. The equatorial monovalent group on one side of Al(III) porphyrin plane built anionic ester or amide bond, while Lewis bases built a metal-ligand equatorial bond on another side of the plane. The superiority over the composition of the compound is that the donor and acceptor sides of the compound are on opposite faces of the porphyrin, which curtails the carrier recombination. Furthermore, the higher energy state π^* orbital of porphyrin and

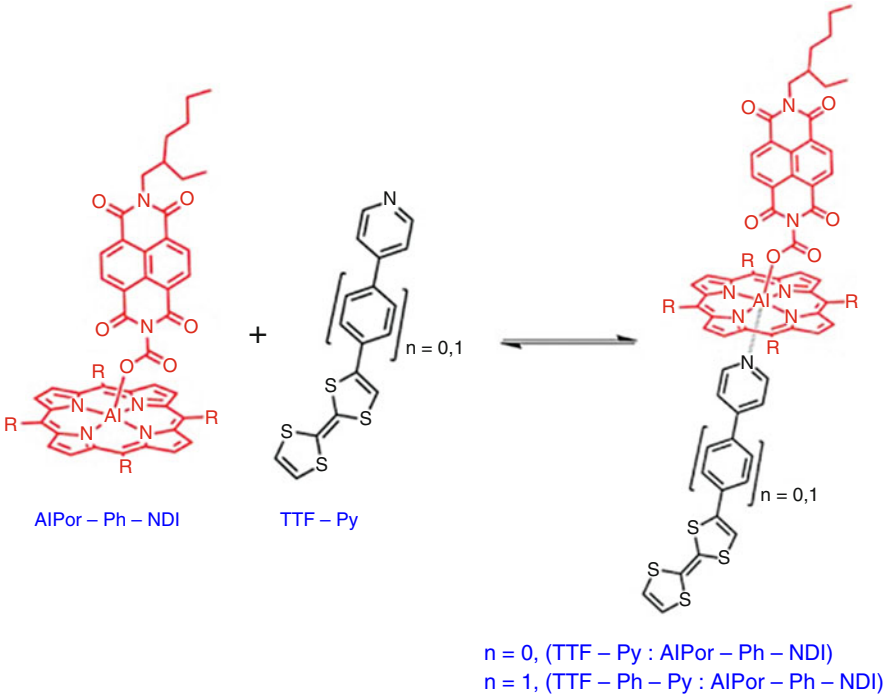

Fig. 5.4 Structure of TTF: AlPor-NDI supramolecular triad

centrically harmonized ligand is in the same space. This leads to an escalation in the charge transfer integral which promotes electron transfer. Puddotoori et al. brought together noncovalent donor-acceptor systems comprising Al(III)Por with centrally bounded naphthalene diimide and tetrathiafulvalene as acceptor and donor as seen in Fig. 5.4, respectively (KC and D'Souza 2016; Lehn 1993; Ding et al. 2016; Guldi 2000; Ohkubo and Fukuzumi 2009; El-Khouly et al. 2004; Hasobe et al. 2004, 2005, 2007; Hosomizu et al. 2007; Imahori et al. 2005a, b, 2006a, b; Sagawa et al. 2010; Shah et al. 2012; Poddutoori et al. 2013).

Building novel artificial photosynthetic systems that can gather and use light from visible and low photon energy range is a difficult task. To achieve it, recently the scientists have focused on building nonionic models based on phthalocyanine chromophores. Figure 5.5 shows a more comprehensive antiaromatic system from heterocyclic macrocycle organic to aromatic macrocyclic compounds. Macrocycles provide a change in transmission minima to longer wavelengths, leading to light harvesting which is more compatible with the optical spectrum of the sun. To sensitize the range of wavelengths from 700 to 900 nm, a benzannulation is brought into phthalocyanine rings, leading to derivatives of phthalocyanine (Kobayashi 2002). Derivatives of phthalocyanine appear to be good molecular building blocks for the artificial photosynthetic systems since they are chemically and thermally more stable and contain more iodide. Also, they can compose coordination

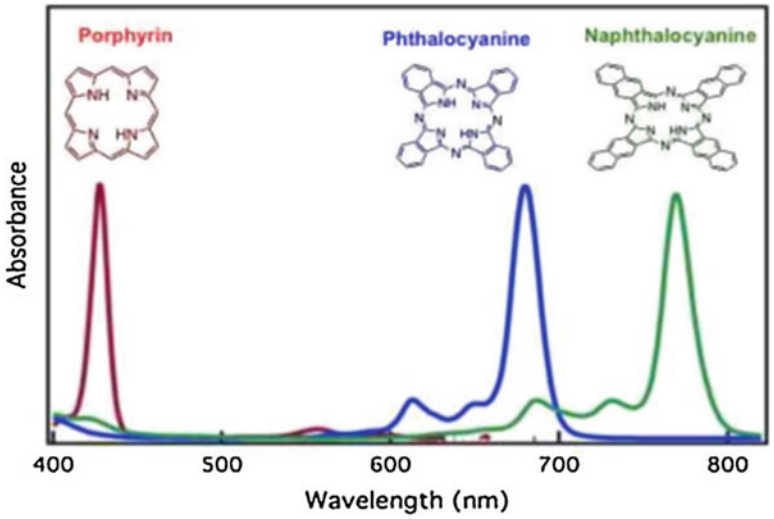

Fig. 5.5 Absorption spectra of porphyrin derivatives, phthalocyanines, and naphthalocyanine

compounds with nearly all metal ions and semi-insulators if adequately brought together by van der Waals interactions (Takeda et al. 2013; Ishii 2012; Macor et al. 2009).

5.4.2 Supramolecular Photosynthetic Complexes Via Crown Ether-Ammonium Cation Interactions

Crown ethers have been considered to be an active group for selective binding to cationic, anionic, and also neural analyst (Deetz et al. 2000; Datta et al. 2004; Mazik et al. 2006) since Pederson developed them (Pederson 1967). Benzo 18-crown-6 has become of particular interest because it composes H-bonding complexes with quaternary alkyl ammonium cations easily (Izzat et al. 1985). Because of its significance, non-ionically linked DASs are consistently investigated to imitate the natural photosynthetic ARC. Studies on metal-ligand coordination are performed only in readily displaced ligands. Therefore, different from the metal-ligand coordination, CEAC binding mode enables scientists to research various media. CEAC binding mode was employed by D'Souza et al. to construct a photosynthetic triad 51 to imitate the artificial reaction center non-ionically. To do this, BODIPY was first ionically joined with a viologen layer with a benzo-18-crown-6 host segment at the opposite end of the porphyrin ring. Second, an ammonium functionalized fullerene was employed to form an organized structure through ion-induced dipole interactions to construct a relatively steady nonionic triad 51 in polar benzonitrile. Studies indicated the presence of energy transmission from antenna BODIPY to the energy

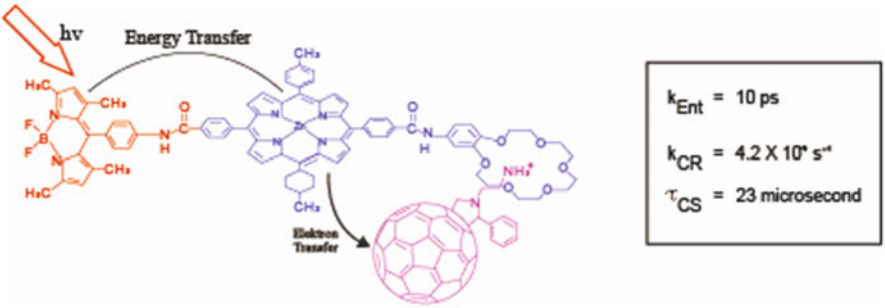

Fig. 5.6 Charge stabilization in the nonionic triad

acceptor zinc porphyrin with a quantum efficiency of ~97%. Afterward, polarization occurred from ^{1}ZnP* to the linked C_{60}, through CEAC interactions to populate a nondurable polarized state. Formation of a triplet polarized state of 23 s was observed, pointing out charge stabilization in the nonionic triad as seen in Fig. 5.6 (El-Khouly et al. 2017; Maligaspe et al. 2009).

Self-assembly with an ammonium ion-crown ether interaction is a robust technique as it provides the great course with energy levels of 100 kJ/mol and more. F. D/Souza, O. Ito et al. stated that the SWNT-ZnP donor-acceptor nanocomposites were assembled by employing ammonium ion-crown ether binding, which is a favorable technique to construct SWNTs bearing donor-acceptor nanocomposites and are instrumental in converting light into energy and applications of photovoltaic (D'Souza et al. 2007).

Noncovalent assembly of boron dipyrrin, zinc porphyrin, and buckyball has been one of the most promising techniques to construct antenna-reaction center models, in which excitation of BDP leads to effective photoinduced electron transfer to ZnP. An electron transfer originates from ZnP to construct ZnP+–C60 radical ion pair. This plan was applied to action constructed compound (D'Souza et al. 2004; Maligaspe et al. 2009, 2010) 1 and 2 and used metal-ligand equatorial coordination technique to bond imidazole buckyball to ZnP of the ionically bounded BDP-ZnP dyads which have approximately four BDP entities (D'Souza et al. 2004; Maligaspe et al. 2010). In model 3, the crown ether-alkyl cation binding technique was used to bring together buckyball with ZnP-BDP dyad (Maligaspe et al. 2009). In these models, the donor and acceptor were located close to each other to promote subsequent energy and electron transfer procedures. Even though electron relay was detected, a stable electron relay state was hard to achieve. In this study, we have deliberately put the antenna unit between zinc porphyrin and buckyball to enhance the gap between them. Taking photo and redox into account, this combination could turn BDP not only into an energy donor but also into a primary electron acceptor from the excited ZnP. In this way, the semiquinone BDP could go through an electrorepulsion to the buckyball or give rise to the construction of higher energy triplet state buckyball where further electron transfer can occur. The eventual consequence of this could be

segregating ZnP+ and C60 species, which is necessary for forming durable polarized species.

This novel concept has been verified in the study conducted by Francis D'Souza et al. by synthesizing and assembling supramolecular triad 4 (D'Souza et al. 2011).

Recently, Zhu et al. reported a new approach for the establishment of donor-acceptor (Si-TCP)n-Ph$C_{60}NH^{3+}$ arrays on indium tin oxide electrode to using as a photoelectrochemical cell. For establishing of new arrays, a Si-O-Si framework-mediated stepwise self-assembly of TCP maintained the vertical growth of porphyrin chains on the indium tin oxide electrode. Then, the fulleropyrrolidine appended with an alkylammonium chain (Ph$C_{60}NH^{3+}$) was self-assembled via crown-ether-alkyl ammonium binding to produce the donor-acceptor arrays. It is engrossing that the (Si-TCP)n-Ph$C_{60}NH^{3+}$ arrays show significantly enhanced photocurrent generation when irradiated with light, and it can be generated reversibly without any decline in the on-off ratio. The enhancement of photocurrent in this supramolecular donor-acceptor conjugate system is found appropriate for potential applications in opto-electronics and light-harvesting systems. This study opened an interesting opportunity for the fabrication of high photocurrent conversion cells through a combination of molecular design and a simple solution processing (Zhu et al. 2018).

5.5 Conclusion

Monetary and ecological elements in recent years have pushed an enthusiasm toward the advancement of scalable technologies to enhance the share of renewable sources into energy portfolio of the world. Artificial photosynthesis systems can simultaneously capture and store the solar energy in the form of fuel. So they are a promising alternative for other fuel types. Photoelectrochemical cell-based systems can use low energy density reactants such as water and carbon dioxide and transform them via light-driven processes into energy-dense hydrogen or carbon-containing fuels. Photoelectrochemical cell-based devices need to incorporate cost-effective components that can perform the light absorption, catalytic reaction, ion transport, and product separation processes. All of these processes need to take place simultaneously, imposing strong interactions and interdependence between all of the components of solar fuel devices. Moreover, these interactions require all of the components to operate stably under appropriate electrolyte composition, pH, irradiation level, and temperature.

As observed in plants, the primary photosynthesis reaction is

$$CO_2 + H_2O + \text{Sunlight} + \text{Nutrients} \rightarrow \text{Carbohydrates} + O_2 \qquad (5.4)$$

Artificial photosynthetic systems refer to any human-made arrangement that carries out this primary reaction in a manner or setting that is different from that of nature. An engineering or industrial realization of the artificial photosynthetic system implies intensification and common and widespread use (and large-scale

application) of reaction (5.4), as potentially thousands of tons of CO_2 in every year could be converted into beneficial products.

There are some essential headlines for the evaluation of artificial photosynthetic systems such as economic value. For the assessment (development) of artificial photosynthetic systems, some of the critical issues are (Martin 2000):

1. Economic value
2. Functional specifications
3. System choice
4. System developments:
   (a) Modulus development
   (b) Integration of modules
   (c) Lab scale testing
5. Lab scale testing
6. Implementation

References

Abrahamson JT, Sen F, Sempere B et al (2013) Excess thermopower and the theory of thermopower waves. ACS Nano 7(8):6533–6544

Aday B, Yildiz Y, Ulus R et al (2016) One-pot, efficient and green synthesis of acridinedione derivatives using highly monodisperse platinum nanoparticles supported with reduced graphene oxide. New J Chem 40:748–754

Akocak S, Sen B, Lolak N et al (2017) One-pot three-component synthesis of 2-amino-4H-chromene derivatives by using monodisperse Pd nanomaterials anchored graphene oxide as a highly efficient and recyclable catalyst. Nanostruct Nano-objects 11:25–31

Alstrum-Acevedo JH, Brennaman MK, Meyer TJ (2005) Chemical approaches to artificial photosynthesis. 2. Inorg Chem 44:6802–6827

Aminur Rahman GM, Lüders D, Rodríguez-Morgade MS et al (2009) Physicochemical characterization of subporphyrazines-lower subphthalocyanine homologues. Chem Sus Chem 2:330–335

Ayranci R, Baskaya G, Guzel M et al (2017a) Enhanced optical and electrical properties of PEDOT via nanostructured carbon materials: a comparative investigation. Nanostruct Nano-objects 11:13–19

Ayranci R, Baskaya G, Guzel M et al (2017b) Carbon-based nanomaterials for high-performance optoelectrochemical systems. Chem Sel 2(4):1548–1555

Balzani V, Moggi L, Scandola F (1987) Towards supramolecular photochemistry: assembly of molecular components to obtain photochemical molecular devices. Supramol Photochem 214:1–28

Balzani V, Credi A, Venturi M (2003) Photoinduced charge separation and solar energy conversion. In: Balzani V, Credi A, Venturi M (eds) Molecular devices and machines: a journey into the Nanoworld. Wiley-VCH, Weinheim, pp 132–173

Baskaya G, Esirden I, Erken E et al (2017a) Synthesis of 5-substituted-1H-tetrazole derivatives using monodisperse carbon black decorated Pt nanoparticles as heterogeneous nanocatalysts. J Nanosci Nanotechnol 17:1992–1999

Baskaya G, Yıldız Y, Savk A et al (2017b) Rapid, sensitive, and reusable detection of glucose by highly monodisperse nickel nanoparticles decorated functionalized multi-walled carbon nanotubes. Biosens Bioelectron 91:728–733

Blankenship RE, Madigan MT, Bauer CE (eds) (1995) Anoxygenic photosynthetic bacteria. Kluwer Academic Publishing, Dordrecht, p 1343

Bozkurt S, Tosun B, Sen B et al (2017) A hydrogen peroxide sensor based on TNM functionalized reduced graphene oxide grafted with highly monodisperse Pd nanoparticles. Anal Chim Acta 989:88–94

Britt RD (1996) Oxygen evolution. In: Yocum CY, Ort D (eds) Advances in photosynthesis: oxygenic photosynthesis, the light reactions. Kluwer Academic Publishers, Amsterdam, pp 137–164

Brothers PJ (2008) Boron complexes of porphyrins and related polypyrrole ligands: fantastic chemistry for both boron and the porphyrin. Chem Commun 18:2090–2102

Cabrera-Espinoza A, Insuasty B, Ortiz A (2018) Novel BODIPY-C60 derivatives with tuned photophysical and electron acceptor properties: isoxazolino[60]fullerene and pyrrolidino[60] fullerene. J Lumin 194:729–738

Celik B, Baskaya G, Karatepe O et al (2016a) Monodisperse Pt(0)/DPA@GO nanoparticles as highly active catalysts for alcohol oxidation and dehydrogenation of DMAB. Int J Hydrog Energy 41:5661–5669

Celik B, Erken E, Eris S et al (2016b) Highly monodisperse Pt(0)@AC NPs as highly efficient and reusable catalysts: the effect of the surfactant on their catalytic activities in room temperature dehydrocoupling of DMAB. Catal Sci Technol 6:1685–1692

Celik B, Kuzu S, Erken E et al (2016c) Nearly monodisperse carbon nanotube furnished nanocatalysts as highly efficient and reusable catalyst for dehydrocoupling of DMAB and C1 to C3 alcohol oxidation. Int J Hydrog Energy 41:3093–3101

Celik B, Yildiz Y, Erken E et al (2016d) Monodisperse palladium-cobalt alloy nanoparticles assembled on poly (N-vinyl-pyrrolidone) (PVP) as highly effective catalyst for the dimethylamine borane (DMAB) dehydrocoupling. RSC Adv 6:24097–24102

Chen T, Dai L (2013) Carbon nanomaterials for high-performance supercapacitors. Mater Today 16 (7–8):272–280

Chitta R (2002) Master thesis, University of Hyderabed

Claessens CG, Gonzalez-Rodríguez D, Torres T (2002) Subphthalocyanines: singular nonplanar aromatic compounds synthesis, reactivity, and physical properties. Chem Rev 102:835–854

Collings AF, Critchley C (eds) (2005) Artificial photosynthesis: from basic biology to industrial application. Wiley-VCH Verlag, Weinheim, p 339

D'Souza F, Ito O (2012) Photosensitized electron transfer processes of nanocarbons applicable to solar cells. Chem Soc Rev 41:86–96

D'Souza F, Smith PM, Zandler ME et al (2004) Energy transfer followed by electron transfer in a supramolecular triad composed of boron dipyrrin, zinc porphyrin, and fullerene: a model for the photosynthetic antenna-reaction center complex. J Am Chem Soc 126:7898–7907

D'Souza F, Chitta R, Sandanayaka ASD et al (2007) Self-assembled single-walled carbon nanotube: zinc–porphyrin hybrids through ammonium ion–crown ether interaction: construction and electron transfer. Chem Eur J 13:8277–8284

D'Souza F, Wijesinghe CA, El-Khouly ME et al (2011) Ultrafast excitation transfer, and charge stabilization in a newly assembled photosynthetic antenna-reaction center mimic composed of boron dipyrrin, zinc porphyrin and fullerene. Phys Chem Chem Phys 13:18168–18178

Danks SM, Evans EH, Whittaker PA (1985) Photosynthetic systems: structure, function, and assembly. Wiley, New York

Dasdelen Z, Yıldız Y, Eris S et al (2017) Enhanced electrocatalytic activity and durability of Pt nanoparticles decorated on GO-PVP hybrid material for methanol oxidation reaction. Appl Catal B Environ 219C:511–516

Datta K, Banerjee M, Mukherjee AK (2004) Comparative study of the host−guest complexes of [60]- and [70]-fullerenes with N,N′-Dibenzyl-1,4,10,13-tetraoxane-7,16-diaza-cyclooctadecane in different solvents. J Phys Chem B 108:16100–16106

Deetz MJ, Shang M, Smith BD (2000) A macrobicyclic receptor with versatile recognition properties: simultaneous binding of an ion pair and selective complexation of dimethylsulfoxide. J Am Chem Soc 122:6201–6207

Deisenhofer J, Norris JR (eds) (1993) The photosynthetic reaction center, 1st edn. Academic, San Diego, p 432

del Rey B, Torres T (1997) Synthesis of highly conjugated boron (III) subphthalocyanines. Tetrahedron Lett 38:5351–5354

del Rey B, Keller B, Torres T et al (1998) Synthesis and nonlinear optical, photophysical, and electrochemical properties of subphthalocyanines. J Am Chem Soc 120:12808–12817

Demir E, Savk A, Sen B et al (2017a) A novel monodisperse metal nanoparticles anchored graphene oxide as a Counter Electrode for Dye-Sensitized Solar Cells. Nanostruct Nano-objects 12:41–45

Demir E, Sen B, Sen F (2017b) Highly efficient nanoparticles and f-MWCNT nanocomposites based counter electrodes for dye-sensitized solar cells. Nanostruct Nano-objects 11:39–45

Demirci T, Celik B, Yıldız Y et al (2016) One-pot synthesis of Hantzsch dihydropyridines using highly efficient and stable PdRuNi@GO catalyst. RSC Adv 6:76948–76956

Ding Y, Zhu WH, Xie Y (2016) Development of ion chemosensors based on porphyrin analogues. Chem Rev 117:2203–2256

El-Khouly ME (2010) Electron transfer reaction of light harvesting zinc naphthalocyanine–subphthalocyanine self-assembled dyad: spectroscopic, electrochemical, computational, and photochemical studies. Phys Chem Chem Phys 12:12746–12752

El-Khouly ME, Ito O, Smith PM et al (2004) Intermolecular and supramolecular photoinduced electron transfer processes of fullerene–porphyrin/phthalocyanine systems. J Photochem Photobiol C 5:79–104

El-Khouly ME, Araki Y, Ito O et al (2006) Subphthalocyanines as light-harvesting electron donor and electron acceptor in artificial photosynthetic systems. J Porphyrins Phthalocyanines 10:1156–1164

El-Khouly ME, Shim SH, Araki Y et al (2008) Effect of dual fullerenes on lifetimes of charge-separated states of subphthalocyanine-triphenylamine-fullerene molecular systems. J Phys Chem B 112:3910–3917

El-Khouly ME, Ryu JB, Kay K-Y et al (2009) Long-lived charge separation in a dyad of closely-linked subphthalocyanine-zinc porphyrin bearing multiple triphenylamines. J Phys Chem C 113:15444–15453

El-Khouly ME, Ju DK, Kay KY et al (2010) Supramolecular tetrad of subphthalocyanine–triphenylamine–zinc porphyrin coordinated to fullerene as an "Antenna-Reaction-Center" mimic: formation of a long-lived charge-separated state in nonpolar solvent. S Chem Eur J 16:6193–6202

El-Khouly ME, Gutierrez AM, Sastre-Santos A et al (2012a) Light harvesting zinc naphthalocyanine–perylenediimide supramolecular dyads: long-lived charge-separated states in nonpolar media. Phys Chem Chem Phys 14:3612–3621

El-Khouly ME, Kim JH, Kay KY et al (2012b) Subphthalocyanines as light-harvesting electron donor and electron acceptor in artificial photosynthetic systems. J Phys Chem C 116:19709–19717

El-Khouly ME, Moiseev AG, van der Est A et al (2012c) Photoinduced electron transfer in zinc naphthalocyanine-naphthalenediimide supramolecular dyads. ChemPhysChem 13:1191–1198

El-Khouly ME, Fukuzumi S, D'souza F (2014) Photosynthetic antenna-reaction center mimicry by using boron dipyrromethene sensitizers. ChemPhysChem 15:30–47

El-Khouly ME, El-Mohsnawy E, Fukuzimi S (2017) Solar energy conversion: from natural to artificial photosynthesis. J Photochem Photobiol C Photochem Rev 31:36–83

Eris S, Dasdelen Z, Sen F et al (2018a) Investigation of electrocatalytic activity and stability of Pt@f-VC catalyst prepared by in-situ synthesis for methanol electrooxidation. Int J Hydrog Energy 43(1):385–390

Eris S, Dasdelen Z, Sen F (2018b) Enhanced electrocatalytic activity and stability of monodisperse Pt nanocomposites for direct methanol fuel cells. J Colloid Interface Sci 513:767–773

Eris S, Dasdelen Z, Yildiz Y et al (2018c) Nanostructured Polyaniline-rGO decorated platinum catalyst with enhanced activity and durability for Methanol oxidation. Int J Hydrog Energy 43 (3):1337–1343

Erken E, Esirden I, Kaya M et al (2015) A rapid and novel method for the synthesis of 5-substituted 1H-tetrazole catalyzed by exceptional reusable monodisperse Pt NPs@AC under the microwave irradiation. RSC Adv 5:68558–68564

Erken E, Pamuk H, Karatepe O et al (2016a) New Pt(0) nanoparticles as highly active and reusable catalysts in the C1–C3 alcohol oxidation and the room temperature dehydrocoupling of dimethylamine-borane (DMAB). J Clust Sci 27:29

Erken E, Yildiz Y, Kilbas B et al (2016b) Synthesis and characterization of nearly monodisperse Pt nanoparticles for C1 to C3 alcohol oxidation and dehydrogenation of dimethylamine-borane (DMAB). J Nanosci Nanotechnol 16:5944–5950

Esirden I, Erken E, Kaya M et al (2015) Monodisperse Pt NPs@rGO as highly efficient and reusable heterogeneous catalysts for the synthesis of 5-substituted 1H-tetrazole derivatives. Catal Sci Technol 5:4452–4457

Fukuzumi S, Imahori H, Yamada H et al (2001) Catalytic effects of dioxygen on intramolecular electron transfer in radical ion pairs of zinc porphyrin-linked fullerenes. J Am Chem Soc 123:2571–2575

Geyer M, Plenzig F, Rauschnabel J et al (1996) Subphthalocyanines: preparation, reactivity and physical properties. Synthesis 9:1139–1151

Giraldo JP, Landry MP, Faltermeier SM et al (2014) A nanobionic approach to augment plant photosynthesis and biochemical sensing using targeted nanoparticles. Nat Mater 13:400–408

Goksu H, Celik B, Yildiz Y et al (2016a) Superior monodisperse CNT-supported CoPd (CoPd@CNT) nanoparticles for selective reduction of nitro compounds to primary amines with NaBH4 in an aqueous medium. Chem Sel 1(10):2366–2372

Goksu H, Yildiz Y, Celik B et al (2016b) Highly efficient and monodisperse graphene oxide furnished Ru/Pd nanoparticles for the dehalogenation of aryl halides via ammonia borane. Chem Sel 1(5):953–958

Goksu H, Yildiz Y, Celik B et al (2016c) Eco-friendly hydrogenation of aromatic aldehyde compounds by tandem dehydrogenation of dimethylamine-borane in the presence of reduced graphene oxide furnished platinum nanocatalyst. Catal Sci Technol 6:2318–2324

Gonzalez Rodríguez D, Bottari GJ (2009) Phthalocyanines, subphthalocyanines and porphyrins for energy and electron transfer applications. Porphyrins Phthalocyanines 13:624–636

Gonzalez-Rodríguez D, Torres T, Guldi DM et al (2002) Energy transfer processes in novel subphthalocyanine-fullerene ensembles. Org Lett 4:335–338

Gonzalez-Rodríguez D, Torres T, Olmstead MM et al (2006) Photoinduced charge-transfer states in subphthalocyanine-ferrocene dyads. J Am Chem Soc 128:10680–10681

Gonzalez-Rodríguez D, Carbonell E, Guldi DM et al (2009) Modulating electronic interactions between closely spaced complementary π surfaces with different outcomes: regio- and diastereomerically pure subphthalocyanine–C60 tris adducts. Angew Chem Int Ed 48:8032–8036

Guldi DM (2000) Fullerenes: three-dimensional electron acceptor materials. Chem Commun 5:321–327

Gust D, Moore TA (1999) Intramolecular photoinduced electron-transfer reactions of porphyrins. In: Gust D, Moore TA (eds) The porphyrin handbook. Academic, New York, pp 153–190

Gust D, Moore TA, Moore AL (1993) Molecular mimicry of photosynthetic energy and electron transfer. Acc Chem Res 26:198–205

Gust D, Moore TA, Moore AL (2001) Mimicking photosynthetic solar energy transduction. Acc Chem Res 34(1):40–48

Hasobe T, Kamat PV, Absalom MA et al (2004) Supramolecular photovoltaic cells based on composite molecular nanoclusters: dendritic porphyrin and C_{60}, porphyrin dimer and C_{60}, and porphyrin-C_{60} dyad. J Phys Chem B 108:12865–12872

Hasobe T, Kamat PV, Troiani V et al (2005) Enhancement of light-energy conversion efficiency by multi-porphyrin arrays of porphyrin-peptide oligomers with fullerene clusters. J Phys Chem B 109:19–23

Hasobe T, Saito K, Kamat PV et al (2007) Organic solar cells. Supramolecular composites of porphyrins and fullerenes organized by polypeptide structures as light harvesters. J Mater Chem 17:4160–4170

Hosomizu K, Imahori H, Hahn U et al (2007) Dendritic effects on structure and photophysical and photoelectrochemical properties of fullerene dendrimers and their nanoclusters. J Phys Chem C 111:2777–2786

Imahori H, Mori Y, Matano J (2003) Nanostructured artificial photosynthesis. J Photochem Photobiol C 4:51–83

Imahori H, Fujimoto A, Kang S et al (2005a) Host-guest interactions in the supramolecular incorporation of fullerenes into tailored holes on porphyrin-modified gold nanoparticles in molecular photovoltaics. Chem Eur J 11:7265

Imahori H, Fujimoto A, Kang S et al (2005b) Supramolecular incorporation of C60 molecules into tailored holes on porphyrin-modified gold nanoclusters. Adv Mater 17:1727–1730

Imahori H, Mitamura K, Shibano Y et al (2006a) A photoelectrochemical device with a nanostructured SnO2 electrode modified with composite clusters of porphyrin-modified silica nanoparticle and fullerene. J Phys Chem B 110:11399–11405

Imahori H, Mitamura K, Umeyama T et al (2006b) Chem Commun 28:406–408

Ishii K (2012) Functional singlet oxygen generators based on phthalocyanines. Coord Chem Rev 256:1556–1568

Izzat RM, Bradshaw JS, Nielson SA et al (1985) Thermodynamic and kinetic data for cation-macrocycle interaction. Chem Rev 85:271–339

Karatepe O, Yildiz Y, Pamuk H et al (2016) Enhanced electrocatalytic activity and durability of highly monodisperse Pt@PPy-PANI nanocomposites as a novel catalyst for electro-oxidation of methanol. RSC Adv 6:50851–50857

KC CB, D'Souza F (2016) Design and photochemical study of supramolecular donor-acceptor systems assembled via metal-ligand axial coordination. Coord Chem Rev 322:104–141

Kietaibl H (1974) The crystal and molecular structure of a new phthalocyanine-like boron complex. Monatsh Chem 105:405–418

Kim D (2012) Multiporphyrin arrays: fundamentals and applications. CRC Press, Boca Raton, p 828

Kim JH, El-Khouly ME, Araki Y et al (2008) Photoinduced processes of subphthalocyanine–diazobenzene–fullerene triad as an efficient excited energy transfer system. Chem Lett 37:544––545

Kim BS, Ma B, Donuru VR et al (2010) Bodipy-backboned polymers as an electron donor in bulk heterojunction solar cells. Chem Commun 46:4148–4150

Kobayashi N (2002) Coord Chem Rev 227:129–252

Kuninobu K, Tsutomu I, Makoto H et al (1996) Structure and some properties of (alkoxo)(subphthalocyaninato)boron(III). Bull Chem Soc Jpn 69:2559–2563

Ladomenou K, Nikolaou V, Charalambidis G et al (2017) Porphyrin-BODIPY-based hybrid model compounds for artificial photosynthetic reaction centers. C R Chim 20:314–322

Lehn JM (1990) Perspectives in supramolecular chemistry-from molecular recognition towards molecular information processing and self-organization. Angew Chem Int Ed 29:1304–1319

Lehn JM (1993) Supramolecular chemistry. Science 260:1762–1763

Liao J, Wang Y, Xu Y et al (2015) Synthesis, optical and electrochemical properties of novel meso-triphenylamine BODIPY dyes with aromatic moieties at 3,5-positions. Tetrahedron 71:5078–5084

Liao J, Zhao H, Xu Y et al (2016) Novel D-A-D type dyes based on BODIPY platform for solution-processed organic solar cells. Dyes Pigments 128:131–140

Liddell PA, Sumida JP, Macpherson AN et al (1994) Preparation and photophysical studies of porphyrin-C60 dyads. Photochem Photobiol 60:537–541

Luhman WA, Holmes RJ (2011) Investigation of energy transfer in organic photovoltaic cells and impact on exciton diffusion length measurements. Adv Funct Mater 21:764–771

Macor L, Fungo F, Tempesti T et al (2009) Near-IR sensitization of wide band gap oxide semiconductor by axially anchored Si-naphthalocyanines. Energy Environ Sci 2:529–534

Maligaspe E, Tkachenko NV, Subbaiyan NK et al (2009) Photosynthetic antenna−reaction center mimicry: sequential energy- and electron transfer in a self-assembled supramolecular triad composed of boron dipyrrin, zinc porphyrin, and fullerene. J Phys Chem A 113:8478–8489

Maligaspe E, Kumpulainen T, Subbaiyan NK et al (2010) Electronic energy harvesting multi BODIPY-zinc porphyrin dyads accommodating fullerene as a photosynthetic composite of antenna-reaction center. Phys Chem Chem Phys 12:7434–7444

Mao M, Zhang X, Cao L et al (2015) Design of Bodipy based organic dyes for high-efficient dye-sensitized solar cells employing double electron acceptors. Dyes Pigments 117:28–36

Martin JN (2000) System engineering guidebook. CRC Press, Boca Raton, p 13

Mazik M, Kuschel M, Sicking W (2006) Crown ethers as building blocks for carbohydrate receptors. Org Lett 8:855–858

Nierengarten JF (2014) Fullerenes and other carbon-rich nanostructures. Springer, Berlin. https://doi.org/10.1007/978-3-642-54854-3

Ohkubo K, Fukuzumi S (2009) Rational design and functions of electron donor-acceptor dyads with much longer charge-separated lifetimes than natural photosynthetic reaction centers. Bull Chem Soc Jpn 82:303–315

Pan B, Zhu Y-Z, Ye D et al (2018) Improved conversion efficiency in dye-sensitized solar cells based on porphyrin dyes with dithieno[3,2-b:2,3-d]pyrrole donor. Dyes Pigments 150:223–230

Panda MK, Labomenou K, Coutsolelos AG (2012) Porphyrins in bio-inspired transformations: light-harvesting to the solar cell. Coord Chem Rev 256:2601–2627

Pederson CJ (1967) Cyclic polyethers and their complexes with metal salts. J Am Chem Soc 89:7017–7036

Poddutoori PK, Zarrabi N, Moiseev AG, Gumbau-Birsa R, Vassiliev S, Est AVD (2013) Chem Eur J 19:3148–3157

Rauschnabel J, Hanack M (1995) New derivatives and homologs of subphthalocyanine. Tetrahedron Lett 36:1629–1632

Romero Nieto C, Medina A, Molina-Ontoria A et al (2012) Towards enhancing light harvesting-subphthalocyanines as electron acceptors. Chem Commun 48:4953–4955

Romero-Nieto C, Guilleme J, Villegas C et al (2011) Subphthalocyanine-polymethine cyanine conjugate: an all organic panchromatic light harvester that reveals charge transfer. J Mater Chem 21:15914–15918

Sagawa T, Yoshikawa S, Imahori H (2010) One-dimensional nanostructured semiconducting materials for organic photovoltaics. J Phys Chem Lett 1:1020–1025

Sahin B, Demir E, Aygun A et al (2017) Investigation of the effect of pomegranate extract and monodisperse silver nanoparticle combination on MCF-7 cell line. J Biotechnol 260C:79–83

Sahin B, Aygun A, Gunduz H et al (2018) Cytotoxic effects of platinum nanoparticles obtained from pomegranate extract by the green synthesis method on the MCF-7 cell line. Colloids Surf B Biointerfaces 163:119–124

Sastre A, Torres T, Diaz-Garcia MA et al (1996) Subphthalocyanines: novel targets for remarkable second-order optical nonlinearities. J J Am Chem Soc 118:2746–2747

Sen F, Boghossian AA, Sen S et al (2013a) Application of nanoparticle antioxidants to enable hyperstable chloroplasts for solar energy harvesting. Adv Energy Mater 3(7):881–893

Sen S, Sen F, Boghossian AA et al (2013b) The effect of reductive dithiothreitol and trolox on nitric oxide quenching of single-walled carbon nanotubes. J Phys Chem C 117(1):593–602

Sen F, Karatas Y, Gülcan M et al (2014a) Amylamine stabilized platinum (0) nanoparticles: active and reusable nanocatalyst in the room temperature dehydrogenation of dimethylamine- borane. RSC Adv 4(4):1526–1531

Sen F, Ulissi ZW, Gong X et al (2014b) Spatiotemporal intracellular nitric oxide signaling captured using internalized, near-infrared fluorescent carbon nanotube nanosensors. Nano Lett 14 (8):4887–4894

Sen B, Kuzu S, Demir E et al (2017a) Hydrogen liberation from the dehydrocoupling of dimethylamine-borane at room temperature by using novel and highly monodispersed RuPtNi nanocatalysts decorated with graphene oxide. Int J Hydrog Energy 42(36):23299–23306

Sen B, Kuzu S, Demir E et al (2017b) Polymer-graphene hybrid decorated Pt nanoparticles as highly efficient and reusable catalyst for the dehydrogenation of dimethylamine-borane at room temperature. Int J Hydrog Energy 42(36):23284–23291

Sen B, Akdere EH, Savk A et al (2018) A novel thiocarbamide functionalized graphene oxide supported bimetallic monodisperse Rh-Pt nanoparticles (RhPt/TC@GO NPs) for Knoevenagel condensation of aryl aldehydes together with malononitrile. Appl Catal B Environ 225 (5):148–153

Shah SM, Kira A, Imahori H et al (2012) Co-grafting of porphyrins and fullerenes on ZnO nanorods: towards supramolecular donor-acceptor assembly. J Colloid Interface Sci 386:268–276

Shimizu S, Nakano S, Hosoya T et al (2011) Pyrene-fused subphthalocyanine. Chem Commun 47:316–318

Solntsev PV, Spurgin KL, Sabin JR et al (2012) Photoinduced charge transfer in short-distance ferrocenylsubphthalocyanine dyads. Inorg Chem 51:6537–6547

Takeda A, Oku T, Suzuki A et al (2013) Fabrication and characterization of fullerene-based solar cells containing phthalocyanine and naphthalocyanine dimers. Synth Met 177:48–51

Torres T (2006) From subphthalocyanines to subporphyrins. Angew Chem Int Ed. 2006 45:2834–2837

Tsuda A, Osuka A (2001) Fully conjugated porphyrin tapes with electronic absorption bands that reach into the infrared. Science 293:79–82

Urban M, Grätzel M, Nazeeruddin MK et al (2014) Meso-substituted porphyrins for dye-sensitized solar cells. Chem Rev 114:12330–12396

Verrett B, Rand BP, Cheyns D et al (2011) A 4% efficient organic solar cell using a fluorinated fused subphthalocyanine dimer as an electron acceptor. Adv Energy Mater 1:565–568

Wheeler RA (2004) Molecular bioenergetics: simulations of electron, proton, and energy transfer. American Chemical Society, Washington, DC. 2004

Yildiz Y, Erken E, Pamuk H et al (2016a) Monodisperse Pt nanoparticles assembled on reduced graphene oxide: highly efficient and reusable catalyst for methanol oxidation and dehydrocoupling of dimethylamine-borane (DMAB). J Nanosci Nanotechnol 16:5951–5958

Yildiz Y, Esirden I, Erken E et al (2016b) Microwave (Mw)-assisted synthesis of 5-substituted 1H-tetrazoles via [3+2] cycloaddition catalyzed by Mw-Pd/Co nanoparticles decorated on multi-walled carbon nanotubes. Chem Sel 1(8):1695–1701

Yildiz Y, Okyay TO, Gezer B et al (2016c) Monodisperse Mw-Pt NPs@VC as highly efficient and reusable adsorbents for methylene blue removal. J Clust Sci 27:1953–1962

Yildiz Y, Pamuk H, Karatepe O et al (2016d) Carbon black hybrid material furnished monodisperse platinum nanoparticles as highly efficient and reusable electrocatalysts for formic acid electro-oxidation. RSC Adv 6:32858–32862

Yildiz Y, Ulus R, Eris S et al (2016e) Functionalized multi-walled carbon nanotubes (f-MWCNT) as highly efficient and reusable heterogeneous catalysts for the synthesis of acridinedione derivatives. Chem Sel 1(13):3861–3865

Yildiz Y, Kuzu S, Sen B et al (2017a) Different ligand based monodispersed metal nanoparticles decorated with rGO as highly active and reusable catalysts for the methanol oxidation. Int J Hydrog Energy 42(18):13061–13069

Yildiz Y, Okyay TO, Sen B et al (2017b) Highly monodisperse Pt/Rh nanoparticles confined in the graphene oxide for highly efficient and reusable sorbents for methylene blue removal from aqueous solutions. Chem Sel 2(2):697–670

Zhao H, Liao J, Peng M et al (2015) Synthesis of fluorene-based di-BODIPY dyes containing different aromatic linkers and their properties. Tetrahedron Lett 56:7145–7149

Zhu P, Song F, Ma P, Li S, Wang Y (2018) Effective photocurrent generation in supramolecular porphyrin-fullerene conjugates assembled by crown ether-alkyl ammonium cation interactions. Dyes Pigments. https://doi.org/10.1016/j.dyepig.2018.01.012

Chapter 6
Polymeric Semiconductors as Efficient Photocatalysts for Water Purification and Solar Hydrogen Production

Sudesh Kumar, Raghava Reddy Kakarla, Ch. Venkata Reddy, Enamul Haque, Veera Sadhu, and S. Naveen

Contents

S. Kumar
Department of Chemistry, Banasthali University, Banasthali Vidyapith, Vanasthali, Rajasthan, India

R. R. Kakarla (✉)
School of Chemical & Biomolecular Engineering, The University of Sydney, Sydney, NSW, Australia

C. V. Reddy (✉)
School of Mechanical Engineering, Yeungnam University, Gyeongsan, South Korea

E. Haque
School of Medicine and Centre for Molecular and Medical Research, Deakin University, Waurn Ponds, VIC, Australia

V. Sadhu (✉)
School of Physical Sciences, Banasthali University, Banasthali Vidyapith, Vanasthali, Rajasthan, India

S. Naveen
School of Basic Sciences, Jain University, Bangalore, India

Inamuddin et al. (eds.), *Nanophotocatalysis and Environmental Applications*,
Environmental Chemistry for a Sustainable World 31,
https://doi.org/10.1007/978-3-030-04949-2_6

Abstract Environmental contamination is one of the serious issues to an environment and human health due to the contamination of a wide range of organic chemicals, industrial dyes and other hazardous substances in the drinking water, air and land. The innovation of the photocatalytic process has been presented to be the green and feasible method for the environmental decontamination.

Photocatalysis has a wide range of application such as wastewater treatment (organic dye degradation), disinfection, solar water splitting, CO_2 reduction and air purification. Many photocatalysts have been developed for the disintegration of water into CO_2, H_2O and other non-harmful substances. Compounds, with the help of O_2, act as clean oxidants. Among various photocatalytic materials, the polymeric semiconducting photocatalysts show highly efficient photocatalytic performance for various photocatalytic applications. For example, oxygenated groups present on the surface of graphene oxide (GO) make it effective in the removal of pollutants such as phenol, chlorophenol and industrial dyes. In this chapter, we discussed various chemical methodologies, properties and photocatalytic applications of polymeric semiconductors (carbon nitride, C_3N_4), graphene and metal-organic framework (MOF)-based hybrid nanostructured photocatalysts for the water purification and the solar hydrogen production. Such efficient photocatalysts are expected to solve the issues of environmental remediation.

Keywords Graphene oxide · Graphitic carbon nitride (g-C_3N_4) · Metal-organic framework (MOF) · TiO_2 · Semiconductors · Functional heterostructured hybrid photocatalysts · Photocatalysis · Antibacterial activity · Photocatalysis fundamentals · Catalysts characterization · Photocatalysts kinetics · Photocatalytic mechanism · Environmental applications · Environmental decontamination · Organic dye degradation · Wastewater purification · Hydrogen evolution reactions · Solar hydrogen production

6.1 Introduction

A common problem spotted across the globe is environmental contamination. It's the burning issue which can't be over sighted. Among all the sort of environmental problems, the one striking at the top of the list is water pollution. Water pollution is probably the most important of the current issues, and the concern still continues for future also. The idea of using the water resources in a manner that it should fulfil our needs for the present inadequacy shouldn't be witnessed in future.

The idea of how to wisely use the available should pop up the head. It's not only the inadequacy of water resources that should concern but also the consequences of consumption of polluted water. With the increasing advancements in technology and changing lifestyles, our natural resources are getting exploited and overconsumed. Water is indispensable for both living and existence. Data states that 88% of the

annual diarrheal occurrence is due to the unsafe water and improper hygiene (Bivins et al. 2017). The cause for this diarrheal outbreak is chiefly the human activity or the polluted water.

Water pollution could be classified under two headings:

1. *Point source*: In point source pollution, there is the direct emission of effluents and contaminants into the water bodies. The discharge could be regulated.
2. *Non-point source*: The pollutants are indirectly discharged into water bodies, and it can't be controlled.

The development of clean environment free from any fossil is very important. Thus, it's essential to think about such technologies which make water resources pollution free.

6.2 Photocatalysis

The catalyst could be defined as a substance which changes the rate of a reaction without being itself involved in the reaction. In other words, the catalyst is the substance which lowers the free activation energy of any reaction (Dasireddy and Likozar 2017). When any reaction is accelerated in the presence of a catalyst, then such reaction is called photocatalysis (Hathway et al. 2009). Photocatalysis is established on the ability of photocatalyst to both adsorb reactant and absorb photon, respectively (Job and Kang 2013).

Photocatalytic innovation has been exhibited to be one of the "green" and practicable systems for the natural remediation. Along these lines, ecological photocatalytic processes, including sanitization of water and air, risky environmental waste remediation, water refinement, freshening up, self-cleaning and antibacterial activity, have caused increasingly consideration as of late. Although, inferable from the low photocatalytic effectiveness and the utilization of light are still exceptionally constrained. Consequently, more examinations are required from the perspective of functional utilize.

The favourable activities including natural tainting, self-clean structures, freshening up, against the bacterial activity, antifogging settling cleaning activity. Moreover, nitrogen oxides (NOx) are noticeable all around, and it is important to remove such harmful air pollutants by oxidizing NOx to nitrates using photocatalysts. As indicated by the overview directed by the research organization, the market of photograph catalysis with respect to the issues of condition increment ceaselessly.

Both the mechanical and financial significance of photocatalysis have expanded extensively over the past decade. An assortment of utilizations extending from antifogging, self-cleaning surfaces via air and water filtration processes and sun-powered actuated hydrogen creation has been produced, and huge numbers of these have advanced into business items. Photocatalysts stimulate or quicken

compound responses coming about, for instance, in a disintegration of natural particles. Because of their expansive surface zone, nanosized particles demonstrate an essentially improved reactivity contrasted with bigger particles or mass material (Chen et al. 2000).

Keeping in mind the end goal to address this critical issue, broad research is in progress to create progressed scientific, physicochemical and biochemical techniques for the portrayal and disposal of risky concoction mixes from contaminated water, air and soil. Semiconductor-based photocatalysis is planned to be both enhancing and reciprocal to a portion of the more traditional methodologies for the pulverization or change of perilous substance squanders, e.g. high-temperature burning, altered enacted slop assimilation, anaerobic absorption and regular physicochemical treatment.

6.2.1 Basic Principles of Photocatalytic Reaction

The word photocatalysis is a combination of photo and catalysis words, in which photo means the light and catalysis defines the process where the substance participates in the rate of a reaction without bringing about any change in its own composition and rate of reaction. Photocatalysis is a process where either direct irradiation or irradiation by catalyst accelerates the reaction.

The photocatalytic reaction could be classified into two categories:

1. *Environment purification*: The reactions occurring under this category are followed by decreasing in Gibbs free energy and are further categories as a lower-state reaction.
2. *High energy conversions*: These are led by a large positive change in the values of Gibbs free energy (Chen and Wang 2012).

The band gap is the difference of energy between conduction band valence bands. It's important to name the knowledge of band gap while studying semiconductor photocatalysis. When semiconductor absorbs photon energy greater than those of band gap, then the valence band electrons excite to the conduction band and leave behind a hole in valence band. These photoexcited electrons have the potential to reduce the substances, whereas the holes of valence band have the potential to oxidize substances (Man et al. 2017). One of most important and efficient technologies for the remediation of the environment is photocatalysis. It's listed in one of the green environmental remediation techniques.

6.2.2 Photocatalytic Properties

Photocatalysis is an emerging advancement that allows a wide range of uses, including degradation of organics dyes, antibacterial activity and production of

fuel splitting of water and carbon dioxide degradation. Numerous inorganic semiconducting materials have been considered as photocatalysts, and the flexibility of these materials have grown in the current years. By understanding the properties of various photochemical materials and their exhibition of reaction forms, it is necessary to plan their combinations.

The main places of interest of the photocatalytic framework are:

(i) Desired band gap
(ii) Appropriate morphological structures
(iii) Large surface area
(iv) Dependability
(v) Reusability

Semiconducting metal oxides, for instance, oxides of vanadium (V), chromium (Cr), titanium (Ti), tin (Sn), zinc (Zn), tungsten (WO) and cerium (Ce) having abovementioned characteristics, take after comparable photocatalytic procedures, for example, light ingestion, which incites an accuse division procedure of the arrangement of positive openings that can oxidize natural substrates. Among these semiconducting metal oxides (TiO_2, ZnO, SnO_2, WO_3 and CeO_2), which are plenteous in nature, have been broadly utilized as the photocatalysts, especially as the heterogeneous photocatalytic materials for very long time. This is due to their unique properties of biocompatibility, extraordinary strength in a variety of conditions and ability to generate the charge transporters when it permits with a measure of light vitality. The positive mix of electronic structure, the properties of charge transport and light absorption and energized functioning period of metal oxides have made it workable for their application as efficient photocatalysts.

Graphene oxide (GO) is a functional form of graphene sheet consist of rich oxygenated groups on their surface. The basal plane of GO is covalently attached by hydroxyl (OH) and epoxy groups, while carboxyl (-COOH) groups are originated at the edges of GO nanosheets. These –OH functional groups make of GO a hydrophilic nature and improve the dispersion in aqueous systems. The band gap of GO can be controlled by modifying the oxidation rate (Kim et al. 2003a). The good dispersion in water and its controllable band gap values motivate to explore this low-cost potential material for the applications in the research area of photocatalysis.

6.2.3 Photocatalytic Mechanism

At the point when a given photocatalyst is illuminated by the light of energy more prominent than the band hole energy of the photocatalytic material, the charge partition happens. At that point, using the electrons and openings produced by the charge division, the photocatalyst stimulates an oxidation-decrease response. Specifically, TiO_2, with generally expansive band hole energy of 3.0–3.2 eV, can

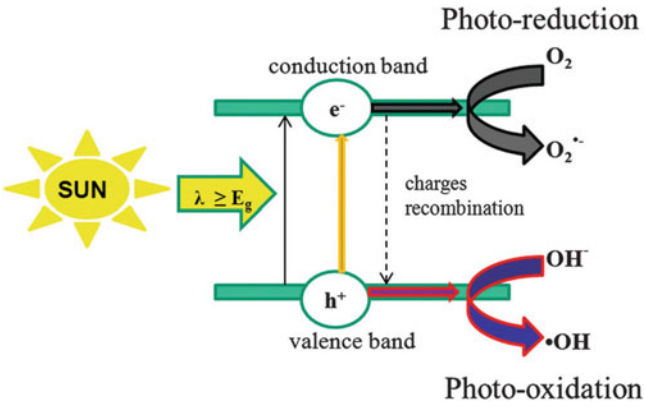

Fig. 6.1 Photocatalytic activation of a semiconductor and primary reactions occurring on its surface. (Reproduction from Colmenares and Luque 2014, Royal Society of Chemistry)

accomplish an effective oxidation-lessening response with the bright beams introduce in our living condition (Szabó et al. 2006).

The effect of the photocatalyst concentration was investigated on the evolution of hydrogen (H_2) and oxygen (O_2) from water (H_2O) under illumination of the light. No photocatalytic material for the part of water has yet been marketed due to a need in proficiency, high generation cost and so forth. In any case, the advance accomplished in the photocatalytic material to date depends on the consequences of these investigations. Different photocatalytic materials for the water disintegration have been revealed and created, a significant number of which use TiO_2 and the cases of which contain TiO_2 particles conveying a metal, for example, platinum or rhodium or an oxide, for example, RuO_2. The general photocatalytic mechanism of a semiconductor and primary reactions take place on its surface are illustrated in Fig. 6.1.

6.3 Photocatalytic Functional Materials: Synthesis, Properties and Applications

6.3.1 Graphitic Carbon Nitride (g-C_3N_4)

6.3.1.1 Synthesis of Polymeric g-C_3N_4

A carbene is found to be a thermal robust compound which is non-volatile up to 600 °C. It possesses one of the highest thermal stability for an organic compound. The thermal stability possessed by this molecule is higher than the entire thermal stable polymer, for example, aromatic polyamides. The thermal stability of polymeric graphite shows variations on the basis of different methods of synthesis and other parameters. The variation observed may be caused by the difference in the

condensation method (Komatsu and Nakamura 2001; Yan et al. 2009; Miller et al. 2002; Gillan 2000). The optimum Van Der Waal interaction between each layer of carbon nitride allows it to be soluble in almost all the samples such as water THF, DMF, alcohol, toluene, etc. Assessment of optical properties could be done by UV-Vis absorption and photoluminescence. Some theoretical calculation explained carbon nitride as a semiconductor. The carbon nitride obtained after self-condensation are macro powders with the small surface area.

6.3.1.2 Photocatalytic Mechanism of g-C_3N_4

The current studies on photocatalysis are primarily focused on the development of the materials having small band gap and desirable positions of band gap for the splitting of water (Gillan 2000). Maximum of the semiconductors are chiefly inorganic metal centred, consisting of metal oxides, sulphides and nitrides (Liang et al. 2017). The metal-based semiconductors are found in nature and in enzyme and act as active sites for photocatalytic degradation of contaminants present in the water. The g-C_3N_4 possesses all the electronic properties suitable for the heterogeneous photocatalyst. This molecule also possesses a band gap of 2.7 eV which further corresponds to the band gap of 460 nm. The energy required for the production of H_2 from H_2O can be calculated as follows:

$$\boxed{\begin{aligned} &2H_2O \rightarrow O_2 + 4H^+ + 4e^- + 0.82V \\ &2H^+ + 4e^- \rightarrow H_2 - 0.41V \end{aligned}}$$

The photo water splitting in presence of photocatalyst, it's important to have a larger band gap. The band gap must be the photo-generated hole that should have enough oxidation strength to oxidize the water to oxygen. The photo-generated electron has sufficient reduction potential to reduce H_2O to H_2 as shown in Fig. 6.2. The visible-light-driven photocatalytic process undergoes three strategies such as (A) H_2 generation from water, (B) photochemical initiation of O_2 and (C) photo-oxidation of organic contaminants present in wastewater.

The position of band gap must be such that photo-generated hole is strengthened enough to oxidize water to oxygen; later this photo-generated electron reduces water to H_2, i.e. the HOMO and LUMO engulfs redox potential of water. This type of engulfing is rarely observed in organic semiconductors, for example, if the semiconductor is stable against water and oxygen, it would be a case of photocorrosion (Wang et al. 2012).

6.3.1.3 Photodegradation of Chemical Pollutants Using g-C_3N_4

The organic pollutants are oxidized into CO_2, water and other non-harmful compounds with the aid of oxygen. O_2 act as a clean oxidant. The above-mentioned

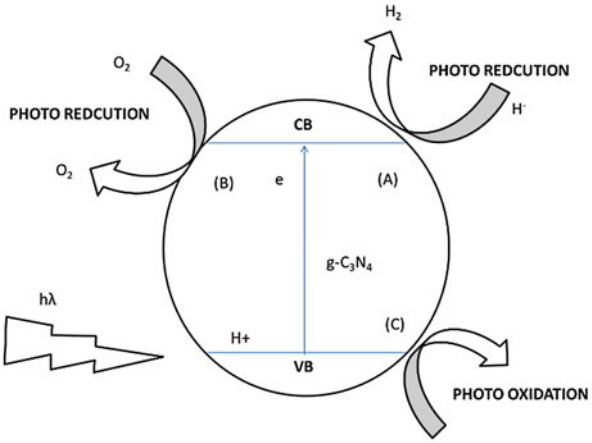

Fig. 6.2 Three strategies to realize visible light-induced photocatalysis. (Reprinted with permission from Wang et al. 2012, copyright (2009) American Chemical Society)

approach is considered as a natural and effective way to remove organic pollutants rapidly. Methyl orange was being degraded using g-C_3N_4 as metal-free photocatalyst (Yan et al. 2009). The studies revealed that the reduction process for degradation of MO over g-C_3N_4 was initiated by photogeneration of electrons. Doping of g-C_3N_4 with boron could improve dye absorption and light absorption. To activate H_2O under visible-light radiation, carbon nitride has been applied as metal photocatalyst. The catalyst was reusable even after activation of water, which ensures clean environment from organic pollutants.

6.3.1.4 Graphene Oxide-Based Hybrid Photocatalysts

To enhance the implementation of photocatalytic semiconductors materials, few steps should be kept in mind. One of the mixtures of promising semiconducting materials is with 3D graphene. Graphene has the capability to act as an electron acceptor. Instead of knowing the face that titanium supported semiconductors hold more value than the graphene-based conductors for the removal of toxins from natural sources. There exist many semiconductors which have been joined to the graphene network with a specific termination objective to watch the adjustment of its impact on the evacuation of natural poisons from the water.

Cuprous oxide (Cu_2O) exists as one of the potential semiconductors to get combined with the graphene. The outcomes demonstrated a critical increment of the photocatalytic movement of the Cu_2O/rGO nanocomposites with regard to nanosize Cu_2O. Such hybrid nanostructured catalysts enhance the absorbance of light and expand the light retention and exchange of photo-generated electrons of Cu_2O to reduced graphene oxide (rGO). This leads to the improvement of charge partition of hybrid catalyst, and it was determined by the photoluminescence spectra.

GO is the most functional form of possessing oxygenated groups. GO is surrounded by epoxy and hydroxyl groups at the basal plane. GO appear as a

hydrophilic material due to the presence of oxygenated groups (Ramirz et al. 2015). The oxidation level can be modified by adjusting the band gap. The above-mentioned properties, i.e. tunable band gap and dispersion in water, encourage exploring the application in the photocatalytic area. 3.26 eV was the calculated band gap of GO. Some of the aromatic compounds such as phenol and chlorophenol were easily removed from water with the help of GO as a photocatalyst.

They also used an efficient adsorbent for the environmental applications. Graphene oxide (GO) and reduced graphene oxide (rGO) were investigated as an adsorbent to think about the adsorption attributes of substantial metal mixes and natural from fluid arrangements. Specialists have tried a wide range of kinds of created adsorbents, for example, activated carbon (AC), polymeric materials, zeolites and hybrid nanomaterials, used as adsorbents for the expulsion of chemical pollutants or heavy metal ions from wastewater. Be that as it may, these adsorbents have been experiencing either low adsorption limits or low performances. Accordingly, incredible exertion has been done as of late to look for a novel class of adsorbents and grow new adsorbent systems.

The carbonaceous nanostructured materials are viable adsorbents to purify water from wastewater through removing the contaminants. Graphene nanosheets are hydrophobic, and, subsequently, stable scatterings in the polar solvents must be acquired with the expansion of appropriate surfactants. Graphene oxides displays oxygen-having useful gatherings, for example, epoxy and hydroxyl (generally situated on the base and best surfaces), and carbonyl (C=O) and carboxyl (-COOH) in the most part of the nanosheets edges, randomly appropriated in the structures graphene nanosheets. These utilitarian gatherings particularly increment the hydrophilic characteristics of GO, making it effortlessly well dispersed in the aqueous system and very stable for a long time under basic ecological conditions.

Rapid industrialization has led to increasing in the discharge of effluents (Castillo et al. 2017). Presence of heavy metals in the water poses threat to the health of the living forms and causes damage to the aquatic life. Metals mainly found in the industrial discharge are chromium, arsenic, zinc, nickel, cobalt, mercury and chromium. These metals are toxic even at the lowest concentrations (Chandana and Subrahmanyam 2017). Several chemical and physical methods have been involved to remove the organic contaminants and metals from the water. Some of the methods are:

- Filtration
- Precipitation
- Coagulation
- Adsorption
- Ion exchange
- Osmosis

These methods are not very efficient and economic. The one used mostly is adsorption, and the reason behind its wide use is its economic and efficient compared to the others. The other most important reason for its popularity is it does not generate any waste in the end.

6.3.2 *Metal-Organic Framework (MOF)-Based Photocatalysts*

6.3.2.1 Principles

In the late 1990s, the disclosure of another sort of permeable mixes has offered extraordinary consideration because of the potential these materials displayed in cutting-edge mechanical applications. These are named as permeable coordination polymers or metal-organic framework (MOF) structures. MOFs are notable to have vast surface regions due to ultrahigh porosity with the measure of their pores running from the smaller scale to mesoporous administration. The structures of MOFs are obtained from natural ligands (alluded to as linkers) and metal groups that act as the connectors.

The main secondary building unit (SBU) is the natural linker, which might be ditopic (having two sorts of coordinative functionalities), tritopic (three composers) or polytopic (more than three kinds). The second SBU is a metal molecule, a limited polyatomic inorganic group with at least two metal iotas, or a boundless inorganic unit, for example, an interminable occasional bar of metal particles. Metal-containing SBUs are produced in situ and can be predesigned because of the sensible decision of response conditions (dissolvable framework, temperature, molar focus, pH). The states of SBUs are characterized by their purposes of expansion (network with natural linker SBU) and can be shown as a polyhedron, polygon or interminable pole. To differentiate, natural linkers are performed to a custom shape. The tasteful science of MOFs relies upon a blend of given metal optional building unit with an assortment of natural SBUs.

6.3.2.2 Photocatalytic Applications of MOFs

With consistently expanding requests of vitality and with petroleum products ending up perpetually lessened, sun-based vitality speaks to an alluring elective arrangement and an extensive group of research which portrays the outfitting and sequestering of vitality from the sun. A few ways to deal with change and store sunlight based vitality as concoction bonds have been proposed, including photochemical methodology, for example, the decrease of CO_2 and H_2O part. The inalienable capacity of plants to trap daylight and change water and CO_2 to sugars (a procedure named photosynthesis) is the wellspring of much motivation for scientists in the field. The advancement of systems to encourage photochemical change has additionally been the subject of huge core interest. Nevertheless, certain materials showing the capacity to part water by outfitting UV light a few confinements on the utilization of the sun-powered range exist. It, in any case, stays of essential significance to plan a steady, capable and practical approach that can change over sun oriented vitality by benefiting from the most extreme sunlight based range.

The retention of light by certain photoactive natural particles makes them experience changes which typically can't be encouraged under standard thermally actuated conditions. Given that the extensive piece of the range isn't utilized by natural mixes, which just retain UV photons, their effectiveness is imperfect. Confinements identified with sun-powered range retention can be alleviated by the utilization of atomic colours which can retain low vitality photons, offering to ascend to new photocatalytic responses under the noticeable light. Three phases include the transformation of sun-powered vitality into helpful compound vitality: the age of charge-isolated energized states by utilizing a photosensitizer to assimilate daylight, the making of redox proportional and resulting exchange to receptive destinations and the nearness of oxidation and lessening half responses at reactant focuses. With the target of combining photosensitizer and reactant segments into covalent fortified dimers, supramolecular structures or polymers a few sorts of mixes have been produced; this approach has a high level of many-sided quality, be that as it may, in that the procedure is difficult and requires many advances, accordingly restricting its pertinence.

MOFs can work as photocatalysts for the fundamental reason that they consolidate photosensitizer and reactant usefulness inside one structure. The previously mentioned three phases of photocatalysis are in this way encouraged inside one strong compound. Through substitution of the standard photocatalyst which ordinarily incorporates substantial metals, photoactive MOFs can work as predominant photocatalysts by limiting sullying and can promptly be recouped and reused because of their strong frame, subsequently giving financial advantages.

In the recent years, MOFs have been well researched for heterogeneous photocatalytic applications. The utilization of MOFs in the photocatalytically determined exploitation of natural poisons and NOx, antibacterial movement and age of sun-powered fills and photoelectrochemical (PEC) vitality features. Furthermore, there are a few announced MOFs that have additionally been utilized in the photocatalytic generation of high-esteem chemicals under mellow conditions. In these reports, the attainability of calibrating the MOF's vitality band structure and surface practical gathering was demonstrated. From the studies, MOFs now remain as an exceptional class of highly efficient photocatalysts due to their tunable characteristics (size, shape, morphology and porosity) compared with the conventional semiconductor photocatalysts.

There are a few incredible surveys that address the advances of MOFs in the photodegradation of natural toxins in wastewater, water part and photoreduction of CO_2, where these materials' security and light retention properties are basically talked about. Although, these audits are constrained as far as outlining the plan rule/criteria and the photocatalytic working instrument, both of which are vital to the advancement of new MOF photocatalysts having attractive properties for acknowledgement in future reasonable applications.

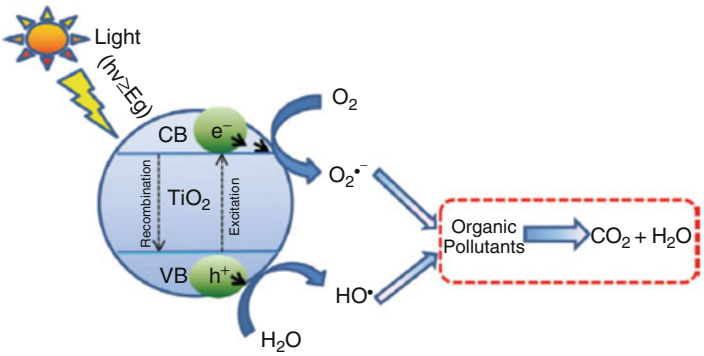

Fig. 6.3 Illustration of photocatalytic activity of TiO_2 photocatalyst. (Reprinted with permission from Samsudin et al. 2015, copyright (2015) Penerbit UKM publisher)

6.3.3 TiO_2-Based Hybrid Photocatalysts

6.3.3.1 Principles

In the framework of environmental issues such as water and air contamination, it is essential to talk about photocatalysis. Photocatalysis has shown great results in the fields of energy storage and depollution of natural sources. Photocatalysis also enables the direct transformation of solar energy into chemical and splitting of water molecules. The importance of photocatalyst is regarded for the solution it gives from the environmental problems such as climate change and greenhouse gas emissions which elevate the need for more developed technologies for the benefit of the environment.

Photocatalytic activity mechanism of TiO_2 photocatalyst is shown in Fig. 6.3. Generally, an electron-hole pair is formed when an electron is moved to the conduction band from the valence band. Then the charge carriers and motivated conduction band electrons are transferred to the TiO_2 surface to make oxidation and reduction procedures. In order to form superoxide ions, the conduction band electrons of TiO_2 are captured by the oxygen molecules. Hydroxyl radicals are formed with an electron-hole pair when the superoxide ions respond with protons or water molecules. Lastly, these formed radicals ultimately lead to the dye degradation into harmless compounds.

6.3.3.2 Different Forms of TiO_2 and Its Physicochemical Properties

TiO_2 shows photocatalytic activity in a non-exhaustive way. It is one of the oldest metal oxides to show the photocatalytic activity. TiO_2 shows exhibit abundant properties for being a good photocatalyst. Some of the properties executed by TiO_2 are as follows:

(i) Non-exhaustive
(ii) Low toxicity
(iii) Great photocatalytic activity
(iv) Chemical stability
(v) Photostability
(vi) Antipollution
(vii) Antibacterial

Great efforts were made to enhance the existing photocatalytic technologies to get the best out of all the existing technologies. A lot of work has been done in order to find out materials that have higher efficiencies for being photocatalysts. TiO_2 has great applications in the fields of photochemistry and nanotechnology.

TiO_2 occurs in three crystallographic phases:

- *Anatase*

  (i) Bipyramidal tetragonal symmetry
  (ii) Photocatalytically active
  (iii) The structure comprises of octahedral

- *Rutile*

  (i) Used as a pigment
  (ii) In coating industry
  (iii) Chemically inert

- *Brookite*

  (i) Limited range of temperature
  (ii) Orthorhombic symmetry

TiO_2 falls under the category of an n-type semiconductor. TiO_2 semiconductors get activated by UV light (Kim et al. 2003b). The real efficiency of TiO_2 depends on the phase composition along with the size, porosity and its composition. TiO_2 shows a tendency to generate the holes and electron in the presence of UV light, due to which it is considered as an authentic material for the green technology.

The TiO_2 which gets activated by visible light could be synthesized by the following methods:

(i) Metal ion implantation
(ii) TiO_2 reduction
(iii) Sensitizing TiO_2 with dyes

Doping of TiO_2 with other materials began in the 1980s. N-doped TiO_2 was reported as light-sensitive photocatalyst. Studies have carried out on the large number of anions such as sulphur, carbon, etc. In the case of N-doped titanate semiconducting catalyst, the origin of visible-light sensitivity is the localized N_{2p} level. The hole movement should be low. The photo-produced hole in the high mobility region in TiO_2's valence band should be used to attain high action under the visible light.

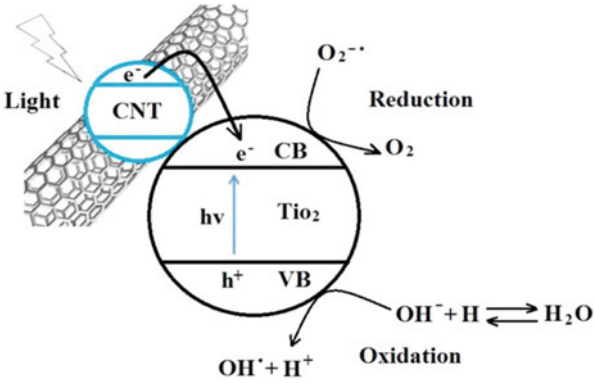

Fig. 6.4 The photocatalytic mechanism of photocatalytic degradation over TiO_2/carbon nanotubes hybrid photocatalyst. (Reprinted with permission from Mohamed et al. 2016, copyright (2016) Elsevier)

6.3.3.3 Structure of TiO_2

Titanium dioxide exists as a polymorphic structure, and as discussed above, it has three polymorphic structures. Anatase and rutile are tetragonal, and brookite is orthorhombic. In anatase, TiO_6 octahedron is a bit distorted with two TiO_2 bonds greater than rest of the O-Ti-O bonds, which show a deviation from 90°. Anatase shows more deviation from rutile. Brookite formation occurs by joining of edges of distorted octahedral. They can find applications such as treatment of wastewater, air pollution control and water splitting.

6.3.3.4 Photocatalytic Mechanism of TiO_2

The mechanism begins with adsorption of photons by an extremely reactive electronically excited molecule. The capability of photochemistry is controlled by the features of light adsorption. The process begins with the formation of charge carriers in the semiconductor materials. Titanium oxide's valence band comprises of oxygen's 2p orbital, whereas the conduction band of titanium comprises of 3d orbitals.

Absorption of photon initiates the photocatalytic mechanism. It should be noted that the energy of photon should be greater than the band gap titanium dioxide, which further causes generation of an electron-hole pair on titanium dioxide surface. The holes are generated in the valence band due to the excited electrons to the conduction band. To dissipate the energy as heat, the excited electrons and holes combine together, by getting trapped in the surface states or by reacting with the electron donors and acceptors which are adsorbed on the surface of the semiconductor (Fig. 6.4.)

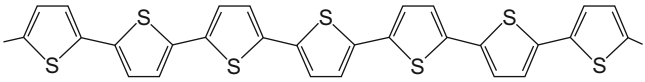

Fig. 6.5 Chemical structure of polythiophene

6.3.3.5 Hybrid Photocatalysts Based on TiO_2 and Organic Conjugated Polymers

6.3.3.5.1 Properties of Polythiophene

The electronic and photonic properties of this polymer are the main cause of drawing and holding on attention. The π conjugation in the electronic structure allows the delocalization of the charge transporters when doping on the mobility of high charge carriers. The delocalized charged structures are responsible for the strong absorptions. Polythiophene comprises of a long chain of alternate double and single bonds (Vukmirovic and Wang 2009). The first and fourth carbons are combined by the sulphur atom which forms a thionyl ring molecule. This leads to increase in the single bond character. Weaker mesomeric effect pushes the band gap of polythiophene to blue. The sulphur groups present in the chain direct the electronic and optical properties, whereas the carbon conjugation directs the spectroscopic properties as shown in Fig. 6.5.

6.3.3.5.2 Properties of Polyaniline

Some of the physicochemical properties of polyaniline are:

(i) High conductivity
(ii) Redox reversibility
(iii) Swift change
(iv) High stability in the air

Polyaniline is one of the most central organic conducting polymers due to the following properties (Vachon et al. 1987):

(i) Outstanding electrical conductivity
(ii) A rich number of intrinsic redox sites
(iii) Easy processability
(iv) Excellent environmental and thermal stability
(v) Excellent physical and chemical characteristics

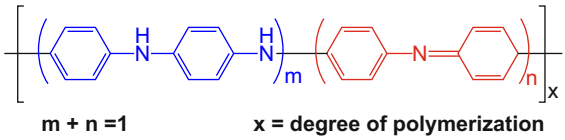

Fig. 6.6 Chemical structure of polyaniline

Polyaniline is the leading conducting polymer to succeed worldwide commercial market for various industrial applications. The chemical structure of polyaniline is shown in Fig. 6.6. Polyaniline exists in a variety of different forms and structures. The green protonated emeraldine (green colour) is the most common, and it has an electrical conductivity on a semiconducting level of the order of 100 S/cm, several orders of magnitude higher than that of common polymeric materials such as polystyrene, polyethylene, etc. ($<10^{-9}$ S/cm), but it is lower than that of typical metallic materials ($>10^{4}$ S/cm). The protonated form of polymer (polyaniline hydrochloride) converts to a semi- or non-conducting emeraldine base (blue colour) when treated with a base such as sodium hydroxide and ammonium hydroxide.

6.3.3.5.3 Properties of Polypyrrole

This chemical compound is formed by connecting a large number of pyrrole rings. Polypyrrole is the conducting materials. They belong to the rigid-rod polymer family; basically, all are derivative of polyacetylene. This was the first polymer to exhibit high conductivity. These are commonly known by the name "pyrrole black". Polypyrrole has also shown natural existence with melanin and polyacetylene. Polypyrrole shows characteristics for radar absorbing material. Polypyrrole can be prepared using the following methods (Xu et al. 2006; Wang et al. 2004; Kilmartin and Wright 2001; Tan and Ge 1996):

- Chemical polymerization
- Electrochemical
- Plasma
- Vapour phase polymerization

Vapour phase polymerization is the most suitable method because it provides suitable thickness and great conductivity along with uniformity to the film.

The drawbacks of other techniques are:

- Poor electrical conductivity
- Demand for the conductive substrates
- Porosity
- Uneven thickness of the film
- Size of substrate

6.3.3.5.4 Synthesis of TiO_2-Based Hybrid Photocatalysts with Different Organic Conjugated Polymers

Synthesis of TiO_2/Polyaniline Hybrid Photocatalysts Titania/polyaniline hybrid catalysts are synthesized by the following method. Two grammes of TiO_2 and 3.3 mL of distilled aniline was taken in a beaker containing 100 mL of 1 M HCl and continued to stir in the ice bath. The oxidant (peroxide) was then added to above solution and sonicate the mixture for an hour, and autoclave it for overnight. Then, the product was filtered and washed with deionized water and acetone in order to get rid of unreacted aniline, by-products and impurities.

Synthesis of TiO_2/Polythiophene Hybrid Photocatalysts Two grammes of TiO_2 and 3.1 mL of distilled thiophene monomer was taken in a beaker containing 5 mL of acetonitrile. The mixer kept in an ice bath (−10 °C) under the magnetic stirring, and then add ferric chloride solution was added dropwise to above solution. The reaction mixture was sonicated and transferred to an autoclave and then heat in the oven for overnight. The product was filtered using the membrane filter and washed several times with an excess of deionized water and acetone to remove unreacted thiophene and by-products.

Synthesis of TiO_2/Polypyrrole Hybrid Photocatalysts Two grammes of TiO_2 and 3.6 ml distilled pyrrole was taken in the beaker containing 10 ml of distilled water. The mixture was kept on an ice bath under constant stirring, and then add ferric chloride solution by dropwise. After sonicating the reaction mixture for an hour, autoclave it, and then keep in the oven for an hour. The obtained product was filtered and washed with an excess of deionized water and acetone to remove unreacted pyrrole and by-products.

6.3.3.5.5 Characterization of TiO_2/Conjugated Polymer-Based Hybrid Catalysts

XRD X-ray diffraction technique is chiefly used for the identification of crystalline material's phase, and it provides the information about the dimension of the unit cell. It could be specifically said that the power of XRD is used for the characterization of polycrystalline phases. The composition of the material is determined by grounding it, and then it's homogenized. Majority of the solid mass is described as crystalline. The diffraction pattern can be obtained when the X-rays comes in contact with the substance.

X-rays are based on the approach of constructive interference of monochromatic light. Generation of x-rays is through cathode ray tube. The use of diffraction technique is chemical analysis. It can further include phase analysis; the widest use of XRD technique is for the determination of the crystalline structure of

unknown crystals. It finds great application in the branch of geology, earth sciences, material sciences, etc. for the characterization of the crystalline material and the identification of the materials.

Cyclic voltammetry:

- Helps in the quantitative determination of organic and inorganic compounds.
- Measures kinetic rate.
- Determines the adsorption process.
- Determines the complexion values.
- It has great use in the pharmacy industry for the quantitative determination of compounds.
- It also helps in defining the thermodynamic properties.
- Helps in the calculation of the number of electrons in a redox reaction.

Raman Spectroscopy The Raman spectroscopy is utilized to determine some low-frequency modes such as rotation and vibration in a system. Raman spectroscopy occurs from inelastic collisions. The frequency difference of incident and scattered light corresponds to the vibrational and rotational spectra. It holds great use in the branch of chemistry because a vibrational spectrum provides authentic information about the bonds of the molecule. The orientation of any crystal could also be found out from the Raman spectroscopy.

6.3.3.5.6 Antibacterial Activity of Photocatalysts

The photocatalytic effect of TiO_2 is theoretically possible since this catalytic material is easy to fabricate with low cost in large scale (Tan and Ge 1996; Cheng et al. 2009). One of the potential applications of TiO_2 photocatalysts is the antibacterial activity. The antibacterial reagents act as an inactivate cell viability, but the pyrogenic and toxic ingredients like endotoxins remain even after the killing of bacteria. The endotoxin is the cell wall constituent of bacteria that consisting of a carbohydrate chain, which is expressed as the complex lipid and O-antigen. Endotoxin is highly toxic and causes serious and risky problems in the manufacturing industries of pharmaceuticals and medical devices (Ishibashi et al. 2000).

The photocatalytic reaction of TiO_2 has been used to inactivate a wide range of microorganisms as explained below (Kim et al. 2003b; Duffy et al. 2004; Chamorn and Yasuyoshi 2006). The certain amount of the photocatalyst was dispersed into saline solution (0.9%) and then sterilized the mixed solution by autoclaving at the high temperature of 1200 °C and pressure of 15 lbs for 30 min. After cooling it to room temperature, the product was mixed with 1 mL of the bacterial cell suspension under the magnetic stirring to avoid the settling of photocatalyst and then irradiated the solution under visible light (150 W ozone-free Xe lamp) that has a wavelength of 420–630 nm. The bacterial suspension was also irradiated in the absence of photocatalyst to determine the antibacterial activity. After irradiation process, 1 mL of catalyst suspension was distributed over the Petri dish that consists of the nutrient agar and incubated it for 2 days at 370 °C, and then it was taken out for the

counting. It was found that the antibacterial efficiency of TiO_2 photocatalyst was increased as the decrease of a number of colonies.

6.3.3.6 Environmental Application of Different Photocatalysts

6.3.3.6.1 Water Purification

The photochemical degradation of hazardous pollutants such as dyes, pharmaceutical effluents and metallic discharge was performed under visible-light irradiation (oriel lamp). The photodegradation % of dyes and 4-nitrophenol was analysed using the equation, $((C_0 - C)/C_0) * 100$, where C_0 and C represent the initial and final concentration of the photocatalysts. Phenol, bisphenol-A and antibiotic sulfamethoxazole were studied using high-performance liquid chromatography (HPLC) with the reverse phase column. The antibacterial studies were also carried out under visible-light irradiation to study *Salmonella typhi* which is the typhoid-causing bacteria. The antibacterial activity was determined using the colony counting technique.

With the growing demand for water and lack of clean sources due of the quick advancement of industrialization, population growth and long dry period have turned into the critical issue around the world. The amount of safe and drinking water for day by day is decreasing slowly, and this issue can be resolved urgently. It is estimated that ~4 billion individuals experience to have no or little access to spotless and purified drinking water supply and a great many individuals passed on of serious waterborne sicknesses yearly. These measurable figures are required to develop in near future, as drastically increasing the water pollution due to the release of organic contaminants and micro hazardous pollutants into water. It is necessary to develop effective clean water technologies to treat the wastewater, resulting in human well-being.

Among the advanced oxidation processes (AOP), the heterostructured photocatalysis utilizing semiconducting catalysts (e.g. TiO_2, CdS, ZnO, GaP, ZnS, ZrO_2, WO_3, Fe_2O_3, etc.) has shown its effectiveness in photodegrading an extensive variety of equivocal headstrong organic pollutants into promptly biodegradable compounds that mineralized in the long-run to the harmless small molecules such as carbon dioxide (CO_2) and water (H_2O). Among various semiconductor photocatalysts, TiO_2 has gotten the best enthusiasm for the research and development of photocatalysis innovation. It has two main crystal phases such as anatase and rutile with the band gap values of 3.2 eV and 2.0 eV. The multifaceted TiO_2 photocatalyst has unique properties such as chemical stability, environmental stability and protection from the synthetic breakdown, and their solid mechanical properties have advanced its wide range of photocatalytic applications in an area of wastewater treatment. Various imperative highlights for the heterostructured photocatalysts which have expanded their potential uses in wastewater treatment are the following (Fujishima et al. 2007): (i) an ambient working environment,

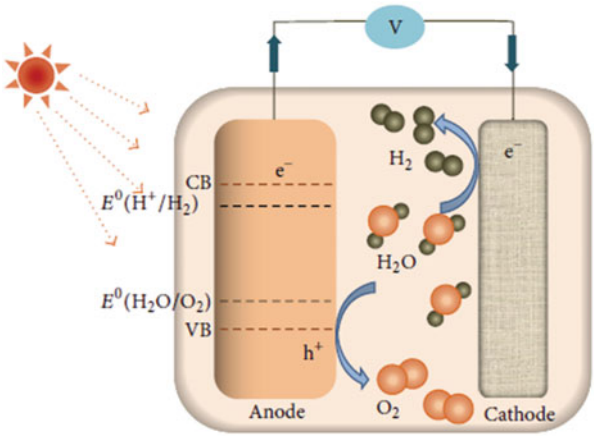

Fig. 6.7 The schematic representation for PEC water splitting of TiO_2. (Reproduced from Kochuveedu 2016, copyright (2016) Hindawi publisher)

(ii) the total mineralization of guardians and it halfway mixes without optional contamination and (iii) the process operates at low cost.

The post-partition of the semiconductor TiO_2 impetus after wastewater treatment stays as the significant hindrance towards the reasonableness as an industrial process. TiO_2 molecule size and its surface vitality make the solid inclination for the impetus aggregates in the middle of an operation process. Such aggregated particles are exceedingly impeding in perspectives of particle measure protection, surface region lessening and its expectancy of recyclability. Other specialized difficulties incorporate into the impetuses improvement with more extensive photoactivity and it's joining with the feasible catalytic reactor framework.

The proposed mechanism for photoelectrochemical water splitting of TiO_2 is shown in Fig. 6.7. Reduction and oxidation are the elementary chemical reactions that ensue through water splitting. As stated, for the evolution of H_2 and O_2, the conduction band and valance band positions of materials have to fit into the water reduction and oxidation potential respectively. Upon light irradiated, the photogenerated electrons are excited to the CB from the VB and leaving the same amount of holes. Finally, the photoexcited electrons and holes are involved in the generation of hydrogen and oxygen.

6.3.4 Graphene Oxide (GO)-Based Photocatalyst for Dye Degradation and H_2 Evolution

Recently, graphene-based composite materials have been considered as a promising candidate in both technical and scientific communities because of its tremendous properties (Zhang et al. 2015; Novoselov et al. 2012). The preparation of graphene-based composite photocatalyst materials has progressed into numerous fields, such as energy storage and transformation, optoelectronics, nanoelectronics, biosensors,

supercapacitors, etc. (Yang and Xu 2016). In detail, the abundance preparations of the graphene-based catalysts for enhancing the solar energy transformation ability have been observed in recent years (Zhang et al. 2014; Yuan et al. 2014; Han et al. 2015; Pan et al. 2014).

Graphene is a suitable material for photocatalyst support and an electron acceptor/trapper due to its huge surface area, greater work function, good optical transmittance and outstanding electronic conductivity (Yang and Xu 2013; Yang et al. 2014; Han et al. 2017). As per literature survey, it is significantly noticed that the addition of a suitable quantity of graphene-associated materials for the photoactive mechanisms is necessary for the conversion of solar energy. Generally, the actual form of graphene in the graphene-based catalysts is different from its original state, which is owing to the existence of defects, oxygenated functional groups and grouping of the graphene sheets. Hence, it is difficult to get maximum properties of graphene. Such a condition intensely advises that (i) the incorporation of graphene with a photocatalyst semiconductor to make new multicomponent composite photocatalyst materials gives a favourable approach for fabricating the next-generation simulated photosynthetic systems and (ii), furthermore, there is still enormous room to increase the catalytic activity of graphene-based composite catalysts through improving the properties of the synthesized graphene composite catalysts.

However, due to its poor photocatalytic performance, different approaches have been suggested to increase its photocatalytic activity. Therefore, graphene and its products have been effectively exposed as a photocatalyst for PEC water splitting reactions. Another method to enlarge its advantages is the hybridization with other compounds like g-C_3N_4 (graphitic carbon nitride). Polymeric g-C_3N_4 shows a graphite-like structure, and it has been developed as a visible-light and metal-free reactive catalyst in the photosynthesis and environmental remediation.

6.3.4.1 Photodegradation of Chemical Pollutants

Photodegradation of pollutants is one of the most potential eco-friendly sanitization technologies owing to its inexpensive, no secondary pollution and simple handling. In this concern, a graphene/g-C_3N_4 hybrid composite is a green visible-light catalyst and has involved significant research attention since its favourable advantages in the dye decomposition of hazardous contaminants, such as dye degradation of organic substance via oxidation, diminished metal ion and NOx reduction. Generally, a photocatalytic decomposition reaction via photocatalytic oxidation of pollutants with O_2 under photo illumination makes CO_2, H_2O or other compounds. To estimate the photocatalytic performance, different organic pollutant dyes have been used as contaminants such as rhodamine B (RhB), methylene orange (MO), congo red (CR) and methyl blue (MB).

Li et al. successfully synthesized cross-linked g-C_3N_4/reduced graphene oxide (rGO) composites using the combination of cyanamide and GO with various weight proportions under thermal treatment (Li et al. 2013). It is observed that a suitable rGO ratio in the g-C_3N_4/rGO nanocomposite caused a positively shifted VB

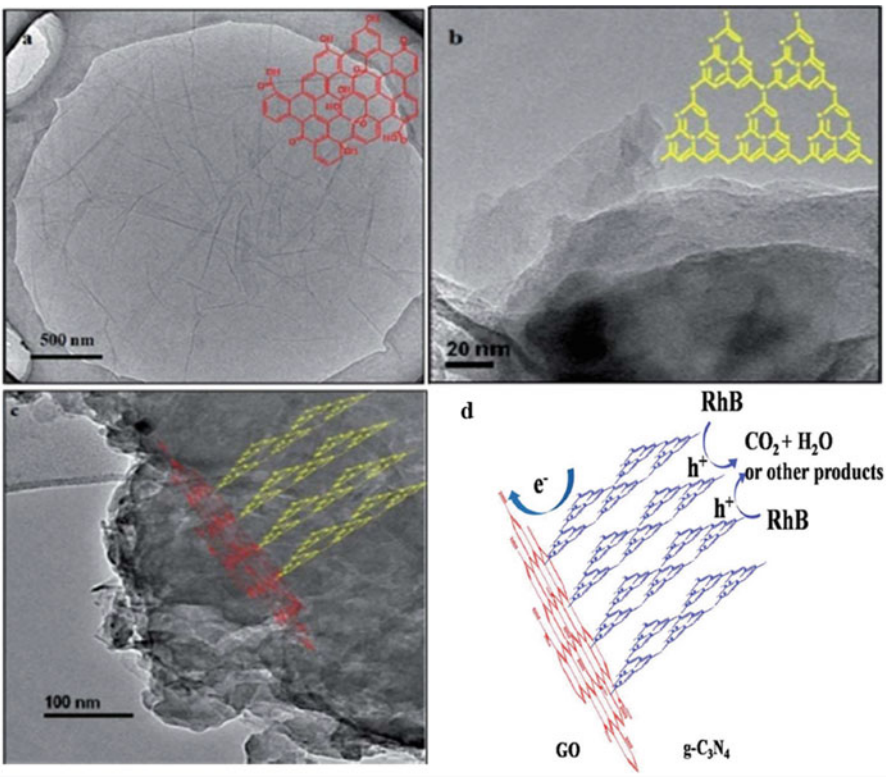

Fig. 6.8 TEM image and schematic representation (inset) of (**a**) GO, (**b**) g-C_3N_4, (**c**) GO/g-C_3N_4 and (**d**) proposed mechanism for charge transfer and photodegradation of RhB for the hybrid nanocomposite. (Reproduced with permission from Liao et al. 2012, copyright (2012) Royal Society of Chemistry)

potential and reveals an improved oxidation ability. Moreover, the hybrid sample exhibited enhanced light absorption capacity, improved conductivity and better electron transport properties due to the existence of rGO. Accordingly, an optimized rGO ratio of 2.5% in the nanohybrid exhibited three times greater photocatalytic degradation of RhB than pristine g-C_3N_4. Furthermore, the optimum photocatalyst was also displayed 2.7 times greater efficient of 4-nitrophenol degradation than bare g-C_3N_4. This enhanced photocatalytic performances could be due to the better utilization of visible light, oxidation power, properties of electron movement, decreased band gap, movement of band edge potential and better electronic conductivity.

A modified GO/g-C_3N_4 nanocomposite has been fabricated by Liao et al. (2012) using a sonochemical synthesis method for superior catalytic activity. The transmission electron microscopic (TEM) images of pristine GO, g-C_3N_4 and GO/g-C_3N_4 hybrid composite are shown in Fig. 6.8a–c. From the result and analysis, it is signifying the GO performances as a separation centre and acceptor of an electron

in the hybrid composite. Under visible-light irradiation, the separation of active photoexcited carriers improved the photocatalytic activity. In case of GO/g-C_3N_4, the evaluated dye degradation rate constants for RhB and 2,4-dichlorophenol were found to be 3.80 and 2.08, which compared with bare GO and g-C_3N_4. Based on the structural, morphological studies and their properties, the effective catalytic activity would be mostly associated with the detachment of charge carriers. Figure 6.8d shows the suggested catalytic activity of hybrid GO/g-C_3N_4 nanocomposite.

Upon light illumination, the photoexcited electrons of g-C_3N_4 moved from the valence band to the conduction band. Due to the heterojunction construction between GO and g-C_3N_4, the photoexcited e^- then moved to the GO sheet, which decreases the possibility of charge carrier's recombination rate and improved the separation competence. Furthermore, this led to ample holes left on the VB of g-C_3N_4. Hence, due to the VB edge potential of g-C_3N_4 (1.57 V vs Ag/AgCl), RhB and 2, 4-DCP was oxidized to CO_2, H_2O or other intermediates. Yu et al. (2014) reported a porous g-C_3N_4/graphene nanocomposite was prepared by mixing graphene with porous g-C_3N_4 for methyl blue dye degradation.

The hybrid sample showed a noticeable improvement of photocatalytic decomposition of MB, and the enhancement was six times higher than that of pristine g-C_3N_4. In another similar work, GO/g-C_3N_4 composite was effectively synthesized using an anchoring exfoliated g-C_3N_4 onto a GO surface by Dai et al. (2014) for methyl blue (MB) organic pollutant dye degradation. The optimal weight fraction of GO hybrid sample was exhibited largely reinforced photocurrent. Thus, the resultant catalytic performance of the hybrid composite was significantly enhanced with the optimized photocurrent. The optimized hybrid composite sample exhibited greater MB dye degradation activity than the pure g-C_3N_4, commercial P25 and the physical mixture of g-C_3N_4 and GO as a photocatalyst.

When compared to binary hybrid composite materials, the development of heterojunction photocatalysts can efficiently detach the photo-induced holes (h^+) and electrons (e^-) and produce more active radical species, which are useful for practical applications. In recent times, heterojunction nanocomposites like g-C_3N_4-Ag_X ($X = VO_4^{3-}$, CO_3^{2-}, PO_4^{3-}, S^{2-}, Cl^-, Br^- and I^-) have been concerned great consideration and broadly studied due to their promising separation of charge carriers and photocatalytic performance (Wang et al. 2014). Apart from the graphene/g-C_3N_4 binary nanohybrid composites, graphene/g-C_3N_4 synthesized ternary heterojunctions have also been studied. In this respect, Li et al. (2015) reported a novel AgBr assisted on g-C_3N_4-deposited N-doped graphene ternary super hybrid (AgBr/g-C_3N_4/NG_{-x}) composite that was successfully developed using a polymerization followed by ion exchange method.

The optimized AgBr/g-C_3N_4/NG-50 photocatalyst sample (the content of g-C_3N_4/NG in AgBr/g-C_3N_4/NG-x was 50 wt%) exhibited the greater photocatalytic degradation activity compared to other samples. Furthermore, when further increased g-C_3N_4/NG content, decreased photocatalytic activity. This result specified that the additional g-C_3N_4/NG generate active sites on the photocatalyst surface and decrease the light diffusion distance in the catalytic reaction process. This enhancement in degradation is due to the effective detachment of charge carriers at

the boundary of AgBr/g-C_3N_4/NG hybrid and enhanced the separation rate of photo-induced holes (h^+) and electrons (e^-), which led to the outstanding catalytic performance of MO dye degradation.

In another report, Liu et al. described Fe(III) incorporated into a graphene/g-C_3N_4 binary nanocomposite was successfully developed in order to introduce the interfacial charge transfer effect by a simple impregnation technique (Liu et al. 2016). Moreover, an innovative ternary nanocomposite (Fe(III)/graphene/g-C_3N_4) has been fabricated by a direct mixing of graphene and the binary Fe(III)/g-C_3N_4 nanocomposite. From the result and analysis, it was observed that the synthesized photocatalyst displayed improved absorption ability of light and decreased the charge separation rate and better photocatalytic performance than the other prepared samples.

It is noticed that the incorporation of graphene and Fe exhibited well organization, small in size, and comparatively high content than the binary composite, and this shows the effect of graphene and Fe species in the composite. Therefore, the ternary Fe(III)/graphene/g-C_3N_4 catalyst exhibited the greater photocatalytic performance than binary composite, due to its better photo immersion ability and detachment of charge carriers. In another study, g-C_3N_4 combined CdS nanoparticles and rGO sheets (g-C_3N_4/CdS/rGO) ternary nanocomposite have been successfully fabricated by Rajendra et al. (2014). Consequently, the prepared g-C_3N_4/CdS/rGO ternary composite exhibited greater dye degradation of RhB and congo red organic pollutants. Significantly, no considerable alteration in the degradation competence was noticed after three sequential cycles, concluding that the g-C_3N_4/CdS/rGO nanocomposite has decent reusability and stability for practical applications. Moreover, noble metal nanoparticles are supported by graphene and g-C_3N_4 and the SPR effect due to the loaded noble metal ions, which can improve the immersion of light capacity. Hence, the total photocatalytic activity has been enhanced.

6.3.4.2 Hydrogen (H_2) Evolution Reaction by g-C_3N_4-Based Functional Photocatalysts

Using a suitable photocatalyst, the hydrogen evolution reaction (HER) is an effective method for hydrogen generation via water electrolysis (Zheng et al. 2015). However, several nonnoble metal photocatalysts suffer intrinsic erosion for the HER, thus resultant in reduced constancy. Nevertheless, carbon-related photocatalysts, particularly nitrogen-/carbon-related materials, are capable substitutes owing to the strong tolerance to acid/alkali surroundings and the improved π bonding to increase their electron donor/acceptor properties (Shalom et al. 2014).

In past years, graphene/g-C_3N_4 hybrid composites have been used as potential catalysts for electrocatalytic HER activity. Qiao et al. (Zheng et al. 2014) established the application of g-C_3N_4/NG hybrid (g-C_3N_4 attached nitrogen-doped graphene) photocatalyst for HER performance through hypothetical investigation and experimental studies. From the experimental observations, it is revealed that the

electrocatalytic properties are initiated from its intrinsic chemicals and electronic coupling, which encourages the adsorption of proton and reduced kinematics.

The preparation of a flexible 3D film by mixing the porous C_3N_4 nanolayers with N-doped graphene sheets was composed through a simplistic process via low-price precursors for HER electrodes without any substrates has been reported (Duan et al. 2015). This nonmetal electrocatalyst has showed unbeatable HER activity with an identical positive onset potential near to commercial Pt (8 mV vs 0 mV of Pt/C vs RHE @ 0.5 mA cm^{-2}), extraordinary conversation current density of 0.43 mA cm^{-2} and remarkable strength (seldom activity loss >5000 cycles). The exhibited outstanding HER activity is due to (i) in-plane pores into C_3N_4 and exfoliation of C_3N_4 into nanosheets, (ii) highly ordered porous structure and (iii) 3D conductive graphene network. Moreover, the prepared material showed an outstanding stability owing to the active lodging of graphene and sheets C_3N_4.

Recently, by using a hydrothermal technique, a 3D nanoribbon construction of g-C_3N_4 nanoribbon-G was prepared (Zhao et al. 2014). SEM and TEM image of the prepared g-C_3N_4 nanoribbon-G is shown in Fig. 6.9a, b. Because of the mass transportation and multipath way of charge, the hybrid composite showed extraordinary HER activity with a Tafel slope of 54 mV $decade^{-1}$ and a low onset overpotential of 80 mV as shown in Fig. 6.9c, d. The g-C_3N_4 nanoribbon-G catalyst with better strength under various scan rates showed a low overpotential of 207 mV to get a 10 mA cm^{-2} HER current density, which is lesser than those of g-C_3N_4/NG hybrids as shown in Fig. 6.9e. Instantaneously, the resulting nanohybrid exhibited outstanding durable constancy that is essential for sensible hydrogen production as shown in Fig. 6.9f.

Bonding of layer materials into 2D single-atom sheets has encouraged excellent properties, because of its greater surface area, great intrinsic charge carrier movement and noticeable modifications in the band structure. Qu et al. synthesized a dual mesh of 2D g-C_3N_4 meshes in situ formed on 2D graphene meshes (g-CN@G MMs) by a direct template-free technique (Han et al. 2016). The unique mesh-on-mesh g-C_3N_4@G MM catalyst composite displays an excellent HER activity, because of its extremely extended surface area, plentiful hydrogen adsorption locations, numerous electron carriage channels and great ability of electron movement. Under visible-light irradiation, the fabricated of single layers g-C_3N_4 shows a H_2 generation rate (8510 μmol h^{-1} g^{-1}) and quantum efficiency (5.1%).

6.4 Conclusion

Through the studies, it was concluded that carbon-based hybrid materials (graphitic carbon nitride and graphene) were found to be efficient in removal of waste from water. They found to be responsible for increasing photocatalytic activity and very effective in decontamination of water. The factors responsible for the decontamination of wastewater are the surface area, temperature, pH and composition. The efficiency could also be improved by functionalization of these nanostructured

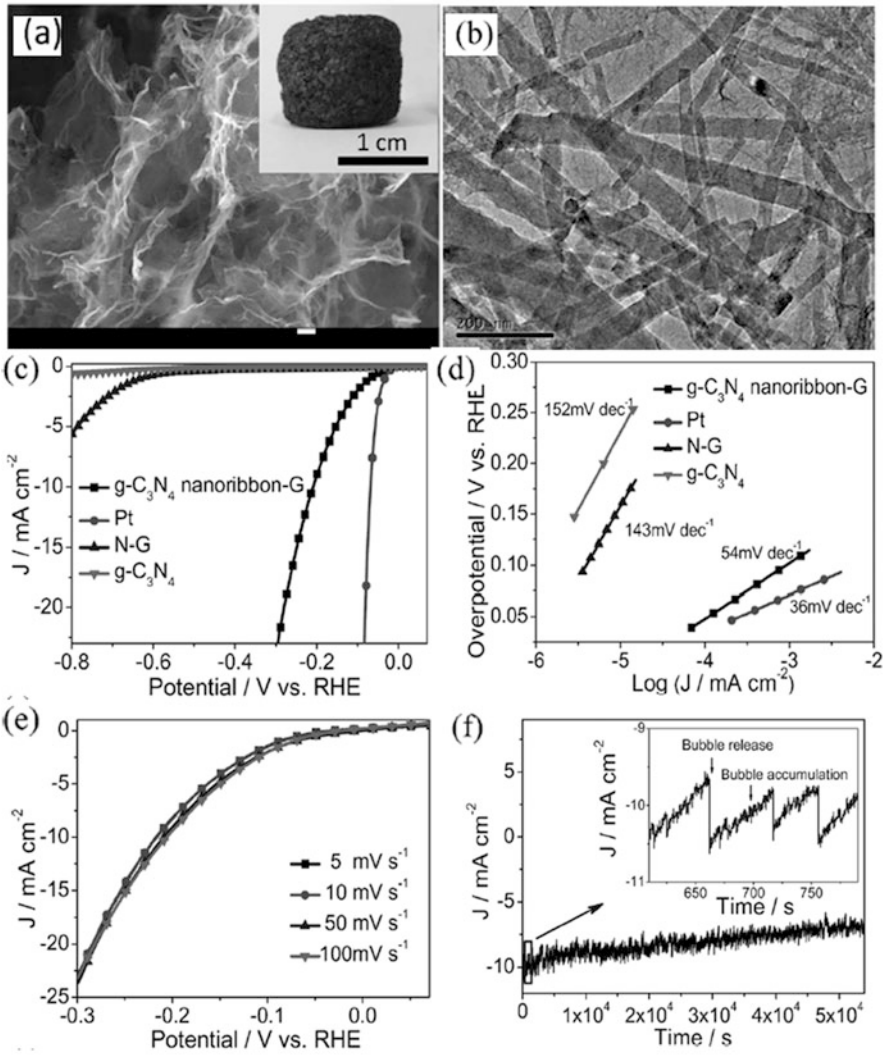

Fig. 6.9 (**a**) SEM images of the synthesized g-C_3N_4 nanoribbon-G. The inset of (**a**) is a photo of the as-prepared g-C_3N_4 nanoribbon-G, (**b**) TEM images of the prepared g-C_3N_4 nanoribbon-G, (**c**) the HER polarization curves, (**d**) the consistent Tafel plots of numerous catalysts (g-C_3N_4 nanoribbon-G, Pt wire, NG and g-C_3N_4, respectively), (**e**) the polarization curves of g-C_3N_4 nanoribbon-G with a scan rate from 5 to 100 mVs^{-1} and (**f**) time dependence of the current density at 200 mV versus RHE. (Reprinted with permission from Zhao et al. 2014, copyright (2014) Wiley)

carbon materials by various kinds of functional groups and with various dopants and semiconducting metal oxides. They show promising results in the photocatalysis process.

References

Bivins AW, Sumner T, Kumpel E, Howard G, Cumming O, Ross I, Nelson K, Brown J (2017) Estimating infection risks and the global burden of diarrheal disease attributable to intermittent water supply using QMRA. Environ Sci Technol 51:7542–7551

Castillo A, Vall P, Baserba MG, Comas J, Poch M (2017) Selection of industrial (food, drink and milk sector) wastewater treatment technologies: a multi-criteria assessment. J Clean Prod 143:180–190

Chamorn M, Yasuyoshi H (2006) Antifungal activity of TiO_2 photocatalysis against Penicillium expansum in vitro and in fruit tests. Int J Food Microbiol 2:99–103

Chandana L, Subrahmanyam C (2017) Non-thermal discharge plasma promoted redox transformation of arsenic (III) and chromium (VI) in an aqueous medium. Chem Eng J 329:211–219

Chen S, Wang LW (2012) Thermo-dynamic oxidation and reduction potentials of photocatalytic semiconductors in aqueous solution. Chem Mater 24:3659–3666

Chen JF, Wang YU, Guo F, Wang XM, Zheng C (2000) Synthesis of nanoparticles with novel technology: high-gravity reactive precipitation. Ind Eng Chem Res 39:948–954

Cheng CL, Sun DS, Chu WC, Tseng YH, Ho HC, Wang JB, Chung PH, Chen JH, Tsai PJ, Lin NT, Yu MS, Chang HH (2009) The effects of the bacterial interaction with visible-light responsive titania photocatalyst on the bactericidal performance. J Biomed Sci 16:7. (10 pgs)

Colmenares JC, Luque R (2014) Heterogeneous photocatalytic nanomaterials: prospects and challenges in selective transformations of biomass-derived compounds. Chem Soc Rev 43:765–778

Dai K, Lu L, Liu Q, Zhu G, Wei X, Bai J, Xuan L, Wang H (2014) Sonication assisted preparation of graphene oxide/graphitic-C_3N_4 nanosheet hybrid with reinforced photocurrent for photocatalyst applications. Dalton Trans 43:6295–6299

Dasireddy VBCC, Likozar B (2017) Activation and decomposition of methane over cobalt-copper and iron-based heterogeneous catalysts for CO_x-free hydrogen and multi walled carbon nanotube production. Energy Technol 5:1344–1355

Duan J, Chen S, Jaroniec M, Qiao SZ (2015) Porous C_3N_4 nanolayers@N-graphene films as catalyst electrodes for highly efficient hydrogen evolution. ACS Nano 9:931–940

Duffy EF, Al Touati F, Kehoe SC, McLoughlin OA, Gill LW, Gernjak W, Mc Guigan KG (2004) A novel TiO_2-assisted solar photocatalytic batch-process disinfection reactor for the treatment of biological and chemical contaminants in domestic drinking water in developing countries. Sol Energy 77:649–655

Fujishima A, Zhang X, Tryk DA (2007) Heterogeneous photocatalysis: from water photolysis to applications in environmental cleanup. Int J Hydrogen Energ 32:2664–2672

Gillan EG (2000) Synthesis of nitrogen-rich carbon nitride networks from an energetic molecular azide precursor. Chem Mater 12:3906–3912

Han C, Chen Z, Zhang N, Colmenares JC, Xu Y-J (2015) Hierarchically CdS decorated 1D ZnO nanorods-2D graphene hybrids: low temperature synthesis and enhanced photocatalytic performance. Adv Funct Mater 25:221–229

Han Q, Wang B, Gao J, Cheng ZH, Zhao Y, Zhang ZP, Qu LT (2016) Atomically thin mesoporous nano mesh of graphitic C_3N_4 for high-efficiency photocatalytic hydrogen evolution. ACS Nano 10:2745–2751

Han Q, Chen N, Zhang J, Qu L (2017) Graphene/graphitic carbon nitride hybrids for catalysis. Mater Horiz 4:832–850

Hathway T, Rockafellow EM, Jenks WS, Chul Oh Y (2009) Photocatalytic degradation using tungsten-modified TiO2 and visible light: kinetic and mechanistic effects using multiple catalyst doping strategies. J Photochem Photobiol A 207:197–203

Ishibashi KI, Fujishima A, Watanabe T, Hashimoto K (2000) Detection of active oxidative species in TiO_2 photocatalysis using the fluorescence technique. Electrochem Commun 2:207–210

Job WK, Kang HJ (2013) Polyacrylonitrile-TiO_2 fibers for control of gaseous aromatic compounds. Ind Eng Chem Res 52:4475–4483

Kilmartin PA, Wright GA (2001) Photoeffects to characterise polypyrrole electrodes and bilayers with polyaniline. Electrochim Acta 46:2787–2794

Kim J, Sohn D, Sung Y, Kim ER (2003a) Fabrication and characterization of conductive polypyrrole thin film prepared by in situ vapor-phase polymerization. Synth Met 132:309–313

Kim B, Kim D, Cho D, Cho S (2003b) Bactericidal effect of TiO_2 photocatalyst on selected food-borne pathogenic bacteria. Chemosphere 52:277–281

Kochuveedu ST (2016) Photocatalytic and photoelectrochemical water splitting on TiO_2 via photosensitization. J Nanomater. http://dx.doi.org/10.1155/2016/4073142

Komatsu T, Nakamura T (2001) Polycondensation/pyrolysis of tris-s-triazine derivatives leading to graphite-like carbon nitrides. J Mater Chem 11:474–478

Li Y, Zhang H, Liu P, Wang D, Li Y, Zhao H (2013) Cross-linked g-C_3N_4/rGO nanocomposites with tunable band structure and enhanced visible light photocatalytic activity. Small 9:3336–3344

Li HY, Gan SY, Wang HY, Han DX, Niu L (2015) Intercorrelated superhybrid of AgBr supported on graphitic-C_3N_4-decorated nitrogen-doped graphene: high engineering photocatalytic activities for water purification and CO_2 reduction. Adv Mater 27:6906–6913

Liang Q, Jin J, Zhang M, Liu Q, Xu S, Yao C, Li Z (2017) Construction of mesoporous carbon nitride/binary metal sulfide heterojunction photocatalysts for enhanced degradation of pollution under visible light. Appl Catal B 218:545–554

Liao G, Chen S, Quan X, Yu H, Zhao H (2012) Graphene oxide modified g-C_3N_4 hybrid with enhanced photocatalytic capability under visible light irradiation. J Mater Chem 22:2721

Liu Q, Guo YR, Chen ZH, Zhang ZG, Fang XM (2016) Constructing a novel ternary Fe(III)/graphene/g-C_3N_4 composite photocatalyst with enhanced visible-light driven photocatalytic activity via interfacial charge transfer effect. Appl Catal B 183:231–241

Man MKL, Margiolakis A, Jones SD, Harada T, Wong EL, Krishna MBM, Madeo J, Winchester A, Lei S, Vajtai R, Ajayan PM, Dani KM (2017) Imaging the motion of electrons across semiconductor heterojunctions. Nat Nanotechnol 12:36–40

Miller DR, Wang J, Gillan EG (2002) Rapid, facile synthesis of nitrogen-rich carbon nitride powders. J Mater Chem 12:2463–2469

Mohamed AA, EI-Sayed R, Osman T, Toprak M, Muhammed M, Uheida A (2016) Composite nanofibers for highly efficient photocatalytic degradation of organic dyes from contaminated water. Environ Res 145:18–25

Novoselov KS, Falko VI, Colombo L, Gellert PR, Schwab MG, Kim K (2012) A roadmap for graphene. Nature 490:192–200

Pan X, Yang MQ, Tang ZR, Xu Y-J (2014) Noncovalently functionalized graphene-directed synthesis of ultralarge graphene-based TiO_2 nanosheet composites: tunable morphology and photocatalytic applications. J Phys Chem C 118:27325–27335

Rajendra CP, Varsha K, Caroline SYL (2014) Hybrid photocatalysts using graphitic carbon nitride/cadmium sulfide/reduced graphene oxide (g-C_3N_4/CdS/RGO) for superior photodegradation of organic pollutants under UV and visible light. Dalton Trans 43:12514–12527

Ramirz KB, Kim D, Cho D, Cho S (2015) 4-chlorophenol removal from water using graphite and graphene oxides as photocatalysts. J Environ Health Sci Eng 13:33. (10pgs)

Samsudin EM, Goh SN, Wu TY, Ling TT, Bee S, Hamid A, Juan JC (2015) Evaluation on the photocatalytic degradation activity of reactive blue 4 using pure anatase nano-TiO_2. Sains Malays 44:1011–1019

Shalom M, Gimenez S, Schipper F, Herraiz-Cardona I, Bisquert J, Antonietti M (2014) Controlled carbon nitride growth on surfaces for hydrogen evolution electrodes. Angew Chem Int Ed 53:3654–3658

Szabó T, Berkesi O, Forgó P, Josepovits K, Sanakis Y, Petridis D, Dékány I (2006) Evolution of surface functional groups in a series of progressively oxidized graphite oxides. Chem Mater 18:2740–2749

Tan SN, Ge H (1996) Investigation into vapour-phase formation of polypyrrole. Polymer 37:965–968

Vachon DD, Angus RO, Lu FL, Nowak M, Liu ZX, Schaffer H (1987) Polyaniline is poly-para-phenyleneamineimine: proof of structure by synthesis. Synth Met 18:297–302

Vukmirovic N, Wang LW (2009) Electronic structure of disordered conjugated polymers: polythiophenes. J Phys Chem B 113:409–415

Wang J, Neoh KG, Kang ET (2004) Comparative study of chemically synthesized and plasma polymerized pyrrole and thiophene thin films. Thin Solid Films 446:205–217

Wang X, Blechert S, Antonietti M (2012) Polymeric graphitic carbon nitride for heterogeneous photocatalysis. ACS Catal 2:1596–1606

Wang S, Li D, Sun C, Yang S, Guan Y, He H (2014) Synthesis and characterization of g-C_3N_4/Ag_3VO_4 composites with significantly enhanced visible-light photocatalytic activity for triphenylmethane dye degradation. Appl Catal B 144:885–892

Xu J, Hou J, Zhang S, Zhang R, Nie G, Pu S (2006) Electrosyntheses of high quality poly (5-methylindole) films in mixed electrolytes of boron trifluoride diethyl etherate and diethyl ether. Eur Polym J 42:1384–1395

Yan SC, Li ZS, Zou ZG (2009) Photodegradation performance of g-C_3N_4 fabricated by directly heating melamine. Langmuir 25:10397–10401

Yang MQ, Xu YJ (2013) Selective photo redox using graphene-based composite photocatalysts. Phys Chem Chem Phys 15:19102–19118

Yang MQ, Xu YJ (2016) Photocatalytic conversion of CO_2 over graphene-based composites: current status and future perspective. Nanoscale Horiz 1:185–200

Yang MQ, Zhang N, Pagliaro M, Xu YJ (2014) Artificial photosynthesis over graphene–semiconductor composites. Are we getting better? Chem Soc Rev 43:8240–8254

Yu Q, Guo S, Li X, Zhang M (2014) Template free fabrication of porous g-C_3N_4/graphene hybrid with enhanced photocatalytic capability under visible light. Mater Technol 29:172–178

Yuan L, Yang MQ, Xu YJ (2014) Tuning the surface charge of graphene for self-assembly synthesis of a $SnNb_2O_6$ nanosheet–graphene (2D–2D) nanocomposite with enhanced visible light photoactivity. Nanoscale 6:6335–6345

Zhang J, Xiao FX, Xiao G, Liu B (2014) Self-assembly of a Ag nanoparticle-modified and graphene-wrapped TiO_2 nanobelt ternary heterostructure: surface charge tuning toward efficient photocatalysis. Nanoscale 6:11293–11302

Zhang N, Yang MQ, Liu S, Sun Y, Xu YJ (2015) Waltzing with the versatile platform of graphene to synthesize composite photocatalysts. Chem Rev 115:10307–10377

Zhao Y, Zhao F, Wang X, Xu C, Zhang Z, Shi G, Qu L (2014) Graphitic carbon nitride nanoribbons: graphene-assisted formation and synergic function for highly efficient hydrogen evolution. Angew Chem Int Ed 53:13934–13939

Zheng Y, Jiao Y, Zhu Y, Li LH, Han Y, Chen Y, Du A, Jaroniec M, Qiao SZ (2014) Hydrogen evolution by a metal-free electrocatalysts. Nat Commun 5:3783

Zheng Y, Jiao Y, Jaroniec M, Qiao SZ (2015) Advancing the electrochemistry of the hydrogen-evolution reaction through combining experiment and theory. Angew Chem Int Ed 54:52–65

Chapter 7
Advances and Innovations in Photocatalysis

Giuseppina Iervolino, Vincenzo Vaiano, and Paolo Ciambelli

Contents

Abstract This chapter is related to the advances and innovations of photocatalytic processes in recent years. In particular, both the innovative aspects of the applicability of photocatalysis and technological advances were considered, with particular attention to the photocatalytic energy recovery, organic synthesis and new reactor configurations.

In particular, the chapter discusses the possibility to produce an energy source such as hydrogen and/or methane from the degradation of organic substance present in wastewater by heterogeneous photocatalysis. Particular attention has been given to the use of photocatalysts active under visible light and to their efficiency in the absence of noble metals. The chapter also reports experimental results in which the simultaneous valorization and purification of food industrial wastewater are

G. Iervolino · V. Vaiano · P. Ciambelli (✉)
Department of Industrial Engineering, University of Salerno, Fisciano, SA, Italy
e-mail: vvaiano@unisa.it; pciambelli@unisa.it

Inamuddin et al. (eds.), *Nanophotocatalysis and Environmental Applications*,
Environmental Chemistry for a Sustainable World 31,
https://doi.org/10.1007/978-3-030-04949-2_7

proposed using structured photocatalysts. Moreover, in this chapter, the application of photocatalysis in the synthesis of organic compounds will be presented. Finally, new reactor configurations, such as photocatalytic membrane reactors (PMRs), will be discussed.

Keywords Photocatalysis · Hydrogen production · Sacrificial agents · Wastewater valorization · Organic synthesis · Selective photocatalysts · Doped photocatalysts · Visible light sources · Photocatalytic membranes · Supported photocatalysts

7.1 Introduction

In recent years, the need to apply efficient technologies for environmental protection and energy recovery has been strongly increased. The presence of contaminants in the ecosystem is a challenge that every day the scientific community, together with the industrial realities, proposes to be able to overcome in order to obtain a better environment for the life and health of human beings. Many studies on these topics have been done, and, among the various proposed technologies, one, in particular, has had a growing interest from the scientific community: "photocatalysis". The peculiarity of heterogeneous photocatalysis lies in its ability to act where other processes have limitations, such as the possibility to obtain the complete mineralization (conversion into CO_2 and H_2O) of pollutants. Furthermore, the advantages of this process are represented by the possibility of operating in mild condition, applying low temperatures and pressures compared to the classic industrial processes. Thanks to its many applications, the studies carried out on photocatalytic processes are different and relate to various topics such as the purification of water, the hydrogen production and the synthesis of organic compounds under mild conditions. These main three innovative aspects are illustrated in the following sections of this chapter.

7.2 Photocatalysts for Hydrogen Production

In recent years, the interest in heterogeneous photocatalysis has increased considerably, demonstrating the remarkable effectiveness of this process for different purposes. In particular, the energy and environmental needs have led to the development of photocatalysis towards different perspectives and progress. For this reason, a phenomenal expansion in the range of investigations conducted on photocatalysis has been observed. As a result, a number of topics have emerged which equally led to several research perspectives. Considering the increase of global need for alternative energy, one of these topics is represented by the photocatalytic production of hydrogen from aqueous solutions. Solar energy can be used to convert photonic and or thermal energy that is stored in the sunlight into hydrogen. Thermochemical,

photobiological and photocatalytic water splitting are some of the examples of hydrogen production from solar water splitting (Xie et al. 2012). Photocatalytic water splitting into H_2 and O_2 using semiconducting catalysts has received much attention due to the potential of this technology, as well as the great economic and environmental interest for the production of the clean fuel H_2 from water using solar energy. Fujishima and Honda described for the first photocatalytic decomposition of water under light radiation demonstrating the potential of TiO_2 semiconductor materials to split water into H_2 and O_2 (Fujishima and Honda 1972).

In general, photocatalysis has been used with the aim to remove, from liquid or gaseous streams, the pollutants and non-biodegradable compounds, which with the conventional processes are not removed. Through photocatalysis, thanks to the presence of hydroxyl radicals, it is possible to obtain the complete mineralization of non-biodegradable substances, managing to obtain as a final product CO_2 and H_2O. Beyond this objective that concerns the removal of pollutants, photocatalysis was (and is still today) investigated as a process for the production of hydrogen. This represents an innovative aspect of the application of heterogeneous photocatalysis. The importance of photocatalysis in the production of hydrogen is represented by the increasing availability of data in the literature, which demonstrate an increase in the interest of the scientific community towards this topic. Photocatalytic water splitting using solar energy for hydrogen production offers a promising option to produce hydrogen, and it has been attracting significant interest in the recent literature because it uses two of the most abundant, clean, renewable and natural energy sources available to us. Photocatalytic hydrogen production, therefore, has been recognized as a potential solution to address excessive utilization, limited reserves and negative environmental impact issues related to fossil fuels (Jang et al. 2012). The prospective benefits of photocatalytic water splitting into hydrogen and oxygen can be listed as economic and environmental advantages because the process uses solar energy and produces hydrogen in a clean way with no greenhouse gas emissions (Acar et al. 2016). Recently, a strong revival of interest in this matter is being observed, since hydrogen economy becomes an increasingly important issue. In order to enhance the hydrogen production, often the water-splitting reaction is provided with the use of a sacrificial agent (organic substance). In fact, photocatalytic water splitting may not be particularly promising; however, production of hydrogen by photocatalytic decomposition of organic wastes appears to be an exciting idea.

Several organic compounds, such as methanol, or other alcohols and sugars can act as sacrificial agents in the photocatalytic hydrogen production. In fact, these substances are able to combine with the valence band holes more effectively than water (Yamakata et al. 2003). In this way the electrons which are located in the conduction band become more available to reduce electron-acceptor species, e.g. H^+, to produce hydrogen (Chiarello and Selli 2014) and the overall reaction turns into the photoreforming of the organic compounds, giving an H_2 and CO_2 mixture. For example, as reported in the literature (Lianos et al. 2009), during the photocatalytic process, a semiconductor is excited by absorption of a photon, which creates an electron-hole pair. Holes oxidize the organic substance and the oxidation process

leads to the production of hydrogen ions and oxidation products. These products are further oxidized until complete mineralization is achieved. For example, in the methanol oxidation and mineralization steps, the following reactions take place:

$$CH_3OH + 2h^+ \rightarrow HCHO + 2H^+ \tag{7.1}$$

$$HCHO + H_2O + 2h^+ \rightarrow HCOOH + 2H^+ \tag{7.2}$$

$$HCOOH + 2h^+ \rightarrow CO_2 + 2H^+ \tag{7.3}$$

Hydrogen ions, in turn, are reduced by excited electrons, producing molecular hydrogen

$$2H^+ + 2e^- \rightarrow H_2 \tag{7.4}$$

The overall chemical reaction is then represented by

$$CH_3OH + H_2O \rightarrow CO_2 + 3H_2 \tag{7.5}$$

It is possible to confirm that the last equation is equivalent to methanol reforming. Reforming is always obtained in the presence of water, and it is mostly known as a high-temperature process (Dauenhauer et al. 2006). In this case, the photocatalytic reforming involves both the alcohol decomposition and mineralization and the water decomposition and hydrogen production. So, it is possible to confirm that the photocatalytic reforming leads simultaneously to the water splitting and water cleaning. It is possible to apply the reforming reaction to an organic substance and the schematic reactions:

$$C_xH_yO_z + (2_{x-z})H_2O \rightarrow xCO_2 + (2_{x-z} + y/2)H_2 \tag{7.6}$$

Christoforidis et al. have proposed the following representation (Fig. 7.1).

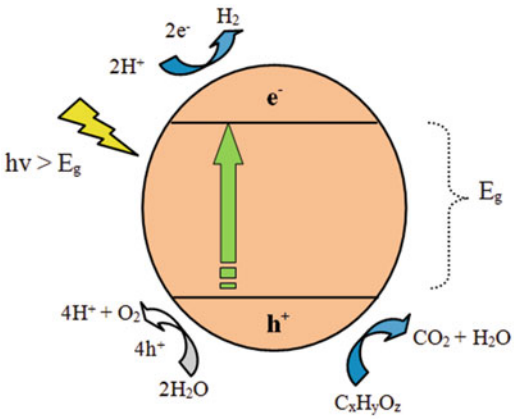

Fig. 7.1 Representation of the redox reactions occurring on the photocatalyst surface following its activation by the light energy (Christoforidis and Fornasiero 2017)

In this figure, water splitting and oxygenate ($C_xH_yO_z$) oxidation occur under anaerobic conditions. The photoreforming reaction is evidenced by blue arrows. However, several literature data have demonstrated that the addition of sacrificial agents, such as methanol, ethanol or sugar (Christoforidis and Fornasiero 2017), can improve the efficiency of hydrogen production (Colmenares et al. 2011; Strataki et al. 2010). Since these early reports, the field of photocatalytic H_2 production from water using carbon-containing compounds as sacrificial agents has gained significant attention (Puga 2016). Recently, research developments have focused mainly on improving the performances of photocatalysts, studying simple configurations for the immobilization of the catalyst and its activation in the presence of visible light.

7.2.1 Nature of Different Sacrificial Agents and Typical Mechanism of Photoreforming

Several organic substances were studied in the photocatalytic hydrogen production process with the aim to enhance the results obtained from photocatalytic water splitting. Photocatalytic reforming or organic compounds may be a good approach since the process can be carried out under ambient conditions and driven by sunlight. The pioneer study was conducted in 1980 by Kawai and Sakata (1980) that reported hydrogen production from carbohydrate on $RuO_2/TiO_2/Pt$ photocatalyst under 500 W Xe lamp irradiation. Subsequently, they indicated that hydrogen could also be obtained from other biomasses, such as cellulose, starch, dead insects and waste materials using the same process, demonstrating the feasibility of producing hydrogen from biomass by a photocatalytic process (Kawai and Sakata 1981). In the following paragraph, the sacrificial substances most used in photocatalytic hydrogen production are presented.

7.2.1.1 Methanol as a Sacrificial Agent

Among the sacrificial substances generally used in photocatalytic reforming for hydrogen production, methanol is considered the model molecule because of its simple atomic structure (one hydroxyl group and one carbon atom). Several studies report the use of methanol for the photocatalytic hydrogen production (Castaneda et al. 2018; Gomathisankar et al. 2014; Miwa et al. 2010; Udani and Ronning 2015). The mechanism proposed by Kawai and Sakata for the production of hydrogen from methanol involves the initial formation of formaldehyde and formic acid (intermediate) and the final production of H_2 and CO_2 (Kawai and Sakata 1980). Another study on the use of metalized TiO_2 as a photocatalyst proposed the oxidation of methanol on the TiO_2 by photogenerated h^+ protons forming HCOH and finally HCOOH (Chen et al. 2007). It was observed that H^+ originating from both H_2O and methanol is used for the H_2 formation (Chen et al. 2007) and that with the increase of

methanol concentration, there is an increase of H_2 production (Strataki et al. 2007). In particular, for 20% of water and 80% of methanol solution, they observed a hydrogen production of 4.5 μmole H_2/min after 250 min of irradiation time. Also Gomathisankar et al. report the photocatalytic hydrogen generation from aqueous methanol solution using TiO_2 in the presence of metal particles. In this work, it was observed that in the presence of methanol, the addition of copper particles in the synthesis of photocatalyst induces an increase of the hydrogen production. Under the optimal conditions, the hydrogen production is about 68 times higher than that obtained with pure TiO_2 (Gomathisankar et al. 2014).

7.2.1.2 Ethanol as a Sacrificial Agent

Another sacrificial agent often reported in literature for photocatalytic hydrogen production is ethanol, mostjy because of its high production on large scale from renewable biomass, including cellulose or lignocellulose (Zinoviev et al. 2010). Ethanol photoreforming takes place through the following reactions:

$$C_2H_5OH + 2h^+ = CH_3CHO + 2H^+ \tag{7.7}$$

$$CH_3CHO + H_2O + 2h^+ = CH_3COOH + 2H^+ \tag{7.8}$$

In these reactions, the formation of intermediates such as acetaldehyde and acetic acid and the simultaneous production of H_2 via H^+ reduction occur. It has been reported that the complete ethanol photoreforming, based on the CO_2/H_2 molar ration produced, was obtained over Pt/TiO_2 catalysts, presenting 50% apparent quantum yield of H_2 evolution at 365 nm (Kondarides et al. 2008).

7.2.1.3 Glycerol as a Sacrificial Agent

Another interesting sacrificial substance studied for the photocatalytic production of hydrogen is glycerol. It is a by-product in the production of biodiesel through catalytic transesterification, and it has already been studied as an effective sacrificial reagent for photocatalytic H_2 production through photoreforming reaction (Sadanandam et al. 2017; Wang et al. 2017). Among the various catalysts studied, the most investigated was TiO_2 (Fu et al. 2011). The photoreforming reaction of glycerol to H_2 and CO_2 occurs through the formation of 2,3-dihydroxypropanal and then the formation of other compounds, such as alcohols or aldehydes (Christoforidis and Fornasiero 2017).

The glycerol photoreforming reaction is reported:

$$C_3H_8O_3 + 3H_2O \rightarrow 3CO + 7H_2 \tag{7.9}$$

Typically, the photoreforming reaction of glycerol takes place under aerate conditions. So, the organic substance is oxidized through the photogenerated holes, while the electrons are released to reduce water to hydrogen. The presence of the organic substance positively affects the production of hydrogen which is higher compared to the photocatalytic water splitting. According to Li et al. (2010), the complete mechanism of glycerol photoreforming can be described as follows: the first step is the excitation of the semiconductor (typically TiO_2) through light, which causes the formation of the h^+ e^- pair, responsible for splitting water into hydroxide ions and hydrogen ions. Simultaneously, the electron generated reduces the hydrogen ions to H_2 gas. Below the main reactions that illustrate the glycerol photoreforming mechanism, typically reported in the literature (Christoforidis and Fornasiero 2017), are shown:

$$\text{Semiconductor} \rightarrow h^+ + e^- \tag{7.10}$$

$$h^+ + H_2O \rightarrow OH^- + H^+ \tag{7.11}$$

$$H^+ + e^- = 1/2\ H_2 \tag{7.12}$$

Glycerol absorbed on the catalyst may react with hydroxyl radical:

$$CH_2OHCHOHCH_2OH + OH = CH_2OHCHOHCHOH \tag{7.13}$$

The $CH_2OHCHOHCHOH$ species reacts with water to form $CH_2OHCHOHCH(OH)_2$ species. These last species are unstable; therefore they are transformed into aldehydes:

$$CH_2OHCHOHCH(OH)_2 \rightarrow CH_2OHCHOHCHO + H_2O \tag{7.14}$$

·OH species then react continuously with the aldehyde:

$$CH_2OHCHOHCHO + OH \rightarrow CH_2OHCHOHCO + H_2O \tag{7.15}$$

$$CH_2OHCHOHCHO + H_2O \rightarrow CH_2OHCHOCOOH + H^+ \tag{7.16}$$

When the species $CH_2OHCHOCOOH$ react with the hole (h^+) induced by the excitation of the catalyst by the action of light, the decarboxylation is obtained:

$$CH_2OHCHOHCOOH + h^+ \rightarrow CH_2OHCHOH + CO_2 + H^+ \tag{7.17}$$

The unstable $CH_2OHCHOH$ species are transformed to obtain CO_2, H_2O and the final products, as reported below:

$$\begin{aligned} &CH_2OHCHOH \rightarrow CH_2OHCH(OH)_2 \rightarrow CH_2OHCHO \rightarrow \\ &CH_2OHCOOH \rightarrow CH_2OH \rightarrow \\ &HCH(OH)_2(HCHO) \rightarrow HCO \rightarrow HCOOH \rightarrow CO_2 + H_2O \end{aligned} \tag{7.18}$$

7.2.1.4 Glucose as a Sacrificial Agent

Photocatalytic H_2 production from sugars, and in particular from glucose, is an interesting process (Iervolino et al. 2016a). It is possible to obtain glucose from cellulose hydrolysis, but it is interesting to note that high content of different kind of sugars is available in wastewaters from food processes (Iervolino et al. 2018). The first study on the mechanism of glucose degradation was reported in 1983 by St. John et al. (1983). They proposed that the photogenerated h^+ oxidizes the -OH and -CHO groups, releases protons and produces -COOH groups, whose decarboxylation occurs with CO_2 evolution. This mechanism is represented by the following equations:

$$R - CHO + H_2O + 2h^+ = R - COOH + 2H^+ \tag{7.19}$$

$$R - CH_2OH + H_2O + 4h^+ = R - COOH + 4H^+ \tag{7.20}$$

$$R - COOH = RH + CO_2 \tag{7.21}$$

The reaction of glucose with $OH^{\bullet}$ has been also proposed for the production of gluconic acid that is further oxidized to CO_2. The presence of this intermediate has been confirmed by several authors (Iervolino et al. 2016a; Li et al. 2010; Mohamed and Aazam 2012; Vaiano et al. 2015). In particular, the results reported by Iervolino et al. show that the formation of CO_2 and H_2 occurs mainly by the reaction of photocatalytic wet reforming of glucose, according to the following reaction:

$$C_6H_{12}O_6 + 6H_2O = 6CO_2 + 12\ H_2$$

Their experiments were carried out with TiO_2 containing noble metal (Pd) on the surface. In particular, the results showed that the presence of Pd resulted in an increased methane production (7.58 μmol) and yield (2%) compared with the TiO_2 catalyst without Pd, for which CH_4 production and yield were about 2.8 μmol and 0.6%, respectively. Considering, therefore, the formation of methane, it has been hypothesized that it comes from the degradation of glucose through the following reaction:

$$C_6H_{12}O_6 = 3CH_4 + 3CO_2 \tag{7.22}$$

The proposed mechanism suggests that the CO_2 mainly comes from the photocatalytic wet reforming of glucose, as confirmed by the molar ratio H_2/CO_2

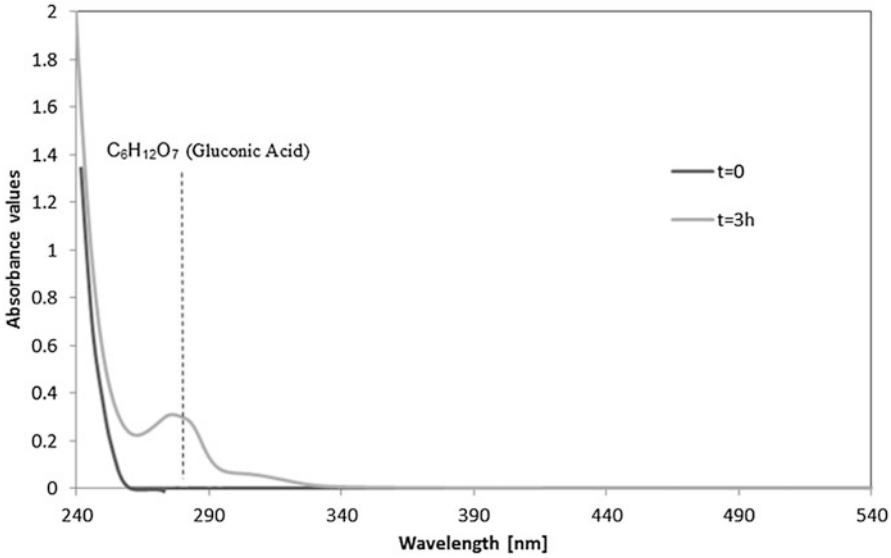

Fig. 7.2 Spectrophotometric analysis of aqueous samples at an initial time $t = 0$ and after 3 h of irradiation time ($t = 3$ h) (Vaiano et al. 2015)

being equal to 2, while CH_4 could be formed through the following reaction, similar to anaerobic digestion:

$$C_6H_{12}O_6 + 6H_2O = 6\,CH_4 + 6O_2 \tag{7.23}$$

The authors confirmed this result by analysing liquid samples taken from the reactor after 3 h of irradiation and demonstrating the presence of gluconic acid represented by a band with a peak at a wavelength of 254 nm (Ramachandran et al. 2006), as reported in Fig. 7.2.

Enhanced photocatalytic hydrogen productions have been obtained by studying methods to optimize the photocatalysts properties. In particular, the studies were directed both on the use of photocatalysts active in the presence of UV light (in particular using Pt, Pd or Au loaded on catalyst surface, or by surface modification using fluorine, with the aim to reduce the charge carrier recombination and to enhance the photocatalytic performance) (Iervolino et al. 2016b; Wu et al. 2008), and also towards catalysts active under visible light (Liu et al. 2006; Sacco et al. 2012). The use of visible or solar light represents an advantage both in terms of economics and application in the use of photocatalytic systems for the hydrogen production. In this case, it is very important to synthesize photocatalysts with a low band gap. About this aspect, interesting results were reached by Iervolino et al., that reported the performance of $LaFeO_3$ prepared with a simple solution combustion synthesis and tested in the photocatalytic hydrogen production from an aqueous solution containing glucose. They obtained good performances in the hydrogen

production both under UV and visible irradiation, using LEDs as light source. The characterization results have shown that the band gap energy of this perovskite was about 2.0 eV. With this photocatalyst hydrogen production equal to 140 μmol after 3 h of irradiation time was achieved, with glucose initial concentration equal to 1000 mg/L. On this $LaFeO_3$ photocatalyst, the proposed mechanism to explain the photocatalytic hydrogen production was not the photoreforming of glucose, since the H_2/CO_2 molar ratio wasn't equal to 2, while the analysis of the aqueous solution evidenced the presence of gluconic acid, underlining that this molecule could be an intermediate in the reaction mechanism, according to the literature (Li et al. 2010). Considering these results, the hydrogen production has been attributed to the produced $H^{\bullet}$ radicals that can form H_2 (Eq. 7.28). In details, glucose (RCHO) adsorbed on the catalyst may react with hydroxyl radicals and by this way, gluconic acid (RCOOH) is produced according to Eqs. (7.24) and (7.25):

$$RCHO + OH^{\bullet} = RCO^{\bullet} + H_2O \tag{7.24}$$

$$RCO^{\bullet} + H_2O = RCOOH + H^{\bullet} \tag{7.25}$$

Simultaneously, the holes react also with glucose, according to Eqs. (7.26) and (7.27):

$$H^{+} + RCHO = RCO^{\bullet} + H^{\bullet} \tag{7.26}$$

$$RCO^{\bullet} + H_2O = RCOOH + H^{\bullet} \tag{7.27}$$

$$H^{\bullet} + H^{\bullet} = H_2 \tag{7.28}$$

Equation (7.28) represents the hydrogen formation from the radical recombination. Hydrogen can be also produced by water-splitting reaction on $LaFeO_3$ (Parida et al. 2010). Hydrogen production of 1.6 mmol/g_{cat}, corresponding to a hydrogen yield equal to 16% was achieved. These results are better than those obtained with Pd/TiO_2-based photocatalyst, where the hydrogen yield was equal to 3%. This confirms the potential of photocatalysis for the production of hydrogen from aqueous solutions containing sugars, and furthermore, they demonstrate the efficiency of noble metal-free photocatalysts in obtaining competitive results with respect to the catalysts loaded with noble metals. $LaFeO_3$ perovskite has shown excellent photocatalytic activity for the hydrogen production under visible light. Moreover, recent literature data have shown that it is possible to enhance the performance of perovskite using ruthenium as a doping metal (Iervolino et al. 2017). With the same photocatalyst, the effect of a different light source (visible LEDs) was evaluated in the hydrogen production evidencing the high effectiveness of the catalyst also in the presence of visible LEDs (Iervolino et al. 2017).

7.2.2 Hydrogen Production from Photocatalytic Wastewater Treatment

Although sacrificial agents such as ethanol and others improve the efficiency of the photocatalytic hydrogen production, the addition of these substances in aqueous solutions leads to an increase in the cost of the process, inevitably linked to the cost of the sacrificial agents themselves (Galinska and Walendziewski 2005). As an alternative to the addition of sacrificial agents, the biomass, which represents a very versatile renewable resource, can also be utilized for the sustainable production of hydrogen. In this case, biomass can be represented by wastewater from agro-food industries or industrial wastewater characterized by the presence of a high content of specific organic substances. It is very interesting that the use of organic pollutants presents wastewater as a sacrificial agent in a simultaneous wastewater treatment and valorization, with H_2 production (Christoforidis and Fornasiero 2017). Examples, in literature, are the results of the degradation of urea or bisphenol A in absence of oxygen with the simultaneous production of H_2 over modified TiO_2 with different metal co-catalysts (Bowker et al. 2009; Kim et al. 2012). The photocatalytic H_2 production under UV irradiation using olive mill wastewater was also reported (Speltini et al. 2015). In these cases, it was observed that the maximum hydrogen production, with a TiO_2 dosage equal to 2 g/L and a solution pH value of 3, was equal to 38 mmol after 2 h of reaction. Simultaneously, chemical oxygen demand was reduced by 92%. These results confirm that the process can be applied as a method for the degradation of organic pollutants with simultaneous H_2 production. Interesting results were also obtained in the application of photocatalysis for the valorization of the wastewater from brewing process (Iervolino et al. 2017). The photocatalytic experiments were carried out in the presence of perovskite-based photocatalyst doped with metal (Ru) and in the presence of visible light irradiation. After 4 h of visible light irradiation, a degradation of maltose equal to 50%, and, in parallel, photocatalytic hydrogen production equal to about 2128 $\mu mol/g_{cat}$ were obtained, confirming the possibility to give value to wastewater from brewing process obtaining hydrogen under visible light (Iervolino et al. 2017). With reference to characteristics of carbohydrates, it was demonstrated that the rate of hydrogen evolution decreases with increasing their molecular weights (i.e. in the soluble order starch<sucrose<glucose) (Fu et al. 2008).

Literature results have shown how the photocatalytic process can also be applied to food industrial wastewater. In particular, studies have been conducted using wastewaters from cherry washing (Iervolino et al. 2018). This wastewater was characterized by the presence of red colour, and it presented also a high sugar content, in particular sorbitol, fructose and glucose. For the application of the photocatalytic process in the treatment of a wastewater on an industrial scale, the photocatalyst (based on metal doped perovskites) was afterwards deposited on nanoparticles with magnetic properties to avoid the drawback related to the separation of a catalyst in powder form after the reaction. The application of the photocatalytic process on this wastewater has allowed to obtain a hydrogen

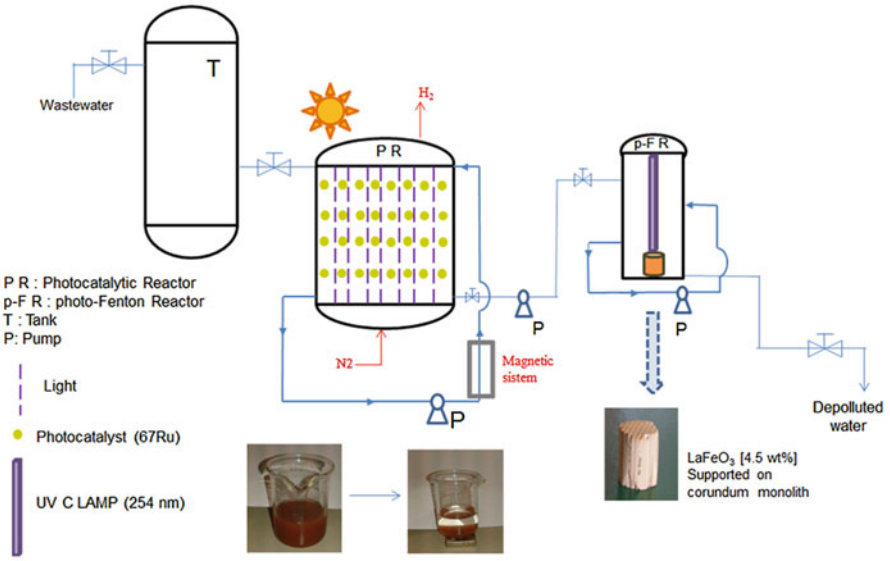

Fig. 7.3 Wastewater valorization process and treatment plant based on AOPs (Iervolino et al. 2018)

production higher than that generally reported in the literature (12,344 μmol/L after 4 h of reaction under visible light irradiation), allowing also the degradation of the high organic content. The water obtained at the end of the process has the characteristics necessary to be disposed of or for reuse in irrigation. In this way different advantages were achieved: in addition to the simultaneous degradation of organic substances and the valorization of wastewater, the simple removal of the photocatalyst at the end of the treatment is also guaranteed, as well as its reuse for several cycles (Iervolino et al. 2018). A possible treatment scheme has been suggested, in which it is possible to foresee the step of valorization of the wastewater by applying advanced oxidation processes (Fig. 7.3).

7.3 Photocatalysts Developed for the Synthesis of Organic Compounds in Mild Conditions

Despite pioneering work on the use of heterogeneous photocatalysis for the synthesis of organic compounds, such as the paper by Teichner on the selective oxidation of alkanes and olefinic compounds (Formenti et al. 1970), the major development on photocatalytic studies in the last century has been mostly restricted to environmental catalysis studies. This research led to commercial photocatalytic processes, activated by UV radiation, for the treatment of wastewater in order to reduce the pollutant's concentration under the limits fixed by environmental current regulations (Herrmann

1999). In more recent years, CO_2 conversion, water splitting, photoelectrochemical processes, solar light-driven photocatalysts and energy generation strongly grew as the subjects of primary interest.

Partial photooxidation of paraffin to aldehydes and ketones with TiO_2 was reported in 1972 (Formenti et al. 1973), and 2 years later, a reactivity scale of carbon in photooxidative reactions (Ctert > Cquat > Csec > Cprim) was determined, and surprisingly high selectivity for hydrocarbon partial oxidation to aldehydes and ketones was reported (n-alkanes 76%, i-alkanes 80%, neo-alkanes 57%) if compared to the unselective total oxidation to CO_2 of the relevant thermal reactions. A reaction mechanism of photocatalytic oxidation, responsible for such unexpected selectivity, was suggested, completely different from those usually involved in catalytic thermal oxidation carried out in the absence of irradiation (Djeghri et al. 1974).

In the same years, parallel innovative results were obtained for the selective photocatalytic oxidation of isopropanol. In particular, the role of photoadsorbed oxygen as a precursor to the photooxidation and a mechanism explaining the role of "adsorbed water" in the process by the action of OH^- ions as traps for photo-holes produced by the illumination were proposed (Bickley et al. 1973).

As above reported, after the work of researchers like the examples reported above, opening new horizons to photocatalysis in the field of selective oxidation of organic compounds, only in the current century, this topic has attracted growing interest, supported by significant results indicating novel perspectives, especially related to visible light-driven processes (Kou et al. 2017; Romero and Nicewicz 2016). It must be also noted that major interest has been addressed to liquid phase systems with respect to gas phase. However, in this part of chapter, an almost unique reactant system, an object of our research for many years, will be treated: the gas-phase heterogeneous photocatalytic selective oxidative dehydrogenation of cyclohexane. Several ways to induce or increase selectivity in these reacting systems such as catalyst modification, experimental conditions, irradiation and type of reactor, finding very unusual results, will be discussed.

7.3.1 The Starting Point

In the framework of a chemical engineering master's thesis on selective heterogeneous photocatalytic oxidation of cyclohexane, we found that literature results mostly concerned the selective conversion to cyclohexanone and cyclohexanol in the liquid phase. As examples, high photooxidative activity by polyoxotungstate anions in slurry reactors was reported (Giannotti and Richter 1999; Maldotti et al. 1997), while isolated tetrahedral vanadyls on alumina are active for converting cyclohexane to cyclohexanone (Teramura et al. 2001). Cyclohexanol, cyclohexanone and polyoxygenated compounds were obtained with silica-supported vanadium or tungsten oxides (Maldotti et al. 1994, 1997; Molinari et al. 1998; Teramura et al. 2001). In these systems the role of solvent is a critical issue, influencing the reaction product distribution even through competitive adsorption (Almquist and

Biswas 2001). However, moving from a paper reporting spectroscopic evidence of spontaneous selective oxidation of cyclohexane to cyclohexanone with metal exchanged zeolite catalyst (Sun et al. 1996), we moved to investigate gas-phase cyclohexane photooxidation.

Really, the first result, as expected, was the good performance of anatase titania for total oxidation of cyclohexane to CO_2 at mild conditions (atmospheric pressure, temperature lower than 100 °C, 1000 ppm inlet cyclohexane concentration, oxygen/cyclohexane inlet ratio = 1.5, fixed bed annular flow reactor, UV lamp for irradiation at 360 nm), i.e. a totally unselective catalyst. Our approach to modifying this performance derived from our consolidated experience with thermal heterogeneous catalytic oxidation on supported metal oxides such as MoO_x and VO_x and aimed at verifying the role of typical aspects of those systems, such as reactant, intermediate and product adsorption in the overall photocatalytic conversion process.

7.3.2 *The Effect of Supporting Metal Oxides on Titania on Selectivity*

We prepared MoO_xTiO_2 catalysts by depositing increasing molybdenum oxide amounts on the supporting unselective titania and tested them at the same experimental conditions. We found a very impressive and clear result: the catalyst turned as selective for the conversion to benzene as MoOx loading increased, reaching a maximum value of 65% selectivity at 15% cyclohexane conversion for 8.0 MoO_3 wt% loading. The unique secondary product was CO_2. However, the catalyst showed fast deactivation (Ciambelli et al. 2005).

Catalyst characterization was performed in order to support a study of the reaction mechanism. Raman spectra clearly demonstrated the increasing formation of surface poly-molybdate species with MoO_3 loading and the progressively higher degree of Mo anions polymerization, the Mo-nuclearity likely ranging from 7 to 12. At higher than 8 wt%, MoO_3 loading segregated MoO_3 crystallites started to form. Based on that evidence, we attributed the selective formation of benzene to the presence of poly-molybdate species supported on the titania surface, suggesting that these species poison unselective sites of titania surface responsible for the total oxidation reaction. Therefore, our most selective catalyst can be described as a poly-molybdate monolayer covered sulphated anatase titania. It is worthwhile that Wachs found for unsulphated titania a molybdenum oxide monolayer coverage of 7.6 μmol/m^2, corresponding to about 7.5 wt% of MoO_3 on our sulphated titania support (Wachs and Weckhuysen 1997). Moreover, polyoxotungstates as catalytically photoactive species in liquid phase were studied in Maldotti et al. (1997).

To rationalize these previous results, we proposed a series-parallel reaction scheme based upon consecutive oxy-dehydrogenation steps occurring on active molybdenum sites in competition with total oxidation on bare titania. The first reaction step is oxy-dehydrogenation of cyclohexane to cyclohexene, followed by

further oxy-dehydrogenation to benzene on the molybdenum oxide active sites (Ciambelli et al. 2008a). The two-step scheme in terms of progressive dehydrogenation also suggested the potential selective conversion to cyclohexene.

7.3.3 The Effect of Titania Dopant

One more input to our goal of enhancing both activity and selectivity of the reacting system came from reported finding on the positive effect of titania dopant such as sulphate in that direction (Ciambelli et al. 2008b). We started to investigate sulphated titania as support in MoO_X/TiO_2 catalyst in comparison with unsulphated one, reaching the conclusion that both sulphate and polymeric molybdate species play an essential role in determining the unusual photocatalytic properties found. Comparing unsulphated and sulphated titania, we found that the steady-state conversion of cyclohexane to carbon dioxide decreased as sulphate load increased, but sulphate was unable to give any selective oxidation, both catalysts being only active for total oxidation to CO_2. On the other hand, on sulphated titania-supported MoOx catalyst, the presence of sulphate species on the surface of titania enhances benzene yield as more as higher is the sulphate content. Therefore, sulphate species together with polymeric molybdate species seem to be necessary to obtain selective cyclohexane photo oxy-dehydrogenation to benzene (Ciambelli et al. 2005).

7.3.4 The Effect of Titania Surface Area

Since the usual goal for a catalytic partial oxidation process is that of maximizing not only selectivity but also reactant conversion, starting from the description of the most selective MoO_X/TiO_2 catalyst, we tried to increase the specific activity by using a nano-titania with higher surface area, aiming at covering this surface with higher load of selective catalytic surface species. Anatase titania with crystallite size ranging from 5 to 10 nm and 345 m^2/g specific surface area (PC 500 provided by Millennium Inorganic Chemicals, UK) was used as catalyst support for various contents of molybdenum oxide and sulphate, deposited through a two-step process. Firstly, nano-titania was impregnated with the ammonium sulphate aqueous solution, followed by drying under stirring at 80 °C and calcination at 300 °C for 3 h. Then, the sulphated sample was impregnated with ammonium heptamolybdate aqueous solution, dried at 120 °C for 12 h and calcined in air at 400 °C for 3 h. By this way we reached maximum sulphate loading of 19 $\mu mol/m^2$, maintaining Mo loading to a concentration corresponding to that for monolayer as previously determined (8 $\mu mol/m^2$), without formation of segregated MoO_3 crystallites. The high sulphate content promoted benzene yield (Fig. 7.4), while cyclohexene was produced in very low concentration, and CO_2 was absent. Sulphate doping increased

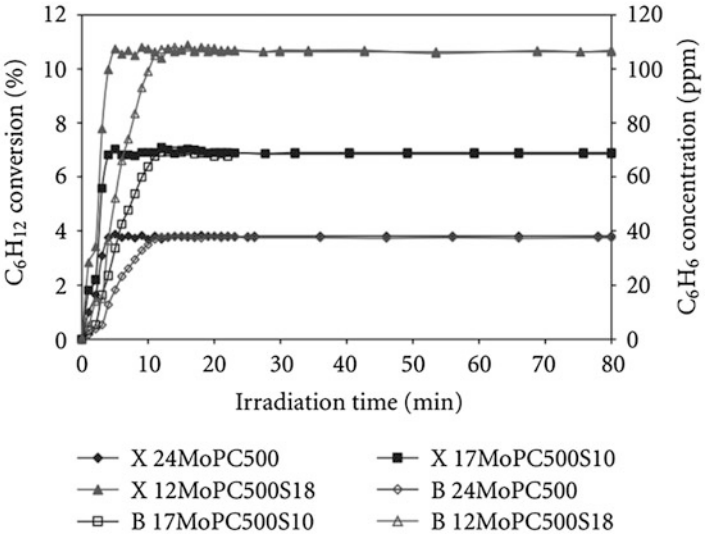

Fig. 7.4 Cyclohexane conversion (X) and benzene outlet concentration (B) on catalysts with different Mo and sulphate loading (Ciambelli et al. 2008b)

cyclohexane adsorption up to 0.22 μmol/m^2, confirming the critical role of acidity for the photoactivity (Fig. 7.5) (Ciambelli et al. 2008b).

7.3.5 The Effect of Substituting Titania

Even more surprising was the result obtained by changing the support from titania to a not photoactive oxide, such as alumina. In fact, neither alumina, sulphated alumina nor $MoO_x/\gamma\text{-}Al_2O_3$ catalyst exhibited any photoactivity for cyclohexane conversion, while sulphated $MoO_x/\gamma\text{-}Al_2O_3$ catalyst was able to selectively convert cyclohexane to cyclohexene, without formation of benzene and CO_x as by-products (Figs. 7.4 and 7.5). Cyclohexene formed simultaneously to cyclohexane conversion after lamp on, reaching steady-state values in only 30 min. Moreover, cyclohexane conversion and cyclohexene yield decreased with the sulphate content. The results show that sulphate strongly enhances the photoactivity of $MoO_x/\gamma\text{-}Al_2O_3$ catalyst, likely due to promoted cyclohexene desorption from the photocatalyst surface controlled by the photocatalyst surface acidity. In this way, selectivity to olefin of 100% was obtained (Ciambelli et al. 2007, 2009). With the same catalyst, formulation styrene was photocatalytically produced from ethylbenzene with 100% selectivity (Sannino et al. 2013b).

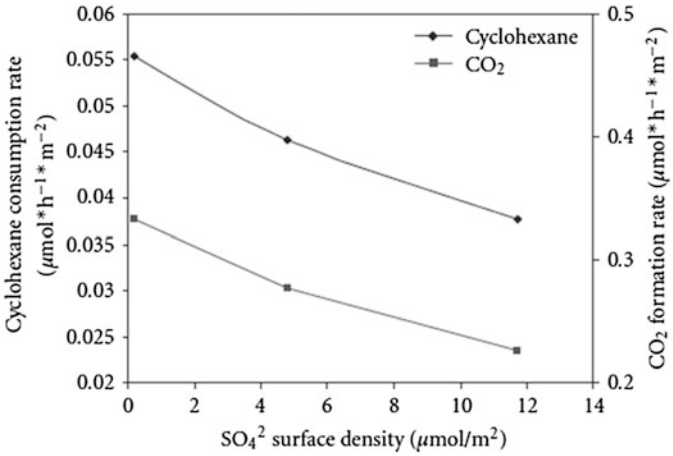

Fig. 7.5 Cyclohexane conversion (X) and benzene outlet concentration (B) on catalysts with different Mo and sulphate loading (Ciambelli et al. 2008b)

7.3.6 The Effect of Reactor and Illumination

It is well known that a critical issue for enhancing the performance of a photocatalyst is the type of photoreactor. Looking for a solution able either to minimize loss of the originally emitted light or maximize uniform irradiance of the entire catalyst surface, contact between catalyst and reagents, removal of reaction products from catalyst surface and heat and mass transfer rate, we moved from a fixed bed annular to a bi-dimensional fluidized bed reactor and introduced a novel solution for irradiation, based on two 365 nm peak UV-light-emitting diode (UV-LED) modules of 40 elements, positioned in front of the Pyrex windows and operated at various forward current values. The UV-LED outputs were adjusted by a power supply. A proportional-integral-differential controller of reactor temperature was also installed into the reactor.

Really, we had to solve the critical issue related to poor fluidizability of titania, which belongs to C group of Geldart distribution. Moreover, the tendency of this type of particles to agglomerate would result in limited light exposition (Geldart 1972). The first solution adopted to enhance the catalyst fluidizability was the use of physical mixtures $MoOx/TiO_2$-α-Al_2O_3 (Ciambelli et al. 2005). Further research on this aspect led to significant enhancement of the catalytic performance using TiO_2-Al_2O_3 mixed oxides as catalytic support and obtaining improved cyclohexane conversion and benzene selectivity with respect to $MoOx/TiO_2$ (Ciambelli et al. 2008b). To further increase the performance of the gas-phase photocatalytic fluidized bed reactor, we prepared the catalyst by using as support a material transparent to ultraviolet radiation, such as TiO_2/SiO_2. With this catalyst, we reached steady-state cyclohexane consumption rate of about 42 μmol h^{-1} g^{-1} (97% benzene

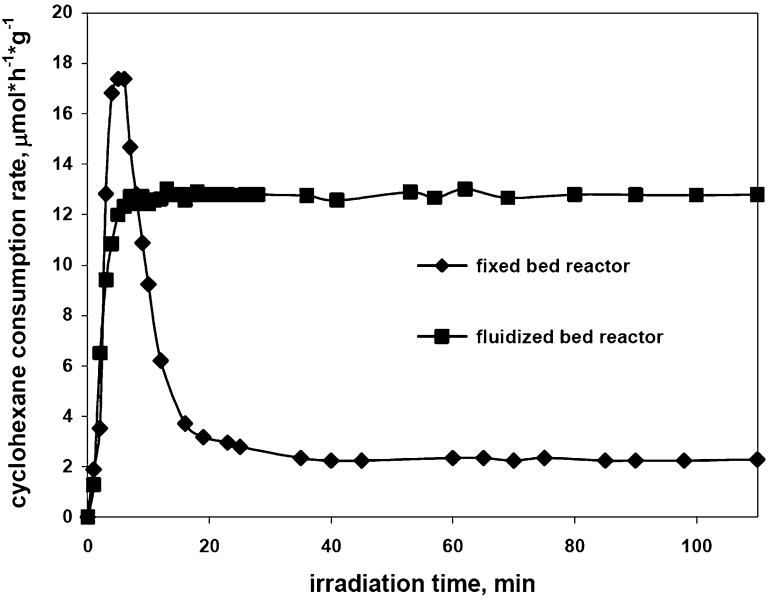

Fig. 7.6 Cyclohexane consumption rate as a function of irradiation time on MoO_x/TiO_2 catalyst using the fluidized bed and fixed bed reactor (Sannino et al. 2011)

selectivity), higher than that obtained (17 µmol h^{-1} g^{-1}) on the optimized formulation for $MoOx/TiO_2$-Al_2O_3 catalysts (Vaiano et al. 2014). The fluidized bed reactor was a good solution for our photocatalytic process, since catalyst particles scattered more and better-utilized light by the mobile catalyst than in a granular fixed bed, resulting in higher light absorption.

Moreover, at the variance of the fixed bed, in the fluidized bed reactor, the catalyst did not deactivate. Deep characterization performed after the photoreactivity test indicated that the catalyst used in fluidized conditions remained active as it maintained the initial sulphur content at the surface. A considerable decrease in the rate of poisoning by carbonaceous species was observed at higher molybdenum and sulphate contents. With fluidized bed reactor, cyclohexane conversion was three times higher at 100 selectivities to benzene (Sannino et al. 2011; Vaiano et al. 2013) (Fig. 7.6).

In Table 7.1 a summary of the best performances obtained for the photocatalytic selective oxidative dehydrogenation of cyclohexane is presented.

Table 7.1 Comparison of photocatalytic performances in different reactions

Reaction	Catalyst	Average crystallite size nm	Reactant conversion %	Selectivity %	Reaction temperature °C	Apparent quantum yield[a] (φ) %	Photoreactivity[b], mol/($m^3_{reactor}$ [a]s)
Cyclohexane to benzene	MoO_3/TiO_2	5	12	99	120	0.44	$3.8*10^{-3}$
Cyclohexane to cyclohexene	MoO_3/Al_2O_3	10	28	100	120	0.56	$3.7*10^{-3}$
Ethylbenzene to styrene	MoO_3/Al_2O_3	10	34	100	120	0.61	$3.9*10^{-3}$

[a]Calculated as the ratio between the number of reacted ethanol molecules per second and the number of photons entering the reactor per second
[b]Calculated as moles of ethanol converted per second and per irradiated volume

7.3.7 *Cyclohexanol and Cyclohexanone by Gas-Phase Photocatalytic Oxidation?*

Coming back to the photocatalytic partial oxidation of cyclohexane to cyclohexanol and cyclohexanone, it is worthwhile to underline that we obtained for the first time this kind of selectivity, typical of the liquid phase, also in the gas phase on gold/titania catalyst prepared by photo deposition on sol-gel TiO_2. Tuning gold content results in a dramatic effect on selectivity (at 100 °C, selectivity to cyclohexanone up to 80% at Au 2.0 wt% load, highest selectivity to cyclohexanol at Au 0.5 wt% load). The only by-product is carbon dioxide. Catalyst deactivation was dramatically reduced at 100 °C (Sannino et al. 2013a).

7.4 Photocatalytic Membrane Reactors

Considering the recent developments reported in the literature, it is possible to state that the heterogeneous photocatalysis is an interesting water treatment technology (Zheng et al. 2017). Several photocatalysts have been studied, starting from TiO_2, and different modification technics have been used to make photocatalysts active under solar or visible light (Hu et al. 2010; Zhang et al. 2010). Despite this very important aspect for the application of photocatalysis on an industrial scale, there are other aspects that limit the applicability of this process. Photocatalysts are generally employed as suspended particles in the reactors. However, the most complicated phase is represented by the separation of the photocatalyst particles from the treated water. In fact, this aspect is the main disadvantage related to the photocatalytic processes (Iglesias et al. 2016).

Therefore, a separation and recovery step is necessary to realize the reuse of photocatalysts. To do this, the membrane technologies used for the first time in water treatment in 1960 were invented (Muhamad et al. 2016). Membrane technology is widely used in wastewater treatment by means of microfiltration, ultrafiltration, nanofiltration and reverse osmosis. Thinking about photocatalysis, and therefore the problem of separation and reuse of catalysts, it is clear how the use of membrane reactors can represent an interesting further application for this technology.

By combining photocatalysis with membrane reactors, photocatalytic membrane reactors are obtained. Membrane technology can offer new opportunities in design, rationalization and optimization of processes and products.

A photocatalytic membrane reactor combines a photocatalyst and a membrane to induce chemical reactions. Photocatalytic membrane reactors are a useful “green” technology able to improve both the performances of classical photoreactors and those ones of membrane-based processes minimizing environmental and economic impacts (Molinari et al. 2017).

Due to the various advantages that can be obtained by applying this technology, the study of photocatalytic membrane reactors has increased (Chester et al. 1993; Sabate et al. 1992).

Considering the type of the photocatalysts, photocatalytic membrane reactor configurations can be divided into two main categories (Zheng et al. 2017):

– Photocatalytic membrane reactors with photocatalyst suspended in feed solution
– Photocatalytic membrane reactors with photocatalyst immobilized in/on the membrane

In the case of slurry reactors, a membrane filtration may be used in a single step for the recovery of catalyst particles from aqueous solution (Augugliaro et al. 2006). The main disadvantage of this configuration is the membrane fouling. To overcome this problem, the use of photocatalytic membranes (photocatalytic membrane reactors with photocatalyst immobilized in/on the membrane) is proposed. However, the immobilization of the photocatalyst often induced a worsening of photoactivity (Geissen et al. 2001). For the photocatalytic membrane reactor design, the choice of the type of membrane has a crucial role. This choice must be made according to the photocatalytic process. This means that, if the photocatalysis is used for the degradation of organic pollutants, the membrane must be able to reject the substrates and their intermediate products, which otherwise pass in permeate. Instead, if the photocatalytic process is used as a synthetic pathway, the main objective of the membrane can be the selective separation of the product, minimizing its successive oxidation which leads to undesirable by-products (Molinari et al. 2017).

The photocatalytic membrane reactor configuration is related to the process mode (dead end or crossflow, batch or continuous flow), membrane technology, membrane module numbers or the type of the light source.

However, the typical photocatalytic membrane reactor configuration is composed of a membrane unit equipped with another unit that is the photoreactor irradiated with a light source, as reported in the literature (Mozia 2010).

In fact, for example, a photocatalytic membrane reactor can be constituted by a first stage with the tank containing the suspended photocatalyst and a second stage where the membrane is present. In particular, in this configuration, the light source is positioned on the additional tank in which the photocatalytic reaction takes place, located between the feed tank and membrane module (Fig. 7.7) (Mozia 2010).

In a photocatalytic membrane reactor using suspended photocatalyst, it is possible to divide the overall plant in two zones: the photocatalytic reactor zone (i.e. the photoreactor) where the photocatalyst is irradiated and the photocatalytic reaction takes place and the membrane separation zone (i.e. the membrane separation unit) where the confining of the photocatalyst and of the unreacted substrate in the reactor happens.

On the basis of this, the distribution of the photocatalytic membrane reactor's volumes between these two zones is another important design parameter that needs to be optimized (Kertesz et al. 2014). Considering these aspects, PMR systems coupled with suspended photocatalyst may be interesting for different aspects related to the use of membranes in the final stage, such as the degradation of dye from

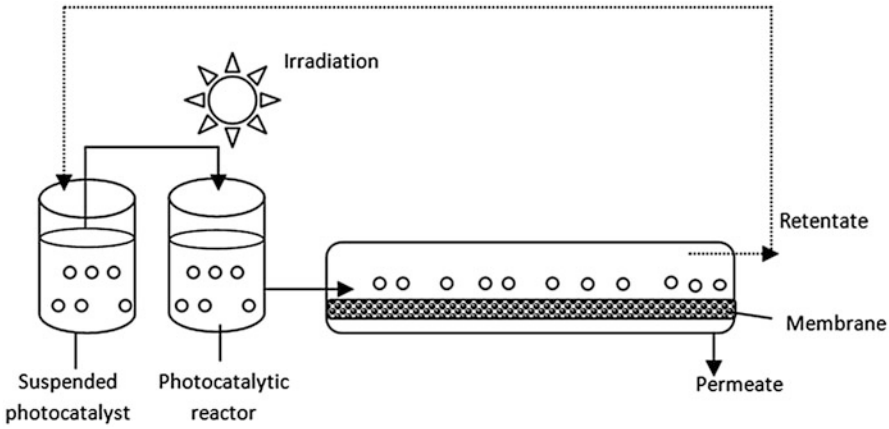

Fig. 7.7 Possible PMR configuration using the irradiation on the second tank (photocatalytic reactor) between the tank for suspended photocatalyst and the membrane (Mozia 2010)

industry wastewater due to the possibility to separate and reuse the photocatalyst, thanks to the membrane action, the possibility to remove also the intermediate generated by the dye degradation obtaining a high-quality permeate and the possibility to operate in continuous mode (Ganiyu et al. 2015) .

Moreover, systems based on the use of suspended catalyst are more efficient than immobilized systems, as typically reported in the literature (Mascolo et al. 2007).

However, membrane photoreactor systems with a suspended photocatalyst have some disadvantages, for example, the fouling, causing the decrease of the performance of the photocatalytic degradation and the necessity of a long time of reaction in addition to an expensive filtration treatment when the recovery of the photocatalyst particles is required (Molinari et al. 2017).

Another possible configuration, as mentioned above, is a photocatalytic membrane reactor where the photocatalyst is immobilized on or within the membrane and the light source is located on the membrane module where the photocatalyst is present (Fig. 7.8). The use of a photocatalyst immobilized on the membrane allows obtaining a photocatalytic membrane able to improve the performance of technology based on the coupling of photocatalysis with membrane filtration in view of real applications. In this configuration the membrane function is twofold: it must support the photocatalyst and it must act as a selective barrier for the contaminants to be degraded.

In Fig. 7.8 it is reported an example of photocatalytic membrane reactors including reactors with photocatalytic membranes.

However, these systems present some limitations such as diffusive limitations on photocatalysts which, for this reason, show a loss of photoactivity, mass transfer limits and limited system duration due to the possible deactivation and washing of the catalyst.

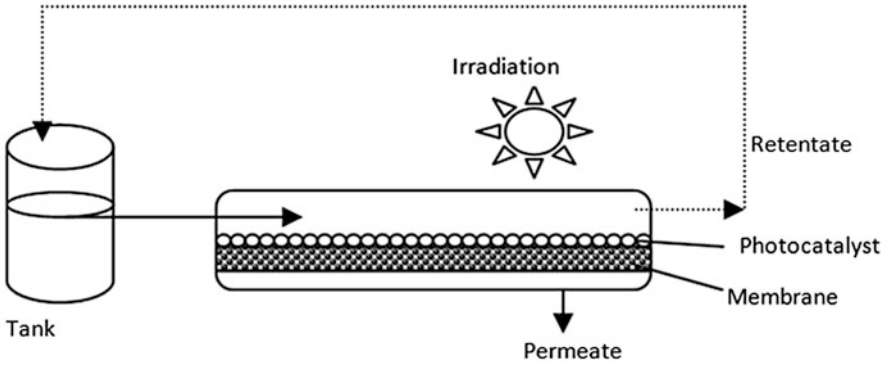

Fig. 7.8 Possible photocatalytic membrane reactor configuration using the irradiation on the photocatalyst immobilize on (or within) the membrane module (Mozia 2010)

Another disadvantage is the possibility of membrane oxidation by the action of •OH radicals. Therefore inorganic membranes could be preferable, thanks to their excellent thermal, mechanical and chemical stability.

Therefore it is preferable to use inorganic membranes because they have excellent properties such as high thermal, chemical and mechanical stability. In the literature, there are several studies in which the applications of various types of membrane photoreactors have been reported and different fields of applications have been examined. For example, the degradation of azo dyes present in industrial wastewaters has been shown in various experimental works based both on the use of slurry photoreactors and in other literature papers describing the use of the photocatalyst immobilized on the membrane (Hairom et al. 2015; Molinari et al. 2004).

Molinari et al. have studied the degradation of two different azo dyes, Congo Red and Patent Blue, present in aqueous solution with a suspended photocatalytic membrane reactor configuration and using TiO_2-P25 as the photocatalyst and a nanofiltration membrane. From experimental results it was possible to observe that very high results were obtained for the photodegradation of Congo Red, evidencing the beneficial effect of the nanofiltration membrane acting as a barrier for both the substrate and the catalyst. However, as regards the Patent Blue degradation, the authors have observed that using a nanofiltration membrane, lower degradation was obtained. This result indicates that the correct selection of the membrane is the key step to improve photocatalytic membrane reactor performance. In addition to TiO_2-P25, other photocatalysts have also been studied, for example, ZnO synthesized via precipitation method and tested in a suspended PMR aimed to industrial dye wastewater treatment (Hairom et al. 2015). In this case, both nanofiltration and ultrafiltration membranes were tested, and their performances in the degradation of azo dye were compared. The results evidenced that very interesting results were obtained using this system for the treatment of industrial wastewater from printing presses. Operating conditions, in particular, the pH of solution, played an important

role for the control of the photocatalytic efficiency and the fouling behaviour in the photocatalytic membrane reactor-based systems.

These results demonstrate how the use of membrane reactors with suspended photocatalysts was an interesting approach to the degradation of dyes present in the industrial wastewaters.

However, there remains a problem linked to membrane fouling, induced by the deposition of the catalyst on the membrane surface. In order to overcome this limitation, different approaches have been considered, such as the use of a hollow fibre membrane and the backwash (Sopajaree et al. 1999). It has been observed that with the use of the hollow fibre membrane-ultrafiltration unit, the photocatalyst is maintained in the reactive environment and completely separated from the treated effluents.

As regards the use of photocatalytic membranes, in the literature it is reported the use of inorganic composite membranes based on TiO_2/Al_2O_3 with photocatalytic capability prepared by the sol-gel technique (Zhang et al. 2006). The obtained photocatalytic membranes allowed to achieve 82% removal efficiency of Direct Black 168 dye after 5 h of UV irradiation. With this membrane, the simultaneous photocatalytic reaction and separation were ensured, obtaining a high permeate flux (82 L m^{-2} h^{-1}) by using a low pressure (0.5 bar), thanks to the high porosity. The necessity to develop a visible light-active system may represent another aspect for the large-scale use of PMR systems, using the direct sunlight. Athanasekou et al. formulated a highly active photocatalytic ceramic UF membranes and tested it under near-UV/vis and visible light irradiation (Athanasekou et al. 2015). The test has demonstrated that this photocatalytic membrane was stable and reusable. Considering these results it is possible to confirm that the coupling with heterogeneous photocatalysis and a membrane-based process could be a promising technology for wastewater treatment. The immobilization of photocatalyst on membrane surface does not require the separation of the photocatalyst and minimize the membrane fouling. However, this last configuration presents low photocatalytic efficiency. Therefore, photocatalytic membrane reactors using suspended photocatalyst particles are actually more suitable for large-scale application aimed at wastewater treatment.

7.5 Concluding Remarks

The topics discussed in the present chapter are related to innovation aspects in the heterogeneous photocatalysis. In particular, it has evidenced the possibility to produce hydrogen from the aqueous solution containing organic compounds using visible light-active “noble metal-free” photocatalysts. Moreover it has presented novel photocatalyst formulations for the synthesis of organic compounds useful in industrial chemistry. Finally it analysed the recent literature about the use of photocatalytic membrane reactors, presenting some solutions to overcome the problem related to the fouling formation during the water and wastewater treatment.

References

Acar C, Dincer I, Naterer GF (2016) Review of photocatalytic water-splitting methods for sustainable hydrogen production. Int J Energy Res 40(11):1449–1473. https://doi.org/10.1002/er.3549

Almquist CB, Biswas P (2001) The photo-oxidation of cyclohexane on titanium dioxide: an investigation of competitive adsorption and its effects on product formation and selectivity. Appl Catal A Gen 214(2):259–271. https://doi.org/10.1016/S0926-860X(01)00495-1

Athanasekou CP, Moustakas NG, Morales-Torres S, Pastrana-Martínez LM, Figueiredo JL, Faria JL, . . . Falaras P (2015). Ceramic photocatalytic membranes for water filtration under UV and visible light. Appl Catal B Environ 178:12–19. https://doi.org/10.1016/j.apcatb.2014.11.021

Augugliaro V, Litter M, Palmisano L, Soria J (2006) The combination of heterogeneous photocatalysis with chemical and physical operations: a tool for improving the photoprocess performance. J Photochem Photobiol C 7(4):127–144. https://doi.org/10.1016/j.jphotochemrev.2006.12.001

Bickley RI, Munuera G, Stone FS (1973) Photoadsorption and photocatalysis at rutile surfaces. II photocatalytic oxidation of isopropanol. J Catal 31(3):398–407. https://doi.org/10.1016/0021-9517(73)90311-4

Bowker M, Davies PR, Al-Mazroai LS (2009) Photocatalytic reforming of glycerol over gold and palladium as an alternative fuel source. Catal Lett 128(3–4):253–255. https://doi.org/10.1007/s10562-008-9781-1

Castaneda C, Tzompantzi F, Rodriguez-Rodriguez A, Sanchez-Dominguez M, Gomez R (2018) Improved photocatalytic hydrogen production from methanol/water solution using CuO supported on fluorinated TiO2. J Chem Technol Biotechnol 93(4):1113–1120. https://doi.org/10.1002/jctb.5470

Chen T, Feng Z, Wu G, Shi J, Ma G, Ying P, Li C (2007) Mechanistic studies of photocatalytic reaction of methanol for hydrogen production on Pt/TiO2 by in situ Fourier transform IR and time-resolved IR spectroscopy. J Phys Chem C 111(22):8005–8014. https://doi.org/10.1021/jp071022b

Chester G, Anderson M, Read H, Esplugas S (1993) A jacketed annular membrane photocatalytic reactor for wastewater treatment: degradation of formic acid and atrazine. J Photochem Photobiol A 71(3):291–297. https://doi.org/10.1016/1010-6030(93)85013-X

Chiarello GL, Selli E (2014) Photocatalytic production of hydrogen. In: Advances in hydrogen production, storage and distribution. Woodhead Publishing, Cambridge, UK, pp 216–247

Christoforidis KC, Fornasiero P (2017) Photocatalytic hydrogen production: a rift into the future energy supply. ChemCatChem 9(9):1523–1544. https://doi.org/10.1002/cctc.201601659

Ciambelli P, Sannino D, Palma V, Vaiano V (2005) Cyclohexane photocatalytic oxidative dehydrogenation to benzene on sulphated titania supported MoOx. Stud Surf Sci Catal 155:179–187

Ciambelli P, Sannino D, Palma V, Vaiano V, Eloy P, Dury F, Gaigneaux EM (2007) Tuning the selectivity of MoOx supported catalysts for cyclohexane photooxidative dehydrogenation. Catal Today 128(3–4):251–257. https://doi.org/10.1016/j.cattod.2007.07.006

Ciambelli P, Sannino D, Palma V, Vaiano V (2008a) The effect of sulphate doping on nanosized TiO2 and MoOx/TiO2 catalysts in cyclohexane photooxidative dehydrogenation. Int J Photoenergy., No pp. given. https://doi.org/10.1155/2008/258631

Ciambelli P, Sannino D, Palma V, Vaiano V, Bickley RI (2008b) Reaction mechanism of cyclohexane selective photo-oxidation to benzene on molybdena/titania catalysts. Appl Catal A Gen 349(1–2):140–147. https://doi.org/10.1016/j.apcata.2008.07.019

Ciambelli P, Sannino D, Palma V, Vaiano V, Mazzei RS, Eloy P, Gaigneaux EM (2009) Photocatalytic cyclohexane oxidehydrogenation on sulphated MoOx/γ-Al2O3 catalysts. Catal Today 141(3–4):367–373. https://doi.org/10.1016/j.cattod.2008.10.020

Colmenares JC, Magdziarz A, Aramendia MA, Marinas A, Marinas JM, Urbano FJ, Navio JA (2011) Influence of the strong metal support interaction effect (SMSI) of Pt/TiO2 and Pd/TiO2 systems in the photocatalytic biohydrogen production from glucose solution. Catal Commun 16(1):1–6. https://doi.org/10.1016/j.catcom.2011.09.003

Dauenhauer PJ, Salge JR, Schmidt LD (2006) Renewable hydrogen by autothermal steam reforming of volatile carbohydrates. J Catal 244(2):238–247. https://doi.org/10.1016/j.jcat.2006.09.011

Djeghri N, Formenti M, Juillet F, Teichner SJ (1974) Photointeraction on the surface of titanium dioxide between oxygen and alkanes. Faraday Discuss Chem Soc 58(0):185–193. https://doi.org/10.1039/DC9745800185

Formenti M, Juillet F, Teichner SJ (1970) Controlled photooxidation of paraffins and olefins over anatase at room temperature. C R Acad Sci Ser C 270(2):138–141

Formenti M, Juillet F, Meriaudeau P, Teichner SJ (1973) Heterogeneous photocatalysis. Partial and total oxidation of hydrocarbons and inorganic compounds at room temperature on solid catalysts under irradiation

Fu X, Long J, Wang X, Leung DYC, Ding Z, Wu L, ... Fu X (2008) Photocatalytic reforming of biomass: a systematic study of hydrogen evolution from glucose solution. Int J Hydrogen Energy 33(22):6484–6491. https://doi.org/10.1016/j.ijhydene.2008.07.068

Fu X, Wang X, Leung DYC, Gu Q, Chen S, Huang H (2011) Photocatalytic reforming of C3-polyols for H2 production. Appl Catal B 106(3–4):681–688. https://doi.org/10.1016/j.apcatb.2011.05.045

Fujishima A, Honda K (1972) Electrochemical photolysis of water at a semiconductor electrode. Nature 238(5358):37–38. https://doi.org/10.1038/238037a0

Galinska A, Walendziewski J (2005) Photocatalytic water splitting over Pt-TiO2 in the presence of sacrificial reagents. Energy Fuel 19(3):1143–1147. https://doi.org/10.1021/ef0400619

Ganiyu SO, van Hullebusch, Eric D, Cretin M, Esposito G, Oturan MA (2015) Coupling of membrane filtration and advanced oxidation processes for removal of pharmaceutical residues: a critical review. Sep Purif Technol 156(Part_3):891–914. https://doi.org/10.1016/j.seppur.2015.09.059

Geissen SU, Xi W, Weidemeyer A, Vogelpohl A, Bousselmi L, Ghrabi A, Ennabli A (2001) Comparison of suspended and fixed photocatalytic reactor systems. Water Sci Technol, 44 (5, Oxidation Technologies for Water and Wastewater Treatment II):245–249

Geldart D (1972) The effect of particle size and size distribution on the behaviour of gas-fluidised beds. Powder Technol 6(4):201–215. https://doi.org/10.1016/0032-5910(72)83014-6

Giannotti C, Richter C (1999) Natural sun light photocatalysed oxidation of adamantane and cyclohexane by W10O32 4. J Phys IV JP 9(3):Pr3-265–Pr263-270

Gomathisankar P, Noda T, Katsumata H, Suzuki T, Kaneco S (2014) Enhanced hydrogen production from aqueous methanol solution using TiO2/Cu as photocatalysts. Front Chem Sci Eng 8 (2):197–202. https://doi.org/10.1007/s11705-014-1417-y

Hairom NHH, Mohammad AW, Ng LY, Kadhum AAH (2015) Utilization of self-synthesized ZnO nanoparticles in MPR for industrial dye wastewater treatment using NF and UF membrane. Desalin Water Treat 54(4–5):944–955. https://doi.org/10.1080/19443994.2014.917988

Herrmann JM (1999) Heterogeneous photocatalysis: fundamentals and applications to the removal of various types of aqueous pollutants. Catal Today 53(1):115–129. https://doi.org/10.1016/S0920-5861(99)00107-8

Hu X, Hu C, Peng T, Zhou X, Qu J (2010) Plasmon-induced inactivation of enteric pathogenic microorganisms with Ag-AgI/Al2O3 under visible-light irradiation. Environ Sci Technol 44 (18):7058–7062. https://doi.org/10.1021/es1012577

Iervolino G, Vaiano V, Murcia JJ, Rizzo L, Ventre G, Pepe G, ... Sannino D (2016a) Photocatalytic hydrogen production from degradation of glucose over fluorinated and platinized TiO2 catalysts. J Catal 339: 47–56. https://doi.org/10.1016/j.jcat.2016.03.032

Iervolino G, Vaiano V, Sannino D, Rizzo L, Ciambelli P (2016b) Production of hydrogen from glucose by LaFeO3 based photocatalytic process during water treatment. Int J Hydrog Energy 41(2):959–966. https://doi.org/10.1016/j.ijhydene.2015.10.085

Iervolino G, Vaiano V, Sannino D, Rizzo L, Palma V (2017) Enhanced photocatalytic hydrogen production from glucose aqueous matrices on Ru-doped LaFeO3. Appl Catal B Environ 207:182–194. https://doi.org/10.1016/j.apcatb.2017.02.008

Iervolino G, Vaiano V, Sannino D, Rizzo L, Galluzzi A, Polichetti M, ... Campiglia P (2018) Hydrogen production from glucose degradation in water and wastewater treated by Ru-LaFeO3/

Fe2O3 magnetic particles photocatalysis and heterogeneous photo-Fenton. Int J Hydrogen Energy 43(4):2184–2196. https://doi.org/10.1016/j.ijhydene.2017.12.071

Iglesias O, Rivero MJ, Urtiaga AM, Ortiz I (2016) Membrane-based photocatalytic systems for process intensification. Chem Eng J (Amsterdam, Neth) 305:136–148. https://doi.org/10.1016/j.cej.2016.01.047

Jang JS, Kim HG, Lee JS (2012) Heterojunction semiconductors: a strategy to develop efficient photocatalytic materials for visible light water splitting. Catal Today 185(1):270–277. https://doi.org/10.1016/j.cattod.2011.07.008

Kawai T, Sakata T (1980) Conversion of carbohydrate into hydrogen fuel by a photocatalytic process. Nature 286(5772):474–476. https://doi.org/10.1038/286474a0

Kawai T, Sakata T (1981) Photocatalytic hydrogen production from water by the decomposition of poly(vinyl chloride), protein, algae, dead insects, and excrement. Chem Lett (1):81–84. https://doi.org/10.1246/cl.1981.81

Kertesz S, Cakl J, Jirankova H (2014) Submerged hollow fiber microfiltration as a part of hybrid photocatalytic process for dye wastewater treatment. Desalination 343:106–112. https://doi.org/10.1016/j.desal.2013.11.013

Kim J, Monllor-Satoca D, Choi W (2012) Simultaneous production of hydrogen with the degradation of organic pollutants using TiO2 photocatalyst modified with dual surface components. Energy Environ Sci 5(6):7647–7656. https://doi.org/10.1039/c2ee21310a

Kondarides DI, Daskalaki VM, Patsoura A, Verykios XE (2008) Hydrogen production by photo-induced reforming of biomass components and derivatives at ambient conditions. Catal Lett 122 (1–2):26–32. https://doi.org/10.1007/s10562-007-9330-3

Kou J, Lu C, Wang J, Chen Y, Xu Z, Varma RS (2017) Selectivity enhancement in heterogeneous photocatalytic transformations. Chem Rev 117(3):1445–1514. https://doi.org/10.1021/acs.chemrev.6b00396

Li Y-X, Wang J-X, Peng S-Q, Lu G-X, Li S-B (2010) Photocatalytic hydrogen generation in the presence of glucose over ZnS-coated ZnIn2S4 under visible light irradiation. Int J Hydrog Energy 35(13):7116–7126. https://doi.org/10.1016/j.ijhydene.2010.02.017

Lianos P, Strataki N, Antoniadou M (2009) Photocatalytic and photoelectrochemical hydrogen production by photodegradation of organic substances. Pure Appl Chem 81(8):1441–1448. https://doi.org/10.1351/PAC-CON-08-07-07

Liu Y, Guo L, Yan W, Liu H (2006) A composite visible-light photocatalyst for hydrogen production. J Power Sources 159(2):1300–1304. https://doi.org/10.1016/j.jpowsour.2005.11.105

Maldotti A, Amadelli R, Varani G, Tollari S, Porta F (1994) Photocatalytic processes with polyoxotungstates: oxidation of cyclohexylamine. Inorg Chem 33(13):2968–2973. https://doi.org/10.1021/ic00091a041

Maldotti A, Amadelli R, Carassiti V, Molinari A (1997) Catalytic oxygenation of cyclohexane by photoexcited (nBu4N)4W10O32: the role of radicals. Inorg Chim Acta 256(2):309–312. https://doi.org/10.1016/S0020-1693(96)05432-1

Mascolo G, Comparelli R, Curri ML, Lovecchio G, Lopez A, Agostiano A (2007) Photocatalytic degradation of methyl red by TiO2: comparison of the efficiency of immobilized nanoparticles versus conventional suspended catalyst. J Hazard Mater 142(1–2):130–137. https://doi.org/10.1016/j.jhazmat.2006.07.068

Miwa T, Kaneco S, Katsumata H, Suzuki T, Ohta K, Chand Verma S, Sugihara K (2010) Photocatalytic hydrogen production from aqueous methanol solution with CuO/Al2O3/TiO2 nanocomposite. Int J Hydrog Energy 35(13):6554–6560. https://doi.org/10.1016/j.ijhydene.2010.03.128

Mohamed RM, Aazam ES (2012) H2 production with low CO selectivity from photocatalytic reforming of glucose on Ni/TiO2-SiO2. Chin J Catal 33(2):247–253. https://doi.org/10.1016/S1872-2067(10)60276-8

Molinari A, Maldotti A, Amadelli R, Sgobino A, Carassiti V (1998) Integrated photocatalysts for hydrocarbon oxidation: polyoxotungstates/ iron porphyrins systems in the reductive activation of molecular oxygen. Inorg Chim Acta 272(1–2):197–203

Molinari R, Pirillo F, Falco M, Loddo V, Palmisano L (2004) Photocatalytic degradation of dyes by using a membrane reactor. Chem Eng Process Process Intensif 43(9):1103–1114. https://doi.org/10.1016/j.cep.2004.01.008

Molinari R, Lavorato C, Argurio P (2017) Recent progress of photocatalytic membrane reactors in water treatment and in synthesis of organic compounds. A review. Catal Today 281 (Part_1):144–164. https://doi.org/10.1016/j.cattod.2016.06.047

Mozia S (2010) Photocatalytic membrane reactors (PMRs) in water and wastewater treatment. A review. Sep Purif Technol 73(2):71–91. https://doi.org/10.1016/j.seppur.2010.03.021

Muhamad MS, Salim MR, Lau WJ, Yusop Z (2016) A review on bisphenol a occurrences, health effects and treatment process via membrane technology for drinking water. Environ Sci Pollut Res 23(12):11549–11567. https://doi.org/10.1007/s11356-016-6357-2

Parida KM, Reddy KH, Martha S, Das DP, Biswal N (2010) Fabrication of nanocrystalline LaFeO3: an efficient sol-gel auto-combustion assisted visible light responsive photocatalyst for water decomposition. Int J Hydrog Energy 35(22):12161–12168. https://doi.org/10.1016/j.ijhydene.2010.08.029

Puga AV (2016) Photocatalytic production of hydrogen from biomass-derived feedstocks. Coord Chem Rev 315:1–66. https://doi.org/10.1016/j.ccr.2015.12.009

Ramachandran S, Fontanille P, Pandey A, Larroche C (2006) Gluconic acid: properties, applications and microbial production. Food Technol Biotechnol 44(2):185–195

Romero NA, Nicewicz DA (2016) Organic photoredox catalysis. Chem Rev 116 (17):10075–10166. https://doi.org/10.1021/acs.chemrev.6b00057

Sabate J, Anderson MA, Aguado MA, Gimenez J, Cervera-March S, Hill CG Jr (1992) Comparison of titanium oxide TiO2 powder suspensions and TiO2 ceramic membranes supported on glass as photocatalytic systems in the reduction of chromium(VI). J Mol Catal 71(1):57–68. https://doi.org/10.1016/0304-5102(92)80007-4

Sacco O, Stoller M, Vaiano V, Ciambelli P, Chianese A, Sannino D (2012) Photocatalytic degradation of organic dyes under visible light on n-doped TiO2 photocatalysts. Int J Photoenergy 2012, Article ID 626759, 8 pages. https://doi.org/10.1155/2012/626759

Sadanandam G, Valluri DK, Scurrell MS (2017) Highly stabilized Ag2O-loaded nano TiO2 for hydrogen production from glycerol: water mixtures under solar light irradiation. Int J Hydrog Energy 42(2):807–820. https://doi.org/10.1016/j.ijhydene.2016.10.131

Sannino D, Vaiano V, Ciambelli P, Eloy P, Gaigneaux EM (2011) Avoiding the deactivation of sulphated MoOx/TiO2 catalysts in the photocatalytic cyclohexane oxidative dehydrogenation by a fluidized bed photoreactor. Appl Catal A 394(1–2):71–78. https://doi.org/10.1016/j.apcata.2010.12.025

Sannino D, Vaiano V, Ciambelli P (2013a) A green route for selective synthesis of styrene from ethylbenzene by means of a photocatalytic system. Res Chem Intermed 39(9):4145–4157. https://doi.org/10.1007/s11164-012-0931-0

Sannino D, Vaiano V, Ciambelli P, Murcia JJ, Hidalgo MC, Navio JA (2013b) Gas-phase photocatalytic partial oxidation of cyclohexane to cyclohexanol and cyclohexanone on Au/TiO2 photocatalysts. J Adv Oxid Technol 16(1):71–82. https://doi.org/10.1515/jaots-2013-0107

Sopajaree K, Qasim SA, Basak S, Rajeshwar K (1999) An integrated flow reactor-membrane filtration system for heterogeneous photocatalysis. Part II: experiments on the ultrafiltration unit and combined operation. J Appl Electrochem 29(9):1111–1118

Speltini A, Sturini M, Maraschi F, Dondi D, Fisogni G, Annovazzi E et al (2015) Evaluation of UV-A and solar light photocatalytic hydrogen gas evolution from olive mill wastewater. Int J Hydrogen Energy 40(12):4303–4310. https://doi.org/10.1016/j.ijhydene.2015.01.182

St. John MR, Furgala AJ, Sammells AF (1983) Hydrogen generation by photocatalytic oxidation of glucose by platinized n-titania powder. J Phys Chem 87(5):801–805. https://doi.org/10.1021/j100228a021

Strataki N, Bekiari V, Kondarides DI, Lianos P (2007) Hydrogen production by photocatalytic alcohol reforming employing highly efficient nanocrystalline titania films. Appl Catal B 77 (1–2):184–189. https://doi.org/10.1016/j.apcatb.2007.07.015

Strataki N, Antoniadou M, Dracopoulos V, Lianos P (2010) Visible-light photocatalytic hydrogen production from ethanol–water mixtures using a Pt–CdS–TiO2 photocatalyst. Catal Today 151 (1):53–57. https://doi.org/10.1016/j.cattod.2010.03.036

Sun H, Blatter F, Frei H (1996) Cyclohexanone from cyclohexane and O2 in a zeolite under visible light with complete selectivity. J Am Chem Soc 118(29):6873–6879. https://doi.org/10.1021/JA953273G

Teramura K, Tanaka T, Yamamoto T, Funabiki T (2001) Photo-oxidation of cyclohexane over alumina-supported vanadium oxide catalyst. J Mol Catal A Chem 165(1–2):299–301. https://doi.org/10.1016/S1381-1169(00)00417-9

Udani PPC, Ronning M (2015) Comparative study on the photocatalytic hydrogen production from methanol over Cu-, Pd-, Co- and Au-loaded TiO2. Oil Gas Sci Technol 70(5):831–839. https://doi.org/10.2516/ogst/2015025

Vaiano V, Sannino D, Almeida AR, Mul G, Ciambelli P (2013) Investigation of the deactivation phenomena occurring in the cyclohexane photocatalytic oxidative dehydrogenation on MoOx/TiO2 through gas phase and in situ DRIFTS analyses. Catalysts 3(4):978–997., 920 pp. https://doi.org/10.3390/catal3040978

Vaiano V, Sannino D, Ciambelli P (2014) Sustainable gas phase selective photocatalytic oxidation of cyclohexane on MoOx/TiO2/SiO2 catalysts. Chem Eng Trans 39(Special Issue):565–570. https://doi.org/10.3303/CET1439095

Vaiano V, Iervolino G, Sarno G, Sannino D, Rizzo L, Murcia Mesa JJ, . . . Navío JA (2015) Simultaneous production of CH4 and H2 from photocatalytic reforming of glucose aqueous solution on sulfated Pd-TiO2 catalysts. Oil Gas Sci Technol 70(5):891–902. https://doi.org/10.2516/ogst/2014062

Wachs IE, Weckhuysen BM (1997) Structure and reactivity of surface vanadium oxide species on oxide supports. Appl Catal A Gen 157(1):67–90. https://doi.org/10.1016/S0926-860X(97)00021-5

Wang C, Cai X, Chen Y, Cheng Z, Luo X, Mo S, . . . Shen Y (2017) Efficient hydrogen production from glycerol photoreforming over Ag2O-TiO2 synthesized by a sol-gel method. Int J Hydrogen Energy 42(27):17063–17074. https://doi.org/10.1016/j.ijhydene.2017.05.183

Wu GP, Chen T, Zhou GH, Zong X, Li C (2008) H2 production with low CO selectivity from photocatalytic reforming of glucose on metal/TiO2 catalysts. Sci China Ser B Chem 51 (2):97–100. https://doi.org/10.1007/s11426-007-0132-7

Xie Q, Wang Y, Pan B, Wang H, Su W, Wang X (2012) A novel photocatalyst LaOF: facile fabrication and photocatalytic hydrogen production. Catal Commun 27:21–25. https://doi.org/10.1016/j.catcom.2012.06.019

Yamakata A, Ishibashi TA, Onishi H (2003) Effects of water addition on the methanol oxidation on Pt/TiO2 photocatalyst studied by time-resolved infrared absorption spectroscopy. J Phys Chem B 107(36):9820–9823

Zhang H, Quan X, Chen S, Zhao H, Zhao Y (2006) Fabrication of photocatalytic membrane and evaluation its efficiency in removal of organic pollutants from water. Sep Purif Technol 50 (2):147–155. https://doi.org/10.1016/j.seppur.2005.11.018

Zhang J, Wu Y, Xing M, Leghari SAK, Sajjad S (2010) Development of modified N doped TiO2 photocatalyst with metals, nonmetals and metal oxides. Energy Environ Sci 3(6):715–726. https://doi.org/10.1039/b927575d

Zheng X, Shen Z-P, Shi L, Cheng R, Yuan D-H (2017) Photocatalytic membrane reactors (PMRs) in water treatment: configurations and influencing factors. Catalysts 7(8):224/221–224/230. https://doi.org/10.3390/catal7080224

Zinoviev S, Mueller-Langer F, Das P, Bertero N, Fornasiero P, Kaltschmitt M, . . . Miertus S (2010) Next-generation biofuels: survey of emerging technologies and sustainability issues. ChemSusChem 3(10):1106–1133. https://doi.org/10.1002/cssc.201000052

Chapter 8
Solar Light Active Nano-photocatalysts

Jesty Thomas and K. S. Ambili

Contents

Abstract Environmental pollution is becoming a serious threat to the human society, and photocatalysis is recognized as an environmental benign technology to remediate organic pollutants from aqueous environment. Mainstream research related to pollutant remediation and energy production is based on heterogeneous photocatalysis, a modified advanced oxidation process. Being a green technology, it can have further applications if the vast and inexpensive solar light can be utilized in place of harmful ultraviolet rays.

This chapter focuses on some important nano-semiconductor photocatalysts like TiO_2, ZnO and graphitic carbon nitride (g-C_3N_4 or CN) and various strategies adopted for improving their photocatalytic activity under sunlight. Different methods for improving visible light active photocatalysts including metal/non-metal doping, the addition of photosensitive materials, incorporation of other nanoparticles, composite formation with other semiconductors and formation of

J. Thomas (✉) · K. S. Ambili
Research Department of Chemistry, Kuriakose Elias College, Kottayam, Kerala, India

Inamuddin et al. (eds.), *Nanophotocatalysis and Environmental Applications*,
Environmental Chemistry for a Sustainable World 31,
https://doi.org/10.1007/978-3-030-04949-2_8

heterojunctions and nanohybrids are discussed. These fundamental information can serve as knowledge base in constructing next-generation photocatalysts with better properties.

Keywords Nano-semiconductor materials · Solar/visible light · Photocatalysts · Pollutant remediation · Advanced oxidation process · TiO_2 · ZnO graphitic carbon nitride · Titanates · Nano-metal sulphides

8.1 Introduction

Solar energy is the most abundant, clean and renewable source of energy available on earth. It was proposed that the amount of sunlight that strikes on earth's surface in an hour is enough to power the world economy for an entire year (Izumi 2013). Sunlight can be effectively employed for energy production and pollutant remediation, two major issues the world is most concerned with. Solar energy utilization techniques have attracted great attention because of low cost, but the developments of materials which can efficiently harvest sunlight require extensive research.

In the development of solar energy utilization technologies, efficient solar energy conversion systems in which solar energy is efficiently used to generate sustainable electrons and holes triggering the reduction and oxidation (redox) reactions are vitally prerequisite. Nowadays advanced oxidation processes (AOPs) offer a feasible strategy to address energy production and pollutant remediation. AOP involves the generation of hydroxyl radicals with very high oxidizing power in an aqueous medium which endorses energy production and degradation of pollutants. UV-mediated ozonation, oxidation using Fenton's reagent (a mixture of H_2O_2 with Fe^{2+}) and electrocoagulation are some common techniques involving AOP. All these techniques produce hydroxyl radicals, which destroy various POPs, present in polluted water via series of chemical reactions. Complete degradation of pollutants, zero waste production and rapid reaction rates are achieved by AOP, but the main drawbacks are inflated cost and reduced efficiency due to the presence of turbidity or UV-absorbing species, i.e. the efficiency of AOP is determined by the wastewater composition and treatment conditions.

Nowadays photocatalysis, a technique based on AOP, has emerged as a fascinating process towards the degradation of various POPs in the environment and also for fuel production, as it is a cost-effective, renewable, non-toxic and versatile technique. According to the IUPAC gold book, photocatalysis is defined as the change in the rate of a chemical reaction or its initiation under the action of light in the presence of a substance called photocatalyst (Glossary of terms used in photochemistry 2006). In 1972, Fujishima and Honda discovered that water can be split into hydrogen and oxygen using TiO_2 electrode under UV light (Fujishima and Honda 1972). This discovery inspired many researchers to work in the area of heterogeneous photocatalysis. Photocatalytic activity is the ability of a material to create an electron-hole pair as a result of exposure to suitable light irradiation. Design and

development of novel photocatalytic systems with high efficiencies have attracted worldwide scientific interests. Semiconductor nanomaterial-based photocatalysis is recognized as a promising alternative to the conventional methods for pollutant removal because it opens green pathways for the complete mineralization of environmental pollutants in the presence of light (Li et al. 2017a).

Photocatalysis is extensively employed in various fields like water and air purification, self-cleaning surfaces, selective and green synthesis of organic compounds, hydrogen generation, etc. Heterogeneous photocatalysts (where photocatalyst and reactants are in different phases) involving nano semiconductors are extensively employed for the remediation of POPs attributed to low cost, non-toxicity, reusability and high stability. TiO_2, ZnO, graphitic carbon nitride (g-C_3N_4 or g-CN), Fe_2O_3, CdS, ZnS, WO_3, $SrTiO_3$, CdTe, MoS_2, ZrO_2, titanates, etc. are the commonly used semiconductors for these purposes (Bhethanabotla et al. 2017; Qin et al. 2017; Liu et al. 2014a, 2017a, b; Shi et al. 2012; Gupta et al. 2017; Shahrokhi 2016; Gao et al. 2013; Hanifehpour et al. 2016; Li et al. 2016a; Basahel et al. 2015).

In this chapter, we discuss some important nano-photocatalysts with a special emphasis on various strategies for improving their photocatalytic activity under visible light in order to exploit sunlight for the photocatalytic degradation of pollutants and also for energy production.

8.2 Mechanism of Semiconductor-Mediated Photocatalysis

Semiconductors are characterized by filled valance band and empty conduction bands. They can act as sensitizers of light-induced redox reactions due to their electronic structure (Hoffmann et al. 1995). Semiconductor photocatalysis is initiated by electron-hole pairs after bandgap excitation. When photocatalyst is irradiated with light whose energy is equal to or greater than bandgap energy of photocatalyst, the valence band electrons (e^-) can be excited to the conduction band, leaving a positive hole (h^+) in the valence band (Fig. 8.1). These excited charge carriers (e^- and h^+) can recombine, releasing the input energy as heat, with no chemical effect. If photoinduced charge carriers travel to the surface of photocatalyst without recombination, they can take part in various redox reactions with surface-absorbed species like oxygen, water and other organic and inorganic species. The valence band holes are powerful oxidants (+1.0 to +3.5 V vs NHE depending on the semiconductor and pH), while the conduction band electrons are good reductants (+0.5 to −1.5 V vs NHE) (Hoffmann et al. 1995). Most organic photodegradation reactions utilize the oxidizing power of the holes either directly or indirectly. These redox reactions are the basic mechanism of photocatalytic energy production, pollutant remediation, water purification, etc.

The bandgap energies and band edge positions of various semiconductors are listed in Fig. 8.2. Wide-bandgap semiconductors like ZnS (3.6 eV), $SrTiO_3$ (3.2 eV), TiO_2 (anatase phase- 3.2 eV; rutile phase-3.0 eV), ZnO (3.2 eV) and ZrO_2 (5.0 eV)

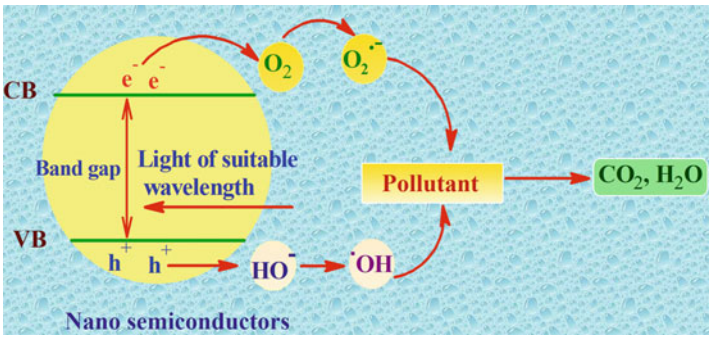

Fig. 8.1 Nano-semiconductor-mediated photocatalytic degradation of pollutants. The photodegradation reactions are caused by the redox reactions of valance band holes and conduction band electrons

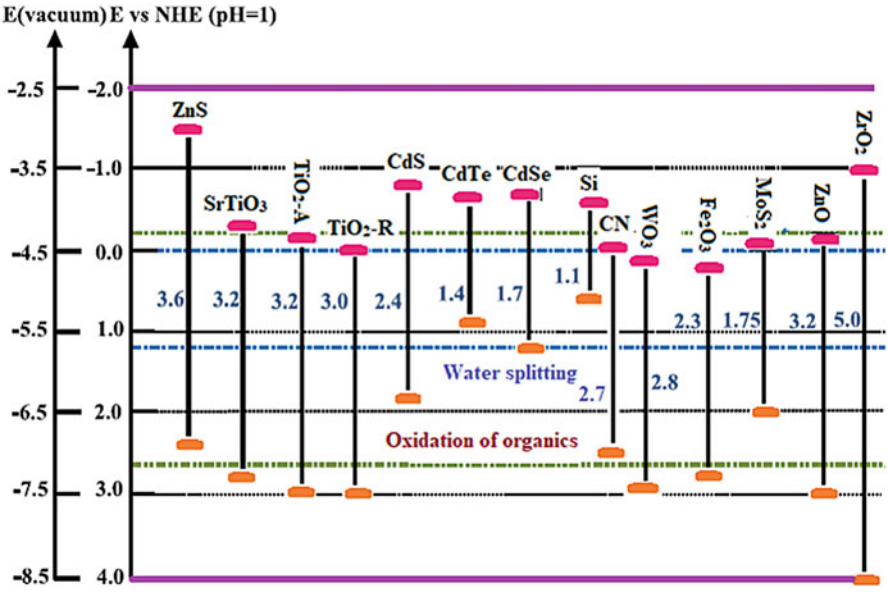

Fig. 8.2 Bandgap energies (eV) and band edge positions of different semiconductors. The wide-bandgap semiconductors uses UV light, and narrow-bandgap semiconductors uses visible light for photocatalysis. (Reprinted from Wu et al. 2015 with permission)

require high-energy UV light for their photocatalytic reactions. However, CdTe (1.4 eV), CdSe (1.7 eV), MoS_2 (1.75 eV), CdS (2.4 eV), Fe_2O_3 (2.3 eV), CN (2.7 eV) and WO_3 (2.8 eV) are narrow-bandgap semiconductors, and they utilize low-energy visible light for photocatalysis. Both wide- and narrow-bandgap semiconductors suffer from disadvantages like rapid recombination and low generation of photoinduced charge carriers. These factors make their photocatalytic efficiency very low. The requirement of harmful UV light for the photocatalytic reactions for

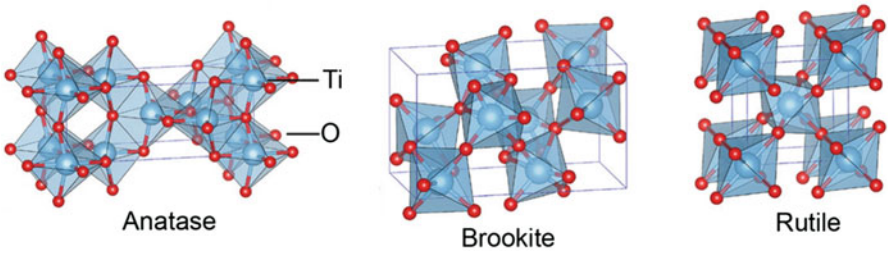

Fig. 8.3 Schematic representations of anatase, brookite and rutile phases of TiO_2. Rutile phase TiO_2 has more chemical stability and high refractive index over anatase phase, but anatase phase TiO_2 is a good photocatalyst (bandgap 3.2 eV). (Reprinted from Haggerty et al. 2017 with permission)

wide-bandgap semiconductors (i.e. low solar energy utilization efficiency) and ultrafast recombination of photoinduced charge carriers are the bottleneck of photocatalysts to satisfy the requirements of applications in a practical way. Use of UV light practically rules out the application of sunlight as an energy source in photocatalysis. Nowadays, research is intensively focused on creating visible/solar light active semiconductor photocatalysts attributed to the fact that sunlight consists of 45% visible light and only 3–5% UV light (rest is other type of electromagnetic radiations). Herein, we present an overview of current research activities that centre on nano-photocatalysts like TiO_2, ZnO and graphitic carbon nitride (g-C_3N_4 or CN).

8.2.1 Nano-TiO_2 as Photocatalysts

Among the different photocatalysts mentioned above, TiO_2 is a widely used photocatalyst for pollutant degradation and energy production as it is cheap, nontoxic and inert. TiO_2 exist mainly in three crystalline phases: anatase, brookite and rutile (Fig. 8.3). Anatase and brookite (kinetic products) will transform to the thermodynamically stable rutile upon calcination at a temperature beyond 600 °C (Hu et al. 2003). Rutile phase has more chemical stability and high refractive index over anatase phase, but despite these advantages, rutile TiO_2 has attracted fewer attention in producing photocatalysts attributed to the lower electrochemical performance than the anatase phase, primarily due to the difference in their electronic structure. Anatase phase TiO_2 is a good photocatalyst, but owing to the wide bandgap of 3.2 eV, it requires UV light for photocatalysis which inhibits its applications in visible light or solar light-mediated photocatalysis. The low photogenerated charge transfer rate is another downside of TiO_2 photocatalysts (Taheri et al. 2017). Reduction of bandgap by introducing energy levels between the conduction band and valence band, using various techniques, permits TiO_2 to be active under the solar light which will be discussed in the following session (Bingham and Daoud 2011).

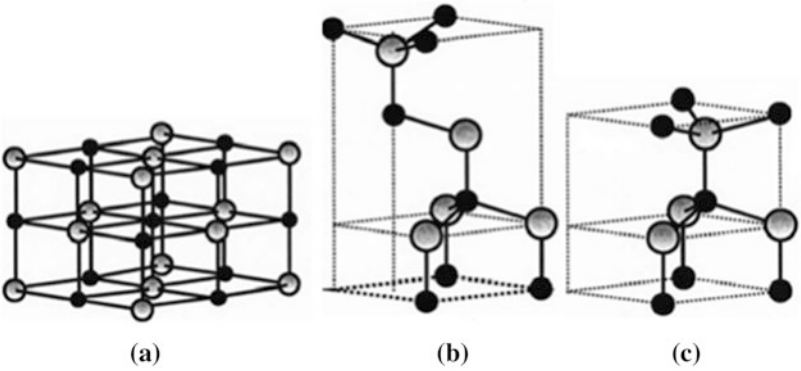

Fig. 8.4 (**a**) Cubic rock salt, (**b**) cubic zinc blende and (**c**) hexagonal wurtzite structure of ZnO crystal (Stick and ball representation). The shaded grey and black spheres denote zinc and oxygen atoms. (Reprinted from (Morkoç and Özg€ur n.d. with permission)

8.2.2 Nano-ZnO as Photocatalysts

ZnO, a wide-bandgap (3.2 eV) semiconductor, has also emerged as a promising candidate in green environmental management system because of its unique characteristics, such as direct bandgap in the near-UV spectral region, strong oxidation ability and good photocatalytic property (Lee et al. 2016; Tripathy et al. 2016). Moreover, it is relatively cheaper compared to TiO_2. As an important semiconductor material, ZnO has been applied in catalysis, paint industries, ceramic bodies, cosmetics, etc. ZnO received much attention in the degradation and complete mineralization of environmental pollutants (Muthulingam et al. 2015; Zyoud et al. 2016; Sun et al. 2016). Since ZnO has almost same bandgap energy as TiO_2, its photocatalytic capability is anticipated to be similar to that of TiO_2. The light absorption of ZnO also is limited in the visible light region due to the wideband energy. Major drawbacks of ZnO are the wide-bandgap energy, photocorrosion and fast recombination of charge carriers which result in the low photocatalytic efficiency (Sun et al. 2016).

ZnO crystallizes in three phases – thermodynamically stable wurtzite, the cubic zinc blende and rock salt (NaCl) structures (Fig. 8.4.). The cubic structures are rarely reported and the rock salt structure is obtained only at relatively high pressure; thus, wurtzite structure is predominant and stable [under ambient conditions, the thermodynamically stable phase is that of wurtzite symmetry]. Wurtzite ZnO belongs to the space group of $P6_{3mc}$ [lattice parameters $a = 0.3296$ and $c = 0.52065$ nm] and has a hexagonal close-packed lattice. Each Zn^{2+} sublattice contains four Zn^{2+} ions surrounded by four O^{2-} ions and vice versa, coordinated at the edges of a tetrahedron, stacked alternately along the *c*-axis (Jagadish and Pearton 2006; Morkoç and Özg€ur n.d.).

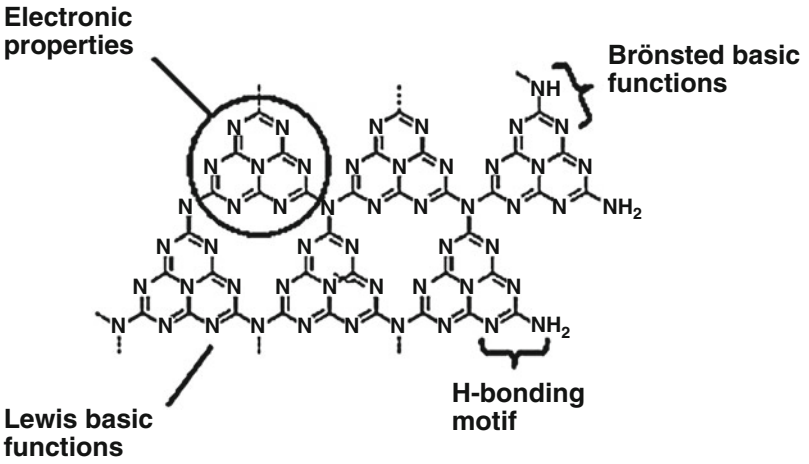

Fig. 8.5 Various functionalities of graphitic carbon nitride. (Reprinted from Thomas et al. 2008 with permission)

8.2.3 Graphitic Carbon Nitride as Photocatalysts

In the year 2009, graphitic carbon nitride (g-C_3N_4), the most stable allotrope among various carbon nitrides, was introduced into the field of heterogeneous catalysis. In the 1830s, Berzelius and Liebig invented "melon", the sprouting form of g-C_3N_4, which is a linear polymer consisting of interconnected tri-s-triazines via secondary nitrogen (Wang et al. 2012). g-C_3N_4 in the form of two-dimensional sheets consists of tri-s-triazines interconnected via tertiary amines (Fig. 8.5) (Zheng et al. 2012a; Thomas et al. 2008).

Graphitic carbon nitride, the metal-free semiconductor photocatalysts, attracted the attention of scientists attributed to their narrow bandgap and aromatic π-conjugated structure. Unlike TiO_2, which is active only under UV region, g-C_3N_4 possesses a bandgap of 2.7 eV (corresponding to visible light of 460 nm) and exhibits promising potential in solar photocatalysis. Hence, g-C_3N_4, an inexpensive and environmentally benign material, is developing as an ideal solar photocatalytic material to replace TiO_2-based materials. Nevertheless, the photocatalytic efficiency of the pristine g-C_3N_4 is still slow under sunlight irradiation because of the high recombination rate of photo-generated electron-hole pairs, low-specific surface area and low visible light utilization efficiency (Thomas et al. 2018). Scientists are now focused on creating novel g-C_3N_4 photocatalysts with enhanced physicochemical properties and high photocatalytic activities under sunlight.

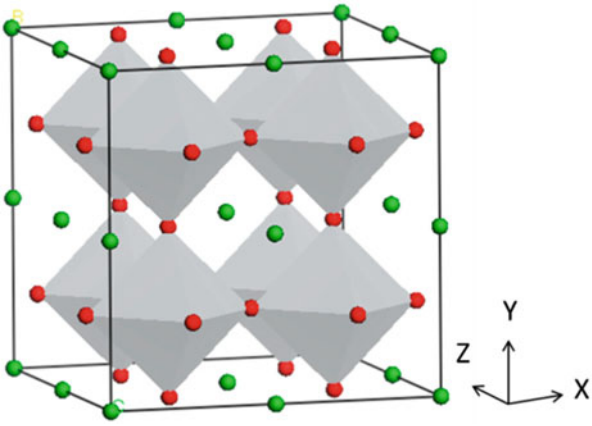

Fig. 8.6 Crystal structure of simple perovskite, $BaTiO_3$ (red, oxygen; green, A site cation; grey, BO_6 octahedra). (Reprinted from Kanhere and Chen 2014 with permission)

8.2.4 Titanates as Photocatalysts

Titanates are another group of widely used photocatalysts (Rutar et al. 2015). They have the general formula, $A_2Ti_nO_{2n+1}$, where A represents ions of metal like Ba, Ca, Sr, Mn, Fe, Co, Ni, etc. In titanates, metal ions occupy the interlayer space resulting in the mobile nature of metal ions. On treatment with acids, they get easily replaced by protons, resulting in the formation of hydrogen titanate. Hence metal titanate can also be used for the synthesis of TiO_2 with different morphologies (Rutar et al. 2015). Titanate perovskites are a class of titanates which have been widely studied for photocatalytic applications for a long time. Perovskites are the class of compounds with general formula ABO_3 in which A site is occupied by the larger cation, while the B site is occupied by the smaller cation. The perovskite crystal structure has corner connected BO_6 octahedra and 12 oxygen coordinated A cations, located in between the eight BO_6 octahedra (Fig. 8.6). $MTiO_3$ (M = Sr, Ba, Ca, Mn, Co, Fe, Pb, Cd, Ni) titanate systems shown excellent photocatalytic properties towards photooxidation reactions and pollutant degradation (Kanhere and Chen 2014).

8.2.5 Nano-metal Sulphides as Photocatalysts

Nanosized metal sulphides like CdS, ZnS and MoS_2 are widely employed for photocatalysis, manufacturing short wavelength light-emitting devices (LED), sensors, etc. CdS is a transition metal sulphide with a bandgap of 2.4 eV with high optical absorption coefficient (Kanhere and Chen 2014). ZnS with a direct bandgap of 3.68 eV makes it suitable for a number of optical applications. MoS_2 with a layered 2D structure similar to carbon nitride (Fig. 8.7) has gained a lot of interest in the area of catalysis and energy production attributed to the van der Waals forces existing between S-Mo-S sandwiches (Shahrokhi 2016; Li et al. 2016a).

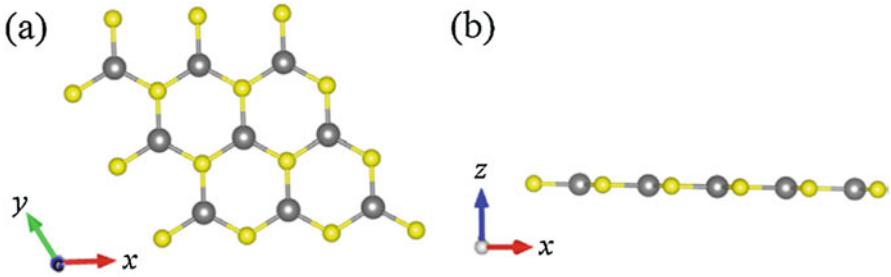

Fig. 8.7 Top (**a**) and side views (**b**) of the graphene-like 2D-ZnS. Big grey and small yellow balls in geometrical models represent zinc and sulphide atoms, respectively. (Reprinted from Shahrokhi 2016 with permission)

8.3 Strategies for Making Solar/Visible Light Active Photocatalysts

As mentioned above, the two major disadvantages in semiconductor-mediated photocatalysis are (i) the ultrafast recombination of photoinduced charge carriers like holes and electrons, which are generated in the valance band and conduction band of photocatalyst after light irradiation, and (ii) requirement of UV light for photocatalysis which accounts for only 3–5% of solar spectrum (Jesty et al. 2011). This charge recombination process results in the reduction of quantum efficiency resulting in the diminution of photocatalytic performance. Extension of the photocatalytically active region of the semiconductor to the visible region will result in widespread real-life applications (Jesty and Yoon 2012). Hence reduction of the recombination process and the improvement of visible light harvest for photocatalytic activity are essential in developing solar light active photocatalyst systems.

Different methods adopted for developing visible light active photocatalysts include metal/non-metal doping, the addition of photosensitive materials, incorporation of other nanoparticles, composite formation with other semiconductors and formation of heterojunctions and nanohybrids (Kumar et al. 2016; Shi et al. 2016; Yao et al. 2015; Moussawi and Patra 2016; Zhu et al. 2015, 2017; Sridharan et al. 2015; Sharma et al. 2016; Bai et al. 2015; Li et al. 2016b, c; Zalfani et al. 2016; Tobajas et al. 2017; Ghasemi et al. 2017) which are discussed below.

8.3.1 Metal/Non-metal Doping

Incorporation of nanoparticles of metals/non-metals is a well-received technique for efficient separation of photoinduced charge carriers and absorption of visible light in semiconductor photocatalysts. Metal-/non-metal-doped semiconductors are more efficient than undoped semiconductor resulting in the improved performance for

photocatalysis. Numerous defects and distortions are introduced into semiconductor system when a dopant is added which result in the changes of electronic properties. The diameters of heteroatoms of dopant must be equal to or smaller than semiconductor atoms (Liu et al. 2016a).

Nanoparticles show properties (both physical and chemical) different from their bulk materials. When nanoparticles of metals/non-metals are incorporated into the photocatalyst, it will exhibit altered properties attributed to the presence of nanoparticles. The strong absorption of visible light caused by the surface plasmon resonance (SPR) of metal nanoparticles has gained considerable attention. When metal nanoparticles are incorporated into the semiconductor, they act as electron trapping sites and diminish the recombination of charge carriers, resulting in the enhanced photocatalytic activity. They also exhibit resonant photon scattering, which in turn increases the interaction time with semiconductor and more electron-hole pairs are generated. Depending upon the nature of neighbouring material or size of metal nanoparticles, changes in photocatalytic performance are expected. Nanoparticles of Au, Ag, Pt, etc. (noble metals) have the ability to absorb visible light owing to localized surface plasmonic resonance. They can redshift the absorption edge of wide-bandgap semiconductors to the visible region when these nanoparticles are doped into semiconductors. For example, Au clusters (formed by the assembly of Au nanospheres and nanorods) doped TiO_2 showed enhanced photocatalytic performance towards the degradation of methylene blue (MB) dye and a hazardous fungicide, carbendazim. Au nanoclusters play dual roles: as a co-catalyst under ultraviolet radiation and as a light harvester in visible light. Compared to bare TiO_2, Au-TiO_2 exhibited enhanced performance attributed to the proficient photo-generated charge separation on the Au-TiO_2 surface served by Au nanostructures (Jesty and Yoon 2012; Thomas and Chitra 2014). Photocatalytic pollutant degradation mechanism by Au-TiO_2 nanoassemblies under UV light irradiation and visible light irradiation is schematized in Fig. 8.8.

Nano-Au-doped ZnO nanoparticles also showed enhanced photocatalytic activity. Glutathione-protected Au nanoparticles with different diameters (1.1, 1.6 and 2.8 nm) were doped into nano-ZnO. The assessment of the photocatalytic performance by monitoring the degradation of dyes like thionine and rhodamine 6G revealed that ZnO-Au nanocomposites showed an increase in photocatalytic activity with an increase in nanogold size (Lee et al. 2011).

Similarly improved photocatalytic activity under visible light was observed in Au nanoparticles (AuNPs) loaded on g-C_3N_4 nanosheets also. The photocatalyst was prepared by ultrasonication-assisted liquid exfoliation of bulk g-C_3N_4 and photoreduction of Au(III) under visible light irradiation. This system showed superior photocatalytic activity under visible light irradiation towards the decomposition of methyl orange compared to bulk g-C_3N_4/g-C_3N_4 nanosheets (Cheng et al. n.d.).

Analogous to nanogold, silver nanoparticles also have been used for improving the visible light activity of the photocatalysts (Jesty et al. 2011). Visible light active nano-Ag/TiO_2 nanocomposites were prepared (Cao et al. 2014) via the combination of a sol-gel process of a titanium ethoxide in inverse mini emulsions and in situ reductions of Ag ions in the $AgBF_4$/TiO_2 by hydrazine. The in situ reduction of Ag ions on the surface of $AgBF_4$/TiO_2 proved that Ag salt content does not influence the

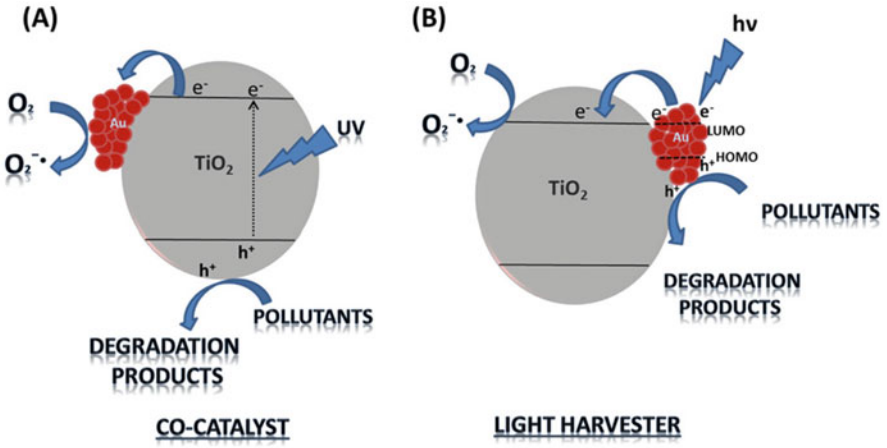

Fig. 8.8 Schematic representation of photocatalytic pollutant degradation mechanism by Au-TiO_2 nanoassemblies under (**a**) UV light irradiation and (**b**) visible light irradiation. (Reprinted from Sharma et al. 2016 with permission)

particle morphology and colloidal stability of the reaction systems. Visible light-induced photocatalytic degradation of rhodamine B (RhB) was studied with respect to different phases of TiO_2 (Ag/rutile or amorphous or anatase TiO_2) and various Ag contents. Nano-Ag/anatase TiO_2 showed enhanced degradation of RhB.

Using a combination of solvothermal technique with photoreduction method, a photocatalyst, Ag-AgBr/TiO_2 heterostructured nanofibres were fabricated on electrospun TiO_2 nanofibres (Sui et al. 2015). Ag-AgBr/TiO_2 heterostructured nanofibres shown enhanced photocatalytic activity towards the degradation of methylene blue dye, attributed to the surface plasmon resonance effect of Ag nanoparticles and the synergetic effect between Ag, AgBr and TiO_2.

It was observed that Ag-doped graphitic carbon nitride films (Ag/g-C_3N_4) synthesized on ITO substrates by a liquid-based reaction process exhibited high photoelectrocatalytic activity for the degradation of methylene blue. Enhancement of photoelectrocatalysis was due to the more visible light harvesting and also due to the easy electron transfer between photo-generated electron and interfacial electron in Ag/g-C_3N_4 film (Qi 2016). Visible light-induced photocatalytic properties of a composite system consisting of silver quantum clusters [$Ag_9(H_2MSA)_7$] (H_2MSA= mercaptosuccinic acid) embedded on graphitic carbon nitride nanosheets (AgQCs-CN) showed extended visible light absorption through multiple single-electron transitions in Ag quantum clusters and an effective electronic structure for hydroxyl radical generation, which enabled increased activity in the photocatalytic degradation of methylene blue and methyl orange dye molecules compared with pristine graphitic carbon nitride (CN) and silver nanoparticle grafted CN (AgNPs-CN). The rate of hydrogen generated using AgQCs-CN was slightly less than that of AgNPs-CN because of surface hydroxyl radical formation (Sridharan et al. 2015).

Effect of different transition metals on the photocatalytic activity of TiO_2 was studied. For this, a series of metal-doped TiO_2 [M/TiO_2 (M = Cu, Ni, Co, Fe, Mn,

Cr)] photocatalysts were prepared via modified precipitation method using corresponding metal nitrates and titanium (IV) butoxide (Kuyumcu et al. 2015). These different metal-doped TiO_2 photocatalysts were used to access the degradation of commercial dyes like methyl orange (MO, azo dye) and methylene blue (MB, thiazine dye group) under visible light. Among the different metals doped TiO_2, Cu/TiO_2 sample exhibited the highest photocatalytic activity under visible light attributed to the low bandgap energy and delayed electron-hole recombination. Cu was found to be a good dopant for CN also. Cu-doped mesoporous graphitic carbon nitride ($Cu/mpg\text{-}C_3N_4$) photocatalysts were prepared using cupric chloride and melamine as precursors. The photocatalytic degradation rate of MO reached 90.2% in 120 min onto Cu^{2+}-doped $mpg\text{-}C_3N_4$. The rate constant for Cu^{2+}−doped $mpg\text{-}C_3N_4$ was two times as high as that of pure $g\text{-}C_3N_4$ due to an increase in the electron/hole separation rate (Le et al. 2016).

Co, Cu and Ni cations were used for ZnO doping and stabilized in aqueous colloidal solutions using different surface capping agents. High PL emission, smallest particle size and most stable colloid were obtained for Co-ZnO showing that Co is the best dopant among three metals. Another photocatalyst, Sn loaded Au-ZnO, was prepared by precipitation-decomposition method (Senthilraja et al. 2016). Sn-Au-ZnO at optimum pH of 11 and catalyst loading of 2 g/L is found to be more efficient than bare ZnO and other commercial catalysts for the mineralization of AR 18 dye under UV-A light (Fig. 8.9). The photocatalytic degradation of

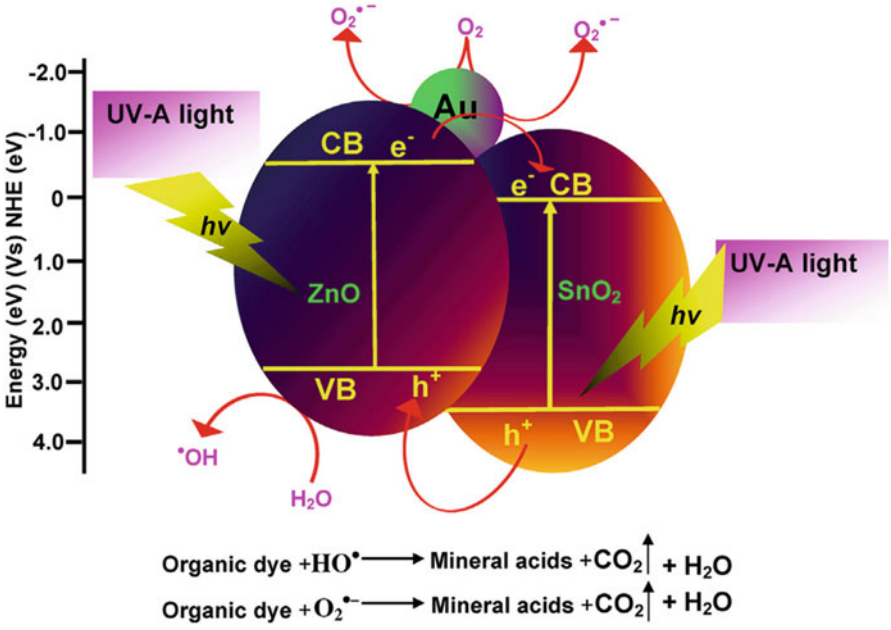

Fig. 8.9 The mechanism for degradation of AR 18 by Sn-Au-ZnO under UV-A light. Catalyst loading of 2 g/L is found to be more efficient than bare ZnO and other commercial catalysts for the mineralization of AR 18 dye. (Reprinted from Senthilraja et al. 2016 with permission)

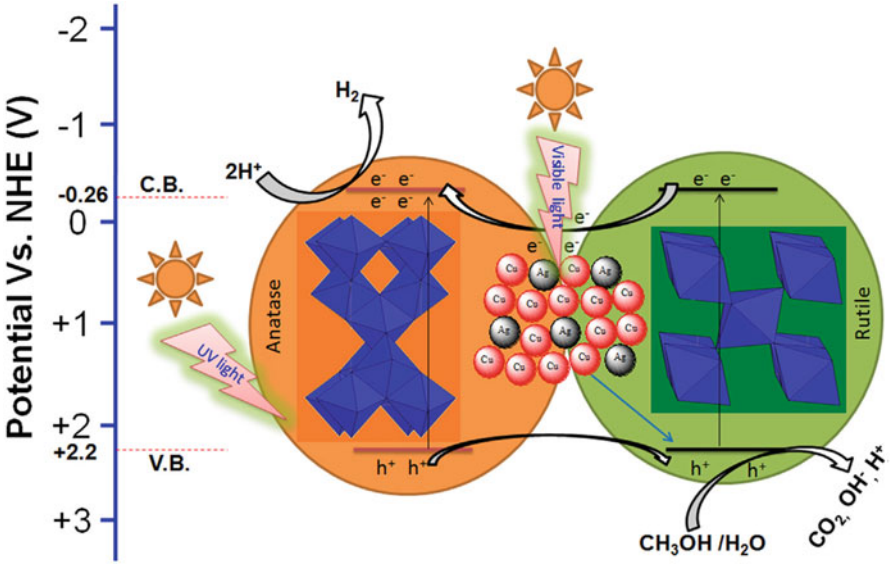

Fig. 8.10 Schematic representation of electron transfer mechanism by surface plasmon resonance in Ag-Cu/TiO_2 and is followed by consecutive electron transfer from Ag-Cu to the valence band of $TiO_2$for H_2 production under solar light irradiation. (Reprinted from Kumar et al. 2016 with permission)

Naphthol Blue Black (NBB) dye in aqueous solution under solar light irradiation was achieved using Ce co-doped Ag-ZnO (Ce-Ag-ZnO) prepared via solvothermal method (Subash et al. 2012). Co-doping of Ce and Ag resulted in the red-shifted absorption edge of ZnO and inhibition of photo-generated charge recombination.

It was found that doping of two or more metals into semiconductors yields enhanced photocatalytic performance; however, their photocatalytic mechanism will be different. Kumar et al. reported a bimetallic-TiO_2 photocatalyst using Cu and Ag metals (Kumar et al. 2016). The bimetallic system shifted the optical response of the TiO_2-based catalyst from UV to the visible region with a shift of bandgap from 3.22 to 2.82 eV. Improved electron-hole separation was also observed as Ag, Cu and/or Ag-Cu metal sites act as electron traps and functioned as co-catalysts. The promotional effect of Ag-Cu particles is induced by plasmon activation under visible light and is followed by consecutive electron transfer from Ag-Cu to the valence band of TiO_2 (Fig. 8.10). The SPR induced local electric field of activated Ag-Cu particles to drive their electrons to combine with the holes on the valance band of TiO_2. Ag-Cu/TiO_2 catalyst was used to study H_2 production (5683 μmoles $g^{-1}h^{-1}$) from H_2O splitting, and the enhanced H_2 production was attributed to additional active sites created by synergetic effect between Ag and Cu nanoparticles.

Rare earth metal oxides are an excellent choice for metal doping attributed to the good thermal stability provided by their 4f multielectron configuration. Lanthanide ions act as electron scavenger and prevent the electron-hole recombination by reaction with superoxide ions which improves the photocatalytic efficiency. The

augmentation in photoluminescence of ZnO co-doped with Li^+ and trivalent rare earth metal ions (RE^{3+}) was studied (Bachir et al. 1997). A series of rare earth metal (La, Ce, Pr, Nd, Sm, Eu, Dy, Gd)-doped TiO_2 were prepared via an ecologically friendly single-step, one-pot, no post-calcination synthesis route for the production of low-cost photocatalytic pigments (Stengl et al. 2009). Among the different rare earth dopants, Nd^{3+} doped TiO_2 showed enhanced performance towards the degradation of orange II dye aqueous solution. Polymer pyrolysis method was employed to synthesize Ln (La^{3+}, Nd^{3+} or Sm^{3+})-doped ZnO nanoparticles (Khatamian et al. 2012) and was used to study the photocatalytic degradation of 4-nitrophenol. The photocatalytic performance of ZnO was enhanced by Ln doping, and 4 wt% Nd-doped ZnO was the most active sample showing high photocatalytic activity for the degradation of 4-nitrophenol. He et al. reported Gd-La co-doped TiO_2 microspheres showing excellent photocatalytic activity towards the degradation of methyl orange dye (Lin et al. 2013). Abundant oxygen vacancies and surface defects for electron trapping and dye adsorption enhanced the performance of Gd-La co-doped TiO_2.

Eu^{3+}-doped graphitic carbon nitride photocatalyst (0.38 wt.% Eu^{3+}) also showed enhanced activity, and near-complete degradation of methylene blue was observed. Eu^{3+} ions act as an electron acceptor and diminish the photoinduced charge recombination ensuing the improved photocatalytic performance. Sm^{3+-}doped g-C_3N_4 nanosheets also showed efficient solar photocatalytic activity due to the decreases in the bandgap and increases in visible light absorption. Here hydroxyl radicals and holes play a significant role in the degradation of dye effluent and salicylaldehyde. Optimization of weight percentage of Sm^{3+} revealed that the degradation of the photocatalytic activities of different samples under sunlight is in the order CN-0.02 wt% Sm^{3+} > CN-0.03 wt% Sm^{3+} > CN-0.05 wt% Sm^{3+} > CN-0.01 wt% Sm^{3+} > g-C_3N_4 (Rutar et al. 2015). It has been found that addition of "Ce" to graphitic carbon nitride also enhanced visible light activity due to the crystal growth inhibition, bandgap reduction and efficient separation of charge carriers (Jin et al. 2015).

Molten metal salts are unique and novel high-temperature ionic liquids that can be used for the development of visible light active photocatalysts. A heterojunction-type g-C_3N_4-based photocatalysts were synthesized using molten salt KCl/LiCl mixtures and melamine in microwave irradiation medium (Liu et al. 2017b). Modified g-C_3N_4 heterojunction showed a visible light-driven photocatalytic hydrogen evolution rate of 1480 μmol $g^{-1}h^{-1}$ and has an apparent quantum yield of 10.7%. This heterojunction provides novel electronic band structures for efficient separation of photoinduced charge carriers, resulting in a large enhancement of hydrogen evolution. Here the synergistic effects of microwave heating and molten salt liquid polycondensation are well employed.

Instead of metals, non-metals are also used for doping in photocatalysts. Atomic orbitals of non-metals have potential energy greater than that of O2p orbital of TiO_2, ZnO, etc.; hence, non-metal doping has attracted much attraction in making visible light active photocatalysts. Non-metals like B, C, O, Si, P, S, halogens, etc. are commonly used for doping in TiO_2, ZnO and graphitic carbon nitride (Shen et al.

2016a; Yu et al. 2016, 2017; Sagara et al. 2016; Zhang et al. 2013; Wang et al. 2017; Suryawanshi et al. 2012; Bu and Chen 2014; Liu et al. 2016b; Qiu et al. 2017; Su et al. 2008; Kwon et al. 2017; Chen et al. 2017; Ansari et al. n.d.; Chaudhuri and Paria 2014; Fan et al. 2017; Samsudin et al. 2016; Carroll et al. 2017; Cai et al. 2016; Han et al. 2015; Bakar and Ribeiro 2016). Previous studies demonstrated that g-C_3N_4 materials showed improved light-harvesting and pronounced changes in the energy band structure when doped with heteroatoms such as sulphur, iodine, boron, phosphorus, oxygen halogens, etc. These dopants may trap electrons and reduce the chances of electron-hole recombination that deactivates the photocatalytic system.

For example, photocatalytic degradation of methylene blue dye was studied by visible light active S-doped TiO_2 nanorods which were synthesized using oxidant peroxide method (Bakar and Ribeiro 2016). Mechanism of MB photocatalytic degradation over S-doped TiO_2 nanorods is outlined in Fig. 8.11. S-doping decreased the crystal size of TiO_2 attributed to the substitution of Ti^{4+} by S^{6+} in the S-doped sample as S^{6+} (0.29 A) has smaller atomic radius compared to Ti^{4+} (0.64 A). S-doping increased the number of adsorbed active groups at the catalyst surface, and the formation of Ti-O-S bond favours the partial transfer of electrons from S to O atoms which helped the electron-deficient S atoms to hold/capture electrons, reducing the electron-hole recombination.

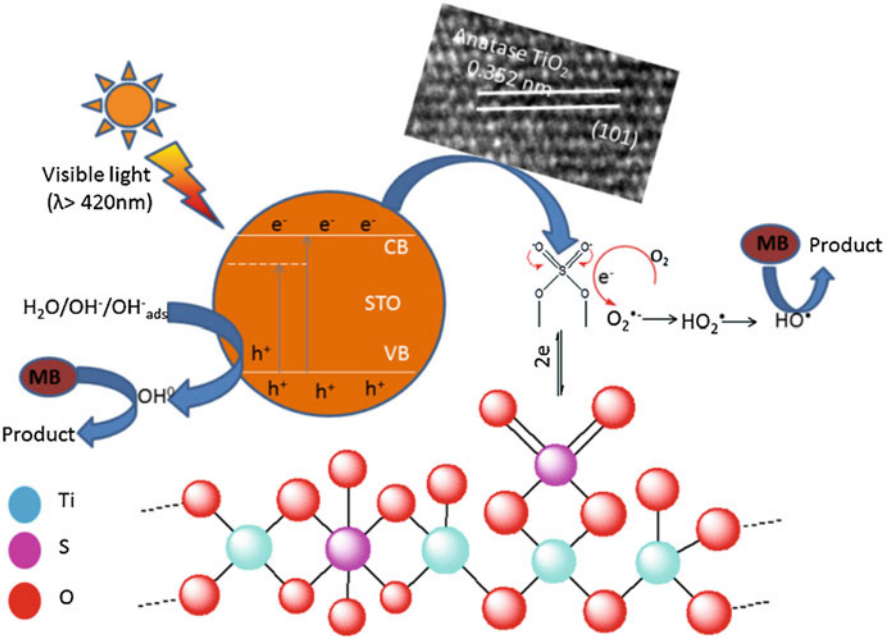

Fig. 8.11 Schematic representation of MB photocatalytic degradation over S-doped TiO_2 nanorods. The transfer of electrons from S to O atoms helped the electron-deficient S atoms to hold/capture electrons thus reducing the electron-hole recombination. (Reprinted from Bakar and Ribeiro 2016 with permission)

S-doped g-C_3N_4 also showed enhanced photocatalytic activity. Nanoporous sulphur-doped g-C_3N_4 microrods were prepared by direct thermal condensation of a melamine-trithiocyanuric acid supramolecular cocrystal. It acts as a highly active photocatalyst for H_2 evolution under visible light irradiation (Feng et al. 2014). Mesoporous sulphur-doped graphitic carbon nitride (MCNS) was synthesized using thiourea and SiO_2 gel solution as a template through a simple thermal condensation method. Among bulk graphitic carbon nitride (g-C_3N_4), undoped g-C_3N_4, sulphur-doped g-C_3N_4 without template and TiO_2 (Degussa P25) samples, the optimized MCNS-4 (sample synthesized at the reaction temperature of 500 °C for 240 min with the SiO_2/thiourea weight ratio of 0.3) illustrated the highest photocatalytic activity towards the removal of MO under visible light irradiation. The enhanced performance was originated from the synergistic effects of high surface area, mesoporous texture, sulphur doping and high visible light absorption, which were helpful for the separation and transportation of the photo-generated electron-hole pairs (Jourshabani et al. 2017). S and O co-doped g-C_3N_4 nanosheets with mesoporous structures synthesized by the polymerization of melamine and H_2O_2-bonded trithiocyanuric acid (TCA) also gave an enhanced photocatalytic performance for RhB degradation. The S-O co-doped g-C_3N_4 gave sixfold increase in the activity, by enhancing visible light adsorption and decreasing its bandgap compared to pristine g-C_3N_4 nanosheets (You et al. 2017).

It was demonstrated that the incorporation of carbon-based materials into semiconductors results in the enhanced photocatalytic performance. Carbon is a good electron acceptor and absorbs over a wide range of visible light. Nanosized carbon materials have higher porosity and various morphologies based on synthesis routes. A series of carbon xerogels-TiO_2 samples were prepared using sol-gel synthesis (García et al. 2017). These samples have homogeneous and three-dimensional mesoporous structure, and the interesting feature is that, even though synthesis route involves the calcination of carbon xerogels-TiO_2 at 900 °C, anatase phase of TiO_2 was stable owing to the good dispersion of TiO_2 in the carbon matrix. During sintering, carbon matrix favoured titania reduction, keeping anatase phase stable. Also, carbon favours electron transfer from TiO_2 nanoparticles, reducing the charge recombination, leading to higher photocatalytic activity. Carbon-doped ZnO at different temperatures was synthesized using commercially available melamine and zinc nitrate hexahydrate as the starting materials. The photocatalytic performance of the as-prepared photocatalyst towards the degradation of a model pollutant, rhodamine B, under visible light irradiation showed that C-doped ZnO exhibited a significantly higher degradation response than bare ZnO due to the narrowing of the bandgap and improved electron/hole separation efficiency (Ansari et al. 2017).

8.3.2 Addition of Photosensitive Materials

Introduction of sensitizers is another popular method because sensitizers can directly absorb visible light and get excited. The excited sensitizers can release electrons to

the conduction band of semiconductors, thus improving the photocatalytic efficiency (Ansari et al. 2017). Photosensitive materials like porphyrins, phthalocyanines, fluorescein, organic dyes, etc. are widely used for enhancing the photocatalytic performance of semiconductors (Radhika and Thomas 2017; Thomasa et al. 2017).

Semiconductivity and visible light photosensitivity of porphyrins/metalloporphyrins make them an important group of photosensitizers. They can boost the separating efficiency of the photoinduced charge carriers by their electron transportability. Their molecules are arranged regularly through the π-π stacking, with which they can form heterojunction structure with semiconductors. Porphyrin compounds (H- or J-type) have good chromophore activities over the solar spectrum and good electron donating properties due to their large π-electron systems. When incorporated into semiconductors, porphyrin aggregates act as light-harvesting assemblies to gather and transfer energy to the assembled devices, resulting in the higher incident photon-to-photocurrent generation efficiency (Li et al. 2010). This was illustrated by the photocatalytic degradation employing copper(II)porphyrin-sensitized TiO_2/ZnO photocatalyst (Li et al. 2010; Yu et al. 2015). Cu (II) porphyrins absorb visible light and act as a small-bandgap semiconductor. When incorporated in TiO_2, it effectively separates the charge carriers and enhances the photocatalytic activity. A porphyrin heteroaggregate ((ZnO/TAPPI-CoTPPS), where TAPPI = tetrakis (4-trimethylaminophenyl) porphyrin and CoTPPS = tetrakis (4-sulfonatophenyl) porphyrin cobalt(II)), has been anchored on the surface of ZnO which forms a strong interaction with the semiconductor. The excited porphyrin heteroaggregate (Por*) injects its excited electrons to the conduction band of ZnO, thus enhancing the photocatalytic performance (Li et al. 2010).

Curcumin, another photosensitive molecule, also was selected as an aspirant to improve the visible light activity of semiconductor photocatalysts. Curcumin-conjugated ZnO nanostructures synthesized by a simple impregnation method showed enhanced photocatalytic performance with a bandgap of 1.2 eV. The enhanced photocatalytic degradation by curcumin-conjugated nano-ZnO compared to bare ZnO was observed depending on the extent of curcumin conjugation. This work has shed some insight into the large-scale utilization of heterogeneous cost-effective photocatalysis via visible light to tackle water contamination and environmental pollution.

Dyes extracted from plants also have been used to sensitize semiconductors. Curcumin (from turmeric), beta-carotene (from root vegetables like carrot, beetroot, etc.), lawsone (from henna leaves), etc. are some useful compounds for this purpose. Ahed Zyoud et al. reported curcumin-sensitized anatase TiO_2 nanoparticles for the photodegradation of organic pollutant (phenazopyridine) under visible light. Curcumin-sensitized anatase TiO_2 was able to completely degrade the pollutant and is a promising alternative for hazardous sensitizing dyes (Zyoud and Hilal 2014).

Phthalocyanines are a group of chromophores having characteristic absorption bands in both UV/blue (Soret band) and the red/near-IR spectral regions (Q band, 650−800 nm). They have excellent photochemical/thermal stability and redox potential, which makes them an attractive candidate for the dye sensitization of

wide-bandgap semiconductors. Zinc phthalocyanine-sensitized polymeric graphitic carbon nitride (Zn-tri-PcNc/g-C_3N_4) photocatalyst was synthesized by impregnation method (Zhang et al. 2014). Zinc phthalocyanine extended spectral response region of g-C_3N_4 from 450 nm to >800 nm. Addition of chenodeoxycholic acid as co-adsorbent to Zn-tri-PcNc/g-C_3N_4 significantly improved photoactivity for H_2 production (125.2 μmol h^{-1}) attributed to the enhancement in electron injection efficiency and impediment of the charge recombination. Photocatalytic degradation of plasticizer dimethyl phthalate (DMP) under xenon-lamp irradiation was achieved by magnetic hybrid photocatalysts formed by layer by layer deposition of Fe_2O_3, SiO_2, TiO_2 and copper phthalocyanine (CuPc) (Chang and Man 2014). The presence of CuPc enhanced the effective inhibition of exciton annihilation and promotion of electron injection into the semiconductors.

Polyoxometalates (POMs) are complex transition metal-oxygen clusters having excellent photoelectrochemical activities which can act as electron pools attributed to their distinctive structures (Sivakumar et al. 2012). These POMs can be incorporated with semiconductors for enhanced photocatalytic performance due to the efficient photo-generated charge separation facilitated by transfer of photo-generated electrons to the d-orbital of POMs, during photocatalysis. Among the different POMs, heteropoly phosphotungstic acid (HPA or HPW, $H_3PW_{12}O_{40}$) is widely used for POM/semiconductor nanocomposites. Visible light active $H_3PW_{12}O_{40}$/TiO_2 (PW_{12}/TiO_2) nano-photocatalyst was synthesized through a modified sol-gel hydrothermal method and the degradation of fuchsin acid, malachite green and p-nitrophenol under simulated sunlight (320 nm< λ <780 nm) irradiation gave first-order rate constants(Zhao et al. 2013). High photocatalytic degradation efficiency was ascribed to the synergistic effect of $H_3PW_{12}O_{40}$ and TiO_2, which resulted in enhanced quantum efficiency and high light-harvesting efficiency. A one-step hydrothermal method was employed for synthesizing PMo_{12}@g-C_3N_4 and PW_{12}@g-C_3N_4 (He et al. 2015). Under UV-vis light irradiations, PMo_{12}@g-C_3N_4-6% showed better photocatalytic performance towards the degradation of methylene blue (MB) and phenol, attributed to the higher surface area and pore volume (He et al. 2015). Phosphotungstic acid ($H_3PW_{12}O_{40}$, HPW) immobilized on mesoporous graphitic carbon nitride (mpg-C_3N_4) contributed a good photocatalyst with high catalytic activity for the oxidative desulfurization process of dibenzothiophene (Zhu et al. 2015). After 15 recycles, catalyst retained its activity towards oxidative desulfurization process, and the Keggin structure of HPW active species was kept after being immobilized on the mpg-C_3N_4 surface.

Organic dye nanoparticles such as perylene nanoparticles (PeNPs) exhibit distinctive optoelectronic properties superior to their bulk counterparts, and they are expected to have higher photosensitization of semiconductors. Stable PeNPs synthesized from perylene-3,4,9,10-tetracarboxylic dianhydride using D-glucosamine hydrochloride are incorporated into g-C_3N_4. The resulting g-C_3N_4-based nanocomposites show greatly enhanced photocatalytic activity under illumination of simulated solar light as compared to those of free g-C_3N_4 and TiO_2 (Degussa P25). When PeNPs – the g-C_3N_4 system (PeNPs-CN) – was irradiated by sunlight, electrons are excited from valance band to conduction band of g-C_3N_4 and generate

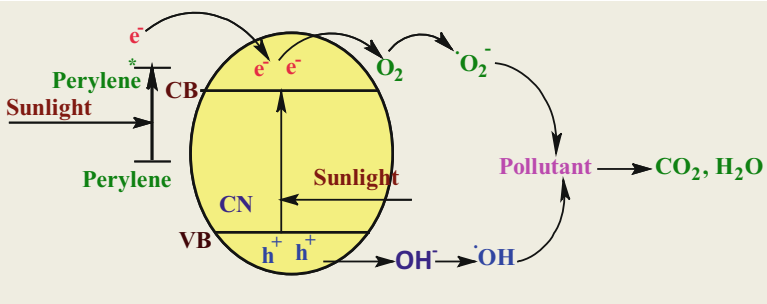

Fig. 8.12 Mechanism of pollutant degradation using PeNPs-CN under sunlight. The photo-generated holes (h+), $^{\cdot}O_2^-$ and $OH^{\cdot}$ radicals formed are mainly responsible for the degradation of pollutants in this system. (Reprinted from Thomasa et al. 2017 with permission)

photoexcited electrons and holes. Perylene nanoparticles get excited (perylene*) under solar light irradiation and rapid e− transfer occur between excited perylene (Perylene*) and g-C_3N_4. The adsorbed perylene* nanoparticles can inject its e− into the conduction band of g-C_3N_4. The photo-generated holes (h+), $^{\cdot}O_2^-$ and $OH^{\cdot}$ radicals formed are mainly responsible for the degradation of pollutants through its successive attacks via the formation of several intermediate products. The mechanism is outlined in Fig. 8.12. (Thomasa et al. 2017).

TiO_2 co-sensitized with copper phthalocyanine (CuPc) and perylene diimide (TiO_2/PTCDI)-CuPc) prepared by hydrothermal method showed higher photocatalytic activity (Zhao et al. n.d.). N,N′-di(octadecyl)perylene-3,4,9,10-tetracarboxylic bisimide (DPBI) is highly fluorescent and exhibited strong absorption and emission in the visible spectral region. Loading of DPBI in TiO2 results in increased absorbance from 400 to 650 nm, and DPBI-loaded TiO_2 showed higher efficiency in Reactive Orange 4 degradation than pure TiO_2 in UV and solar light (Senthilrajaa et al. 2014).

Xanthene dyes are also good sensitizers and tend to be fluorescent, yellow to pink to bluish red depending upon the functional groups on the xanthene moiety (McNaught and Wilkinson 1997). Large absorption, luminescence, excellent light resistance, low toxicity and relatively high solubility in water are the characteristic features of xanthene dyes which makes them excellent choices for optical materials and dye-sensitized solar cells. Fluorescein treatment enhanced the photovoltaic efficiency and inhibited fluorescence quenching in reactant solution. Xanthene dyes like fluorescein, dibromofluorescein, eosin Y and erythrosine B were used to sensitize carbon nitride (Zhang et al. 2015). Picosecond time-resolved fluorescence measurements were employed to derive the electron transfer rate from the LUMO of each photoexcited xanthene dye to the conduction band of carbon nitride. Similar results were obtained from cyclic voltammetry measurements. These results suggest that electron present in LUMO level of these xanthene dyes can inject its electron to the conduction band of C_3N_4 in case of dye-sensitized C_3N_4 composites. On EY sensitization, g-C_3N_4 prepared at 600 °C from urea exhibited the highest

sensitization activity and produced 18.8% hydrogen evolution under optimum conditions (Xu et al. 2013). Factors like pure composition, the higher dye adsorption amount and the lowest defect concentration of the above-mentioned g-C_3N_4 resulted in its highest activity.

8.3.3 Construction of Heterojunctions/Composites

Construction of heterojunction is an effective method for improving the photocatalytic activity of a photocatalyst if the energy band of hetero material is well matched with that of the semiconductor. Heterojunctions can be formed between semiconductors of different bandgap energies. In heterojunctions, photo-generated electrons and holes move into opposite directions by the electric field created in situ, thus overcoming the charge transfer barrier. Cu_2O-TiO_2 nanocomposites were synthesized using a wet impregnation method with TiO_2 nanorods and $CuSO_4$ and showed enhanced hydrogen production (50,339 $mmolh^{-1}g^{-1}$ cat) from biomass-derived glycerol under solar irradiation. TiO_2 nanorods with nanocavities provide a suitable environment for reactions (Kumar et al. 2015). Cu_2O incorporation increased the absorption of UV-visible light from the natural solar spectrum, inhibited the recombination of electron-hole pairs, while TiO_2 nanorods with nanocavities provide multiple internal reflections of light within nanocavities, which improved the surface-interface reactions. Mechanism of photocatalysis of the catalysts is given in Fig. 8.13. Mixed oxide dye-sensitized solar cells (DSSCs) based on CuO-ZnO nanocomposite films as working electrodes with and without titania blocking layer (TBL) were investigated (Habibi et al. 2013)

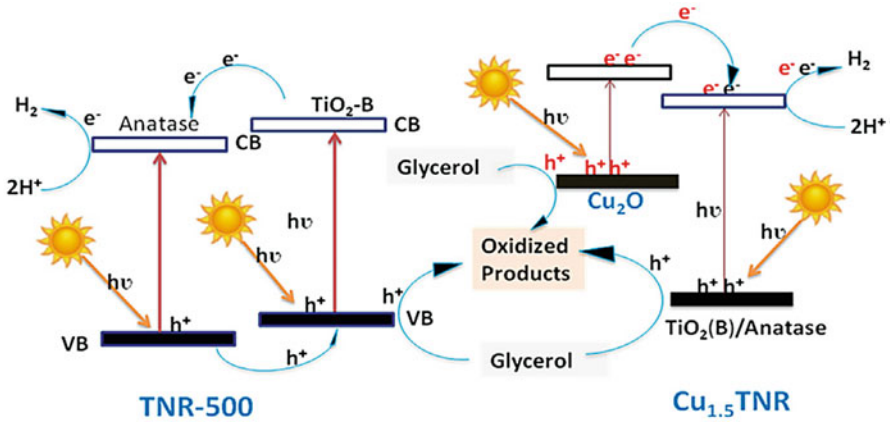

Fig. 8.13 Proposed reaction mechanism of Cu_2O-TiO_2 nanocomposites for photocatalytic H_2 production with aqueous glycerol-water mixture under solar irradiation. (Reprinted from Kumar et al. 2015 with permission)

and found that charge recombination in the working electrode was slow when titania blocking layer was present in DSSC.

Visible light-induced dendritic $BiVO_4/TiO_2$ photocatalysts synthesized using hydrothermal and sol-gel method gave a good result for the photocatalytic degradation of methylene blue (MB) under visible light irradiation. The photocatalyst with a ratio of $BiVO_4/TiO_2$ (mass ratio) equal to 60% prepared at 400 °C exhibited the best photocatalytic activity. In this system $BiVO_4$ acts as a photocatalyst, which can be excited under visible light irradiation, with the generation of holes and electrons. The degradation processes in $BiVO_4/TiO_2$ mainly depended on the synergistic effect of photocatalysis and photosensitization (Li et al. 2016d).

Conjugated polymers are another group of organic semiconductors having wide applications in energy production and pollutant degradation. Based on varying or modifying polymeric monomer, their semiconducting property and light absorption ability can be easily tuned. Poly(benzothiadiazole)-TiO_2-based composite (BBT/TiO_2) is conveniently fabricated through an in situ polycondensation procedure of 4,7-dibromo benzo [1,2,5]thiadiazole and 1,3,5-triethynylbenzene in presence of TiO_2 (Degussa P25) (Hou et al. 2017). BBT/TiO_2 exhibited enhanced visible light photocatalytic activities towards H_2 evolution and ciprofloxacin degradation compared to BBT alone. The enhancement of photocatalytic performance is ascribed to the formation of heterojunction and reduction of the rate of photoinduced charge carriers.

Pure Ag_3PO_4 is a narrow-bandgap (2.33 eV) photocatalyst with inadequate long-term stability due to decomposition in the absence of a sacrificial agent. But when it is incorporated with TiO_2, a highly visible light-responsive Ag_3PO_4/TiO_2 photocatalyst was formed with a molar ratio 75:25(Taheri et al. 2017). Ag_3PO_4/TiO_2 completely degraded bisphenol A pollutant within 4 min of solar irradiation. The synergetic effect between Ag_3PO_4 and TiO_2 which helps in the interfacial charge transfer and suppression of electron-hole recombination resulted in the superior photocatalytic performance of Ag_3PO_4/TiO_2. The visible light-responsive Ag_3PO_4@g-C_3N_4 core shell composites were also synthesized using ultrasonication/chemisorption method (Li et al. 2016b). Photocatalytic degradation of methylene blue (MB) and bisphenol A (BPA) in the presence of these composites showed that Ag_3PO_4@g-C_3N_4 (7.0 wt.%) was able to degrade MB and BPA after visible light irradiation within 30 min. The photocurrent and EIS measurements confirmed the efficient photo-generated charge separation originated from a strong interaction in the intimately contacted interface (Li et al. 2016b).

Graphene having carbon atoms arranged in a honeycomb structure is an excellent electrical conductor. Graphene oxide (GO) with introduced hydroxyl and carboxyl groups also possesses similar properties of graphene. The presence of special surface functional groups makes GO as a good choice for supporting metal or metal oxide particles. High electron mobility and flexible sheet nature of reduced graphene oxide (rGO) make it as a good candidate for photocatalytic applications. They act both as electron-acceptor and as electron-transport material facilitating the migration of photoinduced charge carriers and hinder the charge recombination to enhance the photocatalytic performance during the photocatalysis experiments. Reduced

graphene oxide (rGO) incorporated with semiconductor nanoparticles also showed improved photocatalytic performance (Li et al. 2017b). ZnO microspheres-rGO nanocomposites synthesized via a simple solution method were performed as efficient photocatalysts in comparison with ZnO microspheres and TiO_2 because rGO sheets could reduce the photoinduced charge recombination processes (Li et al. 2017b).

Large Ag cores decorated with small clusters of CuO nanoparticles on the surface of TiO_2 (DegussaP25) (Ag@CuO/TiO_2 nanocomposite), synthesized via radiolytic reduction technique, showed enhanced activity towards phenol degradation and acetic acid oxidation under visible light. Introduction of nanoparticles of CuO decreases the bandgap, and Ag introduces localized surface plasmon resonance which improved the photocatalytic activity of TiO_2 (Medrano et al. 2016). In_2O_3 and WO_3 are well-known semiconductors having bandgaps of 2.8 and 2.7 eV, respectively, with excellent conductivity and stability in aqueous systems. Modified photoelectrodes based on TiO_2/In_2O_3 and TiO_2/WO_3 gave enhanced hydrogen production under visible light conditions. Hydrogen production rates of 11.8 and 13.8 $lh^{-1}m^{-2}$were obtained using TiO_2/In_2O_3 and TiO_2/WO_3, respectively, by these photoelectrodes (Upadhyay et al. 2013). Enhancement in hydrogen production with modified TiO_2 photoelectrodes was due to the improved spectral response resulting from the decrease of energy bandgap. In_2O_3-modified ZnO photocatalyst also showed enhanced activity and stability due to the reduction in both charge recombination and size of ZnO after the loading of In_2O_3, which contributed to the improved hydrogen production from methanol (Martha et al. 2014).

8.3.4 Construction of Nanohybrid Materials

Hybrid materials are composed of two or more components of organic and inorganic origin, which are well dispersed in the molecular level. Hybrid materials of suitable composition are proved as good candidates for visible light active photocatalysts. Lanthanide ion doping and incorporation of photosensitive materials have attracted a lot of interest in the area of solar/visible light photocatalysis. Indeed few reports are available on lanthanide ion doped semiconductor incorporated with photosensitive molecules as hybrid materials. Exploiting the advantages of bandgap reduction by lanthanide ion doping and the electron-hole recombination prevention by incorporation of photosensitive materials, some efficient photocatalytic systems were synthesized (Thomas et al. 2016). Novel photocatalysts, neodymium (Nd^{3+})-doped TiO_2 nanoparticles incorporated with heteropoly phosphotungstic acid (HPA) (Nd^{3+}-TiO_2-HPA) were applied for the degradation of pollutants like methylene blue and organochlorine toxic chemical, 4-chlorophenol in water. Complete mineralization of both the pollutants upon sunlight illumination indicates that Nd^{3+}-TiO_2-HPA nanocomposites would be very useful for cleaning polluted surface water by sunlight through the advanced oxidation process. The enhanced photocatalytic activity of Nd^{3+}-TiO_2-HPA nanocomposites is mainly due to two factors: (i) doping of Nd^{3}

$^{+}$ions decreased the bandgap of TiO_2 (from 3.22 to 2.87 eV) and (ii) HPA addition prevented the recombination of electrons and holes.

Nano-ZnO-based dye-sensitized solar cells were synthesized using zinc porphyrin (an electron donor) and fullerene (C_{60} acid, an electron acceptor) via spin coating method (Hayashi et al. 2009). These dye-sensitized bulk heterojunction solar cells have both features of dye sensitization and bulk heterojunction devices. The porphyrin-fullerene-ZnO nanorod devices exhibited efficient photocurrent generation compared to that of the reference systems. Fullerene can inject its electrons to the conduction band of ZnO and suppresses the recombination of charges. The porphyrin-fullerene composite layer on ZnO surface also efficiently separates the photoinduced charges.

Metal-doped semiconductor incorporated with another semiconductor of low bandgap energy is another way to enhance the visible light-induced photocatalytic performance of a UV light active semiconductor. Such a hybrid nanocomposite, CdS-loaded Ag-ZnO catalyst was obtained using a simple precipitation-thermal decomposition method (Subash et al. 2016). The novel photocatalysts can absorb visible light and has reduced recombination of the photo-generated electron-hole pairs, attributed to the presence of Ag and CdS. Studies showed that loss of Zn during the photocatalytic reaction, one of the main problems associated with nano-ZnO-based photocatalysts, was prevented ascribed to the strong interaction between ZnO with Ag and CdS.

Photosensitizer-metal sulphide-semiconductor nanohybrids show enhanced photocatalytic performance (Yuan et al. 2015). A system for visible light-driven hydrogen evolution was constructed by using Zn(II)-5,10,15,20-tetrakis (4-carboxyphenyl)porphyrin dye-sensitized MoS_2/ZnO as a photocatalyst. It was used for the photocatalytic H_2 production from water in presence of triethanolamine as the sacrificial electron donor under visible light irradiation. MoS_2, having 2D structure, is similar to graphene and is widely used as co-catalyst for photochemical H_2 evolution reaction because of its high edge plane exposure.

It was observed that the incorporation of graphene and nano-Au into TiO_2 significantly enhanced the electron transport and therefore impeded the charge recombination of excited TiO_2 which resulted in the decrease of the crystalline size, an increase of surface area and redshift to the visible region (Ghasemi et al. 2017). Exploiting the surface plasmon resonance of Au nanoparticles and superior electron transport property of carbon nanotubes (CNT), g-C_3N_4-based hybrid (g-C_3N_4/CNTs/Au) was synthesized using ultrasonication method, for water purification and water splitting (Pawar et al. 2015). The large-specific surface area, reduction in the charge recombination and the high visible light absorption due to the SPR of Au nanoparticles were observed in ternary g-C_3N_4/CNTs/Au hybrid. All these properties resulted in the enhancement of photocatalytic activity and photocurrent response of the ternary g-C_3N_4/CNTs/Au hybrid. Photo-generation and electron transport mechanism are shown in Fig. 8.14.

The size-dependent role of metal nanoparticles in hybrid systems for photocatalysis is well explained (Bai et al. 2016). Au nanoparticles having two different sizes (100–150 nm and 10–20 nm) were added to synthesize Au/g-C_3N_4/

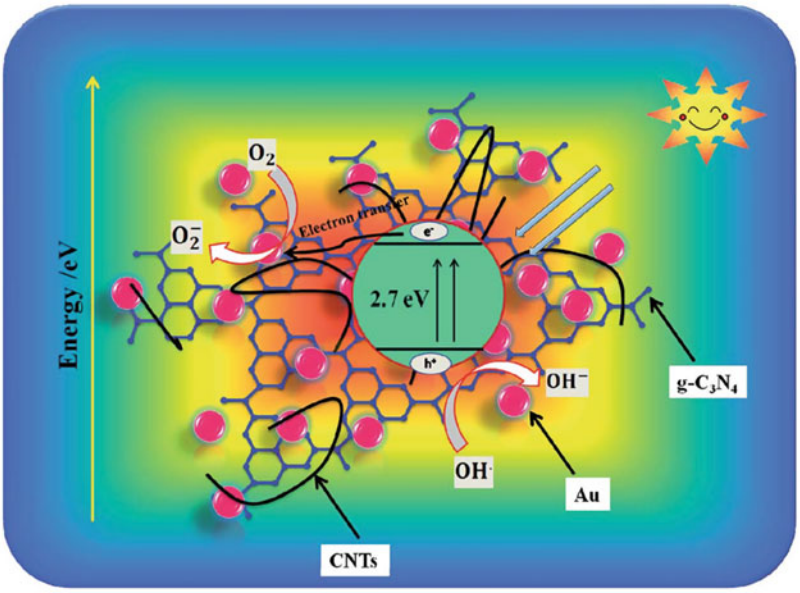

Fig. 8.14 Electron transport mechanism under visible light for the degradation of organic compounds with the ternary g-C_3N_4/CNTs/Au hybrid which showed enhanced photocatalytic activity and photocurrent response. (Reprinted from Pawar et al. 2015 with permission)

BiOBr system (where BiOBr = Bismuth oxybromide). Au/g-C_3N_4/BiOBr system with big Au nanoparticles showed higher photocatalytic activity under UV light (380 nm monochromatic light irradiation) attributed to the Z-scheme bridge roles displayed by big Au nanoparticles. However, Au/g-C_3N_4/BiOBr system with small Au nanoparticles exhibited surface plasmon resonance and showed enhanced performance under visible light (550 nm monochromatic light irradiation). The size-dependent role of Au nanoparticles for the photocatalytic system was due to the SPR effect of small Au nanoparticles and electron transfer centre of big Au nanoparticles.

Synthesis of nanocomposite consisting of metal-organic framework (MOF) and g-C_3N_4 is a new way to improve the drawbacks of the g-C_3N_4 photocatalyst. g-C_3N_4 /Ti-benzenedicarboxylate hybrid nanocomposite {represented as CMTi} was synthesized by employing ultrasonication followed by solvothermal treatment (Wang et al. 2015). The near-complete photocatalytic degradation of RhB was obtained after 60 min of experimental conditions by the hybrid photocatalyst. The enhanced performance of this hybrid nanocomposite was attributed to intervalence electron transfer between Ti^{3+} and Ti^{4+} and synergetic effect between MOF and g-C_3N_4.

Immobilization of photocatalysts on supports like clay, zeolites, MCM-41, silica, etc. not only enhances the photocatalytic performance but also improves the stability of photocatalyst (Belver et al. 2017; Tongon et al. 2014; Vadivel et al. 2016a; Hagura et al. 2011; Suligoj et al. 2016; Wee et al. 2016). Properties like high surface area, layered or fibrous structure and high adsorption capacity have made clay

minerals as one of the extensively used supports in heterogeneous catalysis. Semiconductor-clay composites with superior photocatalytic performance have been reported by many research groups, combining the adsorption capacity of the clay and the photocatalytic ability of semiconductor. The one-step sol-gel route is employed to synthesize solar light active Zr-doped TiO_2 nanoparticles immobilized on delaminated clay materials (Belver et al. 2017). High degradation rates of antipyrine (an analgesic drug) by Zr-doped TiO_2/clay catalyst under solar irradiation show the potential application of this catalyst in environmental remediation. The incorporation of Zr reduced the charge recombination, while the addition of delaminated clay resulted in the high surface area and a disordered mesoporous structure. Construction of novel photocatalysts based on semiconductor-heterojunctions on a delaminated clay surface can enhance their photocatalytic activity, by reducing the probability of electron-hole recombination and promoting the charge carrier migration. Photocatalytic degradation of two widely used pharmaceuticals, acetaminophen and antipyrine, was achieved using TiO_2-ZnO/cloisite photocatalysts based on the heterojunction between semiconductors (TiO_2-ZnO) and delaminated-layered clay (cloisite) (Tobajas et al. 2017). Silica (SiO_2) also is a widely used inorganic supporting material, possessing high chemical stability except towards strong acid or base. SiO_2 has a low refractive index, good light transmission and adsorption of contaminants which result in the enhancement of photoactivity of SiO_2-semiconductor composites. TiO_2-SiO_2 (SBA-15) films free of organic contents were prepared from metatitanic acid as a precursor for TiO2 (Suligoj et al. 2016). TiO2-SiO_2 films were immobilized on glass carriers by brush deposition and showed 100 and 91% decompositions of toluene and formaldehyde, respectively, at room temperature under UV-A irradiation. Six times higher turnover frequency was shown by TiO_2-SiO_2 films in comparison to pure TiO_2. COK-12 (mesoporous silica nanoplatelets having a thickness of 200–300 nm, prepared via spontaneous precipitation of sodium silicate and citrate/citric acid buffered P123 triblock copolymer solutions) support was used to enhance the photocatalytic activity of TiO_2 nanoparticles (Wee et al. 2016). TiO_2-COK-12 photocatalyst has shown excellent photocatalytic activity than Degussa P25. ZnO/silica gel nanocomposite (ZnO/SG) showing the excellent antibacterial property was synthesized via environmentally friendly method by heating a mixture of $ZnCl_2$ and silica gel at 450 °C without the addition of any reducing agent (Lotfiman and Ghorbanpour 2017). The antibacterial test against *Escherichia coli* and *Staphylococcus aureus* revealed that the ZnO/SG prepared in longer deposition times showed improved antibacterial activity due to the enhancement in the contents of ZnO nanoparticles on the silica surface.

Carbon nitride-silica-based hybrid photocatalyst was developed by loading carbon nitride into titanium-incorporated SBA-15 (Ti-SBA15-CN). Photocatalytic reduction of Cr (VI) in aqueous solution and synergistic oxidation of phenol was investigated using Ti-SBA15-CN under visible light irradiation. By introducing Ti into the SBA-15 framework structure, visible light-driven photocatalytic activity of Ti-SBA15-CN can be improved compared to SBA15-CN, and the photocatalytic activity exhibited a rise with the increase of Ti contents. It was because the presence of Ti moiety could promote the separation of the photo-generated charge carriers in

carbon nitride, leading to the enhancement of the photocatalytic activity. The addition of phenol further enhanced the photocatalytic reduction of Cr (VI). Similarly, the presence of Cr (VI) promoted the degradation of phenol. The synergistic effect of the reduction of Cr (VI) and the degradation of phenol provided a salutary method for purification of the complex wastewater and environmental restoration (Liu et al. 2017a).

Visible light-responsive Ag/TiO_2/MCM-41 nanocomposite films were synthesized by an inexpensive and convenient microwave-assisted sol-gel technique (Tongon et al. 2014). Ag/TiO_2/MCM-41 films were used to study the degradation of methylene blue dye and showed degradation rates of 80% and 30% under UV and visible light, respectively. Ag reduced the bandgap energy and prevented recombination of photoinduced charges, whereas adsorption capacity of the nanocomposite films was enhanced by MCM-41. MCM-41 also supplies active hydroxyl radicals attributed to the presence of silanol groups (Si-OH). Graphitic carbon nitride (g-C_3N_4) also showed superior photocatalytic hydrogen evolution when loaded onto the MCM-41 mesoporous silica. 1.2 times higher H_2 evolution was obtained on using MCM-41/g-C_3N_4 compared with pure g-C_3N_4 and is ascribed to the high dispersion of g-C_3N_4 on MCM-41 which in turn lead to the improved separation efficiency of photo-generated charge carriers of g-C_3N_4 (Shen et al. 2016b). Introduction of Ti into the MCM-41 framework structure created (Ti^{4+}-O^{2-}) active centres, resulting in the utilization of visible light.

Semiconductors modified with zeolites, another class of hybrid catalysts, also show enhanced photocatalytic performance attributed to the presence of broad-specific area, high amount of hydrophobic and hydrophilic active sites and adequate crystallinity (Zheng et al. 2012b). The presence of molecular dimensional pores and channels, high surface area, excellent ion exchange properties, etc. nominate zeolite as an excellent candidate in the field of catalysis. Strong acidic functional groups can be introduced in zeolites to incorporate various metals and metal oxides. Functional form of TiO_2-zeolite nanocomposite synthesized via two-step sol-gel method showed a high apparent pseudo-first-order reaction rate constant of 0.0419 min^{-1} at lower dye concentration, following a more adsorption-oriented photocatalytic degradation of water pollutants, which is useful for removing trace and untreated dye compounds in the advanced industrial dye wastewater treatment stage (Chong et al. 2015). Modification of ZnO using different zeolites has potential applications in heterogeneous photocatalysis (Batistela et al. 2017). ZnO photocatalyst modified by supporting on three different zeolites, zeolite Y (NaY), zeolite A (NaA) and zeolite Y ultrastable (USY) showed improved activity. The crystallization of ZnO occurred on the external and internal surfaces of zeolite NaA and zeolites NaY and USY. Zero point charge analysis (ZPC) showed that ZnO modification using NaA caused a significant decrease in ZPC due to synergic effect of ZnO and NaA. ZPC increased in ZnO-NaY and ZnO-USY catalysts indicating that ZnO acts as an integral part of the structure of the catalysts, due to its incorporation into the pores.

Bismuth oxyfluoride (BiOF), a UV-sensitive semiconductor (bandgap of 3.5 eV) which attracted a lot of interest in the area of environmental remediation, was incorporated into other semiconductors to form hybrid materials. Ag modified

BiOF/CN organic-inorganic hybrid photocatalysts exhibited advanced photocatalytic activity towards the degradation of MB under visible light (Vadivel et al. 2016b). The photoinduced electrons can be easily transferred from CN to BiOF ascribed to the fact that conduction band edge potential of CN is more negative than that of BiOF. Ag particles acted as an electron-conduction bridge between CN and BiOF.

$CaFe_2O_4$ belongs to the family of spinel ferrites and is an excellent material showing interesting catalytic properties. Vadivel et al. reported CN-$CaFe_2O_4$ nanocomposites prepared by ultrasonication method (Vadivel et al. 2016a). Among the different synthesized samples, $CaFe_2O_4$ (30%)-CN showed superior photocatalytic activity towards the degradation of methylene blue (MB) under visible light. Addition of $CaFe_2O_4$ leads to strong visible light absorption and efficient charge separation which resulted in the superior photocatalytic activity of CN-$CaFe_2O_4$ nanocomposites.

$ZnIn_2S_4$, a well-known ternary chalcogenide semiconductor having 2D layered structure and the narrow bandgap of 2.6 eV, has been widely studied in photocatalysis. "Sheet-on-sheet" hierarchical nanocomposite consisting of CN and $ZnIn_2S_4$ exhibit remarkably enhanced photocatalytic H_2 production (Zhang et al. 2016). Efficient interfacial photoinduced charge carrier transfer from CN to $ZnIn_2S_4$ resulted in reduced charge recombination in CN and enhanced a number of electrons and holes in $ZnIn_2S_4$.

The photocatalytic degradation of RhB was studied using Fe_2O_3/CN, Co_3O_4/CN and NiO/CN synthesized via one-step pyrolysis of urea and corresponding metal nitrates (Sridharan et al. 2014). During pyrolysis, urea acts as reducing agent and simultaneously gets converted to CN. The resultant photocatalysts have wide absorption in visible spectrum making them suitable choice as optical limiters, which protects eyes from the harmful effects of lasers or other radiations.

8.3.5 Surface Modification

Surface properties of nano-semiconductor photocatalysts have significant effects on their photochemical applications. Especially, in the photocatalytic degradation of organic pollutants, the surface charge of photocatalysts plays a significant role. The point of zero charge (zpc) is a point when electrical charge density on a surface is zero. The semiconductor surface is positively charged below its zpc value and is negatively charged when exceeded its zpc. The zpc values of TiO_2, ZnO and g-C_3N_4 are 6.2 (Wen et al. 2015), 9.5 (Radzimska and Jesionowski 2014) and 5.6, respectively (Fronczak et al. n.d.).

Bird's nest-like anatase TiO_2 microstructure with the exposed highly active surface has been synthesized using a facile one-step solvothermal method (Zhang et al. 2017). Photocatalytic activity of the bird's nest-like sample was more effective than P25 under the simulated solar light for the degradation of MB and was due to

the unique mesoporous structure, high specific surface area and highly active crystal facet exposure.

Anatase TiO_2 nanoparticles with shape controlled bipyramidal morphology (TiO_2-A-bipy) were also reported recently as good photocatalyst (Rémy et al. 2017). The sol-gel method was utilized for the preparation of TiO_2-A-bipy nanoparticles and then used for the photodegradation of three model pollutants – rhodamine B, phenol and formic acid under UV-A radiation exposure. TiO_2-A-bipy showed better photocatalytic activity towards RhB degradation than the commercial TiO_2-P25 attributed to the presence of more acidic sites on the TiO_2-A-bipy surface. However, in the case of phenol and formic acid degradation, commercial TiO_2-P25 showed better activity, may be due to better generation and separation of photo-generated charges. This work proved that dye degradation tests alone cannot confirm the photocatalytic performance of photocatalysts.

The stability of semiconductor nanoparticles can be enhanced by the use of capping agents like polyethylene glycol (PEG), cetyltrimethylammonium bromide (CTAB), etc. However, the photocatalytic activity of capped semiconductor nanoparticles will be different. PEG capped ZnO nanoparticles gave reduced photocatalytic activity than bare ZnO towards the photodegradation of rhodamine B dye (Sudha et al. 2013). But CTAB-modified TiO_2 photocatalysts show enhanced photocatalytic activity than bare TiO_2 attributed to the high separation of photoinduced charge carriers in CTAB-modified TiO2 (Zhong et al. 2013). ZnO with doughnut-like morphology was synthesized via calcination of ZnO-starch biocomposites (Carp et al. 2015). Here starch acted as a template and stabilizing/capping agent. It forces the nucleation and growth of ZnO along polysaccharides regions of high Zn^{2+} concentrations. Complete mineralization and degradation of phenol were obtained using this doughnut-like ZnO photocatalyst under visible light irradiation attributed to the large specific surface area, high crystallinity and narrow bandgap. Mesoporous TiO_2 with the large surface area was synthesized from titanium isopropoxide by sol-gel method using Triton-X and oleic acid as surfactants and diethanolamine as hydrolysis rate controller (Athanasiou et al. 2014). Photocatalytic activity of mesoporous TiO_2 was evaluated by accessing the photocatalytic degradation of methylene blue (MB) solution and NO oxidation.

In the case of graphitic carbon nitride photocatalysts, a proficient approach is exfoliation of bulk g-C_3N_4 (Chang et al. 2014). Exfoliation will create corresponding nanosheets by destroying the multilayer structure of g-C_3N_4. This technique will produce several thin segments having enlarged surface area. Efficient separation of charge carriers along with increased surface area provides a large number of active sites on photocatalysts surface which in turn results in the improved visible light absorption and better photocatalytic activity.

8.4 Conclusion

Growing concern over solar energy utilization and pollutant degradation has generated a strong interest in the development of solar light active photocatalysts, which would provide an environmentally sustainable photocatalytic treatment process for the degradation of organic pollutants and also for energy production using sunlight in place of artificial light. In this chapter we discussed some important photocatalysts, nanosized TiO_2, ZnO and graphitic carbon nitride, and various strategies adopted for improving their photocatalytic efficiency under sunlight. Fundamental information indicated in this chapter about semiconductor photocatalysts would be useful in constructing next-generation photocatalysts with higher spectral response in the visible region for efficient solar energy utilization.

References

Ansari SA, Ansari SG, Foaud H, Cho MH (2017) New J Chem 41:9314–9320. https://doi.org/10.1039/C6NJ04070E

Ansari SA, Ansari MO, Cho MH. Sci Rep, 6:27713. https://doi.org/10.1038/srep27713.

Athanasiou A, Mitsionis A, Vaimakis T, Pomonis P, Petrakis D, Loukatzikou L, Todorova N, Trapalis C, Ladas S (2014) Appl Surf Sci 319:143–150. https://doi.org/10.1016/j.apsusc.2014.06.086

Bachir S, Azuma K, Kossanyi J, Valat P, Haret JCR (1997) J Lumin 75:35–49. https://doi.org/10.1016/S0022-2313(97)00093-8

Bai Z, Yan X, Kang Z, Hu Y, Zhang X, Zhang Y (2015) Nano Energy 14:392–400. https://doi.org/10.1016/j.nanoen.2014.09.005

Bai Y, Chen T, Wang P, Wang L, Ye L, Shi X, Bai W (2016) Sol Energy Mater Sol Cells 157:406–414. https://doi.org/10.1016/j.solmat.2016.07.001

Bakar SA, Ribeiro C (2016) J Mol Catal A Chem 412:78–92. https://doi.org/10.1016/j.molcata.2015.12.002

Basahel SN, Ali TT, Mokhtar M, Narasimharao K (2015) Nanoscale Res Lett 10:73–86. https://doi.org/10.1186/s11671-015-0780-z

Batistela VR, Fogac LZ, Fávaro SL, Caetano W, Machado NRCF, Hioka N (2017) Colloids Surf A Physicochem Eng Asp 513:20–27. https://doi.org/10.1016/j.colsurfa.2016.11.023

Belver C, Bedia J, Rodriguez JJ (2017) J Hazard Mater 322 (233–242. https://doi.org/10.1016/j.jhazmat.2016.02.028

Bhethanabotla VC, Russell DR, Kuhn JN (2017) Appl Catal B Environ 202:156–164. https://doi.org/10.1016/j.apcatb.2016.09.008

Bingham S, Daoud WA (2011) J Mater Chem 21:2041–2050. https://doi.org/10.1039/C0JM02271C

Bu Y, Chen Z (2014) Electrochim Acta 144:42–49. https://doi.org/10.1016/j.electacta.2014.08.095

Cai A, Du L, Wang Q, Chang Y, Wang X, Guo X (2016) Mater Sci Semicond Process 43:25–33. https://doi.org/10.1016/j.mssp.2015.11.017

Cao Z, Zhu S, Qu H, Qi D, Ziener U, Yang L, Yan Y, Yang H (2014) J Colloid Interface Sci 435:51–58. https://doi.org/10.1016/j.jcis.2014.08.021

Carp, Tirsoaga A, Jurca B, Ene R, Somacescu S, Ianculescu A (2015) Carbohydr Polym 115:285–293. https://doi.org/10.1016/j.carbpol.2014.08.061

Carroll JP, Myles A, Quilty B, McCormack DE, Fagan R, Hinder SJ, Dionysiou DD, Pillai SC (2017) J Hazard Mater 324(A):39–47. https://doi.org/10.1016/j.jhazmat.2015.12.038

Chang CF, Man CY (2014) Colloids Surf A Physicochem Eng Asp 441:255–261. https://doi.org/10.1016/j.colsurfa.2013.09.009
Chang F, Zhang J, Xie Y, Chen J, Li C, Wang J, Luo J, Deng B, Hu X (2014) Appl Surf Sci 311:574–581. https://doi.org/10.1016/j.apsusc.2014.05.111
Chaudhuri RG, Paria S (2014) Dalton Trans 43:5526–5534. https://doi.org/10.1039/C3DT53311E
Chen Z, Ge Ma Z, Chen Y, Zhang Z, Zhang J, Gao Q, Meng M, Yuan X, Wang J, Liu GZ (2017) Appl Surf Sci 396:609–615. https://doi.org/10.1016/j.apsusc.2016.10.203
Cheng N, Tian J, Liu Q, Ge C, Qusti A, Asiri A, Al-Youbi A, Sun X. ACS Appl Mater Interfaces 5, 15, 6815–6819. https://doi.org/10.1021/am401802r
Chong MN, Tneu ZY, Poh PE, Jin B, Aryal R (2015) J Taiwan Inst Chem Eng 50:288–296. https://doi.org/10.1016/j.jtice.2014.12.013
Fan Q, Liu J, Yu Y, Zuo S, Li B (2017) Appl Surf Sci 391(B):360–368. https://doi.org/10.1016/j.apsusc.2016.04.055
Feng LL, Zou Y, Li C, Gao S, Zhou LJ, Sun Q, Fan M, Wang H, Wang D, Li G-D, Zou X (2014) Int J Hydrog Energy 39(28):15373–15379. https://doi.org/10.1016/j.ijhydene.2014.07.160
Fronczak M, Krajewska M, Demby K, Bystrzejewski M (n.d.) J Phys Chem C 121 (29):15756–15766. https://doi.org/10.1021/acs.jpcc.7b03674
Fujishima, Honda K (1972) Nature 238:37. https://doi.org/10.1038/238037a0
Gao X, Su X, Yang C, Xiao F, Wang J, Cao X, Wang S, Lu Z (2013) Sensors Actuators B 181:537–543. https://doi.org/10.1016/j.snb.2013.02.031
García EB, Elmouwahidi A, Álvarez MA, Marín FC, Cadenas AFP, Hódar FJM (2017) Appl Catal B Environ 201:29–40. https://doi.org/10.1016/j.apcatb.2016.08.015
Ghasemi S, Hashemian SJ, Alamolhoda AA, Gocheva I, Setayesh SR (2017) Mater Res Bull 87:40–47. https://doi.org/10.1016/j.materresbull.2016.11.020
Glossary of terms used in photochemistry (2006) IUPAC recommendations. 3rd edn., p 384. https://doi.org/10.1351/pac200779030293
Gupta R, Eswar NKR, Modak JM, Madras G (2017) Chem Eng J 307:966–980. https://doi.org/10.1016/j.cej.2016.08.142.
Habibi MH, Karimi B, Zendehdel M, Habibi M (2013) Spectrochim Acta A Mol Biomol Spectrosc 116:374–380. https://doi.org/10.1016/j.saa.2013.07.046
Haggerty JES, Schelhas LT, Kitchaev DA, Mangum JS, Garten LM, Sun W, Stone KH, Perkins JD, Toney MF, Ceder G, Ginley DS, Gorman BP, Tate J (2017) Sci Rep 7:15232. https://doi.org/10.1038/s41598-017-15364-y
Hagura N, Ogi T, Shirahama T, Iskandar F, Okuyama K (2011) J Lumin 131:921–925. https://doi.org/10.1016/j.jlumin.2010.12.024
Han Q, Hu C, Zhao F, Zhang Z, Chen N, Qu L (2015) J Mater Chem A 3:4612–4619. https://doi.org/10.1039/C4TA06093H
Hanifehpour Y, Hamnabard N, Khomami B, Joo SW, Min BK, Jung JH (2016) J Rare Earths 34 (1):45–54. https://doi.org/10.1016/j.molliq.2016.06.076.
Hayashi H, Kira A, Umeyama T, Matano Y, Charoensirithavorn P, Sagawa T, Yoshikawa S, Tkachenko NV, Lemmetyinen H, Imahori H (2009) J Phys Chem C 113:10819–10828. https://doi.org/10.1021/jp902623g
He J, Sun H, Indrawirawan S, Duan X, Tade MO, Wang S (2015) J Colloid Interface Sci 456:15–21. https://doi.org/10.1016/j.jcis.2015.06.003
Hoffmann MR, Martin ST, Choi W, Bahnemannt DW (1995) Chem Rev 95:69–96. https://doi.org/10.1021/cr00033a004
Hou HJ, Zhang XH, Huang DK, Ding X, Wang SY, Yang XL, Li SQ, Xiang YG, Chen H (2017) Appl Catal B Environ 203:563–571. https://doi.org/10.1016/j.apcatb.2016.10.059
Hu Y, Tsai HL, Huangk CL (2003) J Eur Ceram Soc 23:691–696. https://doi.org/10.1016/S0955-2219(02)00194-2.
Izumi Y (2013) Coord Chem Rev 257:171–186. https://doi.org/10.1016/j.ccr.2012.04.018
Jagadish C, Pearton S (2006) Zinc oxide – Bulk, thin films and nanostructures, 1st edn. Elsevier Science, eBook, Amsterdam. ISBN:9780080464039

Jesty T, Yoon M (2012) Appl Catal B Environ 111–112:502–508. https://doi.org/10.1016/j.apcatb.2011.10.039
Jesty T, Kumar KP, Suresh M (2011) Sci Adv Mater 3:59–65. https://doi.org/10.1166/sam.2011.1131
Jin R, Hu S, Gui J, Liu D (2015) Bull Kor Chem Soc 36(1):17–23. https://doi.org/10.1002/bkcs.10001
Jourshabani M, Shariatinia Z, Badie A (2017) Langmuir 33(28):7062–7078. https://doi.org/10.1021/acs.langmuir.7b01767
Kanhere P, Chen Z (2014) Molecules 19:19995–20022. https://doi.org/10.3390/molecules191219995
Khatamian M, Khandar AA, Divband B, Haghighi M, Ebrahimiasl S (2012) J Mol Catal A Chem 365:120–127. https://doi.org/10.1016/j.molcata.2012.08.018
Kumar DP, Reddy NL, Kumari MM, Srinivas B, Kumari VD, Sreedhar B, Roddatis V, Bondarchuk O, Karthik M, Neppolian B, Shankar MV (2015) Sol Energy Mater Sol Cells 136:157–166. https://doi.org/10.1016/j.solmat.2015.01.009
Kumar MK, Bhavani K, Naresh G, Srinivas B, Venugopal A (2016) Appl Catal B Environ 199:282–291. https://doi.org/10.1016/j.apcatb.2016.06.050
Kuyumcu ÖK, Kibar E, Glu KD, Gedik F, Akın AN, Glu ŞÖA (2015) J Photochem Photobiol A Chem 311:176–185. https://doi.org/10.1016/j.jphotochem.2015.05.037
Kwon JH, Park J, Park GS, Zuo JM, Kang SY, Oh JY, Kim M (2017) Curr Appl Phys 17(2):152–156. https://doi.org/10.1016/j.cap.2016.11.013
Le S, Jiang T, Zhao Q, Liu XF, Li Y, Fang B, Gong M (2016) RSC Adv 6:38811–38819. https://doi.org/10.1039/C6RA03982K
Lee J, Shim HS, Lee M, Song JK, Lee D (2011) J Phys Chem Lett 2:2840–2845. https://doi.org/10.1021/jz2013352
Lee KM, Lai CW, Ngai KS, Juan JC (2016) Water Res 88:428–448. https://doi.org/10.1016/j.watres.2015.09.045
Li X, Cheng Y, Kang S, Mu J (2010) Appl Surf Sci 256:6705–6709. https://doi.org/10.1016/j.apsusc.2010.04.074
Li M, Zhang L, Fan X, Wu M, Du Y, Wang M, Kong Q, Zhang L, Shi J (2016a) Appl Catal B Environ 190:36–43. https://doi.org/10.1016/j.apcatb.2016.02.060
Li L, Qi Y, Lu J, Lin S, An W, Liang Y, Cui W (2016b) Appl Catal B Environ 183:133–141. https://doi.org/10.1016/j.apcatb.2015.10.035
Li Z, Wu Y, Lu G (2016c) Appl Catal B Environ 188:56–64. https://doi.org/10.1016/j.apcatb.2016.01.057
Li W, Ze W, Kong D, D D, Zhou M, Y D, Yan T, You J, Kong D (2016d) J Alloys Compd 688:703–711. https://doi.org/10.1016/j.jallcom.2016.07.249
Li J, Xu X, Liu X, Qin W, Wang M, Pan L (2017a) J Alloys Compd 690:640–646. https://doi.org/10.1016/j.jallcom.2016.08.176
Li X, Shen R, Mab S, Chen X, Xie J (2017b) Appl Surf Sci 430:53–107. https://doi.org/10.1016/j.apsusc.2017.08.194
Lin Y, Chai Y, Yang X, Wang DH, Tang Q, Ghoshroy S (2013) Int J Hydrog Energy 38:2634–2640. https://doi.org/10.1016/j.ijhydene.2012.11.100
Liu Y, Wang Z, Wang W, An X, Mi S, Tang J, Huang W (2014a) Appl Surf Sci 315:314–322. https://doi.org/10.1016/j.apsusc.2014.07.143
Liu Y, Wang Z, Wang W, Huang W (2014b) J Catal 310:16–23. https://doi.org/10.1016/j.jcat.2013.03.024
Liu S, Li D, Sun H, Ang HM, Tadé MO, Wang S (2016a) J Colloid Interface Sci 468:176–182. https://doi.org/10.1016/j.jcis.2016.01.051
Liu T, Li X, Yuan X, Wang Y, Li F (2016b) J Mol Catal A Chem 414:122–129. https://doi.org/10.1016/j.molcata.2016.01.011
Liu F, Yu J, Tu G, Qu L, Xiao J, Liu Y, Wang L, Lei J, Zhang J (2017a) Appl Catal B Environ 201:1–11. https://doi.org/10.1016/j.apcatb.2016.08.001

Liu H, Chen D, Wang Z, Jing H, Zhang R (2017b) Appl Catal B Environ 203:300–313. https://doi.org/10.1016/j.apcatb.2016.10.014
Lotfiman S, Ghorbanpour M (2017) Surf Coat Technol 310:129–133. https://doi.org/10.1016/j.surfcoat.2016.12.032
Martha S, Reddy KH, Parida KM (2014) J Mater Chem A 2:3621–3631. https://doi.org/10.1039/C3TA14285J
McNaught AD, Wilkinson A (1997) IUPAC- compendium of chemical terminology, 2nd edn. Blackwell Scientific Publications, Oxford. https://doi.org/10.1351/goldbook.X06695
Medrano MGM, Kowalska E, Lehoux A, Herissan A, Ohtani B, Bahena D, Briois V, Justin CC, López JLR, Remita H (2016) J Phys Chem C 120(9):5143–5154. https://doi.org/10.1021/acs.jpcc.5b10703
Morkoç H, Özg€ur Ü (n.d.) Zinc oxide: fundamentals, materials and device technology. ISBN:978-3-527-40813-9
Moussawi RN, Patra D (2016) Sci Rep 6:24565. https://doi.org/10.1038/srep24565
Muthulingam S, Lee IH, Uthirakumar P (2015) J Colloid Interface Sci 455:101–109. https://doi.org/10.1016/j.jcis.2015.05.046
Pawar RC, Kang S, Ahn SH, Lee CS (2015) RSC Adv 5:24281–24292. https://doi.org/10.1039/C4RA15560B
Qi F, Li Y, Wang Y, Wang Y, Liu S, Zhao X (2016) RSC Adv 6:81378–81385. https://doi.org/10.1039/C6RA17613E.
Qin J, Zhang X, Yang C, Cao M, Ma M, Liu R (2017) Appl Surf Sci 392:196–203. https://doi.org/10.1016/j.apsusc.2016.09.043
Qiu P, Xu C, Chen H, Jiang F, Wang X, Lu R, Zhang X (2017) Appl Catal B Environ 206:319–327. https://doi.org/10.1016/j.apcatb.2017.01.058
Radhika S, Thomas J (2017) J Environ Chem Eng 5:4239–4250. https://doi.org/10.1016/j.jece.2017.08.013
Radzimska AK, Jesionowski T (2014) Materials 7:2833–2881. https://doi.org/10.3390/ma7042833
Rémy SP, Dufour F, Herissan A, Ruaux V, Maugé F, Hazime R, Foronato C, Guillard C, Chaneac C, Durupthy O, Justin CC, Cassaignon S (2017) Appl Catal B Environ 203:324–334. https://doi.org/10.1016/j.apcatb.2016.10.031
Rutar M, Rozman N, Pregelj M, Bittencourt C, Korošec RC, Škapin AS, Mrzel A, Škapin SD, Umek P (2015) Beilstein J Nanotechnol 6:831–844. https://doi.org/10.3762/bjnano.6.86.
Sagara N, Kamimura S, Tsubota T, Ohno T (2016) Appl Catal B Environ 192:193–198. https://doi.org/10.1016/j.apcatb.2016.03.055
Samsudin EM, Hamid SBA, Juan JC, Basirun WJ, Centi G (2016) Appl Surf Sci 370:380–393. https://doi.org/10.1016/j.apsusc.2016.02.172
Senthilraja, Krishnakumar B, Subash B, Sobral AJFN, Swaminathan M, Shanthi M (2016) J Ind Eng Chem 33:51–58. https://doi.org/10.1016/j.jiec.2015.09.010
Senthilrajaa A, Krishnakumara B, Swaminathana M, Nagarajanb S (2014) New J Chem 38:1573–1580. https://doi.org/10.1039/C3NJ01356A
Shahrokhi M (2016) Appl Surf Sci 390:377–384. https://doi.org/10.1016/j.apsusc.2016.08.055.
Sharma V, Kumar S, Krishnan V (2016) ChemistrySelect 1:2963–2970. https://doi.org/10.1002/slct.201600671
Shen SJ, Yang TS, Wong MS (2016a) Surf Coat Technol 303:184–190. https://doi.org/10.1016/j.surfcoat.2016.03.042
Shen S, Zhao D, Chen J, Guo L, Mao SS (2016b) Appl Catal A Gen 521:111–117. https://doi.org/10.1016/j.apcata.2015.11.004
Shi Y, Li H, Wang L, Shen W, Chen H (2012) ACS Appl Mater Interfaces 4:4800–4806. https://doi.org/10.1021/am3011516
Shi L, Wang F, Zhang J, Sun J (2016) Ceram Int 42:18116–18123. https://doi.org/10.1016/j.ceramint.2016.08.124
Sivakumar R, Jesty T, Yoon M (2012) J Photochem Photobiol C: Photochem Rev 13:277–298. https://doi.org/10.1016/j.jphotochemrev.2012.08.001

Sridharan K, Kuriakose T, Philip R, Park TJ (2014) Appl Surf Sci 308:139–147. https://doi.org/10.1016/j.apsusc.2014.04.121.
Sridharan K, Jang E, Park JH, Kim JH, Lee JH, Park TJ (2015) Chem Eur J 21:1–8. https://doi.org/10.1002/chem.201500163
Stengl V, Bakardjieva S, Murafa N (2009) Mater Chem Phys 114:217–226. https://doi.org/10.1016/j.matchemphys.2008.09.025
Su Y, Chen S, Quan X, Zhao H, Zhang Y (2008) Appl Surf Sci 255(5,1):2167–2172. https://doi.org/10.1016/j.apsusc.2008.07.053
Subash B, Krishnakumar R, Velmurugan, Swaminathan M, Shanthi M (2012) Catal Sci Technol 2:2319–2326. https://doi.org/10.1039/C2CY20254A
Subash B, Krishnakumar B, Sobral AJFN, Surya C, John NAA, Senthilraja A, Swaminathan M, Shanthi M (2016) Sep Purif Technol 164:170–181. https://doi.org/10.1016/j.seppur.2016.03.029
Sudha M, Senthilkumar S, Hariharan R, Suganthi A, Rajarajan M (2013) J Sol-Gel Sci Technol 65 (3):301–310. https://doi.org/10.1007/s10971-012-2936-y
Sui Y, Su C, Yang X, Hu J, Lin X (2015) J Mol Catal A Chem 410:226–234. https://doi.org/10.1016/j.molcata.2015.09.018
Suligoj A, Stangar UL, Ristic A, Mazaj M, Verhovsek D, Tusara NN (2016) Appl Catal B Environ 184:119–131. https://doi.org/10.1016/j.apcatb.2015.11.007
Sun Y, Chen L, Bao Y, Zhang Y, Wang J, Fu M, Wu J, Ye D (2016) Catalysts 6:188. https://doi.org/10.3390/catal6120188
Suryawanshi A, Dhanasekaran P, Mhamane D, Kelkar S, Patil S, Gupta N, Ogal S (2012) Int J Hydrog Energy 37:9584–9589. https://doi.org/10.1016/j.ijhydene.2012.03.123
Taheri E, Petala A, Mantzavinos D, Kondarides DI (2017) Catal Today 280:99–107. https://doi.org/10.1016/j.cattod.2016.05.047.
Thomas J, Chitra KR (2014) Adv Mater Res 938:292–296. https://doi.org/10.4028/www.scientific.net/AMR.938.292
Thomas AF, Goettmann F, Antonietti M, Müller JO, Carlsson JM (2008) J Mater Chem 18:4893–4908. https://doi.org/10.1039/B800274F
Thomas J, Radhika S, Yoon M (2016) J Mol Catal A Chem 411:146–156. https://doi.org/10.1016/j.molcata.2015.10.021
Thomas J, Ambili KS, Radhika S (2018) Catal Today 310:11–18. https://doi.org/10.1016/j.cattod.2017.06.029
Thomasa J, Radhika S, Yoon M (2017) Mol Catal 433:274–281. https://doi.org/10.1016/j.mcat.2016.12.016
Tobajas M, Belver C, Rodriguez JJ (2017) Chem Eng J 309:596–606. https://doi.org/10.1016/j.cej.2016.10.002
Tongon W, Chawengkijwanich C, Chiarakorn S (2014) Superlatices Microstruct 69:108–121. https://doi.org/10.1016/j.spmi.2014.02.003
Tripathy N, Ahmad R, Kuk H, Lee DH, Hahn YB, Khang G, Photochem J (2016) Photobiol B: Bio 161:312–317. https://doi.org/10.1016/j.jphotobiol.2016.06.003
Upadhyay R, Tripathi M, Pandey A (2013) High Energy Chem 47(6):308–314. https://doi.org/10.1134/S0018143913060106
Vadivel S, Maruthamani D, Habibi-Yangjeh A, Paul B, Dhar SS, Selvam K (2016a) J Colloid Interface Sci 480:126–136. https://doi.org/10.1016/j.jcis.2016.07.012
Vadivel S, Kamalakannan VP, Kavitha NP, Priya TS, Balasubramanian N (2016b) Mater Sci Semicond Process 41:59–66. https://doi.org/10.1016/j.mssp.2015.07.023
Wang Y, Wang X, Antonietti M (2012) Angew Chem Int Ed 51:68–89. https://doi.org/10.1002/anie.201101182
Wang H, Yuan X, Wu Y, Zeng G, Chen X, Leng L, Li H (2015) Appl Catal B Environ 174–175:445–454. https://doi.org/10.1016/j.apcatb.2015.03.037
Wang S, Zhang X, Li S, Fang Y, Pan L, Zou JJ (2017) J Hazard Mater 331:235–245. https://doi.org/10.1016/j.jhazmat.2017.02.049

Wee LH, Meledina M, Turner S, Custers K, Kerkhofs S, Sree SP, Gobechiya E, Kirschhock CEA, Van Tendeloo G, Martens JA (2016) RSC Adv 6:46678–46685. https://doi.org/10.1039/C6RA06141A
Wen J, Li X, Liu W, Fang Y, Xie J, Xu Y (2015) Chin J Catal 36:2049–2070. https://doi.org/10.1016/S1872-2067(15)60999-8
Wu W, Jiang C, Roy VAL (2015) Nanoscale 7:38–58. https://doi.org/10.1039/C4NR04244A
Xu J, Li Y, Peng S, Lu G, Li S (2013) Phys Chem Chem Phys 15:7657–7665. https://doi.org/10.1039/C3CP44687E
Yao B, Peng C, Zhang W, Zhang Q, Niu J, Zhao J (2015) Appl Catal B Environ 174–175:77–84. https://doi.org/10.1016/j.apcatb.2015.02.030
You R, Dou H, Chen L, Zheng S, Zhang Y (2017) RSC Adv 7:15842. https://doi.org/10.1039/C7RA01036B
Yu MM, Wang C, Li J, Yuan L, Sun WJ (2015) Appl Surf Sci 342:47–54. https://doi.org/10.1016/j.apsusc.2015.03.020
Yu W, Zhang J, Peng T (2016) Appl Catal B Environ 181:220–227. https://doi.org/10.1016/j.apcatb.2015.07.031
Yu Q, Jiang L, Gao S, Zhang S, Ai T, Feng X, Wang W (2017) Ceram Int 43(2):2864–2866. https://doi.org/10.1016/j.ceramint.2016.10.190
Yuan YJ, Tu JR, Ye ZJ, Lu HW, Ji ZG, Hu B, Li YH, Cao DP, Yu ZT, Zou ZG (2015) Dyes Pigments 123:285–292. https://doi.org/10.1016/j.dyepig.2015.08.014
Zalfani M, van der Schueren B, Mahdouani M, Bourguig R, Yu WB, Wu M, Deparis O, Li Y, Su BL (2016) Appl Catal B Environ 199:187–198. https://doi.org/10.1016/j.apcatb.2016.06.016.
Zhang Z, Zhou Y, Zhang Y, Sheng X, Zhou S, Xiang S (2013) Appl Surf Sci 286:344–350. https://doi.org/10.1016/j.apsusc.2013.09.084
Zhang X, L Y, Zhuang C, Peng T, Li R, Li X (2014) ACS Catal 4:162–170. https://doi.org/10.1021/cs400863c
Zhang H, Li S, Lu R, Yu A (2015) ACS Appl Mater Interfaces 7:21868–21874. https://doi.org/10.1021/acsami.5b06309
Zhang Z, Liu K, Feng Z, Bao Y, Dong B (2016) Sci Rep 6:19221–19232. https://doi.org/10.1038/srep19221.
G. Zhang, S. Zhang, L. Wang, R. Liu, Y. Zeng, X. Xia, Y. Liu, S. Luo, Appl Surf Sci 391 (2017) 228–235, https://doi.org/10.1016/j.apsusc.2016.04.095.
Zhao K, Lu Y, Lu N, Zhao Y, Yuan X, Zhang H, Teng L, Li F (2013) Appl Surf Sci 285:616–624. https://doi.org/10.1016/j.apsusc.2013.08.101
Zhao F, Shang J, Liu J (n.d.) Beijing Daxue Xuebao Ziran Kexue Ban/Acta Scientiarum Naturalium Universitatis Pekinensis 46(2):293–297
Zheng Y, Liu J, Liang J, Jaroniec M, Qiao SZ (2012a) Energy Environ Sci 5:6717–6731. https://doi.org/10.1039/C2EE03479D
Zheng Y, Li X, Dutta PK (2012b) Sensors 12:5170–5194. https://doi.org/10.3390/s120405170
Zhong J, Li J, Feng F, Huang S, Zeng J (2013) Mater Lett 100:195–197. https://doi.org/10.1016/j.matlet.2013.03.030
Zhu Y, Zhu M, Kang L, Yu F, Dai B (2015) Ind Eng Chem Res 54:2040–2047. https://doi.org/10.1021/ie504372p
Zhu Y, Shah MW, Wang C (2017) Appl Catal B Environ 203:526–532. https://doi.org/10.1016/j.apcatb.2016.10.056
Zyoud AH, Hilal HS (2014) Phyto Chem Bio Sub J 8(3):127–137. https://doi.org/10.163.pcbsj/2014.8.3.127
Zyoud, Dwikat M, Al-Shakhshir S, Ateeq S, Shteiwi J, Zu'bi A, Helal MHS, Campet G, Park DH, Kwon H, Kim TW, Kharoof M, Shawahna R, Hilal HS (2016) J Photochem Photobiol A Chem 328:207–216. https://doi.org/10.1016/j.jphotochem.2016.05.020

Chapter 9
High-Performance Photocatalysts for Organic Reactions

R. Goutham, K. P. Gopinath, A. Ramprasath, B. Srikanth, and R. Badri Narayan

Contents

Abstract The most important aim of modern organic chemistry is to replace the old, environmentally hazardous, expensive and less efficient processes with new, energy efficient routes of synthesis. In this regard, during the past 10 years, heterogeneous photocatalytic systems have been identified to have made it possible to perform green synthesis of a number of industrially important compounds. This is primarily attributed to its low-cost, ease of availability, simple chemical workup and eco-friendliness. In spite of the significant achievements being made in this field, major challenge pertains to the lack of selectivity. Much of fundamental knowledge pertaining to the reaction conditions such as solvent used, pH, intensity of irradiation, chosen photocatalysts and reaction conditions remain unknown for many synthesis applications. Thus this chapter will review the major achievements that have been made in this field. A review of the state of the art progresses in the use of common photocatalytic materials for the purpose of organic synthesis through four important classes of organic synthesis, namely, oxidation of alcohols, oxidative cleavage of olefins, reduction of nitro compounds, and cyclisation; carbon-hetero bond formation and alkylation will be reviewed.

R. Goutham · K. P. Gopinath (✉) · A. Ramprasath · B. Srikanth · R. Badri Narayan
Department of Chemical Engineering, Sri Sivasubramaniya Nadar College of Engineering, Chennai, Tamil Nadu, India
e-mail: gopinathkp@ssn.edu.in

Inamuddin et al. (eds.), *Nanophotocatalysis and Environmental Applications*,
Environmental Chemistry for a Sustainable World 31,
https://doi.org/10.1007/978-3-030-04949-2_9

Keywords Photoredox catalysis · Organic synthesis · Oxidation · Reduction · Cyclisation · Alkylation · Cross-coupling reactions · Surface plasmon resonance · Metal-organic frameworks · Photosensitisers

9.1 Introduction

Organic compounds form the backbone of numerous valuable products that find extensive application in pharmaceuticals, food processing and pesticide industries and hence form an integral part of everyday life. The synthesis of these compounds has been achieved by conventional routes, and not much have changed about the implementation of these synthetic routes throughout these years. Surprisingly, such organic transformations often require the use of harsh reaction conditions (strong reagents), temperature and pressure. The concept of visible with an increasing emphasis on the environmental impacts posed by such reagents, catalysts used, by-products produced in the reaction; coupled with the need to consider energy costs to remain competitive and handling highly reactive agents has forced manufacturers to look for and incorporate 'greener' synthetic routes. Thus, developing photocatalytic synthesis mechanisms that make use of light as an energy source to drive chemical reactions under much milder reaction conditions is highly desirable. The redox reactions were found to be favourable with the introduction of light which would shift the thermodynamic equilibrium; therefore the chemical synthesis tends to happen under room temperature in addition to prohibiting the thermally induced side reactions (Hagfeldt et al. 2010; Narayanam and Stephenson 2011).

However, the concept of visible light-driven photocatalysis mainly focusses on enhancing the process of molecule activation. More than half of the solar energy has been found to possess infrared radiation followed by visible light and ultraviolet rays. The ultraviolet radiation can be used to directly break or indirectly sensitise the bonds of selected molecules in order to generate highly reactive free radicals that can be used for degradation (Ikeda et al. 2006, 2009) purposes even though the product selectivity is negligible in certain cases (Kumar and Devi 2011). Due to the fact that the infrared radiation possesses inadequate frequency which in turn translates to lower energy, infrared radiation will not be able to provide the necessary energy for a large number of organic reactions. Visible light, in spite of being present in abundance in solar radiation spectrum, doesn't have the potential to drive the reactions directly due to low absorptivity. Therefore, a secondary substance (commonly in the form of a photocatalyst) is introduced, and the visible light photoredox catalysis is fixed as the conventional prototype to bring about the aforementioned energy transfers. Unlike photocatalysis, in photoredox catalysis both donation and acceptance of electrons take place simultaneously, thereby maintaining chemical neutrality (Prier et al. 2013). However, this method would not be feasible for those reactions where stoichiometric chemical oxidants or reductants are required and also in electrochemical reactions.

Generally, the basic mechanism is based on the single-electron transfer (SET) due to the photoexcitation of metallic complexes with organic substrates. Single-electron transfer mechanism often leads to radical ion intermediates with fundamental reactivity patterns differing from their ground state or excited state (Zhang et al. 2012). Moreover, these intermediates cannot be achieved effectively through other methods of activation. The catalysts which are commonly employed for these kinds of processes include azo dyes (Ravelli and Fagnoni 2012; Hari and Konig 2014), semiconducting compounds (Shiraishi et al. 2010; Lang et al. 2014b), noble nanoparticles (Sahoo et al. 2013; Revol et al. 2013), etc. that absorb the visible light to provide a stable and long photoexcited states. The average lifetime of the photoexcited particles is in the scale of 10^{-6} s. There are certain cases where the average excited lifetime of the electrons is hindered due to the possibility of the electrons to undergo bimolecular electron transfer while returning to ground state (Tucker and Stephenson 2012).

Out of the various photo-induced catalytic processes, the heterogeneous visible light catalysis is highly preferred owing to catalyst recoverability which is not possible in other processes. Generally in heterogeneous catalysis, those catalysts with a low band gap energy are preferred as such catalytic materials do only require irradiation with light of lower energy, in order to induce charge separation (Cherevatskaya and König 2014; Lang et al. 2014a). The frequency of the incident photon should synchronise with the overall vibration frequency of conducting electrons of the photoredox catalytic nanoparticles; it is only under this condition optimised absorption of photon takes place as a result of localised surface plasmon resonance (Wang et al. 2012). The overall mechanism can be simply explained as the movement of electrons from valence band to conduction band upon absorption of an incident photon whose energy was greater than the band gap of the catalyst.

In photocatalytic reactions, light energy is selectively irradiated towards a specifically designed photocatalytic agent which gets excited, thereby inducing the accompanying substrate, reagent or secondary catalyst to participate in novel reaction mechanisms that could not be easily attained under thermally controlled conditions. In this reaction pathway, the photocatalyst in its excited state can either remove or donate an electron to an organic or organometallic substrate. This process known as single-electron transfer (SET) facilitates the formation of highly reactive radical species under mild reaction conditions and can also effectively 'switch on' or promote other catalysts that are largely inactive in the absence of a photocatalyst and light energy. Photocatalysts harvest light radiation and convert it into chemical energy and simultaneously carry out the selective molecular activation by means of any one of (i) energy transfer, (ii) organometallic excitation, (iii) light-induced atom transfer and (iv) photoredox catalytic pathways. This review, however, will lay its primary emphasis only on the usage of photoredox catalysis briefly from a mechanistic viewpoint and will discuss the most recently reported impact of this area on the field of organic transformation. However, since the contextual coverage of this paper cannot be exhaustive owing to the tremendous amount of research being reported in this area, particular emphasis has been placed on reports that

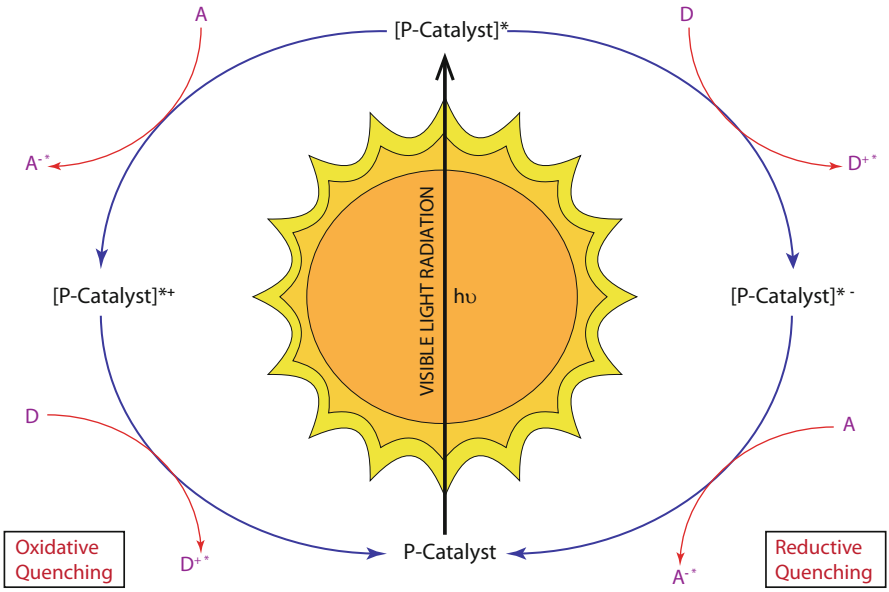

Fig. 9.1 Visible light photoredox catalysis – a schematic representation of the oxidative and reductive quenching cycles (SET pathway)

demonstrate the unique characteristics of photoredox catalysis and at the same time the truly novel nature of the accompanying reactions it can deliver (Fig. 9.1).

Photoredox catalysts are an effective tool to access a distinct reaction environment, wherein simultaneous oxidation and reduction of the organic and organometallic substrates are possible. This strategy is interesting, primarily because the conventional redox agents can bring about reactions that can be singly oxidative, reductive or neutral. Unexpected levels of reactivity have been reported to occur with photoredox catalysis in comparison with traditional reaction manifolds, a feature that is largely attributed to both the aforementioned ability of photoredox catalysts to act as both an oxidant and reductant simultaneously in their excited states and their capacity to convert visible light into equivalent amounts of chemical energy. Specifically, these key features have led to the development of a wide array of redox-neutral organic transformations that were earlier energetically unfeasible under absence of light irradiation. Apart from these potential advantages, a significant advantage also lies in the fact that photoredox reaction manifolds continuously regenerate the excited-state catalyst. The combination of these abilities has wide-reaching implications on designing new synthetic transformations and provides the means to access previously elusive or unknown mechanistic pathways.

This review article mainly focusses on the processes from different perspective through four sections: the oxidation of alcohols, oxidation of amines, carbon-carbon bond formation reactions and carbon-hetero bond formation reactions and other miscellaneous reactions. The application of different types of photoredox catalysts

like metal oxide, metal sulphide, organic semiconductor, plasmonic metal nanoparticles and other novel photoredox catalytic materials in organic synthesis will be illustrated.

9.2 Photocatalytic Oxidation of Alcohols

Carbonyl compounds created from alcohols through varied chemical reaction processes play an important role in synthetic organic chemistry. Compounds like formaldehyde and acetaldehyde that are commercially vital are chiefly used for the production of polymers, resins like carbamide, melamine, 4,4′-diphenylmethane diisocyanate and 2-ethylhexanol and for the manufacture of flavouring agents like vanillin, cinnamaldehyde, (R-)-carvone and benzaldehyde (Maldotti et al. 2002; Dijksman et al. 2003; Augugliaro et al. 2010). For the above conversions, robust oxidising agents like dichromates (Lee and Spitzer 1970) and permanganates (Shaabani et al. 2005) are being employed since yore. However, these oxidising agents were identified to be potentially carcinogenic (Shekhawat et al. 2015; Sahiner et al. 2016) making it indispensable to search for alternative reagents that are environmental friendly, benign and can be effectively used for the large-scale oxidation of alcohols. Thus abundantly available, cheap and nonhazardous photocatalysts which just require sunlight for their excitation have started to draw greater attention (Gil et al. 2013; Abedi and Morsali 2014; DePuccio and Landry 2016; Sadiq et al. 2017; Xu et al. 2017; Li et al. 2017b). However, the application of large band gap semiconductors such as TiO_2 and ZnO for photocatalytic oxidation is restricted, because of their incompatibility to be excited by visible light radiation (Romero et al. 1999; Hernandez-Alonso et al. 2009). In order to optimise the activity of the photocatalyst, various modifications are available in the literature, one such being doping of photocatalyst with metal ions like Fe^{3+}, Mo^{5+}, Ru^{3+}, Os^{3+}, Re^{5+}, V^{4+} and Rh^{3+}. Choi and group have reported that doping TiO_2 with such metal ions in the range of 0.1–0.3 at % increases the photocatalytic activity of TiO_2 (Choi et al. 1994). Many other techniques such as dye sensitisation of the photocatalyst (Zou et al. 2012) and nonmetal doping (Verma et al. 2016) have been performed in order to improve the catalytic activity of the photocatalyst under visible light irradiation.

Jeena et al. reported the selective oxidation of aromatic alcohols catalysed by dye-sensitised ZnO-$AgNO_3$ nanocomposite and 2,2,6,6-tetramethylpiperidine-1-oxyl radical (TEMPO) (Jeena and Robinson 2012). The authors performed the sensitisation of the photocatalyst using Alizarin S dye. This method works on the principle of photoactivation of the dye molecule. The dye then transfers an electron to the conduction band of the semiconducting material. In this case, the injected electrons are taken up by silver ions from $AgNO_3$. Thereby, the Ag^+ ions get reduced to metallic silver. During this process, excited dye molecule returns to its ground state, accompanied with simultaneous oxidation of TEMPO from its radical state to the oxammonium state. The oxammonium salt produced will carry out the oxidisation of the alcohol into the carbonyl group. The use of Ag^+ ions in the form

of $AgNO_3$ will help to stabilise the dye-sensitised photocatalyst, by preventing the detachment of dye molecule from surface of the photocatalyst. The successful utilisation of $ZnO/AgNO_3$/TEMPO system has been reported by the authors, by studying the oxidation of various aromatic compounds as shown in Scheme 9.1a.

The authors had also attempted to scale up this oxidation process to other substrates such as 3,4-dimethoxybenzyl alcohol and benzoin to produce 3,4-dimethoxybenzaldehyde and benzil, respectively. The corresponding reactions are represented as below in Scheme 9.1b.

The visible light-induced aerobic oxidation of alcohols using a coupled photocatalytic system consisting of Alizarin S-sensitised TiO_2 and TEMPO was reported by Ma (Zhang et al. 2008) in the year 2008. In this case, the mechanism of working of the dye-sensitised TiO_2 catalyst is same as that reported by Jeena et al. However, this case only lacks the presence of $AgNO_3$ as electron acceptor. The dye-sensitised electrons will be directly injected into the conduction band of the photocatalyst, which will produce $O_2^{-\bullet}$. The TEMPO-nitroxyl radical will act as electron donor, thereby producing $TEMPO^+$, which will oxidise primary alcohols into aldehydes. It is reported that aromatic alcohols such as *p*-methoxyl benzyl alcohol can be easily oxidised with high selectivity of up to 99%. Allylic alcohols were also oxidised into their corresponding α, β-unsaturated aldehydes with

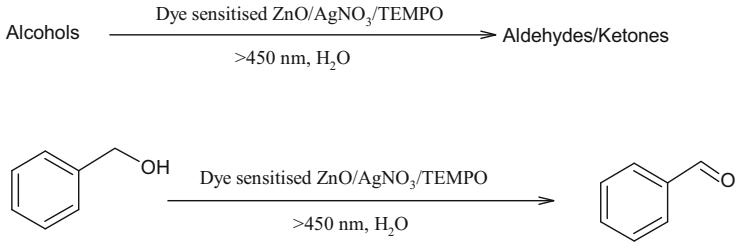

Scheme 9.1a Jeena and Robinson's benzyl alcohol oxidation into benzaldehyde with Alizarin S senstised ZnO-$AgNO_3$ and TEMPO

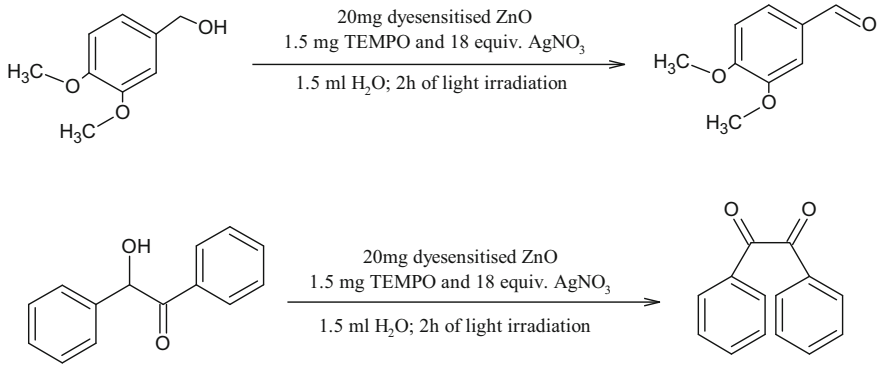

Scheme 9.1b Selective photocatalytic oxidation of alcohols using dye sensitised ZnO (representative reactions)

selectivity ranging from 94% to 98%. The major drawback of the proposed dye sensitised TiO_2-TEMPO system is that it cannot effectively oxidise secondary cyclic alcohols due to the lower chemoselectivity of TEMPO catalysts towards secondary alcohols over primary alcohols. The impressive feature of this system is that nitrogenous alcohols, which are themselves not reactive using transition metal-catalysed reactions (Königsmann et al. 2007), were also easily oxidised using this system. The results observed in this work are as shown below in Scheme 9.2.

Taking this study further, Feng and group have used HNb_3O_8 nanosheets for chemoselective oxidation of alcohols (Liang et al. 2014). Though conventional semiconductor TiO_2 photocatalyst can be modified to make it respond to visible light, more novel photoelectric materials have been found with better photocatalytic efficiency. The typical thickness of the HNb_3O_8 is around 1.1 nm, and it exists as a 2-D monolayer, which introduces surface disorders on HNb_3O_8. Thus, the improved photocatalytic activity of these sheets may emanate from the morphological features of the photocatalyst, namely, molecular thickness, larger surface area and large number of active sites. A surface coordination complex is produced in situ between the Lewis acid sites on the nanocomposite and those of the alcohols. These complexes have been identified to provide means for the effective harvesting of the incident light, and this induces the further photocatalytic reaction. Electron transfer takes place from the surface complex (coordinated alcohol species) to the surface of the Nb catalyst, which will initiate the aerobic oxidation of the alcohol. This process ultimately proceeds with high product selectivity under visible light. The interesting thing to be observed here is that e^- donating groups like $-CH_3$ and $-OCH_3$ groups are more easily oxidised. The oxidation of electron withdrawing groups like halides (-I, -Cl), etc. takes place only to a relatively lesser extent, according to the data in Table 9.1. This suggests that the oxidation reactions proceed via the intermediate carbo-cationic species produced. The observed percentage conversion and selectivity observed by (Liang et al. 2014) are as mentioned below in Scheme 9.3 and Table 9.1.

An interesting class of photocatalysts that are reported for the oxidation of alcohols includes metal-organic frameworks (MOFs). Metal-organic frameworks

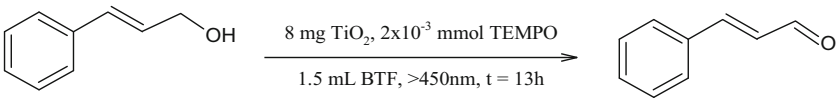

Scheme 9.2 Königsmann's method for photocatalytic oxidation of alcohols using TiO_2 and TEMPO (Königsmann et al. 2007)

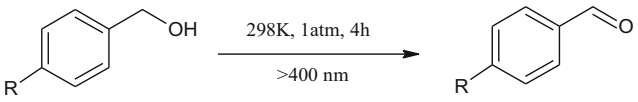

Scheme 9.3 Photocatalytic selective oxidation of benzylic alcohols over HNb_3O_8 nanosheets with visible light irradiation

Table 9.1 Conversions reported for the aerobic chemoselective oxidation of substituted cyclic alcohols using HNb3O8 nanosheets (Liang et al. 2014)
Clearly the oxidation of alcohols containing electron withdrawing groups like halides (-I, -Cl), etc. has taken place only to a relatively lesser extent.
(Reprinted with permission. Copyright 2014, WILEY-VCH)

Catalyst	Substituent	Atmosphere	%Conversion	%Selectivity
HNb_3O_8 nanosheets	$-OCH_3$	O_2	63	85
HNb_3O_8 nanosheets	$-CH_3$	O_2	54	>99
HNb_3O_8 nanosheets	H	O_2	20	>99
HNb_3O_8 nanosheets	Cl	O_2	28	>99
HNb_3O_8 nanosheets	F	O_2	18	>99
Layered HNb_3O_8	$-CH_3$	O_2	1.5	>99
Absence of catalyst[a]	$-CH_3$	O_2	0	0
HNb_3O_8 nanosheets	$-CH_3$	Air	17	>99
HNb_3O_8 nanosheets	$-CH_3$	N_2	2	>99

[a]Photolysis of 4-methylbenzyl alcohol

are porous coordination polymers formed by the self-assembly of metal ion and an organic ligand (Shen et al. 2015b; Fu et al. 2016; Zhen et al. 2016; Wang et al. 2017). Metal-organic frameworks have excellent physicochemical properties such as very high surface area, higher structural flexibility, high porosity and diversiform composition (Cooper 2013). It has been observed that immobilisation of metal-organic frameworks over functionalised organic linkers can increase the visible light sensitivity of the photocatalyst. Such metal-organic frameworks are often immobilised over materials like zeolites (Isaeva and Kustov 2016), graphitic carbon nitride (Huang et al. 2015; Cao et al. 2015; Wang et al. 2015a) and carbon nanotubes (Shen et al. 2015a; Hasan et al. 2016; He et al. 2016). On this note, Xu et al. (2015) have reported hierarchical nano-architectures composed of reduced graphene oxides and photoactive materials (UiO-66-NH_2), which are called as *x*rGO/UiO-66-NH_2, where '*x*' denotes the reduced graphene oxide content. The photoactive metal-organic frameworks were interconnected with reduced graphene oxides (rGO) to produce sandwich nano-architectures, which provide an effective charge separation and charge transfer during the photoredox reactions. This improved activity is attributed due to the unique sandwich structure of the hetero-structure, which ensures the acceleration of photo-generated electron transfer from UiO-66-NH_2 to the reduced graphene oxide layer. Upon irradiation of the nanocomposite with visible light, charge separation takes place in the UiO-66-NH_2 framework, and the electrons get transferred to the graphene layer. The molecular O_2 absorbed on the graphene layer gets reduced by the electrons into $O_2^{\bullet-}$. A simultaneous oxidisation of the aromatic alcohol takes place, due to the deprotonation, which produces the corresponding carbonium ions. Finally, the carbonium ions and the superoxide radicals react to produce the corresponding aldehydes. The oxidation study was carried out using 4-nitrobenzyl alcohol, 4-fluorobenzyl alcohol and 4-methylbenzyl alcohol. In all these cases, the selectivity was found to be 100%. The corresponding

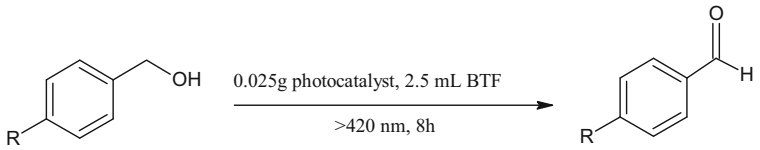

Scheme 9.4 General scheme for the photocatalytic oxidation of alcohols with MOF-rGO nanoarchitectures

Table 9.2 Conversions reported the photoredox catalytic oxidation of alcohols using UiO-66-NH_2-based MOFs (Zhang et al. 2016)
Reaction conditions: 0.5 mmol of the alcohol, 0.025 g of photocatalyst, 2.5 ml Benzotrifluoride as solvent (saturated with O_2), irradiated for up to 8 h under light of wavelength: $\lambda > 420$ nm and intensity: 250 mW
(Reprinted with permission. Copyright 2015, Royal Society of Chemistry)

Substituent group	Photocatalyst	% Conversion
H	UiO-66-NH_2	11.6
NO_2[a]	UiO-66-NH_2	18.9
CH_3	UiO-66-NH_2	2.0
F	UiO-66-NH_2	8.4

[a]4-nitrobenzyl alcohol of 0.05 mmol and BTF solvent of 3.5 ml (due to the lower solubility of 4-nitrobenzyl alcohol in BTF solvent)

conversions as achieved by the authors using pure UiO-66-NH_2 are as mentioned below in Scheme 9.4 and Table 9.2.

Silver-titania-based nanocomposites have also been successfully applied to the photocatalytic oxidation of benzyl alcohol in visible light region. These classes of Ag-TiO_2-based nanocomposites function via surface plasmon resonance (SPR) property, by which noble metals like Au, Ag and Pt absorb visible light radiation. This is demonstrated in the works of Zhang et al. (2016) in which by using nano AgBr@Ag@TiO_2 nanocomposite prepared by a facile three-step procedure, the authors have oxidised benzyl alcohol into benzaldehyde. The AgBr particles anchored over TiO_2 are capable of absorbing light radiation below 475 nm, while the Ag nanoparticles anchored over the TiO_2 surface can absorb light radiation higher than 450 nm due to the surface plasmon resonance. Thus, AgBr@Ag@TiO_2 photocatalyst can exhibit catalytic activity throughout the entire visible light spectrum. TiO_2 and AgBr deposited over it will separate the photolytically produced electron-hole pairs. The electrons thus formed get accumulated on the TiO_2 layer, while the holes get accumulated on AgBr. This is attributed to the reason that the conduction band and valence band edges of AgBr are higher than that of TiO_2 leading to a high degree of charge separation. These electrons, on the surface of TiO_2 layer, will get trapped by the absorbed O_2 molecules to produce $O_2^{\bullet -}$ radicals, which oxidise the benzyl alcohol solution. The conversion of benzyl alcohol (BA) into benzoic aldehyde (BAD) is as represented in Scheme 9.5.

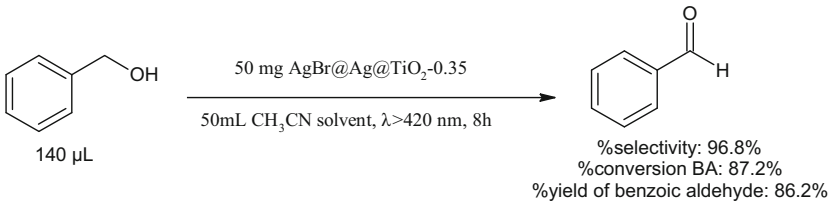

Scheme 9.5 Photocatalytic oxidation of benzylic alcohols with SPR photocatalysts (Ag@AgBr@TiO_2); Zhang et al.

Scheme 9.6 Tanaka's selective oxidation of alcohol groups in *p*-aminobenzyl alcohols using Au doped (SPR enhanced) photocatalysts

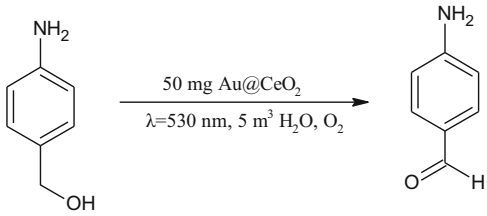

Similarly, Au nanoparticles immobilised over CeO_2 were used by Tanaka et al. (2011) for the photocatalytic oxidation of benzyl alcohol into benzaldehyde under green LED lights ($\lambda = 530$ nm). Here, Au particles of average size 59.3 nm were fixed on CeO_2 particles within a relatively sharp distribution having a standard deviation of 4.9 nm. Owing to surface plasmon resonance of the anchored Au nanoparticles, a strong absorption peak was exhibited at 550 nm. This peak nearly matches the wavelength of the green LED light used for the study. For the study, about 33 μmol of the alcohol, 50 mg of Au@CeO_2, 5cm^3 water, and LED lights at $\lambda = 530$ nm were used. The authors have reported a very high selectivity of about 99% and greater than 99% conversion for the oxidation reaction. Even in the presence of electron withdrawing and electron donating groups, the selectivity has been reported to be fairly high. Thus, halogen derivatives of benzyl alcohols could also be effectively oxidised into their corresponding aldehydes, with very high percentages of conversion. Also, the most important advantage of the Au@CeO_2 catalyst is that it can provide selective oxidation of hydroxyl groups without affecting the other substituents. For example, *p*-aminobenzyl alcohols can be easily oxidised under the similar conditions, to yield *p*-aminobenzaldehyde without affecting the amino group. This is represented in Scheme 9.6.

Apart from the conventional Au nanoparticle-based nanocomposites, free Au nanoparticles can also be employed as visible light photocatalysts for the oxidation of alcohols into their corresponding carbonyl compounds in the presence of H_2O_2 as oxidising agent. This is reported by Hallett-Tapley et al. (2011), wherein the oxidisation of *sec*-phenethyl alcohols was carried out using colloidal Au nanoparticles (mean particle diameter of 15 nm), in presence of H_2O_2 under highly monochromatic radiation (obtained from lasers or LEDs). For this study, lasers

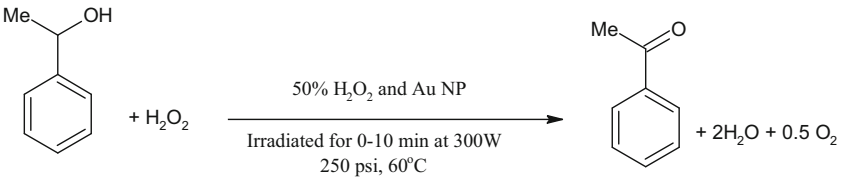

Scheme 9.7a Photocatalytic oxidation of alcohols with free-Au nanoparticles

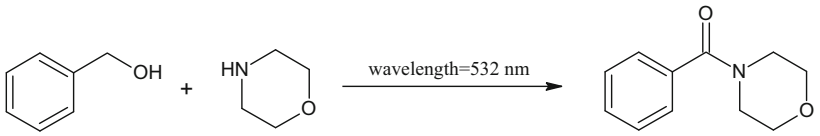

Scheme 9.7b 4-Benzoylmorpholine from benzyl alcohols with gold doped SiO_2 as photocatalysts. Reaction conditions: 0.2 ml benzyl alcohol, 0.2 ml morpholine, 19 ml THF solvent, 1 ml H_2O_2, 0.01 g KOH, 0.025 g Au-SiO_2 catalyst, 4 h reaction time at 25 °C

emitting light radiation at 532 nm and LED lights emitting radiation at 530 nm were employed. The reaction conditions are presented in Scheme 9.7a.

On a similar note, by using Au@SiO_2 heterogeneous catalysts at room temperature using laser emitting light radiation at wavelength of 532 nm, Luque and group carried out a tandem oxidation/amination process. For the synthesis of 4-benzoylmorpholine and morpholine, the reactions proceeded with 99% selectivity and 38% conversion of the reactant within 4 h of reaction time. An insight into this process is mentioned in Scheme 9.7b.

A dual-photosensitiser system for the photocatalytic oxidation of organic compounds was developed by Chao and Fu (2014), wherein a spacer material consisting of a difunctional photocatalyst with two distinct light-absorbing species and one catalytic centre was prepared. In this case, the electron transfer process gets significantly altered, thereby producing an enhanced catalytic efficiency. A ligand, bearing two 2,2′:6′,2″-terpyridine (*tpy*) units and one 2,2′-bipyridine (*bpy*) unit, is linked by C-C single bonds, and the corresponding Ru tri-nuclear complex was synthesised and used. A small quantity of a Co^{3+} was used as a sacrificial electron acceptor, because of the ease of electron transfer from exciting state $^{\bullet}Ru_p^{2+}$ to Co^{3+}. About 0.01 mM of the catalyst, 10 mM of the substrate, 20 mM of the Co^{3+} solution and 5 mL of 0.1 M phosphate buffer at pH = 6.8 under air and argon atmosphere were used to study the effectiveness of the prepared catalysts in oxidising alcohol moieties. The observed reactions under both argon and air atmospheres during the oxidation of various substituted benzyl alcohols as reported by the authors are mentioned in Scheme 9.8. The photocatalytic behaviour of the Ru^{4+} catalysts in this case can be explained to occur due to a complicated, multistep photoredox reactions of the *tpy*, *bpy* and Co^{3+} moieties immobilised over the catalytic centre. A detailed insight into the mechanism can be found in the works of Chao and Fu (2014) and Ohzu et al. (2012). However, the in situ generated $Ru^{c} = O$ moieties are responsible for the oxidation of the substrates.

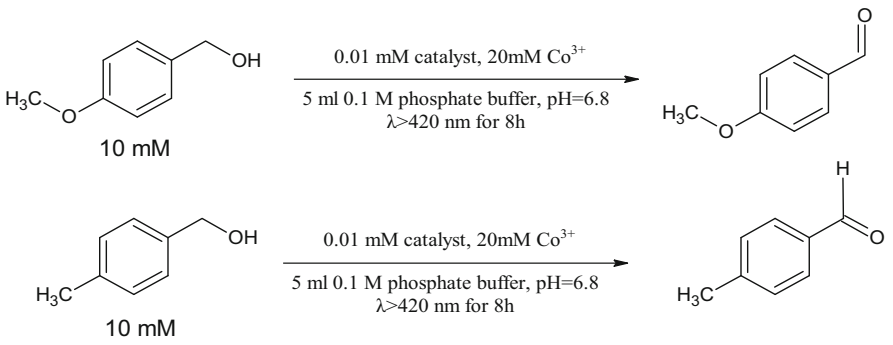

Catalyst used:

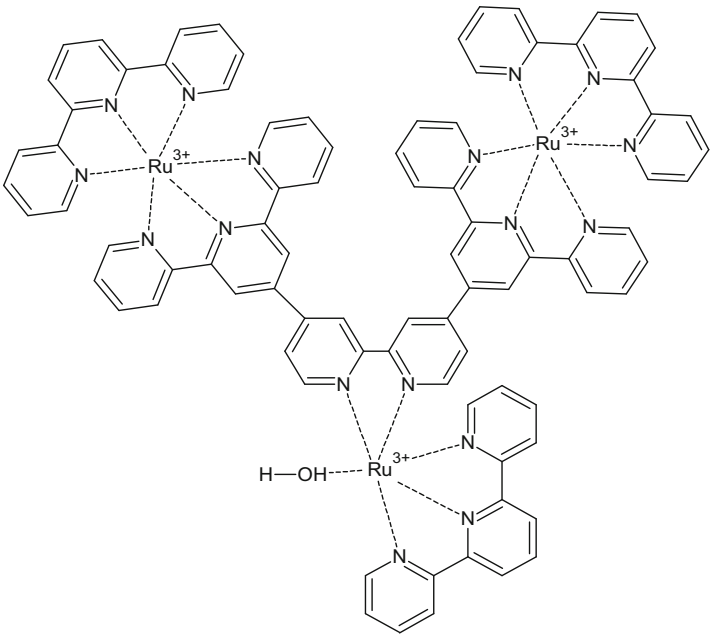

Scheme 9.8 (In all of these reactions, the selectivity was 99% in both Ar and air atmosphere)

Ternary chalcogenides zinc indium sulphides ($ZnIn_2S_4$) synthesised by simple solvothermal method were used for the visible light irradiated, photocatalytic oxidation of aromatic alcohols to aldehydes by Su et al. (2016). The authors synthesised zinc indium sulphides (ZIS) in four different solvent media, namely, EtOH, MeOH, H_2O and ethylene glycol (EG). It has been reported that zinc indium sulphide nanosheets synthesised by using EtOH as solvent showed excellent percentages of selectivity and conversion. The ZIS-EtOH sample showed the highest photocatalytic activity among all the other synthesised catalysts. As an example, the selectivity, conversion and yield values for oxidation of benzyl alcohol to benzaldehyde were

found to be 86.1%, 69.8% and 60.1%, respectively. The interesting point to be observed is that ZIS-MeOH and ZIS-H_2O catalysts also exhibited a similar activity. However, the ZIS-EG catalyst provided a very poor activity, with selectivity, conversion and yield values for oxidation of benzyl alcohol to benzaldehyde being 75.0%, 33.8% and 25.4%, respectively. It is worthwhile to observe that substrates that contain electron donating groups such as -CH_3 and -OCH_3 are more readily oxidised, while the presence of electron withdrawing groups like –X (halogens) retards the oxidation process. However, in case of *meta*- and *ortho*-substituted methoxy groups, the conversion and selectivity were largely decreased. This can be explained due to an increased steric hindrance. By means of band gap structure, the band gap energy for the synthesised samples was reported to be 2.56 eV for ZIS-EG, 2.52 eV for ZIS-EtOH, 2.41 eV for ZIS-MeOH and 2.37 eV for ZIS-H_2O. These band gap values clearly suggest that none of these catalysts are compatible to be used in visible light spectrum for the direct generation of hydroxyl radicals. The possible mechanism of photo-generation of $^{\bullet}OH$ radicals in zinc indium sulphide photocatalytic system is via the interaction of $^{\bullet}O_2^-$ and H_2O_2.

$$e^- + O_2 \rightarrow {}^{\bullet}O_2^- \tag{9.1}$$

$${}^{\bullet}O_2^- + e^- + 2H^+ \rightarrow H_2O_2 \tag{9.2}$$

$${}^{\bullet}O_2^- + H_2O_2 \rightarrow {}^{\bullet}OH + OH^- + O_2 \tag{9.3}$$

$$H_2O_2 \rightarrow 2\,{}^{\bullet}OH \tag{9.4}$$

The photo-generated electron-hole pairs will migrate in the two sub-layers of zinc indium sulphide catalyst, and molecular oxygen trapped in the catalyst surface gets converted to superoxide radical ($^{\bullet}O_2^-$) by the action of e^- from the conduction band of ZIS photocatalyst. The important step involved in the oxidation of benzyl alcohol using zinc indium sulphide photocatalyst is that the superoxide radical formed attacks the substrate followed by alkoxide anion formation. The holes produced during charge separation oxidise the alkoxide to yield benzaldehyde, along with simultaneous elimination of H^+ ions.

The selective oxidation of aromatic alcohols such as benzyl alcohols and its derivatives using O_2, in presence of photocatalysts, is receiving an ever-increasing attention (Long et al. 2013; Niu et al. 2016; Li et al. 2016c; Su et al. 2016). However, these processes involve the simultaneous formation of stoichiometric amounts of H_2O as a by-product. This leads to a situation wherein the atom efficiency is never 100%. The formation of aldehydic compounds by simple dehydrogenation of the corresponding alcohols will be of greater interest because of the simultaneous emission of molecular H_2 which can be collected and be used for various energy or synthetic applications. In this regard, Imamura et al. (2013) reported that atom efficiency in case of simple dehydrogenation is much higher than oxidative dehydrogenation of aromatic alcohols using Pt-TiO_2 in CH_3CN solvent under anaerobic conditions. The authors suggest that whenever H_2 produced, if it is also considered as a valuable product, the overall atom efficiency becomes 100%. Irradiation of

benzyl alcohol in acetonitrile solution using Pt-TiO_2 catalyst for 1 h under Ar atmosphere provided greater than 99% conversion and selectivity. For 50 μmol benzyl alcohol taken with 50 mg Pt-TiO_2, irradiated with UV-LED at $\lambda_{max} = 366$ nm, the H_2 evolution rate was estimated to be 48 μmol, and H_2/benzaldehyde ratio was around 0.94.

Taking this study further, Magdziarz et al. (2016) synthesised a Fe-TiO_2@Zeolite-Y (Fe/TiO_2/ZeSPD) photocatalyst by means of using sono-photo-deposition method. The prepared Fe/TiO_2/SPD was composed of two coupling semiconducting oxides, namely, TiO_2 and Fe_2O_3. The coupling semiconductors cause a vectorial displacement of electrons and holes, thereby enhancing charge separation. In this case, the photocatalytic oxidation study was performed in a 20 ml glass reactor at room temperature. About 54 mg of the catalyst was dispersed in 18 ml benzyl alcohol and 1 mM acetonitrile solution. The mixture was irradiated for 8 h using solar simulating Xe arc lamp. This setup was observed to present a very high selectivity in the order of 95% with a conversion of benzyl alcohol around 48% and yield of around 46%. This yield quantity transcribes to the fact that benzyl alcohol was completely converted into benzaldehyde, and only a negligible amount of unwanted by-products such as CO_2 and benzoic acid was produced. All these facts help to conclude that the prepared Fe-TiO_2/ZeSPD has a much better photonic absorption efficiency under visible light region. Also, due to the increased carbonaceous content on the surface of the Fe-TiO_2/ZeSPD, the hydrophobicity increases, thereby leading to an increased adsorption of benzyl alcohol on the surface of the catalyst (Scheme 9.9).

Water is generally not preferred as solvent for the chemoselective oxidation of alcoholic substances because the holes produced during charge separation may oxidise H_2O molecules to produce hydroxyl radicals. These hydroxyl radicals will cause a non-selective oxidation of the substrates, producing many undesired by-products, thereby decreasing the atom efficiency. However, Zhang and Xu (2014) have made a striking observation that flower-like Bi_2WO_6 semiconducting material provides excellent chemoselectivity during the aerobic oxidation of organic substrates even in the presence of H_2O as solvent. This has been explained by considering that Bi_2WO_6 has a much negative reduction potential of +1.77 V when measured against Ag/AgCl reference electrode. The corresponding reaction conditions studied are presented below in Scheme 9.10.

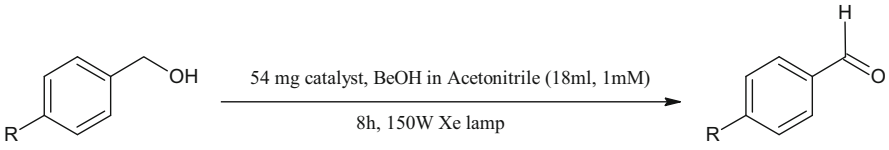

Scheme 9.9 Aromatic aldehydes from benzylic alcohols via photocatalytic dehydrogenation with photo-sono-deposited zeolite-nano-composite photocatalysts; Magdziarz et al. (2016)

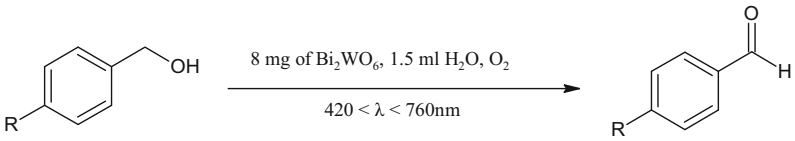

Scheme 9.10 Efficient aqueous media photocatalytic oxidation of benzylic alcohols into corresponding aldehydes with flower-like Bi_2WO_6 photocatalysts

9.3 Selective Oxidation and Oxidative Coupling of Amines

The selective oxidation of amines and especially benzylamines is of particularly high importance in organic chemistry. The resultant imine-based organic compounds are of very high importance in fine chemicals and pharmaceutical industries. Imines have always seen as a promising candidate for synthesis of various bioactive molecules such as alkaloids, nitrogenous heterocyclics, etc. Prochiral imines have often been used in the synthesis of chiral amines (Joyce et al. 2014; Gopula et al. 2014). The other important application of imines is in the field of coordination chemistry, wherein they are used as chelating agents (Kryvoruchko et al. 2002; Tighadouini et al. 2015; Sorour et al. 2016). In conventional processes, such conversion of amines to imines has been performed by condensation of an amine and a carbonyl compound using metal-based catalysts (Zheng et al. 2014; Li et al. 2017a), some non-metallic catalysts (Huang et al. 2012) or even nanocomposite materials (Shimizu et al. 2012; Rana et al. 2015). However, to overcome the excessively active nature of carbonyl group, heterogeneous visible light photocatalysts are widely being employed for the selective oxidation of amines. In these cases, molecular oxygen is used as the oxidant, which can accept an electron from the catalyst, to produce a superoxide anion radical, which initiates the further oxidation of amine group.

A work by Wang et al. (2015b) reported the use of conjugated microporous poly (benzochalcogenadiazoles) (PBCs) for the oxidative coupling of amines under visible light. The authors had prepared a series of PBCs using Sonogashira cross-coupling reaction of 1,3,5-triethynylbenzene as cross-linker and 4,7-dibromo-2,1,3-benzoxadiazole (Br-BO), 4,7-dibromo-2,1,3-2,1,3benzoselenadiazole (Br-BS) and 4,7-dibromo-2,1,3-benzothiadiazole (Br-BT). The PBCs thus produced were designated as B-BO, B-BS and B-BT, respectively. Each of these polymeric networks has reported to contain band gaps of 2.70 eV, 2.41 eV and 2.77 eV, respectively. However, of all the three catalysts, the wide band gap B-BT polymer exhibited a higher conversion rate at reaction conditions of 3 mg B-BT, 1 mmol amine, 3 ml acetonitrile, 1 bar oxygen, blue LED radiation of 460 nm and reaction time of about 3 h. In this case, the photo-generated holes and electrons are made use in the redox reaction cycle. In case of oxidative amine coupling reactions, the superoxide anion radical acts as the terminal oxidising agent. The observed reactions are reported in Scheme 9.11.

In order to overcome the problems associated with wide band gap semiconductors such as TiO_2, many newer photocatalysts have been reported for the selective oxidation of amines. Sun et al. (2015) made use of an amine-functionalised metal-organic framework (MOF), NH_2-MIL-125(Ti), for the visible light-assisted

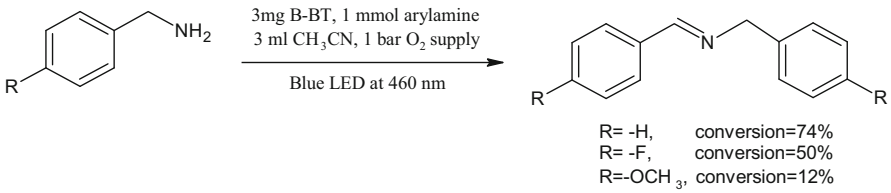

Scheme 9.11 Oxidative coupling of aromatic amines using 4,7-dibromo-2,1,3-benzothiadiazoles

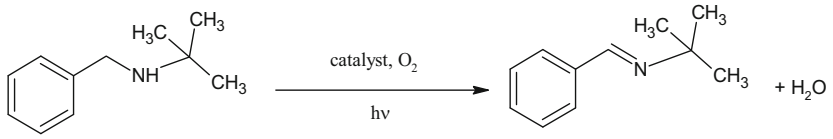

Scheme 9.12 Oxidation of *N*-*t*-butylbenzylamine with BiOCl nanosheets

photocatalytic oxidation of amines to imines. In this case, the in situ generated superoxide radical and Ti^{3+} ions are the main driving force responsible for the oxidation of amine group. For this study, benzylamine was chosen as the substrate. A reaction mixture consists of 0.1 mmol of benzylamine, 5 mg of the synthesised catalyst and 2 mL solvent and visible light radiation for about 12 h under aerobic conditions. The resultant product *N*-benzylidine benzylamine was formed with a moderate conversion rate of 53–73% and a relatively high selectivity of 70–94%. This study was carried out using a variety of solvents such as CH_3CN, $ArCF_3$, DMF and toluene, of which acetonitrile was found to offer an optimum conversion of the amine (~73%) and a very high selectivity towards *N*-benzylidine benzylamine (~86%) after 12 h reaction time.

Bismuth oxyhalides are a group of layer morphology ternary oxide semiconducting materials that are largely being employed in the photodegradation of organic pollutants (Mera et al. 2016; Dong et al. 2016b; Li et al. 2016a). The layered structure of the catalyst reduces the trapping of photo-generated charge carriers and inhibits the recombination of charge carriers due to the internal electric fields between interleaved $[Bi_2O_2]$ slabs and double halogen atoms. Based on this idea, Wu et al. (2015) synthesised a well-defined, colloidal, ultra-thin BiOCl nanosheets by solvothermal process with excellent hydrophobic surface behaviour. These catalysts were then used for the oxidation of secondary amines. *N*-*t*-butylbenzylamine was employed as a model substrate. For a reaction mixture of 0.077 mol catalyst, 0.1 mmol substrate and 4 ml CH_3CN solvent, a conversion of 33% and a selectivity of 99% were observed under visible light radiation ($\lambda > 420$ nm) after 1 h (Scheme 9.12). This suggests the excellent oxidising capability of BiOCl ultra-thin nanosheets under visible light radiation.

It is well known that the product yield in case of primary amine oxidation into imines is quite inefficient using metallic catalysts. Thus the effectiveness of oxidative coupling reactions can be improved under aerobic atmosphere promoted by organocatalysts. Dong et al. (2016a) had reported the oxidation of benzylamines

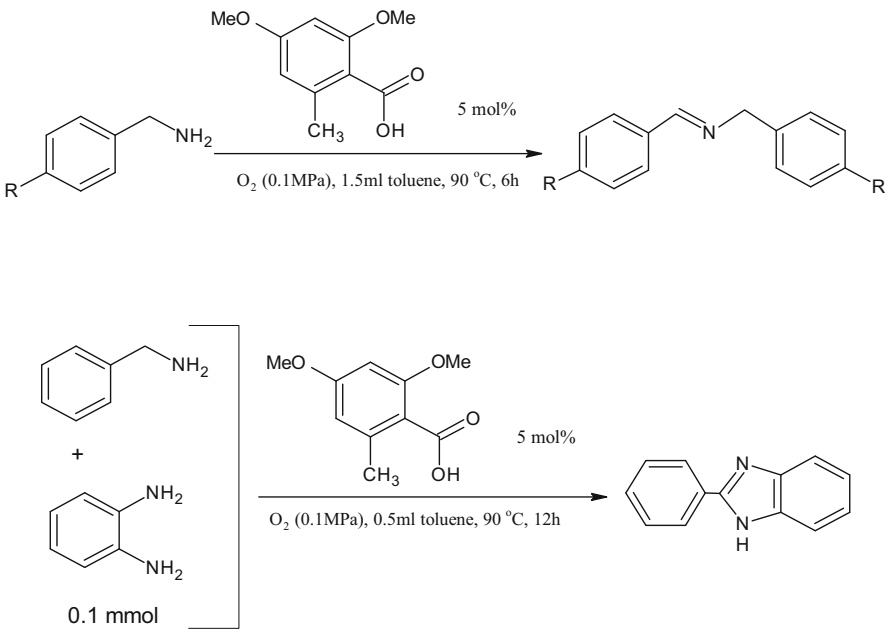

Scheme 9.13 Salicylic acid derivatives promoted oxidative coupling of 1° amines

effectively under oxygen-rich atmosphere promoted by salicylic acid derivatives. The electron-rich 4,6-dihydrosalicylic acid and 4,6-dimethoxysalicylic acid immobilised over 4.7 wt% silica gel have been employed as organocatalysts for the study. Consequently, about 80% yield of the product *N*-benzylidene benzylamine was obtained upon the oxidation of benzylamine. Interestingly, this process is capable of being used for the synthesis of benzimidazole, by the action of benzylamine and 1,2-diamino benzene under similar process conditions with a yield of 83% (Scheme 9.13).

Many heterogeneous catalytic systems such as Au nanoparticles loaded TiO_2 (Naya et al. 2013; Akashi et al. 2016), Nb_2O_5 (Furukawa et al. 2011; Dhakshinamoorthy et al. 2016), metal-organic frameworks (Su et al. 2010; Ahn et al. 2016), mesoporous graphitic carbon nitride (mpg-C_3N_4) (Li et al. 2012; Selvam et al. 2015) and Ru-oxides (Ovoshchnikov et al. 2015; Muthusamy et al. 2016) have been extensively studied and reported in literature. In fact, some of these catalytic systems have been reviewed in this article too. But, using all these catalysts, secondary amines can be effectively oxidised, however only under elevated reaction temperatures of about >363 K. Selvam et al. (2015) had synthesised TiO_2 loaded on Pd nanoparticles in aqueous media. The synthesised catalysts were then reported to have an excellent activity at room temperature, with regard to the photocatalytic oxidation of alcohols, and subsequently were capable of producing imines by condensation with anilines. The catalyst was also capable of reducing the imines into secondary amines with high yields (greater than 80%). The reaction mechanism

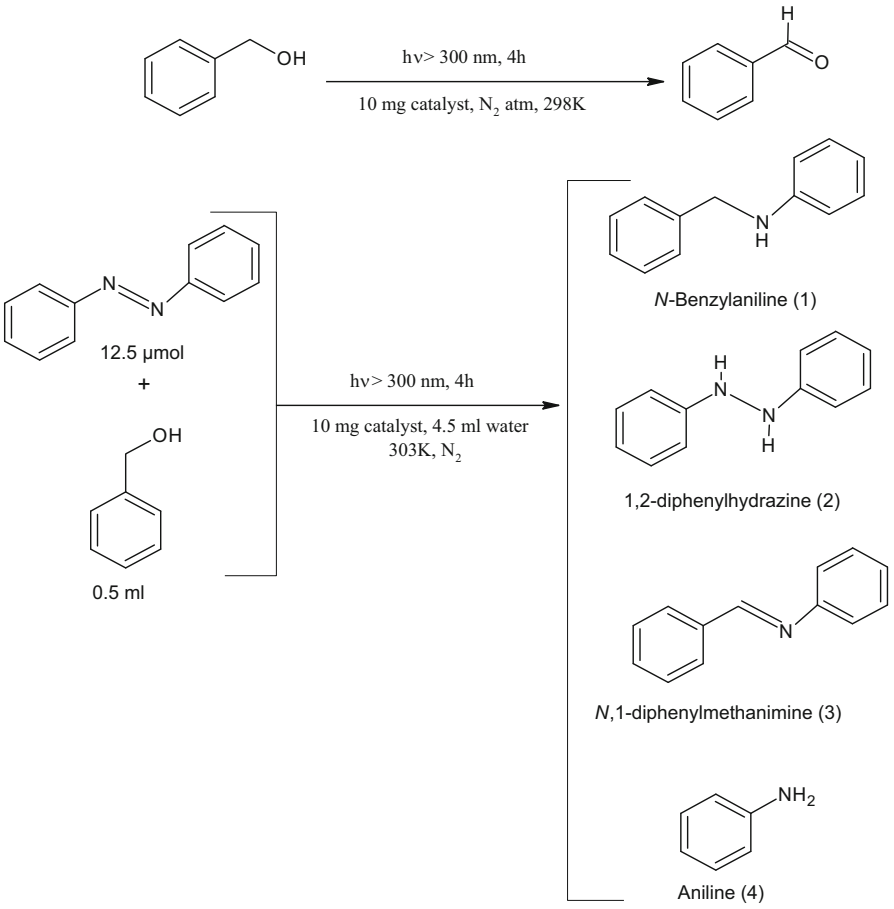

Scheme 9.14 TiO_2 loaded Pd catalysed alcohol oxidation and imine production by condensation reactions; Selvam et al. (2015)

and the actual reaction are depicted by the authors are depicted in Eqs. (9.5, 9.6, 9.7, 9.8, 9.9 and 9.10) and Scheme 9.14 respectively.

The photo-generated holes oxidise alcohols into the corresponding aldehyde along with simultaneous formation of H^+:

$$R_1 - CH_2OH + 2h^+ \rightarrow R_1 - CHO + 2H^+ \tag{9.5}$$

The e^- formed on TiO_2 conduction band will be transferred to the Pd particles, which leads to the reduction of H^+ ions to H atoms. This forms the H-Pd species, which further acts as the reducing agents:

$$H^+ + e^- + Pd \rightarrow H - Pd \tag{9.6}$$

Azobenzene will then be reduced to aniline by the highly active H-Pd intermediate. This reaction takes place through the formation of a hydrazobenzene as an intermediate:

$$R_2 - N = N - R_2 + 2H - Pd \rightarrow R_2 - NH - NH - R_2 + 2Pd \tag{9.7}$$

$$R_2 - NHNH - R_2 + 2H - Pd \rightarrow 2R_2 - NH_2 + 2Pd \tag{9.8}$$

The aldehyde formed is condensed with the aniline produced in Eq. 9.8, to produce an imine. This step proceeds over the active sites over the TiO_2 surface, which acts as a Lewis acid site.

$$R_1 - CHO + R_2 - NH_2 \rightleftharpoons R1 - CH = N - R_2 + H_2O \tag{9.9}$$

The imine thus produced in Eq. 9.9 is then hydrogenated to yield the corresponding secondary amine:

$$R_1 - CH = N - R_2 + 2H - Pd \rightarrow R_1 - CH_2 - NH - R_2 + 2Pd \tag{9.10}$$

This study was carried out with Pd_x/TiO_2 having different weight percentages of Pd ($x = 0.1, 1, 2, 4$). In all these cases, the conversion of azobenzene was found to be greater than 99%. If the main aim of the process is to produce the product **(1)**, then Pd_2/TiO_2 provided the highest yield of 98% for both fresh and reused catalyst. In either of these cases, the yield of aniline **(4)** was, however, zero. The use of Pd_4/TiO_2, however, provided a reasonably high yield of **(1)** (around 68%) and also simultaneously provided up to 12% aniline **(4)**.

Other than the conventional metallic heterogeneous photoredox catalysts such as TiO_2, ZnO and CdS, an increased attention is now being made on fullerenes (Kumar et al. 2016a, b) as catalysts for the selective oxidation of amines to imines. The low solubility of fullerene moieties makes it simple for workup of reactant mixture, and upon completion, the catalysts can be easily isolated from the reaction mixture by simple physical separation techniques such as precipitation or coagulation. Yamakoshi and co-workers had reported the use of photosensitive fullerene (C_{70}) for the photocatalytic oxidation of benzylamines to the corresponding imines (Kumar et al. 2016b). In the study, the photocatalytic activities of two different fullerenes C_{60} and C_{70} as photocatalysts for oxidation of amines were compared. It was reported that C_{60} did not show efficient catalytic activity when compared to TPP (tetraphenylporphyrin), which is a most commonly used photosensitiser. However, C_{70} was found to exhibit much effective activity even under lower intensity light radiation. C_{70} was also reported to be capable of carrying out nucleophilic addition of amines, even under low-energy light radiations. 1,2,3,4-tetrahydroisoquinoline was used as the substrate for oxidation study under white light irradiation obtained from Tungsten lamp (20,000–20,500 lx placed at a distance of 20 cm from the

reactant mixture). In this case, the singlet oxygen ($^1O_2$)-mediated oxidation of amines can be thought to take place from the initial coordination of $^1O_2$ species with amine group to form an exciplex, which is followed by the formation of benzylic radical, which can occur via:

- A single-electron transfers to provide amine radical cation and $O_2^{\bullet-}$ and successive deprotonation at benzyl position
- Direct abstraction of hydrogen

A schematic representation of the processes involved is provided in Fig. 9.2, and the various oxidation reactions using the C_{70} catalysts are mentioned in Scheme 9.15.

Of late, biomimetic quinones are also being employed at large for the dehydrogenation of amines (Samec et al. 2005; Qin et al. 2015; Stahl and Shannon 2016; Goriya et al. 2016). In this context, it has been observed that o-quinone can mimic CuAOs (Cu amine oxidases) and can effectively use green oxidising agents such as

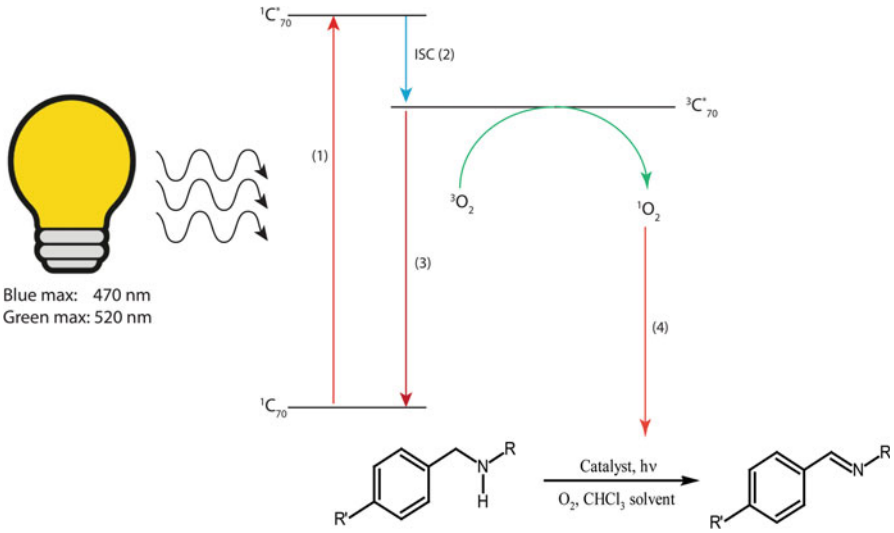

Fig. 9.2 A schematic representation of the photoredox processes involved in oxidation of amine to imines using C_{70} catalysts

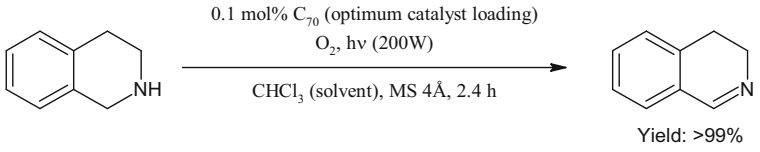

Scheme 9.15 0.38 mmol of reactant subjected to reaction with 5 ml solvent. $CHCl_3$ was saturated with O_2 by bubbling 11.5 mM O_2 in the solvent. Reaction mixture was exposed to air from an open flask. 200 W tungsten filament (white light) lamp placed at a height of 20 cm was used for irradiation

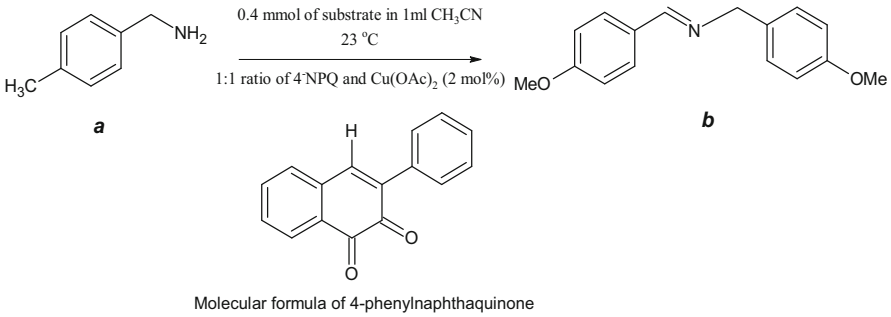

Scheme 9.16a Oxidative coupling of amines in presence of biomimetic quinone (4-NPQ)

molecular oxygen for the dehydrogenation of amines (Goriya et al. 2016). The high redox activity of o-naphthoquinones had been used for the preparation of biomimetic catalysts, which are capable of dehydrogenation of primary amines to convert homo-, cross-coupled amines and secondary amines into imines and ketimines (Goriya et al. 2016). Upon stirring *p*-methoxy benzylamine as a model substrate with various *o*-naphthaquinones, the homo-coupled imine '***b***' (as shown in Scheme 9.16a) was found to be formed with a yield of more than 99% 4-phenyl naphthoquinone (4-NPQ) was employed as catalyst in the presence of CH_3CN solvent and Cu $(OAc)_2$ promoter (2 mol% of both 4-NPQ and $Cu(OAc)_2$).

The equation depicted in Scheme 9.16a are reported to require a longer reaction time of 60 h to achieve completion when performed under ambient air conditions. An interesting observation being the use of hexylamine and 1-phenylethylamine under the aforementioned optimum dehydrogenation condition gave only a meagre imine formation in the order of just >1% and >5%, respectively. This suggests the shortcoming of 4-NPQ as a catalyst for the selective oxidation of primary aliphatic amines. However, the catalyst worked effectively for the selective oxidation as in case of secondary and other unreactive amines (refer Scheme 9.16b), with high yields of target products. Benzimidazole (**3**) was formed with yield of 86%. Secondary amines like tetrahydroisoquinoline were also effectively oxidised in presence of co-catalyst such as Ag_2CO_3. However, aliphatic amines like indoline were inert for most of the process conditions used for the study, and a more theoretical insight into the cooperative catalysis of 4-NPQ and that of $Cu(OAc)_2$, TFA and Ag_2CO_3 as co-catalysts is still required.

In the case of singlet oxygen-assisted oxidation of primary and secondary amines, the selectivity is largely based on the bond dissociation energy of C-H bonds that lie adjacent to the nitrogen atom (Ushakov et al. 2015). This exhibits the case that the oxygen-mediated (aerobic) oxidation proceeds by means of hydrogen abstraction.

Osmium-based complexes, namely, $[Os(fptz)_2(PPhMe_2)_2]$ (**1**), $[Os(fptz)_2(CO)(PPh_3)]$ (**2**) and $[Os(fptz)_2(CO)(Py)]$ (**3**) (where fptz = 3-trifluoromethyl-5-pyridyl-1,2,4-triazole), have been reported to have properties that are conducive to promote the aerobic oxidative coupling of amines into imines (Li et al. 2016b). This type of Os^{2+}-based complexes for the photocatalytic aerobic oxidation is advantageous as

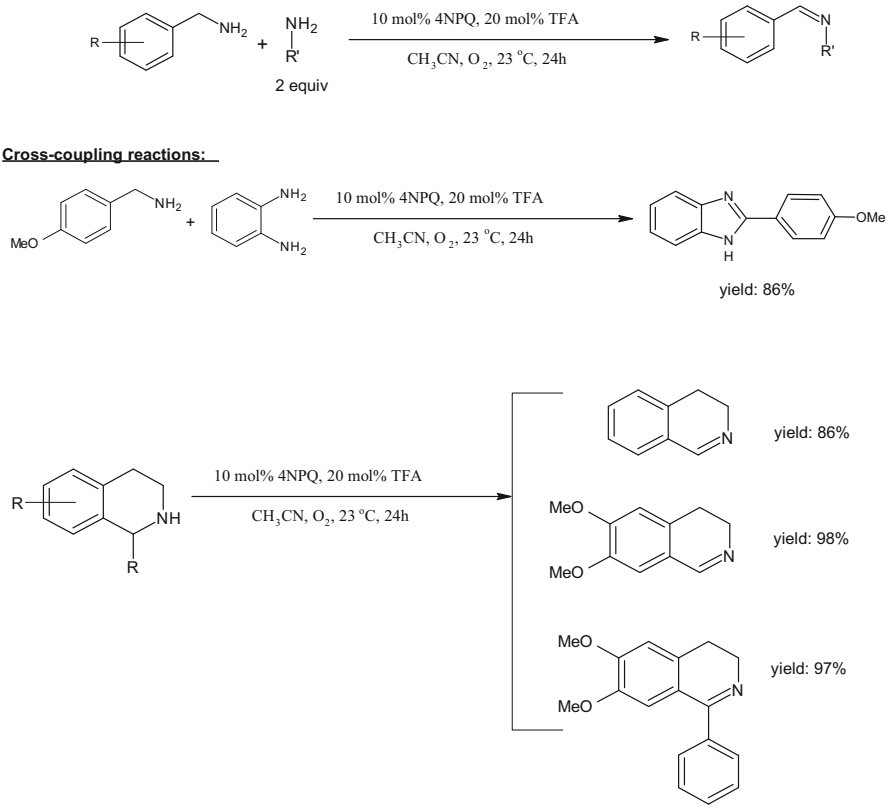

Scheme 9.16b Cross-coupling with biomimetic catalyst (4-NPQ)

they possess a lower energy absorption band, which is capable of absorbing and utilising energy even from the visible light region. However, due to stronger visible light ($\lambda > 420$ nm) absorption and longer lifetime of the triplet state, catalyst (**1**) was capable of functioning as the most effective catalyst for the oxidative coupling of a wide range of amines into their corresponding imines even under very low catalyst loading of 0.06 mol%. For a typical amine oxidation process, the requirements are 2 mmol of substrate, 1 mg of the Os-based catalyst, 50 ml acetonitrile in an open vessel and irradiating with a Xe lamp ($\lambda > 420$ nm) at room temperature. By using this recipe, benzylamine was converted into *N*-benzylbenzaldimine as a sole product with a satisfactory yield of 99%.

9.4 Photocatalytic Cyanation

Organoboron compounds are one of the most important classes of organic compounds that have a wide range of application in organic transformation reactions, and such compounds have been successfully used in organic syntheses for a long time now (Dewar and Kubba 1959; Frisch and Beller 2005; Miyaura 2008; Qiu et al. 2010). Owing to the increasing interest in the use of single-electron transfer (SET) for the organic transformation reactions, Dai et al. (2016) reported the direct photocatalytic cyanation of alkyltrifluoroborates to alkyl nitriles. This is interesting from the view that it is the first ever reported possibility of using photoredox catalysis to transform alkyltrifluoroborates to alkyl nitriles. The reaction involved the use of $[Ru(bpy)_3](PF_6)_2$ as the photocatalyst. Under acidic reaction conditions, the reaction was found to provide a relatively good yield (up to 75%) of desired products (Scheme 9.17a).

The main purpose solved by using an acidic reaction condition (TFA additive) is that it can protonate the carboxyl anion formed from BI-OAc during the reaction, which can quench the excited photocatalyst with that of the reactant (**1**). This photocatalyst has also been successfully applied to deboronative cyanation of secondary and tertiary alkyltrifluoroborates as given in Scheme 9.17b. However, in this case an improved yield of up to 62% was reported.

Though there is an increasing attention being paid towards the usage of organic photocatalysts for the production of novel radical intermediates, the need to use Ru-

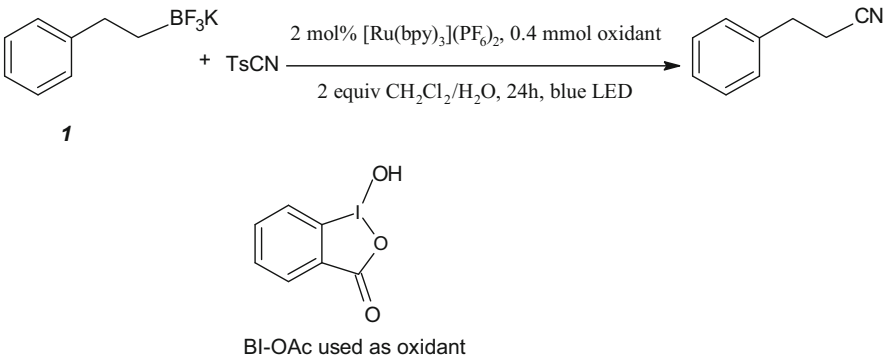

Scheme 9.17a Cyanation of alkyltrifluoroborates to alkyl nitriles with $[Ru(bpy)_3](PF_6)_2$ as photocatalyst

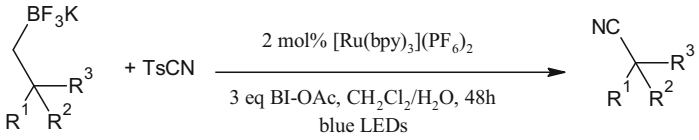

Scheme 9.17b Deboronative cyanation of 2° and 3° alkyltrifluoroborates

and Ir-based compounds as photocatalysts is a major hindrance owing to their recovery and cost. This has often prompted the need to look out for non-metallic photocatalytic materials for organic synthesis applications. Concomitantly in a study by Heitz et al. (2016), eosin-Y dye has used as an inexpensive photoredox catalyst for the coupling of Boc (*t*-butyloxy carbonyl group)-protected potassium α-aminomethyltrifluoroborates (Scheme 9.18a).

However, switching to a stronger oxidising 9-mesityl-10-methacridinium perchlorate ($MesAcr^+$) as photocatalyst has been observed to be able to provide a suitable condition for the nitrile formation without the need to add any external oxidants (Scheme 9.18b).

The photocatalytic cyanation proceeds in a mechanism very similar to that of Fig. 9.2; the photoredox catalyst either Eosin-Y or $MesACr^+$ (as in Schemes 9.18a and 9.18b, respectively) gets excited to singlet excited state, which then undergoes intersystem crossing to excited triplet state (which has a longer lifetime). This radical then appropriately oxidises the potassium alkyltrifluoroborate, forming an alkyl radical.

The visible light-driven photoredox catalysis-based oxidative Strecker reaction of tertiary amines to produce valuable α-aminonitriles has also been reported in

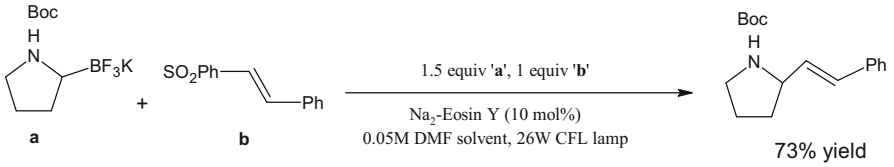

Scheme 9.18a Heitz's photoredox coupling with Eosin-Y dyes as photoredox catalyst

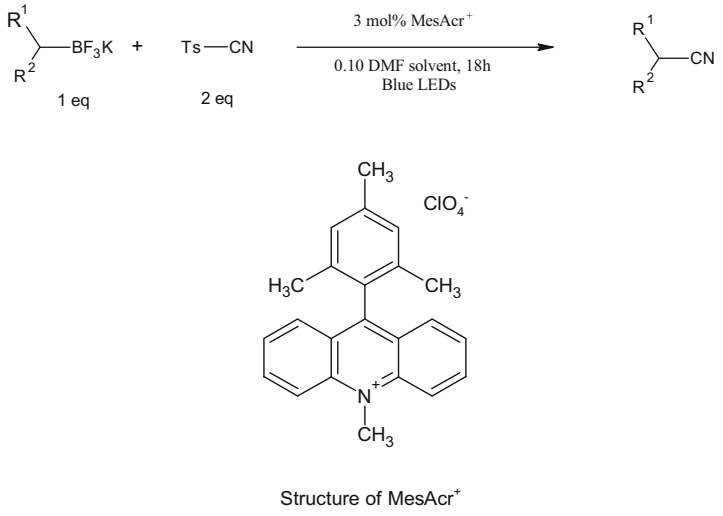

Scheme 9.18b $MesAcr^+$ as photocatalyst for nitrile synthesis

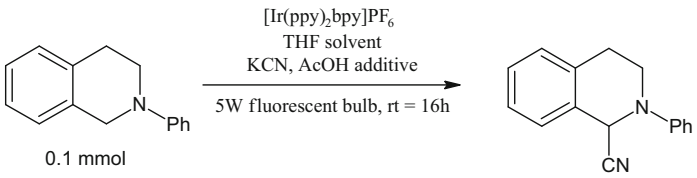

Scheme 9.19 Visible-light photoredox catalysed Strecker reaction of tertiary amines into α-aminonitriles

literature with high efficiencies. Rueping et al. (2011) use a 5 W fluorescent bulb, 0.1 mmol of reactant (2-phenyl-1,2,3,4-tetrahydroisoquinoline) and 1 mol% [Ir(ppy)$_2$bpy]PF$_6$ (ppy = 2-phenyl-pyridine, bpy = 2,2′-bipyridine) photocatalyst in THF solvent (1.0 equiv.), with KCN (1.2 equiv.), in presence of acetic acid (co-catalyst) as a cheap source for CN^- group (read Scheme 9.19). The reaction was capable of producing products with yield as high as 90% for a reaction time of up to 16 h. It was also concluded that the nature of solvents also plays a vital role in determining the effectiveness of the photoredox process, with polar and protic solvents producing poorer results and needing prolonged reaction times.

Several other oxidative cyanation studies similar to the reaction depicted in Scheme 9.19 are present in literature. On a similar note, Kumar et al. (2014) reported an effective visible light-driven photoredox catalysis for the oxidative cyanation of tertiary amines into their corresponding α-aminonitriles using chemically functionalised nanocrystalline TiO_2 grafted Ru(II)-polyazine complex. The synthesised TiO_2 grafted Ru(II)-polyazine complex-based catalysts exhibited a high yield of up to 96% of corresponding α-aminonitrile using 1 mol% of the catalyst within 4 h of reaction time.

Polyoxometalates are also a class of potential candidates for the photoredox catalysts for chemoselective functional group transformation because their properties can be tuned by altering their constituent elements and structures and also by introducing other extraneous metal cations. These advantages are further augmented by the fact that polyoxometalates are stable towards higher temperatures and oxidation than the otherwise commonly used organometallic complexes. Making use of these advantages, Suzuki et al. (2014) synthesised a visible light active tetranuclear cerium(III)-based silicotungstate $TBA_6[\{Ce(H_2O)\}_2\{Ce(CH_3CN)\}_2(\mu_4\text{-}O)(\gamma\text{-}SiW_{10}O_{36})_2]$ (CePOM; TBA= tetra-*n*-butylammonium). This catalyst system upon irradiation with visible light of $\lambda > 400$ nm, the photocatalytic α-cyanation of tertiary amines, is reported to occur smoothly under oxygen-rich atmosphere as sole oxidant and yields of up to 90% within a time period of about 26 h (Scheme 9.20).

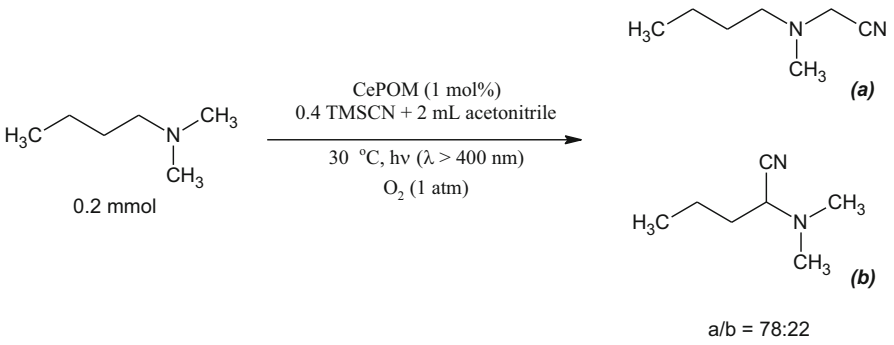

Scheme 9.20 Photocatalytic α-cyanation of tertiary amines with polyoxometalates

9.5 Photocatalytic Cycloaddition and C-C Bond Formation Reactions

Metal-free organic compounds have been employed successfully for the photocatalytic [3+2] cyclo-additive synthesis of pyrrole under visible light radiation (Xuan et al. 2014). Here, a formal [3+2] cycloaddition of 2,3-diphenyl-2*H*-azirine and dimethyl-2-butynediaote was carried out under visible light radiation obtained using 7W blue LEDs, where 9-mesityl-10-methylacridinium perchlorate functioned as the redox catalyst (Scheme 9.21). This reaction is proposed to occur by the single-electron oxidation of 2,3-diphenyl-2*H*-azirine (***a***), followed by the coupling with dimethyl-2-butynediaote (***b***), leading to formation of the desired product (***c***) with up to 98% yield.

The mechanism behind the aforementioned reaction is explained in Scheme 9.21a. Here, the single-electron oxidation by excited photocatalyst and the 2H-azirine **(*a*)** occurs, which leads to ring-opening, to produce 2-aza allyl cation. This 2-aza allyl cation when added to dimethyl-2-butynediaote **(*b*)** produces a zwitterionic intermediate that undergoes intramolecular cyclisation and aromatisation to produce the polysubstituted pyrrole product **(*c*)**.

Notably, the synthesis of highly substituted pyrrole product (***4***) by means of formal [3+2] cycloaddition of vinyl azide (***1***) ($R^1 = R^2 = Ph$) using a photocatalytic cascade process that makes use of both energy transfer and photoredox catalysis has also been reported (Scheme 9.21b, c).

It is to be noted that highly functionalised polycyclic quinoxalines could also be synthesised using visible light photoredox catalysis (He et al. 2014). In a work by Jamison et al., highly functionalised pyrrolo[1,2-a]quinoxalines were synthesised by a novel visible light-driven decarboxylative radical cyclisation of ortho-substituted aryl-isocyanides and radicals produced from phenyliodine (III) dicarboxylate. The reaction involved the photoredox transformation between 1-(2-isocyanophenol)-1*H*-pyrrole (***1***) and phenyliodine(III) dicyclohexanecarboxylate (***2***), using the Ir-based complex [*fac*-Ir(ppy)$_3$] as the photocatalyst (Schemes 9.22a and 9.22b). In this case,

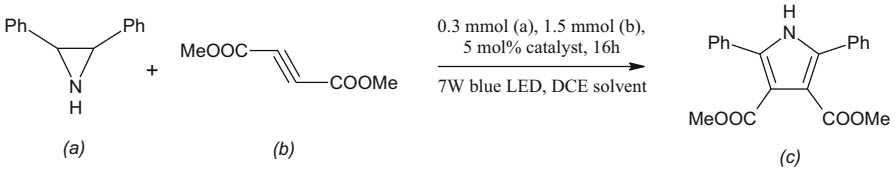

Scheme 9.21a Metal-free organic compounds as photocatalytic [3+2] cyclo-addition reactions; (Xuan et al. 2014)

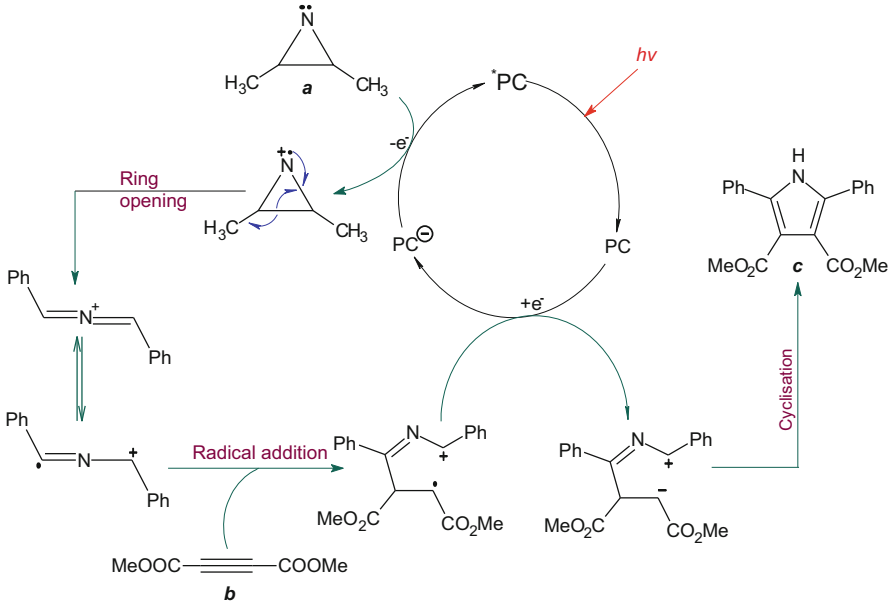

Scheme 9.21b Mechanistic insight into Scheme 9.21a

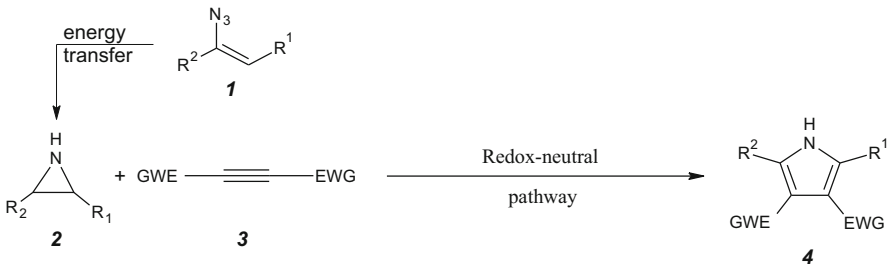

Scheme 9.21c Reaction conditions – 0.3 mmol of (*1*), 1.5 mmol of (*3*), 0.015 mmol of photocatalyst $MesAcr^+$ in 3 mL DCE for 16 h under irradiation of 450–460 nm blue LED

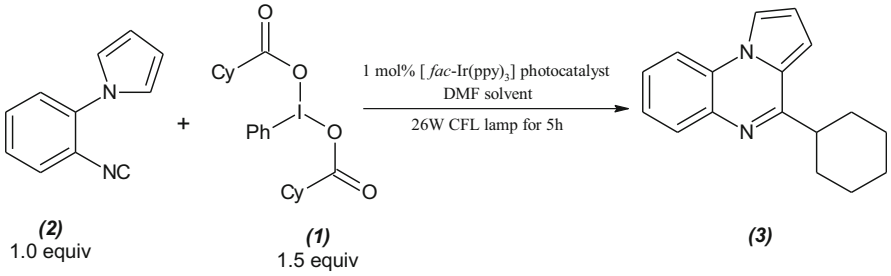

Scheme 9.22a Visible light-driven photocatalytic decarboxylative radical cyclisation

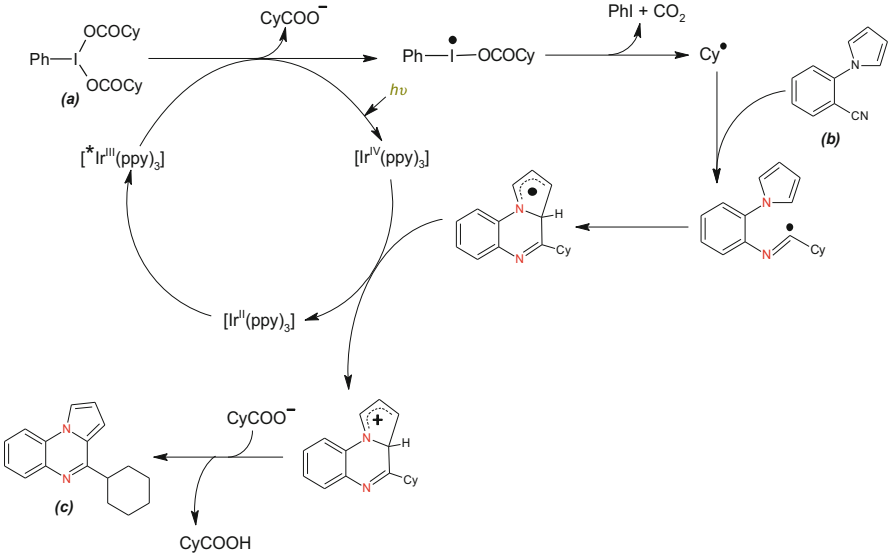

Scheme 9.22b A mechanistic insight into Scheme 9.22a

the resultant 4-cyclohexylpyrrolo[1,2-a]quinoxaline product (***3***) was reported to be formed with a yield of 73%.

Additionally, the [2+2] cycloaddition of bis(enone) has been investigated by means of single-electron reduction of enones by using $Ru(bipy)_3^{2+}$ chromophore under visible light radiation of $\lambda_{max} = 452$ nm (Ischay et al. 2008). This leads to the formation of a photoexcited state $^{\bullet}Ru(bipy)_3^{2+}$, which is a powerful redox catalyst that can oxidise or reduce a variety of organic substrates (Scheme 9.23). Apart from its long excited state of 600 ns, its high quantum efficiency of formation and exceptionally good chemical stability of its ground-state precursors are the prime reasons behind the extensive use of $Ru(bipy)_3^{2+}$ for organic synthesis (Cano-Yelo and Deronzier 1984a, b; Zen et al. 2003; Tyson et al. 2013).

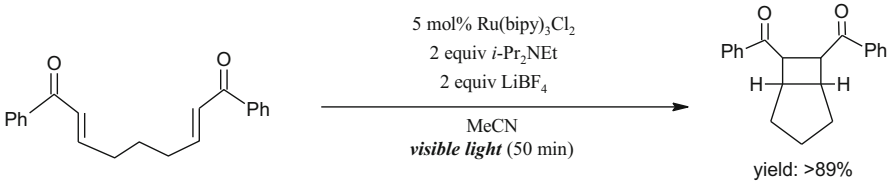

Scheme 9.23 Visible light driven [2+2] cycloaddition of bis(enones); (Ischay et al. 2008)

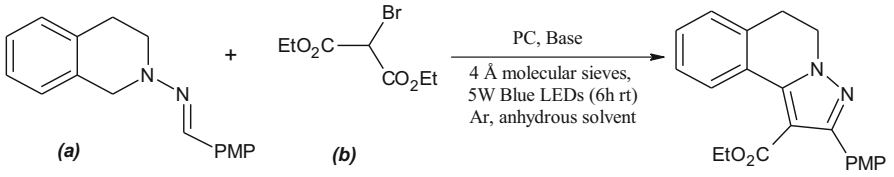

Scheme 9.24a Reaction conditions: 1:2.5 ratio of *a*:*b*, 0.2 mmol of ***a***; 0.002 mmol of 1 mol% photocatalyst; 0.6 mmol (3 equiv) of K_2HPO_4; 2 ml anhydrous acetonitrile solvent; 100 mg of 4 Å molecular sieves; 5 W blue LED irradiation for 16 h; PMP = 4-methoxyphenyl group

It is also interesting to observe that the reaction in Scheme 9.23 has been reported to not occur in the absence of *i*-Pr_2NEt, even at elevated catalyst loadings. This is suggestive that the cycloaddition is not initiated directly by the excited $Ru(bipy)_3^{2+}$ moieties but by the $Ru(bipy)_3^{+}$ moieties produced by the reductive quenching of the amine. Finally, the addition of $LiBF_4$ helps to produce a homogeneous reaction mixture, due to the increased solubility of $Ru(bipy)_3(BF)_4$ in dry acetonitrile.

While it is known that the photoredox synthesis of organic compounds can be carried out by means of adopting either a reductive or an oxidative quenching cycle to accomplish single-electron transfer (Nguyen et al. 2011; Wallentin et al. 2012; Xi et al. 2013; Miyake and Theriot 2014), it has however been reported that multiple quenching cycles can be incorporated in a single reaction (Cheng et al. 2017). This idea has been extended to the purpose of synthesising pyrazole-based compounds by means of formal [4+1] annulation and aromatisation of hydrazones, with diethyl-2-bromomlonate as reactants. The formal addition was carried out by using a mixture of the hydrazone (***1***) with diethyl-2-bromomalonate (in 1:2.5 ratio), with [Ir $(ppy)_2$dtbbpy][PF_6] as the photocatalyst in the presence of anhydrous K_2HPO_4 and 4 Å molecular sieve under blue LED of 5 W rating for a reaction time of 16 h.

The above reaction in Scheme 9.24a takes place via three steps, namely:

1. Oxidative coupling of the hydrazone '***a***' with diethyl-2-bromomalonate via an oxidative quenching cycle to produce a hydrazone '***b***.'
2. The photo-oxidation by the reductive quenching cycle of ***b*** takes place to produce a hydrazinium compound, which is followed by an intramolecular Mannich reaction, to produce dihydropyrazole derivatives '***c***'.
3. Decarboxylation and photo-oxidation of the dihydropyrazole takes place to produce the final pyrazole '***d***', by means of a final reductive quenching cycle.

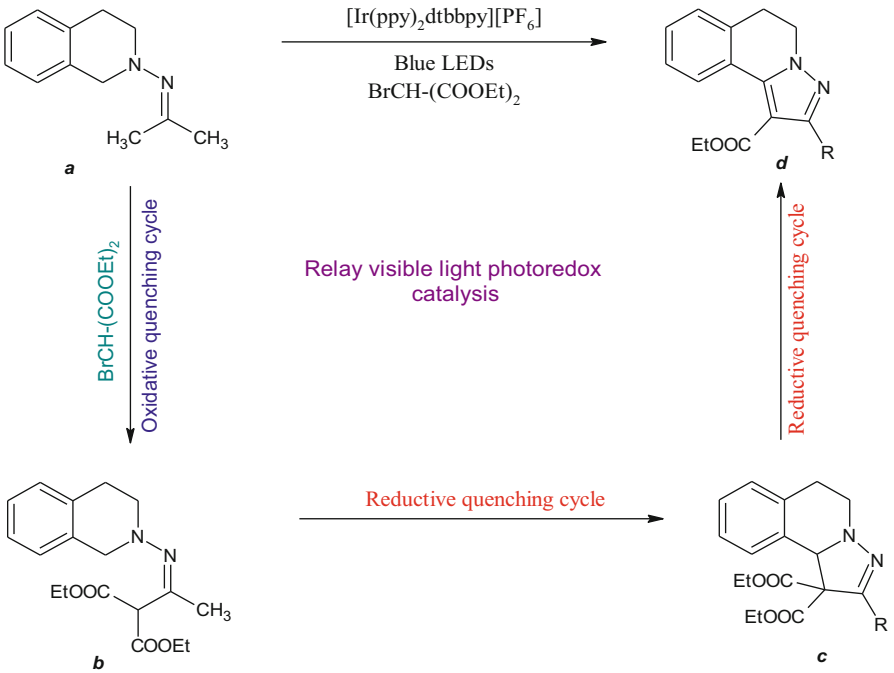

Scheme 9.24b Synthesis of pyrazole based compounds by formal [4+1] annulation and aromatisation of hydrazones

These steps are discussed in Scheme 9.24b.

In case of $Ru(bipy)_3^{2+}$ catalysed intermolecular [2+2] cycloaddition reactions of enones, it is observed that only aryl-enones could be used for the reaction, primarily due to the greater ease of producing the radical anion intermediate; but it can very well be replaced by any other suitable Michael acceptor as the reacting partner. But, in case of intermolecular hetero-coupling processes, it should be observed that the reactant must be a more reactive Michael acceptor than the enone so as to minimise the undesired homo-dimerisation. This has been reported in the work of Du and Yoon (2009), wherein a crossed intermolecular [2+2] cycloadditions of acyclic enones have been carried out under visible light by using $Ru(bipy)_3^{2+}$ as photocatalysts.

Another important feature about the reaction presented in Scheme 9.25 is that the reaction is initiated by the photoexcitation of the $Ru(bipy)_3Cl_2$ catalyst, and it does not access the electronically excited states of enone, thereby avoiding some of the synthetic limitations of cycloadditions, as when conducted by conventional UV photolysis.

A rapid diastereoselective synthesis of quaternary carbon stereo-centres within a cyclopentane scaffold, using visible light photocatalytic [3+2] cycloadditions of aryl cyclopropyl ketones, has also been accomplished successfully using visible light

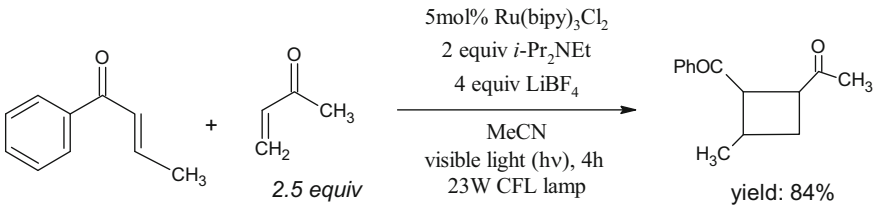

Scheme 9.25 Visible light driven [2+2] cycloaddition of enones

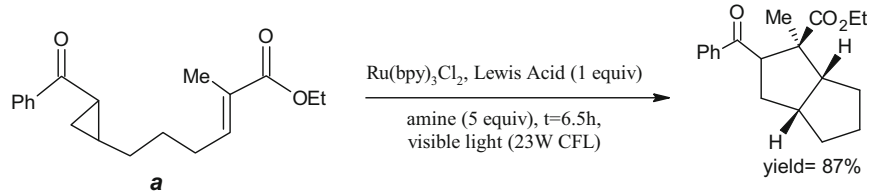

Scheme 9.26a Reaction conditions: $La(OTf)_3$ as lewis acid; $Ru(bpy)_3Cl_2$ (2.5 mol% Ru); TMEDE as amine (5 equiv); 200 wt% $MgSO_4$, MeCN solvent, temperature = 23 °C

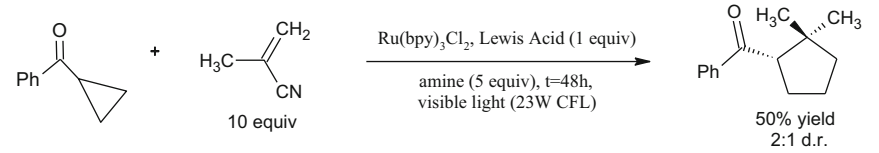

Scheme 9.26b Visible light driven intermolecular [3+2] cycloaddition reaction

irradiation by Lu et al. (2011). The reported reaction involving the single-electron reduction induced formal [3+2] cycloaddition of aryl cyclopropyl ketones with olefinic compounds is capable of producing highly substituted cyclopentane ring systems (Scheme 9.26a). The single-electron reduction of the aryl cyclopropyl ketone produces the corresponding radical anion, which undergoes radical cyclisation that upon oxidation produces the product of the formal intramolecular [3+2] cycloaddition product of '***a***'.

The Lewis acid serves to activate the carbonyl compound '***a***' towards the cycloaddition. Even though the drying agent $MgSO_4$ is not necessary to be included in the reaction, omitting it has been reported to causing a decreased yield of the cyclopentane product and also causes a poorer reproducibility of the reaction. Surprisingly, intermolecular [3+2] cycloaddition reactions were also possible to be conducted under the similar reaction conditions. However, the reaction proceeds to provide only a moderate yield of the cycloadduct along with lower diastereoselectivity (Scheme 9.26b).

Diels-Alder reaction is one of the reactions of paramount importance with regard to C-C bond formation in synthetic organic chemistry. In this regard, it has been

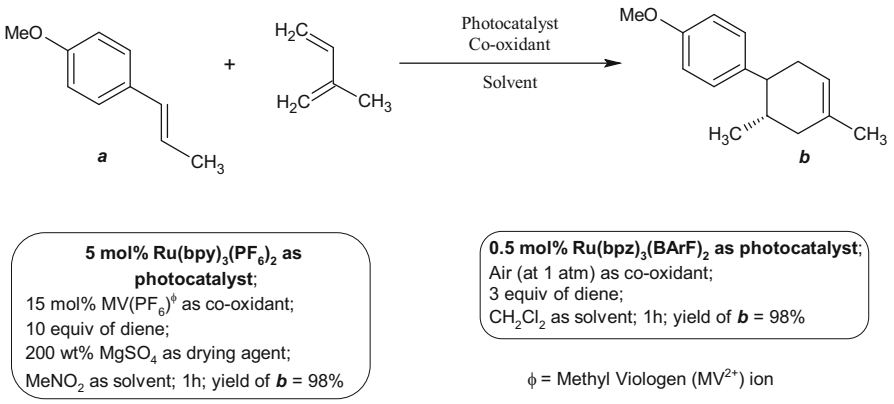

Scheme 9.27 Visible light driven [4+2] cycloaddition via Diels-Alder reaction catalysed by Ru^{2+} polypyridyl complexes

recently reported by Lin et al. (2011) that electron-rich dienophiles can undergo [4 +2] cycloaddition via Diels-Alder reactions, upon irradiation with visible light and Ru^{2+} polypyridyl complexes (Scheme 9.27). This reaction is as a result of the metal to ligand charge transfer (MLCT) in the $Ru(bp)_3^{2+}$ chromophore, upon irradiating with visible light in the region of $\lambda_{max} = 440$ nm. This produces the redox active photoexcited $Ru^{\bullet}(bpy)_3^{2+}$ cations, which oxidise the reactant (***a***) and activate it towards the [4+2] cycloaddition, thereby forming the Diels-Alder product (***b***). Oxygen converts the reduced $Ru(bpy)_3^{+}$ produced in vivo of the reaction, back into the photoactive $Ru(bpy)_3^{2+}$, which can initiate a series of radical cation chains.

Apart from the aforementioned result, the authors have also reported the applicability of the $Ru(bpy)_3^{2+}/MV^{2+}$ catalyst system to be limited, due to the rapid back electron transfer from the reduced MV^{+} cations to the dienophile radical cation. In case of the reactions involving sterically demanding dienes or electron deficient dienophiles, it has been reported that longer reaction times or higher catalyst loading was required to obtain a reasonable yield of the [4+2] cycloadduct.

Guo et al. (2013) reported a photocatalytic system based on iodo-bodipy dyes immobilised on porous siliceous molecular sieve (KIT-1) for the synthesis of pyrrolo [2,1-*a*]isoquinoline from *N*-phenylmaleimides, via a [3+2] photoredox cyclisation reaction. This immobilisation of iodo-bodipy molecules on the molecular sieves allows the recovery and reuse of the photocatalyst, thereby reducing its cost for practical applications. Due to the uniform pore size, three-dimensional structure and high surface area immobilisation of iodo-bodipy molecules on KIT-1 substrate do not have any deleterious effect on the catalytic activity. Also, the triplet excited state of the prepared KIT-1B photocatalyst was found to be 55.3 μs. Thus, the prepared KIT-1B photocatalyst is capable of providing high conversion efficiency of *N*-phenylmaleimides via a single-electron transfer pathway (Scheme 9.28).

Of late, the SET-based [4+2] cyclisation has been reported by a number of research groups (Tucker et al. 2010; Zhang et al. 2014b; Xia et al. 2015). However,

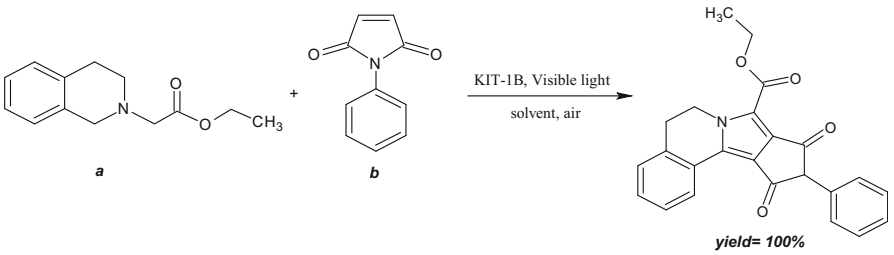

Scheme 9.28 Reaction conditions: 0.12 mmol of '***a***', 0.10 mmol of '***b***', 10 mg of KIT-1B, 1.2 equiv. NBS in 3 ml CH_3CN solvent, 35 W Xe arc lamp as light source, 20 °C, 1 h reaction time

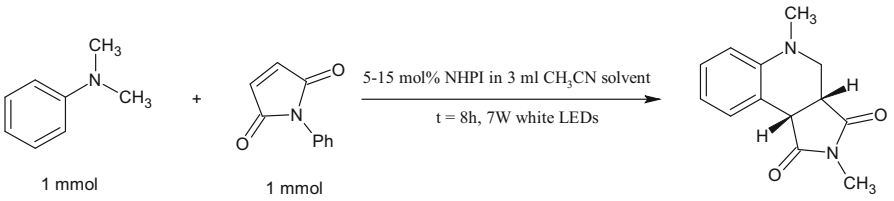

Scheme 9.29 SET-based, metal-free [4+2] radical cyclisation of N-methylaniline with maleimides

it is observable that most of these reactions involve the use of transition metal-based coordination compounds or decomposable dyes as photocatalysts, which are often expensive and also involve harsh reaction conditions. Thus, a metal-free [4+2] radical cyclisation of *N*-methylaniline with maleimides has been reported by Yadav and Yadav (2017), in which *N*-hydroxyphthalimide (NHPI) acts as the visible light photocatalyst. *N*-hydroxyphthalimide (NHPI) under thermal conditions using an oxidant is well known for quite a long time for functionalising C(sp^3)-H bonds to produce alkyl radicals. The *N*-hydroxyphthalimide molecule acts as the precursor for the phthalimide-*N*-oxyl (PINO) radical in the presence visible light due to the homolysis of the O-H bond. The PINO radical thus produced has an excellent ability of C(sp^3)-H activation of *N*-methylanilines to form an α-amino radical without use of any additional oxidants. A very similar, metal-free [4+2] radical cyclisation of *N*-methylaniline with maleimides has also been reported by Tang et al. (2015), in which surface-modified TiO_2 nanoparticles with highly dispersed NiO act as the visible light photocatalyst. This method was found to be capable of producing products with a high yield of up to 86% (Scheme 9.29).

Photocatalytic cascade reaction has also been successfully employed for the purpose of α-amino carbon radical-based cyclisation (radical addition) cascade (Zhao et al. 2016). It has been reported that $[Ir(ppy)_2(dtbby)]^+$-based complexes can act as photocatalysts for the single-electron transfer-based cyclisation between the photo-generated α-amino radical and aroylhydrazones to produce a diverse range of functionalised hydrazide containing chroman-2-ones and dihydroquinolin-2-ones (Scheme 9.30). Consequently, this reaction scheme is also reported to be tolerable

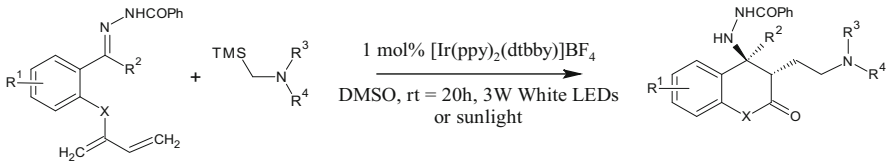

Scheme 9.30 Zhao's photocatalytic cascade reaction for carbon radical-based cyclisation; (Zhao et al. 2016)

towards a wide variety of α-silylamines and aroylhydrazones, thereby capable of producing the corresponding highly functionalised hydrazide-containing chroman-2-ones and dihydroquinolin-2-ones in reasonably impressive yields and commendable diastereoselectivities. This reaction is of high commercial importance due to the fact that chroman-2-ones and dihydroquinolin-2-ones are present in many biologically active natural products and pharmaceuticals (Ronad et al. 2008; Puri et al. 2009; Ingale et al. 2012; Kamat et al. 2015).

Towards the end of 2014, Blechert and co-workers had developed an efficient visible light-induced photocatalysis reaction scheme using mesoporous graphitic carbon nitride (mpg-C_3N_4) for the metal-free radical cyclisation of 2-bromo-1,3-dicarbonyl compounds (Woźnica et al. 2014). A continuous flow reactor had been employed for this reaction, and it has been observed that the reaction time decreased considerably upon using the proposed reaction setup. From Scheme 9.31a, it can be observed that when tetrahydrofuran is used as a solvent for the reaction, the reaction time decreased to a great extent. This suggests that tetrahydrofuran is not just a solvent but also a reagent; and it acts as an electron donor in this reaction.

Initially, the irradiation of mpg-C_3N_4 catalyst leads to charge separation. Consequently, the excited electrons formed by charge separation reduce the activated C-Br bond, to produce the free radical intermediate I, which by means of fast cyclisation forms the radical II. Hydrogen abstraction from II takes place in presence of THF to produce the cyclic compound ***1*** and the tetrahydrofuranyl radical III. The oxidation of the radical III forms the cation IV, which completes the photoredox reaction cycle. A detailed interpretation of the reaction mechanism as reported by the authors is presented in Scheme 9.31b.

In all of the abovementioned studies, one may observe that single-electron transfer (SET) forms an integral part of photocatalytic cycloaddition reaction. The main deciding factor for a successful accomplishment of single-electron transfer is the strict criteria for reduction potentials of the enone (Zeitler 2009). Thus, whenever metal-mediated redox photocatalysts are employed, they can act as effective triplet photosensitisers to carry out the reactions, which are non-conducive for single-electron transfer reactions. This has been reported by Liu et al. (2015), wherein under 3 W blue LED irradiation, the visible light-driven intermolecular [2+2] cycloadditions of coumarin-3-corboxylates and acrylamide derivatives have been carried out. These reactions took place in presence of an iridium complex (FIrPiC) as

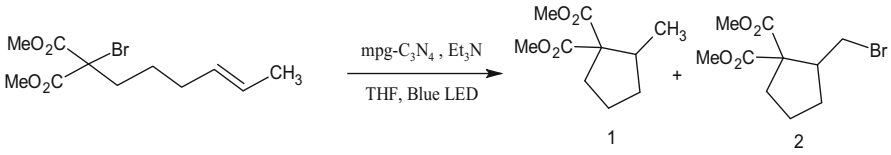

Scheme 9.31a Reaction conditions: reactor with mpg-C_3N_4 (2.5 wt%), '***a***' (0.04 mol), solvent (THF) 5 mL; t_R (reactor residence time) = 5 min; flow rate = 0.124 mL/min; blue LEDs (λ = 420–425 nm); conversion = >99%

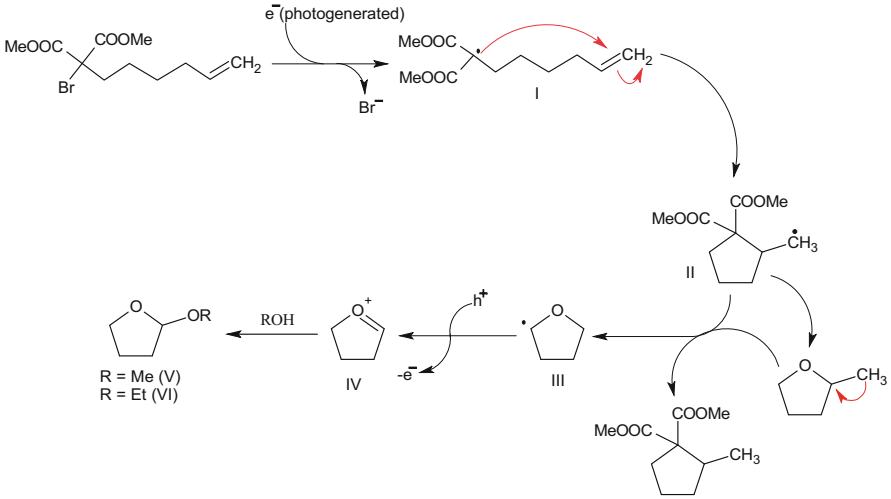

Scheme 9.31b Mechanism of the reaction depicted in Scheme 9.31a

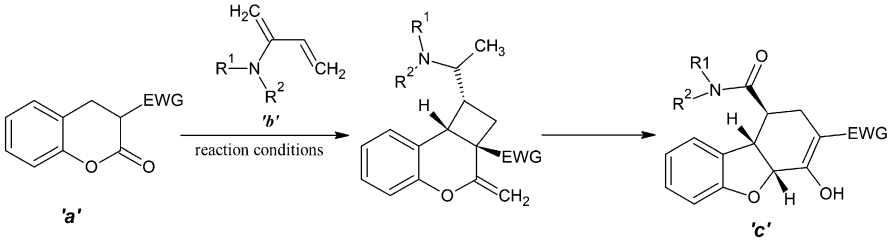

Scheme 9.32 Reaction conditions: 0.20 mmol '***a***' with 0.24 mmol '***b***' in presence of 0.5 mol% photocatalyst in 2 ml solvent, irradiated with 3 W blue LED light at room temperature for 24 h

a photosensitiser, by means of an energy transfer process. In this case, tetrahydrodibenzofurans were produced in excellent yields (Scheme 9.32).

The possibility of using nano-TiO_2 particles as photocatalysts for the selective cyclisation of amino acids in deaerated aqueous suspensions has been known ever since the seminal work published by Ohtani et al. (1990) in the year 1990. Ever

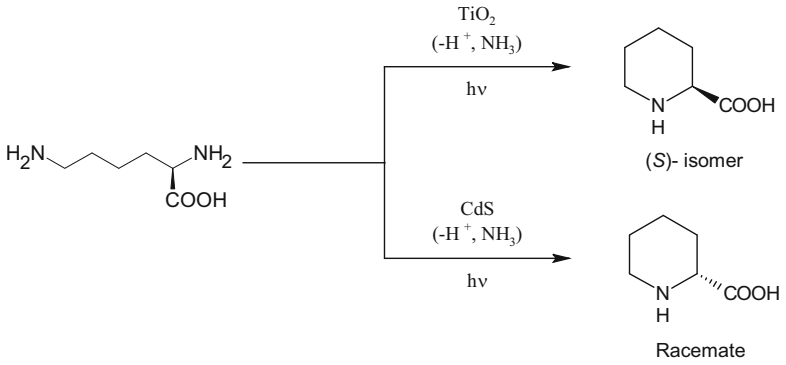

Scheme 9.33 Photocatalytic selective cyclisation of amino acids in deaerated aqueous solutions- a representative reaction

since, in a series of articles by the same research group (Ohtani et al. 1995a, b), a formal, non-redox deamination cyclisation processes were reported. The conversion of lysine into pipecolinic acid (piperidine-2-carboxylic acid) by photoredox cyclisation via the aforementioned process is described in Scheme 9.33 taking Ohtani et al. (2003) as reference. This reaction is reported to be effectively catalysed by both TiO_2 and CdS nanoparticles. When the process was catalysed using TiO_2, the pipecolinic acid (PCA) product retained its (*S*)-configuration entirely. But, a racemic form of the product was formed when CdS was used as photocatalyst. A high value of selectivity of up to 77% and a conversion of 92% was achieved using the hydrothermal crystallised TiO_2. Thus, a one-step diastereoselective synthesis of 2,6-disubstituted piperidine was successfully performed at room temperature by activated CdS particles in their aqueous suspension. This suggests that the photocatalytic selectivity can be tuned by altering the catalyst properties or the experimental conditions of the reaction. In these reactions, one of the amino groups in lysine is oxidised by the photo-generated holes into corresponding imines, which get subsequently hydrolysed into carbonyl derivatives. Finally, the aldehyde/ketone produced is condensed with an amino group on another end of the molecule to form a cyclic Schiff base type of intermediate, from which the desired product PCA is finally obtained by reduction with e^-.

Similarly, a novel photoredox route for the synthesis of coumarins from phenanthrenes using light-irradiated TiO_2 particles was reported by Higashida et al. (2006) in 2006. In this work, an 8% aqueous solution of phenanthrene-acetonitrile mixture in presence of molecular oxygen containing Degussa P25-TiO_2 photocatalysts was irradiated at $\lambda > 340$ nm which in turn provided a product yield of up to 45% after a reaction time of 100 h. The authors have also reported a quantum efficiency of up to 17% at $\lambda = 365$ nm (Scheme 9.34). This reaction is worthy to be noted because of the commercial importance of coumarin-based compounds, as they can act as intermediates to a number of chemicals such as pharmaceuticals and fluorescent dyes (Rohini K and PS 2014). Apart from these uses, coumarins are also used as gain

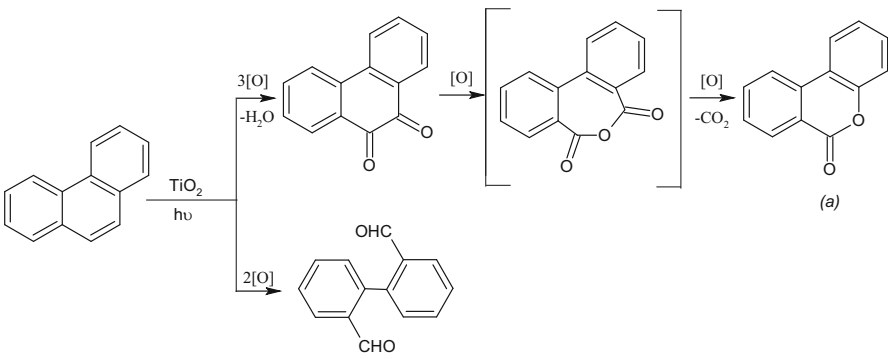

Scheme 9.34 Photoredox synthesis of coumarins from phenanthrenes

media in blue-green tunable organic lasers (Tuccio et al. 1973). The primary advantage of this route is that it can eliminate the numerous steps involved in synthesis of **(*a*)** from commercial reagents by using conventional synthesis techniques (Togo et al. 1995; Bowman et al. 2000).

9.6 Miscellaneous Reactions

In the year of 2014, Baar and Blechert (2015) reported the application of heterogeneous photoredox catalysis for the fluoroalkylation applications. Under a visible light irradiation obtained using a 60 W energy saving bulb and a reaction time of 48 h in presence of mpg-C_3N_4 as photocatalyst, trifluoromethylation and perfluoroalkylations of various arenes have been reported to take place successfully. The reaction was carried out in presence of CF_3SO_2Cl as the precursor to CF_3 radicals (Scheme 9.35).

A radical (cationic) pathway-based trifluoromethylation of enecarbamates has been reported by Carboni et al. (2014). Here, a three-component reaction of an enecarbamate, alkyl halide and an alcohol had been realised using $[Ru(bpy)_3(PF_6)_2]$ as the photoredox catalyst, while Togni's reagent served as the source for -CF_3 group (Scheme 9.36). This is important because of the potential biological activity of β-trifluoromethyl amine derivatives. The irradiation of the system with visible light excites the photocatalyst ($[Ru(bpy)_3^{2+}]$ into $^{\bullet}Ru(bpy)_3^{2+}$ species that are capable of acting as strong reducing agent. These photo-generated $^{\bullet}Ru(bpy)_3^{2+}$ species undergo single-electron transfer to liberate $^{\bullet}CF_3$ radicals from Togni's reagent. Consequently, the electrophilic $^{\bullet}CF_3$ adds regioselectively to the reactant '***a***' (an enecarbamate), to form an α-amido radical, which is rapidly oxidised into *N*-acyliminium cation by single-electron transfer from $Ru(bpy)_3^{3+}$. Finally, by means of nucleophilic trapping by the alcohol '***c***' in presence of KCN forms the respective trifluoromethylated product '***d***'.

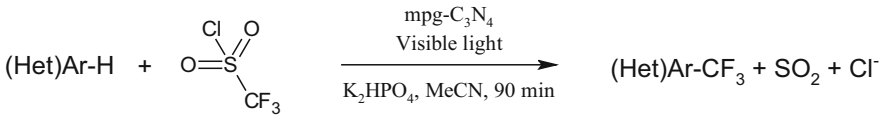

Scheme 9.35 Reaction conditions: 0.25–0.5 mmol of substrate, 1.2–2 equiv TfCl, mpg-C_3N_4 (15–25 mg/0.25 mmol substrate), 3 equiv. K_2HPO_4, MeCN (2 ml/0.25 mmol substrate), 60 W energy saving bulb, $t = 90$ min-3 day

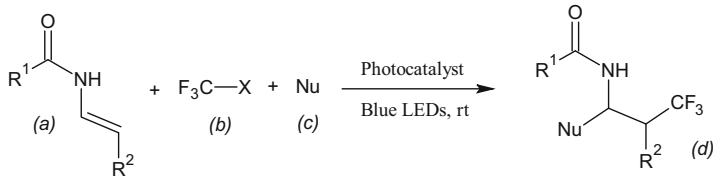

Scheme 9.36 Photocatalytic radical pathway-based trifluoromethylation of enecarbamates

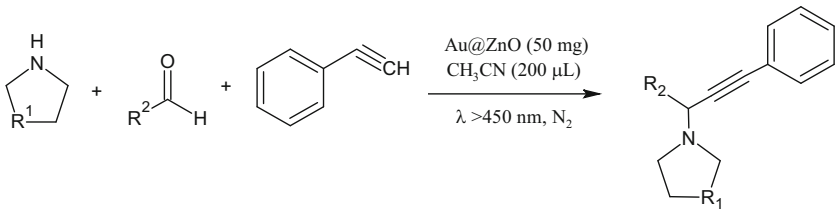

Scheme 9.37 Photocatalytic ternary coupling of aldehydes-amines and phenylacetylenes

On a similar note, the ternary coupling of an aldehyde, an amine and phenylacetylene to produce propargylamines using gold nanoparticles (Au-NPs) is also possible (Trost and Weiss 2009). However, this process is reported to proceed via a surface plasmon resonance (SPR) mechanism. In this case, the aldehyde reacts with the amine to produce enamines. The phenylacetylene then gets activated by Au-NP and then reacts with the enamine, to produce the corresponding propargylamines, by a one-pot ternary coupling (Scheme 9.37). The presence of ZnO along with Au-NPs provides a synergistic effect for the propargylamine synthesis. This is because of the constructive effect played by Zn-salts on alkynyl additions (Zani and Bolm 2006; Trost and Weiss 2009). Initially in the Au-NP@ZnO, the alkyne groups of phenylacetylene get adsorbed on Au-NPs due to their alkynophilicity (Engel and Dudley 2006; Patil et al. 2012) and also on ZnO. Lastly, the enamine produced between the aldehyde and the amine reacts with the alkynyl–[Au-NP@ZnO] complex to form the intended propargylamine.

In 2016, Zhang and co-workers unprecedentedly developed a photo-induced metal-free atom transfer radical polymerisation (ATRP) as a promising technique to eliminate the usage of transition metal-based catalysts in the synthesis of polymeric materials (Huang et al. 2016). The rationale for this concept is exhibited in

Scheme 9.38a. This work reportedly made use of 1,2,3,5-tetrakis(carbazol-9-yl)-4,6-dicyanobenzene (4CzIPN) as the organic photocatalyst for polymerisation of methyl methacrylate at ppm level dosage under blue LED lighting. The reaction was successfully carried out at room temperature with ethyl-α-bromophenyl acetate as the typical polymerisation initiator. The primary difficulty in this process is that a large quantity of the catalyst is required to control the molecular weight and the molecular weight distribution of the polymer. This can be due to the fact that the photocatalyst (4CzIPN) provides a long region absorbance ($\lambda \leq 480$ nm) and a strong reduction potential at excited state which allows the establishment of reversible deactivation equilibrium for an effective control of molecular weights and molecular weight distributions.

The reported polymerisation proceeded via four steps, namely, photoexcitation, activation, propagation and deactivation (Scheme 9.38b). When the photocatalyst

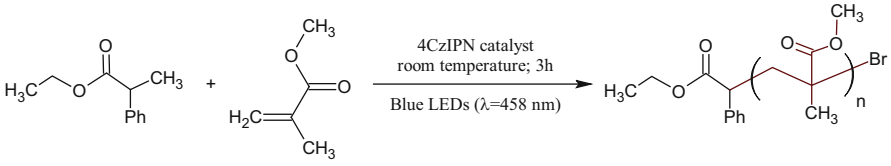

Scheme 9.38a Light driven metal-free atmon transfer radical polymerisation (ATRP) reaction

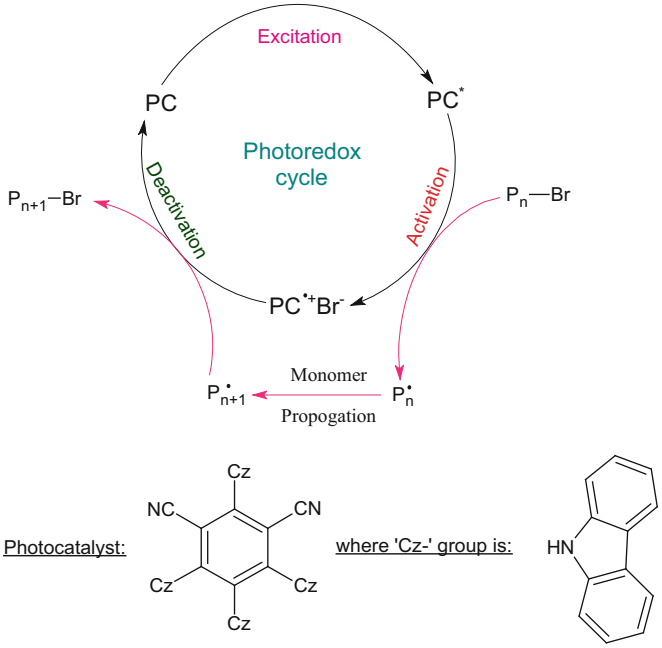

Scheme 9.38b Mechanism of the reaction depicted in Scheme 9.38a

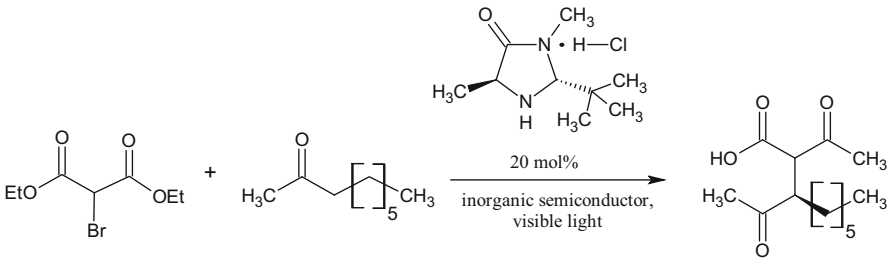

Scheme 9.39 Synergistic activity of organocatalysis and photoredox catalysis for enantioselective alkylation of aldehydes

(PC) was irradiated with light from the blue LEDs, it gets excited to $PC^{\bullet}$. These excited $PC^{\bullet}$ then activates the alkyl bromide $P_n^{\bullet}$, which initiates the further chain propagation. The intermediate state $PC^{\bullet+}Br^{-}$ moieties deactivate the $P_{n+1}^{\bullet}$ and return back to the ground state simultaneously.

In 2012 the successful merger of two unrelated types of catalysis, namely, photoredox catalysis and organocatalysis, was performed by Cherevatskaya and co-workers, in their effort to achieve the enantioselective α-alkylation of aldehydes by using MacMillan's chiral secondary amine (Cherevatskaya et al. 2012). The rationale behind this reaction is illustrated in Scheme 9.39. The reaction proceeds by means of photoredox mechanism. An electron transfer occurs from the conduction band of the photocatalyst (PC) to the halogenated carbonyl compound, causing a loss of a bromide anion and producing a α-carbonyl radical, which adds to the enamine obtained by condensation of the MacMillan catalyst with octanal. The α-amino radical is then oxidised by a hole from the valence band of photocatalyst, yielding the iminium ion that releases the product and regenerates the catalyst.

The direct C−H borylation with or without the use of transition metal catalysts has been presented in numerous works (Ishiyama et al. 2003; Yan et al. 2010; Zhang et al. 2014a). In many of these works, aromatic, nitrogenous compounds like amines, diazonium salts and triazenes are employed as the starting materials to prepare the alkyl boronic acid derivatives. In spite of the versatility of these techniques, limited substrates, harsh reaction conditions and long reaction periods are often an impediment to the process. Interestingly, photoredox catalysis has been employed by Jiang et al. (2016) for the borylation of aryl halides and subsequent aerobic oxidative hydroxylation. This reaction had been carried out using bis(pinacolato)diboron with *fac*-$Ir(ppy)_3$ as the photoredox catalyst to produce corresponding arylboronic esters and phenols. This reaction is interesting from the point that arylboronic acid and esters are of great importance in formation of aryl C-C or C-hetero bonds (Scheme 9.40).

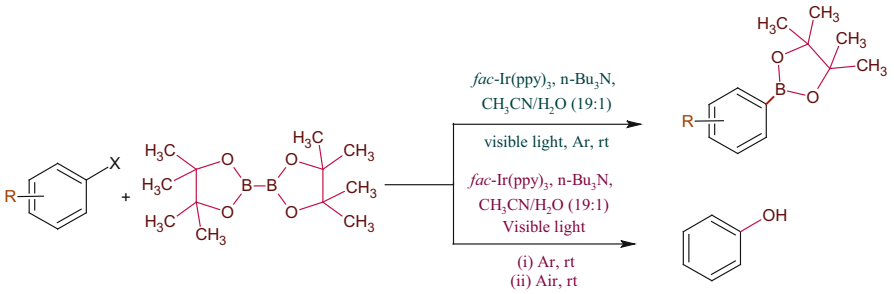

Scheme 9.40 Metal-free photocatalytic direct C-H borylation of aryl halides

9.7 Outlook

The usage of heterogeneous photoredox catalysis for synthesis of organic compounds involves a number of challenges as compared to its application in mineralisation of pollutants. Nevertheless, since photoredox catalysis is driven by means of a series of photo-induced charge transfers ($e^{-}-h^{+}$) to and from the surface of the photocatalyst that act as oxidising and reducing agents, a primary challenge to be addressed is to control and manipulate the charge transfer process so as to achieve selective transformation of functional groups, without producing undesirable transformations in the substrate. Similarly, the synergistic combination of two or more catalysis techniques itself presents an inherent advantage of identifying possible novel reaction mechanisms. The benign reaction conditions provided by photoredox catalysis provide the grounds to effectively combine it with a number of other catalysis techniques. This has been evident in case of the works by Macmillan, Sanford and Rovis. As has been envisaged, such novel combination of catalysis has made it possible for the development of brand new modes of reactions, with greater product yield.

Currently major gaps in knowledge pertaining to the application of photoredox catalysis technology for organic synthesis involve the proper selection and tuning of catalyst surface for improving the selectivity and yield of products. As observed by Friedmann et al. (2016), proper selection of photocatalyst is often required for optimised, selective synthesis, and this necessitates the selection of the photocatalyst to be performed on a case-by-case basis. This requires a detailed study with regard to understanding the property of the substrate, so as to select an appropriate photocatalyst that does not cause over-oxidation or non-selective transformation of the substrate. Such studies might include the matching of the CB and VB potentials with that of the organic compound of interest. The possibility of developing multicatalytic strategies that incorporate photoredox catalysis with a secondary catalytic system has gained interest as this technique can provide room for multisubstrate activation. Combined ‘dual’ photoredox-transition metal-catalysed syntheses are hence being investigated vigorously (Tellis et al. 2016; Skubi et al.

2016). Consequently, experimental studies are also to be performed with a mixture of different photocatalysts in a single reaction system so as to identify novel reaction pathways, which might in turn produce products with higher yields and selectivity.

Yet another main direction which future investigations should focus will be the scaling-up of these photoredox reaction mechanisms for industrial applications to produce valuable chemicals. Recent reports on flow chemistry of photoredox catalysis demonstrate the promising feasibility and potential solution of large-quantity industrial production (Tucker et al. 2012; Nguyen et al. 2013; Wang et al. 2013; Kertalli et al. 2016). However, the usage of other novel materials such as dyestuffs as the photoredox catalyst is also an interesting area for research. This is because, with a number of articles being published on photocatalytic degradation of dyestuffs (Dong et al. 2015), a synergistic approach to use such dyestuff in effluents to catalyse the synthesis of organic compounds will come a long way in achieving the potential gains of developing a green, potentially visible light-driven organic synthesis strategies. Nonetheless, a detailed investigation unto the mechanism of such photoredox reactions will pave way for organic chemists to better understand the process and optimise it for the better.

9.8 Conclusion

Thus the usage of hazardous chemicals and less effective synthetic methods can be replaced by the more efficient heterogeneous photocatalysis for the synthesis of organics to a greater extent. It can also be studied that the application of heterogeneous photoredox catalysis in organic synthesis is not only pertained to the conversion of organic functional groups but can also provide complex carbon-hetero and carbon-carbon coupling reactions. Here both chemical and electrical neutrality are maintained due to the donation and reception of electrons taking place simultaneously. Another advantage of using visible light heterogeneous catalyst is that the whole process can be made energy efficient. In spite of huge advancement, a lot of challenges still remain in this area. A major issue in photoredox catalysis is associated to the substrate scope, which is less general than that of the respective classical methods. As a lot of current photoredox catalytic reactions depend on tertiary amine and halogen compounds for initiation of reaction, other substrates which depend on this type of activation are yet to be discovered. Heterogeneous photocatalysis is still not practically applicable from the view of catalytic activity and selectivity, which therefore has reduced its application in organic chemical synthesis. These limitations instigate the development of various catalyst systems of wider generality. The high selectivity of the products can be obtained by the synergistic catalysis of various catalysts. For instance, the introduction of organic chiral catalyst into the heterogeneous catalysis system can improve the selectivity of the products. Combined heterogeneous and homogeneous visible light catalysis may be an intriguing research topic in future. At the same time, the design and development of a novel heterogeneous catalyst are also an important gateway to the future. Furthermore,

photoredox catalysis has been incorporated along with other modes of catalytic activation, such as enamine catalysis and N-heterocyclic carbene catalysis, to attain enantioselective transformations, and has been integrated with transition metal catalysis to achieve those bond constructions that were earlier regarded to be elusive.

In spite of it still being impractical to achieve the large-scale practical transformation of organic compounds (from alcohols, amines, etc.) into valuable compounds by using photoredox catalysis, promising results obtained from certain catalytic systems consisting of quinone-based biomimetic systems, non-noble metal catalysts such as versatile $Fe(NO_3)_2$/TEMPO, high active CeO_2, Al-based MOF-253 and carbon-based materials make this an interesting problem to be considered. Nevertheless, the problems associated with performing photoredox catalysis effectively on large scales are being addressed using 'continuous flow chemistry'. With the development of much novel multifunctional catalysts, which have a higher activity, exploration of the reaction mechanisms will remain to be the primary issues to be addressed with regard to photoredox organic synthesis.

As the application of photoredox catalysis for organic transformation continues to mature, it will lead to redefining synthesis strategies and will serve to influence and strengthen these endeavours well into the future. We firmly believe that this review can act as a brief guidance for those research directed towards this area and inspire more creative techniques to be reported and implemented.

References

Abedi S, Morsali A (2014) Ordered mesoporous metal–organic frameworks incorporated with amorphous TiO2 as photocatalyst for selective aerobic oxidation in sunlight irradiation. ACS Catal 4:1398–1403. https://doi.org/10.1021/cs500123d

Ahn S, Thornburg NE, Li Z et al (2016) Stable metal–organic framework-supported niobium catalysts. Inorg Chem 55:11954–11961. https://doi.org/10.1021/acs.inorgchem.6b02103

Akashi R, Naya S, Negishi R, Tada H (2016) Two-step excitation-driven Au–TiO2–CuO three-component plasmonic photocatalyst: selective aerobic oxidation of cyclohexylamine to cyclohexanone. J Phys Chem C 120:27989–27995. https://doi.org/10.1021/acs.jpcc.6b08774

Augugliaro V, Caronna T, Di Paola A et al (2010) TiO2-based photocatalysis for organic synthesis. In: Anpo M, Kamat PV (eds) Environmentally benign photocatalysts: applications of titanium oxide-based materials. Springer, New York, pp 623–645

Baar M, Blechert S (2015) Graphitic carbon nitride polymer as a recyclable photoredox catalyst for fluoroalkylation of arenes. Chem Eur J 21:526–530. https://doi.org/10.1002/chem.201405505

Bowman WR, Mann E, Parr J et al (2000) Bu3SnH mediated oxidative radical cyclisations: synthesis of 6H-benzo[c]chromen-6-ones †. J Chem Soc Perkin Trans 1(62):2991–2999. https://doi.org/10.1039/b002539i

Cano-Yelo H, Deronzier A (1984a) Photocatalysis of the Pschorr reaction by tris-(2{,}2[prime or minute]-bipyridyl)ruthenium(II) in the phenanthrene series. J Chem Soc Perkin Trans 2:1093–1098. https://doi.org/10.1039/P29840001093

Cano-Yelo H, Deronzier A (1984b) Photo-oxidation of some carbinols by the Ru(II) polypyridyl complex-aryl diazonium salt system. Tetrahedron Lett 25:5517–5520. https://doi.org/10.1016/S0040-4039(01)81614-2

Cao K, Jiang Z, Zhang X et al (2015) Highly water-selective hybrid membrane by incorporating g-C3N4 nanosheets into polymer matrix. J Membr Sci 490:72–83. https://doi.org/10.1016/j.memsci.2015.04.050

Carboni A, Dagousset G, Magnier E, Masson G (2014) Photoredox-induced three-component oxy-, amino-, and carbotrifluoromethylation of enecarbamates. Org Lett 16:1240–1243. https://doi.org/10.1021/ol500374e

Chao D, Fu W-F (2014) Insight into highly selective photocatalytic oxidation of alcohols by a new trinuclear ruthenium complex with visible light. Dalton Trans 43:306–310. https://doi.org/10.1039/C3DT52157E

Cheng J, Li W, Duan Y et al (2017) Relay visible-light photoredox catalysis: synthesis of pyrazole derivatives via formal [4 + 1] annulation and aromatization. Org Lett 19:214–217. https://doi.org/10.1021/acs.orglett.6b03497

Cherevatskaya M, König B (2014) Heterogeneous photocatalysts in organic synthesis. Russ Chem Rev 83:183

Cherevatskaya M, Neumann M, Füldner S et al (2012) Visible-light-promoted stereoselective alkylation by combining heterogeneous photocatalysis with organocatalysis. Angew Chem Int Ed 51:4062–4066. https://doi.org/10.1002/anie.201108721

Choi W, Termin A, Hoffmann MR (1994) The role of metal ion dopants in quantum-sized TiO2: correlation between photoreactivity and charge carrier recombination dynamics. J Phys Chem 98:13669–13679. https://doi.org/10.1021/j100102a038

Cooper AI (2013) Covalent organic frameworks. Cryst Eng Comm 15:1483. https://doi.org/10.1039/C2CE90122F

Dai J-J, Zhang W-M, Shu Y-J et al (2016) Deboronative cyanation of potassium alkyltrifluoroborates via photoredox catalysis. Chem Commun 52:6793–6796. https://doi.org/10.1039/C6CC01530A

DePuccio DP, Landry CC (2016) Photocatalytic oxidation of methanol using porous Au/WO3 and visible light. Cat Sci Technol 6:7512–7520. https://doi.org/10.1039/C6CY01449F

Dewar MJS, Kubba VP (1959) New heteroaromatic compounds—IV. Tetrahedron 7:213–222. https://doi.org/10.1016/S0040-4020(01)93188-6

Dhakshinamoorthy A, Asiri AM, García H (2016) Metal-organic framework (MOF) compounds: photocatalysts for redox reactions and solar fuel production. Angew Chem Int Ed 55:5414–5445. https://doi.org/10.1002/anie.201505581

Dijksman A, Arends IWCE, Sheldon RA (2003) Cu(ii)-nitroxyl radicals as catalytic galactose oxidase mimics. Org Biomol Chem 1:3232–3237. https://doi.org/10.1039/B305941C

Dong S, Feng J, Fan M et al (2015) Recent developments in heterogeneous photocatalytic water treatment using visible light-responsive photocatalysts: a review. RSC Adv 5:14610–14630. https://doi.org/10.1039/C4RA13734E

Dong C, Higashiura Y, Marui K et al (2016a) Metal-free oxidative coupling of benzylamines to imines under an oxygen atmosphere promoted using salicylic acid derivatives as organocatalysts. ACS Omega 1:799–807. https://doi.org/10.1021/acsomega.6b00235

Dong S, Pi Y, Li Q et al (2016b) Solar photocatalytic degradation of sulfanilamide by BiOCl/reduced graphene oxide nanocomposites: mechanism and degradation pathways. J Alloys Compd 663:1–9. https://doi.org/10.1016/j.jallcom.2015.12.027

Du J, Yoon TP (2009) Crossed intermolecular [2+2] cycloadditions of acyclic enones via visible light photocatalysis. J Am Chem Soc 131:14604–14605. https://doi.org/10.1021/ja903732v

Engel DA, Dudley GB (2006) Olefination of ketones using a gold(III)-catalyzed Meyer−Schuster rearrangement. Org Lett 8:4027–4029. https://doi.org/10.1021/ol0616743

Friedmann D, Hakki A, Kim H et al (2016) Heterogeneous photocatalytic organic synthesis: state-of-the-art and future perspectives. Green Chem 18:5391–5411. https://doi.org/10.1039/C6GC01582D

Frisch AC, Beller M (2005) Catalysts for cross-coupling reactions with non-activated alkyl halides. Angew Chem Int Ed 44:674–688. https://doi.org/10.1002/anie.200461432

Fu Y, Sun L, Yang H et al (2016) Visible-light-induced aerobic photocatalytic oxidation of aromatic alcohols to aldehydes over Ni-doped NH2-MIL-125(Ti). Appl Catal B Environ 187:212–217. https://doi.org/10.1016/j.apcatb.2016.01.038

Furukawa S, Ohno Y, Shishido T et al (2011) Selective amine oxidation using Nb2O5 photocatalyst and O2. ACS Catal 1:1150–1153. https://doi.org/10.1021/cs200318n

Gil S, Marchena M, Fernández CM et al (2013) Catalytic oxidation of crude glycerol using catalysts based on Au supported on carbonaceous materials. Appl Catal A Gen 450:189–203. https://doi.org/10.1016/j.apcata.2012.10.024

Gopula B, Chiang C-W, Lee W-Z et al (2014) Highly enantioselective Rh-catalyzed alkenylation of imines: synthesis of chiral allylic amines via asymmetric addition of potassium alkenyltrifluoroborates to N-Tosyl imines. Org Lett 16:632–635. https://doi.org/10.1021/ol4035897

Goriya Y, Kim HY, Oh K (2016) O-naphthoquinone-catalyzed aerobic oxidation of amines to (Ket) imines: a modular catalyst approach. Org Lett 18:5174–5177. https://doi.org/10.1021/acs.orglett.6b02697

Guo S, Zhang H, Huang L et al (2013) Porous material-immobilized iodo-Bodipy as an efficient photocatalyst for photoredox catalytic organic reaction to prepare pyrrolo[2{,}1-a]isoquinoline. Chem Commun 49:8689–8691. https://doi.org/10.1039/C3CC44486D

Hagfeldt A, Boschloo G, Sun L et al (2010) Dye-sensitized solar cells. Chem Rev 110:6595–6663. https://doi.org/10.1021/cr900356p

Hallett-Tapley GL, Silvero MJ, González-Béjar M et al (2011) Plasmon-mediated catalytic oxidation of sec-phenethyl and benzyl alcohols. J Phys Chem C 115:10784–10790. https://doi.org/10.1021/jp202769a

Hari DP, Konig B (2014) Synthetic applications of eosin Y in photoredox catalysis. Chem Commun 50:6688–6699. https://doi.org/10.1039/C4CC00751D

Hasan Z, Cho D-W, Chon C-M et al (2016) Reduction of p-nitrophenol by magnetic co-carbon composites derived from metal organic frameworks. Chem Eng J 298:183–190. https://doi.org/10.1016/j.cej.2016.04.029

He Z, Bae M, Wu J, Jamison TF (2014) Synthesis of highly functionalized polycyclic quinoxaline derivatives using visible-light photoredox catalysis. Angew Chem 126:14679–14683. https://doi.org/10.1002/ange.201408522

He Y, Shang J, Zhao Q et al (2016) A comparative study on conversion of porous and non-porous metal–organic frameworks (MOFs) into carbon-based composites for carbon dioxide capture. Polyhedron 120:30–35. https://doi.org/10.1016/j.poly.2016.05.027

Heitz DR, Rizwan K, Molander GA (2016) Visible-light-mediated alkenylation, allylation, and cyanation of potassium alkyltrifluoroborates with organic photoredox catalysts. J Organomet Chem 81:7308–7313. https://doi.org/10.1021/acs.joc.6b01207

Hernandez-Alonso MD, Fresno F, Suarez S, Coronado JM (2009) Development of alternative photocatalysts to TiO2: challenges and opportunities. Energy Environ Sci 2:1231–1257. https://doi.org/10.1039/B907933E

Higashida S, Harada A, Kawakatsu R et al (2006) Synthesis of a coumarin compound from phenanthrene by a TiO2-photocatalyzed reaction. Chem Commun 36:2804. https://doi.org/10.1039/b604332a

Huang H, Huang J, Liu Y-M et al (2012) Graphite oxide as an efficient and durable metal-free catalyst for aerobic oxidative coupling of amines to imines. Green Chem 14:930–934. https://doi.org/10.1039/C2GC16681J

Huang S, Xu Y, Xie M et al (2015) Synthesis of magnetic CoFe2O4/g-C3N4 composite and its enhancement of photocatalytic ability under visible-light. Colloids Surf A Physicochem Eng Asp 478:71–80. https://doi.org/10.1016/j.colsurfa.2015.03.035

Huang Z, Gu Y, Liu X et al (2016) Metal-free atom transfer radical polymerization of methyl methacrylate with ppm level of organic photocatalyst. Macromol Rapid Commun. https://doi.org/10.1002/marc.201600461

Ikeda S, Fubuki M, Takahara YK, Matsumura M (2006) Photocatalytic activity of hydrothermally synthesized tantalate pyrochlores for overall water splitting. Appl Catal A Gen 300:186–190. https://doi.org/10.1016/j.apcata.2005.11.007

Ikeda S, Kobayashi H, Ikoma Y et al (2009) Structural effects of titanium(IV) oxide encapsulated in a hollow silica shell on photocatalytic activity for gas-phase decomposition of organics. Appl Catal A Gen 369:113–118. https://doi.org/10.1016/j.apcata.2009.09.008

Imamura K, Tsukahara H, Hamamichi K et al (2013) Simultaneous production of aromatic aldehydes and dihydrogen by photocatalytic dehydrogenation of liquid alcohols over metal-loaded titanium(IV) oxide under oxidant- and solvent-free conditions. Appl Catal A Gen 450:28–33. https://doi.org/10.1016/j.apcata.2012.09.051

Ingale N, Maddi V, Palkar M et al (2012) Synthesis and evaluation of anti-inflammatory and analgesic activity of 3-[(5-substituted-1,3,4-oxadiazol-2-yl-thio)acetyl]-2H-chromen-2-ones. Med Chem Res 21:16–26. https://doi.org/10.1007/s00044-010-9494-z

Isaeva VI, Kustov LM (2016) Metal-organic frameworks and related materials. In: Zeolites and zeolite-like materials. Elsevier, San Diego, pp 33–109

Ischay MA, Anzovino ME, Du J, Yoon TP (2008) Efficient visible light photocatalysis of [2+2] enone cycloadditions. J Am Chem Soc 130:12886–12887. https://doi.org/10.1021/ja805387f

Ishiyama T, Takagi J, Yonekawa Y et al (2003) Iridium-catalyzed direct borylation of five-membered heteroarenes by Bis(pinacolato)diboron: regioselective, stoichiometric, and room temperature reactions. Adv Synth Catal 345:1103–1106. https://doi.org/10.1002/adsc.200303058

Jeena V, Robinson RS (2012) Convenient photooxidation of alcohols using dye sensitised zinc oxide in combination with silver nitrate and TEMPO. Chem Commun 48:299–301. https://doi.org/10.1039/C1CC15790F

Jiang M, Yang H, Fu H (2016) Visible-light photoredox borylation of aryl halides and subsequent aerobic oxidative hydroxylation. Org Lett 18:5248–5251. https://doi.org/10.1021/acs.orglett.6b02553

Joyce LA, Sherer EC, Welch CJ (2014) Imine-based chiroptical sensing for analysis of chiral amines: from method design to synthetic application. Chem Sci 5:2855–2861. https://doi.org/10.1039/C4SC01006J

Kamat DP, Tilve SG, Kamat VP, Kirtany JK (2015) Syntheses and biological activities of chroman-2-ones. A review. Org Prep Proced Int 47:1–79. https://doi.org/10.1080/00304948.2015.983805

Kertalli E, Schouten JC, Nijhuis TA (2016) Direct synthesis of propylene oxide in the liquid phase under mild conditions. Appl Catal A Gen 524:200–205. https://doi.org/10.1016/j.apcata.2016.06.021

Königsmann M, Donati N, Stein D et al (2007) Metalloenzyme-inspired catalysis: selective oxidation of primary alcohols with an iridium–aminyl-radical complex. Angew Chem Int Ed 46:3567–3570. https://doi.org/10.1002/anie.200605170

Kryvoruchko A, Yurlova L, Kornilovich B (2002) Purification of water containing heavy metals by chelating-enhanced ultrafiltration. Desalination 144:243–248. https://doi.org/10.1016/S0011-9164(02)00319-3

Kumar SG, Devi LG (2011) Review on modified TiO2 photocatalysis under UV/visible light: selected results and related mechanisms on interfacial charge carrier transfer dynamics. J Phys Chem A 115:13211–13241. https://doi.org/10.1021/jp204364a

Kumar P, Varma S, Jain SL et al (2014) A TiO2 immobilized Ru(ii) polyazine complex: a visible-light active photoredox catalyst for oxidative cyanation of tertiary amines. J Mater Chem A 2:4514. https://doi.org/10.1039/c3ta14783e

Kumar R, Gleissner EH, Tiu EG V., Yamakoshi Y (2016a) ChemInform abstract: C $_{70}$ as a photocatalyst for oxidation of secondary benzylamines to imines. ChemInform 47. https://doi.org/10.1002/chin.201622157

Kumar R, Gleißner EH, Tiu EGV, Yamakoshi Y (2016b) C70 as a photocatalyst for oxidation of secondary benzylamines to imines. Org Lett 18:184–187. https://doi.org/10.1021/acs.orglett.5b03194

Lang X, Chen X, Zhao J (2014a) Heterogeneous visible light photocatalysis for selective organic transformations. Chem Soc Rev 43:473–486. https://doi.org/10.1039/C3CS60188A

Lang X, Ma W, Chen C et al (2014b) Selective aerobic oxidation mediated by TiO2 photocatalysis. Acc Chem Res 47:355–363. https://doi.org/10.1021/ar4001108

Lee DG, Spitzer UA (1970) Aqueous dichromate oxidation of primary alcohols. J Organomet Chem 35:3589–3590. https://doi.org/10.1021/jo00835a101

Li X-H, Wang X, Antonietti M (2012) Solvent-free and metal-free oxidation of toluene using O2 and g-C3N4 with nanopores: nanostructure boosts the catalytic selectivity. ACS Catal 2:2082–2086. https://doi.org/10.1021/cs300413x

Li J, Sun S, Qian C et al (2016a) The role of adsorption in photocatalytic degradation of ibuprofen under visible light irradiation by BiOBr microspheres. Chem Eng J 297:139–147. https://doi.org/10.1016/j.cej.2016.03.145

Li Y-H, Liu X-L, Yu Z-T et al (2016b) Osmium(ii) complexes for light-driven aerobic oxidation of amines to imines. Dalton Trans 45:12400–12408. https://doi.org/10.1039/C6DT02331B

Li Y, Miao J, Sun X et al (2016c) Mechanochemical synthesis of Cu-BTC@GO with enhanced water stability and toluene adsorption capacity. Chem Eng J 298:191–197. https://doi.org/10.1016/j.cej.2016.03.141

Li M, Hao Y, Cárdenas-Lizana F, Keane MA (2017a) Gold promoted imine production by selective gas phase reductive coupling of nitrobenzene and benzaldehyde. Appl Catal A Gen 531:52–59. https://doi.org/10.1016/j.apcata.2016.11.037

Li M, Wu S, Yang X et al (2017b) Highly efficient single atom cobalt catalyst for selective oxidation of alcohols. Appl Catal A Gen 543:61–66. https://doi.org/10.1016/j.apcata.2017.06.018

Liang S, Wen L, Lin S et al (2014) Monolayer HNb_3O_8 for selective photocatalytic oxidation of benzylic alcohols with visible light response. Angew Chem 126:2995–2999. https://doi.org/10.1002/ange.201311280

Lin S, Ischay MA, Fry CG, Yoon TP (2011) Radical cation Diels–Alder cycloadditions by visible light photocatalysis. J Am Chem Soc 133:19350–19353. https://doi.org/10.1021/ja2093579

Liu Q, Zhu F-P, Jin X-L et al (2015) Visible-light-driven intermolecular [2+2] cycloadditions between coumarin-3-carboxylates and acrylamide analogs. Chem Eur J 21:10326–10329. https://doi.org/10.1002/chem.201501176

Long B, Ding Z, Wang X (2013) Carbon nitride for the selective oxidation of aromatic alcohols in water under visible light. ChemSusChem 6:2074–2078. https://doi.org/10.1002/cssc.201300360

Lu Z, Shen M, Yoon TP (2011) [3+2] cycloadditions of aryl cyclopropyl ketones by visible light photocatalysis. J Am Chem Soc 133:1162–1164. https://doi.org/10.1021/ja107849y

Magdziarz A, Colmenares JC, Chernyayeva O et al (2016) Iron-containing Titania photocatalyst prepared by the sonophotodeposition method for the oxidation of benzyl alcohol. ChemCatChem 8:536–539. https://doi.org/10.1002/cctc.201501250

Maldotti A, Molinari A, Amadelli R (2002) Photocatalysis with organized systems for the oxofunctionalization of hydrocarbons by O2. Chem Rev 102:3811–3836. https://doi.org/10.1021/cr010364p

Mera AC, Contreras D, Escalona N, Mansilla HD (2016) BiOI microspheres for photocatalytic degradation of gallic acid. J Photochem Photobiol A Chem 318:71–76. https://doi.org/10.1016/j.jphotochem.2015.12.005

Miyake GM, Theriot JC (2014) Perylene as an organic photocatalyst for the radical polymerization of functionalized vinyl monomers through oxidative quenching with alkyl bromides and visible light. Macromolecules 47:8255–8261. https://doi.org/10.1021/ma502044f

Miyaura N (2008) Metal-catalyzed cross-coupling reactions of organoboron compounds with organic halides. In: Metal-catalyzed cross-coupling reactions. Wiley-VCH Verlag GmbH, Weinheim, pp 41–123

Muthusamy S, Kumarswamyreddy N, Kesavan V, Chandrasekaran S (2016) Recent advances in aerobic oxidation with ruthenium catalysts. Tetrahedron Lett 57:5551–5559. https://doi.org/10.1016/j.tetlet.2016.11.024

Narayanam JMR, Stephenson CRJ (2011) Visible light photoredox catalysis: applications in organic synthesis. Chem Soc Rev 40:102–113. https://doi.org/10.1039/B913880N

Naya S, Kimura K, Tada H (2013) One-step selective aerobic oxidation of amines to imines by gold nanoparticle-loaded rutile titanium(IV) oxide plasmon photocatalyst. ACS Catal 3:10–13. https://doi.org/10.1021/cs300682d

Nguyen JD, Tucker JW, Konieczynska MD, Stephenson CRJ (2011) Intermolecular atom transfer radical addition to olefins mediated by oxidative quenching of photoredox catalysts. J Am Chem Soc 133:4160–4163. https://doi.org/10.1021/ja108560e

Nguyen JD, Reiß B, Dai C et al (2013) Batch to flow deoxygenation using visible light photoredox catalysis. Chem Commun 49:4352–4354. https://doi.org/10.1039/C2CC37206A

Niu H, Liu S, Cai Y et al (2016) MOF derived porous carbon supported Cu/Cu2O composite as high performance non-noble catalyst. Microporous Mesoporous Mater 219:48–53. https://doi.org/10.1016/j.micromeso.2015.07.027

Ohtani B, Tsuru S, Nishimoto S et al (1990) Photocatalytic one-step syntheses of cyclic imino acids by aqueous semiconductor suspensions. J Organomet Chem 55:5551–5553. https://doi.org/10.1021/jo00308a005

Ohtani B, Iwai K, Kominami H et al (1995a) Titanium(IV) oxide photocatalyst of ultra-high activity for selective N-cyclization of an amino acid in aqueous suspensions. Chem Phys Lett 242:315–319. https://doi.org/10.1016/0009-2614(95)00740-U

Ohtani B, Kawaguchi J, Kozawa M et al (1995b) Effect of platinum loading on the photocatalytic activity of cadmium(II) sulfide particles suspended in aqueous amino acid solutions. J Photochem Photobiol A Chem 90:75–80. https://doi.org/10.1016/1010-6030(95)04084-S

Ohtani B, Pal B, Ikeda S (2003) Photocatalytic organic syntheses: selective cyclization of amino acids in aqueous suspensions. Catal Surv from Asia 7:165–176. https://doi.org/10.1023/A:1025389725637

Ohzu S, Ishizuka T, Hirai Y et al (2012) Mechanistic insight into catalytic oxidations of organic compounds by ruthenium(iv)-oxo complexes with pyridylamine ligands. Chem Sci 3:3421–3431. https://doi.org/10.1039/C2SC21195E

Ovoshchnikov DS, Donoeva BG, Golovko VB (2015) Visible-light-driven aerobic oxidation of amines to nitriles over hydrous ruthenium oxide supported on TiO2. ACS Catal 5:34–38. https://doi.org/10.1021/cs501186n

Patil NT, Shinde VS, Thakare MS et al (2012) Exploiting the higher alkynophilicity of Au-species: development of a highly selective fluorescent probe for gold ions. Chem Commun 48:11229–11231. https://doi.org/10.1039/C2CC35083A

Prier CK, Rankic DA, MacMillan DWC (2013) Visible light photoredox catalysis with transition metal complexes: applications in organic synthesis. Chem Rev 113:5322–5363. https://doi.org/10.1021/cr300503r

Puri S, Kaur B, Parmar A, Kumar H (2009) Ultrasound-promoted greener synthesis of 2H-chromen-2-ones catalyzed by copper perchlorate in solventless media. Ultrason Sonochem 16:705–707. https://doi.org/10.1016/j.ultsonch.2009.04.002

Qin Y, Zhang L, Lv J et al (2015) Bioinspired organocatalytic aerobic C–H oxidation of amines with an ortho-quinone catalyst. Org Lett 17:1469–1472. https://doi.org/10.1021/acs.orglett.5b00351

Qiu D, Mo F, Zheng Z et al (2010) Gold(III)-catalyzed halogenation of aromatic boronates with N-halosuccinimides. Org Lett 12:5474–5477. https://doi.org/10.1021/ol102350v

Rana S, Maddila S, Yalagala K, Jonnalagadda SB (2015) Organo functionalized graphene with Pd nanoparticles and its excellent catalytic activity for Suzuki coupling reaction. Appl Catal A Gen 505:539–547. https://doi.org/10.1016/j.apcata.2015.07.018

Ravelli D, Fagnoni M (2012) Dyes as visible light photoredox organocatalysts. Chem Cat Chem 4:169–171. https://doi.org/10.1002/cctc.201100363

Revol G, McCallum T, Morin M et al (2013) Photoredox transformations with dimeric gold complexes. Angew Chem Int Ed 52:13342–13345. https://doi.org/10.1002/anie.201306727

Rohini KSP, S PS (2014) Therapeutic role of coumarins and coumarin-related compounds. J Biofertilizers Biopestic 5:1–3. https://doi.org/10.4172/2157-7544.1000130

Romero M, Blanco J, Sánchez B et al (1999) Solar photocatalytic degradation of water and air pollutants: challenges and perspectives. Sol Energy 66:169–182. https://doi.org/10.1016/S0038-092X(98)00120-0

Ronad P, Dharbamalla S, Hunshal R, Maddi V (2008) Synthesis of novel substituted 7-(Benzylideneamino)-4-,ethyl-2 *H* -chromen-2-one derivatives as anti-inflammatory and analgesic agents. Arch Pharm (Weinheim) 341:696–700. https://doi.org/10.1002/ardp.200800057

Rueping M, Zhu S, Koenigs RM et al (2011) Visible-light photoredox catalyzed oxidative Strecker reaction. Chem Commun 47:12709. https://doi.org/10.1039/c1cc15643h

Sadiq M, Saeed K, Sadiq S et al (2017) Liquid phase oxidation of cinnamyl alcohol to cinnamaldehyde using multiwall carbon nanotubes decorated with zinc-manganese oxide nanoparticles. Appl Catal A Gen 539:97–103. https://doi.org/10.1016/j.apcata.2017.04.007

Sahiner N, Demirci S, Sahiner M, Yilmaz S (2016) Application of superporous magnetic cationic cryogels for persistent chromate (toxic chromate and dichromate) uptake from aqueous environments. J Appl Polym Sci 133:n/a-n/a. https://doi.org/10.1002/app.43438

Sahoo B, Hopkinson MN, Glorius F (2013) Combining gold and photoredox catalysis: visible light-mediated oxy- and aminoarylation of alkenes. J Am Chem Soc 135:5505–5508. https://doi.org/10.1021/ja400311h

Samec JSM, Éll AH, Bäckvall J-E (2005) Efficient ruthenium-catalyzed aerobic oxidation of amines by using a biomimetic coupled catalytic system. Chem Eur J 11:2327–2334. https://doi.org/10.1002/chem.200401082

Selvam K, Sakamoto H, Shiraishi Y, Hirai T (2015) Photocatalytic secondary amine synthesis from azobenzenes and alcohols on TiO2 loaded with Pd nanoparticles. New J Chem 39:2856–2860. https://doi.org/10.1039/C5NJ00158G

Shaabani A, Tavasoli-Rad F, Lee DG (2005) Potassium permanganate oxidation of organic compounds. Synth Commun 35:571–580. https://doi.org/10.1081/SCC-200049792

Shekhawat K, Chatterjee S, Joshi B (2015) Chromium toxicity and its health hazards. Int J Adv Res 3:167–172

Shen C, Zhao C, Xin F et al (2015a) Nitrogen-modified carbon nanostructures derived from metal-organic frameworks as high performance anodes for Li-ion batteries. Electrochim Acta 180:852–857. https://doi.org/10.1016/j.electacta.2015.09.036

Shen L, Liang R, Wu L (2015b) Strategies for engineering metal-organic frameworks as efficient photocatalysts. Chin J Catal 36:2071–2088. https://doi.org/10.1016/S1872-2067(15)60984-6

Shimizu K, Shimura K, Tamagawa N et al (2012) Sulfur promoted Pt/SiO2 catalyzed cross-coupling of anilines and amines. Appl Catal A Gen 417–418:37–42. https://doi.org/10.1016/j.apcata.2011.12.019

Shiraishi Y, Sugano Y, Tanaka S, Hirai T (2010) One-pot synthesis of benzimidazoles by simultaneous photocatalytic and catalytic reactions on Pt@TiO2 nanoparticles. Angew Chem 122:1700–1704. https://doi.org/10.1002/ange.200906573

Skubi KL, Blum TR, Yoon TP (2016) Dual catalysis strategies in photochemical synthesis. Chem Rev 116:10035–10074. https://doi.org/10.1021/acs.chemrev.6b00018

Sorour MH, Hani HA, Shaalan HF, El-Sayed MMH (2016) Experimental screening of some chelating agents for calcium and magnesium removal from saline solutions. Desalin Water Treat 57:22799–22808. https://doi.org/10.1080/19443994.2015.1111595

Stahl AEW, Shannon S (2016) Quinones in hydrogen peroxide synthesis and catalytic aerobic oxidation reactions. In: Liquid phase aerobic oxidation catalysis: industrial applications and academic perspectives: industrial applications and academic perspectives. Wiley-VCH Verlag GmbH & Co. KGaA, Weinheim

Su F, Mathew SC, Lipner G et al (2010) mpg-C3N4-catalyzed selective oxidation of alcohols using O2 and visible light. J Am Chem Soc 132:16299–16301. https://doi.org/10.1021/ja102866p

Su L, Ye X, Meng S et al (2016) Effect of different solvent on the photocatalytic activity of ZnIn2S4 for selective oxidation of aromatic alcohols to aromatic aldehydes under visible light irradiation. Appl Surf Sci 384:161–174. https://doi.org/10.1016/j.apsusc.2016.04.084

Sun D, Ye L, Li Z (2015) Visible-light-assisted aerobic photocatalytic oxidation of amines to imines over NH2-MIL-125(Ti). Appl Catal B Environ 164:428–432. https://doi.org/10.1016/j.apcatb.2014.09.054

Suzuki K, Tang F, Kikukawa Y et al (2014) Visible-light-induced photoredox catalysis with a tetracerium-containing silicotungstate. Angew Chem Int Ed 53:5356–5360. https://doi.org/10.1002/anie.201403215

Tanaka A, Hashimoto K, Kominami H (2011) Selective photocatalytic oxidation of aromatic alcohols to aldehydes in an aqueous suspension of gold nanoparticles supported on cerium (iv) oxide under irradiation of green light. Chem Commun 47:10446–10448. https://doi.org/10.1039/C1CC13801D

Tang J, Grampp G, Liu Y et al (2015) Visible light mediated cyclization of tertiary anilines with maleimides using nickel(II) oxide surface-modified titanium dioxide catalyst. J Organomet Chem 80:2724–2732. https://doi.org/10.1021/jo502901h

Tellis JC, Kelly CB, Primer DN et al (2016) Single-electron transmetalation via photoredox/nickel dual catalysis: unlocking a new paradigm for sp^3–sp^2 cross-coupling. Acc Chem Res 49:1429–1439. https://doi.org/10.1021/acs.accounts.6b00214

Tighadouini S, Radi S, Bacquet M et al (2015) Synthesis of 1-(furan-2-yl) imine functionalized silica as a chelating sorbent and its preliminary use in metal ion adsorption. Sep Sci Technol 50:710–717. https://doi.org/10.1080/01496395.2014.959134

Togo H, Muraki T, Yokoyama M (1995) Remote functionalization (1): synthesis of γ- and δ-lactones from aromatic carboxylic acids. Tetrahedron Lett 36:7089–7092. https://doi.org/10.1016/0040-4039(95)01432-H

Trost BM, Weiss AH (2009) The enantioselective addition of alkyne nucleophiles to carbonyl groups. Adv Synth Catal 351:963–983. https://doi.org/10.1002/adsc.200800776

Tuccio SA, Drexhage KH, Reynolds GA (1973) cw laser emission from coumarin dyes in the blue and green. Opt Commun 7:248–252. https://doi.org/10.1016/0030-4018(73)90021-7

Tucker JW, Stephenson CRJ (2012) Shining light on photoredox catalysis: theory and synthetic applications. J Organomet Chem 77:1617–1622. https://doi.org/10.1021/jo202538x

Tucker JW, Narayanam JMR, Krabbe SW, Stephenson CRJ (2010) Electron transfer photoredox catalysis: intramolecular radical addition to indoles and pyrroles. Org Lett 12:368–371. https://doi.org/10.1021/ol902703k

Tucker JW, Zhang Y, Jamison TF, Stephenson CRJ (2012) Visible-light photoredox catalysis in flow. Angew Chem Int Ed 51:4144–4147. https://doi.org/10.1002/anie.201200961

Tyson EL, Ament MS, Yoon TP (2013) Transition metal photoredox catalysis of radical Thiol-ene reactions. J Organomet Chem 78:2046–2050. https://doi.org/10.1021/jo3020825

Ushakov DB, Plutschack MB, Gilmore K, Seeberger PH (2015) Factors influencing the regioselectivity of the oxidation of asymmetric secondary amines with singlet oxygen. Chem Eur J 21:6528–6534. https://doi.org/10.1002/chem.201500121

Verma S, Baig RBN, Nadagouda MN, Varma RS (2016) Selective oxidation of alcohols using photoactive VO@g-C3N4. ACS Sustain Chem Eng 4:1094–1098. https://doi.org/10.1021/acssuschemeng.5b01163

Wallentin C-J, Nguyen JD, Finkbeiner P, Stephenson CRJ (2012) Visible light-mediated atom transfer radical addition via oxidative and reductive quenching of photocatalysts. J Am Chem Soc 134:8875–8884. https://doi.org/10.1021/ja300798k

Wang P, Huang B, Dai Y, Whangbo M-H (2012) Plasmonic photocatalysts: harvesting visible light with noble metal nanoparticles. Phys Chem Chem Phys 14:9813–9825. https://doi.org/10.1039/C2CP40823F

Wang X, Cuny GD, Noël T (2013) A mild, one-pot Stadler-Ziegler synthesis of arylsulfides facilitated by photoredox catalysis in batch and continuous-flow. Angew Chem 125:8014–8018. https://doi.org/10.1002/ange.201303483

Wang H, Yuan X, Wu Y et al (2015a) Synthesis and applications of novel graphitic carbon nitride/metal-organic frameworks mesoporous photocatalyst for dyes removal. Appl Catal B Environ 174–175:445–454. https://doi.org/10.1016/j.apcatb.2015.03.037

Wang ZJ, Garth K, Ghasimi S et al (2015b) Conjugated microporous poly (benzochalcogenadiazole)s for photocatalytic oxidative coupling of amines under visible light. Chem Sus Chem 8:3459–3464. https://doi.org/10.1002/cssc.201500827

Wang X, Ding S, Wang H et al (2017) Conversion of propionic acid and 3-pentanone to hydrocarbons on ZSM-5 catalysts: reaction pathway and active site. Appl Catal A Gen 545:79–89. https://doi.org/10.1016/j.apcata.2017.07.037

Woźnica M, Chaoui N, Taabache S, Blechert S (2014) THF: an efficient electron donor in continuous flow radical cyclization photocatalyzed by graphitic carbon nitride. Chem Eur J 20:14624–14628. https://doi.org/10.1002/chem.201404440

Wu Y, Yuan B, Li M et al (2015) Well-defined BiOCl colloidal ultrathin nanosheets: synthesis{,} characterization{,} and application in photocatalytic aerobic oxidation of secondary amines. Chem Sci 6:1873–1878. https://doi.org/10.1039/C4SC03229B

Xi Y, Yi H, Lei A (2013) Synthetic applications of photoredox catalysis with visible light. Org Biomol Chem 11:2387–2403. https://doi.org/10.1039/C3OB40137E

Xia X-D, Ren Y-L, Chen J-R et al (2015) Phototandem catalysis: efficient synthesis of 3-Ester-3-hydroxy-2-oxindoles by a visible light-induced cyclization of diazoamides through an aerobic oxidation sequence. Chem Asian J 10:124–128. https://doi.org/10.1002/asia.201402990

Xu J, He S, Zhang H et al (2015) Layered metal-organic framework/graphene nanoarchitectures for organic photosynthesis under visible light. J Mater Chem A 3:24261–24271. https://doi.org/10.1039/C5TA06838J

Xu J, Shang J-K, Chen Y et al (2017) Palladium nanoparticles supported on mesoporous carbon nitride for efficiently selective oxidation of benzyl alcohol with molecular oxygen. Appl Catal A Gen 542:380–388. https://doi.org/10.1016/j.apcata.2017.05.036

Xuan J, Xia X-D, Zeng T-T et al (2014) Visible-light-induced formal [3+2] cycloaddition for pyrrole synthesis under metal-free conditions. Angew Chem 126:5759–5762. https://doi.org/10.1002/ange.201400602

Yadav AK, Yadav LDS (2017) Visible light photoredox catalysis with N-hydroxyphthalimide for [4+2] cyclization between N-methylanilines and maleimides. Tetrahedron Lett 58:552–555. https://doi.org/10.1016/j.tetlet.2016.12.077

Yan G, Jiang Y, Kuang C et al (2010) Nano-Fe2O3-catalyzed direct borylation of arenes. Chem Commun 46:3170–3172. https://doi.org/10.1039/B926945B

Zani L, Bolm C (2006) Direct addition of alkynes to imines and related C[double bond{,} length as m-dash]N electrophiles: a convenient access to propargylamines. Chem Commun:4263–4275. https://doi.org/10.1039/B607986P

Zeitler K (2009) Photoredox catalysis with visible light. Angew Chem Int Ed 48:9785–9789. https://doi.org/10.1002/anie.200904056

Zen J-M, Liou S-L, Kumar AS, Hsia M-S (2003) An efficient and selective photocatalytic system for the oxidation of sulfides to sulfoxides. Angew Chem 115:597–599. https://doi.org/10.1002/ange.200390134

Zhang Y, Xu Y-J (2014) Bi2WO6: a highly chemoselective visible light photocatalyst toward aerobic oxidation of benzylic alcohols in water. RSC Adv 4:2904–2910. https://doi.org/10.1039/C3RA46383D

Zhang M, Chen C, Ma W, Zhao J (2008) Visible-light-induced aerobic oxidation of alcohols in a coupled photocatalytic system of dye-sensitized TiO_2 and TEMPO. Angew Chem Int Ed 47:9730–9733. https://doi.org/10.1002/anie.200803630

Zhang C, Tang C, Jiao N (2012) Recent advances in copper-catalyzed dehydrogenative functionalization via a single electron transfer (SET) process. Chem Soc Rev 41:3464–3484. https://doi.org/10.1039/C2CS15323H

Zhang L-S, Chen G, Wang X et al (2014a) Direct borylation of primary C□H bonds in functionalized molecules by palladium catalysis. Angew Chem Int Ed 53:3899–3903. https://doi.org/10.1002/anie.201310000

Zhang N, Samanta SR, Rosen BM, Percec V (2014b) Single electron transfer in radical ion and radical-mediated organic, materials and polymer synthesis. Chem Rev 114:5848–5958. https://doi.org/10.1021/cr400689s

Zhang P, Wu P, Bao S et al (2016) Synthesis of sandwich-structured AgBr@Ag@TiO2 composite photocatalyst and study of its photocatalytic performance for the oxidation of benzyl alcohols to benzaldehydes. Chem Eng J 306:1151–1161. https://doi.org/10.1016/j.cej.2016.08.015

Zhao Y, Chen J-R, Xiao W-J (2016) Synthesis of hydrazide-containing chroman-2-ones and dihydroquinolin-2-ones via photocatalytic radical cascade reaction of aroylhydrozones. Org Lett 18:6304–6307. https://doi.org/10.1021/acs.orglett.6b03174

Zhen W, Ma J, Lu G (2016) Small-sized Ni(111) particles in metal-organic frameworks with low over-potential for visible photocatalytic hydrogen generation. Appl Catal B Environ 190:12–25. https://doi.org/10.1016/j.apcatb.2016.02.061

Zheng Z, Chen C, Bo A, et al (2014) Visible-light-induced selective photocatalytic oxidation of benzylamine into imine over supported Ag/AgI photocatalysts. ChemCatChem 6:n/a-n/a. https://doi.org/10.1002/cctc.201301030

Zou Y-Q, Chen J-R, Liu X-P et al (2012) Highly efficient aerobic oxidative hydroxylation of arylboronic acids: photoredox catalysis using visible light. Angew Chem 124:808–812. https://doi.org/10.1002/ange.201107028

Index

Inamuddin et al. (eds.), *Nanophotocatalysis and Environmental Applications*,
Environmental Chemistry for a Sustainable World 31,
https://doi.org/10.1007/978-3-030-04949-2